Metabolic flux analysis of the nitrogen-fixing bacterium *Azorhizobium caulinodans*

Khushboo Borah

Department of Plant Sciences

Keble College

University of Oxford

A thesis submitted for the degree of

Doctor of Philosophy

Michaelmas Term 2017

Supervisors**:**

Professor R. George Ratcliffe

Dr. Nicholas J. Kruger

Professor Philip S. Poole

Abstract

Metabolic flux analysis of the nitrogen-fixing bacterium *Azorhizobium caulinodans*

Khushboo Borah, Keble College

Submitted for the degree of D.Phil, Michaelmas Term 2017

Symbiotic nitrogen fixation in rhizobial-legume symbioses is important for agriculture and the establishment of a successful symbiosis depends on the metabolic integration of the rhizobia inside the host nodules. This study aims to understand the metabolic adaptations in a rhizobium during nitrogen fixation. The study uses ^{13}C-metabolic flux analysis to derive carbon fluxes across the metabolic network of the model diazotrophic rhizobium, *Azorhizobium caulinodans* ORS571. The flux maps obtained for aerobic, micro-aerobic and nitrogen-fixing free-living cultures identified these metabolic adjustments as an increase in polyhydroxybutyrate synthesis and tricarboxylic acid cycle fluxes required to sustain growth and metabolism during micro-aerobic nitrogen fixation. Flux maps for bacteroids, isolated from the root and stem nodules of *S. rostrata*, highlighted reduced tricarboxylic acid cycle fluxes and increased flux through the methyl malonate semialdehyde pathway relative to the free-living N_2-fixing cultures. Polyhydroxybutyrate was indispensable for nitrogen fixation and diazotrophic growth in free-living cultures, and for establishment of effective symbiosis with the host, but it was less important for the growth of non-nitrogen fixing free-living cultures under aerobic and micro-aerobic conditions. Deletion of polyhydroxybutyrate under aerobic conditions resulted in slow growth and caused changes in biomass synthesis, mainly affecting lipids and exo-polysaccharide. Under micro-aerobic conditions, deletion of polyhydroxybutyrate also resulted in slow growth and increased fluxes through the tricarboxylic acid cycle, gluconeogenesis, and the pentose phosphate pathway. There was a significant rise in lipid production that potentially substituted for polyhydroxybutyrate and maintained redox balance during micro-aerobic growth. The combined findings from the flux maps highlight the adjustments in central carbon metabolism associated with free-living and symbiotic nitrogen fixation. This knowledge is important for research aimed at improving the existing symbiosis and developing synthetic symbioses between rhizobia and non-legumes, which will reduce dependence on chemical nitrogen fertilizers.

Acknowledgements

I am grateful to my supervisors Professor George Ratcliffe, Dr. Nick Kruger and Professor Philip Poole for providing me with the opportunity to work on this project and for their guidance, patience and support throughout.

I would like to thank Dr. Vinoy Ramachandran, Dr. Carmen Canizares, Professor Hugh Dickinson, Mr Pedro Bota and Dr. Andrez Tckaz for their support with equipment and laboratory work.

I acknowledge the assistance provided by Louis Dreyfus Weidenfeld scholarship and leadership programme.

Finally, I would like to thank my parents Kusha and Santana, my fiancé, Chris Slater, and friends for their understanding, encouragement and invaluable support.

Abbreviations

Ac: Acetate

AcCoA: Acetyl-CoA

ADP: Adenosine diphosphate

AKG: α-Ketoglutarate

AMP: Adenosine monophosphate

ANOVA: Analysis of variance

ATP: Adenosine triphosphate

Ala: Alanine

Asn: Asparagine

Arg: Arginine

Asp: Asparate

Cit: Citrate

CoA: Coenzyme A

Cys: Cysteine

CTP: Cytidine triphosphate

DOT dissolved oxygen tension

DCW: Dry cell weight

DOF: Degrees of freedom

DNA: Deoxyribonucleic acid

DHAP: Dihydroxyacetone phosphate

ED: Entner–Doudoroff

EMP: Embden-Meyerhof-Parnas

EPS: Exo-polysaccharide

E4P: Erythrose-4-phosphate

EC: Enzyme component

FAD: Flavine adenine dinucleotide

$FADH_2$: Dihydroflavine-adenine dinucleotide

Fum: Fumarate

F6P: Fructose-6-phosphate

FBP: Fructose-1,6-bisphosphate

FTHF: Formyltetrahydrofolate

G6P: Glucose-6-phosphate

Glu: Glutamate

Gly: Glycine

Gln: Glutamine

GC: Gas chromatography

GC-MS: Gas chromatography mass spectrometry

GDP: Guanosine diphosphate

GTP: Guanosine triphosphate

GAP: Glyceraldehyde-3-phosphate

GS/GOGAT: Glutamine synthetase/ Glutamate synthase

His: Histidine

ICit: Isocitrate

Ile: Isoleucine

IMP: Inosine monophosphate

INCA: Isotopomer network compartmental analysis

Kb: kilo bases

KDPG: 2-Keto-3-deoxy-6-phosphogluconate

Leu: Leucine

Lys: Lysine

LL_DAP: L,L-diaminopimelate aminotransferase

LPS: Lipopolysaccharide

MFA: Metabolic flux analysis

MSDH: Methylmalonate semialdehyde dehydrogenase

Met: Methionine

MI: Mass isotopomer

MID: Mass isotopomer distribution

MSTFA: N-methyl-N-trimethylsilyl trifluroacetamide

Mal: Malate

METHF: Methyltetrahydrofolate

MEETHF: Methylenetetrahydrofolate

MS: Mass spectrometry

ME: Malic enzyme

NAD: Nicotinamide adenine dinucleotide

NADH: Dihydronicotinamide adenine dinucleotide

NADP: Nicotinamide adenine dinucleotide phosphate

NADPH: Dihydronicotinamide adenine dinucleotide phosphate

OAA: Oxaloacetate

PPP: Pentose phosphate pathway

PCR: Polymerase chain reaction

Pro: Proline

PG6: 6-Phosphogluconate

PEP: Phosphoenolpyruvate

Pepck: Phophoenolpyruvate carboxykinase

Pyr: Pyruvate

PHB: Polyhydroxybutyrate

PG3: 3-Phosphoglycerate

Phe: Phenylalanine

RNA: Ribonucleic acid

Ru5P: Ribulose-5-phosphate

R5P: Ribose-5-phosphate

ROS: Reactive oxygen species

SEM: Standard error of the mean

SD: Standard deviation of the mean

S7P: Sedoheptulose-7-phosphate

SSR: Sum of squared residual

Ser: Serine

Suc: Succinate

Suc_nat: Unlabelled succinate

SucCoA: Succinyl CoA

TIC: Total ion counts

Thr: Threonine

Tyr: Tyrosine

Trp: Tryptophan

TBDMS: N-tert-butyldimethylsilyl-N-methyl trifluoroacetamide

TCA: Tricarboxylic acid cycle

UMP: Uridine monophosphate

Val: Valine

X5P: Xylulose-5-phosphate

Table of contents

1. Introduction

Nitrogen is indispensable for plant growth and productivity; hence it is an important factor for agricultural systems. All the major cultivated food and cash crops require large inputs of nitrogen in the soils to sustain their growth and productivity. Di-nitrogen available in the atmosphere cannot be used directly by plants but they assimilate nitrogen in the form of nitrate and ammonia. This demand for nitrate and ammonia is fulfilled by commercially available synthetic nitrogen fertilizers. With the increasing human population, the demand for food production increases, and so the dependence on the fertilizers in the agricultural systems increases to enhance crop yields. But nearly 60 % of the total fertilizer applied is not absorbed by the crops and it ultimately leaks into underground water systems and sea, negatively affecting marine life (Cheng, 2008; Conley, 2012). Also the production of synthetic fertilizers is expensive and poses serious environmental threat (Peoples et al., 1995; Cheng, 2008; Tkacz & Poole, 2015; Dent & Cocking, 2017). Certain soil micro-organisms perform biological nitrogen fixation (BNF), where they convert atmospheric di-nitrogen to ammonia and enrich nitrogen content of the soil. BNF is also carried out in a rhizobial-legume symbiosis, where rhizobia, a group of nitrogen (N_2) fixing bacteria that belongs to the class of α-proteobacteria, enters into an efficient symbiotic association with the plants of the Leguminosae family. This symbiosis is of great biological and ecological importance and a major contributor to the global nitrogen cycle (Okazaki et al., 2016). Rhizobia can be found as free-living organisms in the soil or as nitrogen-fixing symbionts inside their host plant (Gage, 2004). Plants benefit from the fixed nitrogen in exchange for the carbon substrates supplied to the associated rhizobia.

Legume plants increase the fertility of the soil with fixed nitrogen, so it is also used in crop rotation practice with food crops like rice, wheat and maize (Boddey et al., 1997; Graham & Vance, 2000; Bar et al., 2000). Decomposition of legumes and also their root exudates and nodule necrosis adds nitrogen to the soil and improves soil quality

(Chen et al., 2003; Herridge et al., 2008; Fustec et al., 2010; Berrada & Fikri-Benbrahim, 2014; Carranca et al., 2015). So, this symbiotic association is of great significance in agricultural systems for enriching soil nitrogen and has the potential to substitute for synthetic nitrogen fertilizers and reduce their use (Ghosh & Bhat, 1998; López-López et al., 2010; Peoples et al., 2009). Rhizobia used as biofertilizers for crops such as rice and wheat increased the photosynthetic rates of the plants and grain yield (Yanni et al., 1997; Biswas et al., 2000; Peng et al., 2002; El-Sirafy et al., 2005). Consequently, symbiotic nitrogen fixation is an intensive research area and there is particular interest in finding ways to extend the process to non-N_2 fixing plants such as cereal crops for the development of sustainable agricultural systems (Mus et al., 2016; Gopalakrishnan et al., 2015). Such engineered symbiosis in non-legumes in addition to the existing rhizobial-legume symbiosis would increase the sustainability of agricultural systems and improve food security.

1.1 Symbiotic interaction between rhizobia and legumes

The symbiotic association between rhizobia and legumes involves a sequence of interaction and invasion stages that result in the development of a N_2 fixing nodule (Figure 1.1). The process begins with the induction of *Nod* genes in rhizobia in response to the secretion of flavonoids by the host plant. *Nod* genes are responsible for the production of rhizobial signal molecules or nod factors that play an important role in the early stages of interaction between the plant and bacteria. Nod factors (NFs) are lipochitoligosaccharides that are responsible for nodule organogenesis in the host plant (Geelen et al., 1995; Suzuki et al., 2007). Rhizobia colonize legume roots and NFs induces calcium signaling in the root hairs causing alterations in the root hair cytoskeleton which ultimately results in morphological changes like curling and swelling of the root hairs (Chang et al., 2009). After attachment, rhizobia enter the host plant through a tubular structure called the infection thread which is composed of structural

components from both symbiotic partners (Rae et al., 1992; Gage, 2004; Montiel et al., 2016). Exo-polysaccharides- succinoglycan (EPS I), EPS II and K antigen synthesized by the rhizobium, *Sinorhizobium meliloti* are reported to play a role in the initiation and extension of the infection threads (Fraysse et al., 2003). The rhizobia in the infection threads are finally released into the cytoplasm of nodule primordial cells (Mylona et al., 1995). This mode of infection results in nod factor-induced calcium oscillations which in turn trigger the expression of “sym “genes, *SymRK* and *CCaMK.* These genes are responsible for nodule organogenesis and infection thread progression (Oldroyd et al., 2011; Oldroyd, 2013; Downie, 2014).

An alternative-mode of bacterial infection called lateral root invasion or crack entry is also observed in some rhizobia that induce stem nodulation on the host plant (Capoen, 2010). This type of infection does not require the primary nod factor signaling pathway; instead this intercellular colonization involves ethylene and reactive oxygen species induced cell death at the lateral root bases. Rhizobia proliferate in the infection pockets formed as a result of cell death and are eventually internalized in the nodule primordial cells through infection threads which require the common sym pathway (Capoen, 2010).

Irrespective of the route of infection, after internalization in the host, rhizobia are accommodated in an intracellular compartment called the symbiosome within the nodule where they differentiate into nitrogen fixing bacteroids (Lee et al., 2008; Capoen, 2010; Oldroyd et al., 2011; Denison & Kiers 2011; Terpolilli et al., 2016). The differentiation of rhizobia was reported to be a host directed process, where the nodule cells release symbiotic peptides and activate differentiation of rhizobia into elongated and polyploid bacteroids with loss of cell division ability (Van de Velde et al., 2010; Farkas et al., 2014; Maroti & Kondorosi, 2014). Nodules formed as a result of rhizobia-legume symbiotic interaction can be of two types- determinate and indeterminate. The major difference is the presence of a persistent meristematic activity in the

indeterminate nodules but not in the determinate nodules. Legumes like *Medicago truncatula*, *Medicago sativa* (alfalfa), *Pisum sativum* (pea), *Vicia* species (vetches) and *Trifolium* species (clovers) forms indeterminate nodules, elongated in shape and they continue to form new nodule cells which are subsequently infected by the rhizobia for N_2 fixation (Timmers et al., 1999; Webb et al., 2014; Xiao et al., 2014). This type of nodule shows developmental stages with young meristem at the nodule tip to the older senescent tissue near the origin of the nodule near the root. Determinate nodules are round in shape, lack persistent meristematic activity and does not have gradient developmental stages. Legumes like *Glycine max* (soybean), *Vicia faba* (bean), *Sesbania rostrata* and *Lotus japonicus* which are mostly tropical in origin forms determinate nodules (Handberg & Stougaard, 1992; Ndoye et al., 1994; Gage, 2004).

The stages of infection thread formation and nodule meristem activity during nodule development was also reported to be dependent on the generation of reactive oxygen species (ROS), and the antioxidant defense system in the host and rhizobia. ROS has been reported to act as the signaling molecules for rhizobial invasion and nodule senescence (Montiel et al., 2016). In the tropical legume, *Sesbania rostrata*, ROS was reported to be crucial for formation of infection pockets and initiation of nodule primordia (D'haeze et al., 2003). Rhizobia defective in antioxidant defense systems showed reduced capacity to fix N_2 in the nodules, suggesting that the rhizobia adapts to the altered environment inside the nodules (Chang et al., 2009). N_2 fixation in the nodules was also affected by environmental factors like drought, and salt stress which modifies the oxygen (O_2) balance in the nodules. This shows the process of nodule formation to be complex and is controlled by host, rhizobial and environmental factors.

Rhizobia possess a nitrogenase enzyme complex that reduces atmospheric N_2 into ammonia, according to the reaction:

$$N_2 + 8H^+ + 8e^- + 16ATP \longrightarrow 2NH_3 + H_2 + 16ADP + 16Pi$$

This is a highly reductive and energy consuming process hence the process of nitrogen fixation is largely dependent on bacterial respiration. Rhizobia, being obligate aerobes, require oxygen for energy metabolism under N_2 fixing conditions. The nitrogenase enzyme is extremely oxygen sensitive, so a low oxygen or micro-aerobic environment is maintained inside the nodule to prevent its inactivation (Udvardi & Poole, 2013). Leghemoglobin, a plant protein with high affinity for oxygen provides reduced amounts of O_2 to the bacteroids at concentration of 3 to 22 nM for bacteroid respiration inside the nodules (Hunt & Layzell, 1993; Batut & Boistard, 1994; White et al., 2007). Rhizobia thus maintain a balanced carbon and energy metabolism to sustain cellular activity as well as to fuel nitrogen fixation in a low O_2 environment.

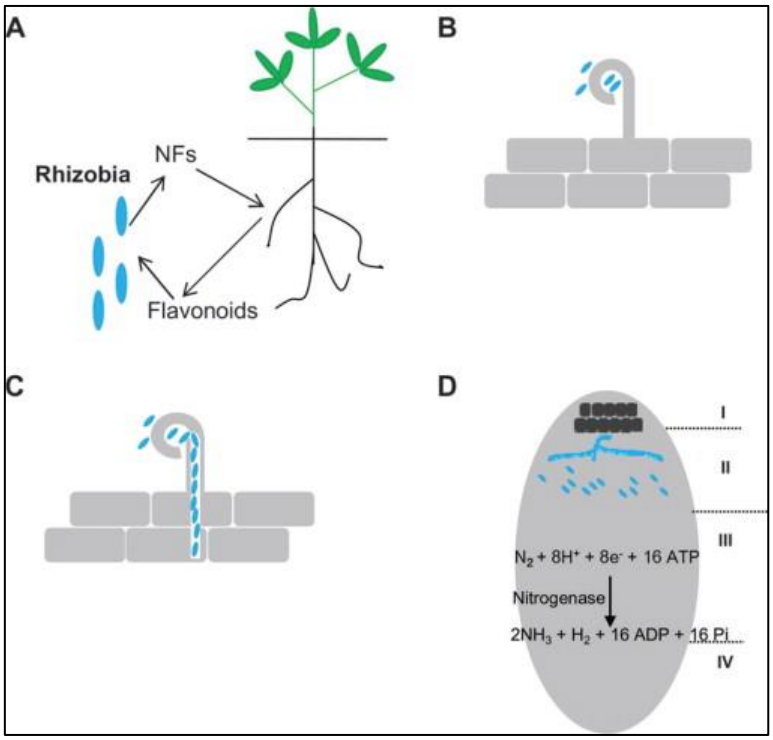

Figure 1.1**: Different stages involved during the rhizobial-legume symbiosis**. A shows the recognition of rhizobia by its respective host plant; B shows rhizobial attachment and root hair curling in the host; C shows the growth of infection thread; D shows *M. truncatula* nodule with (I) meristematic (II) infection (III) N_2 fixing and (IV) Senescent zone (Chang et al., 2009).

1.2 Metabolism of rhizobia under free-living conditions

The metabolic behavior of rhizobia in the free living state differs from that of bacteroids inside the plant nodule. Rhizobia exhibit diversity in carbon nutrition and can be classified into fast and slow growers. Fast growing rhizobia are able to metabolize a wide range of carbon sources like hexoses, pentoses, di-saccharides, tri-saccharides and organic acids while slow growers exhibit optimum growth on sugar alcohols and aromatic compounds (Stowers, 1985). Enzymatic and radiorespirometric analysis has been used to study central carbon metabolism under aerobic conditions in both fast and slow growing rhizobia. Hexoses are mainly metabolized by the Entner-Doudoroff (ED) pathway and the pentose phosphate pathway (PPP) as rhizobia lack the activity of enzymes of the Embden-Meyerhof-Parnas (EMP) pathway (Stowers, 1985; Romanov, et al., 1994). The presence of an extracellular glucose oxidation by a periplasmic pyroloquinoline quinine (PQQ) dependent glucose dehydrogenase (GDH) was also reported to be an alternative pathway to ED for glucose metabolism in *S. meliloti* rhizobial strains (Bernardelli, et al., 2001). In *Rhizobium tropici* free-living cultures grown on sucrose as the carbon source, high activities of the enzymes of the PPP (glucose-phosphate dehydrogenase and phosphogluconate dehydrogenase) and ED pathway were detected, whereas a key enzyme phosphofructokinase of the EMP pathway had low activity (Romanov et al., 1994). It was also reported that gluconeogenesis in *R. tropici* cultures grown with glutamate or malate as the carbon source was mediated by the activities of PEP carboxykinase and fructose-6-phosphate aldolase. Similar metabolic behaviour was reported in *S. meliloti* free-living cultures grown on complex medium, where ED was the primary pathway for glucose catabolism, both oxidative and non-oxidative branch of the PPP generated pentose-5-phosphate precursors for biomass synthesis along with higher activities reported for the tricarboxylic acid (TCA) cycle (Fuhrer, et al., 2005).

In the free living state, *Rhizobium. etli* adopted a fermentation-like metabolism under oxygen limited conditions where it excreted organic acids and amino acids with a concomitant decrease of the TCA cycle activity (Encarnación et al., 1995). It was proposed that the fermentative state of *R. etli* might be similar to that adopted when it enters into symbiotic association with the host (Encarnación et al., 1995).

1.3 Metabolism of rhizobia during symbiotic association

The N_2 fixing bacteroid inside the plant nodule has to undergo metabolic adjustments depending on the range of respiratory substrates supplied by the host, to meet the energy requirement for symbiotic nitrogen fixation. Bacteroid metabolism is primarily dependent on the exchange of metabolites and nutrients with the host including carbon compounds, N_2, O_2, amino acid and ions such as phosphorus, sulfur, molybdenum in the symbiosome space of the nodule (White et al., 2007; Terpolilli et al., 2012; Brear et al, 2013; Emerich & Krishnan, 2014; Lira et al., 2015; Cheng et al., 2016). Most rhizobia cannot synthesize homocitrate, an essential component of the iron-molybdenum co-factor of nitrogenase. In this condition, the activation of nitrogenase in the bacteriod depends entirely on the supply of homocitrate from the host (Terpolilli et al., 2012; Clarke et al., 2014). In return for essential metabolites and nutrients, the bacteroid delivers fixed N_2 in the form of ammonia which is assimilated into amino acids by the host (Lodwig & Poole, 2003; Udvardi & Poole, 2013). The diagrammatic representation of this complex interaction between rhizobia and host plant in the symbiosome is shown in Figure 1.2.

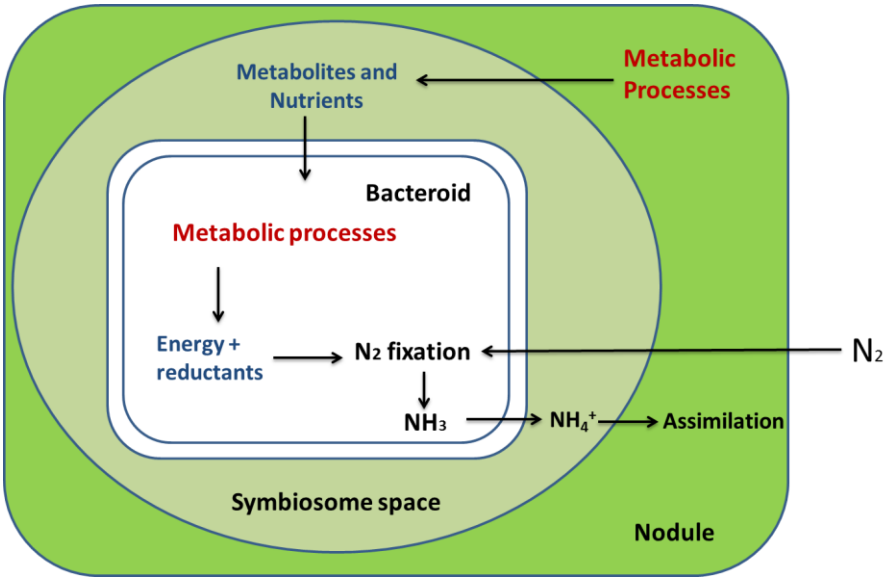

Figure 1.2**: Metabolic co-operation between the bacteroid and host inside the nodule**.

1.3.1 Carbon provision to bacteroids

Plant photosynthate primarily in the form of sucrose, is transported to the nodules where sucrose is converted to glucose by sucrose synthase. Glucose then enters the glycolytic or oxidative pentose phosphate pathway to form phosphoenolpyruvate (PEP). PEP is then converted to oxaloacetate by phosphoenolpyruvate carboxylase (PEPC) and then to the di-carboxylic acid malate by a reaction catalyzed by malate dehydrogenase (MDH) (Gordon, et al., 1999). From the nodule cytoplasm, malate is then transported though the peribacteroid membrane and metabolized by the bacteroid to generate energy and reductants that are required for N_2 fixation in the nodules (White et al., 2007). The peribacteroid membrane is reported to be impermeable to sugars like sucrose, glucose and fructose but rapid transport of di-carboxylic acids is facilitated through the di-carboxylic acid transport (Dct) system. Previous studies showed that bacteroids defective for the Dct system are unable to establish effective symbiotic nitrogen-fixation (Finan et al., 1983; Reid et al., 1996). Thus di-carboxylic acids mainly are the principal carbon source for bacteroid respiration that meets the energy requirement for N_2 fixation (McAllister & Lepo, 1983; Stowers, 1985; Romanov et al., 1994; Lodwig & Poole, 2003; White et al., 2007).

1.3.2 Carbon metabolism

Previous studies based on enzymatic, mutation and radioisotope-labeling strategies suggest that organic acids can be metabolized by a fully functional TCA cycle in isolated bacteroids (Stovall & Cole, 1978). Higher activities of TCA cycle enzymes and malic enzyme was also observed in bacteroids as reported in previous studies (McKay et al,, 1988; Romanov et al., 1994). The TCA cycle has also been shown to be active in pea bacteroids and was essential for fully effective for symbiotic N_2-fixation (Terpolilli et al., 2016). The capacity to synthesize sugars through gluconeogenesis is proposed to be an absolute requirement for nitrogen fixation in most rhizobial species during symbiosis. Rhizobia with mutations in their glycolytic and gluconeogenesis enzymes exhibited reduced N_2 fixing activity in the host during symbiosis (Udvardi & Poole, 2013). One of the studies proposed that glucose metabolism also occurs extracellularly in the periplasmic space of the bacteroid via periplasmic pyroloquinoline quinine (PQQ) dependent glucose dehydrogenase. In this process, glucose is initially converted into gluconate which can then be metabolized via the PPP or ED pathways in the bacteroid (Bernardelli et al., 2001). Glucose metabolism in a bacteroid might be necessary for the synthesis of polysaccharides or storage polymers and it is not clear if their synthesis increases the efficiency of N_2 fixation during symbiosis. It was shown that *R. tropici* bacteroids had similar or elevated activities of carbohydrate catabolizing enzymes as compared to free-living cells. The activity of phosphogluconate dehydrogenase enzyme that catalyzes the generation of ribulose-5-phosphate from phosphogluconate in oxidative pentose phosphate pathway was observed to have a higher activity in the bacteroids than free-living cells (Romanov et al., 1994). Whereas, enzymatic studies performed on *Bradyrhizobium strain* 32H1 showed no detectable expression of hexose catabolizing enzymes of EMP, ED and oxidative PPP (Stowers & Elkan, 1984). This suggests that a N_2 fixing bacteroid undergoes metabolic adaptations in the nodule, but the metabolic behaviour in bacteroids can be species dependent.

Myo-inositol is abundant in the nodules of certain legumes like pea, alfalfa and soybeans and is mainly supplied to the bacteroids by the host during symbiosis. Myo-inositol catabolism in rhizobia has been reported to affect its competitiveness in the host during symbiosis (Fry et al., 2001). An overview of the proposed inositol catabolic pathway in *S. meliloti* is represented in Figure 1.3.

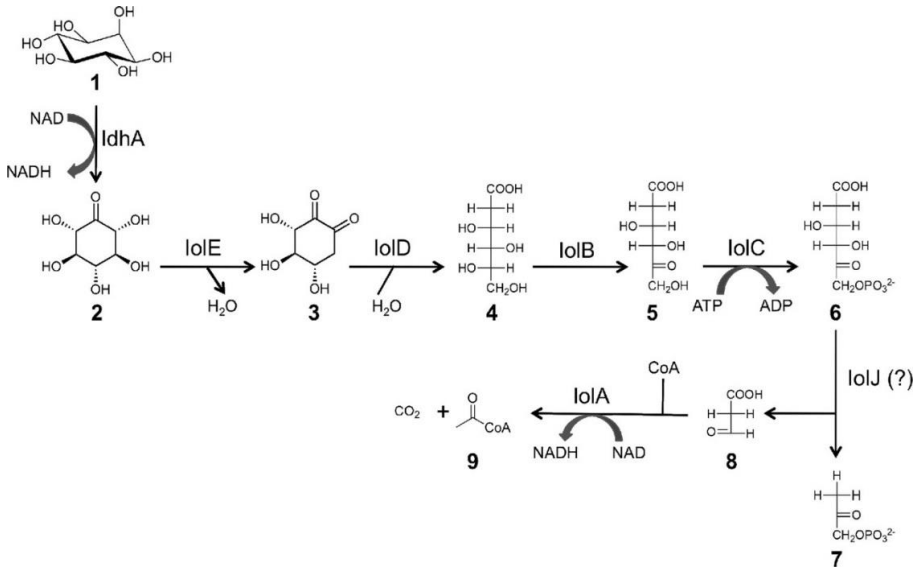

Figure 1.3: **The proposed myo-inositol catabolic pathway in *Sinorhizobium meliloti***. 1,myo-inositol(MI); 2, 2-keto-myo-inositol; 3, 3D-(3,4/5) trihydroxycyclohexane-1,2-dione (THcHDO); 4, 5-deoxy glucuronic acid (5DG); 5, 2-deoxy-5-keto-d-gluconic acid (DKG); 6, DKGP; 7, dihydroxyacetone phosphate (DHAP); 8, malonic semialdehyde (MSA); 9, acetyl coenzyme A (acetyl-CoA). Enzymes: IdhA, myo-inositol dehydrogenase; IolE, 2KMI dehydratase; IolD, THcHDO hydrolase; IolB, 5DG isomerase; IolC, DKG kinase; IolJ aldolase; IolA, MSA dehydrogenase (Kohler et al., 2010).

Rhizopine, a compound synthesized from myo-inositol by symbiotic *S. meliloti* and *R. leguminosarum* by. *viciae* strains serves as a growth substrate for free living rhizobia located within the infection threads and rhizosphere. This acts as a selective growth substrate provided by the host plant to the free-living rhizobia that is able to establish effective symbiotic N_2-fixation. This provides competitive advantage to the rhizobia over other bacterial strains during colonization and nodulation of host roots and stem (Poole et al., 1994; Murphy et al., 1995; Fry et al., 2001; Kohler et al., 2010).

1.3.3 Nitrogen metabolism

Free-living rhizobia take up nitrogen sources such as ammonia from the external environment and assimilate it either via glutamate dehydrogenase or the combined activities of glutamine synthetase and glutamate synthase (GS/GOGAT). But under nitrogen limiting conditions, the assimilation of ammonia in the rhizobial species- *R. leguminosarum*, *R. trifolli* and *R. japonicum* occurred mainly via GS/GOGAT pathway (Brown & Dilworth, 1975). During symbiotic N_2 fixation, the ammonium assimilatory enzymes of the GS/GOGAT pathway were down-regulated in the bacteroids inside the nodule suggesting that bacteroids do not assimilate the fixed N_2 but supply it to the host (Brown & Dilworth, 1975; Patriarca et al., 2002; Udvardi & Poole, 2013). Ammonium is reported to be the primary export product of N_2 fixation in many rhizobial species, that is supplied to the plant through the peribacteroid membrane transport system (Allaway et al., 2000; Udvardi & Poole, 2013). A diagrammatic representation of nitrogen metabolism in the symbionts inside the nodule is shown in Figure 1.4. Due to the down-regulation of the ammonium assimilation pathway, the bacteroid also becomes auxotrophic for amino acid during symbiosis and depends on the host for the supply of amino acids. Mutation of the amino acid transporters Aap and Bra, that are responsible for the transport of branched chain amino acid results in defective growth and development of bacteroids during symbiosis (Udvardi & Poole, 2013). Mulley et al. (2011) showed that mutation of GOGAT in pea bacteroids prevents bacteroid development and N_2 fixation; this was due to the inability of the bacteroids to synthesize or transport amino acids. Mulley et al. (2011) also showed that sufficient amino acids were supplied to the bacteroids by the host plant and *de novo* ammonium assimilation was not necessary in pea bacteroids.

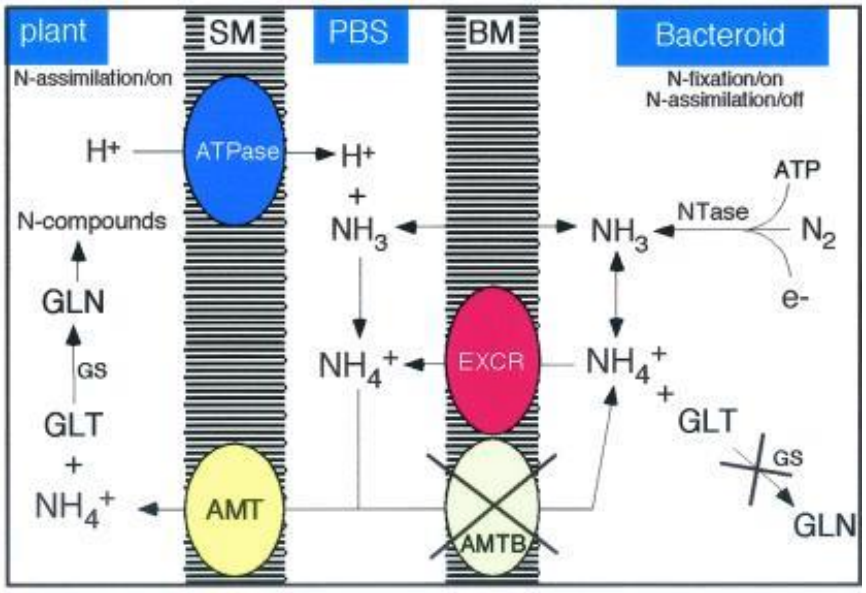

Figure 1.4: **NH_4^+ flux and assimilation inside the nodule.** NH_3 produced through nitrogenase (Ntase) action diffuses freely through the bacteroid membrane (BM). NH_4^+ is excreted probably by an active mechanism (EXCR) into the peribacteroid space (PBS), where an ATPase present on the symbiosome membrane (SM) pumping protons keeps a high NH_4^+/NH_3 ratio, and a transport system for NH_4^+ uptake (AMT) moves NH_4^+ to the plant cytoplasm, where it is assimilated. In bacteroids, the NH_4^+ transporter Amt B is not expressed (Patriarca et al., 2002).

1.3.4 Synthesis of bacteroid storage polymers

The majority of carbon supplied to the bacteroids by the host is channeled towards energy production for N_2 fixation while some of the carbon is also employed for production of intracellular storage polymers like glycogen and polyhydroxybutyrate (PHB) (Lodwig et al., 2005; Trainer & Charles, 2006). These storage compounds act as carbon and energy reserves that can be utilized under conditions of carbon starvation. They might also provide competitive advantage to the rhizobia over other soil microbes helping to establish symbiosis with their respective legume host (Trainer & Charles, 2006). The synthesis and metabolism of storage polymers have also been shown to fuel bacteroid differentiation in the nodules (Lodwig et al., 2005).

Glycogen synthesis from ADP-glucose is catalyzed by glycogen synthase subsequently forming α-1,6-glycosidic linkages (Lodwig & Poole, 2003; Wang et al., 2007). The

glycogen synthesis pathway in rhizobia is represented in Figure 1.5. *R. leguminosarum* by. *viciae* mutant unable to synthesize glycogen, had unaltered N_2 fixation ability in the nodules of pea plants in comparison to the wild type. There was an increased accumulation of starch throughout the nodules, which suggested that bacteroids unable to synthesize glycogen required less photosynthates from the host cell and so the excess carbon from the host was stored as starch in the nodules (Lodwig & Poole, 2003; Lodwig et al., 2005). In contrast, a *S. meliloti* glycogen mutant resulted in a reduced symbiotic efficiency for nodulation and N_2 fixation on older nodules of alfalfa (Wang et al., 2007).

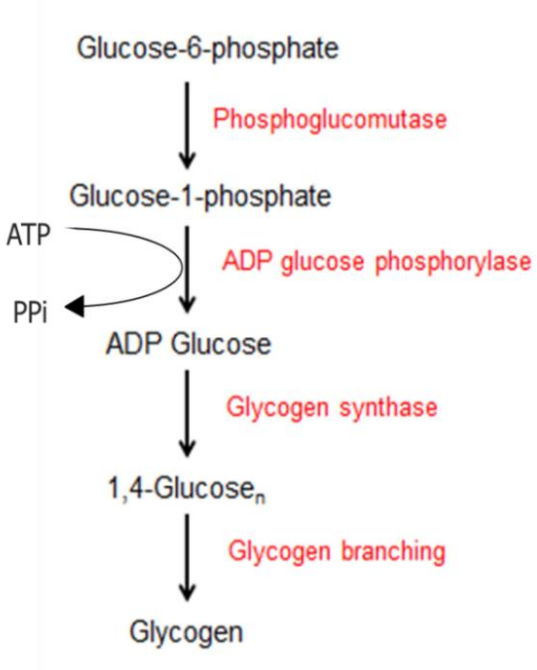

Figure 1.5: **Glycogen synthesis pathway**. The precursors and intermediates of the pathway are represented in black; enzymes catalyzing each step are represented in red.

Most rhizobia accumulate PHB in both the free-living state under oxygen limiting conditions and as bacteroids in mature nodules during symbiosis (Stowers, 1985; Pauling et al., 2001). PHB is synthesized by the condensation of two acetyl-CoA molecules to form acetoacetyl-CoA which is then reduced to form β-hydroxybutyryl-CoA (Steinbuchel & Schlegel, 1991; Mandon et al., 1998). Finally the β-hydroxybutyryl

residues are polymerized to form the polyester (Steinbuchel & Schlegel, 1991; Mandon et al., 1998) . From a study in *R. tropici* bacteroids, it was confirmed that the activity of the enzyme β-hydroxybutyrate dehydrogenase, which was responsible for degradation of PHB, was significantly higher as compared to the free-living cells. This study suggests the presence of an active PHB synthesis and degradation pathway operating in *R. tropici* bacteroids (Romanov et al., 1994). The schematic representation of PHB synthesis pathway in rhizobia is represented in Figure 1.6.

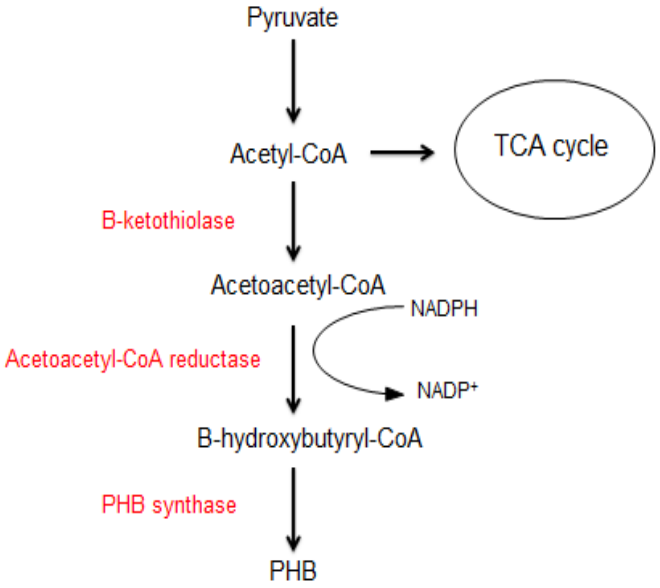

Figure 1.6: **PHB synthesis pathway**. The precursors, reaction intermediate, reductants and product of the pathway are shown in black; enzymes catalyzing each step of the pathway are shown in red.

Bacteroids from the determinate nodules in beans and soybeans showed significant accumulation of PHB while bacteroids in indeterminate nodules of chick peas, did not show accumulation of the polymer (Kim & Copeland, 1996). Free-living and symbiotic forms of *S. meliloti* were observed to degrade and utilize PHB under carbon starvation conditions (Ratcliff et al., 2008). A defect in the PHB synthesis pathway in *S. meliloti* results in reduced symbiotic performance of the rhizobia with its hosts *Medicago truncatula* and alfalfa affecting infection, competition and N_2 fixation efficiency (Wang et al., 2007). Similarly, *Bradyrhizobium japonicum* mutants defective for

polyhydroxyalkanoate (PHA) synthesis showed reduced competitiveness for nodulation on the host plant (Quelas et al., 2013). A different study reported that inhibition of PHB synthesis in *S. meiloti* PHB resulted in a reduced cellular ratio of NAD^+/NADH and the mutant was defective for exopolysaccharide (EPS)- succinoglycan synthesis (Aneja et al., 2004). PHB was also reported to improve tolerance to high temperatures, H_2O_2 exposure, UV irradiation, desiccation and osmotic stress (Kadouri et al., 2003). These results indicate that PHB metabolism potentially regulates metabolic and cellular activities in some rhizobia and is required to establish effective symbiotic competition with the host.

PHB deficient strains of *Rhizobium leguminosarum* by. *viciae* and *Rhizobium leguminosarum* by. *phaseoli* which nodulate pea and bean plants respectively, did not show any change in symbiotic efficiency or growth defect of the plant, when inoculated on to the host, in comparison to the plants inoculated with the wild type strains. This suggests that defect in PHB metabolism may not affect the N_2 fixation ability of the pea and bean bacteroids *inplanta*. During symbiosis, PHB granules were observed in the wild type *R. leguminosarum* by. *viciae*, in the infection threads but not in the mature bacteroids, suggesting that the bacteria used PHB reserve when leaving the infection thread and differentiating into bacteroids (Lodwig et al., 2005). A PHB mutant in *R. etli* was reported to exhibit increased nitrogenase activity than the wild type and improved host plant productivity (Cevallos et al., 1996). Also, *Sinorhizobium meliloti* mutants, which do not synthesize PHB, were observed to remain unaffected in their symbiotic N_2-fixation capabilities in the nodules (Povolo et al., 1994; Cai et al., 2000). In contrast, the diazotroph, *Azorhizobium caulinodans*, was growth defective and compromised for N_2 fixation under both free-living and symbiotic conditions (Mandon et al., 1998). This shows that the effect of PHB metabolism in N_2 fixing activity of rhizobia can be species dependent. Besides providing competitive advantage to the rhizobia over other rhizosphere microbes, PHB accumulation has been reported to act as an electron and

carbon sink in bacteroids that regulates TCA cycle operation and redox balance of the cell under micro-aerobic conditions or low O_2 conditions (Mandon et al., 1998; Trainer & Charles, 2006; Terpolilli et al., 2016). Under micro-aerobic conditions, such as in the nodules, the NAD(P)H generated by the central metabolism increases in the cell which leads to inhibition of the TCA cycle enzymes- NADP-isocitrate dehydrogenase and citrate synthase. In order to prevent inhibition of TCA cycle activity, acetyl-CoA and NADPH is channeled towards PHB synthesis which acts as an electron acceptor (Senior & Dawes, 1971; Jackson & Dawes, 1976;). Conversely, the degradation of PHB produces acetyl-CoA which can be assimilated by the TCA cycle and glyoxylate shunt (Senior & Dawes, 1971). NADH is also generated during degradation of PHB, which can be utilized to generate energy via oxidative phosphorylation.

The synthesis of storage polymers and N_2 fixation both require reductants and energy sources. Hence PHB and glycogen synthesis might potentially compete with N_2 fixation for the same carbon source. Also, in some rhizobial species, the function of glycogen and PHB has been reported to play an important role in metabolism under free-living and symbiotic conditions. So, the relationship between the metabolism of storage polymers in bacteroids and N_2 fixation is complex and can be species dependent. The understanding of the metabolic interaction between these processes during symbiosis is currently limited.

1.4 Metabolic flux analysis

Metabolism is a complex process involving multiple biochemical reactions that maintain cellular activity. Each metabolic pathway comprises of a set of chemical reactions that converts substrate into end products through a series of intermediate compounds. The rate of metabolite interconversion in a chemical reaction is termed a metabolic flux and the distribution of fluxes across the network defines a flux map (Kruger & Ratcliffe, 2015). The quantification of metabolic fluxes helps in understanding the metabolic

phenotype of an organism under different environmental conditions. This is helpful in identifying the target pathways to improve productivity in organisms of interest.

The study of metabolic pathways/metabolism has gained high importance for metabolic engineering in the field of medicine and biotechnology. For instance, the study of the metabolic behavior of a pathogen during invasion of the host can help to identify possible pathways that can be targeted to reduce cellular activity of the pathogen during infection (Beste et al., 2011). Metabolic studies of industrially important micro-organisms like *Corneybacterium glutamicum*, *Escherichia coli*, *Saccharomyces cerevisiae* have provided strategies to improve the strains for enhanced biofuel production (Toya & Shimizu, 2013; He et al., 2014).

1.4.1 Methods for measurement of metabolic fluxes

Quantification of metabolic fluxes requires a good understanding of the metabolic network stoichiometry followed by computational, mathematical and experimental analysis. At present, there are two main approaches for determining fluxes based on the stoichiometry of the metabolic network. The first is metabolic network analysis (MNA) which explores the solution space of stoichiometric equations based on theoretical information to predict all fluxes and construct a model under steady state conditions. Genome scale metabolic modeling is a widely used method based on MNA to study microbial metabolism with the help of genomic information of the metabolites in a biochemical pathway. Flux balance analysis (FBA) is one of the most prominent mathematical methods used to predict fluxes through the metabolic network. FBA is computationally fast and can be used for prediction of large models with many thousands of reactions. It is a constraint based approach that requires reaction stoichiometry, an objective function and biomass composition constraints for prediction of fluxes. However, FBA metabolic models are based on assumptions about the system, specifically that the metabolite concentrations are constant over time, and it

also requires a predefined objective function like maximization of biomass or maximization of ATP. A biological system may function with different or multiple objective functions hence the choice of an appropriate objective function is crucial for FBA (Edwards & Palsson, 2000; Kauffman et al., 2003; Resendis-Antonio et al., 2007; Weitzel et al., 2007; Chen et al., 2011; Toya et al., 2011).

The second approach is metabolic flux analysis (MFA) which involves the quantification of intracellular fluxes using an experimental approach under *in vivo* conditions. Steady state MFA is based on isotopic labelling studies where the fluxes are measured by introducing a labelled precursor to the network and determining the re-distribution or flow of label throughout the network (Wiechert et al., 2001; Ratcliffe & Shachar-Hill, 2006; Antoniewicz, 2015). Unlike FBA it can be used to study complex biological networks consisting of cyclic, parallel or reversible reactions (Wiechert, 2001). In ^{13}C-MFA the system is incubated with a ^{13}C labelled substrate and the isotopic enrichment or redistribution of label into metabolites and end-products is measured when system has reached at a metabolic and isotopic steady state using mass spectrometry (MS) or nuclear magnetic resonance (NMR) techniques (Kruger & Ratcliffe, 2009; Kruger et al., 2012; Young et al., 2014; Kruger & Ratcliffe, 2015). It is important that the system under study is at metabolic and isotopic steady state because the mass isotopomer distributions of metabolic intermediates are determined by the isotopic substrate used and the fluxes through the network (Antoniewicz et al., 2007c). The rates of substrate uptake and biomass accumulation are also measured to provide the external boundaries of the system and hence to deduce the intracellular fluxes using the label patterns of network metabolites. A stoichiometric model is first constructed from the isotopomer balance equations for intracellular metabolites and this isotopic network model is simulated to obtain best fit flux maps of carbon and energy flow through the metabolic network. (Wendisch et al., 1997; Wiechert, 2001; Ratcliffe & Shachar-Hill,

2006; Weitzel et al., 2007; Chen et al., 2011; Srour et al., 2011; Toya et al., 2011; Toya & Shimizu, 2013). An overview of ^{13}C-MFA strategy is shown in Figure 1.7.

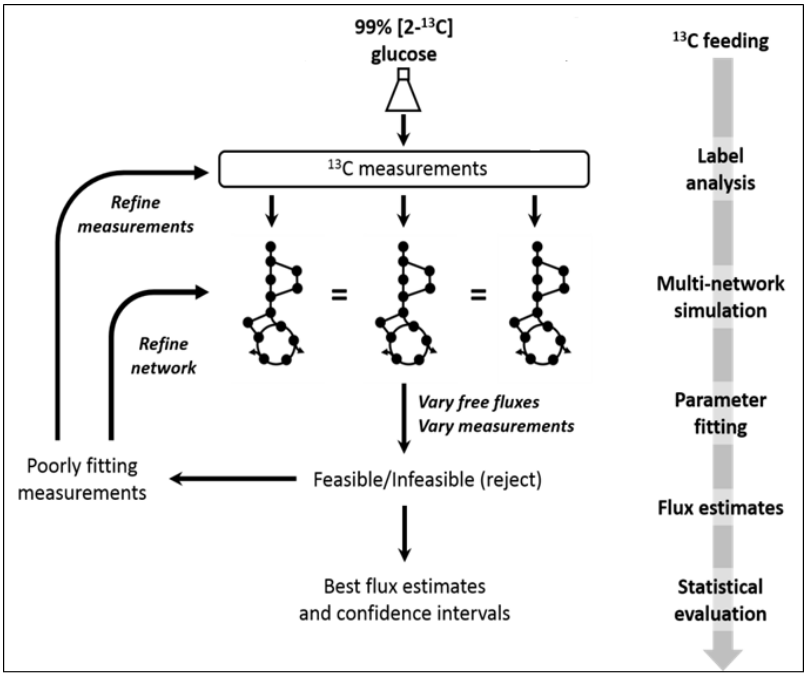

Figure 1.7**: Outline strategy for ^{13}C-metabolic flux analysis** (Kruger et al., 2014)

1.4.2 Prediction of metabolic fluxes in rhizobia

The first metabolic network model of a nitrogen fixing bacterium, *Rhizobium etli* CFN42*,* inside the nodule was reconstructed from the annotated genome of the bacterium and the fluxes were predicted using FBA. The objective function used for the analysis was to maximize the steady state production of symbiotic N_2 fixation products. This metabolic model predicted the activity of oxidative phosphorylation, gluconeogenesis, and the PHB biosynthesis pathways in the bacteroid. Myo-inositol catabolism was predicted to increase symbiotic N_2 fixation. The model predicted zero flux through the ED, PP and ammonium assimilatory pathway under micro-aerobic conditions. Minimal flux was predicted through the TCA cycle in agreement with the experimental data in *Bradyrhizobium japonicum* bacteroids, which suggests that an incomplete use of TCA cycle can still result in N_2 fixation at low oxygen uptake rates in *R. etli*. However, the prediction disagreed with the proteomic data from *B. japonicum* bacteroids that reported the presence of several PP pathway enzymes during N_2 fixation. As the

spectrum of amino acid produced in *R. etli* during N_2 fixation is not well characterized, this in silico prediction of amino acid production was compared with the experimentally observed amino acids in *B. japonicum* bacteroids. The model predictions disagreed with the experimental data reporting the synthesis of asparagine, methionine, leucine, isoleucine, glycine, glutamine and serine. Detailed experimental information about the amino acids of *R. etli* will be required for the validation of the model. Nevertheless, this metabolic reconstruction was able to predict the metabolic behaviour of *R. etli* during symbiosis to a considerable extent and also suggested that gene deletion in PHB synthase and glycogen synthase could potentially increase symbiotic N_2 fixation (Resendis-Antonio et al., 2007). This in silico analysis for prediction of intracellular fluxes of the metabolic network in *R. etli* was based on an assumed objective function and requires integration of experimental data to improve the reconstructed model.

A metabolic network model of *Sinorhizobium meliloti* 1021 during symbiotic N_2 fixation was developed using predictive modelling, FBA which showed the key pathways participating during this symbiosis. The model showed N_2 fixation to be dependent on nutrient and co-factor exchange between the rhizobia and host cell for carbon and energy metabolism. The objective functions used for this study involved nutrient sharing between symbionts and nitrogenase reaction in bacteroids. The model predicted a complete TCA cycle and gluconeogenesis, also active PPP, glyoxylate shunt, malic enzyme activity and amino acid cycling which were shown to agree with the experimentally measured enzymatic and proteomic data for *S. meliloti* (Figure 1.8). In the absence of PHB, the model predicted incomplete utilization of TCA and inactive PPP, sulfur porphyrin, chlorophyll metabolism pathways during symbiotic N_2 fixation. However this predicted metabolic phenotype did not agree with the experimental evidences (Zhao et al., 2012). Nevertheless, this study predicted activity of the pathways involved during symbiotic nitrogen fixation in *S. meliloti* but lacks the quantitation of fluxes through the predicted pathways which can be done using ^{13}C-

MFA. A combined genome scale model of the clover plant Medicago truncatula and its rhizobial symbiont *S. meliloti* was generated to predict fluxes through the model during symbiotic nitrogen-fixation using FBA. This model shows that when glutamate is imported as the carbon source in the bacteroid, the TCA cycle was fed with ketoglutarate to produce one ATP. On the other hand, dicarboxylic acid malate imported to the bacteroids, produced less ATP and less NADH, which reduced the flux through the respiratory chain, allowing the symbiont to sustain N_2 fixation under low O_2 conditions (Pfau et al., 2016). The fluxes predicted for the genome scale models of rhizobia using FBA provides optimum activity of the metabolic network required to maximize or minimise an assumed objective function and lacks measurement of metabolically active fluxes supported by experimental data, so these predicted fluxes may not be an exact representation of the metabolic phenotype.

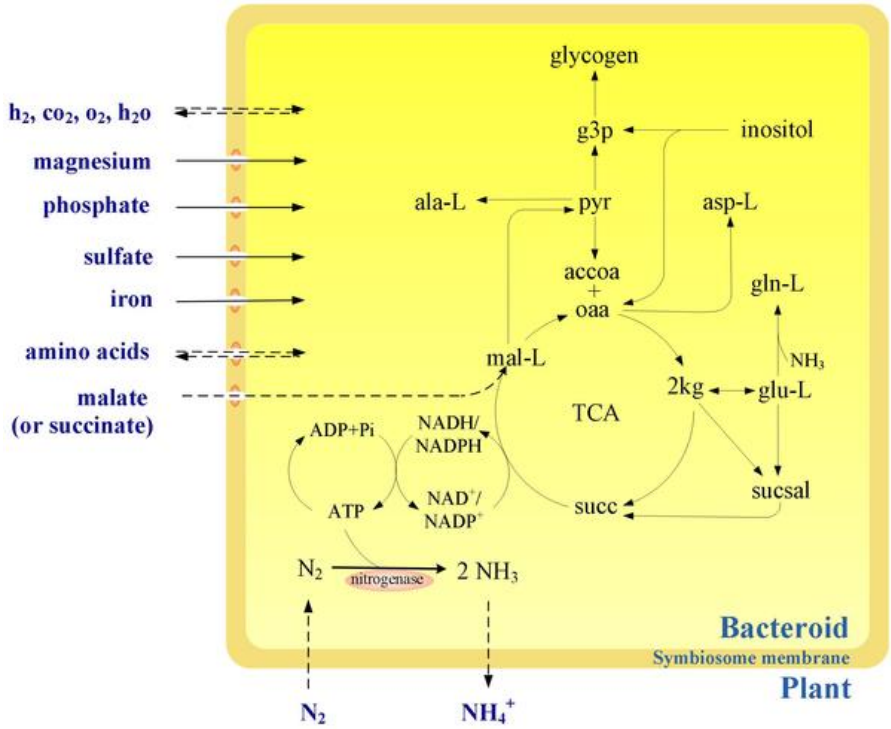

Figure 1.8: **Metabolic network of *S. meliloti* 1021 during SNF**. The model shows nutrient (carbon, ammonium, co-factors) sharing between the symbionts, nitrogenase reaction, TCA cycle, gluconeogenesis, amino acid cycling (Zhao et al., 2012).

1.4.3 Steady state ^{13}C-MFA of microbial system

Steady state ^{13}C-MFA, which allows the measurement of intracellular fluxes has been widely used to study central carbon metabolism in industrially important microbial systems such as *Escherichia coli*, *Actinobacillus succinogenes, Bacillus subtilis, Corynebacterium glutamicum* and *Saccharomyces cerevisiae* (McKinlay et al., 2007; Toya & Shimizu, 2013; Guo et al., 2015; Gonzalez et al., 2017). According to the flux maps obtained from ^{13}C labeling experiments on *Agrobacterium tumefacians, Pseudomonas fluorescens, Pseudomonas putida, Sinorhizobium meliloti, Rhodobacter sphaeroides, Zymomonas mobilis and Paracoccus versutus*, the ED pathway was identified as the sole route for glucose metabolism in all species (Fuhrer et al., 2005). In a different study, the metabolism of *Mycobacterium tuberculosis* responsible for pathogenesis of tuberculosis was investigated using ^{13}C-MFA. This study was the first to identify a novel metabolic pathway (the 'GAS' pathway) that utilizes the glyoxylate shunt, anaplerotic reactions for pyruvate oxidation and succinyl CoA synthetase for the generation of succinyl CoA and is functional under the slow growth conditions of the pathogen in the host (Beste et al., 2011). ^{13}C-MFA has been successfully used to study the metabolism of the free-living, *Rhizobium leguminosarum* by. Viciae (Rlv3841) growing aerobically on [$^{13}C_4$]succinate as the carbon source (Terpolilli et al., 2016). This study reported the metabolic fluxes of the free-living rhizobia but does not report about the metabolic fluxes in rhizobia during N_2-fixation. ^{13}C-MFA has also been used to measure complex and highly compartmentalized fluxes in the plant metabolic network (Roscher et al., 2000; Kruger & Ratcliffe, 2009; Masakapalli et al., 2010; Masakapalli et al., 2013) . Flux studies on globally important food crops have provided an insight into the plant metabolic processes responsible for increased biomass production. For instance, the fluxes into fatty acid metabolism that affect the efficiency of developing *Zea mays* embryos to accumulate starch and fatty acid as seed storage reserves were quantified using MFA. The flux through the plastidic NADP-dependent

malic enzyme was identified to play a key role in supplying carbon and NADPH for fatty acid metabolism (Alonso et al., 2010). MFA has proved to be effective in previous studies that investigated the metabolic alterations in plants due to nutritional changes and environmental perturbations. In one of these studies, MFA was used to investigate the impact of carbon and nitrogen supply on the flux through primary metabolism that ultimately results in diverse storage composition of *Glycine max* seeds (Allen & Young, 2013). The flux maps of central metabolic pathways in *Arabidopsis thaliana* revealed complex metabolic responses of the system to the changes in nitrogen nutrition (Masakapalli et al., 2013). Other studies have also used ^{13}C-MFA strategy to study metabolism in mammalian cell lines (Young, 2013; Ahn & Antoniewicz, 2011; Hiller & Metallo, 2012; Walther et al., 2012; Jiang et al., 2016). As ^{13}C-MFA has proven to be successful for understanding the metabolic state of a system in the previous studies that involved microbial, plant and mammalian systems, this approach was chosen to analyse the effect on the rhizobial metabolic network due to N_2-fixation. This study is the first to use *Azorhizobium caulinodans* ORS571- the diazotroph and micro-symbiont of the tropical legume, *Sesbania rostrata* as the model organism for steady state ^{13}C-MFA.

1.5 ORS571- *S. rostrata* symbiotic system

As ORS571 has the ability to fix nitrogen in both free-living state and in symbiosis with *S. rostrata*, this model system was ideal for the investigation of the metabolic phenotype of the rhizobium under N_2-fixing and non N_2-fixing conditions. Symbiotic ORS571 is able to form two different types of nodules on the stem and root of the host. This makes it an attractive system to study the impact on the metabolic behaviour of this rhizobium in different nodule types. ORS571 was previously shown to colonize the roots of rice, wheat and arabidopsis. This provides an opportunity to explore the endophytic role of this rhizobium in non-legumes and the possible alterations for establishing a N_2 fixing symbiosis.

1.5.1 Taxonomic and physiological characteristics of ORS571

ORS571 is taxonomically distinct from other rhizobial species; it belongs to the class of α-proteobacteria, family - *Xanthobacteraceae*, genus- *Azorhizobium*, species- *caulinodans* and is closely related to *Xanthobacter autotrophicus* and the rhizobial genus *Bradyrhizobium* (Elmerich et al., 1982; Tsukada et al., 2009). *Azorhizobium* was also reported to differ from the genus *Rhizobium* and *Bradyhrizobium* in genetic, phenotypic and metabolic characteristics. Unlike the other two groups of rhizobia, ORS571 has a cell size of 1-2 microns in length and possess a lateral flagellum in liquid medium as shown in Figure 1.9. They form relatively small colonies on both rich and minimal media agar plates. Although ORS571 is closely related to *Bradyrhizobium*, they show comparatively faster growth characteristics. Unlike the other two rhizobial groups, they do not metabolize sugars and alcohols but prefers organic acids as their best carbon substrates (Dreyfus et al., 1988; Pauling et al., 2001). ORS571 also has the unique ability to survive and grow in a wide range of temperatures from 12ºC to 44ºC (Scott & Ludwig, 2004).

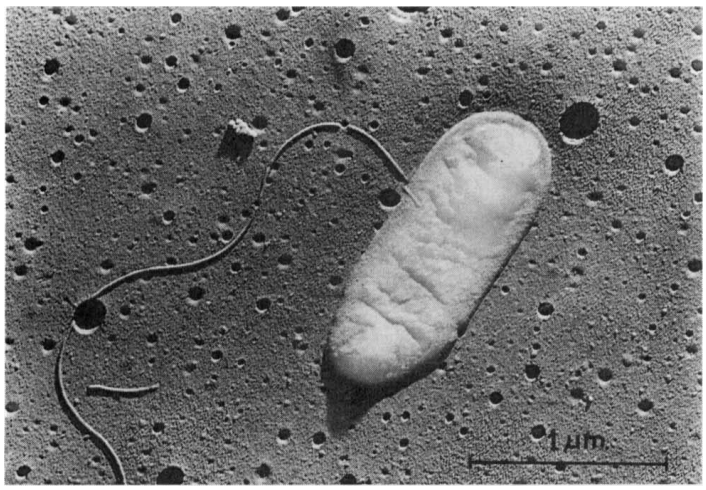

Figure 1.9: ***Azorhizobium caulinodans*** **ORS571 grown in liquid media** (Dreyfus et al., 1988)

1.5.2 Genetic organization of ORS571

ORS571 has a singular circular genome of size 5.37 Mb with an overall GC content of 67% and 4714 protein encoding genes dedicated for functions such as transport and

regulation, chemotaxis, metabolism, synthesis of surface polysaccharides, biofilm formation, symbiotic interaction with host and N_2-fixation. 96.3% of these protein encoding genes have homologs while 3.7% were unique to ORS571. The genes for the metabolic pathways ED, TCA, gluconeogenesis and PPP were reported to be present in the genome. The organism does not perform EMP or glycolysis due to the absence of a gene encoding phosphofructokinase that catalyses the phosphorylation of fructose-6-phosphate to fructose-1,6-bisphosphate. The genome also consists of genes responsible for N_2 fixation, which encodes for functions like nitrogenase assembly, synthesis of MoFe cofactor and FeS clusters, and electron transport. The genes for oxidizing hydrogen *hup*, *hyp* and *hox*A enables ORS571 to utilize the by-product hydrogen as an ATP source generated during nitrogenase reaction. A distinct symbiosis region of 87.6 kb was reported which consists of nodulation genes (*nod* ABCSUIJ), amino acid uptake, chemotaxis and type IV secretion system genes (Elmerich et al., 1982; Lee et al., 2008).

1.5.3 Regulation of N_2 fixation

N_2 fixation reaction is catalysed by the enzyme nitrogenase complex which is controlled by *nifHDK* genes. The enzyme complex is composed of dinitrogenase (MoFe protein) and dinitrogenase reductase (Fe protein). Dinitrogenase, encoded by *nifD* and *nifK* gene, is a heterotetramer composed of two pairs of two metalloclusters– P-cluster and iron molybdenum cofactor (FeMo-co). Dinitrogenase reductase, encoded by *nifH* gene, is a homodimer containing a single [4Fe-4S] cluster (Igarashi & Seefeldt, 2003). Dinitrogenase reductase transfers electrons to dinitrogenase component at the expense of MgATP for reduction N_2 to $2NH_3$. ORS571 has duplicated *nifH* genes, where *nifH1* is reported to be crucial mainly for N_2 fixation in free living conditions and *nifH2* mainly during symbiosis (Iki et al., 2007; Norel & Elmerich, 1987). Both the components of nitrogenase complex are irreversibly oxidised by O_2, resulting in the

inactivation of nitrogenase (Robson & Postgate, 1980). Thus N_2-fixation requires a micro-aerobic environment for the protection of nitrogenase from O_2.

ORS571 has a complex set of regulatory networks for expression of *nif* and *fix* genes that are responsible for N_2 fixation. This regulatory network has been reported to bear resemblance with *Klebsiella pneumoniae* and *Rhizobium meliloti* (Kaminski et al., 1991). The transcriptional activator NifA which is controlled by σ^{54} dependent type promoter controls the expression of *nif* and *fix* genes for both free living and symbiotic N_2 fixation (Ratet et al., 1989). The expression of NifA is controlled by regulatory genes that sense nitrogen and oxygen concentrations in the organism and the environment. The regulatory genes *fixL*, *fixJ* and *fixK* confer O_2 sensitivity to NifA and mediate its expression under O_2 limiting conditions (Kaminski et al., 1991). The two component nitrogen regulatory proteins NtrBC and NtrXY senses intracellular and extracellular nitrogen concentrations and mediate the transcription of NifA under nitrogen starving conditions (Lee et al., 2008; Pawlowski et al., 1991; Pawlowski et al., 1987). The genetic regulation of N_2 fixation in ORS571 is shown in Figure 1.10.

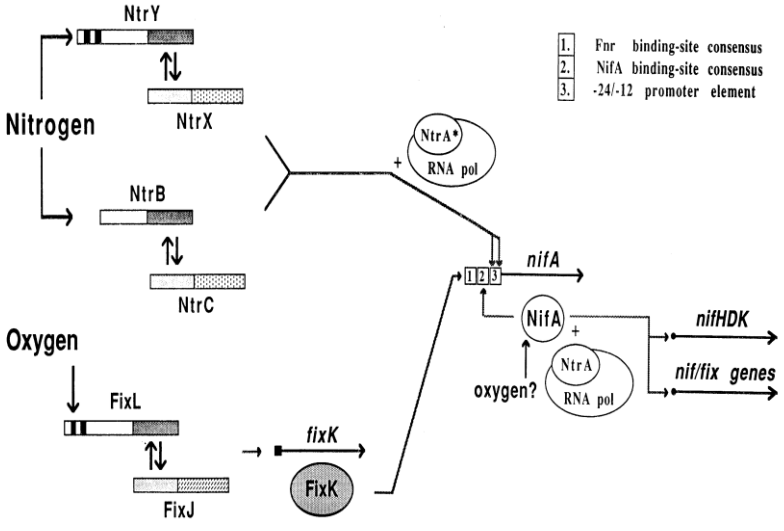

Figure 1.10: **The expression of NifA that regulates Nif/Fix genes is dependent on the nitrogen and oxygen concentrations in the system and in the environment.** The regulatory proteins NtrB, NtrC, Ntr X and NtrY senses intracellular and extracellular N concentrations and mediates NifA expression. The oxygen sensitivity of NifA is conferred through *fix* L, *fix* J and *fix*

K genes and mediates NifA expression under O_2 limiting (micro-aerobic) conditions (Stigter et al., 1993). The expression of NifA under N starving and O_2 limiting conditions regulates the expression of *nif*/*fix* genes in order to enable N_2-fixation in ORS571 under free-living and symbiotic conditions.

1.5.4 N_2 fixation in ORS571

ORS571 has the ability to fix N_2 both as a diazotroph and as a micro-symbiont. Unlike *Rhizobium* and *Bradyrhizobium*, ORS571 fixes N_2 in free living cultures in the absence of a fixed nitrogen source in the media, under micro-aerobic or low oxygen conditions with an oxygen tolerance up to 10% in the atmosphere (Dreyfus et al., 1988; Lee et al., 2008). Most rhizobia do not possess *nifV* gene that encodes homocitrate synthase and hence are auxotrophic for homocitrate, the Fe-Mo co-factor in nitrogenase. These rhizobia are able to express nitrogenase only during symbiosis with their host legume where the rhizobia depend on the exogenous supply of homocitrate from the host plant (Hakoyama et al., 2009). But ORS571 possess a functional *nifV* that enables it to express nitrogenase in free living cultures under nitrogen limiting conditions.

The generation of hydrogen (H_2) by nitrogenase is an energy consuming process and a considerable fraction of the energy from photosynthates is utilised for H_2 evolution. This decreases the efficiency of nitrogenase reaction for reducing N_2 resulting in a net loss of energy supplied to nitrogenase (Allen et al., 1991). H_2 oxidation improves the efficiency of N_2 fixation process by maximizing the electron flux to nitrogenase for reduction of N_2 (Schubert & Evans, 1976). ORS571 has been shown to utilise the H_2 generated as a by-product of N_2 fixation by its hydrogenase system expressed both under micro-aerobic free living conditions and as endosymbionts (Dreyfus & Dommergues, 1981; de vries et al., 1984). The hydrogenase system, encoded by *hup* and *hyp* gene cluster reoxidizes the H_2 produced to generate ATP, which enables ORS571 to perform efficient N_2 fixation (Das & Lodha, 1998). Besides ATP generation, it was also proposed that hydrogenase system also functions to improve respiratory

protection from oxygen inactivation of nitrogenase and prevents accumulation of H_2 at the active site of nitrogenase that could inhibit N_2 reduction (Allen et al., 1991).

The maximum nitrogenase activity in free living cultures was observed at a dissolved oxygen tension (DOT) of 10 µM and the activity decreases at oxygen concentrations below 1 µM (Gebhardt et al., 1984). However, the nitrogenase activity of the bacteroids form of ORS571 was observed at oxygen concentrations of 0.02 µM in the nodules (Bergersen et al., 1986; Bergersen et al, 1988). The nitrogenase activity under different oxygen tensions differs in the free living and symbiotic forms of ORS571. It was suggested that this was due to the presence of different micro-aerobic respiration pathways for the different O_2 concentrations under free living and symbiotic conditions. ORS571 expresses four terminal oxidases cytochrome aa3 (cyt*aa3*), cyt*d*, cyt*o* and FixNOQP which mediates electron transport for oxidative phosphorylation. Cytochrome *d* has been reported to be essential for micro-aerobic respiration during N_2-fixation in free living cultures while both FixNOQP and cyt*d* were necessary for symbiotic N_2 fixation (Kitts & Ludwig, 1994; Mandon, et al., 1994; Boogerd et al., 1998).

1.5.5 Symbiotic function of ORS571

ORS571 is a micro-symbiont of the fast growing annual tropical legume *Sesbania rostrata* and it is able to nodulate both the roots and stem of the host (Boogerd et al., 1998; Dreyfus, et al., 1988; Suzuki et al., 2007). This legume is well adapted to survive in water logged or submerged soil and has adventitious root primordia on the stem where the bacterial invasion occurs through the cracks. The stem nodules were reported to fix high amounts of N_2 as compared to other legumes like soybean, which makes this legume ideal as a green manure to be used in rotation with rice cultivation in the wetlands (Dreyfus et al., 1985; Lee et al., 2008). The mode of infection occurs by intracellular invasion in both the root and stem of *S. rostrata* in flooded or waterlogged soils. While the mode of infection in non-flooded soil occurs by the common root hair

curling process on the roots of the host (Dreyfus et al., 1985; D'Haeze et al., 2004; Herder et al., 2006). Previous studies on the genes essential for nodulation in the host and symbiotic N_2 fixation were reported to be *nod*, *nif*, *fix*, hydrogen uptake *(hup and hyp)*, lipopolysaccahride (LPS), and exopolysaccharide (EPS) biosynthesis, chemotaxis, sulphur and carbon uptake genes, which were more highly expressed in bacteroid forms than in free-living cells (Suzuki et al., 2007; Tsukada et al., 2009). ORS571 was also shown to colonize establish an endophytic interaction in the xylem of its host *S. rostrata* other than the nodules (O'Callaghan et al., 1997).

ORS571 was able to colonize the intracellular infection pockets located in the cortex of the roots and xylem of *Arabidopsis thaliana* and wheat and was not a nod factor dependent (Gough et al., 1997; Sabry et al., 1997; Stone et al., 2001). Similarly ORS571 was also shown to colonize rice and *Brassica napus* (oil seed rape) roots by lateral root crack invasion which was nod factor independent colonization. This colonization was observed to be stimulated and significantly enhanced in the presence of the flavonoid naringenin in both the plants (O'Callaghan et al., 2000; Jain & Gupta, 2003). However, there is no evidence of detectable N_2 fixation in the roots of non-legumes colonized by ORS571 in any of the studies mentioned above. This shows that ORS571 is able to establish only endophytic relationship with non-legumes and further research is required to explore the potential for a N_2 fixing symbiosis between this rhizobia and non-legumes.

1.5.6 PHB metabolism in ORS571

The carbon storage polymer PHB was previously reported to play an important role in the growth and metabolism of ORS571. In one of the studies, free-living chemostat cultures were observed to degrade PHB under carbon limitation conditions and it was suggested that the degradation of PHB provides carbon and energy source for synthesis of biomass and other cellular functions. But under oxygen-limiting growth

conditions, no PHB degradation was observed irrespective of the presence and absence of a carbon source; this suggests that the metabolism of PHB was O_2 dependent. Addition of nitrogen sources like ammonia or atmospheric N_2 in oxygen-limited cultures was also reported to stimulate PHB degradation. This could potentially provide competition benefit for ORS571 during the initial period of symbiosis with the host and also in the rhizosphere (Stam et al., 1986). In a different study on a PHB mutant of ORS571, rapid synthesis of the polymer in the wild type was observed during exponential growth stage, which was mainly dependent on the physiological nitrogen source. The PHB mutant showed reduced growth and impaired *nif*A expression, resulting in the lack of nitrogenase activities of ORS571 both as free living cultures and as bacteroids in the nodules of the host plant (Mandon et al., 1998). This suggests that besides acting as a redox regulator in cellular metabolism, PHB metabolism was important for the expression of key genes necessary for N_2 fixation in ORS571.

1.6 Metabolic flux analysis of ORS571

From the previous studies it is evident that central carbon metabolism and energy generation in a bacteroid during symbiosis differs from that of the free living rhizobia to meet the demands of N_2 fixation. Despite substantial progress in identifying genes and signalling molecules of the symbionts that are responsible for establishing successful symbiosis, the current challenge lies in understanding the exact metabolic characteristics of the symbionts. Transcriptomic, proteomic and metabolomic approaches to decipher the complex metabolic interactions between the host and rhizobium that sustains nitrogen fixation do not reveal these interactions. However, the metabolic integration of rhizobia inside the nodule and the host plant that provides energy and reductants for nitrogen fixation is complex and still unclear. Understanding this process requires detailed biochemical and metabolic analysis to investigate the intracellular fluxes that describes the true metabolic phenotype of the symbionts involved during N_2 fixation. This understanding will help in identifying potential targets in

the symbionts that could enhance the efficiency of the process and also to engineer synthetic symbiosis between rhizobia and non-legumes.

The metabolic activity of a bacteroid *in planta* that interacts with the host processes and supports the energetic state of the cell under N_2 fixing conditions requires detailed biochemical and metabolic analysis. From the aforementioned metabolic studies, steady state MFA has proved to be a very powerful method for measuring multiple fluxes in the central metabolic network of an organism and for assessing redox and energy balance in the network. The flux maps generated in these studies provides insights into metabolic control, identification of novel metabolic routes and strategies for rational design in metabolic engineering.

Owing to the potentials of ^{13}C-MFA, this approach was chosen for the first objective of this study- to establish the method in free-living aerobic cultures of ORS571. Chapter 3 includes step by step explaination of the methods established for steady state ^{13}C-MFA and generation of flux maps. The second objective was to use steady state ^{13}C-MFA and generate flux maps for ORS571 free-living cultures under aerobic, micro-aerobic and N_2 fixing conditions. The results presented in chapter 4 highlight the active pathways and the adjustments in metabolic fluxes of these pathways due to N_2 fixation under micro-aerobic conditions. The third objective was to generate flux maps for symbiotic ORS571 (bacteroid) isolated from the root and stem nodules of the host plant. The results presented in chapter 5 shows the metabolic behaviour of the bacteroid during N_2 fixation under symbiotic conditions and the changes in the metabolic fluxes of the bacteroid as compared to the free-living N_2-fixing ORS571. The final objective was to generate flux maps for a PHB less strain of ORS571 under aerobic and micro-aerobic metabolism (chapter 6). This was to assess the behaviour of the metabolic network in the absence of PHB- a metabolically important carbon and electron sink in rhizobia.

2. General Materials and methods

2.1 Antibiotics, chemicals and kits

Antibiotics nitrofurantoine, kanamycin (Km), neomycin (Neo) were purchased from Sigma Aldrich. Tryptone yeast (TY) and Luria Bertani (LB) growth medium were purchased from Sigma Aldrich. Universal minimal salts medium (UMS) was prepared in the lab and the composition of UMS media is shown in Table 2.1. Plasmid isolation, gel extraction and PCR purification kits were purchased from Thermo Scientific. Genomic DNA isolation kit for rhizobia was purchased from Qiagen. The enzymes and buffers for molecular biology work were purchased from New England Biolabs (NEB) and the primers were obtained from Eurofins Genomics. Go taq green master mix and Phusion PCR kits for PCR amplification were purchased from Promega and NEB respectively. For labelling experiments, the substrate [U-$^{13}C_4$]succinic acid was purchased from CK Isotopes Ltd, USA. The samples for gas chromatography mass spectrometry (GC-MS) were prepared using two derivatisation reagents, N-tert-butyldimethylsilyl-N-methyl trifluoroacetamide with 1% tert-butyldimethylchlorosilane (TBDMS), purchased from Sigma Aldrich and N-methyl-N-(trimethylsilyl) trifluoroacetamide (MSTFA), purchased from Fluka Analytical. For gas chromatography (GC) experiments, four gases - acetylene, nitrogen, air and hydrogen were purchased from BOC and consumables such as Schott bottles, universal bottles, needles and rubber seals were purchased from Sigma Aldrich. A special gas mixture of 3% oxygen and 97% nitrogen was also purchased from BOC.

Table 2.1 **UMS media composition**

Compound	Amount (mg/L)	MW	Final Concentration
K_2HPO_4	87.4	174.18	0.5 mM
$MgSO_4.7H_2O$	500	246.47	2 mM
NaCl	500	58.44	8.5 mM
MOPS	4190	209.3	20 mM

Compound	Amount (mg/L)	MW	Final Concentration
EDTA-Na_2	0.375	372.24	1.0 µM
$ZnSO_4.7H_2O$	0.16	287.53	0.6 µM
$Na_2MoO_4.2H_2O$	0.2	241.9	0.8 µM
H_3BO_3	0.25	61.83	4.0 µM
$MnSO_4.4H_2O$	0.2	223.07	0.9 µM
$CuSO_4.5H_2O$	0.02	249.7	0.08 µM
$CoCl_2.6H_2O$	1	237.93	4.2 µM
$CaCl_2.2H_2O$	75	147.01	0.51 mM
$FeSO_4.7H_2O$	12	278.05	0.04 mM
Thiamine hydrochloride	1	337.27	3.0 µM
D-Pantothenic acid Ca salt	2	476.53	4.2 µM
Biotin	0.1	241.31	0.4 µM

2.2 Bacterial strains and plasmids

The list of bacterial strains and plasmid used for this study is shown in Table 2.2

Table 2.2: **Strains and plasmids**

Strain or plasmid	Description	Source or reference
ORS571	Wild type strain of *Azorhizobium caulinodans* (Model organism for the study)	Dreyfus et al., 1988
OPS0865	ORS571 *phbC*::pK18; Neo^r/Km^r	This work
DH5α	F_ *80lacZ_M15* _(*lacZYA-argF*) *U169 recA1 endA1 hsdR17* (rK_ mK_) *phoA supE44 thi-1 gyrA96 relA1*	Invitrogen
pRK2013	ColEI replicon with RK2 *tra* genes, helper plasmid used for mobilizing plasmids; Km^r	Karunakaran et al., 2010
pK18mob	pK18mob pUC19 derivative lacZ mob plasmid; Km^r	Schäfer et al., 1994; Karunakaran et al., 2010
pOPS0391	pK18mob containing internal fragment of *A. caulinodans phbC* gene; Neo^r/Km^r	This work

Wildtype *Azorhizobium caulinodans* ORS571 was used as the model system to study the metabolic characteristics during free-living and symbiotic N_2-fixation with *Sesbania rostrata*. *E. coli* strains DH5α and pRK2013 were used for cloning and conjugation studies.

2.3 16SrRNA PCR and phylogenetic analysis

ORS571 was inoculated into TY liquid medium with the antibiotic nitrofurantoine (10 μg ml^{-1}) and was grown overnight for genomic DNA isolation. 16S ribosomal RNA (rRNA) PCR was performed using four universal phylogeny primers: 27F (forward primer), 1492R (reverse primer) that binds at the start and end of the 16SrRNA gene. Primers V_4F (forward primer) and V_4R (reverse primer) bind in the middle which are the variable regions of the gene among the species. The details of the primers used are shown in Table 2.3. The PCR was done using genomic DNA of ORS571 as the template and using three combinations of primers: (i) 27F and V_4R; (ii) V_4F and 1492R; and (iii) 27F and 1492R. The PCR products of reactions 1 and 2 have a product of 600-750 bp, while the product of reaction 3 is of size 1.2 kb. The reactions were set up using the Go Taq reaction kit purchased from Promega. The PCR products were analysed by gel electrophoresis to confirm the correct product sizes for each reaction. The PCR products were sequenced using the services from Eurofins Genomics. These sequences were analysed by BLAST to find the best match to the sequences and to confirm the rhizobial phylogeny. A neighbour joining tree was constructed using the software MEGA6 and the instructions available in the manual.

Table 2.3: **Phylogenetic primers**

Primers	Sequences 5' to 3'	Source or reference
27F	AGAGTTTGATCMTGGCTCAG	Lane, 1991

Primers	Sequences 5' to 3'	Source or reference
V_4F	GTGCCAGCMGCCGCGGTAA	Tremblay et al., 2015
V_4R	GGACTACHVGGGTWTCTAAT	Tremblay et al., 2015
1492R	TACGGYTACCTTGTTAYGACTT	Lane, 1991

2.4 Bacterial growth conditions

2.4.1 ORS571 free-living aerobic growth conditions

ORS571 was streaked on a TY slope containing 10 µg/ml nitrofurantoine to select for ORS571 and the slope was grown for 2-3 days at 37ºC. The slope was washed three times in UMS medium and was inoculated into the same medium with a carbon source, 10 mM ammonium chloride (NH_4Cl) and 1 mM vitamin stock to start liquid cultures. 0.3 mM nicotinic acid was also added to the UMS medium as it is required to support the growth of ORS571 in minimal media (Elmerich et al., 1983). The cultures were kept at a growth temperature of 37ºC in an incubator shaker at 200 rpm.

2.4.2 ORS571 free-living micro-aerobic growth conditions

ORS571 cultures were grown in 500 ml water jacketed bioreactors in a micro-aerobic or low O_2 chamber purchased from Belle Technology. This chamber was connected to a nitrogen cylinder which maintained the desired levels of N_2 and O_2 inside the chamber. The bioreactors were connected to a circulating water bath which maintained a temperature of 37ºC. The cultures were continuously sparged with the atmosphere inside the chamber using a fish pump under sterile conditions. The cultures were also stirred using magnetic stirrers to allow homogenous mixing of nutrient media. The experimental set up is shown in Figure 2.1.

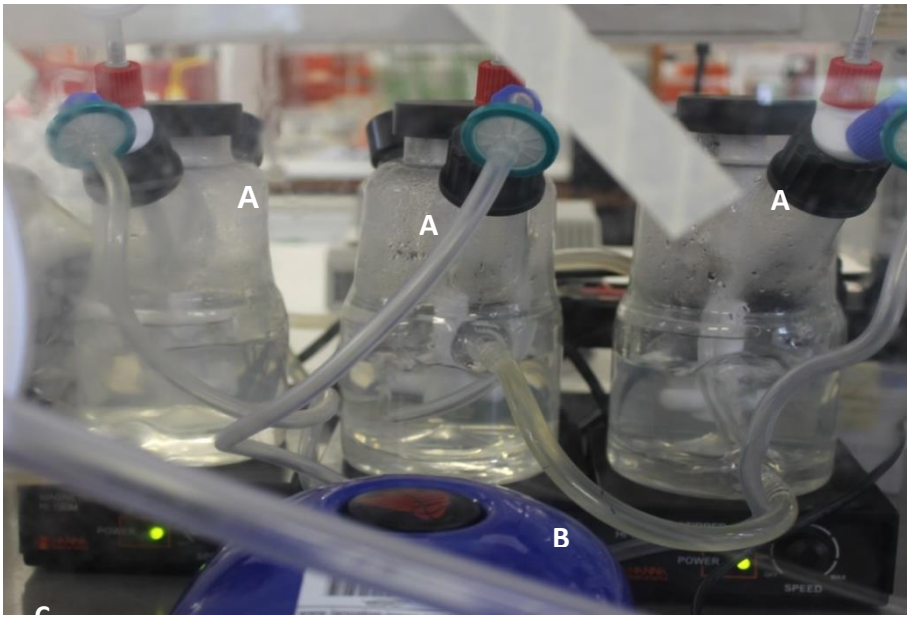

Figure 2.1: **Establishment of ORS571 micro-aerobic free-living cultures.** Bioreactors (A) were connected to a fish pump (B) and were placed on stirrers (C) for mixing of cultures.

2.4.3 Mini-reactor set up

Small scale cultures (10 ml) were grown in the mini-reactor set up shown in Figure 2.2 for aerobic condition and Figure 2.3 for micro-aerobic conditions. Cultures were grown in 28 ml universal bottles, sealed with rubber caps and fitted with an 8-10 cm needle for inlet of air and an outlet needle for equalizing the air pressure. A fish pump was used for continuous sparging of the cultures, with air (21% O_2) through the inlet needles to grow ORS571 under aerobic conditions. For micro-aerobic conditions, the cultures were sparged with 3% O_2-97% N_2 gas from a gas cylinder connected to the system. A water bath was used for maintaining the growth temperature of 37ºC. The cultures were also connected to humidifiers which maintained moisture in the air that was sparged into the cultures.

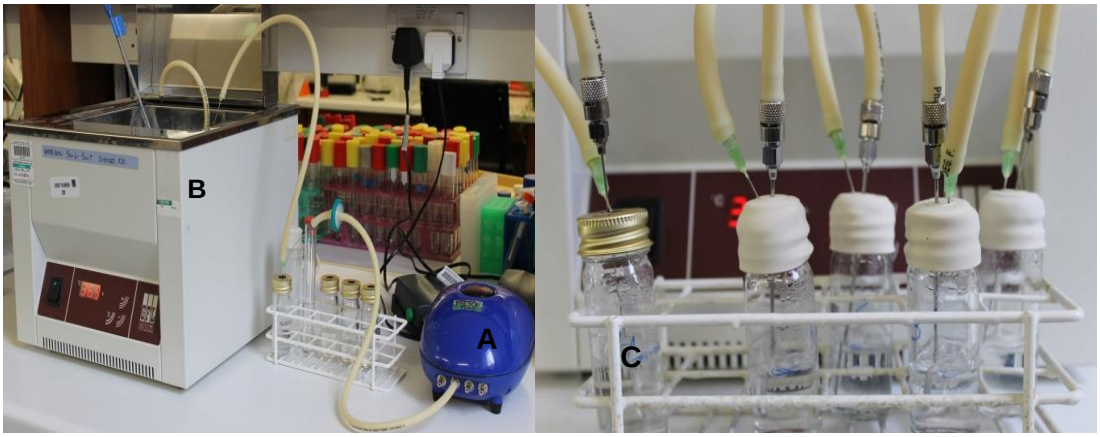

Figure 2.2: **Mini-reactor set up for aerobic growth condition**. Fish pump (A) was used to sparge air into the cultures and the water bath (B) maintained a growth temperature of 37ºC. The cultures were connected to humidifiers (C).

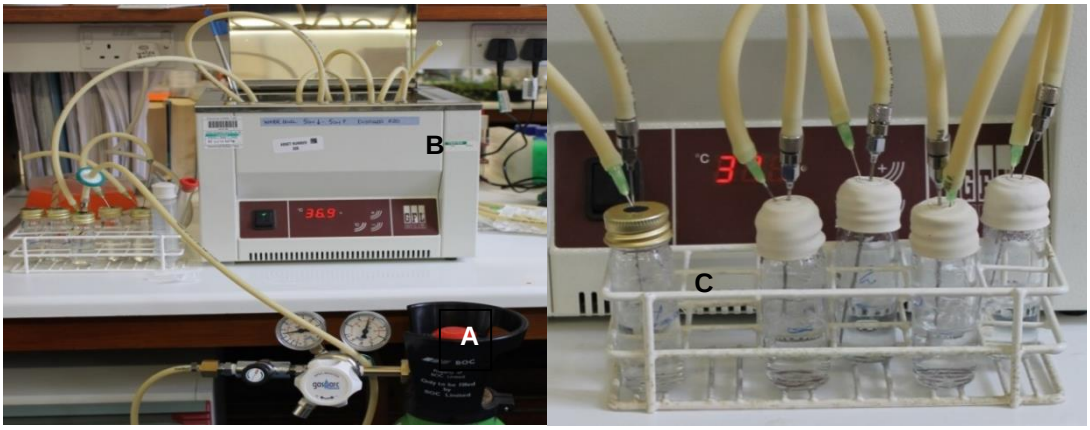

Figure 2.3: **Mini-reactor set up for micro-aerobic growth condition**. Gas cylinder (A) was used to sparge 3 % O_2-97 % N_2 gas mixture into the cultures and water bath (B) maintained a growth temperature of 37ºC. The cultures were connected to humidifiers (C).

2.4.4 *E. coli* growth conditions

E. coli strains were grown on LB agar plates with Km (50 µg/ml) at an incubation temperature of 37ºC. Liquid cultures in LB media were kept in an incubator shaker at 200 rpm and 37ºC.

2.5 Plant growth conditions

Sesbania rostrata seeds purchased from Sunshine Seeds and Hutton institute Dundee, were scarified by soaking in concentrated sulphuric acid for 10-15 min and

washed three times before being placed in agar plates (4 % (vol/vol). Agar plates were sealed with micropore tape and kept in the growth room for 2-3 days until they germinated. Fine vermiculite was mixed with nitrogen free rooting solution containing the ingredients listed in Table 2.4. The vermiculite with the rooting solution was autoclaved before use. After germination, seeds were placed on fine vermiculite media, and kept in a plant growth room with a photoperiod of 16 hours and at a temperature of 21ºC. Nodulation in *S. rostrata* was obtained by inoculation with ORS571 on the root and shoot of 1-week-old plants. The plants were watered once a week and given rooting solution every 3 weeks.

Table 2.4: **Nutrient composition of nitrogen free rooting solution**

Chemical	**Stock concentration**	**Stock Volume**	**Final concentration**	**Volume in 2.5 l**
$CaCl_2.2H_2O$	1M	72.51 g/500ml	1 mM	2.5
KCl	100 mM	3.73 g/ 500ml	100 µM	2.5
$MgSO_4$	800 mM	98.59 g/500ml	800 µM	2.5
Fe EDTA	10 mM	1.84 g/ 500ml	10 µM	2.5
H_3BO_3	350 mM	2.16 g/ 500ml	35 µM	0.25
$MnCl_2.4H_2O$	90 mM	1.78 g/ 500ml	9 µM	0.25
$ZnCl_2$	8 mM	0.109 g/500ml	0.8 µM	0.25
$Na_2MoO_4.2H_2O$	5 mM	0.121 g/500ml	0.5 µM	0.25
$CuSO_4.5H_2O$	3 mM	0.075 g/500ml	0.3 µM	0.25
KH_2PO_4		25 g		1.25
Na_2HPO_4		28.4 g		1.42

2.6 Isolation of bacteroids from *S. rostrata* by the differential spin method

Root and shoot nodules from *S. rostrata* were picked in the low O_2 cabinet that maintained a micro-aerobic environment with an oxygen concentration of < 1 %. Isolation of bacteroids was done according to the method described in Tsukada et al., 2009, modified for this study. The nodules were homogenised with a mortar pestle in

MMS buffer (pH 7.0) containing 40 mM MOPS (morpholinepropanesulfonic acid), 20 mM KOH, 2 mM $MgSO_4$, 0.3 M sucrose and polyvinylpyrrolidone (PVP) (4 % vol/vol). The homogenate was filtered through four layers of muslin cloth and centrifuged at 500 g for 5 min to remove plant debris. The supernatant was collected in a fresh tube and centrifuged again at 5000 g for 10 min. The supernatant was removed and the bacteroid pellet was washed with MMS buffer containing 25% PVP to remove any remaining plant material. The pellet was then washed with MMS buffer containing no PVP at 5000 g for 2 min. The bacteroid pellet was re-suspended in UMS media with a carbon source for subsequent assays.

2.7 Nitrogenase assay using GC

2.7.1 Nitrogenase assay for free-living ORS571

The nitrogenase activity in free-living cultures of ORS571 was measured by the acetylene reduction assay (ARA) adapted from the method described in Trinick et al., 1976. A 200 ml culture was grown in bioreactors under micro-aerobic condition and a 5-10 ml volume was withdrawn from the culture and transferred to a 28 ml universal bottle and capped with rubber seals to stop any gas exchange. 2% acetylene (C_2H_2) was injected into the bottle by removing 680 µl air and injecting 560 µl of acetylene gas with a 1 ml syringe. Incubation with 2% acetylene was done for various lengths of time and the amount of ethylene (C_2H_4) production was measured by injecting 1 ml of air into the GC Perkin Elmer Clarus 480. The peak areas for ethylene produced were recorded and the rate of nitrogenase activity was expressed as nanomoles C_2H_4 h^{-1} OD_{600}^{-1}.

2.7.2 Nitrogenase assay for plants

6 to 8-week-old *S. rostrata* and 4-week-old soybean plants were used for ARA assay. The assay was adapted from the method described in Trinick et al., 1976. The plants were taken out of the pots and placed in 250 ml to 1000 ml Schott bottles (depending

on the size of the plants). The bottoms of the Schott bottles were dampened with a moist wipe before placing the plants inside. 2% C_2H_2 was injected into the Schott bottles and the amount of air to be removed and the amount of acetylene to be injected was calculated according to the capacity or volume of the bottle used. The plants were incubated for up to 2 hours and C_2H_4 produced was detected using GC Perkin Elmer Clarus 480. The rate of nitrogenase activity was expressed as nanomoles C_2H_4 h^{-1} per jar.

2.7.3 Nitrogenase assay in isolated bacteroids and nodule sections

Nodules isolated in the low O_2 cabinet were cut into thin sections with a razor blade and were re-suspended in UMS media with 10 mM succinate as the carbon source. Both nodule sections and isolated bacteroids from *S. rostrata* plants were assayed for nitrogenase activities by the method described in 2.7.1.

2.8 Biomass composition measurement

2.8.1 Dry cell weight measurement

Free-living liquid cultures of ORS571 were used to obtain dry cell weight measurements. Cells were harvested at different growth stages and the optical density of the culture was recorded at a wavelength of 600 nm with a spectrophotometer purchased from Thermo Scientific. Cultures were spun down, supernatant was discarded and the pellet was freeze-dried in a lyophilizer overnight to prepare dry cell pellets. The dry weight was calculated by subtracting the weight of the tubes with the dry cell pellet from the empty tubes.

2.8.2 Protein estimation

Dry cell pellets were used for protein estimation by the bicinchoninic acid assay (BCA assay) (Smith et al., 1985). Bovine serine albumin (BSA) was used as the standard protein to prepare a standard protein curve for the estimation of protein in samples. The standards were prepared in milliQ water in a range of concentration

from 0 to 1 mg ml^{-1}. The standards and dry cell pellets were mixed with of 2 N NaOH and incubated at 100°C for 10 min. After incubation, the standards were directly used for the BCA assay while the samples were cooled, centrifuged at 13000 rpm for 30 min and the supernatant was used for the assay. 4% copper sulphate and 1 ml BCA solution were added to both the standards and samples, followed by mixing and incubation at 60°C for 30 min. The absorbance for both the standards and samples was recorded at 562 nm using water as the blank in a spectrophotometer.

2.8.3 Lipid estimation

The amount of lipid in the samples was determined by the sulpho-phospho vanillin assay using linolenic acid as the standard (Izard & Limberger, 2003; Cheng et al., 2011; McMahon et al., 2013). Linolenic acid was dissolved in chloroform and used to prepare the standards in a range from 0 to 1 mg ml^{-1} for the assay. Only glass vials were used for this assay. The standards were evaporated to dryness by incubating them at 90°C for 10 min. Dry cell pellets were dissolved in phosphate buffer saline and both the standards and samples were incubated at 95°C for 20 min in a 2 ml of concentrated sulphuric acid. The tubes were cooled on ice, vortexed and the absorbance was recorded at 535 nm. Phosphoric acid vanillin reagent was prepared by dissolving 0.12 g of vanillin in 20 ml of water, and the volume was adjusted to 100 ml with 85 % phosphoric acid. 5 ml of this reagent was added to both standard and samples, mixed well and incubated at 37°C for 10 min in the dark. The absorbance was read again at 535 nm and the increase in absorbance showed the detection of lipid by phosphoric acid vanillin reagent.

2.8.4 Nucleic acid estimation

Dry cell pellets were re-suspended in milliQ water in ribolyser tubes which were filled with 0.2 mm silica and glass beads up to $1/4^{th}$ of the volume of the tubes. The cell pellets were disrupted using a Fast prep FP120 ribolyser. After disruption, cells were

centrifuged at 8000 rpm for 5 min and supernatant was collected separately for quantitation of DNA and RNA. The quantitation was performed using Qubit fluorescence assay kit from Thermo Fisher Scientific. Samples were mixed with DNA and RNA detection dyes and the concentration of each was calculated using standard curves.

2.8.5 Polyhydroxybutyrate (PHB) estimation

The amount of PHB in rhizobial cultures was estimated using Law and Slepecky's spectrophotometric method with a few minor changes (Law & Slepecky, 1961). Dry cell pellets were dissolved in 1 ml of sodium hypochlorite solution (10-15% chlorine) and incubated at 37°C for 1 hour. After incubation, 4 ml of milliQ water was added to the samples and mixed well. 1 ml of this suspension was centrifuged at 4000 rpm for 20 min, supernatant removed and the pellet was washed with 1 ml of acetone followed by 1 ml of ethanol. After complete removal of ethanol, the pellet was re-suspended in 1 ml of chloroform and transferred to glass tubes. The tubes were placed in a boiling water bath at 100°C for 1-2 min to extract PHB with chloroform. The tubes were immediately placed on ice and the chloroform was collected in a separate glass tube. The extraction was performed twice with 1 ml of chloroform and the total chloroform extract was filtered using 0.2 µM Whatman PTFE (polytetrafluoroethylene) supported membrane filters. 100 µl of the filtrate was evaporated to dryness and 5 ml of concentrated sulphuric acid was added to these tubes. Tubes were vortexed and incubated in a boiling water bath at 100°C for 20 min. PHB in the presence of sulphuric acid at a high temperature forms crotonic acid, which has an absorbance at 235 nm (Law & Slepecky, 1961). The absorbance at 235 nm was recorded and the amount of PHB in the samples was calculated from a standard curve, prepared from sodium 3-hydroxybutyrate.

2.8.6 Carbohydrate estimation

Total carbohydrates in the cells were extracted by a method described by Ionescu & Belkin, 2009. Dry cell pellets were mixed with 400 µl of milliQ water and 800 µl chloroform followed by vigorous mixing. The samples were centrifuged at 13000 rpm for 10 min to obtain a lower and upper layer phase separation. The upper aqueous layer contained carbohydrates and 300 µl of this layer was collected separately and mixed with 200 µl of milliQ water. Carbohydrate quantitation was performed using the anthrone assay (Seifter et al., 1950). Anthrone reagent was prepared by dissolving 0.5 g of anthrone powder purchased from Sigma Aldrich in to 10 ml of ethanol followed by addition of 240 ml of 75 % sulphuric acid. 500 µl of sample was taken in glass tube and 1 ml of 75 % sulphuric acid was added followed by 2 ml of anthrone reagent. The samples were vortexed and incubated at 100ºC for 10 min. Tubes were cooled and the absorbance was recorded at 620 nm. The amount of carbohydrates was calculated from a glucose standard curve.

2.8.7 Exo-polysaccharide (EPS) estimation

ORS571 cultures were harvested at specific growth stages and the extraction of EPS secreted into the media was adapted from the method described by Zevenhuizen, 1971. The medium was filtered using 0.22 µm Millipore filters and three volumes of absolute ethanol were added to the medium to precipitate the carbohydrates. This was followed by incubation at -20ºC for an hour, followed by centrifugation at 4000 rpm for 10 min. The supernatant was discarded and the pellet was washed with 40 ml cold absolute ethanol followed by centrifugation at 3000 rpm for 3 min. The supernatant was discarded and the pellet was left to dry overnight. The dry pellet was re-suspended in 1 ml of milliQ water and dialysed against 1 l of milliQ water overnight. EPS was detected using the anthrone assay as described in 2.9.6 and the amount of EPS was quantitated using a galactose standard curve.

2.9 Scanning electron microscopy (SEM) imaging

Liquid cultures of ORS571 were grown under aerobic and micro-aerobic conditions using the experimental set up described in section 2.4.3. The cultures were harvested at a late exponential growth stage and 2-3 ml of the cultures was spun down at 12,000 rpm for two min and washed three times with milliQ water. The cells were re-suspended in 50 µl of glutaraldehyde (2 % vol/vol) in phosphate buffer saline (PBS). The cell suspension was placed on glass slides (size 1 cm approx.) coated with poly-lysine and the slides incubated in small round petri dishes at 4ºC for 1.5 hours. After incubation, the glass slide was washed twice in PBS and the remaining buffer was aspired from the petri dish. The samples were dehydrated in an alcohol gradient using 30 %, 50 %, 70 %, 85 %, 95 % and 100 % ethanol with an incubation period of 15 min for each gradient. The slides were then dried using a critical point drying (CPD) instrument. After drying, the slides were coated with gold-palladium with a sputter coater and imaged by scanning electron microscope (SEM) Jeol JSM 5510.

2.10 Statistical tests

Two sample t-test assuming unequal variance was performed using Microsoft excel with the significance level or the critical value α fixed at 0.05. Two measurements were considered statistically different if the p-value for the comparison was < 0.05. A line of best fit for was produced using Microsoft excel comparing measurements obtained under two conditions. The coefficient of determination, and slope close to 1 indicates a good agreement between the measurements and confirming that the measurements are identical. ANOVA (analysis of variance), Tukey's and sidak's multiple comparison tests were performed using Graph pad prism 7 software and comparisons with p-value < 0.05 were considered significantly different.

2.11 Extraction of metabolites from free-living cultures and bacteroids

Free-living cultures of ORS571 were harvested at exponential growth phase by filtration of cells using 0.45 µm Millipore membrane filters containing nitrocellulose and a vacuum-aided filtration unit. Isolated bacteroid suspensions in UMS were harvested using the same procedure for free-living cultures. The filter paper containing harvested cells was dipped in a pre-chilled mixture containing 3 ml methanol and 1.5 ml chloroform in the ratio of 2:1 in a glass tube, which broke the cells and released metabolites into the methanol chloroform mix. The tube was incubated on ice for 30 min with frequent mixing during the incubation. The filter paper was then removed and 3 ml of milliQ water was added to the tube, vortexed and centrifuged at room temperature, 2000 rpm for 15 min to allow phase separation as shown in Figure 2.5.

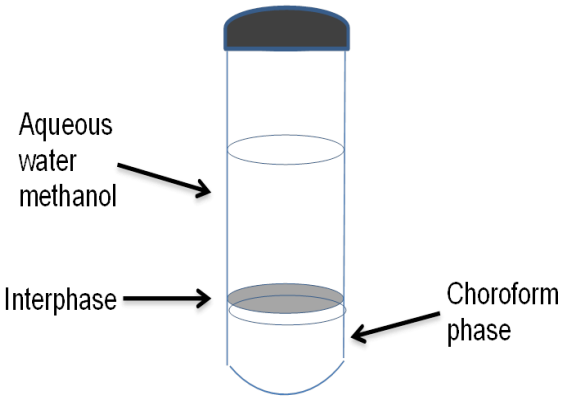

Figure 2.5: **Phase separation of metabolites obtained by methanol chloroform extraction.**

2.12 Preparation of samples for GC-MS

2.12.1 Metabolites soluble in aqueous phase

2 ml of the aqueous upper layer containing soluble metabolites was mixed with 5 µl internal standard mixture of norvaline and ribitol present at a concentration of 0.2 mg ml^{-1}, and the samples were dried using a speed vacuum centrifuge. The dried material was then mixed with the solvent pyridine and derivatised with the chemical TBDMS to improve the suitability, efficiency and detection of metabolites in GCMS

(Orata, 2012). The dried material was mixed with 25 µl of pyridine and mixed in a thermomixer at 900 rpm, 37°C for 30 min. The samples were briefly spun and 35 µl of MSTFA, derivatization reagent was added. The samples were mixed for another 30 min at 900 rpm and 37°C. After this incubation, samples were briefly spun, transferred to GC-MS vials and sealed. 1 µl of this sample was injected into the GC at an injection port temperature of 230 °C. The oven temperature was constant at 70 °C for 5 min, followed by an increase to 330 °C for 5 min at 120 °C/minute. The temperature was then decreased to 70 °C for 1 minute at 120 °C/minute. The carrier gas was helium and the flow was maintained at 1.3 ml /minute. The total run time of each sample was 69.33 min, including a solvent delay of 10 min. The scan parameters for the MS detector were set to 50 for a low mass and 600 for a high mass.

2.12.2 Metabolites insoluble in aqueous phase

The intermediate and bottom layers were obtained in a single phase by adding 2:1 methanol chloroform mixture and 1 ml- 2ml of this mixture was centrifuged at 10,000 rpm for 30 min. The supernatant was discarded, and the pellet was boiled in 500 µl 6M hydrochloric acid for 24 hours at 100°C. The hydrolysate was centrifuged at 13000 rpm for 15 min and the supernatant was collected in a fresh tube. The supernatant was spun again and 200-500 µl of this supernatant was mixed with 5 µl of 0.2 mg ml^{-1} internal standard and left to dry. 25 µl of pyridine was added to the dried material, followed by mixing in a thermomixer at 900 rpm for 30 min and at 37°C. The samples were spun briefly and derivatised with 35 µl of TBDMS reagent. The samples were spun briefly, transferred to GC-MS vials and sealed. 1 µl of this sample was injected into the GC-MS Agilent 7890A (GC coupled to 5975C mass spectrophotomter (VL MSD) with triple axis detector) at an injection port temperature of 230 °C. The oven temperature was constant at 120 °C for 5 min, followed by an increased to 270 °C at 4 °C/minute and was held at this temperature for 3 min. The temperature was further

increased to 310°C at 20 °C/minute and was held at this temperature for 1 minute. The temperature was then again decreased to 120 °C at 60 °C/minute. The carrier gas was helium and the flow was maintained at 1.3 ml /minute. The total run time of each sample was 51.667 min, including a solvent delay of 10 min. The scan parameters for the MS detector were set to 150 for low mass and 600 for high mass.

2.13 Analysis and processing of GC-MS data

2.13.1 Extraction of GC-MS data

Raw data files were analysed using Chemstation, a GC-MS data analysis software provided by Agilent. For each GC peak of a metabolite or a compound, extraction of m/z values was done by integration/scan across the whole peak. For each metabolite, the m/z values and their respective ion counts were extracted as a Microsoft Excel file.

2.13.2 Baseline correction of raw data

The correction of MS (mass spectrometry) data for detector and chemical noise was done using MetAlign software. Raw data files were entered into the software and correction was performed with a pre-set baseline and noise elimination parameters (Lommen, 2009).

2.13.3 Identification of metabolites

Identification of soluble phase metabolites (amino acids, organic acids and sugars) derivatised using MSTFA was done in AMDIS (Automated mass spectral deconvolution and identification system) developed at the National Institute of Standards and Technology (NIST). The software identifies a metabolite by referring to its mass spectral database. TBDMS derivatised metabolites (amino acids and PHB) were identified by their characteristic fragmentation patterns and m/z values as

reported in the literature (Rosenblatt et al., 1992; Dauner & Sauer, 2000; Molnár-Perl & Katona, 2000; Halket et al., 2005).

2.13.4 Quantification of amino acids

Standards were prepared using amino acids in a range of concentrations and were derivatized according to the method described in 2.13.2. A known amount of twenty different amino acids were used to set up the quantitation method in the Chemstation software and the amount of each amino acid in the samples was quantified from the respective standard curve.

2.14 ^{13}C labelling experiments

2.14.1 Labelling experiments in free-living ORS571 cultures

A TY slope of ORS571 was grown for 2-3 days and washed with UMS minimal media three times and cells were re-suspended in 5 ml of UMS. 0.5-1 % vol/vol of the culture suspension was inoculated in 10 ml of UMS media containing 20% [$^{13}C_4$]succinic acid and 80% unlabelled sodium succinate at an overall concentration of 10 mM as the carbon source along with vitamins, ammonium chloride and nicotinic acid as described in section 2.4. These non N_2-fixing cultures were grown in either aerobic conditions (21% O_2) and or micro-aerobic conditions (3% O_2, 97% N_2) up to late exponential growth stages, followed by extraction of metabolites and ^{13}C isotopomer analysis using GC-MS. For N_2-fixing ORS571, free-living cultures were grown under micro-aerobic conditions (3% oxygen, 97% nitrogen) containing 20% [$^{13}C_4$] succinic acid and 80% unlabelled sodium succinate at an overall concentration of 10 mM as the carbon source along with vitamins and nicotinic acid. These cultures were also grown up to the late exponential stage, followed by extraction of metabolites and ^{13}C isotopomer analysis.

2.14.2 Labelling experiments in bacteroids

Isolated bacteroids were re-suspended in UMS media containing 20% [$^{13}C_4$] succinic acid and 80% unlabelled sodium succinate at an overall concentration of 10 mM. Bacteroid suspensions were placed in a shaker incubator for 24 hours at 200 rpm and 37°C. After incubation, the bacteroids were harvested for metabolite extraction and ^{13}C isotopomer analysis.

2.15 Mass isotopomer analysis

2.15.1 Mass correction of MS spectra

The mass spectra of TBDMS derivatized metabolites, obtained from the labelling experiments were baseline-corrected and the m/z values with ion counts were extracted for trehalose, amino acid and hydroxybutyrate. The MS data provided information on the labelling pattern i.e the ^{13}C incorporation in the metabolites. However, this mass isotopomer distribution of carbon atoms in a labelled metabolite were overlaid by mass effects from naturally-occurring stable mass isotopes like ^{1}H, ^{2}H, ^{16}O, ^{17}O, ^{29}Si from the metabolite and derivatization chemical. A MATLAB-based mass correction tool called MSCorr was used to correct the MS spectra and eliminate the isotopic effects from non-carbon atoms of the metabolite and derivatization chemicals except for ^{13}C in the metabolite fragment (Wahl et al., 2004). The MS data after mass correction provided fractional abundance of mass isotopomer families in each fragment of a metabolite along with errors associated with each measurement. The average ^{13}C incorporation (%) in the molecular fragments i.e the average enrichment per carbon atom, was calculated from the fractional abundance of the mass isotopomers after mass correction. An example of the calculation for average ^{13}C incorporation in M-57 fragment of alanine-2TBDMS is described in Table 2.5.

Table 2.5: **Average ^{13}C calculation in alanine-2TBDMS (M-57 fragment)**

Mass isotopomer	No of ^{13}C	Fractional abundance from MSCorr	Total ^{13}C in the fragment
M + 0 (M0)	0	0.7148	0 X 0.7148
M + 1 (M1)	1	0.0852	1 X 0.0852
M + 2 (M2)	2	0.0441	2 X 0.0441
M + 3 (M3)	3	0.1559	3 X 0.1559
Average			0.2137
Average ^{13}C (%)			21.37 %

2.15.2 Validation of molecular fragments used for flux analysis

TBDMS-derivatised fragments of amino acid and PHB along with MSTFA-derivatised fragments of trehalose were used for flux analysis. The fragments after mass correction were validated or chosen using the following criteria: (i) average ^{13}C (%) incorporation in the fragments close to the expected value (% of labelled substrate provided in the media) (ii) small errors of measurement on the fractional abundance of isotopomers after mass correction (iii) fragments with non-negative fractional abundance for isotopomers after mass correction (iv) fragments with no overlapping m/z values with any other fragments (v) valid fragments already reported in the literature.

2.16 Steady state ^{13}C-MFA using INCA

2.16.1 Metabolic modelling

The metabolic network model for ORS571 free-living cultures and bacteroids was built in Isotopomer network compartmental analysis (INCA), a MATLAB based software obtained from Vanderbilt university USA, according to the procedure described in the manual (Young, 2014). The reactions of the model included steady state mass balance or elementary metabolite unit (EMU) balance equations based on reaction stoichiometry, reversibility and carbon atom transition information. The model was

constrained by a biomass equation that was unique for each of the free-living and bacteroid models and was completely dependent on the biomass composition of the organism measured under different conditions.

2.16.2 Experimental data input and steady state ^{13}C-MFA

The mass isotopomer data obtained from labelling experiments was entered into the metabolic model along with initial flux values and isotope tracer information. Flux estimation was performed in INCA by minimizing the sum of squared residuals (SSR) between simulated and experimental measurements. The best fit flux solutions will have a statistically acceptable SSR. The goodness of flux maps or the validation of flux estimates was assessed by using inbuilt statistics in INCA, called parameter continuation, an algorithm that calculates confidence intervals for each of the fluxes measured (Young, 2014).

2.17 Succinate consumption assay

Succinate consumption rates were measured in the free-living cultures using a GC-MS assay. A 1/1000 dilution of the original 10 mM succinate stock was chosen for this assay to avoid saturation of the detector. Different amounts ranging from 0 to 1000 nanomoles of succinate was run through the GC-MS and the total ion count (TIC) of succinate peak (m/z 289) was recorded for each of the standards. The standard curve prepared from the different amounts of succinate and their respective TICs was used to estimate the amount of succinate left in the medium that was used to grow ORS571. Liquid cultures were set up under aerobic, micro-aerobic and N_2-fixing conditions and grown up to stationary phase. 1 ml of the cultures was withdrawn at different time intervals and the OD_{600nm} and dry cell weight was also recorded for each of the time intervals. The cultures were spun and the media was collected in a fresh tube. The medium was diluted to 1/1000 fold and 500 µl was run through the GC-MS. The amount of succinate present in the medium for the culture harvested at a particular OD and time interval was calculated from the standard curve.

The specific substrate consumption rate (q_s) was determined using a procedure based on the logarithmic method (Görgens et al., 2005).

$$q_s = exp\left(\frac{ln\left(\frac{s-s_0}{m_0-m}\right)}{t}\right)$$

where s_0 and s are the total amount of substrate at, respectively, the beginning of the culture and at a specific time, t, in the culture cycle, and m_0 and m are the biomass at the corresponding times. During exponential growth, q_s remains constant and is estimated by linear regression of $ln\left(\frac{s-s_0}{m_0-m}\right)$ against t which yields a plot with a gradient = ln (q_s). q_s was used to obtain absolute flux maps for ORS571.

2.18 Construction of a PHB mutant

The strategy involving a single cross over integration mutation in the *phbC* gene (AZC_1845) was used to develop a PHB mutant in ORS571. The schematic of the strategy is shown in Figure 2.6. pK18 mobilizable vector (pK18*mob*) of size ~3.79 kb and carrying kanamycin/neomycin resistance (Kan^R/Neo^R) gene and *lacZ* gene was used to construct the integration mutant. The list of primers used for this study is shown in Table 2.6

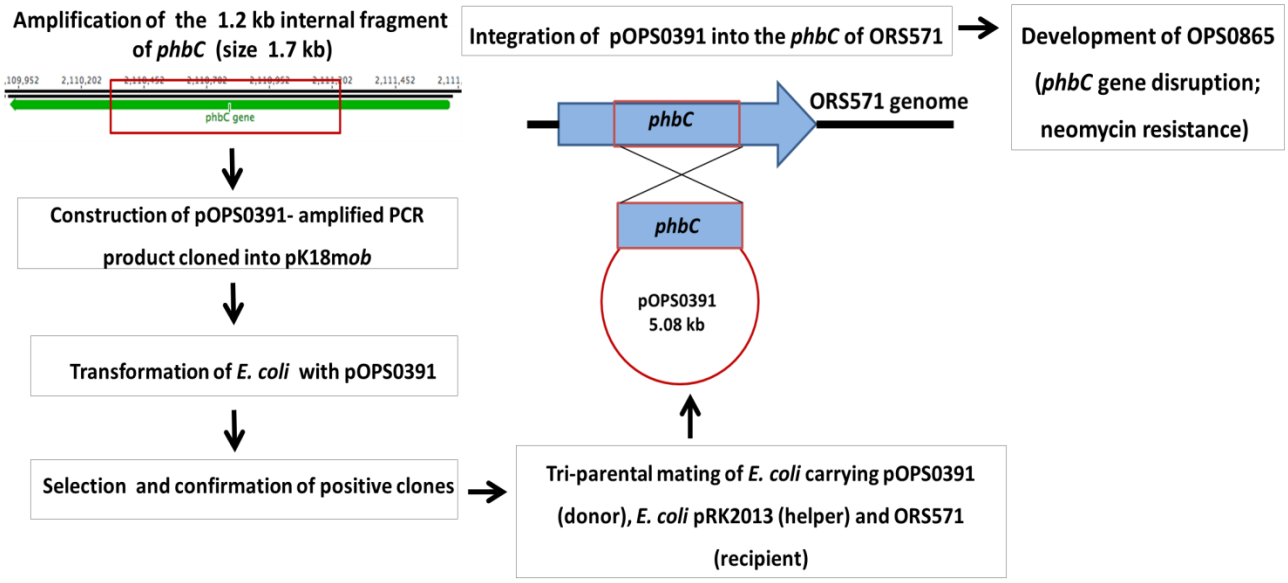

Figure 2.6: **Strategy for the development of a PHB mutant in ORS571**

Table 2.6: **Primers used for constructing the PHB mutant**

Primer	Sequence (5' to 3')	Function	Source of reference
Oxp1218	TGATTACGCCAAGCTATAAGCGGAGTTGGGCGG	*phbC* PCR primer for internal gene fragment	This work
Oxp1219	GCAGGCATGCAAGCTGTTCTTCGACGCCCTGAAGC	*phbC* PCR primer for internal gene fragment	This work
M13 forward	CACGACGTTGTAAAACGA	Sequencing primer for the insert cloned in pUC derivative-pK18	Bahar et al., 1998
M13 reverse	GGATAACAATTTCACACAGG	Sequencing primer for the insert cloned in pUC derivative-pK18	Bahar et al., 1998
Oxp0394	GCAGTTTCTTCGCCTGAG	*nifA* PCR primer	This work
Oxp0395	AAGCCGTCCGTTGTCTC	*nifA* PCR primer	This work
pK18A	ATCAGATCTTGATCCCCTGC	pK18*mob* mapping primer	Karunakaran et al., 2010
pK18B	GCACGAGGGAGCTTCCAGGG	pK18*mob* mapping primer	Karunakaran et al., 2010
Oxp1043	TTTTTGGTACCATGGAGGCGTTCGCCCAGAA	*phbC* mapping primer	This work

2.18.1 Construction of pOPS0391

A 1.12 kb internal fragment of *phbC* gene was PCR amplified using primers oxp1218 (forward) and oxp1219 (reverse). Both forward and the reverse primers included a 15 bp linker containing a *HindIII* site compatible with pK18. The PCR reaction composition and amplification conditions were set up according to the manufacturer's recommendations (Phusion(R) High-Fidelity DNA Polymerase kit, NEB) as defined in Table 2.7 and Table 2.8 respectively. The size of the PCR products was confirmed by 1 % agarose gel electrophoresis. The PCR products were purified for subsequent reactions using PCR purification kit.

Table 2.7: **Reaction composition for *phbC* amplification**

Component	Volume (µl)
Water	13.5
GC buffer	4
DMSO	0.6
Primer oxp1218 (10 pmoles)	0.4
Primer oxp1219 (10 pmoles)	0.4
dNTPs	0.4
Phusion DNA polymerase	0.2
ORS571 genomic DNA	0.5

Table 2.8: **Amplification conditions for *phbC***

Step	Temperature (°C)	Time	Number of cycles
Initial degradation	98	2 min	1
Denaturation	98	10 seconds	35
Annealing	76	30 seconds	
Extension	72	3 min 50 seconds	
Final extension	95	7 min	1
Soak	95	Infinity	1

The pK18*mob* vector was obtained by digesting pK18 with *Hind*III using standard conditions (Table 2.9) at 37ºC for 1 h.

Table 2.9: **Restriction digest reaction composition**

Component	Volume (µl)
pK18*mob* vector	100
NEB Buffer 2	30
*Hind*III	10
Water	160

The product was purified using PCR purification kit. The amplified *phbC HindIII* fragment was cloned into the pK18*mob* vector using BD In-Fusion cloning kit (BD Biosciences). The reaction conditions for a volume of 5 µl are shown in Table 2.10. The reaction set up was carried out in PCR tubes, which was incubated at 50 ºC for 15 min. The total size of the final construct pOPS0391 is 5.08 kb.

Table 2.10: **BD in-Fusion cloning reaction composition**

Component	Volume (µl)
Insert (*phbC HindIII*)	2
Vector (pK18 *HindIII* digested)	1
In-fusion BD master mix	1
Water	1

2.18.2 Transformation of *E. coli* with pOPS0391

Home-made DH5α competent cells were used for the transformation. 5 µl of pOPS0391 was mixed with 50 µl of the competent cells in a microfuge tube and then incubated on ice for 30 min. The mixture was then heat shocked at 42 ºC for 40 seconds after which 1 ml of warm LB SOC (super optimal LB broth media with added glucose) was immediately added to the reaction, followed by incubation in a shaker incubator at 37ºC for 1 h at 200 rpm. 100 µl of the 1ml reaction was plated onto LB agar plates containing kanamycin (50 µg ml^{-1}) and X-Gal (40 µg ml^{-1}). The remaining 900 µl was centrifuged and re-suspended in 100 µl of LB media and plated onto LB agar plates containing kanamycin and X-Gal. The plates were incubated for 24 h at 37ºC.

2.18.3 Identification of positive clones

The positive clones of *E. coli* carrying pOPS0391 plasmid was identified by the white colour of the colonies. The white colour of the colonies was due to the disrupted expression of *lacZ* in pK18 carrying *phbC* gene in the *HindIII* site. Six white colonies were chosen for colony PCR analysis to check for the presence of *phbC* insert in pK18

vector. Universal primers, M13 forward and M13 reverse were used for the PCR amplification in the reaction set up of 50 µl is shown in Table 2.11. 50 µl of the PCR reaction mix was added to each PCR tubes containing a fraction of the white colony picked with the help of a tooth pick. The amplification conditions are shown in Table 2.12.

Table 2.11: **Reaction composition for colony PCR**

Component	Volume (µl)
2X Go Taq Green Master Mix	20
M13 forward primer (10 pmoles)	5
M13 reverse primer (10 pmoles)	5
Water	20

Table 2.12: **Amplification condition for colony PCR**

Step	Temperature (ºC)	Time (minute)	Number of cycles
Initial denaturation	95	10	1
Denaturation	95	1	30
Annealing	57	1	
Extension	72	2	
Final extension	72	10	1
Soak	4	Infinite	1

The PCR products were confirmed by 1 % agarose gel electrophoresis. The six white colonies were inoculated into LB liquid media with kanamycin and grown overnight at 37ºC. Plasmids were isolated from these cultures and were screened for the presence of appropriate insert by restriction digest analysis using diagnostic *Nco*I sites. There are two sites for *Nco*I in the pOPS0391 and the restriction digests yielded two products of size 3.78 kb and 1.3 kb respectively. The identity of the insert was confirmed by sequencing of the plasmid construct pOPS0391 (performed by Eurofins Genomics).

2.18.4 Conjugation of pOPS0391 into ORS571

The plasmid pOPS0391 was introduced into ORS571 by conjugation using tri parental mating. DH5α containing pOPS0391 was used as the donor *E. coli* (Kan^R), pRK2013

carrying *tra* genes was used as the helper *E. coli* (Kan^R) and WT ORS571 was the recipient rhizobium ($Carb^R$) for the conjugation. The conjugation was done by two different methods. The first method involved growing liquid cultures of donor, helper and recipient strains with respective antibiotics in the media to the late exponential stage. The donor and helper strains were subcultured into fresh LB media with antibiotics and grown for 3-4 h until the cultures reach exponential stage. 1 ml each of donor, recipient and helper strains were spun down at 6000 rpm for 5 min in a bench top centrifuge. The strains were washed with fresh TY 3 times. A sterile 1.5 ml microcentrifuge tube containing 400 µl of donor, 200 µl helper and 400 µl of the recipient was set up. The tube was centrifuged at 6000 rpm for 5 min and the cells were re-suspended in 30 µl of fresh TY media. The 30 µl suspension was spotted on to a TY plate with no antibiotics and was incubated at 37ºC for 24 h. Following incubation, the culture was scooped out and suspended in 1 ml of fresh TY liquid media with no antibiotics. 4 dilutions of the suspension-10^0, 10^{-1}, 10^{-2} and 10^{-3} were prepared and 100 µl of each was spread plated on TY plates containing antibiotics carbenicillin at 200 µg ml^{-1} and neomycin 100 µg ml^{-1} to select conjugants of ORS571 containing pK18*mob* integration.

The second method involved mixing the donor, helper and recipient strains with sterile loops on to a TY plate with no antibiotics and incubated at 37ºC for 24 h. Following incubation, the mixture of strains was streaked onto TY plates containing antibiotics carbenicillin at 200 µg ml^{-1} and neomycin 100 µg ml^{-1} to select conjugants of ORS571 containing pK18 integration.

2.18.5 Confirmation of OPS0865

ORS571 colonies resistant to both carbenicillin and neomycin were obtained from both types of conjugation methods. The colonies were streaked onto a fresh TY plate containing selective antibiotics and incubated for 2 days at 37ºC. After incubation,

single colonies were picked and inoculated into TY liquid media with selective antibiotics. Genomic DNA was prepared from the overnight cultures and was used as a template for PCR amplification of *nifA* gene using primers oxp0394 (forward) and oxp0395 (reverse). The PCR reaction was done using Phusion(R) High-Fidelity DNA Polymerase (NEB). The PCR reaction composition and amplification condition are shown in Tables 2.13 and 2.14 respectively.

Table 2.13: **Reaction composition for amplification of *nifA***

Component	Volume (µl)
Water	13.5
GC buffer	4
DMSO	0.6
Primer oxp0394 (10 pmoles)	0.4
Primer oxp0395 (10 pmoles)	0.4
dNTPs	0.4
Phusion DNA polymerase	0.2
ORS571 genomic DNA	0.5

Table 2.14: **Amplification conditions for *nifA***

Step	Temperature (ºC)	Time	Number of cycles
Initial degradation	98	2 min	1
Denaturation	98	10 seconds	35
Annealing	61	30 seconds	
Extension	72	2 min 50 seconds	
Final extension	72	7 min	1
Soak	4	Infinity	1

The PCR products obtained were confirmed to be of correct size (3.1 kb) by 1% agarose gel electrophoresis. The genomic DNA obtained from the conjugants was also

used for the PCR amplification of 16SrRNA gene for confirmation of the phylogenetic identity of the strain as described in 2.3.

Integration of the pOPS0391 plasmid into the *phbC* gene of ORS571 was confirmed by mapping PCR using primers oxp1043 and pK18mob-specific primer (pK18 A and pK18 B). The PCR reaction composition and the amplification conditions are shown in Tables 2.15 and 2.16 respectively. The size of the PCR products (1.5 kb) was confirmed by 1% agarose gel electrophoresis.

Table 2.15: **Reaction composition for mapping PCR**

Component	Volume (µl)
2X Go Taq Green Master Mix	10
Primer oxp1043 (10 pmoles)	2
Primer pK18A/pK18B (10 pmoles)	2
Genomic DNA	2
Water	4

Table 2.16: **Amplification conditions for mapping PCR**

Step	Temperature (ºC)	Time (minute)	Number of cycles
Initial denaturation	95	10	1
Denaturation	95	1	
Annealing	58	1	30
Extension	72	5	
Final extension	72	10	1
Soak	4	Infinite	1

The inactivation of *phbC* gene in the conjugants was confirmed by PCR using primers oxp1043 (forward primer) and oxp1044 (reverse primer). The reaction composition and amplification conditions are shown in Tables 2.17 and 2.18 respectively. The size of the PCR products was confirmed by 1 % agarose gel electrophoresis.

Table 2.17: **Reaction composition for *phbC* amplification**

Component	Volume (µl)
2X Go Taq Green Master Mix	10
Primer oxp1043 (10 pmoles)	2
Primer oxp1044 (10 pmoles)	2
Genomic DNA	2
Water	4

Table 2.18: **Amplification conditions for *phbC* amplification**

Step	Temperature (ºC)	Time (minute)	Number of cycles
Initial denaturation	95	10	1
Denaturation	95	1	
Annealing	58	1	
Extension	72	5	30
Final extension	72	10	1
Soak	4	Infinite	1

2.19 Radioactivity assay

Root and stem nodules were harvested from *S. rostrata* inside the low O_2 cabinet and bacteroids were harvested by a differential spin method. Bacteroids were suspended in 1 ml UMS media without any carbon, nitrogen or vitamin source. The suspension was transferred to glass vials fitted with a GF/F glass microfiber filter paper (purchased from whatman) dipped in 10% potassium hydroxide (KOH) and sealed with rubber caps. The vials were taken to the radioactivity room for the assay. [2, 3-^{14}C]succinic acid (purchased from American Radiolabelled Chemicals) was used as the radioactive substrate (specific activity- 55 mCi/mmol) for this assay. Non-radioactive, succinate was used to the bacteroid suspensions at a final concentration of 2 mM, followed by the addition of the [2,3-^{14}C]succinic acid at a final amount of 1 µCi for 1 ml of the sample. The bacteroid suspensions were incubated for 0h, 1h and 2h, and the radioactivity was measured in the metabolic CO_2 output and intracellular metabolites. The amount of ^{14}C in the metabolic CO_2 output from the bacteroids was measured in

the CO_2 trapped in the GF filter. The filter was transferred to a scintillation vial (Perkin Elmer) and 35µl of Scintillation fluid (ScintiSafe3 Liquid Scintillation Cocktail – Fisher) was added to each vial. The amount of ^{14}C in the intracellular metabolites was measured by spinning down 100 µl of the sample at 8000 rpm for 2 minutes. The pellet was re-suspended in 1 ml of ice cold trichloroacetic acid (TCA), mixed well and incubated for 30 minutes on ice. Following incubation, the TCA suspension was filtered using GF/F filter, and transferred to the scintillation vial with 35ul scintillation fluid. The vials were left overnight and the radioactivity was counted the following day, using Trilux microbeta scintillation counter. The counts per minute (CPM) was recorded for each of the sample and the uptake of ^{14}C succinic acid (nmol) was calculated as below:

$$^{14}C\ \text{Uptake} = \frac{(CPM\text{-}B * A) / S}{(CPM*A)/V / ((X*A) + (Y/Z*1000))}$$

Where CPM-B: CPM for blank; A: Assay volume (ml); S: Sample volume (ml); V: Standard volume (ml); X: Substrate concentration (µM); Y: Isotope (µCi); Z: Specific activity (mCi $mmol^{-1}$)

2.20 Calculation of growth rate and doubling times

Growth curves for ORS71 grown under specific growth conditions were generated from OD_{600} measurements recorded at specific time intervals. Growth rate and doubling times were calculated from the graph of log OD vs time using the following equations

$$\mu = \frac{\ln OD_2 - \ln OD_1}{t_2 - t_1} \quad (1)$$

$$t_D = \frac{\ln 2}{\mu} \quad (2)$$

Where µ: growth rate; OD_1, OD_2: two points (optical densities) that lie on the line of best fit for the graph log OD vs time; t_1, t_2: time at which OD_1 and OD_2 were measured t_D: doubling time

3. Development of ^{13}C-MFA in ORS571 free-living cultures

3.1 Introduction

Rhizobial metabolism has been previously studied using FBA- the in silico method which predicted fluxes through the network in *R. etli* and *S. meliloti* based on assumed objective function (Resendis-Antonio et al., 2007; Zhao et al, 2012; Pfau et al., 2016). The fluxes reported in these papers were studied from theoretical perspectives, which lack measurement of metabolically active fluxes supported by experimental data. ^{13}C-MFA is a powerful technique that uses experimental measurements for quantification of intracellular fluxes (Crown & Antoniewicz, 2013; Gomes & Simoes, 2012). ^{13}C-MFA has been previously used to study the metabolism of *R. leguminosarum*, growing on succinate as the carbon source (Terpolilli et al., 2016) and *S. meliloti* growing on glucose as the carbon source (Fuhrer et al., 2005). These studies report fluxes in rhizobial systems during aerobic growth conditions, but do not report fluxes during N_2 fixing conditions.

Diazotroph *A. caulinodans* was chosen for this study, as it is an ideal rhizobial model system that provides an opportunity for ^{13}C-MFA in the free-living cultures under N_2-fixing conditions. To perform ^{13}C-MFA in ORS571 during N_2 fixation, it was first necessary to establish the growth conditions that would provide maximum growth of free-living cultures, and also to establish methods that would produce reliable measurements required for ^{13}C-MFA. So, the aim of this chapter was to establish the methodology of ^{13}C-MFA at an appropriate growth stage of ORS571 free-living cultures that can be used to quantify fluxes under various growth conditions.

The first section of the chapter describes the establishment of best growth conditions (growth temperature, nicotinic acid requirement, and carbon source) for ORS571 free-living cultures under aerobic (21% O_2) conditions for biomass

measurements and ^{13}C labelling experiments. The biomass measurements were used to construct the biomass reaction which constrained the model for flux analysis. The chapter also describes the establishment of ^{13}C labelling experiments and the methods for processing GC-MS data and extraction of reliable MS measurements for metabolites isolated from ORS571. For the labelling experiments, ORS571 was grown on a ^{13}C labelled substrate until it reached metabolic and isotopic steady state, and the label was distributed throughout the network of the organism into primary metabolites like sugars, organic acids, amino acids and other biomass outputs. The MS measurements that includes labelling pattern of the biomass outputs provide information about their precursors and intermediates of the active metabolic pathways and estimation of intracellular fluxes (Sauer et al., 1999).

The final section of the chapter describes the use of INCA for performing ^{13}C-MFA and generation of statistically robust flux maps showing the distribution of carbon fluxes throughout the metabolic network of ORS571 under free-living aerobic conditions. A metabolic network of ORS571 which contains all the reactions of central carbon metabolism and biosynthesis of cellular components was constructed based on the genetic, molecular and metabolic information available in literature. This model along with the MS and biomass measurements was simulated using the software INCA for ^{13}C-MFA, to obtain an optimized flux pattern in the network under a specific growth condition, followed by statistical validation of the flux maps. The overall experimental design for ^{13}C-MFA is shown in Figure 3.1.

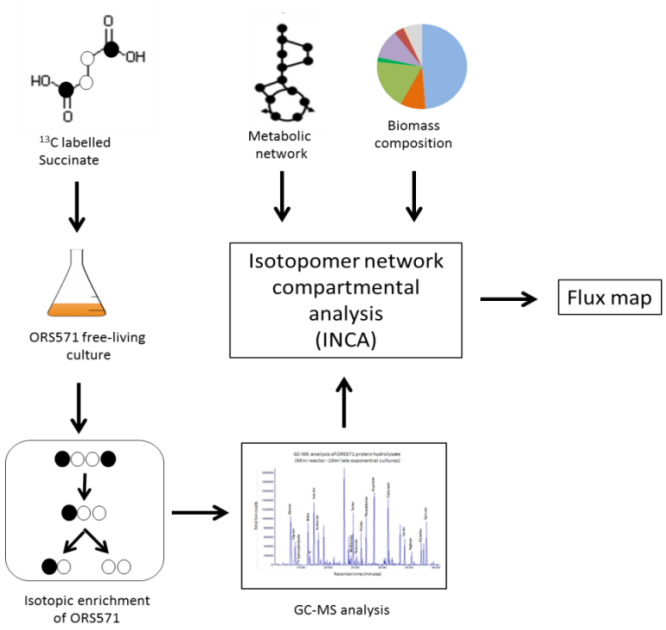

Figure 3.1: **Overall experimental design for ^{13}C-MFA in ORS571.**

3.2 Physiological characteristics of ORS571

3.2.1 Identification of the strain using 16SrRNA analysis and its relationship to the other rhizobial species

The 16S rRNA gene which encodes 16S ribosomal RNA of the small subunit of the prokaryotic ribosome is widely used for the study of bacterial phylogeny (Turner et al., 2013). The taxonomic classification of the model organism for the current study was confirmed based on 16S rRNA gene sequencing (Rout, 2014). The 16S rRNA PCR and phylogenetic analysis was done according to the method described in section 2.3. The PCR products obtained from the amplification of three different regions in the 16S rRNA gene of the strain are shown in Figure 3.2. PCR product 3 (size 1.2 kb) was sequenced and the alignment statistics of the sequence is listed in the appendix A1. The sequence was used to construct the neighbour joining tree in Figure 3.3, which shows that the strain is placed in the family of Xanthobactaraceae, genus- *Azorhizobium* and species- *caulinodans*.

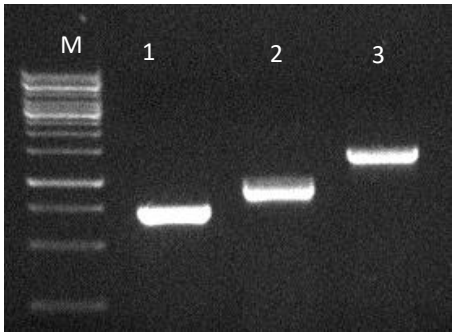

Figure 3.2: **Agarose gel electrophoresis showing the products of 16SrRNA PCR**. M stands for 1kb DNA ladder, 1 for the PCR product obtained using the primer pair 27F and V_4R, 2 for V_4F and 1492R and 3 for 27F and 1492R.

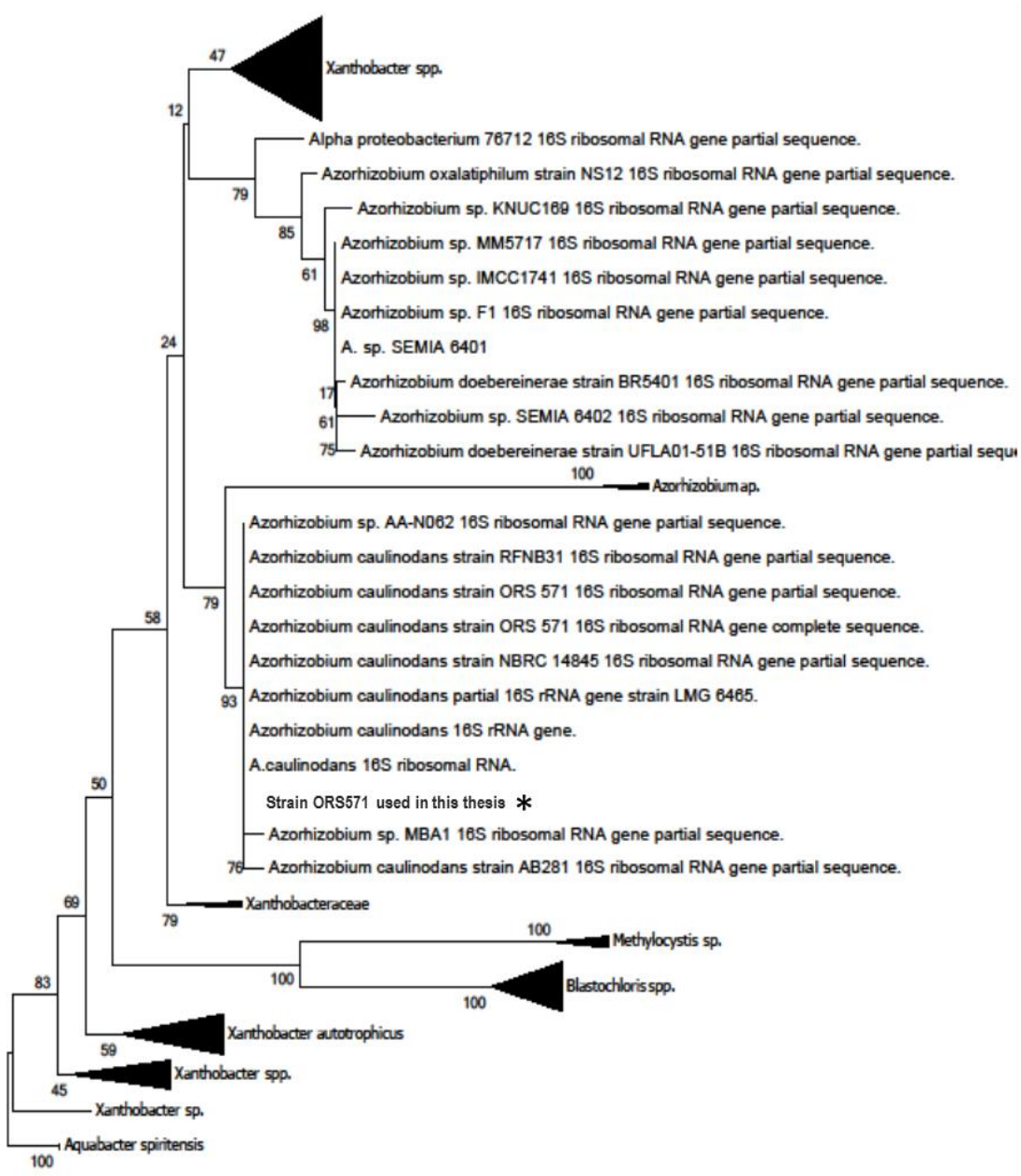

Figure 3.3: **Taxonomic classification of ORS571**. Neighbour joining tree showing the taxonomic position of the strain ORS571 used in this thesis (marked with *) and its close relatives. The strain used for the analyses described in this report groups with other ORS571 sequences and is closely placed to *Azorhizobium caulinodans* strains in the family Xanthobacteraceae.

3.2.2 Symbiotic interaction of ORS571 with the host legume

S. rostrata plants were grown in nitrogen free vermiculite and ORS571 was used to inoculate the roots and stem of the plants. *S. rostrata* plants with and without inoculation are shown in Figure 3.4. Upon inoculation with ORS571, *S. rostrata* forms N_2-fixing nodules on the stem and root (Figure 3.5). Nitrogenase activity of plants inoculated with and without with ORS571 was measured using the ARA assay as described in 2.7.2 (Figure 3.6). The plant inoculated with ORS571 grew in the absence of any nitrogen source in the medium, whereas the uninoculated control plant showed very poor growth. Nitrogenase activity was detected in the plant inoculated with ORS571. This experiment confirms that the ORS571 strain used throughout this study interacts with *S. rostrata* and is able to facilitate effective symbiotic N_2 fixation in both root and stem nodules.

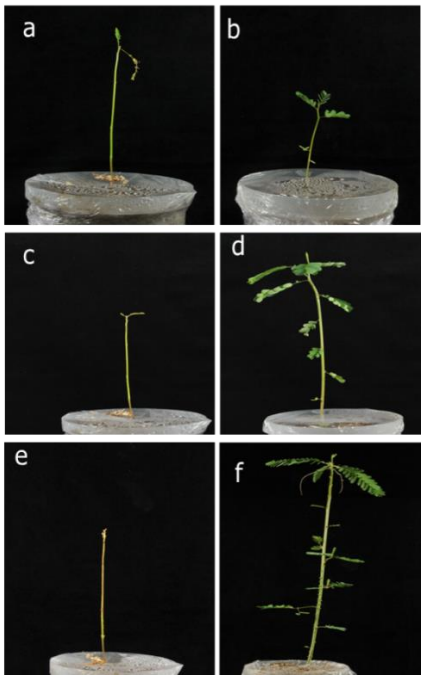

Figure 3.4: **Symbiotic interaction between *S. rostrata* and ORS571.** Uninoculated control *S. rostrata* plants:- (a) 5 week old, (c) 8 week old and (e) 11 week old show very poor growth due to the absence of nitrogen in the growth medium. *S. rostrata* inoculated with ORS571:- (b) 5 week old, (d) 8 week old and (f) 11 week old shows vigorous growth in absence of a nitrogen source in the growth medium.

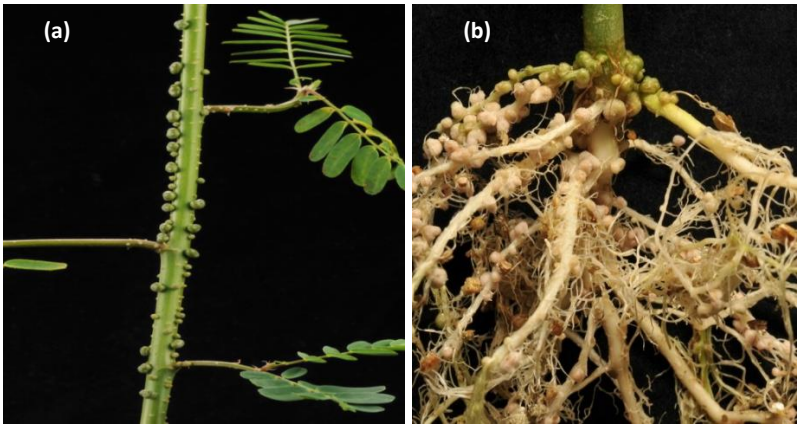

Figure 3.5: **Nodulation in *S. rostrata***. (a) Stem nodules on 11 week old *S .rostrata* inoculated with ORS571; (b) root nodules on 16 week old *S. rostrata* inoculated with ORS571.

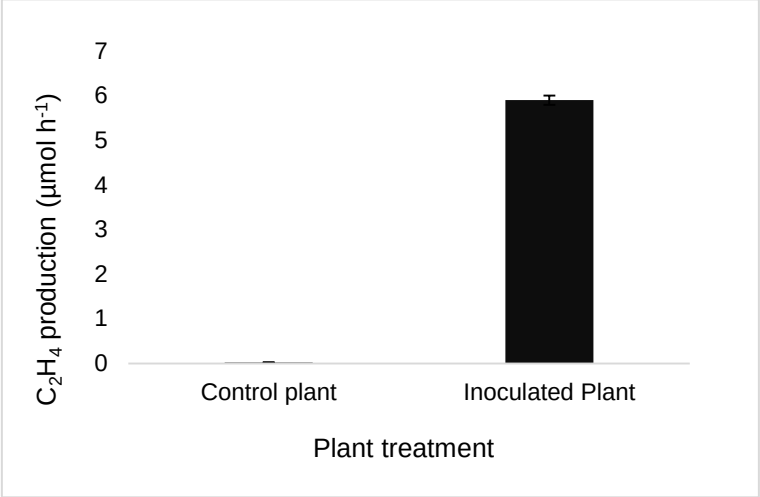

Figure 3.6: **Nitrogenase activity in 8 week old *S. rostrata* plants**. Activity was measured in uninoculated control plant and plant inoculated with ORS571. Values are the mean of two determinations ± SD (standard deviation of the mean).

3.3 Establishment of growth conditions for free-living ORS571 cultures

3.3.1 Growth temperature

ORS571 has been previously reported to grow above 28ºC, which is an ideal growth temperature of most other rhizobial species under laboratory conditions (Scott & Ludwig, 2004). For the labelling experiments, a suitable temperature is desired that increases the rate of production of biomass and decreases the time needed for the

system to be at isotopic equilibrium. For this purpose, ORS571 was grown in rich medium, Tryptone yeast (TY) at 28ºC and 37ºC to select the better growth temperature for flux studies. It was observed that ORS571 exhibited a faster growth at 37ºC compared to 28ºC and so 37ºC was used as the growth temperature for growing free-living cultures. The growth curves of ORS571measured at 28º and 37ºC is shown in Figure 3.7.

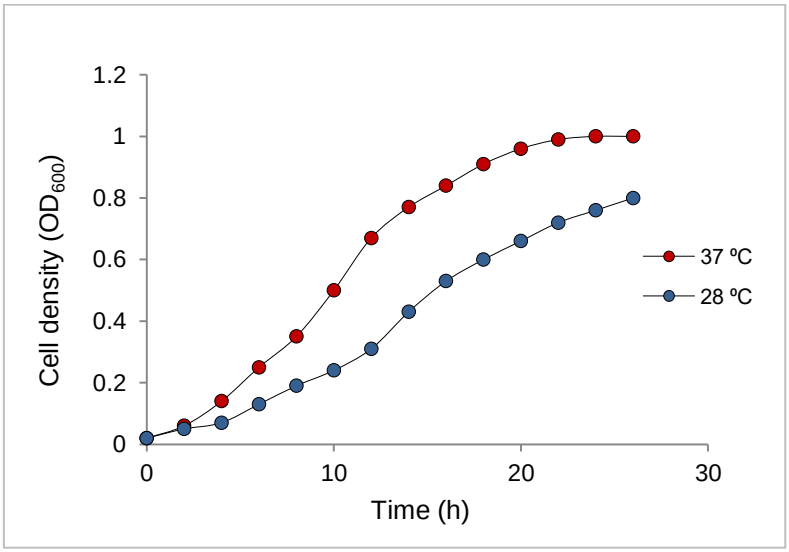

Figure 3.7: **Effect of temperature on the growth of ORS571**. Growth curves of ORS571 at 28 and 37ºC grown in TY media over a period of 26 h. Cell growth was monitored by measuring the optical density of cultures at 600nm at specific time intervals. The measurements for the growth curves are from individual cultures.

3.3.2 Nicotinic acid as a growth requirement

ORS571 was previously reported to be auxotrophic for nicotinic acid, which was a growth limiting factor, for free-living cultures grown in the presence of either ammonia or N_2 as the nitrogen source (Elmerich et al., 1983). ORS571 lacks quinolinate synthase (Nad A) and so is unable to synthesize NAD^+ from aspartate (Figure 3.8) (Kitts et al., 1989). ORS571 acquires nicotinate from exogenous nicotinic acid and this requirement for the growth of ORS571 in a minimal media supplemented with carbon, nitrogen and vitamin sources was confirmed from the

growth curves shown in Figure 3.9. Cultures without nicotinic acid failed to grow, confirming that nicotinic acid is required as a growth factor for ORS571 when grown in minimal media.

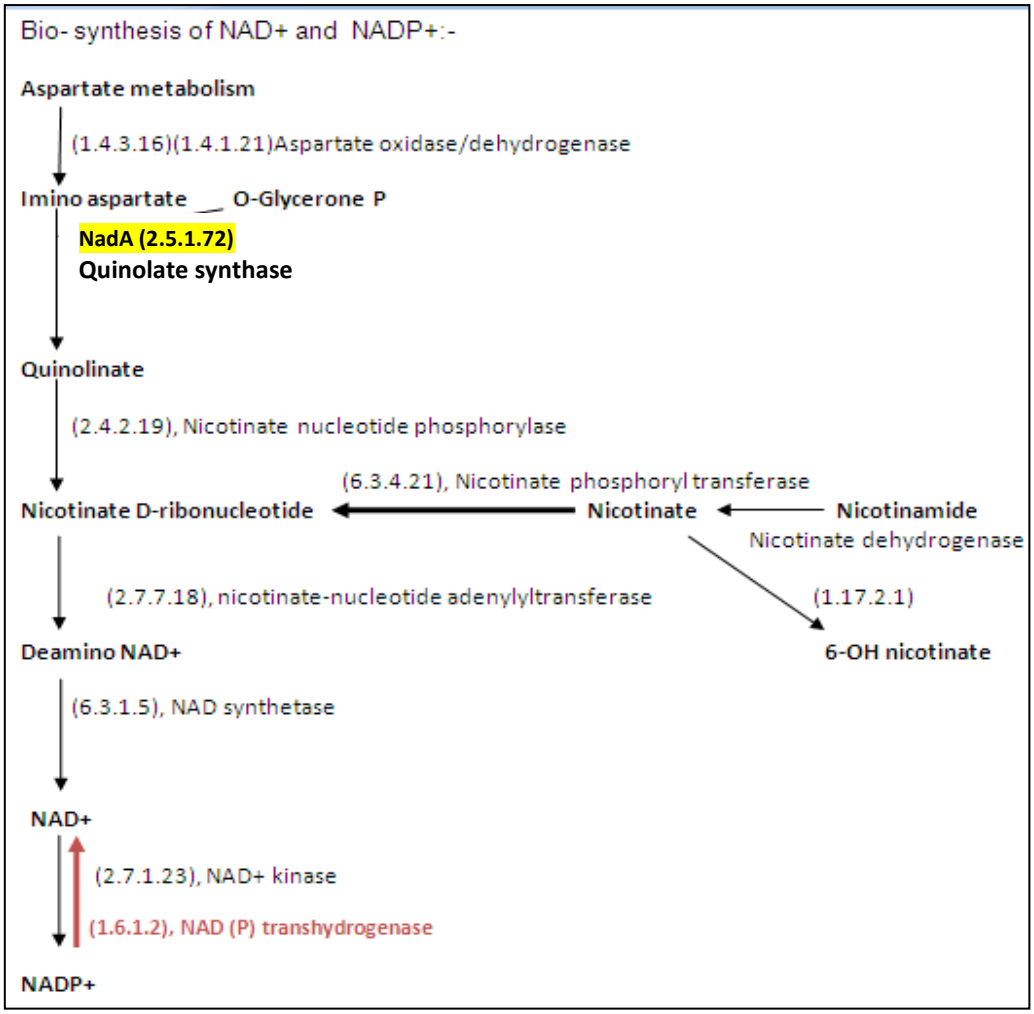

Figure 3.8: **NAD^+ and $NADP^+$ synthesis pathway in ORS571.** The pathway shows the intermediates, end products and enzymes for each reaction of the pathway. The activity of quinolinate synthase (NadA) highlighted in yellow, is not reported in ORS571 thus preventing *denovo* synthesis of NAD^+. ORS571 depends on the uptake of exogenous nicotinic acid for the synthesis of NAD^+. Figure adapted from the KEGG database.

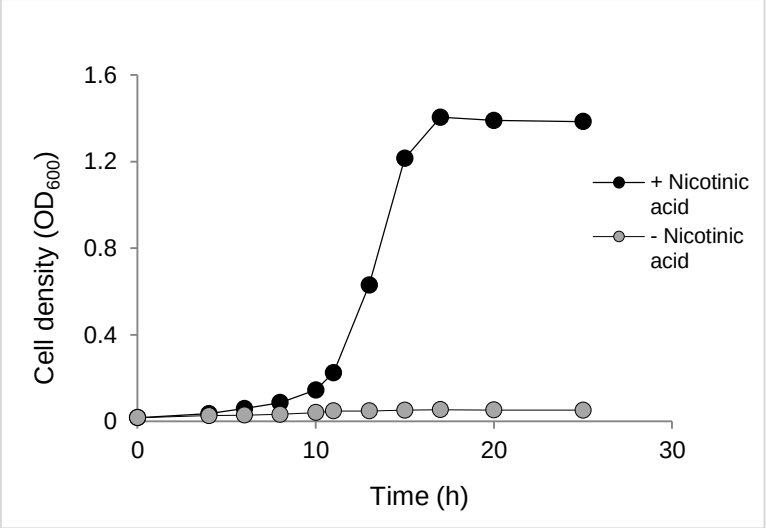

Figure 3.9: **Nicotinic acid requirement by free-living cultures of ORS571.** Growth curve of ORS571 in the presence and absence of nicotinic acid (0.3 mM) in minimal growth media. The measurements for the growth curves are the mean of two determinations.

3.3.3 Carbon substrate

Carbon compounds that are reported to be present in the symbiosome space of the nodule were supplied as carbon sources in UMS minimal media to test the growth of ORS571 cultures at 37ºC (White et al., 2007; Emerich & Krishnan, 2014; Libault 2014). From the growth curves of ORS571 on different carbon sources (Figure 3.10) it was evident that the di-carboxylic acids succinate and malate were readily utilized by ORS571 cultures. Growth rates (appendix FigureA29) and doubling times (Figure 3.11) were calculated from ln OD_{600} vs time plots (appendix Figure A28) as described in 2.20. Cultures grown on succinate had the shortest doubling time in comparison to the other carbon substrates. From this experiment, succinate was chosen as the major carbon source for subsequent growth and labelling studies.

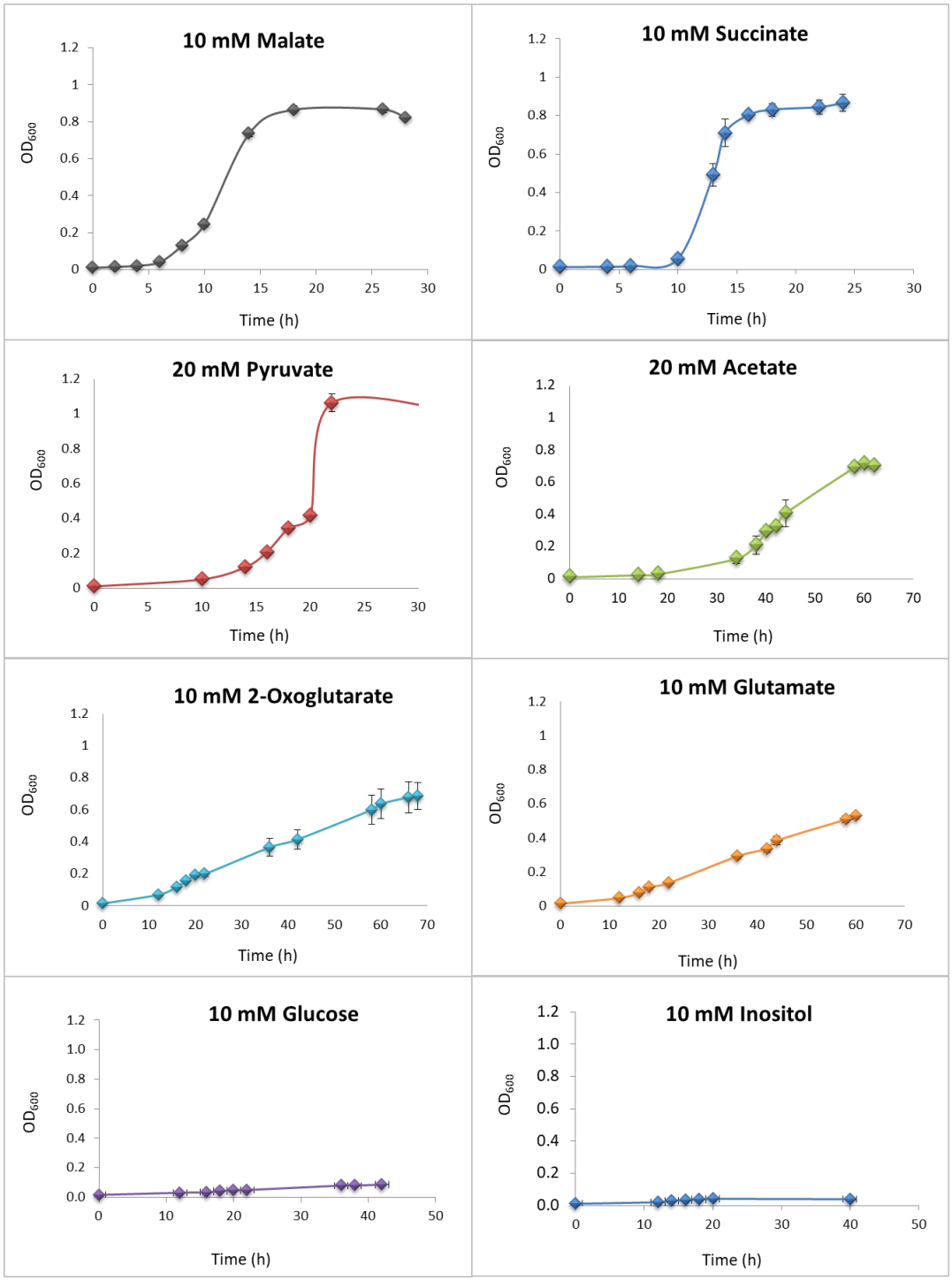

Figure 3.10: **Effect of carbon substrate on the growth of ORS571**. Growth curves of ORS571 on succinate (10 mM), malate (10 mM), pyruvate (20 mM), acetate (20 mM), 2-oxoglutarate (10 mM), glutamate (10 mM), glucose (10 mM) and inositol (10 mM). All measurements are the mean ± SEM (standard error of the mean) of three biological replicates.

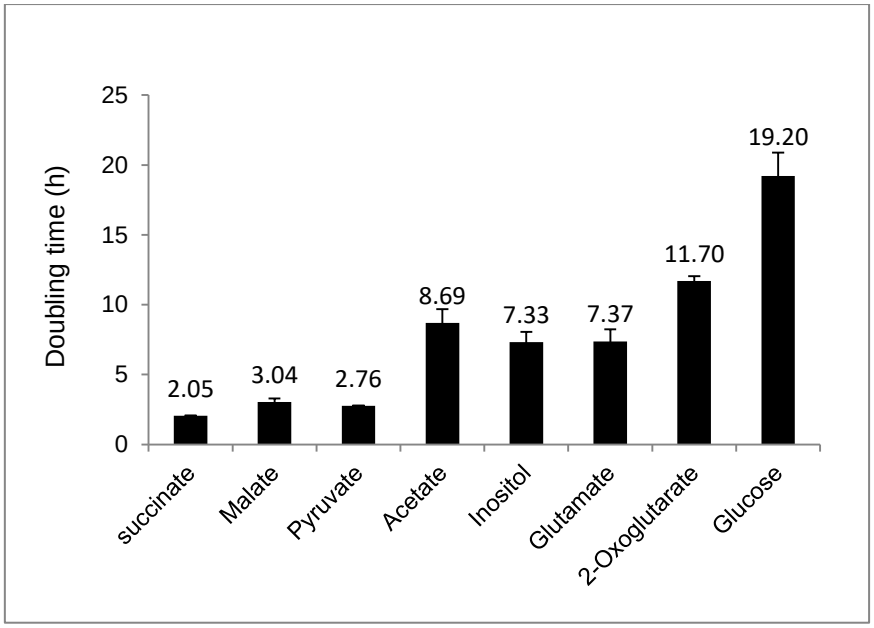

Figure 3.11: **Comparison of the doubling time of ORS571 cultures grown with various carbon sources**. Values were calculated from the growth curves shown in Figure 3.10 and are the mean ± SEM of three biological replicates.

3.3.4 Succinate concentration

ORS571 was grown on succinate concentrations ranging from 1 to 20 mM in minimal media at 37ºC to optimize the concentration for labelling studies (Figure 3.12). 10 and 20 mM succinate concentrations supported the highest cell density during the exponential growth phase whereas 1 mM, 2 mM and 5 mM concentrations resulted in lower cell densities presumably due to substrate limitation. A proportional increase in the final cell density of the cultures at stationary phase was observed for the succinate concentrations from 1 to 10 mM. However, the cultures grown on 20 mM succinate did not show a similar proportional increase in the final cell density achieved, suggesting that the growth on 20 mM succinate might be inhibited due to an increase in growth inhibitory by-products secreted into the culture medium at high cell densities. Cultures grown on 10mM succinate showed a a proportional increase in the final cell density at stationary phase and was selected over the other substrate limiting and growth inhibiting succinate concentrations.

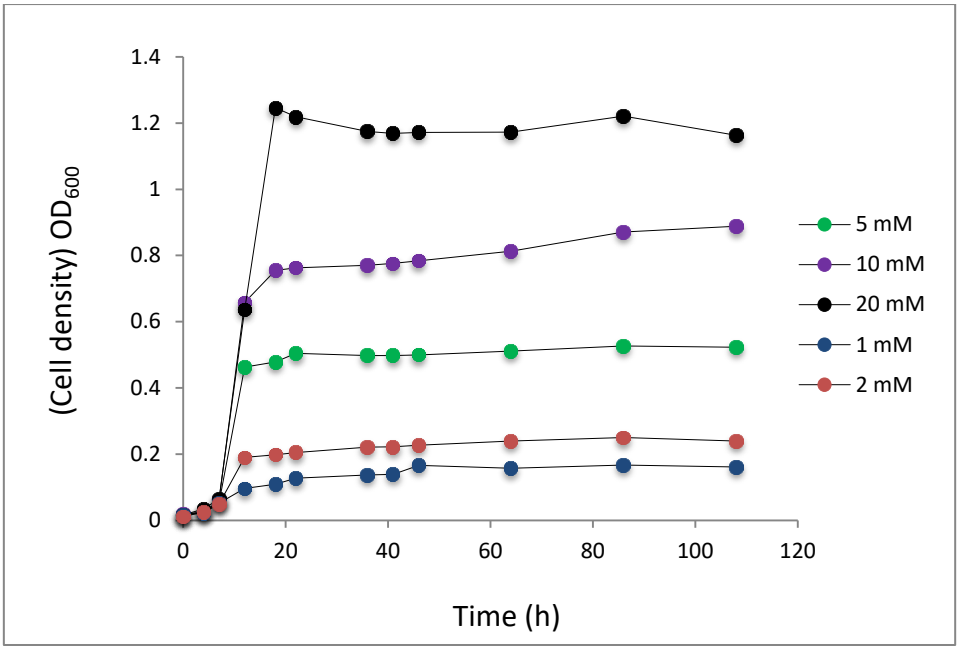

Figure 3.12: **Effect of succinate concentration on the growth of ORS571.** Growth curves of ORS571 on various concentrations of succinate in minimal media.

3.4 Biomass composition

ORS571 cultures were grown under the aerobic growth conditions (section 2.4.1) with 10mM succinate as the carbon source, nicotinic acid and at growth temperature of 37ºC as established in the previous section of this chapter. The cultures were harvested at early and late exponential growth phases, defined by optical density of 0.2-0.25 and 0.75-0.80, respectively, to measure the biomass composition (Figure 3.13). The amount of protein, lipid, nucleic acid (DNA and RNA), PHB, carbohydrate and EPS were measured for both the growth stages using methods described in section 2.8. Dry cell weight (DCW) for ORS571 cultures harvested at early and late exponential growth stages was measured according to the method described in section 2.8.1, and the amounts of protein, lipid, DNA, RNA, PHB, carbohydrate and EPS were expressed as a percentage of the DCW (Table 3.1). The biomass compositions obtained for ORS571 during early and late exponential phases are represented as pie charts in Figures 3.14. Protein constituted the largest proportion of the cell dry weight followed by RNA, lipids and PHB. DNA, carbohydrate and EPS

were each a minor proportion of the cell dry weight. The component labelled- "others" presumably includes mainly additional cell wall materials, polyamines, ions and polyphosphates which were not measured directly in this study.

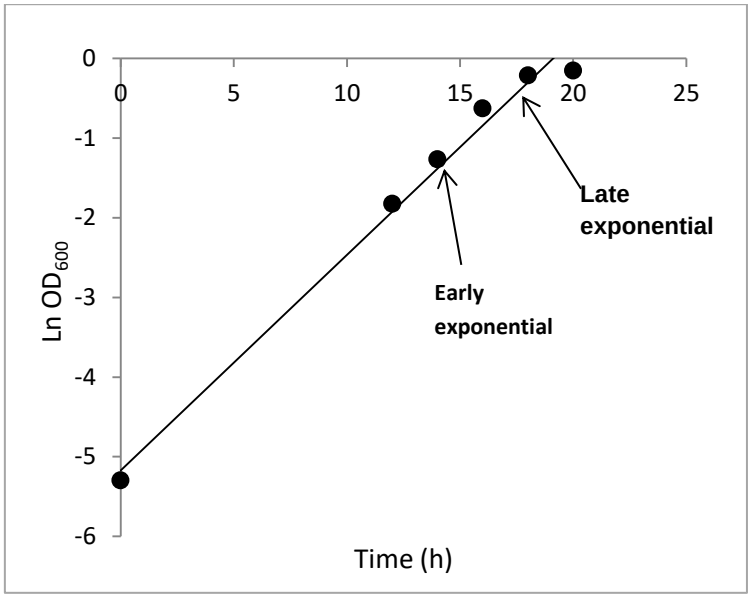

Figure 3.13: **Growth stages of ORS571 cultures used for biomass measurements**. The early and late exponential growth stages used for biomass measurements are shown with arrows.

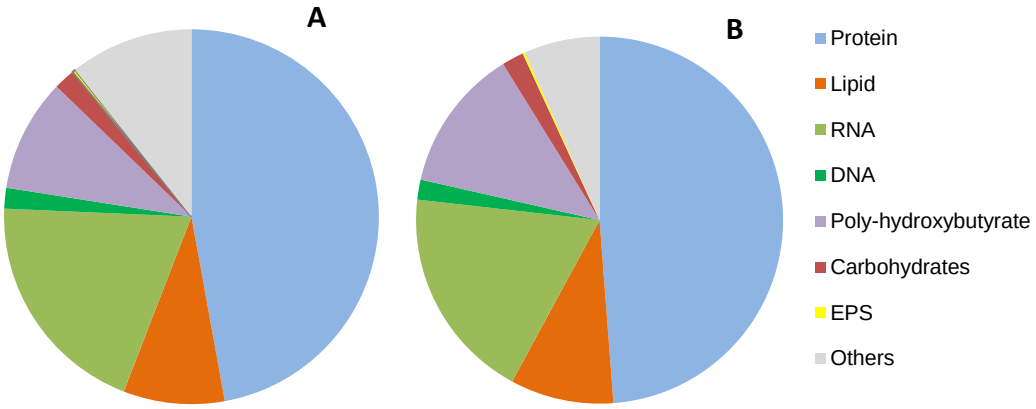

Figure 3.14: **Biomass composition of ORS571 during early (A) and late (B) exponential growth phase**. Each of the components is expressed as the proportion of dry cell weight. Values for protein, lipid, DNA, RNA, PHB, carbohydrates and EPS are the mean of six determinations.

3.4.1 Assessment of metabolic steady state

The biomass measurements from early and late exponential cultures were compared to assess if there were metabolic differences between the two growth stages. The results of t-tests done on the measurements shows no significant differences in the biomass measurements obtained at the two growth stages. This indicates that ORS571 free-living cultures were at a metabolic steady state during exponential growth.

Table 3.1: **Comparison of biomass measurements between early and late exponential ORS571 cultures**

Biomass component	Proportion of biomass (% w/w)		
	Early exponential cultures	Late exponential cultures	P-value
Protein	47.1 ± 2.64	48.7 ± 2.78	0.70
Lipid	8.73 ± 1.26	9.10 ± 1.24	0.85
RNA	23.8± 3.41	18.8 ± 1.75	0.27
DNA	1.78 ± 0.24	1.76 ± 0.23	0.95
PHB	9.73 ± 1.54	12.6 ± 0.94	0.44
Carbohydrates	1.83 ± 0.39	1.93 ± 0.21	0.75
EPS	0.282 ± 0.01	0.186 ± 0.03	0.07

The biomass measurements for early and late exponential cultures are the mean ± SEM of six biological replicates.

3.5 Choice of isotope substrate for ^{13}C labelling experiment

In section 3.3.3, it was observed that ORS571 free-living cultures showed the fastest doubling in succinate, therefore [$^{13}C_4$]succinic acid was chosen as the ^{13}C isotopic substrate for labelling experiments. A previous study on *E. coli* showed that the varying amounts of label 0%, 20%, 40%, 60%, 80% and 100% used for labelling experiments, did not affect the growth rate and biomass synthesis (Leighty & Antoniewicz, 2012). This shows the metabolic behaviour of a system does not depend on the amount of ^{13}C labelled substrate used for labelling experiments. Also, the flux estimates obtained were consistent for the different amounts of isotope

substrates used (Leighty & Antoniewicz, 2012). A different study on Arabidopsis suspension cultures also showed that varying ^{13}C-enrichment of the growth substrate did not affect the metabolic fluxes (Kruger et al., 2007).

Based on these previous studies, it was clear that the amount of isotope supplied does not affect flux estimates.

A previous study used 20% [$^{13}C_4$]succinate as the substrate for ^{13}C-MFA of *R. leguminosarum* and successfully measured fluxes through the network (Terpolili et al., 2016). The isotope substrate amount of 20% was commonly used for ^{13}C-MFA in microbial and plant systems (Masakapalli et al., 2010; Masakapalli et al., 2014; Terpolili et al., 2016)

Based on the reports from previous studies, the isotope substrate for this study was used as a combination of 20% [$^{13}C_4$]succinate and 80% unlabelled succinate.

3.6 Metabolic profiling of ORS571

The extraction of metabolites from free-living cultures was done by the methanol-chloroform-water method as described in section 2.11. The soluble metabolites in the aqueous methanol phase were derivatised with the MSTFA reagent and were identified by GC-MS analysis using AMDIS software. The aqueous phase included organic acids, free amino acids and sugars, and the representative profile obtained from late exponential cultures is shown in Figure 3.15. The metabolites that were insoluble in the aqueous phase r were derivatised using the TBDMS reagent and the metabolites were identified from their characteristic molecular fragmentation pattern as reported elsewhere (Molnár-Perl & Katona, 2000). The representative profile shown in Figure 3.16 was obtained from late exponential cultures and the metabolites mainly consisted of proteinogenic amino acids, lipid and 3-hydroxybutyric acid, the monomeric units of the polymer, PHB. The metabolite profile obtained for early exponential culture (data not shown) was similar to that of the late exponential cultures. From this analysis, it is confirmed that the method used

for metabolite extraction and detection by GC-MS was able to produce a series of prominent, well resolved peaks of cellular metabolites. The profile consists predominantly of free pool and protein-derived amino acids, which were comparable to those resolved in similar analyses of other microbial samples (Christensen & Nielsen, 1999; Antoniewicz et al., 2007a; Antoniewicz et al.2007b; He et al., 2014; Okahashi et al., 2014). In addition trehalose and 3-hydroxybutyric acid derived from precursors of central carbon metabolism will provide information on mass isotopomer distribution of the precursors, which will be useful for ^{13}C-MFA.

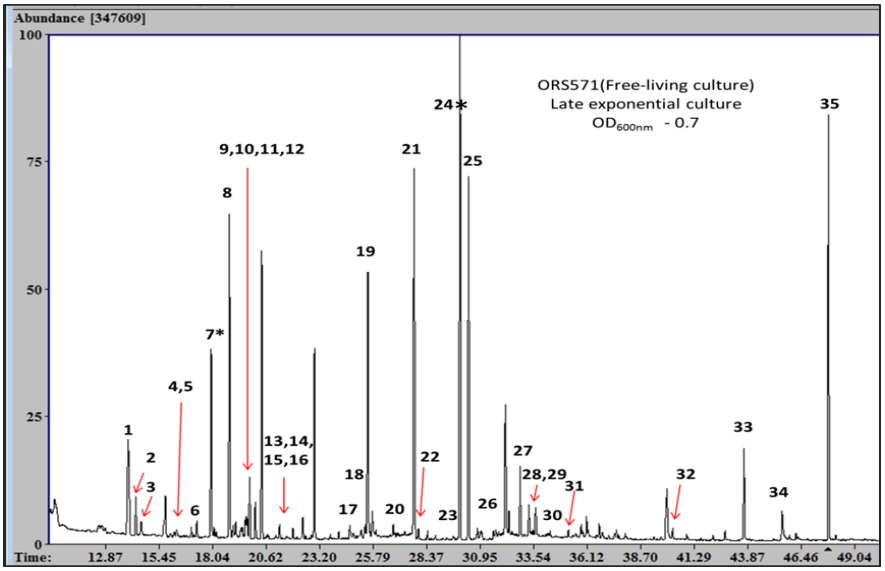

1. Alanine- 2TMS
2. Valine-1TMS
3. Glycine-2TMS
4. Butanoic acid, 2-amino-2TMS
5. Proline-1TMS
6. Valine-2TMS
7. Norvaline-2TMS*
8. Phosphoric acid-3TMS
9. Leucine-2TMS
10. Nicotinic acid-1TMS
11. Glycine-3TMS
12. Succinic acid-2TMS
13. Uracil-2TMS
14. Alanine-3TMS
15. Threonine-3TMS
16. Thymine-2TMS
17. Nicotinamide-1TMS
18. Methionine-2TMS
19. Pyroglutamic acid-2TMS
20. Nicotinic acid, 6 hydroxy-2TMS
21. Glutamic acid-3TMS
22. Phenylalanine-2TMS
23. Glucose, 1,6-anhydro,beta-3TMS
24. Ribitol-5TMS*
25. Putreschine-4TMS
26. Glycerol-3-phosphate-3TMS
27. Lysine-3TMS
28. Adenine-2TMS
29. Tyrosine-2TMS
30. Mannitol-6TMS
31. Hexadecanoic acid-1TMS
32. Octadecanoic acid-1TMS
33. Uridine-3TMS
34. Inosine-4TMS
35. Trehalose, alpha alpha-D-8TMS

Figure 3.15: **Separation of aqueous soluble metabolites derivatised with MSTFA.** The peak marked with * is an exogenous compound used as internal standard for GC-MS.

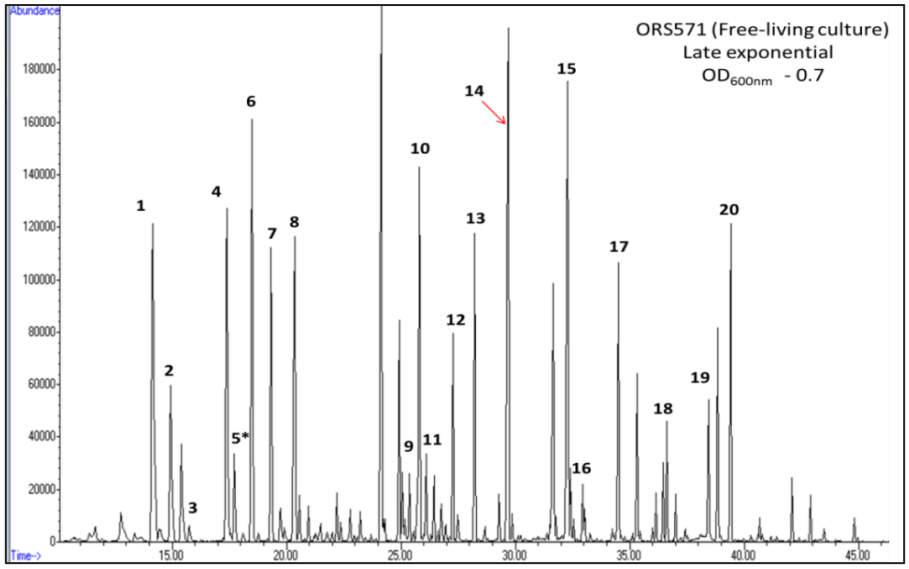

Figure 3.16: **Separation of aqueous insoluble metabolites derivatized with TBDMS.** The peak marked with * is an exogenous compound used as internal standard for GC-MS.

3.7 Analysis of GC-MS measurements of metabolites extracted from cells following stable isotope labelling

3.7.1 Integration interval for GC signal

GC-MS files were processed using the data analysis software provided by Agilent Technologies. The MS measurement or MS profile for a metabolite containing MID information (m/z and their respective ion counts) was obtained by integrating over the GC peak. The choice of integration region of the GC peak for extraction of MS profile was optimized for the amino acid alanine isolated from late exponential cultures (Figure 3.17). GC-MS raw data files were baseline corrected using the software MetAlign as described in section 2.13.2 and the average ^{13}C enrichment of

the fragments was calculated after mass correction using MSCorr software as described section 2.15.1.

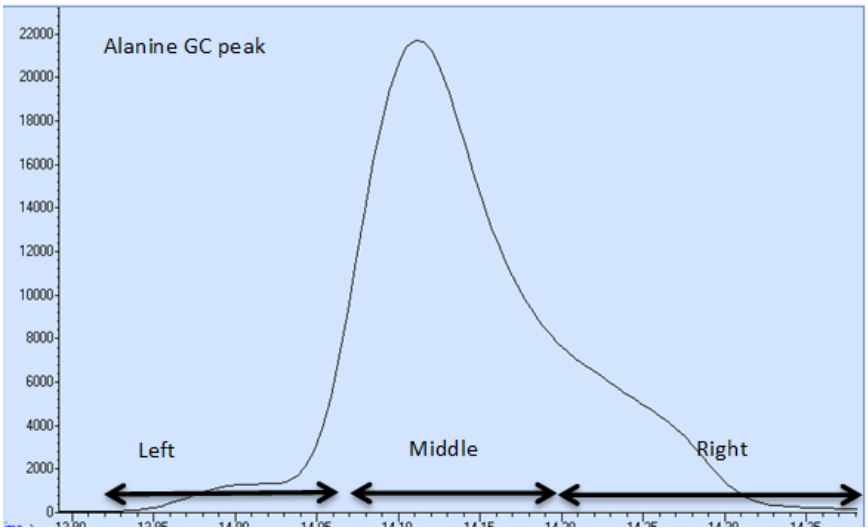

Figure 3.17: **GC peak of the amino acid alanine, showing the three integration regions (left, middle and right) used for measuring ^{13}C enrichment across the peak.**

A discrepancy was observed in the average ^{13}C enrichment across different sections of the amino acid alanine from both early and late exponential cultures. The expected average ^{13}C enrichment of the metabolite fragments obtained from the labelling experiment was 20% based on the label (20% [$^{13}C_4$]succinic acid) supplied to the cultures. However the average ^{13}C abundance after mass correction was different for the same fragment from the three regions of the GC peak (Figure 3.18). The earliest eluting (left tail) region of the GC peak showed the highest deviation from the expected average ^{13}C enrichment. The middle section had an average ^{13}C enrichment which was closer to the expected value in comparison to the left tail region. The right tail of the peak had the closest ^{13}C enrichment to the expected value in comparison to the other two regions. The same discrepancy was observed for other fragments of alanine from the same sample (Figure 3.18) and for other amino acids derived from hydrolysis of protein extracted from labelled ORS571 cultures (data not shown).

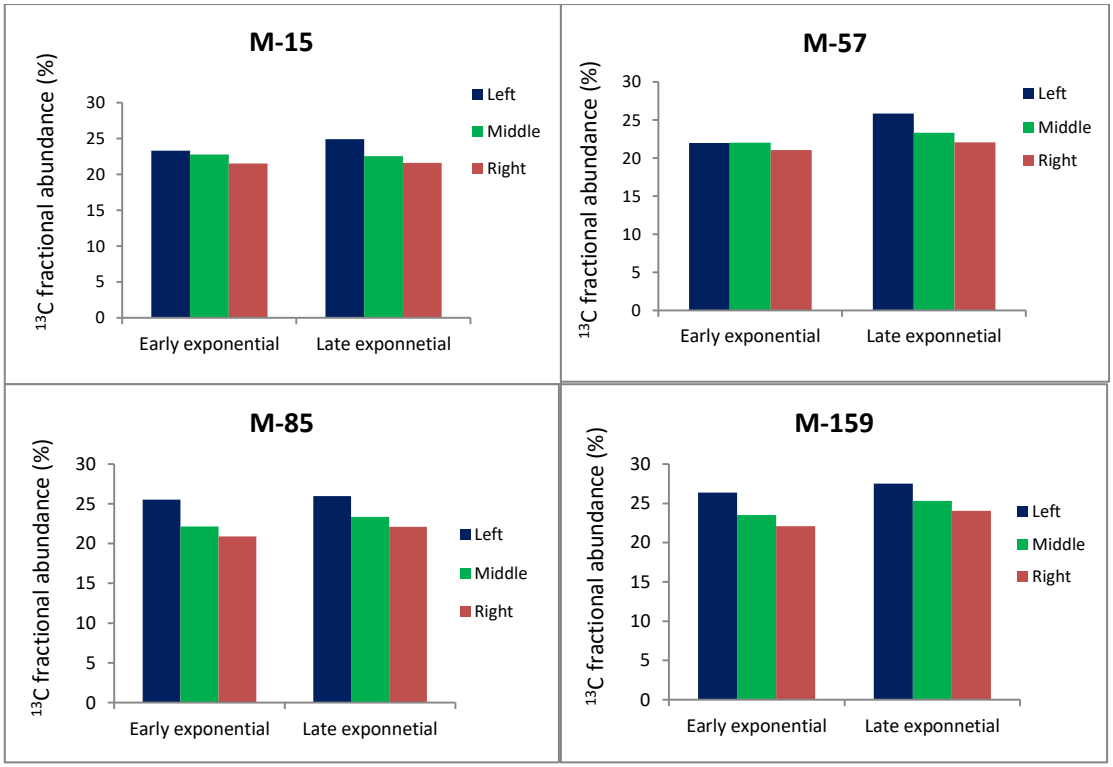

Figure 3.18: **^{13}C enrichments of TBDMS molecular fragments extracted from different sections of the alanine peak**. There was a difference in the average ^{13}C incorporation in the left, middle and right region of the alanine peak and this was observed in the characteristic TBDMS fragments, M-15, M-57, M-85 and M-159 of alanine, for both early and late exponential cultures.

To understand this variation in ^{13}C enrichment across different regions of GC peak, the first attempt was to check for saturation of the detector which may result in under-estimates of the amount of the most abundant mass isotopomer (typically M0 in this study) of the fragment. But no instance of saturation of the detector was found when the ion counts were checked for each individual scan for a particular region of the peak. Another possible cause was suspected to be the choice of degrees of freedom used to correct for the contribution of natural abundance of atoms other than native amino acid C atoms to the MID using the MSCorr program. To test this, the degrees of freedom were varied in the range from 1 to 10 for all the three sections of the peak. From this analysis, the average ^{13}C enrichment after mass

correction was still found to be different across the three sections of the peak, with the right tail region showing the closest ^{13}C fractional abundance to the expected value. This shows that the discrepancy in ^{13}C enrichment of different regions of the alanine peak was not due to mass correction. The third analysis was to check for the interfering ions or chemical compounds (due to the column bleed in GC) which might occur as a noise in the MS profile. However, the abundance of other ions in any particular scan of the GC peak occurred in relatively low abundance as compared to the mass isotopomers of interest. So it unlikely that the discrepancy of ^{13}C enrichment across different regions of the peak was due to the presence of interfering compounds in the MS profile.

An alternative explanation for the discrepancy observed in ^{13}C enrichments across different regions of the GC peak is the commonly recognised isotopic fractionation effect during GC separation, which results in a variation of the ^{12}C and ^{13}C composition of metabolite profiles eluting from the column. The source of isotopic fractionation can be the GC inlet, the method of derivatisation, dispersion of chromatographic peak caused by the presence of different mass isotopomers or gas transfer (Sessions, 2006; Allen & Ratcliffe, 2009; Zhang et al., 2012b). This variation in isotopic composition of ^{12}C and ^{13}C results in discrepancies of ^{13}C enrichment across different regions of the GC peak. To avoid bias from isotopic discrimination, the integration interval was set to the full peak width for the metabolites to extract their respective MS profile for mass correction. This method was adopted from the recommendations in Dauner & Sauer, 2000 and Antonieweicz et al., 2007a.

3.7.2 Mass correction of MS measurements

Baseline corrected GC-MS data for amino acids, PHB and trehalose from extracts of cells that had been labelled with 20% [$^{13}C_4$]succinate were mass corrected using MSCorr to eliminate the contribution to the ^{13}C enrichment of the fragments from the C atoms introduced during derivatization and the mass effects resulting from the

natural abundance of isotopes of atoms other than carbon (Wahl et al., 2004). The MID obtained after mass correction consists of mass isotopomers and their respective fractional abundance in a molecular fragment. The reliability of these MIDs obtained after mass correction was dependent on the degrees of freedom that were chosen for correction. The degrees of freedom refer to the number of mass isotopomers used in the correction algorithm. The results presented below shows how the implementation of the MSCorr program was optimized to produce reliable MIDs for molecular fragments of a metabolite required for flux analysis. The ratio of chi square value to the chi square critical, was used to check for MS data consistency and validation of the MID obtained for a metabolite after mass correction. The backward degrees of freedom refer to the region corresponding to the m/z less than expected for the completely unlabelled fragment and this degree of freedom was fixed to be 1. The optimization was required for the forward degrees of freedom that refer to an isotopomer family, with one or more ^{13}C. The analysis was done for optimizing the forward degrees of freedom by correction of four different molecular fragments of alanine-2TBDMS and glutamate-3TBDMS obtained from late exponential cultures grown in 20% [$^{13}C_4$]succinate. The ratio of chi square value to critical value for both alanine (Figure 3.19) and glutamate (Figure 3.20) decreased as forward degrees of freedom were varied from 1 to 10, while keeping the backward fixed at 1, during mass correction. A small ratio of chi square value to chi square critical indicates that the MIDs of the molecular fragment remained consistent after mass correction and were considered reliable for flux analysis. The ratio decreased by seven fold (approximately) from 1 to 2 degrees of freedom and the ratio continued to decrease from 2 to 10 degrees of freedom. The ratio was found to be further decreased if the forward degrees of freedom were increased beyond 10. Since the ratio decreased significantly at 2 forward degrees of freedom, and no significant reduction was observed from 3 to 10, backward 1 and forward 2 degrees

of freedom were chosen as the default values for mass correction of MS measurements from both early exponential cultures. While the reliability of MIDs in the molecular fragments of a metabolite depends on the degrees of freedom allowed during mass correction, the ^{13}C fractional abundance in the molecular fragment after mass correction does not vary significantly with the number of degrees of freedom as shown for alanine-2TBDMS (Figure 3.21) and glutamate-3TBDMS (Figure 3.22).

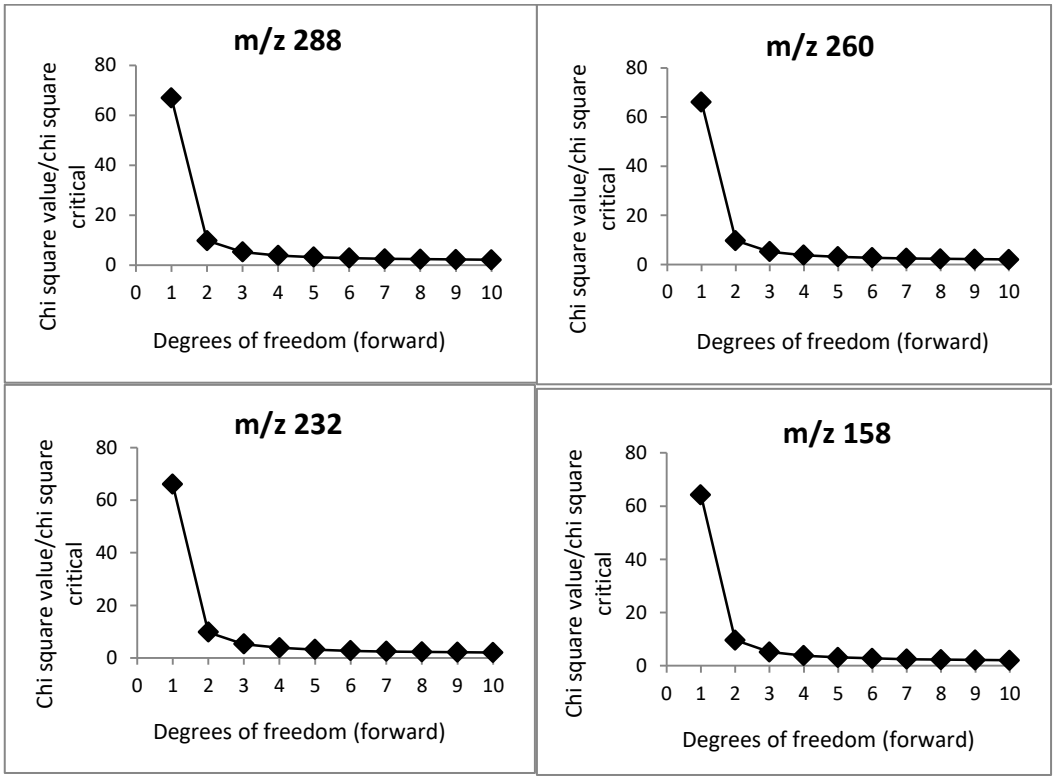

Figure 3.19: **The ratio of chi square value to chi square critical calculated for alanine-2TBDMS fragments- 288, 260, 232 and 158**. All of the ratios are calculated as a mean of four individual measurements.

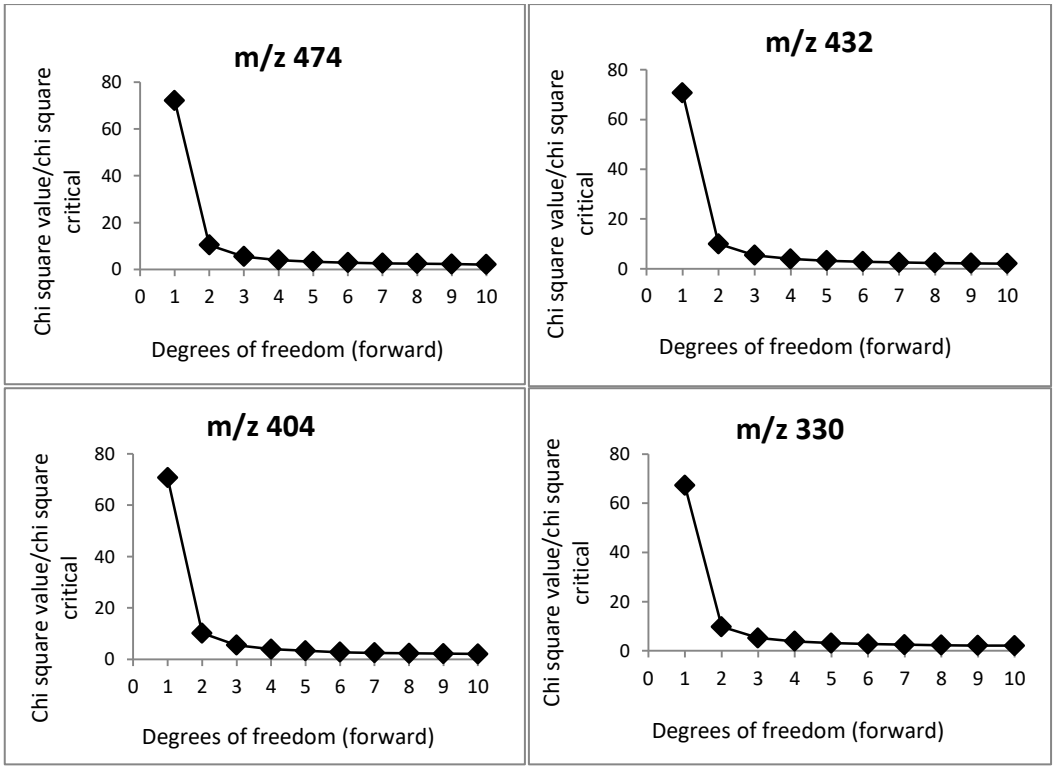

Figure 3.20: **The ratio of chi square value to chi square critical calculated for glutamate-3TBDMS fragments- 474, 432, 404 and 330**. All of the ratios are calculated as a mean of four individual measurements.

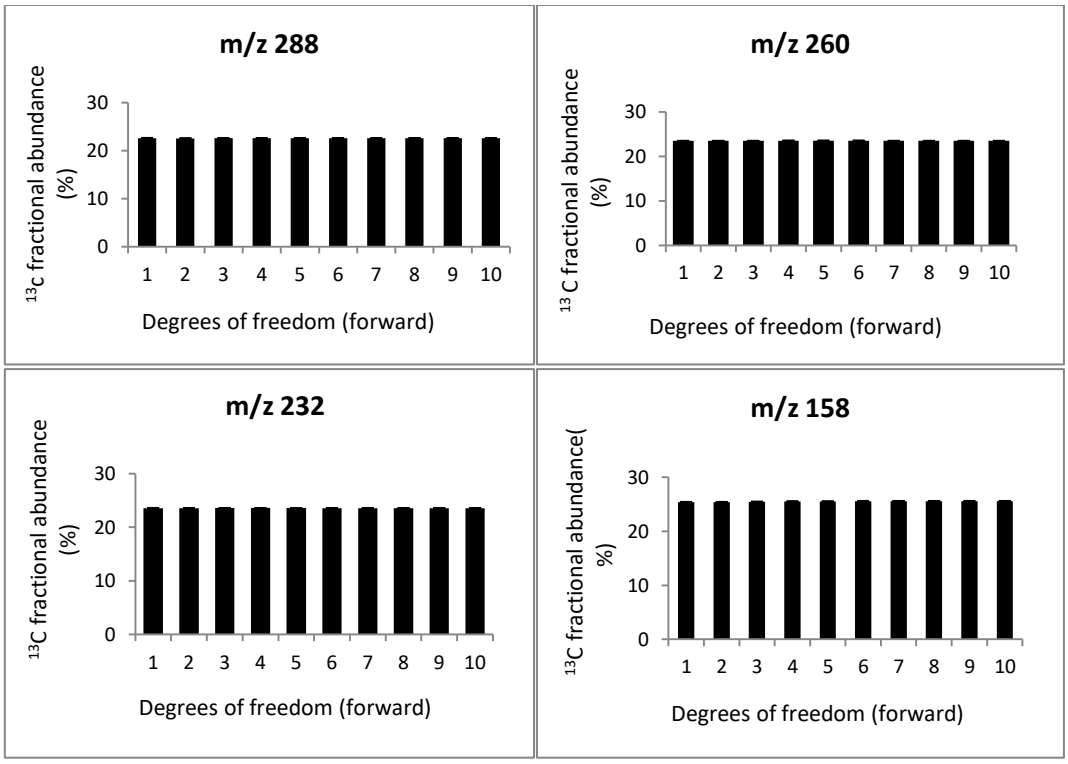

Figure 3.21: **^{13}C enrichments calculated for alanine-2TBDMS fragments- 288, 260, 232 and 158 after mass correction**. The average ^{13}C enrichment calculated for each forward degree of freedom in a fragment is a mean of four determinations ± SEM.

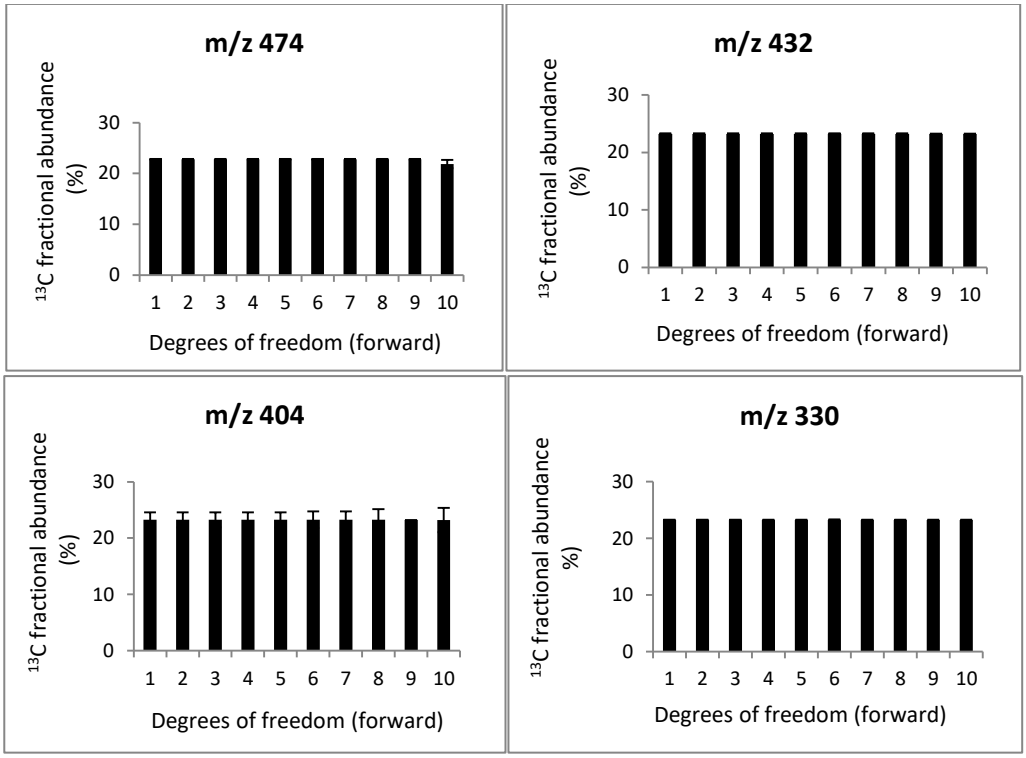

Figure 3.22: **^{13}C fractional abundances calculated for glutamate-3TBDMS fragments- 474, 432, 404 and 330 after mass correction**. The average ^{13}C enrichment calculated for each forward degree of freedom in a fragment is a mean of four determinations ± SEM.

3.7.3 Effect of metabolite concentration on MID

Antoniewicz et al. (2007a) reported that the measured MID of TBDMS-derivatized amino acids varied depending on the amount of the sample analyzed. They found that the intensity of the most abundance isotopomer decreased and the intensity of the lower abundance mass isotopomers increased with the increase in the amount of amino acids analyzed. Similar concentration effects on the MID for fatty acids was reported by Fagerquist et al., 2001. But in a different study, no concentration effect was observed for TBDMS- derivatised amino acids (Dauner & Sauer, 2000). The concentration effect on the MID was suggested to be mass spectrometer dependent by Antoniewicz et al. (2007a) and they proposed a correction for this effect by

extrapolation of GC-MS data to a theoretical infinite dilution. So, it was necessary to check, if there was a concentration effect on the MIDs of the metabolites analyzed by the GC-MS instrument used for this study. To perform this check, two amounts of hydrolysate- 25 µl and 200 µl containing different amounts of protein-derived amino acids were chosen. The MIDs showing fractional abundance of individual mass isotopomers were extracted from the molecular fragments of TBDMS derivatised amino acids- alanine, glycine, glutamate and valine in 25 µl and 200 µl hydrolysates. The MID measured for each amino acid in the two hydrolysate amounts were compared using a line of best fit for the measurements (Figure 3.23). For each amino acid analysed, the coefficient of determination, R^2 value was close to 1, which indicated that the mass isotopomer fractional abundances measured in the two different amounts of hydrolysate showed a good agreement (Figure 3.24). This analysis confirms that the MID of TBDMS amino acids in two different amounts of hydrolysate were identical. So, the MID of the amino acids did not vary depending on the amount of sample analyzed by the GC-MS.

The metabolites detected in 25 µl hydrolysate had a lower abundance (data not shown) and so, there was a risk of the metabolites being lost during baseline correction of the peaks. The metabolites detected in 200 µl hydrolysate had higher abundance and were preferred over 25 µl hydrolysate to obtain maximum abundance of metabolites.

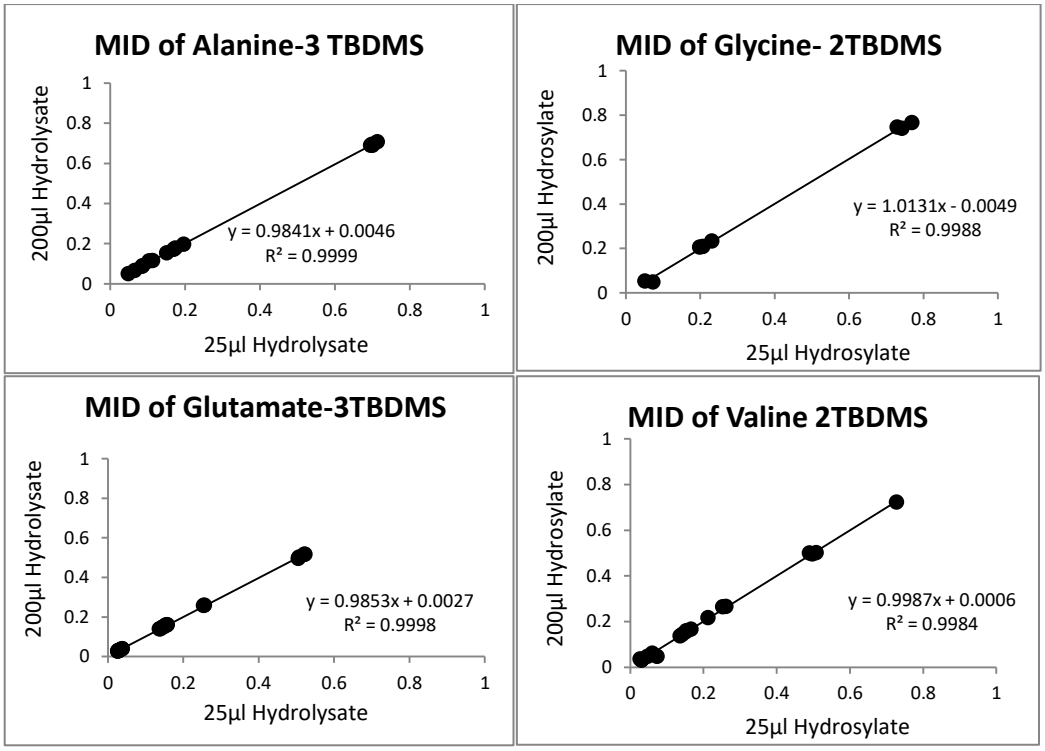

Figure 3.23: **Comparison of mass isotopomer fractional abundance in the amino acids from 25 µl and 200 µl hydrolysate.** The mass istopomers of the amino acid fragment used in these analyses are: alanine-2TBDMS, M-15, m/z 302-305, C0-3; M-57, m/z 260-263, C0-3; M-85, m/z 232-234, C0-2; M-159, m/z 158-160, C0-2; glycine-2TBDMS, M-15, m/z 288-290, C0-2; M-57, 247-248, C1-2;M-85, m/z 218-219, C0-1; valine-2TBDMS, M-15, m/z 330-335, C0-5; M-57, m/z 289-293, C1-5; M-85, m/z 260-264, C0-4; M-159, m/z 186-190, C0-4; glutamate-3TBDMS, M-15, m/z 474-479, C0-5; M-57, m/z 433-437, C1-5; M-85, m/z 404-408, C0-4; M-159, m/z 330-334, C0-4. The measurements for the mass isotopomers for each amino acid are the mean of four determinations.

3.8 Isotopic steady state analysis

For steady state ^{13}C-MFA, ideally the system under study should be at an isotopic steady state. But corrections can be made for biomass components that do not reach isotopic steady state due to pre-existing unlabelled pools (Kruger et al., 2012). Isotopic steady state is achieved when ^{13}C fractional enrichment of the metabolic intermediates from which biomass is synthesized remain constant over time (Antonieweicz, 2015; Williams et al., 2008). To assess if the ORS571 cultures grown

with 20% [$^{13}C_4$]succinic acid, achieved isotopic steady state during exponential growth, the fractional abundance of individual mass isotopomers from 16 protein-derived amino acids were compared using a line of best fit for the measurements (Figure 3.24). The gradient for the line of best fit was close to 1, which confirms that the mass isotopomer proportions measured in the amino acids from early and late exponential cultures were identical. Also, the coefficient of determination, R^2 value of 0.991, showed a strong positive linear correlation and hence a good agreement between the fractional abundance of the mass isotopomers measured in early and late exponential cultures. This analysis, therefore, shows no significant difference in the fractional abundance of mass isotopomers measured in early and late exponential cultures. The average ^{13}C fractional abundance was calculated for the mass corrected molecular fragments of the amino acids according to the method described in section 2.15.1. Statistical analysis (Table 3.2) shows that the average ^{13}C fractional abundance measured in the amino acids from early and late exponential cultures were not significantly different. These two analyses confirm that the ORS571 batch cultures fed with [$^{13}C_4$]succinic acid achieved isotopic steady state during exponential growth.

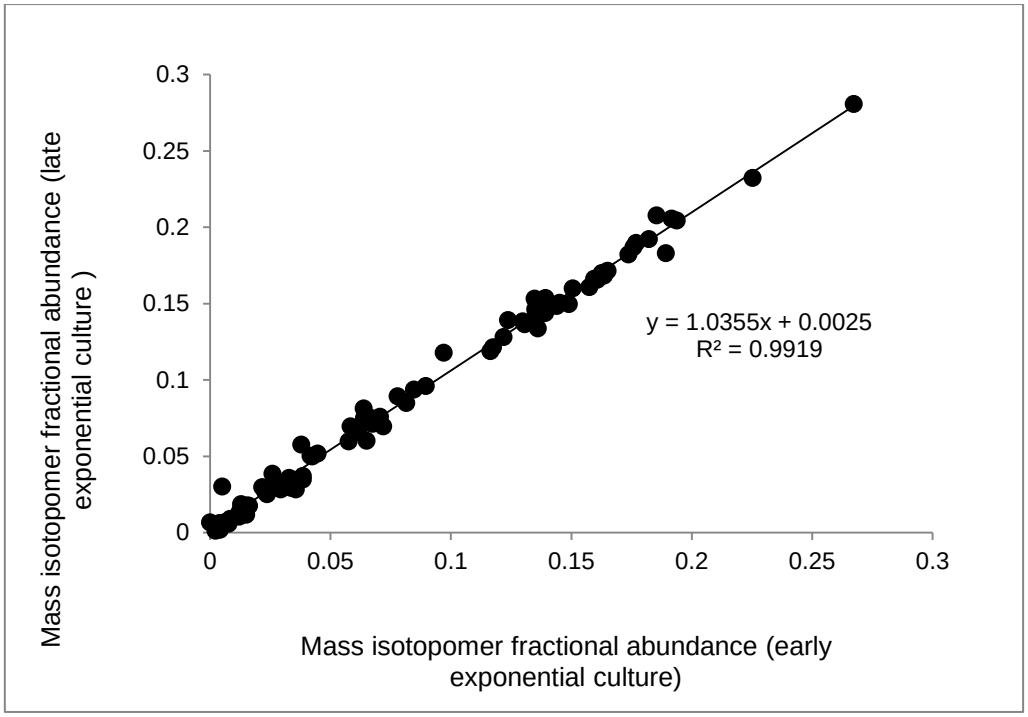

Figure 3.24: **Comparison of the fractional abundance of mass isotopomers from protein-derived amino acids in early and late exponential cutlures**. The mass istopomers of the amino acid fragment used in these analyses are: alanine-2TBDMS, M-57, m/z 261-263, C1-3; glycine-2TBDMS, M-57, 247-248, C1-2; valine-2TBDMS, M-57, m/z 289-293, C1-5; leucine-2TBDMS, M-57, m/z 303-308, C1-6; isoleucine-2TBDMS, M-57, m/z 303-308, C1-6; methionine-2TBDMS, M-57, m/z 321-325, C1-5; serine-3TBDMS, M-57, m/z 391-393, C1-3; threonine-2TBDMS, M-57, m/z 405-408, C1-4; proline-2TBDMS, M-57, m/z 287-291, C1-5; phenylalanine-2TBDMS, M-57, m/z 337-345, C1-9; aspartate-3TBDMS, M-57, m/z 419-422, C1-4; glutamate-3TBDMS, M-57, m/z 433-437, C1-5; lysine-2TBDMS, M-57, m/z 432-438, C1-6; arginine-3TBDMS, M-57, m/z 443-448, C1-6; histidine-3TBDMS, M-57, m/z 441-446, C1-6; tyrosine-3TBDMS, M-57, m/z 467-475, C1-9. For clarity, the fractional abundance of unlabelled mass isotopomers are excluded from the plot. The measurements for each individual mass isotopomer was the mean of three determinations.

Table 3.2: **Comparison of ^{13}C fractional abundance of amino acids in early and late exponential cultures**

Protein-derived amino acids	^{13}C fractional abundance (%)		P-value
	Early exponential cultures	Late exponential culture	
Alanine	21.9 ± 0.08	21.8 ± 0.08	0.85
Glycine	21.0 ± 0.07	21.4 ± 0.09	0.06
Valine	21.3 ± 0.16	22.5 ± 0.65	0.28
Leucine	19.7 ± 0.10	20.0 ± 0.03	0.15
Isoleucine	16.5 ± 0.15	16.3 ± 0.06	0.43
Methionine	21.8 ± 0.41	21.4 ± 0.09	0.47
Serine	19.6 ± 0.39	21.9 ± 0.02	0.11
Threonine	21.7 ± 0.42	21.9 ± 0.04	0.76
Phenylalanine	21.6 ± 0.11	21.8 ± 0.04	0.51
Aspartate	22.0 ± 0.14	22.2 ± 0.08	0.37
Glutamate	21.5 ± 0.13	21.5 ± 0.06	0.99
Lysine	21.1 ± 0.85	22.0 ± 0.08	0.49
Arginine	20.8 ± 0.18	21.2 ± 0.06	0.30
Histidine	18.5 ± 0.57	21.5 ± 0.15	0.06
Tyrosine	21.7 ± 0.28	21.4 ± 0.09	0.49
Proline	22.4 ± 0.47	21.8 ± 0.10	0.39

The molecular fragments of amino acids used for this analysis are- alanine-2TBDMS, M-57, m/z 261-263, C1-3; glycine-2TBDMS, M-57, 247-248, C1-2; valine-2TBDMS, M-57, m/z 289-293, C1-5; leucine-2TBDMS, M-57, m/z 303-308, C1-6; isoleucine-2TBDMS, M-57, m/z 303-308, C1-6; methionine-2TBDMS, M-57, m/z 321-325, C1-5; serine-3TBDMS, M-57, m/z 391-393, C1-3; threonine-2TBDMS, M-57, m/z 405-408, C1-4; proline-2TBDMS, M-57, m/z 287-291, C1-5; phenylalanine-2TBDMS, M-57, m/z 337-345, C1-9; aspartate-3TBDMS, M-57, m/z 419-422, C1-4; glutamate-3TBDMS, M-57, m/z 433-437, C1-5; lysine-2TBDMS, M-57, m/z 432-438, C1-6; arginine-3TBDMS, M-57, m/z 443-448, C1-6; histidine-3TBDMS, M-57, m/z 441-446, C1-6; tyrosine-3TBDMS, M-57, m/z 467-475, C1-9.The measurements for the average ^{13}C fractional abundance in the protein derived amino acids of early and late exponential cultures are the mean ± SEM of four determinations.

3.9 Choice of metabolites to be used for ^{13}C-MFA

3.9.1 Total ion counts (TIC) of metabolites detected in GC-MS

Amino acids from ORS571 grown with 20% [$^{13}C_4$]succinic acid which were extracted in both aqueous and aqueous insoluble phase were used for this analysis. From GC-MS analysis, it was observed that the amino acids extracted in the aqueous soluble phase had a lower TIC as compared to the protein-derived amino acids, which were extracted in the aqueous insoluble phase (Figure 3.25). The issue with the low TIC was that there was a risk of eliminating the metabolite signal during baseline correction (noise elimination) of GC-MS spectra. So, the protein-derived amino acids gave a more abundant signal for extraction and reliable quantification of MID as compared to the free amino acids.

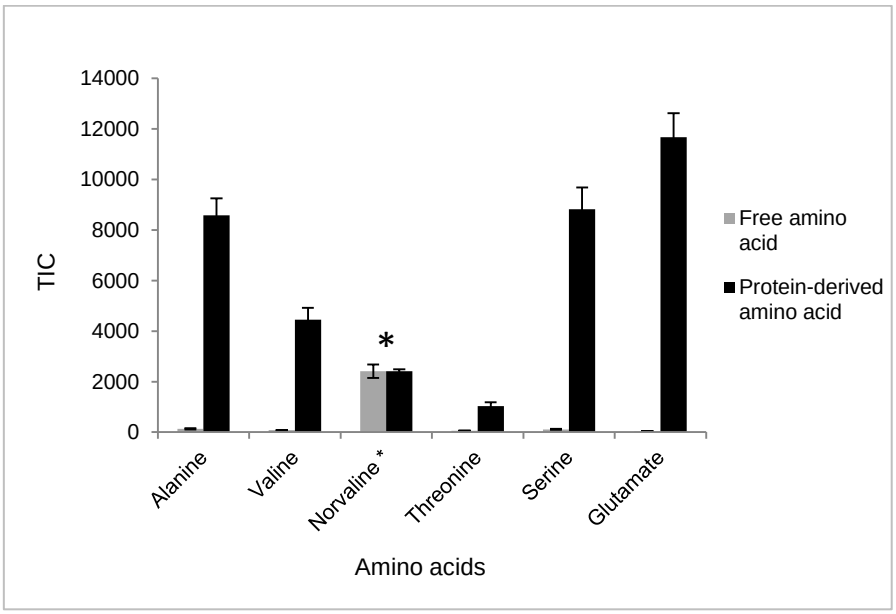

Figure 3.25: **TIC of free amino acids and protein-derived amino acids detected by GC-MS**. The free amino acid molecular fragments used in this analysis are- Alanine-2TMS, M-117, m/z 116-118; valine-2TMS, M-117, m/z 144-148; norvaline-2TMS, M-117, m/z 144- 148; threonine-2TMS, M-218, m/z 117-119; serine-3TMS, M-117, m/z 204-206; glutamate-3TMS, M-117, m/z 246-250. The protein-derived amino acid molecular fragments used for this analysis are- alanine-2TBDMS, M-57, m/z 260-263; valine-2TBDMS, M-57, m/z 288-293;

norvaline-2TBDMS, M-57, m/z 288-293; threonine-2TBDMS, M-57, m/z 404-408; serine-3TBDMS, M-57, m/z 390-393; glutamate-3TBDMS, M-57, m/z 432-437. Norvaline was added used as an internal standard in GC-MS and is marked with an *. The measurements are the mean ± SEM of four determinations.

3.9.2 Comparison of ^{13}C enrichments in aqueous and chloroform soluble metabolites

Amino acids that were detected in GC-MS were integrated over the whole peak width to extract their MS measurements. These MS measurements were corrected for natural isotopic effects using MSCorr according to the methods established in the previous section 3.7.2. The ^{13}C fractional abundance measured in free amino acids was observed to be comparatively lower than the fractional abundance measured in protein-derived amino acids (Figure 3.26). The issue with the ^{13}C fractional abundance calculated in the free amino acids is with accuracy and the minimum TIC required for an accurate measurement of a MID. The free amino acid MIDs are clearly inaccurate and hence unusable because they are less reliable than the MIDs for the protein-derived amino acids. So, MIDs from protein-derived amino acids were chosen for flux analysis. Also, trehalose extracted in the aqueous phase and hydroxybutyrate, the monomer of PHB recovered in the aqueous insoluble phase, showed ^{13}C enrichment close to 20% and were chosen for flux analysis. The mass spectra (MS) of 16 protein-derived amino acids, trehalose and hydroxybutyrate are included in the appendix (Figure A2). The MS profiles in Figure A2 are shown for late exponential cultures, and equivalent profiles were obtained for metabolites extracted from early exponential cultures (data not shown).

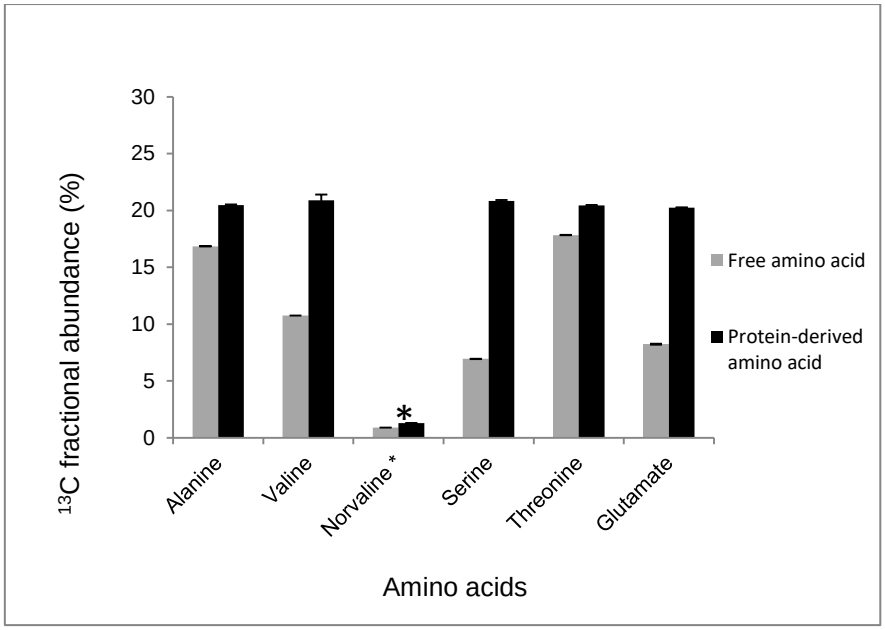

Figure 3.26: **Comparison of ^{13}C enrichment in aqueous phase free-amino acid pools and protein-derived amino acids**. The free amino acid molecular fragments used in this analysis are- Alanine-2TMS, M-117, m/z 116-118; valine-2TMS, M-117, m/z 144-148; norvaline-2TMS, M-117, m/z 144- 148; threonine-2TMS, M-218, m/z 117-119; serine-3TMS, M-117, m/z 204-206; glutamate-3TMS, M-117, m/z 246-250. The protein-derived amino acid molecular fragments used for this analysis are- alanine-2TBDMS, M-57, m/z 260-263; valine-2TBDMS, M-57, m/z 288-293; norvaline-2TBDMS, M-57, m/z 288-293; threonine-2TBDMS, M-57, m/z 404-408; serine-3TBDMS, M-57, m/z 390-393; glutamate-3TBDMS, M-57, m/z 432-437. Norvaline was added used as an internal standard in GC-MS and is marked with an *. The measurements are the mean ± SEM of four determinations.

3.10 Choice of valid molecular fragments for ^{13}C-MFA

The amino acids, PHB and trehalose formed multiple molecular fragments after electron ionization in GC-MS. The MIDs from all of the molecular fragments were extracted after mass correction of the MS profiles. The most reliable molecular fragments of a metabolite were chosen according to the validation critera described in 2.15.2. It was important to use MID from valid molecular fragments of metabolites to generate statistically reliable flux maps. The list of valid molecular fragments for each of the metabolites chosen for ^{13}C-MFA of early and late exponential cultures is shown

in Table 3.3 and the MID for each of the fragments are listed in the appendix (Table A3). The metabolites from early exponential cultures produced fewer valid molecular fragments as compared to late exponential cultures. This was due to the comparatively lower TIC of metabolites from early exponential cultures which results in molecular fragments with less reliable MIDs after mass correction.

Table 3.3: **Valid molecular fragments of metabolites used for ^{13}C-MFA in early and late exponential cultures of ORS571**

Metabolite	Molecular fragments (m/z)	
	Early exponential cultures	Late exponential cultures
Alanine	260, 232	260, 232
Glycine	246, 218	246, 218
Valine	288	288, 260, 186
Leucine	274	274, 200
Isoleucine	200	274, 200
Methionine	320, 292, 218	320, 292, 218
Serine	362, 288, 302	390, 362, 288, 302
Threonine	404	404, 376
Proline	286, 258, 184	286, 258, 184
Phenylalanine	336,302	336, 308, 234, 302
Aspartate	418, 390, 316, 302	418, 390, 316, 302
Glutamate	432, 404, 330	432, 404, 330
Lysine	329	329
Arginine	442	442, 414, 340
Histidine	-	440, 412, 338
Tyrosine	466, 302	466, 364, 302
PHB	275	275
Trehalose	361	361, 271

3.11 ^{13}C-MFA using INCA

Firstly the metabolic model was written in INCA, according to the procedure described in 2.16.1. This was followed by the entry of experimental data into INCA from the labelling experiments on ORS571 free-living cultures with 20% [$^{13}C_4$]succinic acid i.e. the MID measurements for the valid molecular fragments of amino acids, PHB and trehalose. The input flux for entry of succinate into the metabolic network was fixed at 100 and the model was initiated with arbitrary values for internal network fluxes that

were varied during the fitting procedure. Flux estimation was repeated 100 times starting with the arbitrary values to find a global flux solution. A detailed description of each stage is reported below.

3.11.1 Metabolic modelling

The metabolic model for ORS571 was constructed using the genome and metabolic pathway information available from both the literatures and databases (KEGG and BiocCyc) (Figure 3.27). The model consisted of six categories of reactions: (i) succinate input flux to the TCA cycle; (ii) reactions for central carbon metabolism, which includes TCA, ED, PPP, gluconeogenesis, anaplerotic pathways via malic enzyme and PEP carboxykinase; (iii) an additional pathway for AcCoA synthesis in ORS571 using the enzyme (methyl) malonate semialdehyde dehydrogenase (MSDH) (Pauling et al., 2001); (iv) pathways for biosynthesis of amino acid (AA) and PHB; (v) a biomass synthesis reaction (section 3.11.2) composed of biomass measurements for protein, lipids, nucleic acids (DNA and RNA), carbohydrates, EPS and PHB to constrain the model; (vi) additional reactions to compensate for the presence of naturally occurring ^{12}C pools that diluted the ^{13}C label incorporation in protein-derived amino acids and PHB (Masakapalli et al., 2013; Kruger et al, 2014). A full definition of the reactions in the model is provided in Table A4 of the appendix.

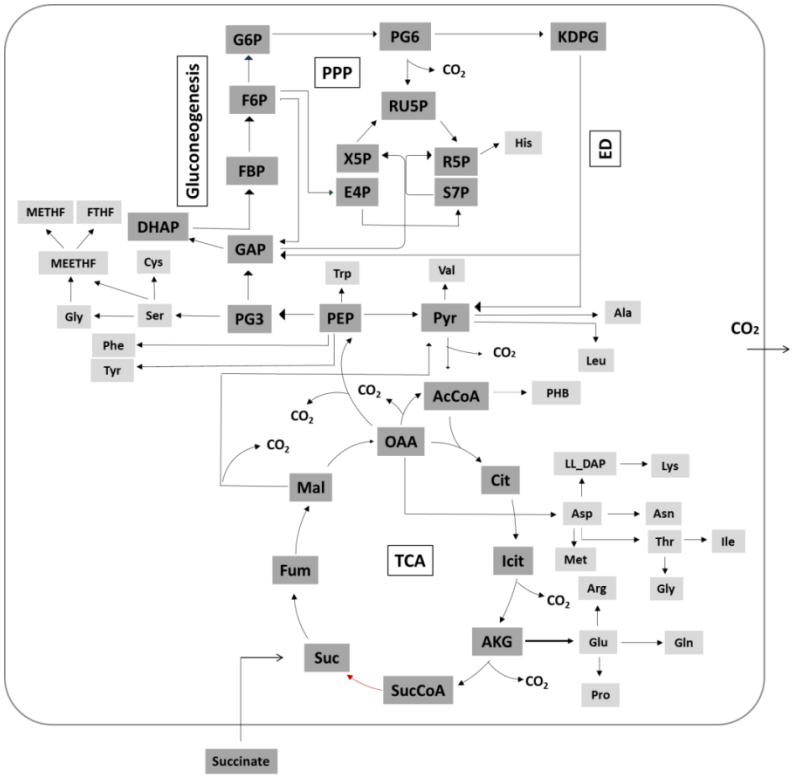

Figure 3.27: **Metabolic model of ORS571 used for ^{13}C-MFA using INCA**

3.11.2 Formulation of biomass synthesis reaction

The biomass synthesis reaction, which constrains the model, was constructed based on the biomass composition measured in early and late exponential cultures (Table 3.1). The amount of each precursor was expressed in mmol/ g dry weight of cells, which was calculated by dividing the amount of precursor that forms the biomass component by its molecular weight. The amount of each precursor was multiplied by the number of carbons atoms it contains to calculate the total carbon atom contribution to biomass synthesis. The composition of the reaction from biomass components and their precursors, measured in early and late exponential cultures is shown below.

i) Protein: The amino acid composition for the protein was calculated based on the general consideration of the amino acid composition previously reported for the gram negative *E. coli* (Long & Antoniewicz, 2014). The contributions from each

of the amino acids towards the synthesis of total protein for early and late exponential cultures are shown in Table 3.4.

Table 3.4: **Amino acid composition for early and late exponential ORS571 cultures**

Amino acid	Proportional abundance of total protein (% w/w)	Protein-derived amino acid content of biomass (mmol g dry wt^{-1})	
		Early exponential cultures	Late exponential cultures
Alanine	6.39	0.42	0.43
Arginine	8.18	0.24	0.25
Asparagine	5.17	0.21	0.22
Aspartic acid	5.17	0.21	0.22
Cysteine	2.53	0.11	0.12
Glutamic acid	7.18	0.26	0.27
Glutamine	7.18	0.26	0.26
Glycine	4.77	0.39	0.40
Histidine	2.05	0.07	0.07
Isoleucine	4.91	0.20	0.21
Leucine	8.39	0.35	0.36
Lysine	6.98	0.25	0.26
Methionine	2.69	0.09	0.10
Phenylalanine	4.29	0.13	0.14
Proline	3.37	0.16	0.17
Serine	3.98	0.21	0.22
Threonine	4.78	0.22	0.23
Tryptophan	1.56	0.04	0.04
Tyrosine	4.12	0.11	0.12
Valine	6.18	0.29	0.30

The proportional abundance of amino acids was adopted from *E. coli* measurements by Long & Antoneiweicz 2014. The amino acid content of biomass was calculated by dividing the amount of each amino acid (mg) by its respective anhydrous molecular weight (g mol^{-1}).

ii) Lipid: The lipid composition and the amount of precursors was calculated based on the whole cell fatty acid composition for *Azorhiozbium caulinodans* as reported in the previous literature (Lang et al., 2013). Table 3.5 shows the composition of the types of lipid, composition of component fatty acids and the overall lipid composition of biomass in ORS571. The amount of lipid was measured by sulfo-phospho vanillin method in terms of linolenic acid equivalents, and was composed of 4% lipopolysaccharide

and 96% phospholipids (75% phosphatidylethanolamine and 25% phosphatidylglycerol).

Table 3.5: **Lipid composition in early and late exponential ORS571 cultures**

Components	Type of fatty acid	Precursors	Lipid content of biomass (mmol g dry wt^{-1})	
			Early exponential cultures	Late exponential cultures
Lipopolysaccharides	C14, C16	Acetyl coenzyme A (AcCoA)	2.65	2.76
Phospholipid (fatty acids)	C18, C20	Acetyl coenzyme A (AcCoA)	0.13	0.13
Phospholipid (ethanolamine)	-	3-phosphoglyceric acid (3-PGA)	0.22	0.19
Phospholipid (glycerol)	-	Dihydroxyacetone phosphate (DHAP)	0.18	0.11

The lipid content of biomass was calculated by dividing the amount of the precursors for each of the lipid component (mg) by its respective molecular weight (g mol^{-1}).

iii) Nucleic acids: The proportion of nucleotides, adenine, guanine, cytidine and thymine that constitutes DNA was calculated based on the GC content in the genome of ORS571 available in the NCBI database (Table 3.6). Table 3.7 shows the precursor metabolites their amounts required for the synthesis of DNA content of biomass for both early and late exponential ORS571 cultures.

Table 3.6: **Nucleotide base composition of DNA in ORS571**

Nucleotide base	% of DNA
Adenine	16.5
Thymine	16.5
Guanine	33.5
Cytidine	33.5

Table 3.7: **Precursor metabolites required for the synthesis of DNA in early and late exponential cultures**

Precursor metabolites	DNA content of biomass (mmol g dry wt^{-1})	
	Early exponential cultures	Late exponential cultures
3-Phosphoglyceric acid	0.028	0.027
Folate	0.028	0.027
Oxaloacetate	0.030	0.030
MEETHF	0.010	0.010
Ribulose 5-phosphate	0.058	0.057

The DNA content of biomass was calculated by dividing the amount of the precursors required for DNA synthesis (mg) by its respective molecular weight (g mol^{-1}).

RNA: The proportion of nucleotides, adenine, guanine, cytosine and uracil required for the synthesis of RNA in ORS571 is shown in Table 3.8. Table 3.9 shows the amount of precursors required for the synthesis of RNA content of biomass in early and late exponential ORS571 cultures.

Table 3.8: **Nucleotide base composition of RNA in ORS571**

Nucleotide base	% of RNA
Adenine	26.56
Guanine	34.26
Cytidine	18.80
Uridine	20.36

The nucleotide base composition of RNA in ORS571 was adapted based on the general consideration of the standard nucleotide base composition reported in the gram negative *E .coli* (Neidhart, 1987).

Table 3.9: **Precursor metabolites required for the synthesis of RNA in early and late exponential cultures**

Precursor metabolites	RNA content of biomass (mmol g dry wt^{-1})	
	Early exponential cultures	Late exponential cultures
3-Phosphoglyceric acid	0.43	0.34
Folate	0.86	0.67
Oxaloacetate	0.30	0.24
Ribulose 5-phosphate	0.73	0.58

The RNA content of biomass was calculated by dividing the amount of the precursors required for RNA synthesis (mg) by its respective molecular weight (g mol^{-1}).

iv) PHB: The PHB synthesis pathway involves condensation of two AcCoA molecules to form 3-hydroxybutyrate units, followed by polymerisation of form 3-hydroxybutyrate to synthesize the polymer (Mandon et al., 1998). Table 3.10 shows the amount of the precursor, 3-hydroxybutyrate used to synthesize the PHB content of the biomass.

Table 3.10: **Precursor metabolites required for the synthesis of PHB in early and late exponential cultures**

Precursor metabolite	PHB content (mmol g dry wt^{-1})	
	Early exponential	Late exponential
3-hydroxybutyrate	1.13	1.46

The PHB content of biomass was calculated by dividing the amount of 3-hydroxybutyrate (mg) by its respective molecular weight (g mol^{-1}).

v) Carbohydrates and EPS: Glucose 6-phosphate is the precursor for the synthesis of carbohydrates and EPS, and the amount of this precursor required is shown in Table 3.11.

Table 3.11: **Precursor metabolites required for the synthesis of carbohydrates and EPS in early and late exponential cultures**

Biomass component	Precursor metabolite	Carbohydrate and EPS content of biomass (mmol g dry wt^{-1})	
		Early exponential cultures	Late exponential cultures
Carbohydrates	Glucose 6-phosphate (G6P)	0.102	0.107
EPS	Glucose 6-phosphate (G6P)	0.015	0.010

The carbohydrate and EPS content of the biomass was calculated by dividing the amount of G6P (mg) by its respective molecular weight (g mol^{-1}).

vi) Final reaction: The total amount of metabolic intermediates required for biomass (expressed in C atom equivalents) was obtained by summing the product of the estimated molar contribution of each component of biomass and the carbon

atom content of the component. The final biomass reactions for early and late exponential cultures are shown as reaction A and B respectively:-

Reaction A- 0.424*Ala + 0.395*Gly + 0.294*Val + 0.349*Leu + 0.204*Ile + 0.163*Pro + 0.096*Met + 0.215*Ser + 0.223*Thr + 0.137*Phe + 0.212*Asn + 0.212*Asp + 0.262*Glu + 0.262*Gln + 0.256*Lys + 0.07*His + 0.119*Tyr + 0.247*Arg + 0.115*Cys + 0.039*Trp + 2.78*AcCoA + 0.184*DHAP + 0.604*PG3 + 0.284*OAA + 0.749*MEETHF + 0.667*R5P + 0.117*G6P + 1.13*PHB = 38.95*Biomass

Reaction B- 0.439*Ala + 0.408*Gly + 0.304*Val + 0.362*Leu + 0.211*Ile + 0.169*Pro + 0.1*Met + 0.223*Ser + 0.231*Thr + 0.142*Phe + 0.219*Asn + 0.219*Asp + 0.271*Glu + 0.271*Gln + 0.265*Lys + 0.073*His + 0.123*Tyr + 0.255*Arg + 0.119*Cys + 0.041*Trp + 2.9*AcCoA + 0.192*DHAP + 0.482*PG3 + 0.801*MEETHF + 0.272*OAA + 0.638*R5P + 0.117*G6P + 1.46*PHB = 40.7*Biomass

3.12 Generation of flux distributions

After construction of the metabolic model, MS measurements from the labelling experiments in early and late exponential cultures were entered in INCA as described in the Young, 2014. Generally, an error of 0.1-5 mol % has been applied to MS measurements (MIDs) in other ^{13}C-MFA studies (Young et al., 2008; Metallo et al., 2009; Zamboni et al., 2009; Masakapalli et al., 2010; Adebiyi et al., 2014; Long et al., 2016; Gonzalez et al., 2017). However, an error of 1.1 mol % was used for all MS measurements in this study, because this corresponds to the natural abundance of the ^{13}C isotope on Earth. Flux optimisations were performed beginning from random initial flux estimates and best-fit flux distributions were calculated by minimising the residuum between the simulated and experimentally obtained MS measurements. The fluxes were calculated relative to the succinate uptake flux which was fixed at 100. The net fluxes and their associated 95% confidence limits for the two growth phases are shown in Table 3.12. The individual fluxes for synthesis of lipids, nucleic acids, carbohydrates and EPS were calculated separately by multiplying the flux through the reaction R61 (Table A4 in appendix) for biomass synthesis by the amount of precursors derived in section 3.11.2.

Table 3.12: **Net fluxes and their associated 95% confidence limits measured for ORS571 free-living cultures at early and late exponential growth stages**

Reaction step (s)	Symbol	Molar flux (relative to succinate uptake)	
Net fluxes		**Early exponential**	**Late exponential**
Uptake fluxes			
Total uptake of succinate (constrained)	*upt3*	100	100
Tricarboxylic acid cycle			
Succinate dehydrogenase	*tca1*	139 (136, 143)	143 (140, 146)
Fumarase	*tca2*	141 (137, 144)	144 (141, 147)
Malate dehydrogenase	*tca3*	86.0 (68.9, 116)	114 (108, 147)
Citrate synthase	*tca4*	43.4 (40.4, 46.4)	46.9 (43.9, 49.7)
Aconitase	*tca5*	43.4 (40.4, 46.4)	46.9 (43.9, 49.7)
Isocitrate dehydrogenase	*tca6*	43.4 (40.4, 46.4)	46.9 (43.9, 49.7)
2-Oxoglutarate dehydrogenase	*tca7*	39.8 (36.8, 43.0)	43.5 (40.4, 46.5)
Succinyl-CoA synthetase	*tca8*	38.5 (35.1, 41.8)	42.2 (39.1, 45.3)
Pyruvate dehydrogenase	*tca9*	65.9 (0, 67.8)	68.9 (1.33, 70.4)
Anaplerotic pathways			
NAD-dependent malic enzyme	*mal*	55.0 (0, 74.6)	30.5 (0, 37.8)
Phosphoenolpyruvate carboxykinase	*pepck*	35.6 (16.0, 91.2)	60.7 (53.5, 61.7)
Methylmalonate-semialdehyde dehydrogenase	*msdh*	0 (0, 67.5)	0 (0, 68.9)
Glycolysis			
Pyruvate kinase	*gly1*	0 (0, 44.2)	39.6 (0, 46.9)
Gluconeogenesis			
Phosphoglycerate kinase	*glu1*	33.3 (13.8, 55.9)	19.0 (11.8, 29.1)
Glyceraldehyde-3-phosphate dehydrogenase	*glu2*	26.7 (7.60, 49.5)	13.2 (6.78, 23.5)
Triosephosphate isomerase	*glu3*	22.3 (3.36, 45.26)	9.2 (3.02, 19.5)
Fructose-bisphosphate aldolase	*glu4*	21.5 (2.69, 44.5)	8.62 (2.38, 18.8)
Fructose-1,6-bisphosphatase	*glu5*	21.5 (2.69, 44.5)	8.62 (2.38, 18.8)
Phosphoglucose isomerase	*glu6*	19.2 (0.43, 48.5)	6.52 (0.40, 21.7)
Pentose phosphate pathway			
Glucose-6-phosphate dehydrogenase	*ppp1*	18.7 (0, 48.0)	6.11 (0, 21.3)
6-phosphogluconate dehydrogenase	*ppp2*	0 (0, 8.13)	0.00 (0, 8.03)

Reaction step (s) Net fluxes	Symbol	Molar flux (relative to succinate uptake) Early exponential	Late exponential
Ribulose-phosphate 3-epimerase	*ppp3*	-2.36 (-2.50, 4.22)	-2.10 (-2.23, 3.28)
Ribose 5-phosphate isomerase	*ppp4*	2.36 (2.24, 5.07)	2.1 (1.99, 4.34)
Transketolase- C5/C3 conversion	*ppp5*	-2.36 (-2.50, 4.22)	-2.10 (-2.23, 3.28)
Transketolase- C6/C4 conversion	*ppp6*	1.75 (-1.55, 1.85)	1.58 (-1.11, 1.68)
Transketolase- C7/C5 conversion	*ppp7*	0.61 (-3.94, 0.65)	0.51 (-2.12, 0.54)
Transaldolase- C6/C3 conversion	*ppp8*	0.61 (-3.94, 0.65)	0.51 (-2.12, 0.54)
Transaldolase- C7/C4 conversion	*ppp9*	-0.61 (-0.65, 3.94)	-0.51 (-0.54, 2.12)
Entner-Doudoroff pathway			
6-Phosphogluconate dehydratase	*ed1*	18.7 (0, 39.7)	6.11 (0, 14.5)
2-keto-3-deoxy-6-phosphogluconate aldolase	*ed2*	18.7 (0, 39.7)	6.11 (0, 14.5)
Amino acid synthesis			
Glutamate dehydrogenase	*glt*	21.8 (20.7, 25.1)	20.5 (19.2, 23.0)
Glutamine synthetase	*gln*	2.37 (2.25, 2.51)	2.23 (2.08, 2.36)
Proline synthesis	*pro*	0.62 (0.59, 0.66)	0.59 (0.55, 0.62)
Arginine synthesis	*arg*	0.95(0.90, 1.00)	0.89 (0.83, 0.94)
Aspartate transaminase	*asp*	5.85 (5.55, 11.08)	5.4 (5.13, 8.94)
Asparagine synthase	*asn*	0.81 (0.77, 0.86)	0.76 (0.71, 0.80)
Alanine aminotransferase	*ala*	1.63(1.54, 1.72)	1.53 (1.43, 1.62)
Serine synthesis	*ser*	4.31 (1.74, 4.52)	4.09(2.51, 4.32)
Serine hydroxymethyltransferase	*glc1*	2.52 (-0.01, 2.66)	2.41 (0.81, 2.54)
MEETHF synthesis	*meethf*	1.00 (0.94, 3.56)	0.98 (0.92, 2.65)
Threonine aldolase	*glc2*	0 (0, 5.07)	0 (0, 3.27)
Cysteine synthesis	*cys*	0.81 (0.77, 0.85)	0.76 (0.71, 0.80)
Lysine synthesis	*lys1*	0.98 (0.93, 1.04)	0.92 (0.86, 0.97)
Lysine synthesis	*lys2*	0.98 (0.93, 1.04)	0.92 (0.86, 0.97)
Threonine synthesis	*thr*	1.64 (1.55, 6.76)	1.54 (1.44, 4.86)
Methionine synthesis	*met*	0.36 (0.35, 0.39)	0.34 (0.32, 0.36)
Valine synthesis	*val*	1.13 (1.07, 1.19)	1.06 (0.99, 1.12)
Leucine synthesis	*leu*	1.34 (1.27, 1.42)	1.26 (1.18, 1.33)
Isoleucine synthesis	*ile*	0.78 (0.74, 0.83)	0.73 (0.68, 0.78)

Reaction step (s)		Molar flux (relative to succinate uptake)	
Net fluxes	Symbol	Early exponential	Late exponential
Phenylalanine synthesis	*phe*	0.52 (0.50, 0.55)	0.49 (0.46, 0.52)
Tyrosine synthesis	*tyr*	0.45 (0.43, 0.48)	0.42 (0.40, 0.45)
Tryptophan synthesis	*trp*	0.15 (0.14, 0.15)	0.14 (0.13, 0.15)
Histidine synthesis	*his*	0.26 (0.25, 0.28)	0.25 (0.23, 0.26)
METHF synthesis	*methf*	0.36 (0.35, 0.39)	0.34 (0.32, 0.36)
FTHF synthesis	*fthf*	0.26 (0.25, 0.28)	0.25 (0.23, 0.26)
Metabolic CO_2 output (net)	*co2.out*	246 (238, 250)	257 (248, 263)
PHB synthesis	*accoa1*	4.34 (4.12, 4.59)	4.46 (4.17, 4.73)
Biomass synthesis	*biomass*	3.84 (3.65, 4.06)	3.49 (3.26, 3.69)
Lipid synthesis	*accoa2*	11.5 (10.15, 11.31)	10.2 (9.53, 10.79)
DNA synthesis	*r5p1*	0.20 (0.21, 0.23)	0.20 (0.18, 0.21)
RNA synthesis	*r5p2*	2.30 (2.19, 2.44)	2.03 (1.89, 2.35)
Carbohydrates synthesis	*g6p1*	0.41 (0.39, 0.43)	0.37 (0.34, 0.40)
EPS synthesis	*g6p2*	0.03 (0.03, 0.04)	0.03 (0.03, 0.04)

The fluxes are presented as best-fit estimates calculated using MS measurements from three determinations for both early and late exponential cultures. The 95% confidence limits for the fluxes were calculated using parameter continuation analysis in INCA and presented as (lower bound, upper bound) of the confidence limits. All fluxes were expressed on a molar basis relative to a succinate uptake of 100.

3.13 Statistical analysis of fluxes

INCA performs chi square test to assess the validity of a flux map. Flux solutions provide an acceptable description of the MS measurements if the sum of the squared residual (SSR) lies in the expected range of residuals as defined by the critical chi square values. The final SSR is calculated from the individual SSR associated with the experimentally measured MS data used for flux estimation. The residuals are the differences between the experimental and simulated MS measurements. Table 3.13 shows the SSRs obtained for the flux maps for early and late exponential cultures. The assessment of goodness of fit for the flux maps was performed by the comparison of simulated MS measurements with that of experimentally measured values. This comparison of MS measurements for the early and late exponential flux

maps is shown in Figure 3.28 and Figure 3.29. The simulated and experimentally determined MS measurements for both the flux maps differ from each other, but the extent of variation is no greater than the estimated errors inherent in the MS analysis. There were no obvious inconsistencies between the measured MID of any molecular fragment and the distribution of ^{13}C predicted from the flux map.

Table 3.13 **SSRs obtained for the flux maps of ORS571 at early and late exponential growth stages**

Growth stage for ORS571 cultures	Obtained SSR	Expected SSR range	Degrees of freedom (DOF)	Comment
Early exponential	274.3	263.1 – 360.7	310	Fit accepted
Late exponential	452.3	486.9 – 616.9	550	Fit accepted

The SSR of the flux map for late exponential cultures was lower than the lower limit of the expected SSR range. This indicated that the experimental MS measurements fitted the model better than expected. This may have been due to an over-estimate of the amount of error of 1.1% used for the experimentally determined MS measurements. This meant that the MS measurements actually had an error less than 1.1% and hence the MS measurements produced a better fit to the model than expected.

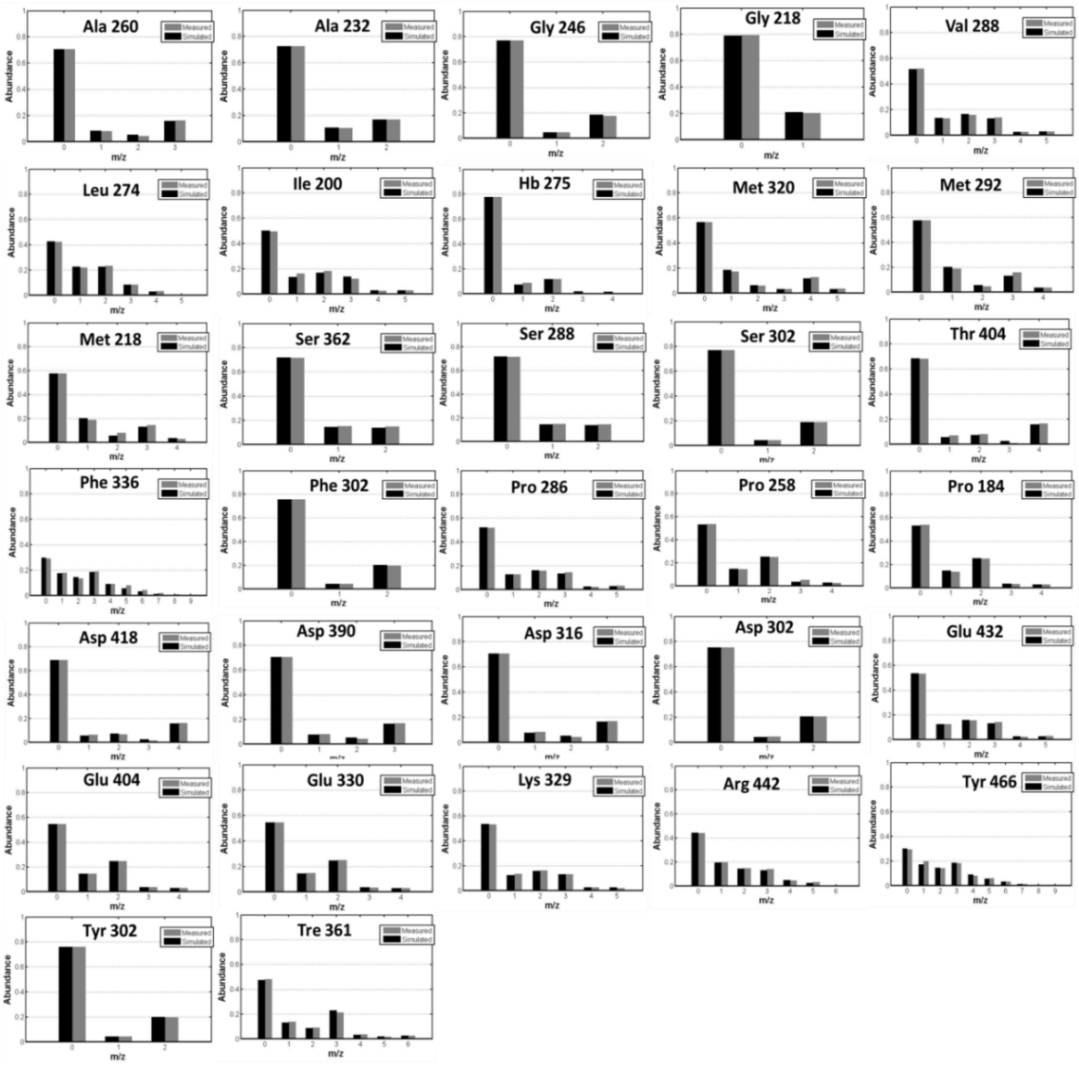

Figure 3.28: **Comparison of the simulated and experimentally measured MS measurements used for flux analysis in ORS571 early exponential cultures**. The simulated (black bars) and measured (grey bars) are plotted with MI on X-axis and abundance of MI on Y-axis. There was no significant difference between the simulated and measured values, which shows the goodness of fit of the flux map. A total of 32 valid MS fragments were used- alanine (Ala 260, Ala 232), glycine (Gly 246, Gly 218), valine (Val 288), leucine (Leu 274), isoleucine (Ile 200), PHB (Hb 275), methionine (Met 320, Met 292, Met 218) serine (Ser 362, Ser 288, Ser 302), threonine (Thr 404), phenylalanine (Phe 336, Phe 302), proline (Pro 286, Pro 258, Pro 184), aspartate (Asp 418, Asp 390, Asp 316, Asp 302), glutamate (Glu 432, Glu 404, Glu 330), lysine (Lys 329), arginine (Arg 442), tyrosine (Tyr 466, Tyr 302) and trehalose (Tre 361).

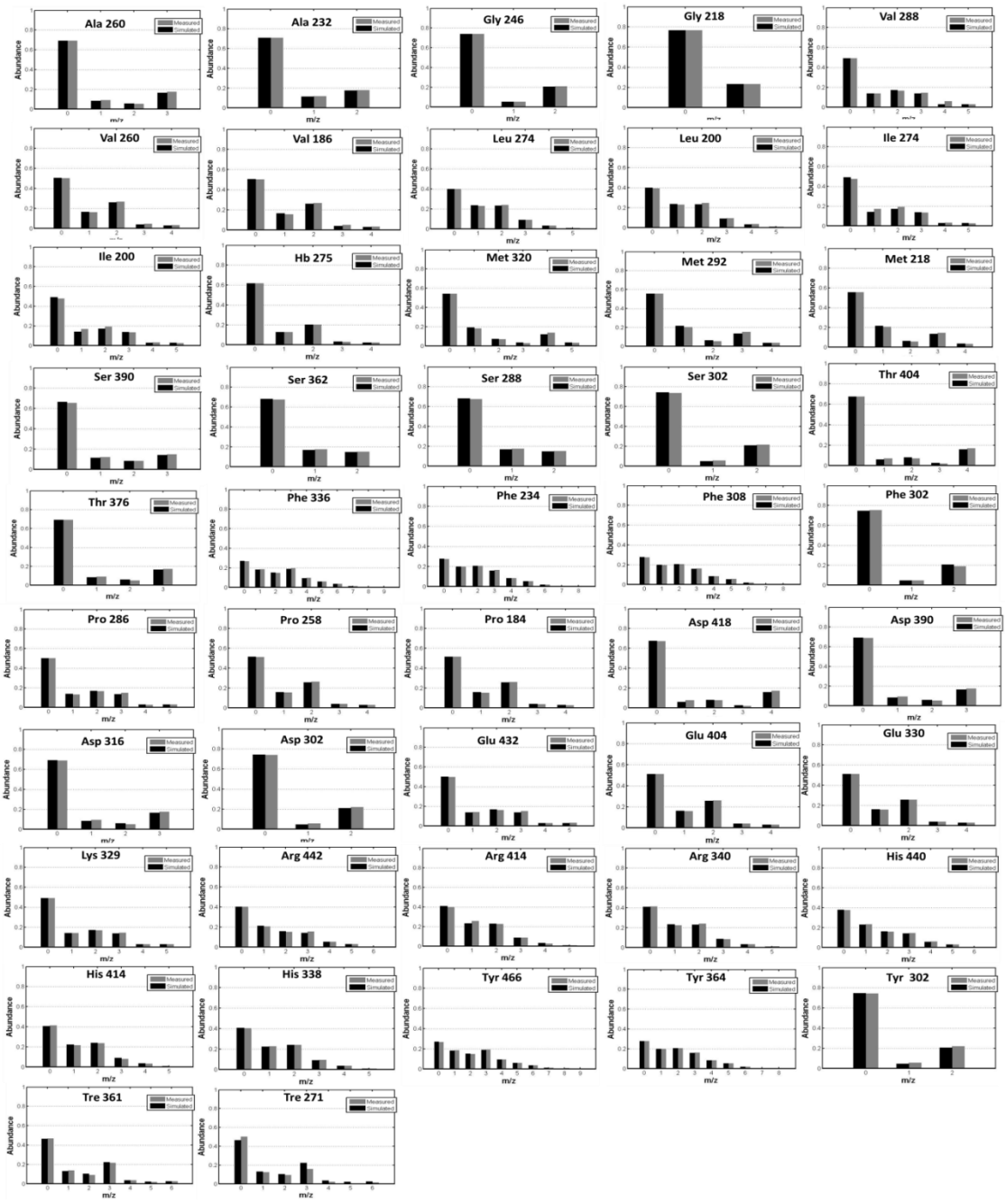

Figure 3.29: **Comparison of the simulated and experimentally measured MS measurements used for flux analysis in ORS571 late exponential cultures**. The simulated (black bars) and measured (grey bars) are plotted with MI on X-axis and abundance of MI on Y-axis. There was no significant difference between the simulated and measured values, which shows the goodness of fit of the flux map. A total of 47 valid MS fragments were used- alanine (Ala 260, Ala 232), glycine (Gly 246, Gly 218), valine (Val 288, Val 260, Val 186), leucine (Leu 274, Leu 200), isoleucine (Ile 274, Ile 200), PHB (Hb 275), methionine (Met 320, Met 292, Met 218) serine (Ser 390, Ser 362, Ser 288, Ser 302),

threonine (Thr 404, Thr 376), phenylalanine (Phe 336, Phe 308, Phe 234, Phe 302), proline (Pro 286, Pro 258, Pro 184), aspartate (Asp 418, Asp 390, Asp 316, Asp 302), glutamate (Glu 432, Glu 404, Glu 330), lysine (Lys 329), arginine (Arg 442, Arg 414, Arg 340), tyrosine (Tyr 466, Tyr 364, Tyr 302) and trehalose (Tre 361, Tre 271).

3.14 Comparison of fluxes

Fluxes were compared based on their nonlinearized 95% confidence limits. Parameter continuation was performed in INCA to calculate the lower and upper bounds of the 95% confidence limits for each flux (Young et al., 2014). The 95% confidence limits were calculated for each of the fluxes by determining the sensitivity of the SSR as a function of the flux value (Antoniewicz et al., 2006). This statistical method was chosen because, linear statistics are inappropriate to analyse statistical significance due to inherent non linearities of the system (Antoniewicz et al., 2006). This method was shown to calculate confidence limits for the non-linear isotopic system accurately and efficiently in comparison to the linearized confidence limits calculated from the local estimates of standard deviations (Antoniewicz et al., 2006). The 95% confidence limits calculated by parameter continuation for a flux under two different conditions shows the statistically acceptable range of values for that flux under the two conditions. For this study, a particular flux was considered to be significantly different, if the confidence limits calculated under the two conditions did not overlap.

The confidence limits for each of the fluxes in early and late exponential cultures of ORS571 overlapped and so, the fluxes were not significantly different. This suggests that there is no significant change in the metabolic behaviour of ORS571 during exponential growth phase. The confidence limits for the flux estimates obtained for early exponential cultures were comparatively wider and less well-defined than that for late exponential cultures, which probably reflects the fewer and generally less

reliable MS measurements available for flux analysis of early exponential ORS571 cultures (section 3.10).

3.15 Analysis of flux distributions

The distribution of fluxes in the metabolic network of ORS571 at early (A) and late (B) exponential growth stages are represented as flux maps in Figure 3.30. The flux maps describe the metabolic behaviour of ORS571 as free-living cultures grown under aerobic, non N_2-fixing conditions. Fluxes of the TCA cycle (*tca1*, *tca2*, *tca3*, *tca4*, *tca5*, *tca6*, *tca7*, *tca8*, *tca9*) were comparatively higher than the other carbon catabolising fluxes of ED (*ed1*, *ed2*), gluconeogenesis (*glu1*, *glu2*, *glu3*, *glu4*, *glu5*, *glu6*) glycolysis (*gly1*) and PPP (*ppp1*, *ppp2*, *ppp3*, *ppp4*, *ppp5*, *ppp6*, *ppp7*, *ppp8*, *ppp9*) pathways. This indicates that the complete TCA cycle is active during aerobic metabolism of ORS571 when grown on succinate as the sole carbon source. Consequently, the flux to overall metabolic CO_2 release was also high. Anaplerotic fluxes *mal* was comparatively higher than *msdh* which confirmed that NAD(P)-ME was the preferred route of malate decarboxylation to AcCoA during aerobic growth. AcCoA was utilised via the TCA cycle and was also used for PHB and lipid synthesis. There was a considerable flux via *pepck* and the PEP synthesized by this pathway was utilised via gluconeogenesis and also to synthesize pyruvate, which produced AcCoA for the TCA cycle. The flux for metabolic CO_2 output, *co_2.out* was comparatively higher than the flux for biomass synthesis, *biomass*. The carbon conversion efficiency (CCE) defined as the proportion of substrate (in this case succinate) converted to biomass was calculated to be 37.4% and 34.3% for early and late exponential cultures. The comparatively low CCE indicates majority of the succinate was utilised for the network reactions during the exponential growth of ORS571 under aerobic conditions.

Flux *glt* for the synthesis of glutamate was observed to be comparatively higher than the fluxes to the rest of the amino acids (*gln*, *pro*, *arg*, *asp*, *asn*, *ala*, *ser*, *glc1*,

meethf, *glc2*, *cys*, *lys1*, *lys2*, *thr*, *met*, *val*, *leu*, *ile*, *phe*, *tyr*, *trp*, *his*); PHB synthesis (*accoa1*); lipid synthesis (*accoa2*); nucleic acid synthesis (*r5p1*, *r5p2*), carbohydrate and EPS synthesis (*g6p1*, *g6p2*).

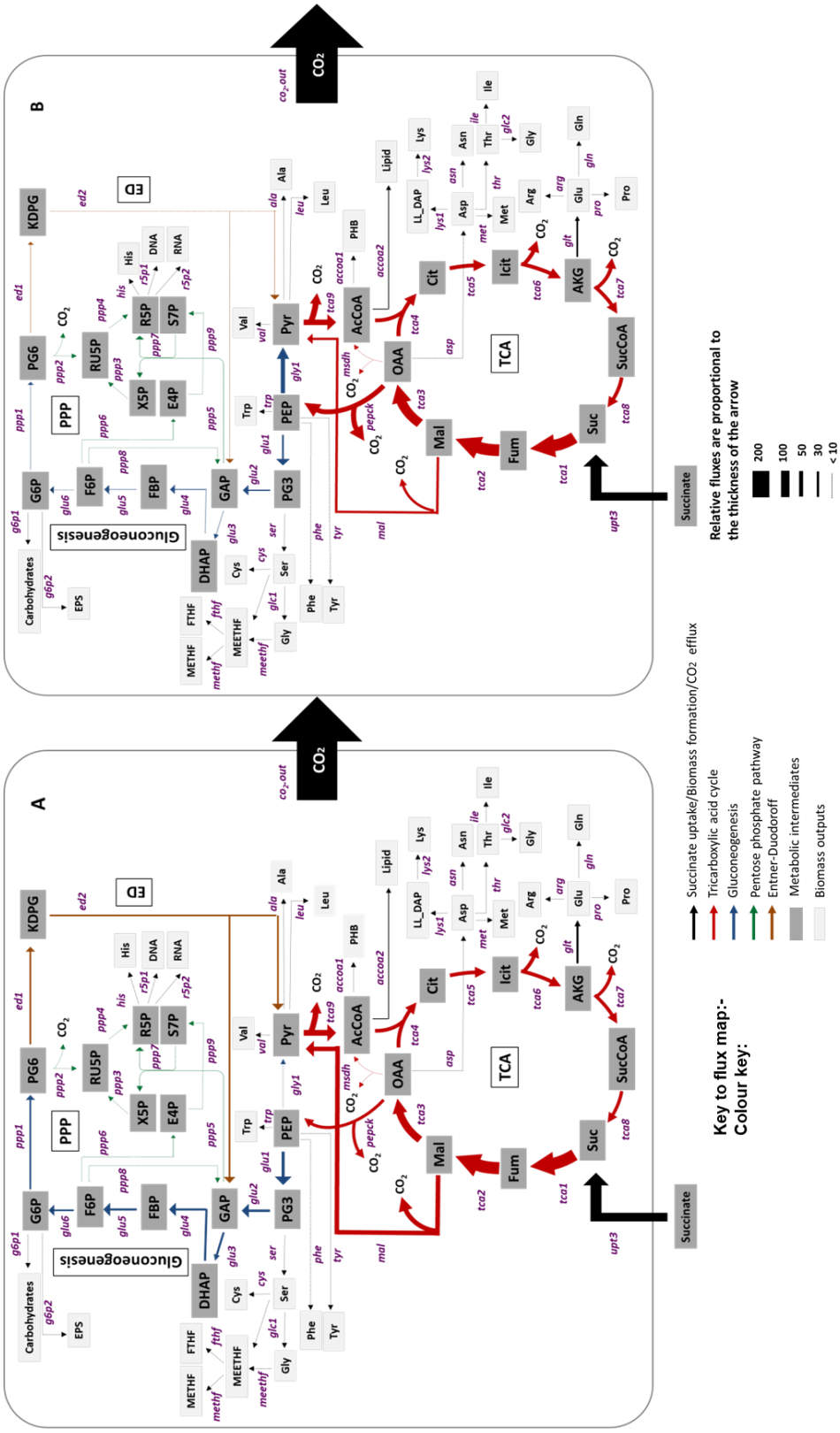

Figure 3.30: **Flux maps of ORS571 cultures at early (A) and late (B) exponential growth stages**. The flux maps represent statistically valid best-fit flux values expressed on a molar basis relative to succinate uptake for early exponential (A) and late exponential (B) cultures. The thickness of the each arrow in the flux maps is proportional to the relative molar flux. Fluxes < 10% of succinate uptake is indicated by dotted arrows. Metabolic intermediates and biomass outputs are shown in rectangular boxes with distinct colour key. The different pathways of the network are specified by colours as described in the colour key. The symbols for fluxes defined in Table 3.12 are shown in *italics*.

3.16 Improvement of poorly defined fluxes

The flux values obtained were either poorly or well defined based on the length of the confidence interval associated with each flux. Fluxes *tca3*, *tca9*, *mal*, *pepck*, *msdh*, *gly1*, *glu1*, *glu2*, *glu3*, *glu4*, *glu5*, *glu6*, *ppp1*, *ed1* and *ed2* obtained for both early and late exponential flux maps had wider confidence limits and were the most poorly defined fluxes in the network. In an attempt to better resolve these fluxes, a labelling experiment was performed in late exponential free-living cultures with 20% [$^{13}C_6$]glucose and 80% unlabelled glucose. The cultures were grown in the presence of unlabelled succinate as ORS571 showed poor growth on glucose as the sole carbon source (section 3.3.3). Two 50 ml late exponential cultures grown with unlabelled succinate (10 mM), one of the cultures supplemented with unlabelled glucose (10 mM) and the other with a mixture of unlabelled and 20% [$^{13}C_6$]glucose (10 mM). However, the cultures grown with [$^{13}C_6$]glucose failed to reach isotopic steady state and the MS measurements obtained from the protein-derived amino acids, trehalose and hydroxybutyrate showed only limited ^{13}C fractional abundance, and hence could not be used to improve the poorly defined fluxes for the gluconeogenesis, ED or PP pathway. The comparison of average ^{13}C fractional abundance in the molecular fragments of the amino acids- alanine, serine, phenylalanine, histidine and tyrosine, from cultures grown with unlabelled glucose, [$^{13}C_6$]glucose and [$^{13}C_4$]succinate is shown in Figure 3.31.

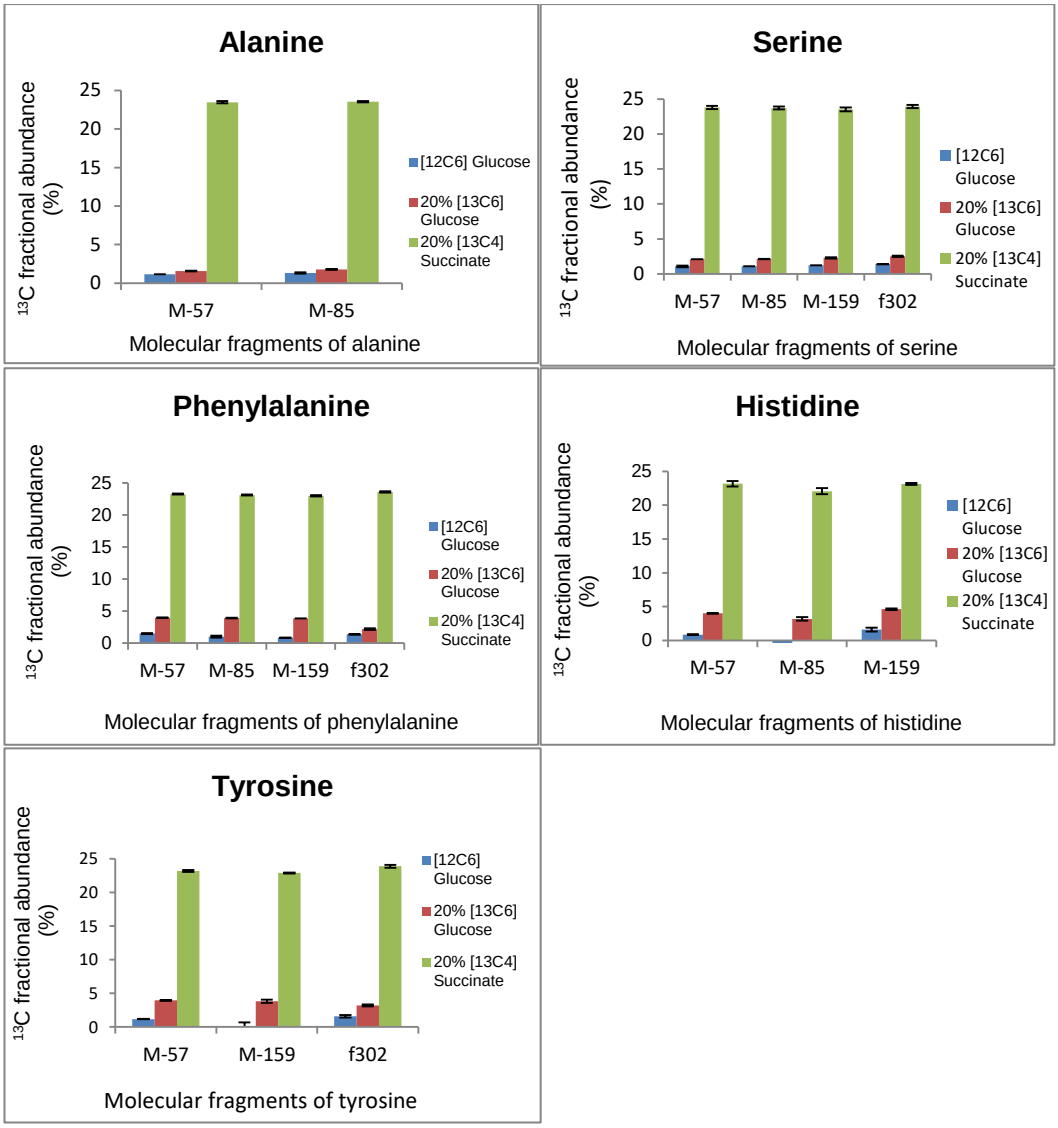

Figure 3.31: **Comparison of average ^{13}C fractional abundance (%) in the amino acids- alanine, serine, phenylalanine, histidine and tyrosine from late exponential cultures grown with unlabelled [$^{12}C_6$]glucose, [$^{13}C_6$]glucose and [$^{13}C_4$]succinate**. The molecular fragments of amino acids used for this analysis are- alanine M-57 (*m/z* 260), M-85 (*m/z* 232); serine M-57 (*m/z* 390), M-85 (*m/z* 362), M-159 (*m/z* 288), f302 (*m/z* 302); phenylalanine M-57 (*m/z* 336), M-85 (*m/z* 308), M-159 (*m/z* 234), f302 (*m/z* 302); histidine M-57 (*m/z* 440),M-85 (*m/z* 412), M-159 (*m/z* 338); tyrosine M-57 (*m/z* 466), M-159, (*m/z* 364), f302 (*m/z* 302). The measurements for unlabelled [$^{12}C_6$]glucose and 20% [$^{13}C_6$]glucose labelling experiments were the mean of 2 individual determinations while the measurements for 20% [$^{13}C_4$]succinate were the mean of 3 determinations ± SD (standard deviation of the mean).

3.17 Co-enzyme analysis

The co-enzyme balances for ATP, NADH, $FADH_2$ and NADPH were calculated for each of the flux maps. Firstly, the reactions in the model that use the co-enzymes were identified (Table 3.14) and the corresponding fluxes were used to calculate the total fluxes for production or consumption of co-enzymes. Co-enzyme specificity of the reactions in the network of ORS571 was confirmed from the information available in the previous literature (Lee et al., 2008) and from KEGG database. The flux values define the direction of these reactions and hence whether a reaction produces or consumes a co-enzyme. The fluxes for co-enzyme utilisation during the synthesis of lipids and nucleic acids were calculated from the amount of their precursor metabolites used for biomass synthesis. Figure 3.32 and Figure 3.33 shows the co-enzyme utilisation (production and consumption) by early and late exponential cultures respectively. Since there were no statistically significant differences between the flux maps obtained for early and late exponential cultures, the minor differences in co-enzyme metabolism reflect the small fluctuations between the flux maps.

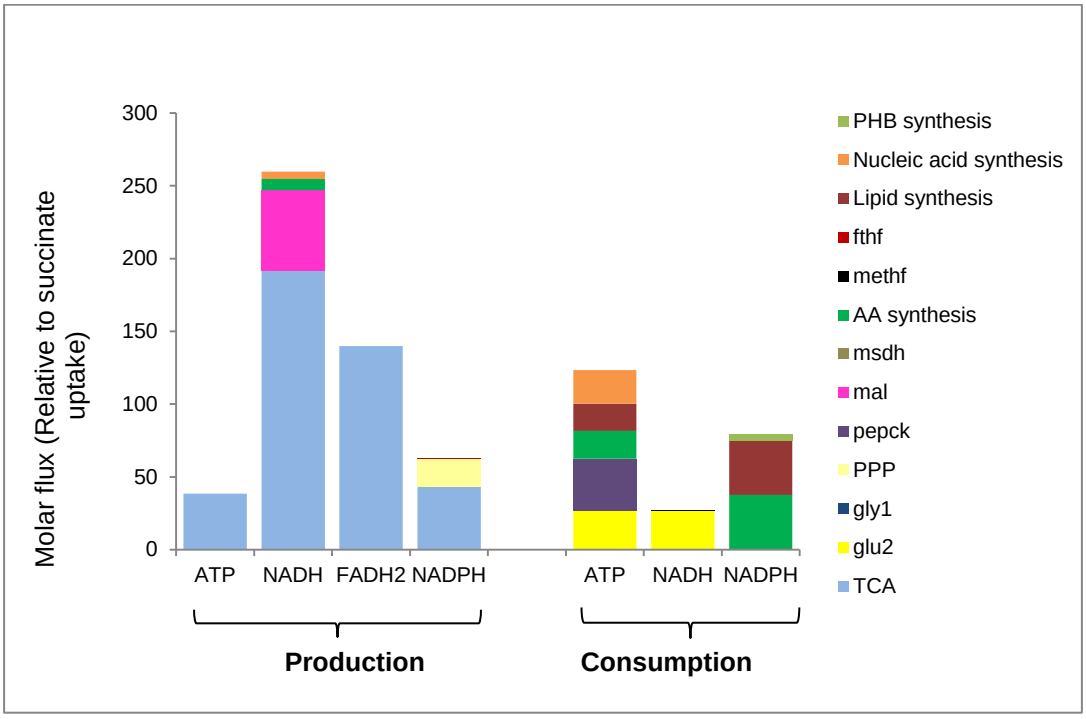

Figure 3.32: **Co-enzyme utilisation in early exponential cultures of ORS571**. The production and consumption of ATP (ATP + GTP), NADH, $FADH_2$ and NADPH by the network was determined from net fluxes in the best-fit flux solution for early exponential cultures shown in Table 3.12. All values are molar fluxes expressed relative to succinate uptake.

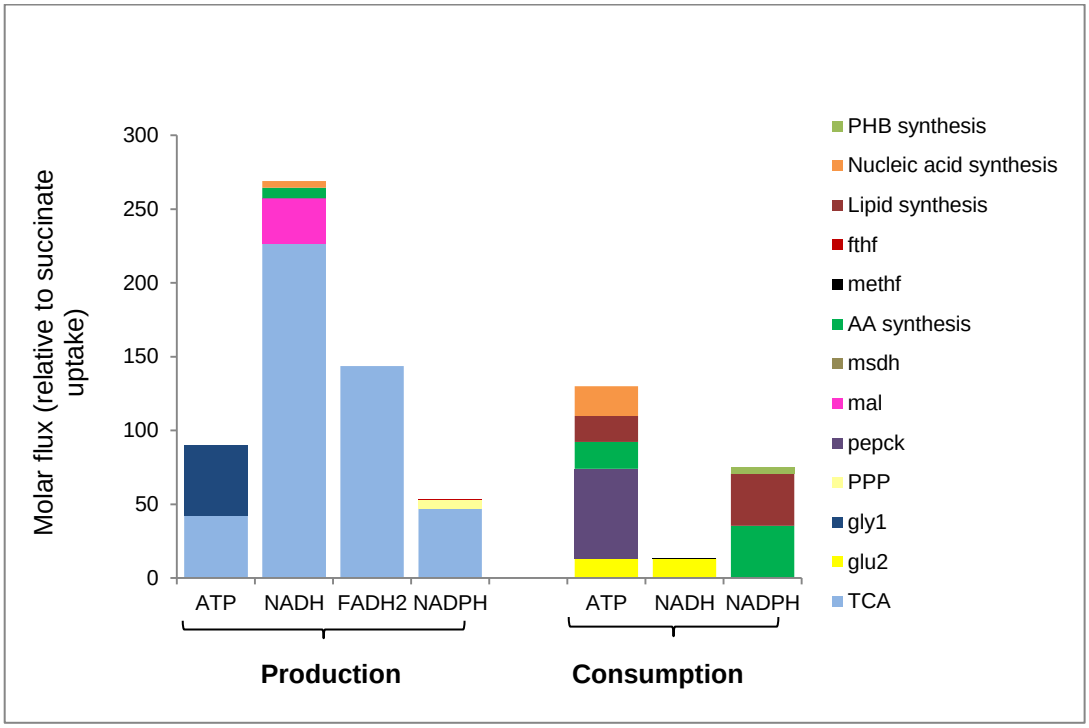

Figure 3.33: **Co-enzyme utilisation in late exponential cultures of ORS571**. The production and consumption of ATP (ATP + GTP), NADH, $FADH_2$ and NADPH by the network was determined from net fluxes in the best-fit flux solution for early exponential cultures shown in Table 3.12. All values are molar fluxes expressed relative to succinate uptake.

The majority of the ATP in the early exponential cultures was produced by *tca8* flux of the network, while in the late exponential cultures both *gly1* and *tca8* produced 53% and 47% of the total ATP in the network. More than 50% of the ATP (51% for early exponential and 57% for late exponential cultures) was used by the reactions *glu2* and *pepck*, and the remaining ATP was used for amino acid, lipids and nucleic acid production.

ORS571 has been previously reported to possess a $NADP^+$-dependent isocitrate dehydrogenase (Tsukada et al., 2009); based on this, the *tca6* reaction of the TCA cycle was considered to produce NADPH and a large proportion of the NADPH in the network was produced by *tca6* – 70% in early exponential and 88% in the late exponential cultures. The remaining NADPH was produced by *ppp1* and *ppp2* reactions of the oxidative PPP reaction (30% in early exponential cultures and 11% in the late exponential cultures). Out of the total NADPH consumed, amino acid and lipid synthesis reactions used the majority (84%) and the remaining was used for PHB synthesis.

The majority of NADH was produced by *tca2*, *tca7*, *tca8* and *tca9* reactions of the TCA cycle (74% in early and 84% in late exponential cultures) and the remainder by *mal, msdh, glc2, ser, leu, tyr, his* and nucleic acid synthesis reactions. Co-enzyme $FADH_2$ was produced solely by the *tca1* reaction of the network. Out of the total NADH consumed, majority was used by *glu2* reaction in the network.

For both early and late exponential cultures, this analysis showed that the total ATP and NADPH consumed was greater than that produced by the network reactions. However, the total NADH and $FADH_2$ produced was greater than that consumed by the network reactions. Therefore, it is likely that the excess NADH and $FADH_2$ produced by the network fluxes can be used to synthesize ATP via oxidative phosphorylation to achieve the additional ATP required for network reactions and biomass production. Also, it is probable that, via transhydrogenase reactions, the excess NADH can be used to produce the NADPH required for biomass production.

Co-enzyme analysis of the early and late exponential ORS571 cultures was limited to the reactions specified in the models. Therefore, this analysis does not show either the production of co-enzymes by oxidative phosphorylation and transhydrogenase reactions, or the utilisation of co-enzymes by functions related to

system maintenance. In other work, it was reported that ATP was required to meet the growth-associated and non-growth-associated maintenance costs in microbial systems (Feist AM, et al., 2007; Neidhart et al., 1990). Also, in heterotrophic Arabidopsis cultures, both ATP and NADPH were reported to support transport costs of the cell associated with transporting ions and metabolites, and to enable processes associated with maintenance costs, such as macromolecule turnover and recycling of unwanted metabolites, (Cheung et al., 2013). Additionally, it has been hypothesized that NADH can be used to support cellular activities such as growth and cell-division (Terpolilli et al., 2016). Therefore, it is expected that the excess NADH and $FADH_2$ produced by the network reactions could be used to synthesize co-enzymes- ATP and NADPH to support maintenance-associated activities of the system.

Table 3.14: **Reactions used for calculation of co-enzyme utilisation in ORS571**

Fluxes	Reactions	Co-enzymes produced	Co-enzymes consumed
upt1	Suc_$^{13}C_4$ -> Suc_in	-	-
upt2	Suc_nat -> Suc_in	-	-
upt3	Suc_in -> Suc	-	-
tca1	Suc + FAD^+ -> Fum + $FADH_2$	1 $FADH_2$	-
tca2	Fum + H_2O <-> Mal	-	-
tca3	Mal + NAD^+ -> OAA + NADH + H^+	1 NADH	-
tca4	OAA + AcCoA + H_2O -> Cit + HsCoA + H^+	-	-
tca5	Cit + H_2O -> Icit	-	-
tca6	Icit + NADP+ -> AKG + CO2 + NADPH	1 NADPH	-
tca7	AKG + NAD+ + CoA -> SucCoA + CO_2 + NADH	1 NADH	-
tca8	SucCoA + GDP + Pi -> Suc + GTP	1 GTP	-
tca9	Pyr + CoA + NAD+ -> AcCoA + CO_2 + NADH	1 NADH	-
mal	Mal + NAD+ -> Pyr + CO_2 + NADH	1 NADH	-
pepck	PEP + CO_2 +ADP <- OAA + ATP	-	1 ATP
msdh	OAA + NAD^+ -> AcCoA + CO_2 + CO_2 + NADH	1 NADH	-
gly1	PEP + ADP + Pi -> Pyr + ATP	1 ATP	-

Fluxes	Reactions	Co-enzymes produced	Co-enzymes consumed
glu1	PEP + H_2O <-> PG3	-	-
glu2	PG3 + ATP + NADH -> GAP + ADP + NAD^+	-	1 ATP, 1NADH
glu3	GAP <-> DHAP	-	-
glu4	DHAP + GAP <-> FBP	-	-
glu5	FBP + H_2O -> F6P	-	-
glu6	F6P <-> G6P	-	-
ppp1	G6P + $NADP^+$ -> PG6 + NADPH	1 NADPH	-
ppp2	PG6 + $NADP^+$ -> Ru5P + CO_2 + NADPH	1 NADPH	-
ppp3	Ru5P <-> X5P	-	-
ppp4	Ru5P <-> R5P	-	-
ppp5	X5P <-> GAP + EC2	-	-
ppp6	F6P <-> E4P + EC2	-	-
ppp7	S7P <-> R5P + EC2	-	-
ppp8	F6P<-> GAP + EC3	-	-
ppp9	S7P<-> E4P + EC3	-	-
ed1	PG6 + H_2O -> KDPG	-	-
ed2	KDPG -> Pyr + GAP	-	-
glt	AKG + NH_4 + NADPH -> Glu + NADP + H_2O + ADP	-	1 NADPH
gln	Glu + NH_4 + ATP -> Gln + ADP + Pi	-	1 ATP
pro	Glu + ATP +2NADPH -> Pro + 2NADP+ + ADP	-	1 ATP, 2 NADPH
arg	Glu + CO_2 + Gln + Asp + AcCoA + 5ATP + NADPH -> Arg + AKG + Fum + Ac + 5ADP + $1NADP^+$	-	5 ATP, 1 NADPH
asp	OAA + Glu -> Asp + AKG	-	-
asn	Asp + 2ATP + NH_4 -> Asn + 2ADP	-	2 ATP
ala	Pyr + Glu -> Ala + AKG	-	-
ser	PG3 + Glu + NAD^+ -> Ser + AKG + NADH	1 NADH	-
glc1	Ser + THF <-> Gly + MEETHF	-	-
meethf	Gly + THF + NAD <-> CO2 + MEETHF + NADH + NH_4	-	-
glc2	Thr + NAD -> Gly + AcCoA + NADH	1 NADH	-
cys	Ser + AcCoA + 3ATP + 4NADPH + SO_4 -> Cys + Ac + 3ADP + $4NADP^+$	-	3 ATP, 4 NADPH

Fluxes	Reactions	Co-enzymes produced	Co-enzymes consumed
lys1	Asp + Pyr + Glu + SucCoA + ATP + 2NADPH -> LL_DAP + AKG + Suc + $2NADP^+$ + ADP	-	1 ATP, 2 NADPH
lys2	LL_DAP -> Lys + CO_2	-	-
thr	Asp + 2NADPH + 2ATP -> Thr + 2ADP + 2NADP+	-	2 ATP, 2 NADPH
met	Asp + METHF + Cys + SucCoA + ATP + 2NADPH -> Met + Pyr + Suc + ADP + $2NADP^+$	-	1 ATP, 2 NADPH
val	Pyr + Pyr + Glu + NADPH -> Val + CO2 + AKG + $NADP^+$	-	1 NADPH
leu	AcCoA + Pyr + Pyr + Glu + NADPH + NAD^+ -> Leu + CO2 + CO2 + AKG + $NADP^+$ + NADH	1 NADH	1 NADPH
ile	Thr + Pyr + Glu + NADPH -> Ile + CO2 + AKG + NH_4 + $NADP^+$	-	1 NADPH
phe	PEP + PEP + E4P + Glu + ATP + NADPH -> Phe + CO2 + AKG + ADP + $NADP^+$	-	1 ATP, 1NADPH
tyr	PEP + PEP + E4P + Glu + ATP + NADPH + NAD^+ -> Tyr + CO_2 + AKG + ADP +$NADP^+$ + NADH	1 NADH	1 ATP, 1 NADPH
trp	Ser + R5P + PEP + E4P + PEP + Gln + 3ATP + NADPH -> Trp + CO2 + GAP + Pyr + Glu + 3ADP + $NADP^+$	-	3 ATP, 1 NADPH
his	R5P + FTHF + Gln + Asp + 5ATP + $2NAD^+$ -> His + AKG + Fum + 5ADP + 2NADH	2 NADH	5 ATP
methf	MEETHF + NADH -> METHF + NAD^+	-	1 NADH
fthf	MEETHF + $NADP^+$ -> FTHF + NADPH	1 NADPH	-
co_2.out	CO_2 -> CO_2_ext	-	-
accoa1	AcCoA + AcCoA + NADPH -> PHB + 2CoA + $NADP^+$	-	1 NADPH
Lipid synthesis	7AcCoA + 6ATP + 12NADPH -> LPS + 6ADP + $12NADP^+$	-	6 ATP, 12 NADPH
Lipid synthesis	9AcCoA + 8ATP + 16NADPH -> Phospholipid + 8ADP $^+$ $16NADP^+$	-	8 ATP, 16 NADPH
Nucleic acid synthesis	R5P + 4ATP +$4NH_4$ -> IMP + 4ADP	-	4 ATP
Nucleic acid synthesis	IMP + GTP + NH_4 -> AMP + GDP	-	1 GTP
Nucleic acid synthesis	IMP + NAD+ + ATP + NH_4 -> GMP + NADH + ADP	1 NADH	1 ATP
Nucleic acid synthesis	carbamoyl phosphate+ 3ATP + HCO_3^- + R5P + $2NH_4$ -> UMP + NADH + 3ADP	1 NADH	3 ATP
Nucleic acid synthesis	UTP + NH_4 + ATP + NH_4 -> CTP + ADP	-	1 ATP
Nitrogen fixation	N_2 + $8H^+$ + $8e^-$ + 16ATP -> $2NH_3$ + H_2 + 16ADP + 16Pi		8 NADPH, 16ATP
Oxidative phosphorylation	NADH + ½ O2 → 3 ATP	3 ATP	1 NADH

Fluxes	Reactions	Co-enzymes produced	Co-enzymes consumed
Oxidative phosphorylation	FADH2 + ½ O2 → 2 ATP	2 ATP	1FADH2
Transhydrogenase	NADH -> NADPH	1 NADPH	1 NADH

3.18 Discussion

^{13}C-MFA is a powerful tool to measure the system-wide intracellular flux distributions which provides an understanding of the metabolic behaviour of the system under specific conditions of growth, nutrition and environment (Wiechert, 2001; Choudhary et al., 2011). The study presented in this chapter uses ^{13}C-MFA to produce flux maps showing metabolic behaviour of the diazotroph, ORS571. The growth conditions established in this chapter for ORS571 free-living cultures (growth temperature and carbon substrate), was a pre-requisite to perform steady state ^{13}C-MFA of ORS571. The growth conditions established in this chapter will also be used in the subsequent chapters to maintain consistency in the experimental design that shall allow comparison of flux maps. This study established that di-carboxylic acids are the preferred carbon source for free-living cultures. Notably, ORS571 showed poor growth on sugars- glucose and inositol, when supplied as the sole carbon source thus confirming previous studies which reported poor growth of ORS571 on glucose (Kitts et al., 1989; Lee et al., 2008; Donald & Ludwig, 1984). ORS571 was auxotrophic for the vitamin nicotinic acid in minimal media which agrees with the observations as reported in Dreyfus et al. (1983). The biomass compositions measured at early and late exponential growth stages, were not significantly different thereby establishing that biomass production was not altered during exponential growth and implying that the system was at metabolic steady state over this phase of the culture cycle. Protein constituted the major proportion of the dry weight of cells, while the other substantial components were DNA, RNA, lipids, carbohydrates, EPS and PHB. There was also a minor

proportion of the biomass composition, unaccounted for by this analysis, and this was assumed to be mainly cell wall components and mineral salts. The biomass measurements were used to formulate a reaction defining biomass production which was used to constrain the ORS571 metabolic model. Labelling experiments performed in early and late exponential cultures using 20% [$^{13}C_4$]succinate produced ^{13}C enrichment in the protein-derived amino acids, which confirmed the isotopic steady state of ORS571 during exponential growth phase. The MS measurements from labelling experiments, biomass measurements and the metabolic model developed for this study enabled the generation of flux maps for early and late exponential cultures of ORS571 using the approach of ^{13}C-MFA and the software, INCA. The assessment of goodness of fit for the flux maps confirmed statistical validation of the flux maps. The flux maps showed quantitative fluxes in ORS571 at early and late exponential growth stages and the flux maps were not significantly different. This indicates that the distribution of metabolic fluxes in ORS571 was not altered during exponential growth phase of the cultures.

The fluxes through the TCA cycle were comparatively higher than the other central carbon catabolising pathways, which confirm it to be actively involved during aerobic growth of ORS571 on succinate. From the current and previous studies, it was observed that ORS571 prefers di-carboxylic acids as a carbon source to sugars (Dreyfus et al., 1988). These results agree with the higher fluxes through the TCA cycle previously reported for the Rlv3841 growing aerobically on succinate as the carbon source (Terpolilli et al., 2016). Co-enzyme analysis done for this study, showed the TCA cycle reactions *tca1*, *tca2*, *tca6*, *tca7*, *tca8* and *tca9* was the major source for production of ATP, NADH, $FADH_2$ and NADPH by the network, which reflected the comparatively higher fluxes through the TCA cycle.

The flux maps for ORS571 showed restricted fluxes through glucose catabolizing pathways (ED, PPP, and gluconeogenesis). This was in contrast to Rlv3841, where

higher fluxes were reported via gluconeogenesis pathway (Terpolilli et al., 2016). A large flux through the anaplerotic reaction catalysed by NAD(P)-ME was also observed for ORS571 which suggests the pathway was active during aerobic metabolism. The flux for the overall metabolic CO_2 output was comparatively higher than the biomass synthesis, which indicates that the majority of the carbon substrate was consumed by the network reactions to support metabolism in aerobic ORS571.

3.19 Conclusion

This study establishes the experimental methodology for performing steady state ^{13}C-MFA in ORS571 to produce flux maps describing the metabolic phenotype of ORS571. The flux maps obtained were statistically robust and represent the distribution of carbon fluxes in ORS571 during exponential growth under aerobic conditions. There was no significant difference in the distribution of fluxes between early and late exponential growth stages, although those for late exponential growth stage were generally statistically more reliable due to the greater range and precision of MID measurements. In view of this, I decided to use late exponential cultures for all subsequent labelling experiments and flux analyses which are described in the ensuing chapters. In summary, the results presented in this chapter establish a robust protocol for the analysis of intermediary metabolism in free-living *A. caulinodans* and a platform for investigating its metabolic phenotype under different growth conditions. This will be exploited in the next chapter for the comparison of metabolic behaviour of ORS571 during aerobic, micro-aerobic and nitrogen-fixing growth conditions.

4. Metabolic behaviour of ORS571 during N_2 fixation

4.1 Introduction

ORS571 is a diazotroph able to fix atmospheric N_2 as a free-living culture in the absence of a nitrogen source in the growth media at a DOT of ≤ 10μM (Pauling et al., 2001). This ability of ORS571 makes it an ideal model system to study the metabolic behaviour during N_2 fixation using ^{13}C-MFA under laboratory conditions. The nitrogenase enzyme is irreversibly inhibited by O_2 and so a low O_2 or micro-aerobic environment is required to prevent inhibition of nitrogenase activity (Bergersen et al., 1986). The concentration of O_2 inside *S. rostrata* nodules, which support N_2 fixation activity of ORS571 bacteroids, was reported to be 10-20 nM (Pauling et al., 2001). The aim of the work described in this chapter was to characterise the anticipated metabolic adjustments needed to support growth and N_2 fixation under these low O_2 conditions.

A transcriptomics analysis of the free-living ORS571 grown in rich and minimal media and bacteroids isolated from the host plant has been previously reported by Tsukada et al., 2009. It was suggested that the acquisition and metabolism of a variety of sulphur and carbon sources supported higher rates of N_2 fixation by ORS571 bacteroids in the stem nodules. In a different study, the genes and enzymes that were essential for N_2 fixation in ORS571 free-living cultures and bacteroids were identified (Suzuki et al., 2007). These studies provide information about the genetic elements required for N_2 fixation in ORS571 but how these genetic elements co-operate with each other to support N_2 fixation in not clear. The activities of the pathways involving the essential genes identified, and their interactions with different parts of the metabolic network during N_2 fixation, need to be understood.

In other diazotrophic bacteria, like *Klebsiella* and *Azotobacter*, cytochrome d (cyt*d*) oxidase was reported to be essential for N_2 fixation under aerobic and micro-aerobic

conditions (Hill et al, 1990; Kelly et al., 1990; Smith et al., 1990). But ORS571 cyt*d* mutants retained their N_2 fixation ability at reduced rates under both free-living and symbiotic conditions (Kitts & Ludwig, 1994). Additionally an alternative cytochrome c oxidase was reported to be active during diazotrophic growth at a DOT ranging from 0.5 to 3% but not during aerobic growth of ORS571 (Pronk et al., 1993). Aerobic growth in ORS571 can be sustained by quinol oxidases alone but growth during N_2 fixation required both quinol and cytochrome oxidases (Kitts & Ludwig, 1994). Unlike other rhizobia, the ability of ORS571 to adapt and fix N_2 under low O_2 conditions was conferred by its flexibility to alter respiratory terminal oxidase composition in response to changing O_2 concentrations (Kitts & Ludwig, 1994). Since there are adaptations in the energy metabolism of ORS571 during diazotrophic growth, it is likely that there would be changes in the manner of carbon utilization via the central metabolic pathways as well. During N_2 fixation, metabolism of ORS571 has to adjust to the low O_2 environment and to the change in nitrogen supply. Identification of these metabolic adjustments will enhance our understanding of how ORS571 metabolic network supports carbon and co-enzyme requirements for its nitrogenase activity in addition to growth, biomass synthesis and other cellular functions.

To identify the metabolic adjustments in N_2-fixing ORS571, the strategy was to compare the metabolic network fluxes by conducting ^{13}C-MFA under three conditions: aerobic (21% O_2), micro-aerobic (3% O_2) free-living cultures grown with NH_4Cl as nitrogen source, and micro-aerobic (3% O_2) free-living cultures grown with atmospheric di-nitrogen as the nitrogen source (Figure 4.1). The comparison of fluxes obtained under aerobic and micro-aerobic conditions should reveal the metabolic adjustments in ORS571 that occur due to the shift to the low O_2 environment. The comparison of fluxes obtained under micro-aerobic and N_2-fixing conditions should reveal the metabolic adjustments in ORS571 that are specifically associated with N_2 fixation.

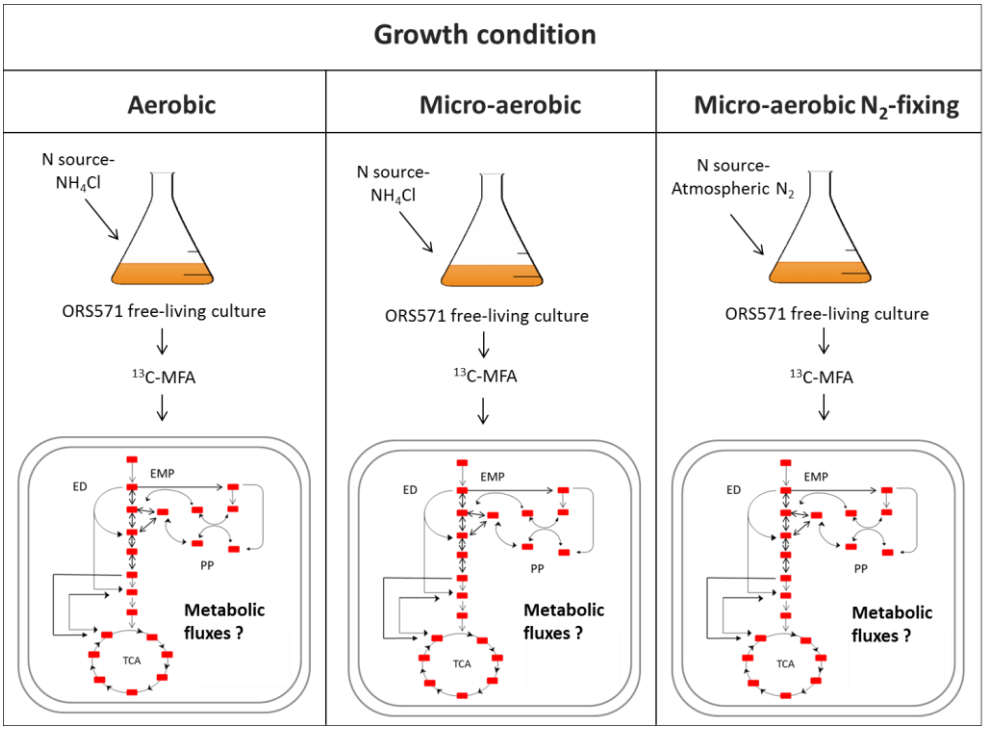

Figure 4.1: **Strategy to study the metabolic adjustments in ORS571 required during N_2fixation**

4.2 Establishment of micro-aerobic growth conditions with atmospheric N_2 as the nitrogen source

The micro-aerobic environment for growing ORS571 free-living cultures with atmospheric N_2 as the sole nitrogen source was established using the experimental set up described in section 2.4.2. A range of micro-aerobic conditions with O_2 levels of 1-6% was maintained inside the micro-aerobic chamber and the level of N_2 were adjusted accordingly. The growth curves obtained under these micro-aerobic conditions are shown in Figure 4.2.

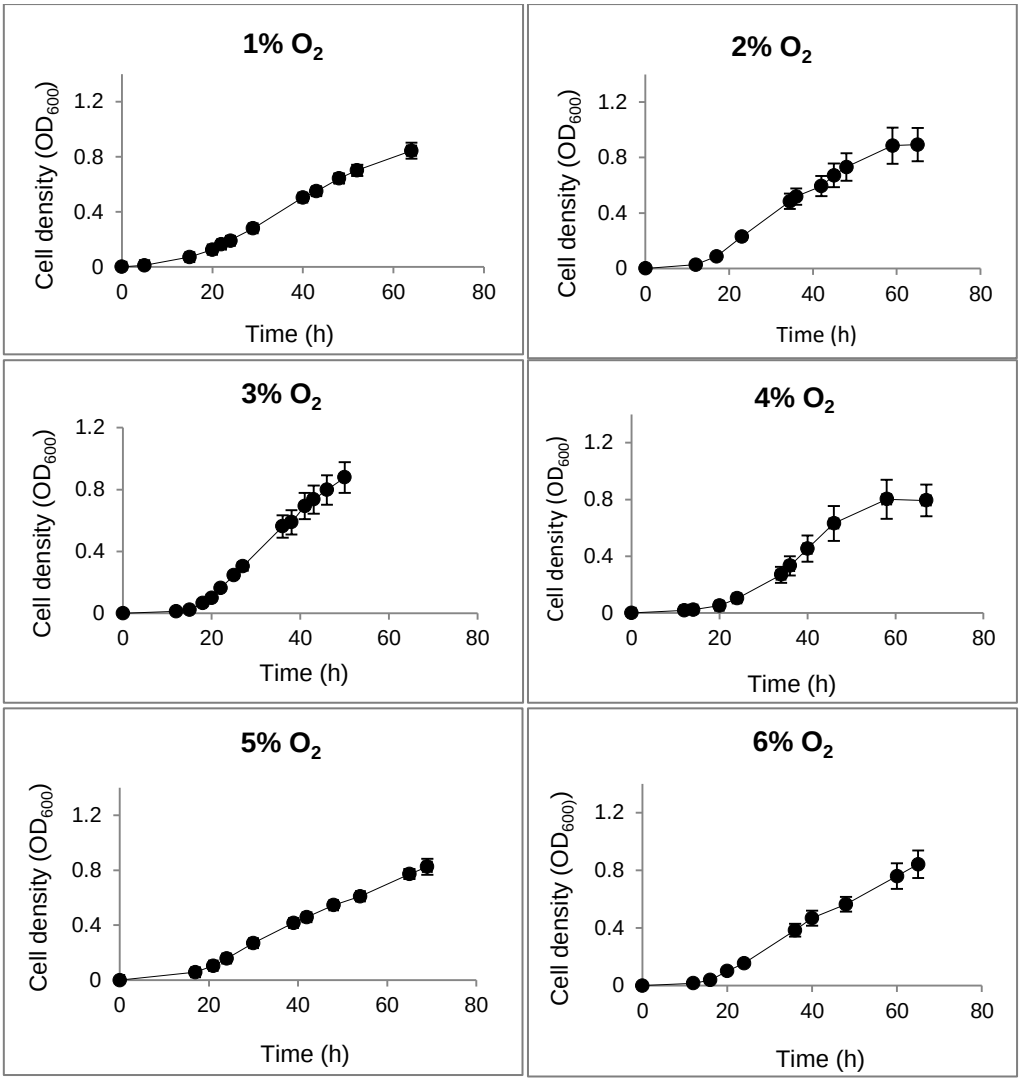

Figure 4.2: **Effect of O_2 concentration on growth of N_2-fixing ORS571 under micro-aerobic condition**. The growth of cultures was monitored by measuring the absorbance of the cultures at 600 nm (OD_{600}). Values are the mean ± SEM from three biological replicates.

Free-living cultures were able to grow and utilize atmospheric N_2 as the nitrogen source under micro-aerobic conditions. The growth rates (appendix Figure A31) and doubling times of ORS571 (Figure 4.3) under the various micro-aerobic conditions was calculated from the growth curves (appendix A30) as described in section 2.20. The comparison in Figure 4.3 confirms N_2-fixing cultures growing at 3% O_2 concentration to exhibit the least doubling time of 6.29 h ± 0.33.

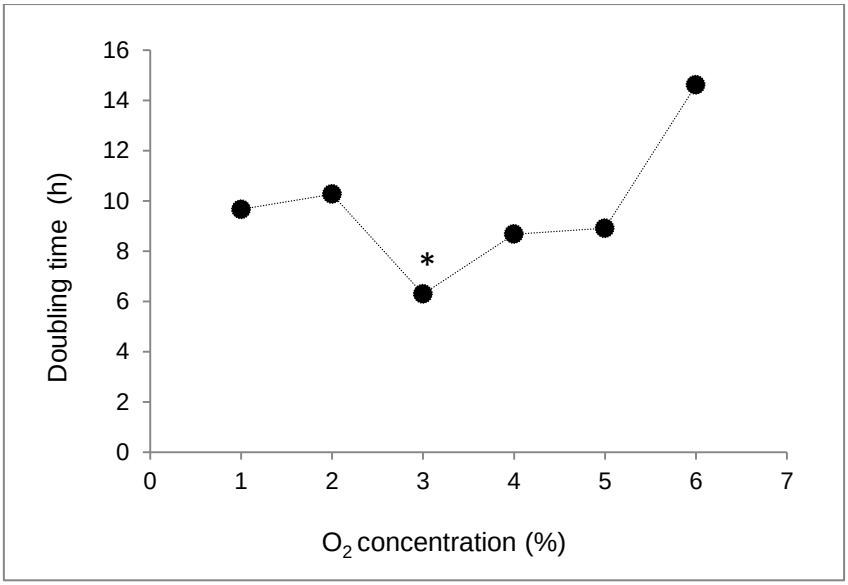

Figure 4.3: **Effect of O_2 on the doubling time of N_2-fixing ORS571 cultures.** The doubling time of ORS571 micro-aerobic cultures at 3% O_2 was significantly lower than observed for the other O_2 concentrations as determined by t-test * (P value < 0.05). Values are the mean ± SEM from three biological replicates.

The nitrogenase activity of the free-living cultures was measured using ARA under the micro-aerobic conditions as described in section 2.7.1. The N_2 fixation rate expressed in terms of the amount of C_2H_4 produced per hour per OD_{600} of cells was maximum at 3% O_2, 0.5 h after C_2H_2 incubation (Figure 4.4).

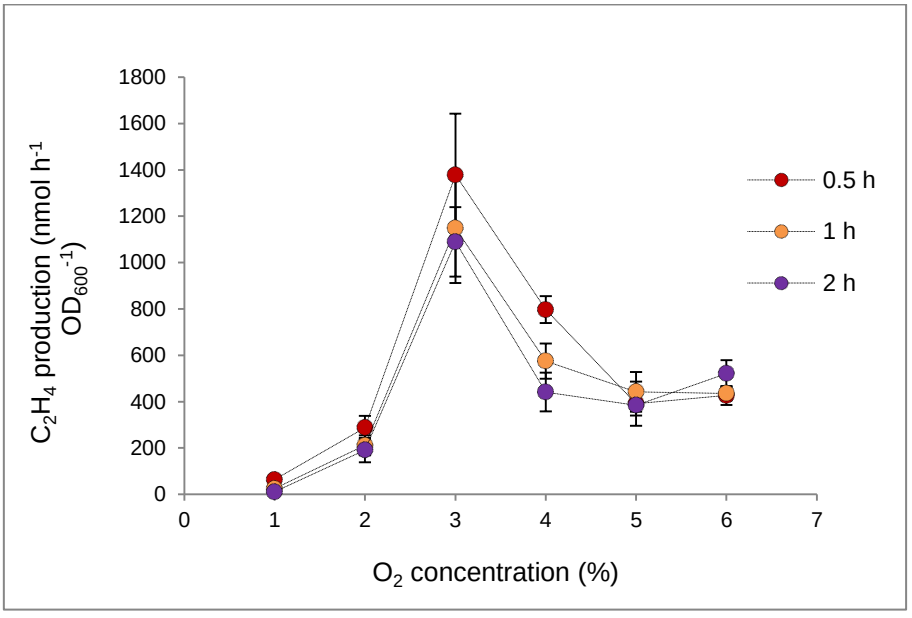

Figure 4.4: **Effect of O_2 concentration on the nitrogenase activity of ORS571 cultures.** The amounts of ethylene (C_2H_4) produced by the nitrogenase actvities of the cultures was measured at 0.5 h, 1 h and 2 h after adding acetylene (C_2H_2). Values are the mean ± SEM from three biological replicates.

Subsequently 3% O_2 was chosen for ^{13}C-MFA of ORS571 under micro-aerobic conditions since N_2-fixing free-living cultures showed the fastest growth with the shortest doubling time and maximum N_2 fixation at 3% O_2.

4.3 Establishment of micro-aerobic growth with NH_4Cl as the nitrogen source

Free-living cultures were grown in the bioreactors with NH_4Cl as the nitrogen source under the micro-aerobic conditions established in section 4.2. The doubling time of the cultures was 3.31 h ± 0.09 and no nitrogenase activity was detectable in these cultures (Figure 4.5).

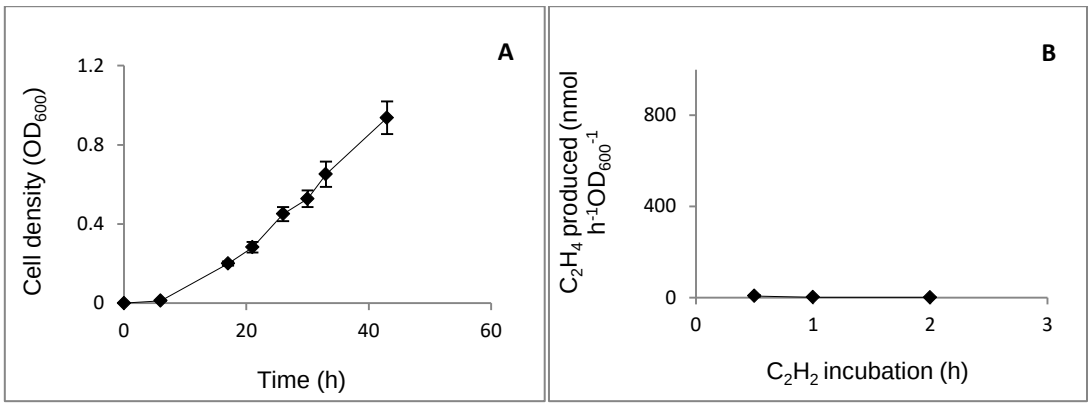

Figure 4.5: **Growth and nitrogenase activity of micro-aerobic ORS571 cultures grown on NH_4Cl as a nitrogen source**. Values are the mean ± SEM from three biological replicates.

4.4 Biomass composition of ORS571 under micro-aerobic conditions

The amount of protein, lipid, RNA, DNA, PHB, carbohydrates and EPS in ORS571 cultures grown under micro-aerobic conditions was determined using established methods (section 2.8). For micro-aerobic cultures, whether grown with NH_4Cl or N_2 as the nitrogen source, PHB and protein constituted the largest proportion of the cell dry

weight followed by RNA, carbohydrate and lipids with DNA and EPS as minor components (Figure 4.6).

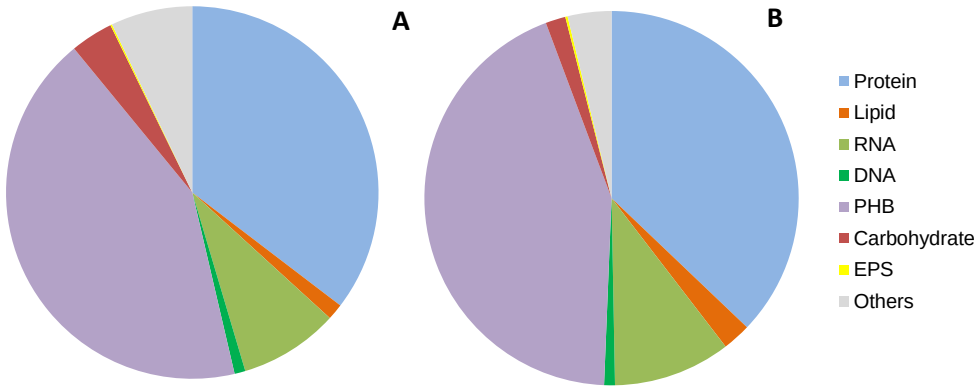

Figure 4.6: **Biomass composition of ORS571 under micro-aerobic conditions.** Cultures were grown with NH_4Cl (A) and N_2 (B) as the nitrogen source. The measurements for protein, lipid, RNA, DNA, PHB, carbohydrates and EPS are expressed as percentage of dry cell weight. Values are the mean from three biological replicates.

4.5 Changes in growth and biomass synthesis during micro-aerobic conditions

The growth characteristics of ORS571 were compared between aerobic and micro-aerobic conditions (Figure 4.7). ORS571 cultures showed slower growth under micro-aerobic conditions with a longer doubling time in comparison with the cultures grown under aerobic conditions. Additionally, N_2-fixing ORS571 free-living cultures showed even slower growth, with a significantly higher doubling time, when compared to the micro-aerobic cultures grown with NH_4Cl as the nitrogen source.

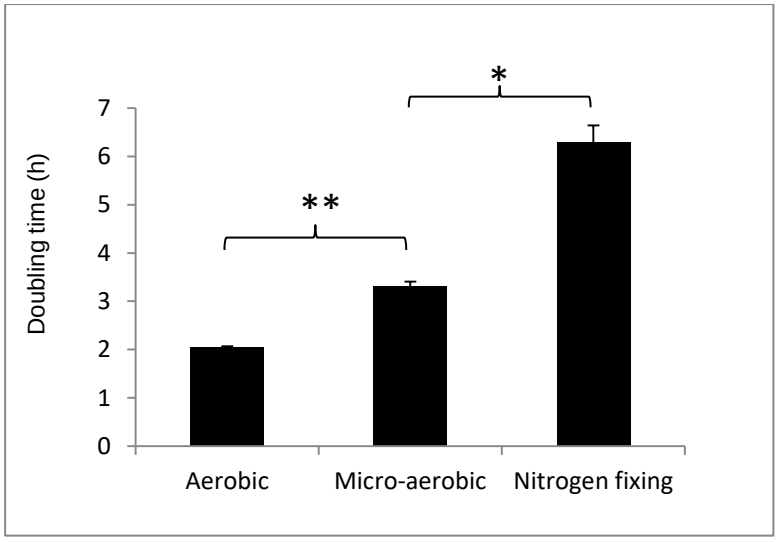

Figure 4.7: **Comparison of the doubling times of ORS571 cultures between aerobic and micro-aerobic conditions**. Values marked with * shows a statistically significant increase confirmed by t-test (** p-value < 0.01; * p-value < 0.05). Values are the mean ± SEM from three biological replicates.

Comparison of ORS571 cultures by scanning electron microscopy revealed no obvious difference in gross morphology between cells grown under aerobic and micro-aerobic conditions with NH_4Cl as the nitrogen source (Figure 4.8).

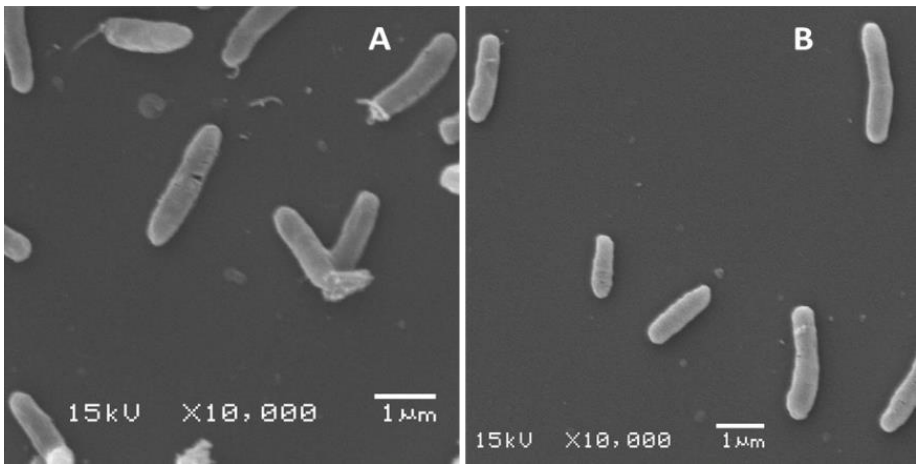

Figure 4.8 **Morphology of ORS571 grown under aerobic and micro-aerobic conditions**. Images are shown for ORS571 grown under aerobic (A) and micro-aerobic (B) with NH_4Cl as the nitrogen source.

The biomass composition of micro-aerobic cultures differed significantly from aerobic cultures (Figure 4.9). Specifically there was a significant decrease in the amount of protein, lipid, RNA and DNA, when ORS571 cultures were shifted from aerobic to micro-aerobic growth conditions; while the amount of PHB increased over 3-fold. The results confirm that although there were no significant morphological changes in ORS571 under aerobic (21% O_2) to micro-aerobic (3% O_2) conditions, there were changes in the biomass outputs between the two conditions.

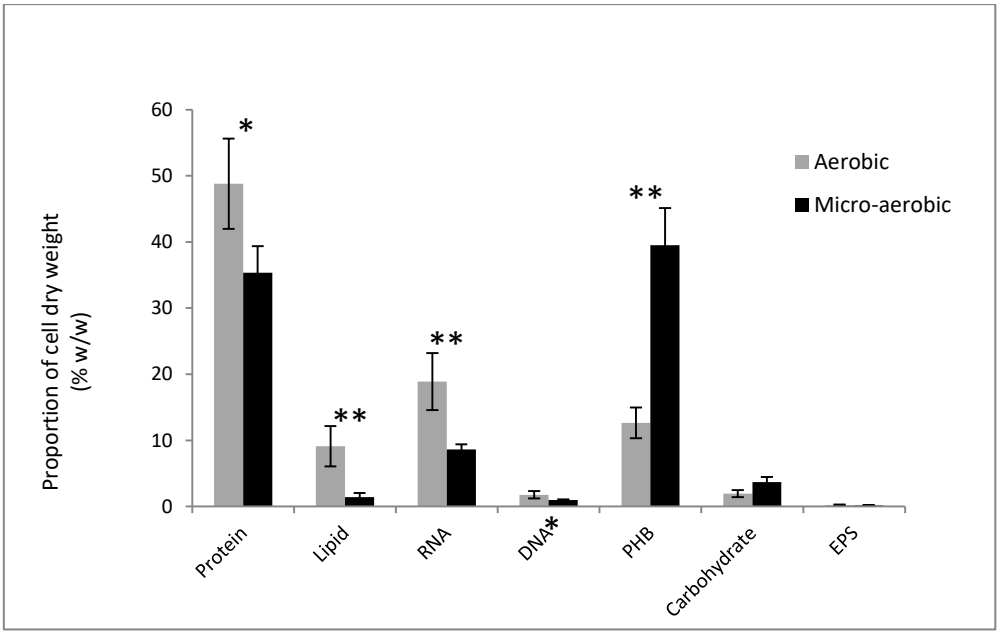

Figure 4.9: **Biomass composition of ORS571 under aerobic and micro-aerobic condition**. The measurements for micro-aerobic cultures were compared to the previously determined measurements for late exponential aerobic cultures (Section 3.4) Values determined for ORS571 grown under aerobic conditions are the mean ± SEM from six biological replicates and for those under micro-aerobic condition are the mean ± SEM from three biological replicates. Significant differences in the biomass measurements between aerobic and micro-aerobic growth conditions as determined by t-tests are indicated: *, p-value < 0.05; **, p-value < 0.01.

The biomass composition determined for the two micro-aerobic conditions were compared to identify changes that arose solely during N_2 fixation (Figure 4.10). The

only significant change was in the amount of carbohydrate (which reduced by 53% during N_2 fixation), although this was only a minor component of the dry cell weight.

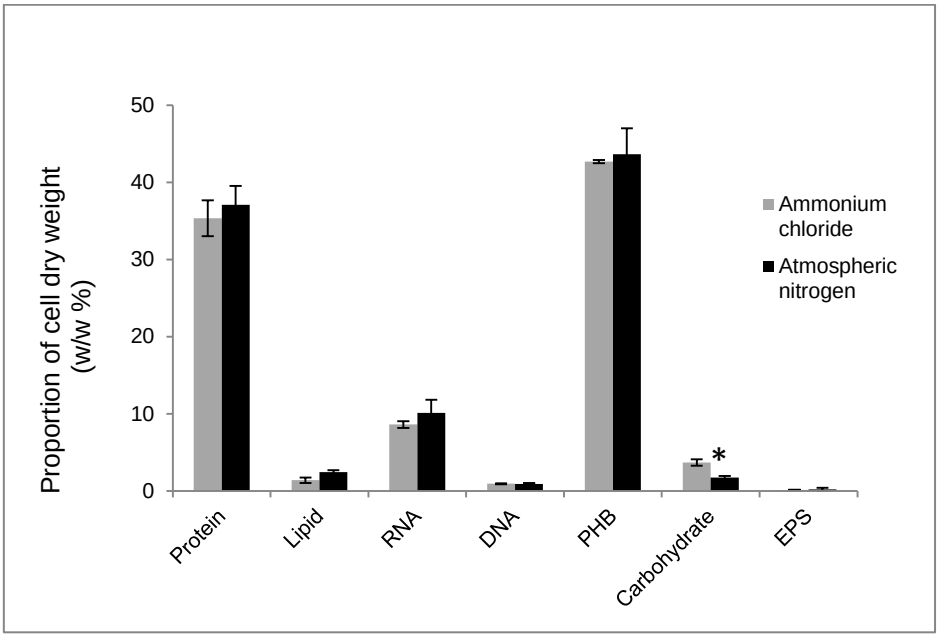

Figure 4.10: **Biomass composition of ORS571 grown with ammonium chloride (NH_4Cl) or atmospheric nitrogen (N_2) as the nitrogen source under micro-aerobic conditions**. Values are the mean ± SEM from three biological replicates. Significant differences in the measurements between the micro-aerobic conditions as determined by t-tests are indicated: *, p-value < 0.05; **, p-value < 0.01.

The results in this section show those there were significant alterations in growth and biomass synthesis of ORS571 under micro-aerobic conditions and these implied possible alterations in the central carbon metabolic fluxes during micro-aerobic growth. Therefore, ^{13}C-MFA was undertaken in order to determine the changes in fluxes through the central metabolic network that were needed to support the differences in growth and biomass composition observed under the micro-aerobic conditions.

4.6 Growth characteristics of ORS571 in mini-reactor

To reduce the cost of ^{13}C carbon substrate and to be able to perform labelling studies on biological replicates, it was desirable to grow cultures in small volumes (10 ml). To

determine whether growth of the small volume of cultures was different to those obtained under the previously established growth conditions, growth curves were generated for ORS571 cultures in the mini reactors (Figure 4.11). The doubling time for 10 ml cultures was calculated as described in section 2.20 and is 2.25 h ± 0.09, under aerobic growth conditions, 3.17 h ± 0.11 under micro-aerobic conditions and 6.6 h ± 0.36 for cultures under micro-aerobic N_2-fixing conditions. There were no significant differences between the growth rate of cultures in mini reactors and larger volume batch cultures establishing that the growth characteristics are unaffected by the change in cultures size.

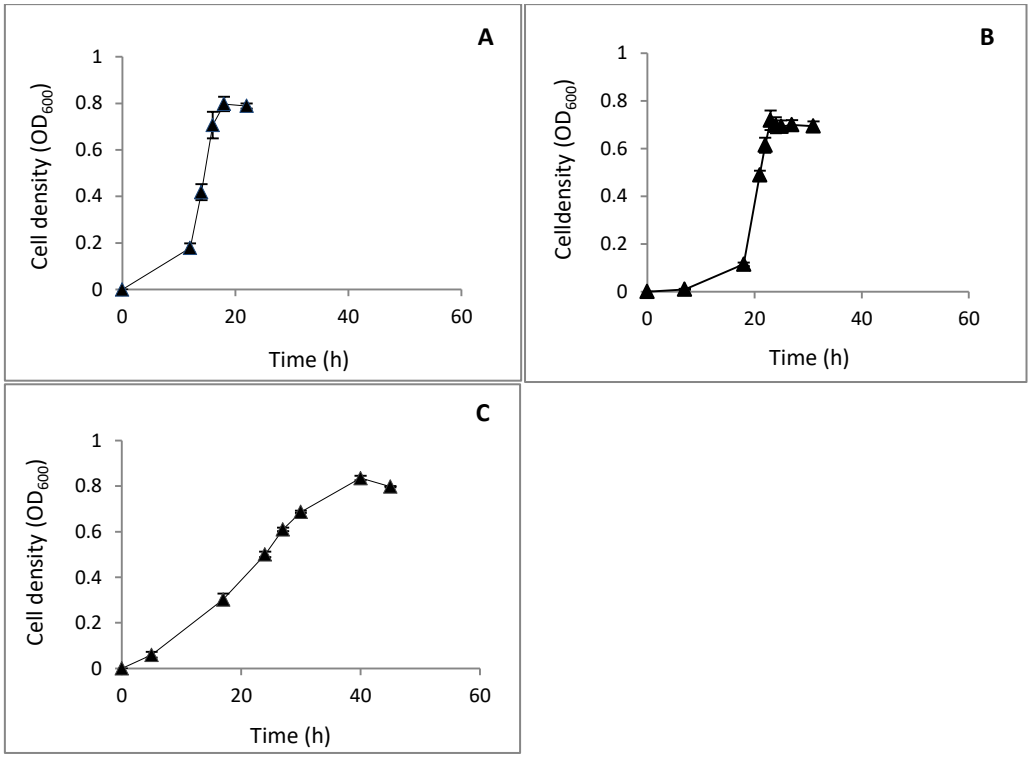

Figure 4.11: **Growth curves of ORS571 under aerobic (A), micro-aerobic (B) and micro-aerobic N_2-fixing (C) conditions in the mini-reactor**. Values are mean ± SEM from three biological replicates.

4.7 Steady state ^{13}C-MFA of ORS571 under aerobic and micro-aerobic condition

The labelling experiments were performed in the mini-reactor using 20% [$^{13}C_4$]succinate as the tracer for free-living cultures grown under (i) aerobic (21 % O_2)

conditions with NH_4Cl as the nitrogen source (ii) micro-aerobic with NH_4Cl as the nitrogen source, and (iii) micro-aerobic conditions with atmospheric N_2 as the nitrogen source. It was shown in chapter 3 that ORS571 cultures subcultured into labelled medium had achieved metabolic and isotopic steady state by early exponential growth phase. So, the cultures were grown in triplicates for each of the three conditions and were harvested at late exponential growth stage. Reliable MS measurements were obtained from the extracted metabolites according to the methods established in chapter 3 and are listed in the appendix (Table A5, Table A6 and Table A7). The metabolic model used for flux analysis under the three conditions was constructed as described in section 3.11.1. The biomass reaction used to constrain the models for each condition was formulated according to the method established in section 3.11.2. The reaction for cultures grown under aerobic condition was derived from the biomass measurements obtained in section 3.4.1 for late exponential cultures. The biomass measurements shown in section 4.4 were used to formulate the biomass reaction for micro-aerobic and micro-aerobic N_2-fixing cultures. The models used for generating flux maps under the three conditions, are included in the appendix (Table A8). The fluxes and their corresponding 95% confidence limits calculated for the three conditions are listed in Table 4.1.

Table 4.1: **Flux distributions for ORS571 free-living cultures under aerobic, micro-aerobic and N_2-fixing conditions**

Reaction step (s)	Symbol	Molar flux (relative to succinate uptake)		
		Aerobic ORS571	**Micro-aerobic ORS571**	**Micro-aerobic N_2-fixing ORS571**
Uptake fluxes				
Total uptake of succinate (constrained)	*upt3*	100	100	100
Tricarboxylic acid cycle				
Succinate dehydrogenase	*tca1*	142 (138, 144)	140 (137, 141)	**165 (160, 168)**
Fumarase	*tca2*	143 (140, 146)	140 (138, 142)	**165 (160, 168)**

Reaction step (s)	Symbol	Molar flux (relative to succinate uptake)		
		Aerobic ORS571	**Micro-aerobic ORS571**	**Micro-aerobic N_2-fixing ORS571**
Malate dehydrogenase	*tca3*	70.3 (67.0, 146)	110 (55.0, 111.7)	74.6 (72.5, 79.1)
Citrate synthase	*tca4*	45.6 (42.5, 48.3)	42.4 (40.3, 44.0)	**66.4 (61.6, 69.5)**
Aconitase	*tca5*	45.6 (42.5, 48.3)	42.4 (40.3, 44.0)	**66.4 (61.6, 69.5)**
Isocitrate dehydrogenase	*tca6*	45.6 (42.5, 48.3)	42.4 (40.3, 44.0)	**66.4 (61.6, 69.5)**
2-Oxoglutarate dehydrogenase	*tca7*	42.2 (38.9, 44.9)	40.1 (37.9, 41.6)	**65.0 (60.1, 68.2)**
Succinyl-CoA synthetase	*tca8*	40.9 (37.6, 43.7)	39.2 (37.0, 40.7)	**64.5 (59.4, 67.7)**
Pyruvate dehydrogenase	*tca9*	67.5 (0, 69.9)	79.2 (0, 80.1)	87.9 (0, 89.2)
Anaplerotic pathways				
NAD-dependent malic enzyme	*mal*	73.0 (0, 77.0)	30.7 (0, 85.2)	90.8 (0, 91.6)
Phosphoenolpyruvate carboxykinase	*pepck*	16.4 (12.2, 29.1)	63.4 (7.74, 63.5)	**5.71 (4.09, 6.09)**
Methylmalonate-semialdehyde dehydrogenase	*msdh*	(0, 69.7)	0 (0, 79.8)	0 (0, 1.36)
Glycolysis				
Pyruvate kinase	*gly1*	0.29 (0, 77.1)	53.6 (0, 85.2)	0 (0, 53.8)
Gluconeogenesis	*glu1*			
Phosphoglycerate kinase		13.9 (10.1, 21.3)	8.27 (6.23, 11.4)	4.85 (3.28, 15.2)
Glyceraldehyde-3-phosphate dehydrogenase	*glu2*	8.93 (6.89, 15.6)	5.20 (4.55, 8.36)	2.98 (2.77, 13.3)
Triosephosphate isomerase	*glu3*	4.91 (3.07, 11.6)	2.53 (1.92, 5.64)	1.55 (1.47, 11.8)
Fructose-bisphosphate aldolase	*glu4*	4.23 (2.42, 10.9)	2.43 (1.82, 5.54)	1.46 (1.38, 11.7)
Fructose-1,6-bisphosphatase	*glu5*	4.23 (2.42, 10.9)	2.43 (1.82, 5.54)	1.46 (1.38, 11.7)
Phosphoglucose isomerase	*glu6*	2.09 (0.39, 12.9)	2.51 (0, 6.94)	1.85 (1.83, 17.6)
Pentose phosphate pathway				
Glucose-6-phosphate dehydrogenase	*ppp1*	1.67 (0, 12.5)	1.76 (0, 6.17)	1.59 (0, 17.4)
6-phosphogluconate dehydrogenase	*ppp2*	0 (0, 6.26)	1.76 (0, 3.90)	1.59 (0, 10.5)

Reaction step (s)	Symbol	Molar flux (relative to succinate uptake)		
		Aerobic ORS571	Micro-aerobic ORS571	Micro-aerobic N_2-fixing ORS571
Ribulose 5-phosphate 3-epimerase	*ppp3*	-2.13 (-2.29, .10)	0.07 (-1.16, 1.49)	0.38 (0.28, 6.35)
Ribose 5-phosphate isomerase	*ppp4*	2.13 (2.03, 4.23)	1.68 (1.07, 2.41)	1.20 (1.14, 4.19)
Transketolase- C5/C3 conversion	*ppp5*	-2.13 (-2.29, .10)	0.07 (-1.16, 1.49)	0.38 (0.28, 6.35)
Transketolase- C6/C4 conversion	*ppp6*	1.61 (-0.50, 1.73)	0.33 (-0.36, 0.97)	0.02 (-2.95, 0.10)
Transketolase- C7/C5 conversion	*ppp7*	0.52 (-1.56, 0.56)	-0.41 (-1.12, 0.18)	-0.41 (-3.39, -.39)
Transaldolase- C6/C3 conversion	*ppp8*	0.52 (-1.56, 0.56)	-0.41 (-1.12, 0.18)	-0.41 (-3.39, -.39)
Transaldolase- C7/C4 conversion	*ppp9*	-0.52 (-0.56, .56)	0 (0, 1.12)	0.41 (0.39, 3.39)
Entner-Doudoroff pathway				
6-Phosphogluconate dehydratase	*ed1*	1.67 (0, 6.64)	0 (0, 2.43)	0 (0, 7.92)
2-keto-3-deoxy-6-phosphogluconate aldolase	*ed2*	1.67 (0, 6.64)	0 (0, 2.43)	0 (0, 7.92)
Amino acid synthesis				
Glutamate dehydrogenase	*glt*	**21.7 (19.5 ,25.5)**	13.9 (13.5, 16.3)	**8.10 (7.39, 10.4)**
Glutamine synthetase	*gln*	**2.26 (2.12, 2.43)**	1.55 (1.52, 1.65)	**0.90 (0.82, 1.05)**
Proline synthesis	*pro*	**0.59 (0.56, 0.64)**	0.41 (0.40, 0.43)	**0.23 (0.21, 0.27)**
Arginine synthesis	*arg*	**0.90 (0.84, 0.97)**	0.62 (0.60, 0.65)	**0.36 (0.32, 0.42)**
Aspartate transaminase	*asp*	7.29 (5.22, 12.1)	3.83 (3.74, 7.29)	2.22 (2.02, 4.66)
Asparagine synthase	*asn*	**0.77 (0.72, 0.83)**	0.53 (0.52, 0.56)	**0.31 (0.28, 0.36)**
Alanine aminotransferase	*ala*	**1.55 (1.45, 1.67)**	1.06 (1.04, 1.12)	**0.62 (0.56, 0.72)**
Serine synthesis	*ser*	3.30 (1.26, 4.32)	2.44 (0.91, 2.55)	1.44 (0.54, 1.68)
Serine hydroxymethyltransferase	*glc1*	1.59 (-0.47, 2.54)	1.26 (-0.29, 1.31)	0.76 (-0.14, 0.88)
MEETHF synthesis	*meethf*	1.86 (0.93, 4.17)	0.26 (0.26, 1.90)	0.19 (0.17, 1.25)
Threonine aldolase	*glc2*	1.71 (0, 6.19)	0 (0, 3.24)	0 (0, 2.07)
Cysteine synthesis	*cys*	**0.77 (0.72, 0.83)**	0.53 (0.52, 0.56)	**0.31 (0.28, 0.36)**
Lysine synthesis	*lys1*	**0.93 (0.87, 1.00)**	0.64 (0.63, 0.68)	**0.37 (0.34, 0.43)**
Lysine synthesis	*lys2*	**0.93 (0.87, 1.00)**	0.64 (0.63, 0.68)	**0.37 (0.34, 0.43)**
Threonine synthesis	*thr*	3.28 (1.46, 7.87)	1.07 (1.05, 4.38)	0.62 (0.56, 2.80)

Reaction step (s)	Symbol	Molar flux (relative to succinate uptake)		
		Aerobic ORS571	Micro-aerobic ORS571	Micro-aerobic N_2-fixing ORS571
Methionine synthesis	*met*	**0.35 (0.33, 0.38)**	0.24 (0.23, 0.25)	**0.14 (0.12, 0.16)**
Valine synthesis	*val*	**1.07 (1.00, 1.15)**	0.74 (0.72, 0.78)	**0.42 (0.39, 0.50)**
Leucine synthesis	*leu*	**1.28 (1.20, 1.37)**	0.87 (0.85, 0.93)	**0.51 (0.46, 0.59)**
Isoleucine synthesis	*ile*	**0.74 (0.70, 0.80)**	0.51 (0.50, 0.54)	**0.29 (0.27, 0.34)**
Phenylalanine synthesis	*phe*	**0.50 (0.47, 0.54)**	0.34 (0.33, 0.36)	**0.20 (0.18, 0.23)**
Tyrosine synthesis	*tyr*	**0.43 (0.40, 0.46)**	0.29 (0.29, 0.31)	**0.17 (0.15, 0,20)**
Tryptophan synthesis	*trp*	**0.14 (0.13, 0.15)**	0.10 (0.09, 0.10)	**0.05 (0.05, 0.06)**
Histidine synthesis	*his*	**0.25 (0.24, 0.27)**	0.17 (0.17, 0.18)	**0.10 (0.09, 0.11)**
Other outputs				
METHF synthesis	*methf*	**0.35 (0.33, 0.38)**	0.24 (0.23, 0.25)	**0.14 (0.12, 0.16)**
FTHF synthesis	*fthf*	**0.25 (0.24, 0.27)**	0.17 (0.17, 0.18)	**0.10 (0.09, 0.11)**
PHB synthesis	*accoa1*	**5.17 (4.84, 5.56)**	16.6 (16.2, 17.6)	**9.41 (8.59, 11.0)**
Biomass synthesis	*biomass*	3.54 (3.31, 3.81)	3.35 (3.27, 3.55)	**1.85 (1.69, 2.17)**
Lipid synthesis	*accoa2*	**10.2 (9.63, 11.0)**	1.52 (1.49, 1.61)	1.45 (1.32, 1.69)
DNA synthesis	*r5p1*	**0.20 (0.19, 0.20)**	0.10 (0.10, 0.10)	**0.05 (0.05, 0.06)**
RNA synthesis	*r5p2*	**2.06 (1.93, 2.21)**	0.89 (0.87, 0.94)	**0.57 (0.53, 0.67)**
Carbohydrates synthesis	*g6p1*	**0.38 (0.35, 0.40)**	0.72 (0.71, 0.77)	**0.18 (0.17, 0.21)**
EPS synthesis	*g6p2*	0.03 (0.03, 0.04)	0.03 (0.03, 0.03)	**0.07 (0.06, 0.08)**
CO_2 output (net)	*co_2.out*	252 (246, 257)	261 (253, 262)	**320 (306, 321)**

Fluxes are presented as best-fit estimates calculated using MS measurements extracted from three individual labelling experiments for each growth condition. The 95% confidence limits for the fluxes were calculated using parameter continuation analysis in INCA and are presented as (lower bound, upper bound) of the confidence limits. All fluxes are expressed on a molar basis relative to a succinate uptake flux of 100. Fluxes measured under two different growth conditions were considered to be significantly different if the confidence intervals associated with the fluxes do not overlap. Fluxes shown in **red** and **blue** represents significant differences under aerobic and N_2-fixing conditions, respectively, relative to the fluxes determined under micro-aerobic conditions.

4.7.1 Statistical analysis of the fluxes

The flux distributions obtained for ORS571 free-living cultures under the three conditions had statistically acceptable SSRs (Table 4.2) as described in section 3.13. The statistical validation of the goodness of fit for the flux distributions under the three conditions is included in the appendix (Figures A9-A11) where the experimentally derived MS measurements for amino acids, PHB and trehalose are compared with the simulated measurements predicted by the corresponding flux distributions. The comparisons confirmed that all measured and simulated isotopomer values are broadly comparable and that the analysis is not distorted by a small number of outlier measurements.

Table 4.2: **SSRs obtained for the fluxes of ORS571 free-living cultures under aerobic, micro-aerobic and N_2-fixing growth conditions**

Growth conditions	Obtained SSR	Expected SSR	Degrees of freedom (DOF)	Comment
Aerobic	446.5	470-597.8	532	Fit accepted
Micro-aerobic	452.2	458.7- 585.1	520	Fit accepted
N_2-fixing	371.2	329.7- 438	382	Fit accepted

4.8 Influence of O_2 concentration on metabolic flux phenotype of ORS571

The comparison of the flux maps determined for aerobic and micro-aerobic ORS571 grown with NH_4Cl is shown in Figure 4.12.

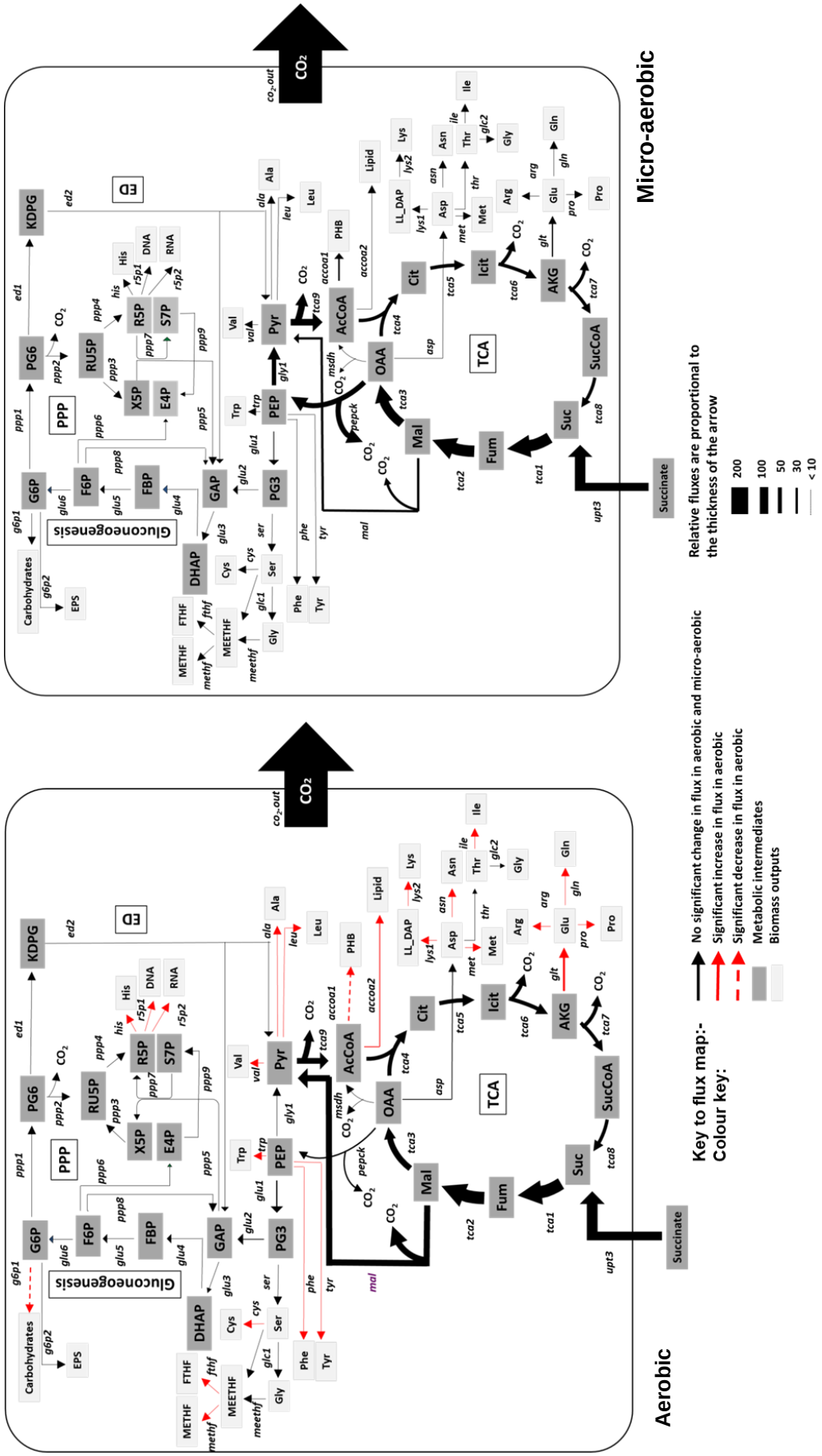

Figure 4.12: **Comparison of flux maps of ORS571 obtained under aerobic and micro-aerobic conditions**. The flux maps represent statistically valid best-fit models based on the redistribution of label following metabolism of [$^{13}C_4$]succinate by ORS571 cultures under aerobic and micro-aerobic condition with NH_4Cl as the nitrogen source. The thickness of the each arrow in the flux maps is proportional to the relative molar flux. Metabolic intermediates and biomass outputs are shown in rectangular boxes with distinct colour key. The symbols for fluxes are shown in *italics* (defined in Table 4.1). Statistically significantly changes in fluxes for ORS571 growing under aerobic condition as compared to that under micro-aerobic condition are shown with distinct colour key. Significant increase in fluxes for aerobic ORS571 (*glt, gln, pro, arg, asn, ala, cys, lys1, lys2, met, val, leu, ile, phe, tyr, trp his, methf, fthf, accoa2, r5p1, r5p2*) are shown as solid lines and a significant decrease in flux (*accoa1, g6p1*) is shown as a dotted line.

The biomass fluxes determined under the two conditions are defined by the biomass compositions. PHB was the greater proportion of the biomass measured during micro-aerobic growth, therefore, the flux *accoa1* for PHB synthesis increased significantly under micro-aerobic conditions. A previous study reported that the accumulation of PHB during low O_2 conditions was required to maintain the balance of reducing power of the cell (Mandon et al., 1998). The excess AcCoA and reducing equivalents (NADH, NADPH) produced under low O_2 conditions were diverted into PHB synthesis to maintain an unrestricted activity of the TCA cycle. Similar findings were reported for the diazotroph, *Azotobacter* which accumulated large amounts of PHB under low O_2 conditions in order to maintain the redox balance and TCA cycle activity (Senior & Dawes, 1971).

Flux *g6p1* for the synthesis of carbohydrates was also significantly higher under micro-aerobic conditions. The fluxes for the synthesis of amino acids- glutamate (*glt*), glutamine (*gln*), proline (*pro*), arginine (*arg*), asparagine (*asn*), alanine (*ala*), cysteine (*cys*), lysine (*lys1*, *lys2*), methionine (*met*), valine (*val*), leucine (*leu*), isoleucine (*ile*), phenylalanine (*phe*), tyrosine (*tyr*), tryptophan (*trp*) and histidine (*his*) were significantly reduced during micro-aerobic growth of ORS571. Fluxes *methf*, *fthf* that were involved in amino acid synthesis, *accoa2* for lipid synthesis, *r5p1* for DNA and *r5p2* for RNA synthesis were reduced under micro-aerobic conditions. These reduced output fluxes are affected by the significantly reduced proportions of protein, lipids and nucleic acids synthesized during micro-aerobic growth.

Flux *tca9* of the TCA cycle produced AcCoA, the precursor for lipids and PHB synthesis. The TCA cycle fluxes (*tca3*, *tca6*), gluconeogenesis flux (*glu1*, *glu*6), glycolysis flux (*gly1*), anaplerotic fluxes (*mal*, *pepck*) and PPP flux (*ppp4*) produced metabolic intermediates for amino acid and nucleic acid synthesis. Because the fluxes to biomass outputs are significantly different, the fluxes that produced the precursors

for these outputs are also expected to vary. But there were no statistically significant differences in the fluxes *tca9*, *tca3*, *tca6*, *glu1*, *glu6*, *gly1*, *mal*, *pepck* and *ppp4* determined under the two conditions. However, these fluxes were relatively poorly defined (the confidence limits with these fluxes were large), so it was possible for the central carbon utilisation fluxes changes under micro-aerobic conditions, but in this study, the changes in these fluxes were not found to be statistically significant between the two conditions.

Anaplerotic fluxes *mal* and *msdh* and the associated flux *tca9* were not significantly different under the two conditions. The confidence limits associated with these fluxes were large and the flux estimates may be unreliable. The possible explanation for this is an identifiability problem at the anaplerotic node of the network. Similar observations were reported for the anaplerotic node involving metabolites PEP, pyruvate, OAA and malate in *Corynebacterium glutamicum* where the large confidence limits obtained for the anaplerotic fluxes was due to the structural identifiability problem of the anaplerotic node (Kappelmann et al., 2015). This identifiability problem may arise due to the insufficient labelling information for the anaplerotic node, low sensitivity of the flux variables to the MS measurements provided or the structure of the network used for ^{13}C-MFA. In this instance, a comparison of the proteomic and transcriptomic profiles of the metabolic intermediates and enzymes may help by restricting the potential permutation of reactions available to support interconversion of metabolites in this section of the network, thus allowing fluxes to be uniquely resolved.

The CCE measured under aerobic and micro-aerobic conditions were 36% and 34% respectively. The total metabolic CO_2 output was not significantly different between the growth conditions. This indicates that the overall utilisation of succinate was not significantly different under the two conditions although its allocation to individual biomass outputs was altered during micro-aerobic growth.

4.9 Influence of N_2-fixation on the metabolic flux phenotype of ORS571 under micro-aerobic conditions

The comparison of the flux maps determined for micro-aerobic ORS571 grown with either NH_4Cl or N_2 as the nitrogen source is shown in Figure 4.13.

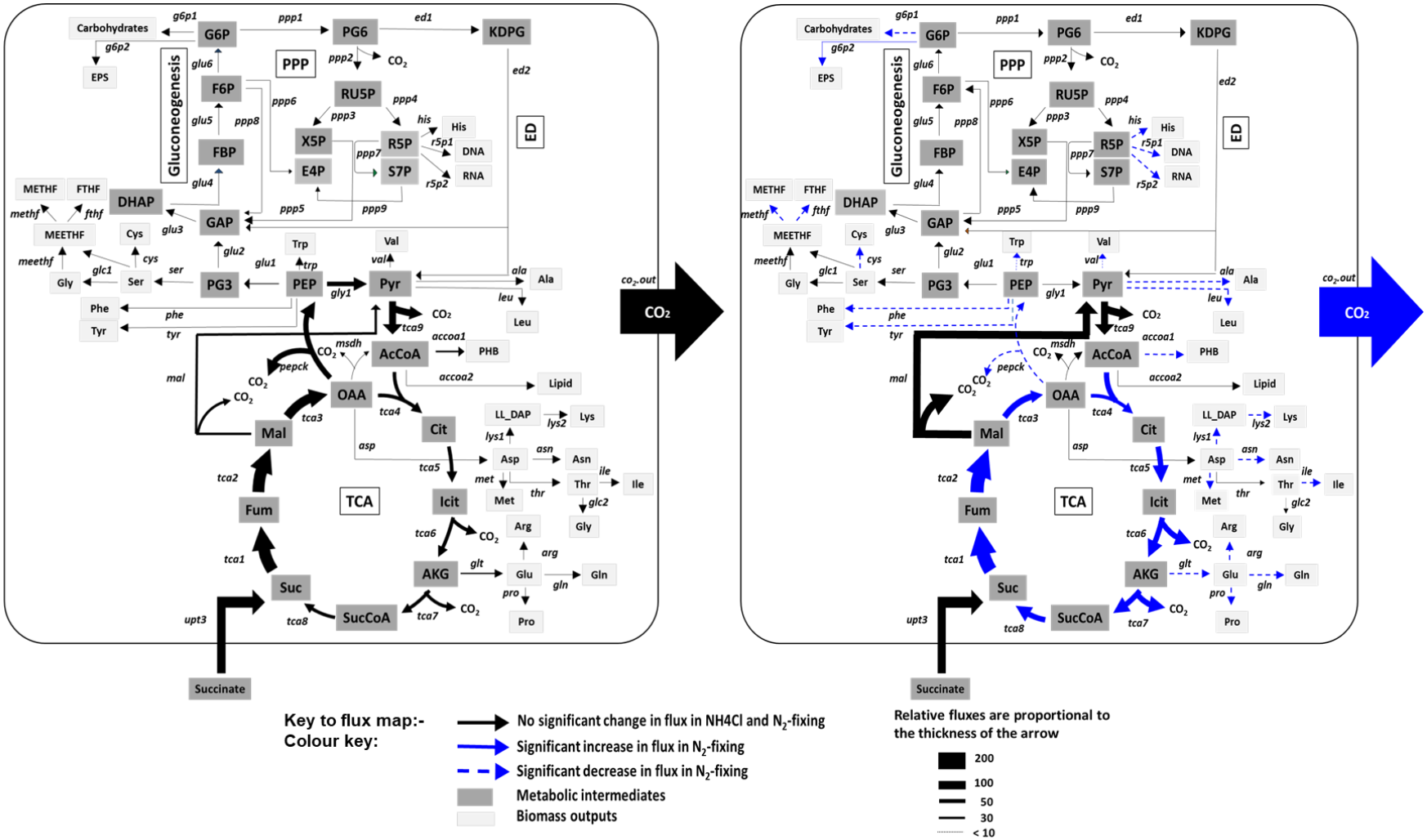

Figure 4.13: **Comparison of flux maps of ORS571 obtained under micro-aerobic and N_2-fixing conditions**. The flux maps represent statistically valid best-fit models based on the redistribution of label following metabolism of [$^{13}C_4$]succinate by ORS571 cultures under micro-aerobic condition grown with NH_4Cl and N_2 as the nitrogen source. The thickness of the each arrow in the flux maps is proportional to the relative molar flux. Metabolic intermediates and biomass outputs are shown in rectangular boxes with distinct colour key. The symbols for fluxes are shown in *italics* (defined in Table 4.1). Statistically significant changes in fluxes for N_2-fixing ORS571 as compared to that grown with NH_4Cl are shown with a distinct colour key. A significant increase in fluxes for N_2-fixing ORS571 (*tca1*, *tca2*, *tca4*, *tca5*, *tca6*, *tca7*, *tca8* and g6p2) are shown as solid line and a significant decrease in fluxes (*pepck*, *glt*, *gln*, *pro*, *arg*, *asn*, *ala*, *cys*, *lys1*, *lys2*, *met*, *val*, *leu*, *ile*, *phe*, *tyr*, *trp his*, *methf*, *fthf*, *accoa1*, *g6p1*, *r5p1* and *r5p2*) are shown as dotted line.

There were changes in the distribution of fluxes through the TCA cycle when ORS571 fixed N_2 under micro-aerobic conditions. Fluxes *tca1*, *tca2*, *tca4*, *tca5*, *tca6*, *tca7* and *tca8* significantly increased during N_2 fixation, while there were no statistically significant changes in fluxes via ED, PPP and gluconeogenesis pathways. The results show the TCA cycle to be the primary succinate utilisation pathway under the micro-aerobic growth conditions and the increase in fluxes through the TCA could be necessary to support the growth and metabolism during N_2 fixation. There was a significant increase in the overall metabolic CO_2 output flux (*co_2.out*) for the N_2 fixing cultures. The CCE of the N_2 fixing cultures (20%) was lower than that measured for micro-aerobic cultures (34%).

The TCA cycle produced metabolic intermediates- PEP, pyruvate, AcCoA, OAA and AKG and co-enzymes which were used for amino acids and PHB synthesis. The fluxes through the TCA cycle being significantly higher during N_2-fixing condition but the biomass synthesis being significantly reduced suggests that the increased TCA cycle fluxes were probably not required to support higher biomass production, but rather that these were needed to maintain other cellular functions.

N_2 fixation is an energetically expensive biochemical reaction requiring 16 moles of ATP and eight moles of NADPH for reduction of one mole of di-nitrogen. Therefore, N_2-fixation will have increased the demand for ATP and reducing power and so, an increase in the TCA cycle fluxes was observed to meet these demands.

Flux *pepck* that directs flux into gluconeogenesis was significantly reduced during N_2 fixation. Although anaplerotic flux *mal* and *tca9* were not statistically different under the two conditions, flux through *pepck* was significantly reduced in the presence of N_2. This was related to the difficulty in resolving fluxes around the anaplerotic node of the network leading to large confidence intervals for individual reactions and thus a lack of power in establishing the significance of any differences in fluxes. Flux *msd*h was lower

than *mal* and *tca3* fluxes under both micro-aerobic conditions, which indicates that fluxes *mal* and *tca3* were the preferential route for decarboxylation of malate.

The fluxes for the synthesis of amino acids- glutamate (*glt*), glutamine (*gln*), proline (*pro*), arginine (*arg*), asparagine (*asn*), alanine (*ala*), cysteine (*cys*), lysine (*lys1*, *lys2*), methionine (*met*), valine (*val*), leucine (*leu*), isoleucine (*ile*), phenylalanine (*phe*), tyrosine (*tyr*), tryptophan (*trp*), and histidine (*his*) were significantly reduced under N_2-fixing conditions. Fluxes *methf* and *fthf* involved in amino acid synthesis were also reduced. It was previously shown that ammonium assimilatory pathways via glutamine synthetase (GS) and glutamate synthase (GOGAT) had a regulatory effect on N_2 fixation; the activities of GS and GOGAT were required to induce N_2 fixation in the free-living cultures (Donald & Ludwig, 1984). In this study, the fluxes *glt* and *gln* that were catalysed via GOGAT and GS respectively were found to be significantly reduced during N_2 fixation. The reduced fluxes via GOGAT and GS and also for the rest of the amino acids are explained by the reduced protein content measured as a proportion of biomass.

Fluxes accoa1 for PHB synthesis, g6p1 for carbohydrate synthesis, r5p1 for DNA and r5p2 for RNA synthesis were also reduced in N_2-fixing cultures. Flux g6p2 for EPS biosynthesis was significantly higher in the N_2-fixing cultures. These differences in fluxes reflect the changes in biomass compositions between the micro-aerobic and N_2-fixing cultures.

4.10 Co-enzyme analysis

Co-enzyme analysis for the flux maps of ORS571 obtained under aerobic, micro-aerobic and N_2-fixing conditions was performed according to the method previously established in chapter 3, section 3.17. This analysis showed the production and consumption of co-enzymes by different parts of the network. Significant changes in co-enzyme utilisation by a reaction under different growth conditions were determined

based on the significant change in the flux through the particular reaction. This analysis was done solely for the fluxes of the metabolic network that were determined in this study. So, this analysis is limited only to the co-enzyme generation and production by the network specified for this study, and does not include production of co-enzymes via oxidative phosphorylation and utilisation of co-enzymes for functions like growth and maintenance.

4.10.1 Comparison of co-enzyme production in ORS571 under different growth conditions

The production of co-enzymes by the network of ORS571 growing under aerobic, micro-aerobic and N_2-fixing conditions is shown in Figure 4.14.

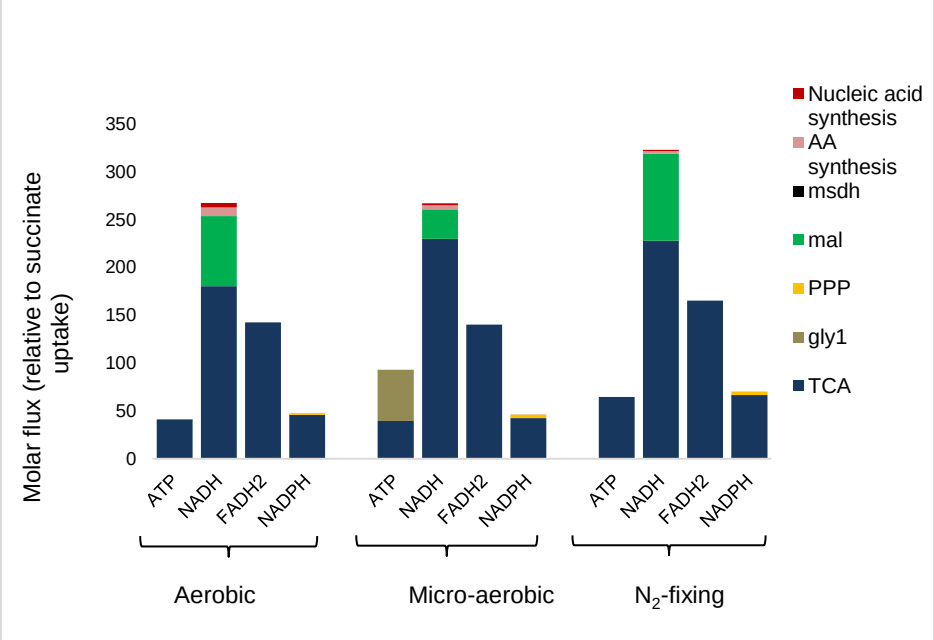

Figure 4.14: **Production of co-enzymes by ORS571 growing under aerobic, micro-aerobic and N_2-fixing conditions**. The production of ATP, NADH, $FADH_2$ and NADPH by the network was determined from the sum of individual fluxes that produced co-enzymes in the flux distributions obtained for ORS571 cultures under the three growth conditions (Table 4.1). All values are molar fluxes expressed relative to succinate uptake.

During growth of ORS571 under aerobic conditions, the majority of the ATP (99%) was synthesized by *tca8* reaction of the TCA cycle and a minor amount (0.7%) by *gly1* of the network. Under micro-aerobic conditions, around 42.2% of ATP was produced by *tca8* and 57.8% was produced by *gly1*, while during N_2 fixation, all of the ATP was produced by the reaction *tca8*. Although there was an increase in production of ATP by *gly1* via pyruvate kinase during micro-aerobic growth, there was no statistically significant difference between the fluxes measured under the three conditions. So, the ATP production by pyruvate kinase under the three conditions was considered to be the same. There was a significant increase in the production of ATP by the TCA cycle during N_2-fixing conditions, which was 65% and 57.3% higher than produced under micro-aerobic and aerobic growth conditions respectively.

Fluxes *tca3* (malate dehydrogenase), *tca7* (2-oxoglutarate dehydrogenase) and *tca9 (*pyruvate dehydrogenase) of the TCA cycle produced majority of the NADH in ORS571-67.5% under aerobic, 86.1% under micro-aerobic and 71% under N_2-fixing conditions. Flux *mal* contributed 27%, 12% and 28% of the total NADH produced under aerobic, micro-aerobic and N_2-fixing conditions. The remaining minor proportion was produced by amino acid (*ser*, *meethf*, *leu*, *glc2*, *tyr*, *his*) and nucleic acid synthesis reactions. Fluxes *tca3*, *tca9*, *mal* were not significantly different under the three conditions, so the contribution of NADH by these reactions were similar. But flux via 2-oxoglutarate dehydrogenase being significantly higher in the N_2-fixing ORS571, the contribution of NADH from this flux also increased significantly.

Co-enzyme $FADH_2$ was produced solely by *tca1* reaction in ORS571 under all three growth conditions. The production of $FADH_2$ by *tca1* was significantly higher in N_2-fixing ORS571- 18% and 16% higher than that produced in micro-aerobic and aerobic ORS571 respectively.

Majority of the NADPH was produced by *tca6* (isocitrate dehydrogenase) under the three growth conditions (Tsukada et al., 2009). The production of NADPH by the flux via isocitrate dehydrogenase higher under N_2-fixing conditions increased significantly by 56% and 46% relative to that produced under micro-aerobic and aerobic conditions, respectively. PPP fluxes, *ppp1* and *ppp2* produced only a minor proportion (< 10%) of the total NADPH generated by the network.

The TCA cycle of the network was the major pathway for production of co-enzymes under the three growth conditions. The production of co-enzymes by the TCA cycle fluxes- ATP (*tca8*), NADH (*tca7*), $FADH_2$ (*tca1*) and NADPH (*tca6*) increased significantly during growth of ORS571 under N_2-fixing conditions. This increased production of co-enzymes reflects the significant increase in fluxes of the TCA cycle during N_2-fixing conditions.

4.10.2 Comparison of co-enzyme consumption in ORS571 under different growth conditions

The consumption of co-enzymes needed for net biosynthesis by ORS571 growing under aerobic, micro-aerobic and N_2-fixing conditions is shown in Figure 4.15.

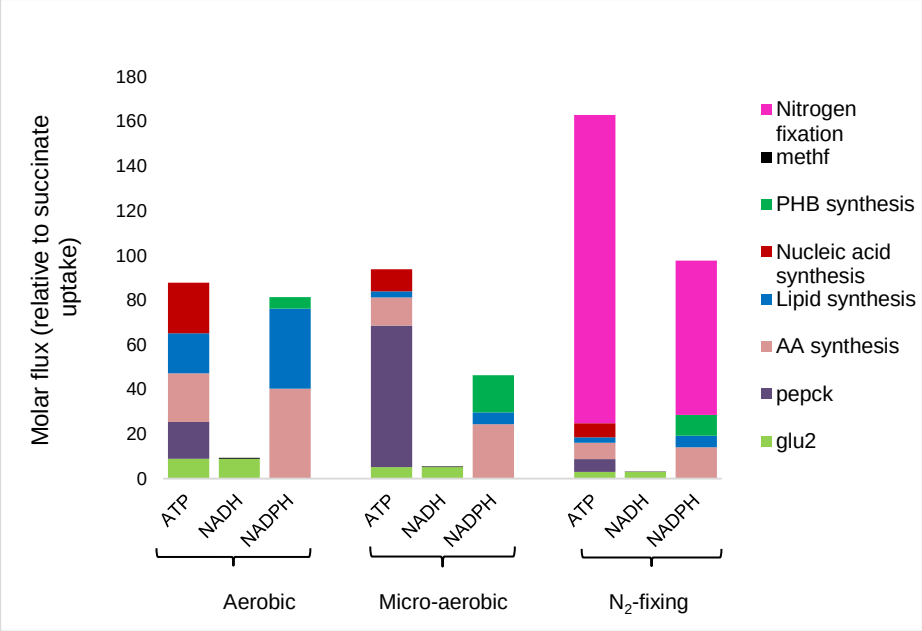

Figure 4.15: **Consumption of co-enzymes by ORS571 growing under aerobic, micro-aerobic and N_2-fixing conditions**. The consumption of ATP, NADH, $FADH_2$ and NADPH by the network reactions was determined from the sum of individual fluxes that used co-enzymes in the flux distributions obtained for ORS571 cultures under the three growth conditions (Table 4.1). All values are molar fluxes expressed relative to succinate uptake.

In aerobic cultures, a large proportion of the ATP (71%) required by the network, was utilised for biomass- nucleic acids, lipids and amino acids (glutamate, glutamine, proline, arginine, asparagine, cysteine, lysine, threonine, methionine, valine, leucine, isoleucine, phenylalanine, tyrosine, tryptophan and histidine). For the micro-aerobic cultures, only 27% of the ATP by substrate level phosphorylation was used for biomass synthesis. For the N_2-fixing cultures, there was a significant reduction in the ATP used for biomass (10%), which is explained by the significantly reduced flux to biomass synthesis. Only a minor proportion of the ATP, (10% for aerobic, 6% for micro-aerobic and 2% for N_2-fixing) was used for the reaction *glu2*. In the micro-aerobic cultures, 68% of the total ATP was consumed by *pepck*. There was no significant difference between the ATP consumed by *pepck* between aerobic and micro-aerobic cultures; but the ATP consumption by *pepck* decreased significantly by 91% in the N_2-fixing cultures relative

to that determined for micro-aerobic cultures. In the N_2-fixing cultures, out of the total ATP utilised by the network reactions, 85% was consumed by the reaction catalysed by nitrogenase enzyme.

The majority of NADH (≥ 95%) was consumed in the reaction via glyceraldehyde-3-phosphate dehydrogenase (*glu2*) under the three growth conditions, only a minor proportion (≤ 5%) was consumed for the reaction *methf* and none was used for net biosynthesis.

About half of the total NADPH produced by the network was consumed for amino acid synthesis in aerobic and micro-aerobic ORS571 but this proportion decreased to only 14% in the N_2-fixing cultures. NADPH used for lipid synthesis significantly decreased by 86% in the micro-aerobic and N_2-fixing cultures as compared to that determined for aerobic cultures. The flux for PHB synthesis was significantly higher for micro-aerobic cultures; therefore the consumption of NADPH for PHB was 3.2 and 1.7 fold higher than aerobic and N_2-fixing cultures.

Nitrogen fixation reaction required electrons; for each molecule of di-nitrogen reduced by nitrogenase, 8 moles of electrons were required. The source of electrons for nitrogenase is not well understood in rhizobia. In the classical model for a N_2-fixing rhizobium, NADH was considered to donate electrons to ferredoxin and then to nitrogenase. However Terpolilli et al. (2016), suggested that NADH was unlikely to transfer electrons to ferredoxin and then to nitrogenase, owing to its standard redox potential. Instead low potential electrons produced by the interaction between electron transferring flavoprotein (ETF) and FixABCX complex could be used for nitrogenase but there was no experimental evidence for this electron donation pathway (Terpolilli et al., 2016). In a different study, it was shown that NADPH was involved in transferring electrons to nitrogenase in *Klebsiella pneumonia* (Yoch, 1974). Based on these previous studies, NADPH was considered to be the source of reducing power for N_2

fixation in ORS571. A large proportion, 71% of the total NADPH was consumed in the reaction catalysed by nitrogenase.

The total consumption of ATP and NADPH for aerobic, micro-aerobic and N_2-fixing conditions was higher than that produced by the metabolic network reactions (substrate level phosphorylation). The consumption of ATP was higher than production by 112% in aerobic, 1.08% in micro-aerobic and 151% in N_2-fixing cultures. For NADPH, the consumption was higher than the production by 71% in aerobic, 0.5% in micro-aerobic and 40% in N_2-fixing cultures. The requirements for the additional ATP and NADPH could potentially be fulfilled by using NADH and $FADH_2$ that are produced in excess by the network. Only a minor proportion of NADH (≤ 5% of the total produced) was consumed for *glu2* and *methf* reactions. $FADH_2$ produced was not consumed in any of the reactions of the network. The excess NADH could produce ATP and NADPH via oxidative phosphorylation and transhydrogenase reactions, while the excess $FADH_2$ could be used to generate ATP via oxidative phosphorylation. Around 30% of the NADH and $FADH_2$ was utilized to produce the additional ATP and NADPH required by the network reactions and biomass production, and the remaining major proportion (> 60%) of the NADH and $FADH_2$ was available for the system that might be required for cellular functions like growth, cell division and maintenance purposes.

4.11 Measurement of absolute fluxes

The relative flux maps obtained under aerobic, micro-aerobic and micro-aerobic N_2-fixing condition were converted to absolute flux maps by using the specific substrate consumption rate (section 2.17) for each condition. The consumption rates for the three conditions and the doubling times of the cultures are shown in Table 4.3. It was clear that substrate consumption rate increased with an increase in the doubling time of the cultures. There were changes in the metabolic fluxes and co-enzyme utilisation in the

micro-aerobic N_2-fixing cultures with longer doubling times and presumably these changes in the metabolic behaviour required increased substrate consumption.

There were differences in the absolute fluxes measured for ORS571 free-living cultures under aerobic, micro-aerobic and N_2-fixing conditions, which suggest differences in metabolic behaviour between the three growth conditions. The changes in the absolute fluxes between the three conditions were consistent with the changes reported in the relative fluxes between the three conditions. For instance, the absolute flux for PHB synthesis in ORS571 during micro-aerobic growth was significantly higher than that measured during aerobic growth. The TCA cycle fluxes *tca1*, *tca2*, *tca4*, *tca5*, *tca6*, *tca7*, *tca8* under N_2-fixing conditions was significantly higher than that measured under micro-aerobic conditions (Table 4.4). The absolute fluxes for ORS571 under the three conditions are listed in the appendix (Table A12).

Table 4.3: **Specific substrate consumption rate and doubling times of ORS571 free-living cultures**

Growth condition	Specific substrate consumption rate (μmol h^{-1} g dry weight of $cells^{-1}$)	Doubling time (h)
Aerobic	0.9 ± 0.02	2.35 ± 0.09
Micro-aerobic	0.97 ± 0.04	3.49 ± 0.04
Micro-aerobic N_2-fixing	1.03 ± 0.01	5.96 ± 0.23

The measurements are the mean ± SEM from three biological replicates.

Table 4.4: **Absolute flux determined for ORS571 cultures under aerobic, micro-aerobic and N_2-fixing conditions**

Fluxes	Absolute flux values measured (µmol h^{-1} g dry weight of $cells^{-1)}$		
	Aerobic condition	**Micro-aerobic condition**	**N_2-fixing condition**
tca1	128.03	135.89	**170.04**
tca2	129.07	136.67	**170.52**
tca4	41.11	41.18	**68.45**
tca5	41.11	41.18	**68.45**
tca6	41.11	41.18	**68.45**
tca7	38.03	38.89	**67.04**
tca8	36.86	38.03	**66.51**
accoa1	**4.65**	16.13	**9.69**
co_2.out	227.12	253.98	**329.65**

4.12 Discussion

The results presented in this chapter provide an understanding of the metabolic adjustments in ORS571 that accompany N_2-fixation under micro-aerobic conditions. Nitrogenase is irreversibly inhibited by molecular O_2, so low O_2 is an absolute requirement for N_2-fixing rhizobia (Bergersen et al., 1986; Allen et al., 1991). The comparison of flux maps obtained under aerobic and micro-aerobic condition highlights the metabolic changes that occur due to the low O_2 environment rather than N_2 assimilation itself.

Under low O_2 conditions, there was an increase in accumulation of the polymer PHB which constituted around 40% of the total cell dry weight. The increase in PHB did not lead to significant alterations in the internal fluxes of the network, but the other biomass output fluxes were reduced. There was also a simultaneous decrease in the amounts of protein, lipids and nucleic acids synthesized in the micro-aerobic cultures.

Accumulation of PHB has been reported in ORS571 and other diazotrophs like *Azotobacter* under conditions of O_2 limitation (Mandon et al., 1998; Jackson & Dawes, 1976; Senior & Dawes, 1971; Pauling et al., 2001). This observation also agrees with a previous study which showed that PHB degradation in ORS571 free-living cultures did not occur under micro-aerobic conditions while PHB was actively degraded and utilized under aerobic conditions (Stam et al., 1986). The degradation of PHB under aerobic conditions might be essential to fulfil the requirements of carbon and energy for growth and survival under the conditions of carbon starvation in the rhizosphere (Stam et al., 1986; Ratcliff et al., 2008). While under micro-aerobic conditions, such as those inside nodules, the increased flux to PHB synthesis can be explained as a metabolic requirement to maintain redox balance of the cell as described by Trainer & Charles (2006). Under low O_2 conditions, the redox potential of the cell decreases and there is a concurrent rise in cellular NAD(P)H levels. The excess NAD(P)H inhibits the enzymes of the TCA cycle- NADP-isocitrate dehydrogenase, pyruvate dehydrogenase, citrate synthase and 2-oxoglutarate dehydrogenase, so, to prevent inhibition of TCA cycle activity, the excess acetyl-CoA and NAD(P)H are diverted away from the TCA cycle and into PHB synthesis (Senior et al., 1972; Senior & Dawes, 1973; Smith et al., 1974; Jackson & Dawes, 1976; Chohan & Copeland, 1998; Schöder et al., 1998; Trainer & Charles, 2006). Thus, PHB metabolism in ORS571 appears to be an oxygen controlled process and the organism accumulates a greater amount of PHB in a low O_2 environment. It was also recently argued by Terpolilli et al. (2016) that NAD(P)H produced by oxidation of AcCoA in the TCA cycle was balanced by storing it as PHB and lipid in pea bacteroids. In a different study, flux balance analysis of *R. etli* bacteroids also predicted that synthesis of storage polymers such as PHB and glycogen was required during N_2-fixation (Resendis-Antonio et al., 2011). In silico simulations showed that deletion of PHB synthesis in *R. etli* bacteroids resulted in increased accumulation of the polymer glycogen (Resendis-Antonio et al., 2011).

Therefore, the results obtained in the current study for ORS571 and those from previous studies confirm that there is an association of N_2 fixation and synthesis of PHB, glycogen and lipids in rhizobial and bacteroid systems under low O_2 concentrations.

The fluxes for the synthesis of biomass components were further reduced in N_2-fixing cultures as compared to the micro-aerobic cultures grown with NH_4Cl. Clearly, during N_2 fixation the metabolic network of ORS571 altered the distribution of carbon and co-enzyme between the biomass synthesis, N_2 fixation and other cellular activities.

The process of N_2-fixation in the free-living cultures of ORS571 was observed to cause changes in the internal fluxes of the network, with fluxes through the TCA cycle reactions (*tca1*, *tca2*, *tca4*, *tca5*, *tca6*, *tca7* and *tca8*) increasing significantly. The TCA cycle was the primary carbon utilisation pathway in N_2-fixing ORS571 during growth on succinate and also the major source for production of ATP, NADH, $FADH_2$ and NADPH for the system. Reduction of N_2 by nitrogenase consumed a significant proportion of the co-enzymes produced by the TCA cycle; 85% of the total ATP and 71% of the total NADPH was used for N_2 reduction and only a small proportion was used for biomass production (< 20%). This was in contrast to micro-aerobic ORS571 grown with NH_4Cl where the majority of the ATP produced by the network was utilised via *pepck* followed by biomass production. Also, all of the NADPH produced by the network reactions was used for biomass production in the micro-aerobic cultures (53% amino acid, 12% lipid and 36% for PHB synthesis). In addition to N_2 reduction, autoprotection or oxygen protection activity of the nitrogenase enzyme in ORS571 also consumes ATP and reducing equivalents (Boogerd et al., 1998). This autoprotection mechanism of the Fe component of nitrogenase reduced inactivation of nitrogenase by O_2 during diazotrophic growth (Boogerd et al., 1998). Hydrogen production during N_2 fixation also consumed additional energy and reducing equivalents (Schubert & Evans 1976; Bothe et al., 1977; Pacovsky et al., 1984; Stam et al., 1987). In another diazotroph, *Kelbsiella*

pneumoniae, hydrogen evolution during N_2 reduction by nitrogenase has been reported to be an ATP consuming process which affects the efficiency of N_2 fixation (Hill, 1976). Although ORS571 possesses a hydrogenase uptake system which recycled the hydrogen produced by nitrogenase activity but the energy produced by reoxidation of hydrogen was not enough to regain the energy invested in H_2 production or for N_2 reduction. (Stam et al., 1984; Stam et al., 1987; Baginsky et al., 2004). Therefore, the process of N_2 fixation and its associated activities of oxygen protection and hydrogen evolution require significant amounts of energy and reducing equivalents in ORS571.

The TCA cycle was the primary metabolic pathway that supported growth and N_2 fixation process in the free-living diazotrophic ORS571. These results agree with the previous reports on bacteroids of fast growing rhizobia, *Sinorhizobium meliloti* and *Rhizobium leguminosarum*, which required a complete TCA cycle to drive N_2 fixation (Dunn, 1998; White et al., 2007). The involvement of the TCA cycle in diazotrophic ORS571, also agreed with the results from flux balance analysis (FBA) of *R. etli* bacteroids and *S. meliloti* which predicted active TCA cycle, for utilisation of di-carboxylates- the primary carbon source for the bacteroids (Resendis-Antonio et al., 2011; Zhao et al., 2012). Zhao et al. (2012) suggested that a tight coupling between the TCA cycle, electron transport and N_2 fixation was required to establish effective symbiotic N_2 fixation in the host nodules. While in a different study, *Bradyrhizobium japonicum* mutants defective for TCA cycle enzymes like isocitrate dehydrogenase and aconitase, were reported to retain N_2 fixation activity in the host (Thöny-Meyer & Kunzler, 1996; Shah & Emerich, 2006). This suggests that the involvement of TCA cycle to support N_2 fixation in rhizobia can be species dependent and there should exist alternative pathways, which can bypass the full TCA cycle activity for rhizobial metabolism during N_2 fixation. A different study performed ^{13}C-MFA of photosynthetic and N_2-fixing cyanobacteria and identified greater flux via TCA cycle and oxidative PPP, that synthesized reducing equivalents and precursors required for N_2 fixation

(Alagesan et al., 2013). The study showed a slower growth of the organism under N_2-fixing conditions (Alagesan et al., 2013). The results obtained in this study for diazotrophic ORS571 were comparable to the above study in photosynthetic cyanobacteria in that slower growth and increased fluxes via the TCA cycle were associated with the process of N_2 fixation.

In this study, higher fluxes were measured for the two reactions catalysed by NAD(P)-ME (*mal*) and PDH (*tca9*) under micro-aerobic N_2 fixation conditions, making this the preferred pathway for AcCoA synthesis. There were no statistically significant differences in these fluxes between micro-aerobic and N_2-fixing conditions because of the limitations of this analysis to produce well defined confidence limits for these fluxes. Despite these limitations, the involvement of these two fluxes during N_2 fixation cannot be ignored. The flux via *mal* and *tca9* during N_2 fixation was likely to channel carbon towards AcCoA synthesis that was ultimately partitioned to TCA cycle, PHB and lipid synthesis. Previously, it was reported that NAD(P)-ME enzyme mutants of ORS571 were able to maintain N_2-fixing activity as free-living cultures but completely lost its symbiotic N_2-fixing ability on the host plant (Suzuki et al., 2007). However, in a subsequent study $NAD(P)^+$-ME mutants of *S. meliloti* still maintained symbiotic N_2-fixation in the host (Zhang et al., 2012a). This suggests that the requirement of NAD(P)-ME under symbiotic N_2-fixation is species dependent. There was a report on PDH mutants of ORS571 which maintained N_2-fixation in cultures but lost the symbiotic ability to fix N_2 on the host (Pauling et al., 2001) and an alternative pathway for AcCoA synthesis from malate or succinate via MSDH activity was proposed to explain this observation. The flux through this alternative pathway was observed to be minimal during N_2 fixation in the free-living ORS571 cultures. This suggests that the alternative pathway could potentially operate in the absence of NAD(P)-ME and PDH activity to sustain N_2 fixation in the free-living cultures under micro-aerobic condition.

A significant increase in the net CO_2 output and reduced CCE was observed for the micro-aerobic N_2-fixing cultures. A different study showed that the CCE of *E. coli* growing on glucose was lower during anaerobic growth (24.1%) as compared to that during aerobic growth (51.7%) (Chen & Sachar-Hill, 2012). This study reported an increase in the glucose uptake rates and in the internal fluxes via glycolysis but reduced growth rate and reduced production of biomass under anaerobic conditions. Also, the intracellular maintenance costs for the anaerobic *E. coli* cultures (51.1%) were reported to be higher than in aerobic cultures (37.2%) (Chen et al., 2011). The increased maintenance costs for the anaerobic *E. coli* cultures were reported to be associated with the protons secreted during fermentative metabolism. The results obtained in this study can be related to the study by Chen et al. (2011), where the micro-aerobic N_2-fixing cultures had longer doubling times, reduced CCE and required an increase in the internal fluxes (TCA cycle) to support nitrogenase activity and its associated maintenance costs.

4.13 Conclusion

This study used ^{13}C-MFA to determine the metabolic adaptations in ORS571 required for N_2 fixation. The flux maps were obtained using the methods established in chapter 3, and they provide an understanding of the metabolic changes in ORS571 that occur during micro-aerobic N_2 fixation. This process of N_2 fixation requires a low O_2 environment in order to function. Due to the low O_2 conditions, the fluxes to biomass outputs of the metabolic network changed significantly. An increase in flux to PHB synthesis was necessary, presumably to maintain redox potential of the cell during growth under low O_2 conditions, and a simultaneous decrease in fluxes to protein, lipids and nucleic acid synthesis was required to balance against the increased PHB accumulation in the cell. The process of N_2 fixation also requires a sufficient source of ATP and NADPH; the metabolic network meets this requirement by a significant increase in fluxes through seven reactions of the TCA cycle involving succinate

dehydrogenase, fumarase, citrate synthase, aconitase, isocitrate dehydrogenase, 2-oxoglutarate dehydrogenase and succinyl-CoA synthetase. The TCA cycle utilised the majority of the carbon and produced the majority of the ATP, NADH and NADPH that were ultimately used for N_2 fixation, growth, cell division, biomass synthesis and maintenance activities of the system. The major adaptations in the metabolic network identified in this chapter highlight the two central pathways - the TCA cycle and PHB synthesis - that were important to establish N_2 fixation in ORS571. This information will be necessary while designing or engineering a synthetic symbiont for non-legume plants. To assess the extent to which the metabolic adjustments during N_2 assimilation observed for free-living ORS571 reflects the conditions during a natural symbiosis, it is necessary to obtain flux maps for ORS571 in association with its host legume *Sesbania rostrata*. The next chapter focuses on MFA of symbiotic ORS571, allowing comparison of the flux maps under free-living and symbiotic N_2-fixing condition.

5. Metabolic behaviour of ORS571 during symbiosis

5.1 Introduction

The semiaquatic tropical legume, *S. rostrata* can harbour ORS571 in both root and stem nodules during symbiosis (Choma, et al., 2012). The phenotypic characteristics of stem nodules are different from those of the root nodules. The mechanism of root nodulation in *S. rostrata* was described as intermediate between determinate and indeterminate nodule types and was previously reported to occur in four developmental stages (Goormachtig et al., 2004). The root nodules formed in *S. rostrata* are non-green and localized at the base of lateral roots and root hairs. Under aerated and non-flooded soils, infection of the host roots occurs by root hair curling invasion (Goormachtig et al., 2004). In flooded or waterlogged soils, the bacteria enter the host by intercellular invasion through cracks on the lateral root base and proliferate in the infection pockets. The bacteria move through the infection threads originating from infection pockets and are finally released into the nodule primordia. Stem nodules are localized at the site of lateral root primordia on the stems and are green due to the presence of chloroplasts in the nodule cortex (Gebhardt et al., 1984; Denduluri & Bal, 1995) . Unlike root nodules, the stem nodules exhibit photosynthetic activity along with N_2 fixation. Similar to lateral root base invasion in waterlogged root nodules, ORS571 enters the host stem by intercellular invasion; via cracks at the base of root primordia which are present along the length of the stem (Ndoye et al., 1994; D'Haeze et al., 1998). The bacteria proliferate in the epidermal fissures at the lateral root primordia followed by the formation of cortical infection pockets. From these pockets, the bacteria move along the infection thread and finally enter the nodule primordia, where they differentiate into N_2-fixing bacteroids (Goormachtig et al., 2004; Suzuki et al., 2007).

There are differences in the nitrogenase activities of the root and stem nodules, and the higher nitrogenase rates exhibited by the stem nodules was attributed to their photosynthetic activity (Hungria et al.,1992; Saraswati et al., 1992). An azorhizobial

outer membrane autotransporter (AoaA) was previously identified to be associated with the high nitrogenase activity of the bacteroids in the stem nodules (Suzuki et al., 2008). AoaA was proposed to play an important role in supressing plant defence responses; and ORS571 defective for AoaA showed reduced EPS production which compromised the symbiotic interaction between the symbionts (Suzuki et al., 2008). The lipopolysaccharides-protein complexes in the outer membrane of ORS571 was also reported to be responsible for the biotic and abiotic stress tolerance of the stem nodules (Sharma et al., 2011). Lipid accumulation in the form of oleosomes in the stem nodules was reported to be significantly higher than in the root nodules. It was suggested that triacylglycerol, synthesized from photosynthetically derived sucrose in the stem nodules resulted in higher accumulation of lipids while the lower lipid content of root nodules was due to the lower availability of photosynthates (Denduluri & Bal, 1995).

From these previous studies, it is clear that there are physiological and metabolic differences between the two nodule types of *S. rostrata*, but there is little information on the extent to which the bacteroids in the two nodule types differ in their metabolic behaviour. It is also unclear whether the metabolic phenotype of ORS571 bacteroids differs from that of the free-living N_2-fixing state. The aim of this chapter was to use ^{13}C-MFA to measure the metabolic fluxes of the bacteroids that fixed N_2 in the stem and root nodules. The flux maps obtained for the two types of bacteroid were compared to identify metabolic differences arising from the different nodule phenotypes. The flux maps for the bacteroids were also compared to that obtained for free-living N_2-fixing ORS571 to identify the metabolic adaptations in the symbiotic forms of ORS571 (Figure 5.1).

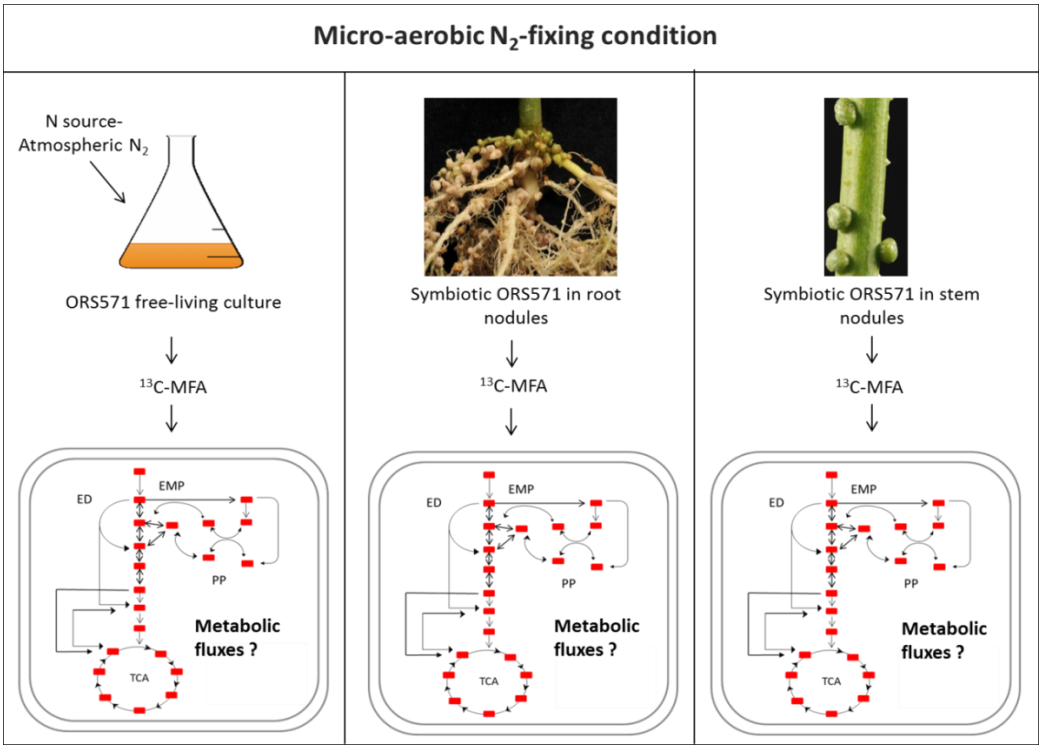

Figure 5.1: **Strategy to study the metabolic adjustments in ORS571 during symbiotic N_2-fixation in root and stem nodules of *S. rostrata*.**

5.2 Physiological characteristics of ORS571 bacteroids

5.2.1 N_2 fixation ability of isolated bacteroids

ORS571 nodulated both roots and stem of *S. rostrata* within two to three weeks after inoculation of the plant. Isolation of bacteroids was done according to the method described in section 2.6 at a much reduced O_2 concentration (< 1%) to prevent inhibition of nitrogenase activity. Nitrogenase activity was measured by the method described in section 2.7.3 and the rates were compared with that of free-living cultures (Figure 5.2).

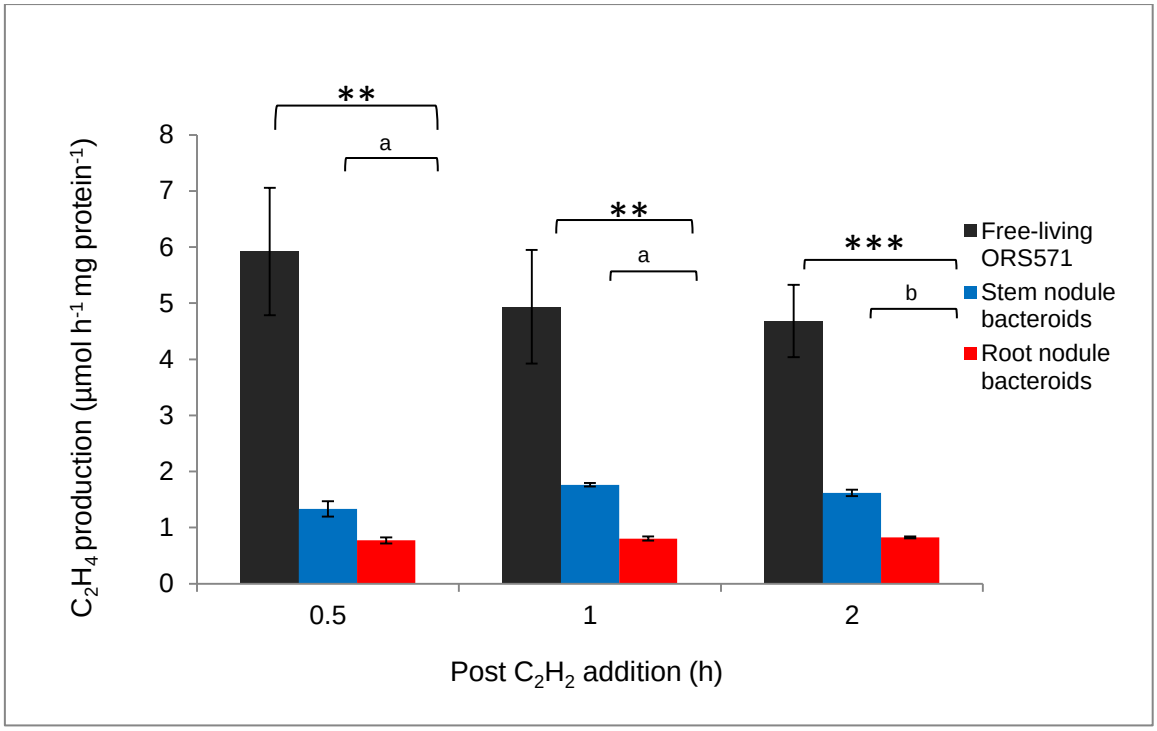

Figure 5.2: **Comparison of nitrogenase activities between free living and symbiotic forms of ORS571.** The amounts of ethylene (C_2H_4) produced by the nitrogenase actvities of the cultures and bacteroids was measured at 0.5 h, 1 h and 2 h after adding acetylene (C_2H_2). Significant differences in the rates measured for the bacteroids and the free-living cultures as determined by ANOVA are indicated: **, p-value < 0.01; ***, p-value < 0.001. Significant differences in the rates measured for stem and root nodule bacteroids as determined by t-test are indicated: a, p-value < 0.05; b, p-value < 0.01. Values are the mean ± SEM from three biological replicates for the cultures and three technical replicates for the bacteroids.

Both stem and root nodule bacteroids had significantly lower nitrogenase activities than the free-living cultures. Also, the rate measured for stem nodule bacteroids was higher than of the root nodule bacteroids. These results confirm that there were differences in the rates of N_2-fixation between the free-living and symbiotic forms of ORS571.

5.2.2 Stability of nitrogenase activity

This analysis was done to check if the bacteroids were stable and retained their nitrogenase activities after isolation from the root and stem nodules (Figure 5.3).

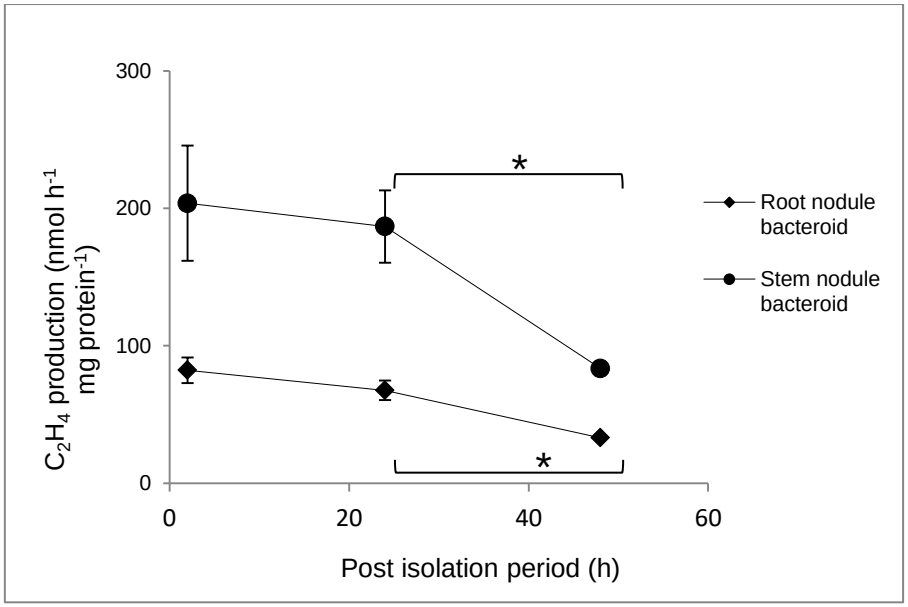

Figure 5.3: **Stability of nitrogenase activity in isolated bacteroids.** Values are the mean ± SEM from three determinations. Significant differences in the rates measured at 24 h and 48 h for both root and stem nodule bacteroids as determined by t-test are indicated: *, p-value < 0.05.

Nitrogenase rates were detected even at 48 h post isolation, however there was a decrease from 2 to 48 h. Between 2 and 24 h the rate reduced by 16% and 20.5% for root and stem nodule bacteroids respectively. Between 24 to 48 h, the rate further decreased by 44.5% and 48.5% for root and stem nodule bacteroids respectively. Clearly, the bacteroids retained their nitrogenase activities post isolation but there was a slow decrease that became significant after 48 h. From this analysis, it was confirmed that the nitrogenase activity of the isolated bacteroids decreased after isolation over time and this puts a limit on the time available for the labelling experiment. So, a labelling duration of 24 h was chosen to allow sufficient ^{13}C incorporation into the biomass of the bacteroids, while minimising the loss of nitrogenase activity.

5.2.3 Growth characteristics of bacteroids

In contrast to free-living cultures, bacteroids isolated from both root and stem nodules showed no growth. The non-dividing state of the bacteroids was confirmed by

measuring the dry weight of the bacteroids at 2 h, 24 h and 48 h post isolation (Figure 5.4). This indicates that unlike the ORS571 free-living N_2-fixing cultures, the N_2-fixing bacteroids do not multiply in mature nodules.

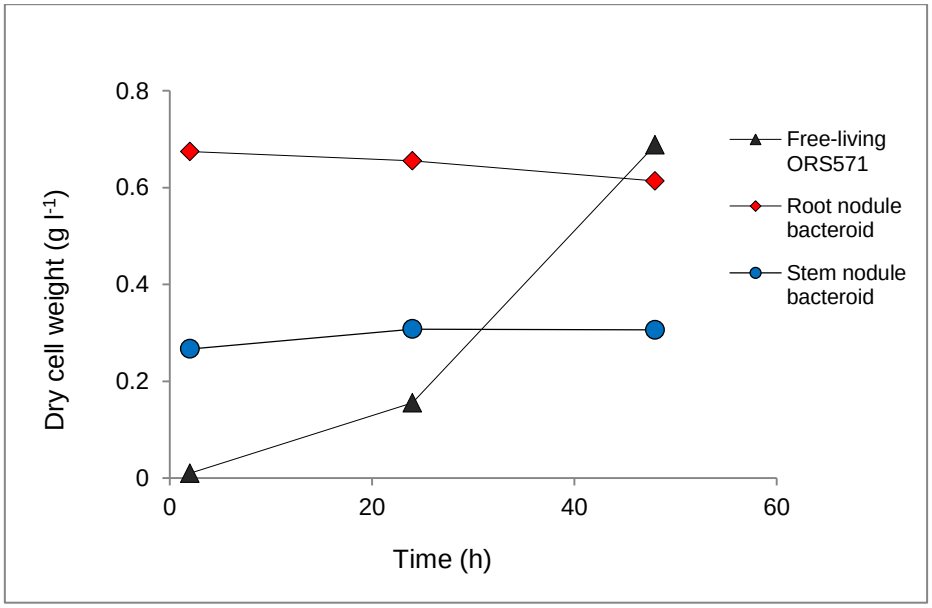

Figure 5.4: **Comparison of dry cell weight of bacteroids isolated from root and stem nodules with measurements of free-living cultures during N_2-fixation.** Values are the mean of three determinations for the free-living ORS571 and single measurements for the bacteroids.

5.3 Metabolic characteristics of isolated bacteroids

5.3.1 Biomass composition

The biomass composition of the bacteroids post isolation from the nodules was measured according to the methods described in section 2.8. Around 50% of the cell dry weight of the bacteroids was made of PHB, followed by protein, lipid, RNA, EPS and carbohydrate, with DNA as a minor component (Figure 5.5).

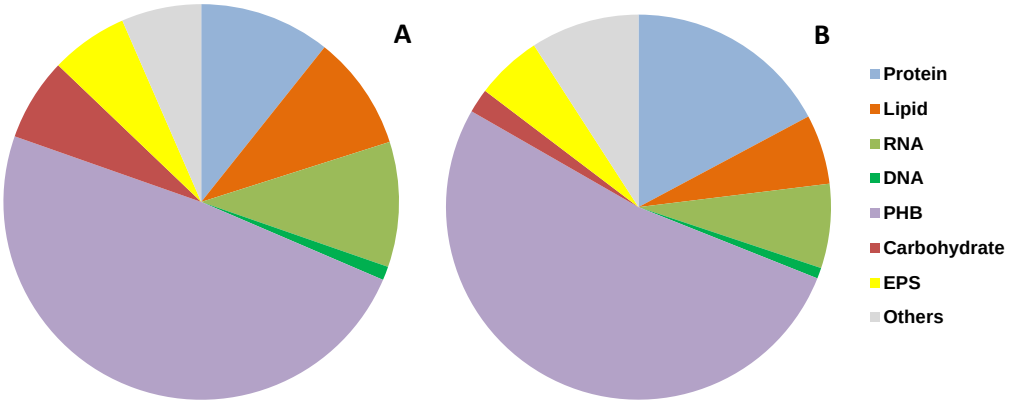

Figure 5.5: **Biomass composition of ORS571 bacteroids.** Measurements for protein, lipid, RNA, DNA, PHB, carbohydrate and EPS are expressed as percentage of dry cell weight for bacteroids isolated from root (A) and stem (B) nodule. Values are the mean of three determinations.

5.3.2 Comparison of biomass composition

The comparison of biomass composition of the bacteroids and micro-aerobic, N_2-fixing free-living cultures (chapter 4) is shown in Figure 5.6. The bacteroids isolated from root and stem nodules showed no significant differences in the amounts of protein, lipid, RNA, DNA, PHB, carbohydrate and EPS synthesized from the two nodule types. The amounts of protein, lipid and EPS of the bacteroids differed significantly as compared to the free-living cultures.

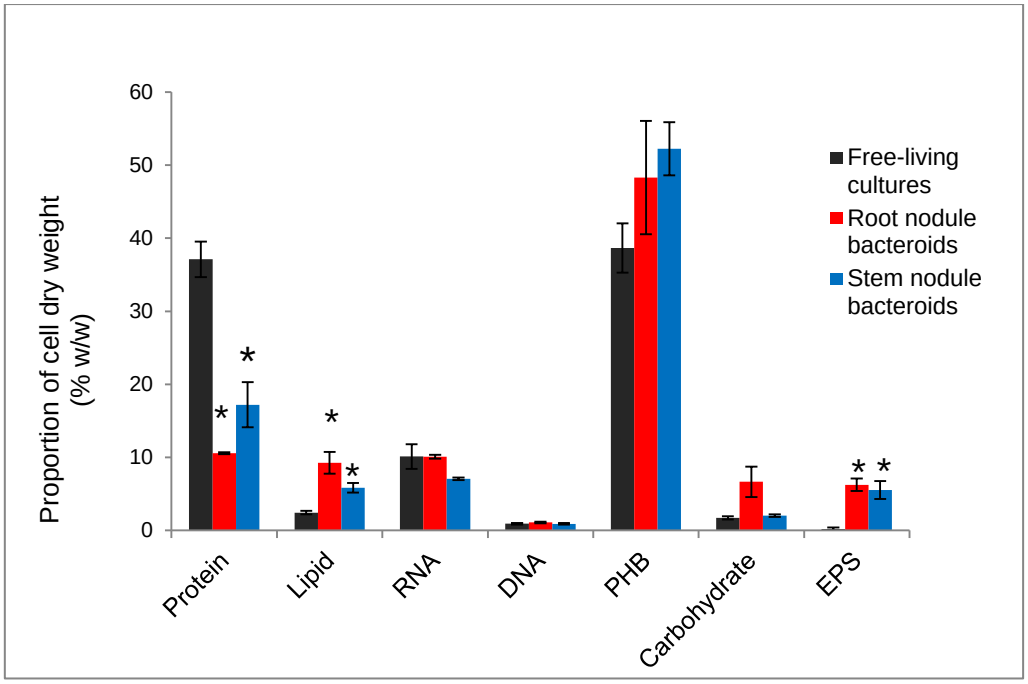

Figure 5.6: **Comparison of biomass composition between bacteroids and free-living cultures**. Values are the mean ± SEM of three determinations. Statistically significant differences in the measurements between the bacteroids and free-living cultures as determined by t-test are indicated: *, p-value < 0.05.

The amounts of lipid and EPS increased significantly over 3-fold and 31-fold, while the amount of protein reduced over 3-fold in root nodule bacteroids. In the stem nodule bacteroids, the amount of lipid and EPS increased over 2-fold and 27-fold, along with a significant reduction in the amount of protein over 2-fold.

5.3.3 Metabolite profiling of isolated bacteroids

Metabolites were extracted from root and stem nodule bacteroids according to the method described in section 2.11. GC-MS analysis and identification of metabolites was done according to the methods described in section 2.12 and 2.13. The profiles of the aqueous soluble metabolites consisted predominantly of free amino acids and sugars and are shown in Figure 5.7 and Figure 5.8. The profiles of the protein-derived amino acids and hydroxybutyrate obtained from hydrolysis of PHB present in insoluble residue after methanol-chloroform extraction for root and stem nodule bacteroids are

shown in Figure 5.9 and Figure 5.10 respectively. This analysis confirmed that the method previously established for extraction and detection of metabolites in the free-living cultures could be applied to bacteroids. The metabolite profile obtained for the bacteroids was similar to that of free-living cultures. This analysis identified metabolites that could be used to extract the mass isotopomer distributions required for ^{13}C-MFA.

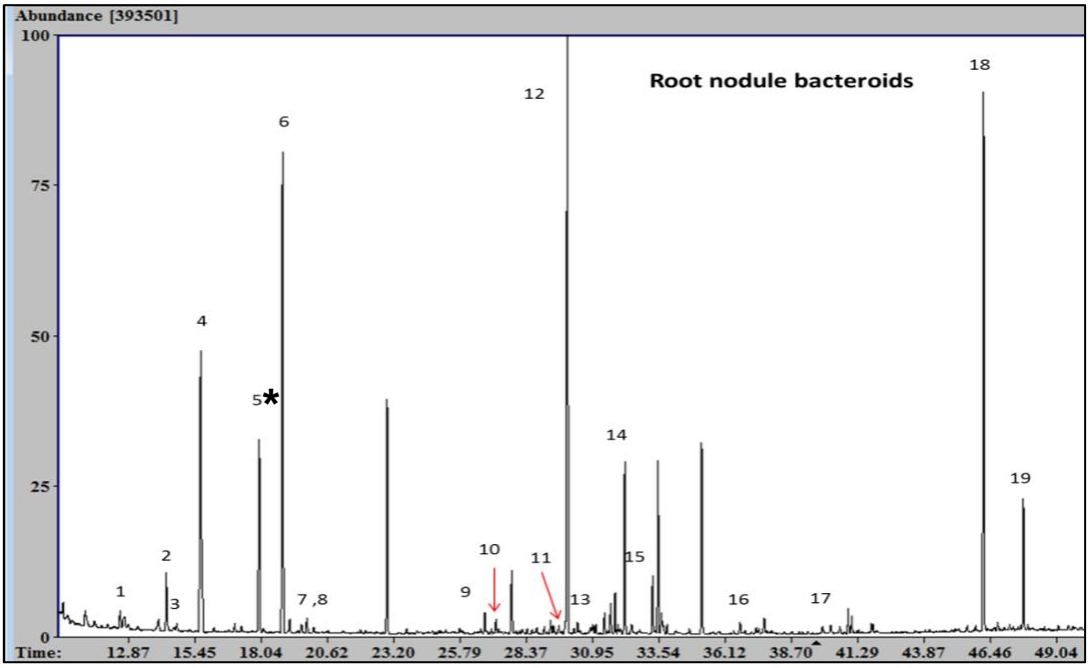

1. Glycolic acid-2TMS
2. Valine-1TMS
3. Pyruvic acid-2TMS
4. Butanoic acid, 3-hydroxy-2TMS
5. Norvaline, DL-2TMS *
6. Glycerol-3TMS
7. Imidiazole 4 acetic acid, 1-methyl-1TMS
8. Glycine-3TMS
9. Galactopyranoside, 1-0-methyl-alpha-4TMS
10. Mannopyranoside, 1-0-methyl-alpha-4TMS
11. Glucose, 1,6-anhydro beta-3TMS
12. Ribitol-5TMS
13. Putreschine, D-5TMS
14. Pinitol, D-5TMS
15. Glucopyranoside, 1-0-methyl alpha-4TMS
16. Hexadecanoic acid-1TMS
17. Octadecanoic acid-1TMS
18. Sucrose-8TMS
19. Trehalose, alpha alpha D-8TMS

Figure 5.7: **MSTFA derivatised soluble phase metabolites from root nodule bacteroids**. The peak marked with * is an exogenous compound used as internal standard for GC-MS.

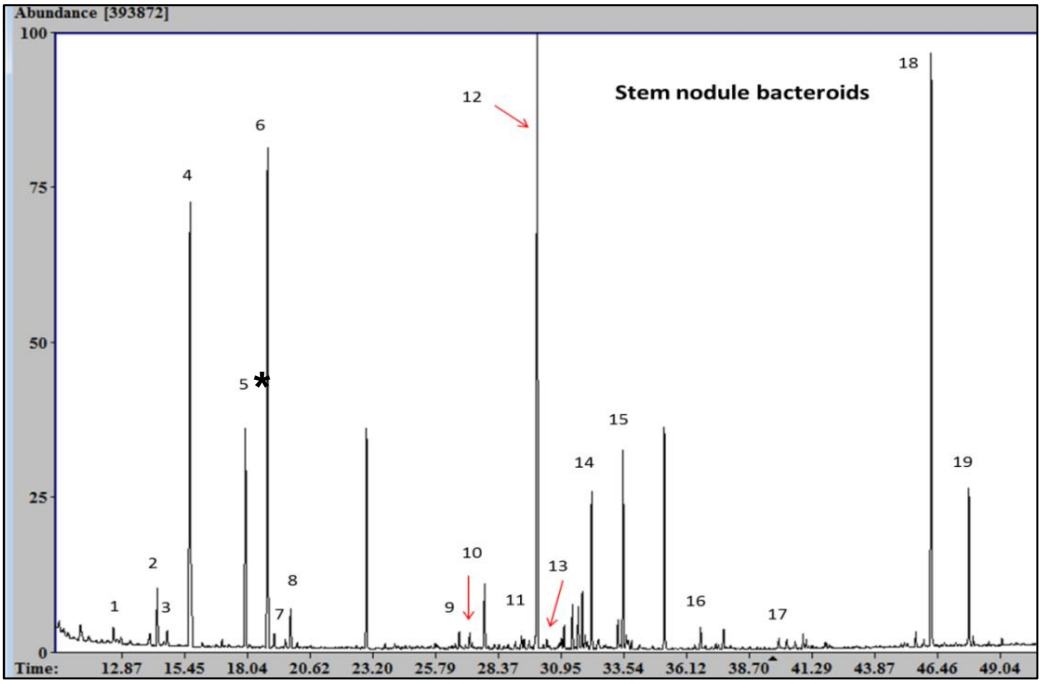

1. Glycolic acid-2TMS
2. Valine-1TMS
3. Pyruvic acid-2TMS
4. Butanoic acid, 3-hydroxy-2TMS
5. Norvaline, DL-2TMS *
6. Glycerol-3TMS
7. Imidiazole 4-acetic acid, 1-methyl-1TMS
8. Glycine-3TMS
9. Galactopyranoside,1-O-methyl alpha-4TMS
10. Mannopyranoside 1-O-methyl alpha-4TMS
11. Glucopyranoside D-5TMS
12. Ribitol-5TMS
13. Putreschine-4TMS
14. Pinitol, D-5TMS
15. Glucopyranose D-5TMS
16. Hexadecanoic acid-1TMS
17. Octadecanoic acid-1TMS
18. Sucrose-8TMS
19. Trehalose, alpha alpha-D-8TMS

Figure 5.8: **MSTFA derivatised soluble phase metabolites from stem nodule bacteroids**. The peak marked with * is an exogenous compound used as internal standard for GC-MS.

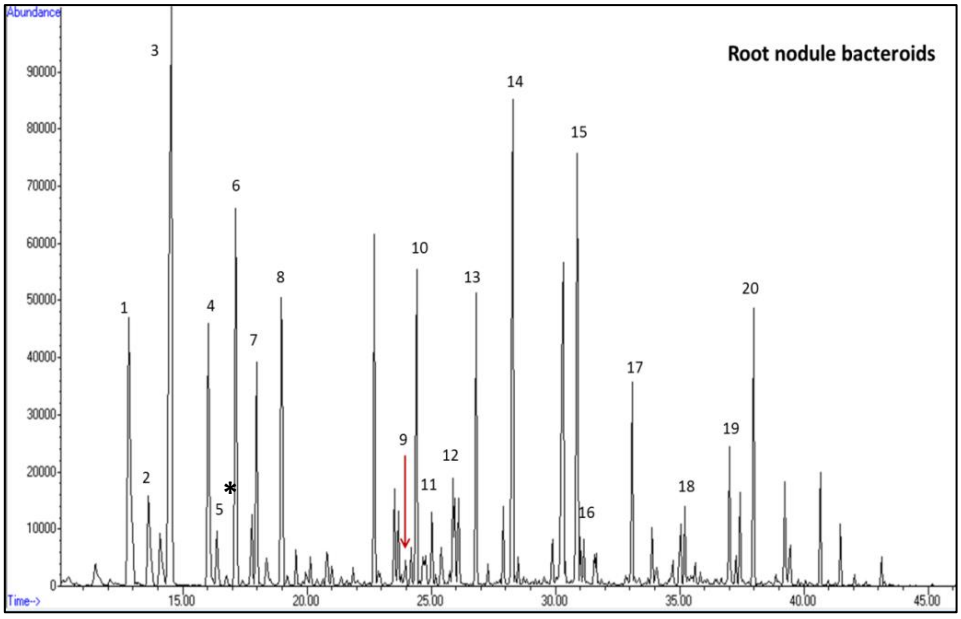

1. Alanine-2TBDMS
2. Glycine-2TBDMS
3. 3-Hydroxybutyric acid-2TBDMS
4. Valine-2TBDMS
5. Norvaline-2TBDMS*
6. Leucine-2TBDMS
7. Isoleucine-2TBDMS
8. Succinic acid-2TBDMS
9. Methionine-2TBDMS
10. Serine-3TBDMS
11. Threonine-2TBDMS
12. Proline-2TBDMS
13. Phenylalanine-2TBDMS
14. Aspartic acid-3TBDMS
15. Glutamic acid-3TBDMS
16. Proline-2TBDMS
17. Lysine-2TBDMS
18. Arginine-3TBDMS
19. Histidine-3TBDMS
20. Tyrosine-3TBDMS

Figure 5.9: **Identification of chloroform soluble metabolites from root nodule bacteroids.**

The peak marked with * is an exogenous compound used as internal standard for GC-MS.

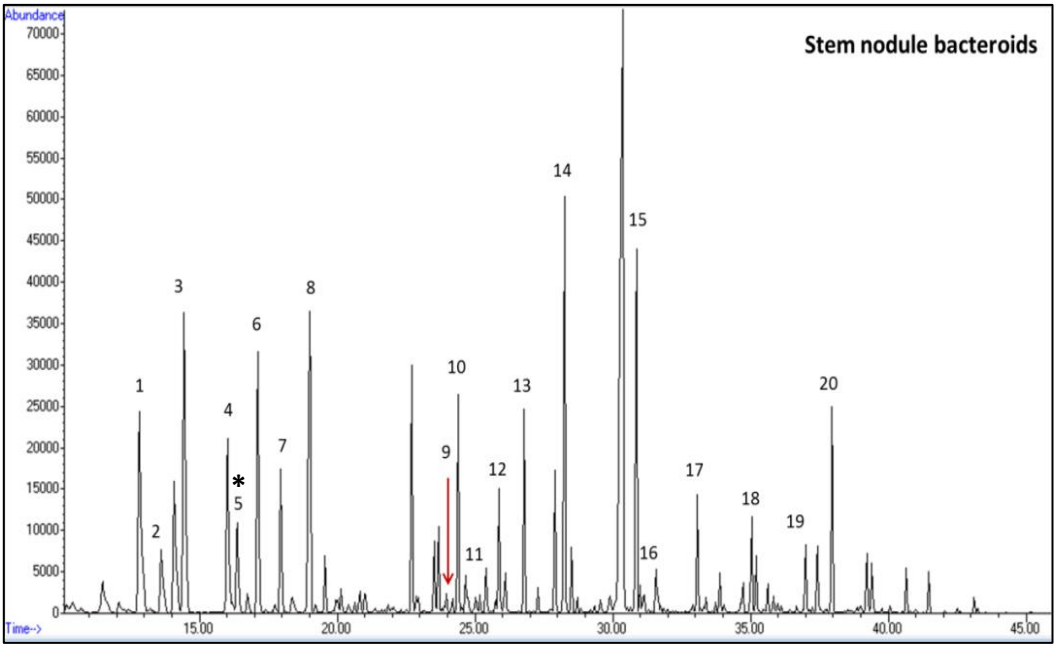

1. Alanine-2TBDMS
2. Glycine-2TBDMS
3. 3-Hydroxybutyric acid-2TBDMS
4. Valine-2TBDMS
5. Norvaline-2TBDMS*
6. Leucine-2TBDMS
7. Isoleucine-2TBDMS
8. Succinic acid-2TBDMS
9. Methionine-2TBDMS
10. Serine-3TBDMS
11. Threonine-2TBDMS
12. Proline-2TBDMS
13. Phenylalanine-2TBDMS
14. Aspartic acid-3TBDMS
15. Glutamic acid-3TBDMS
16. Proline-2TBDMS
17. Lysine-2TBDMS
18. Arginine-3TBDMS
19. Histidine-3TBDMS
20. Tyrosine-3TBDMS

Figure 5.10: **Identification of chloroform soluble metabolites from stem nodule bacteroids.** The peak marked with * is an exogenous compound used as internal standard for GC-MS.

5.4 Establishment of labelling experiments in bacteroids

5.4.1 Selection of symbiotic material for ^{13}C labelling experiments

The nitrogenase activity of symbiotic ORS571 was measured in three different states: intact root nodules excised from the host plant; sections prepared by slicing the root nodule; and isolated bacteroids (Figure 5.11). This aim of this comparison was to identify the tissue preparation with the highest nitrogenase activity given that it was impracticable to perform ^{13}C labelling experiments on whole plants.

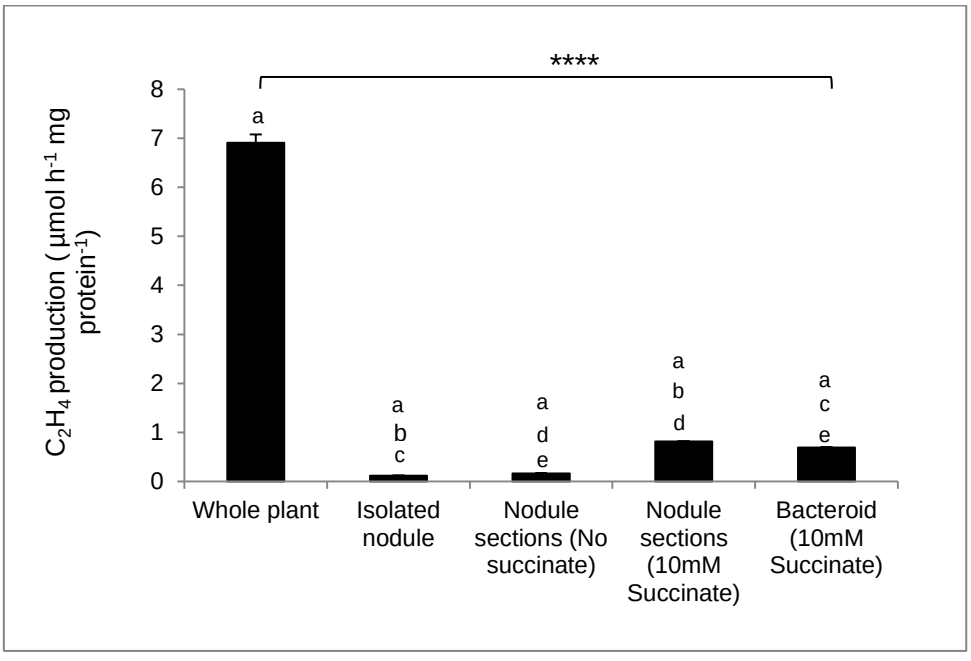

Figure 5.11: **Comparison of nitrogenase activities in symbiotic ORS571**. The measurements for the nitrogenase assay on whole plant, isolated nodule, nodule sections and bacteroids were obtained from five individual (six weeks old) *S. rostrata* plants. Values are the

mean ± SEM from three determinations. Significant differences between the five symbiotic materials as determined by ANOVA are indicated: ****, p-value < 0.0001. Different letters above the bars indicate significant pairwise differences determined by Tukey's multiple comparisons test and are indicated: a, p-value < 0.0001; b, p-value < 0.001; c, p-value < 0.01; d, p-value < 0.001; e, p-value < 0.01.

All the nodule preparations had markedly lower nitrogenase activities than that measured for the nodules insitu (the whole plant). C_2H_4 produced by nodule sections and isolated bacteroids supplemented with succinate had higher rates than the nodules and nodule sections without succinate. This suggests that a supply of carbon maintained higher nitrogenase activities in the symbiotic forms post isolation from the host plant. C_2H_4 production in isolated nodules and nodule sections without succinate accounted for only 2% and 2.3% of the whole plant activity respectively. While, the rates for those supplied with succinate were 12% and 10% of the whole plant activity respectively. This comparison identified the whole plant, nodule sections and isolated bacteroids to be better symbiotic forms for labelling experiments.

5.4.2 Choice of isotope tracer for ^{13}C labelling experiments

The impracticality of labelling the bacteroids in situ arises because: (i) there is no obvious way to introduce the labelled succinate used previously into the nodules; and (ii) labelling the plant with $^{13}CO_2$ to generate endogenously labelled substrate for the bacteroids will generate uniformly labelled substrates which will be uninformative in a steady state analysis (Roscher et al., 2000). Also, using a label other than [$^{13}C_4$]succinate would be inconsistent with the previously established methodology for ^{13}C-MFA in chapters 3 and also the results will not be comparable to that obtained in chapter 4. In section, 5.4.1, it was observed that nodule sections and bacteroids showed higher nitrogenase activities in the presence of succinate. So, to confirm that the bacteroids were able to utilise succinate, a radioactivity assay was done using [2,3-^{14}C]succinate as described in section 2.19 (Figure 5.12).

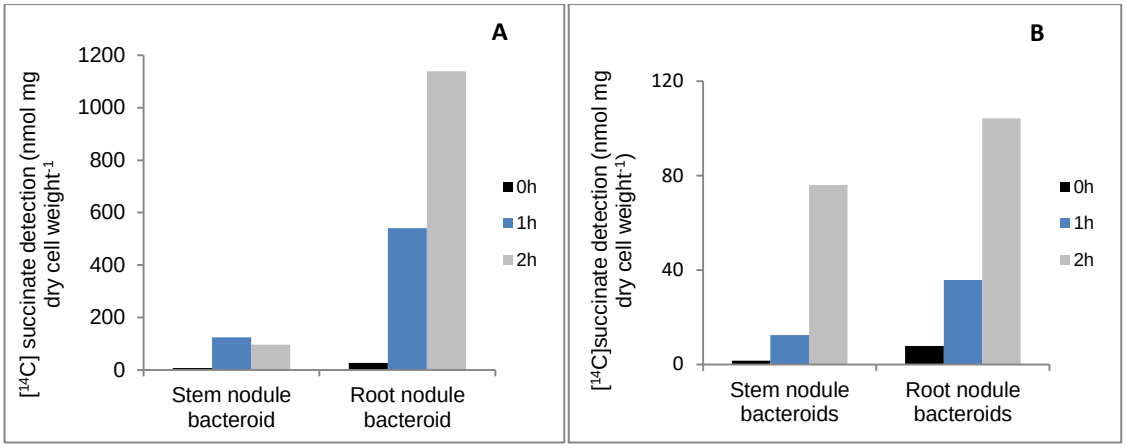

Figure 5.12: **[^{14}C]succinate detection in the in the metabolic CO_2 released (A) and intracellular metabolites (B)**. Measurements are individual determinations and were done on the bacteroids isolated from the root and stem nodule of a six-seven week old *S. rostrata* plants.

Both root and stem nodule bacteroids were able to take up and assimilate [^{14}C]succinate that was detected in the CO_2 output and in the intracellular metabolites (Figure 5.12). This analysis confirmed that succinate could be used as the tracer for labelling experiments in the bacteroids.

5.4.3 Comparison of ^{13}C incorporation in the bacteroids

From previous analyses, 5.4.1 and 5.4.2, it was observed that nodule sections and isolated bacteroids showed higher nitrogenase activities in the presence of succinate and that the bacteroids were able to metabolise succinate. So, nodule sections and isolated bacteroids were incubated with 20% [$^{13}C_4$]succinate and the ^{13}C incorporation in these symbiotic forms was compared (Figure 5.13). The aim of this analysis was to choose the symbiotic material that showed maximum ^{13}C incorporation into the biomass of the bacteroids. Labelling experiments were performed as described in section 2.14.2. Bacteroids were isolated from the nodule sections after incubation with the labelled substrate for 24 h, and the ^{13}C fractional abundance in the protein-derived amino acids of the bacteroids was calculated according to the method described in section 2.13.

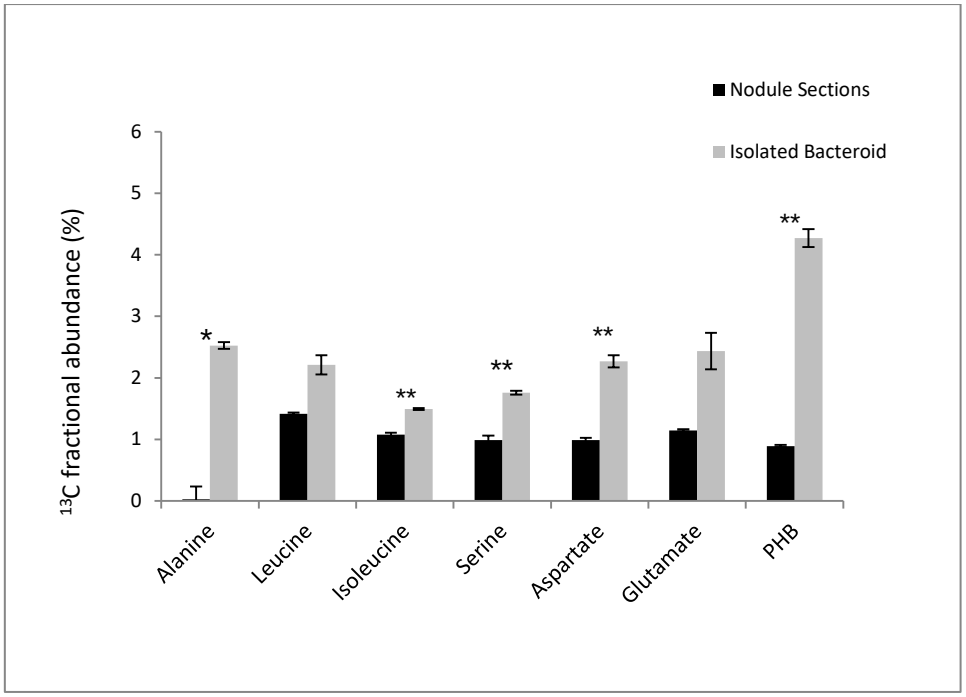

Figure 5.13: **^{13}C fractional abundance of protein-derived amino acids and PHB after labelling the bacteroids of nodule sections and isolated bacteroids.** Measurements are shown for the nodule sections and isolated bacteroids prepared from four-five week old nodules. The protein-derived amino acid molecular fragments used for this analysis are-alanine-2TBDSM, M-57, m/z 260; leucine-2TBDMS, M-85, m/z 274; isoleucine-2TBDMS, M-85, m/z 274; serine-3TBDMS, M-57, m/z 390, aspartate-3TBDMS, M-57, m/z 418; glutamate-3TBDMS, M-57, m/z 432; and PHB-2TBDMS, M-57, m/z 275. Significant differences in the measurements was determined by t-test and are indicated:*, p-value < 0.05; **, p-value < 0.01. Values are the mean ± SEM from three determinations.

Both nodule sections and isolated bacteroids had low fractional abundances of ^{13}C. This can be explained by the non-growing state of bacteroids and hence reduced turnover of protein, which showed lower ^{13}C fractional abundances. Isolated bacteroids showed higher ^{13}C fractional abundance than the bacteroids from the nodule sections (Figure 5.13). The reduced ^{13}C incorporation in the bacteroids of the nodule sections was probably due to the restricted diffusion to the host cells. Bacteroids have greatly reduced intercellular air spaces and thus tighter packing of the host cells making it difficult for the succinate to penetrate the tissue. But, bacteroids isolated from the

nodules were able to access the substrate directly and therefore, showed a higher incorporation of ^{13}C in the protein-derived amino acids. From this analysis, isolated bacteroids from the roots of *S. rostrata* were preferred over the nodule sections to be used as the appropriate symbiotic system for labelling experiments.

5.4.4 Influence of nodule age on ^{13}C incorporation in the bacteroids

To check if the ^{13}C fractional abundance measured in the isolated bacteroids depended on the age of the nodules, labelling experiments were performed on isolated bacteroids from root nodules varying in age. Root nodules were harvested from the plants after three, four, six and eight weeks post inoculation with ORS571. The incorporation of ^{13}C in the metabolites of isolated bacteroids was observed to vary with the age of the nodules (Figure 5.14). Bacteroids isolated from mature or old nodules showed minimal ^{13}C fractional abundance in the protein-derived amino acids and PHB. The probable explaination for this was the comparatively reduced turnover of protein and PHB in the bacteroids of the mature nodules. Early or young nodule bacteroids (three weeks post inoculation with ORS571) showed higher ^{13}C fractional abundance as compared to the bacteroids in mature nodules. Similar differences in ^{13}C fractional abundance was observed for the bacteroids isolated from three week and eight week old stem nodules (Figure 5.15). Based on this analysis, three week old nodules were chosen as the best stage for isolation of bacteroids from the root and stem nodules for labelling experiments.

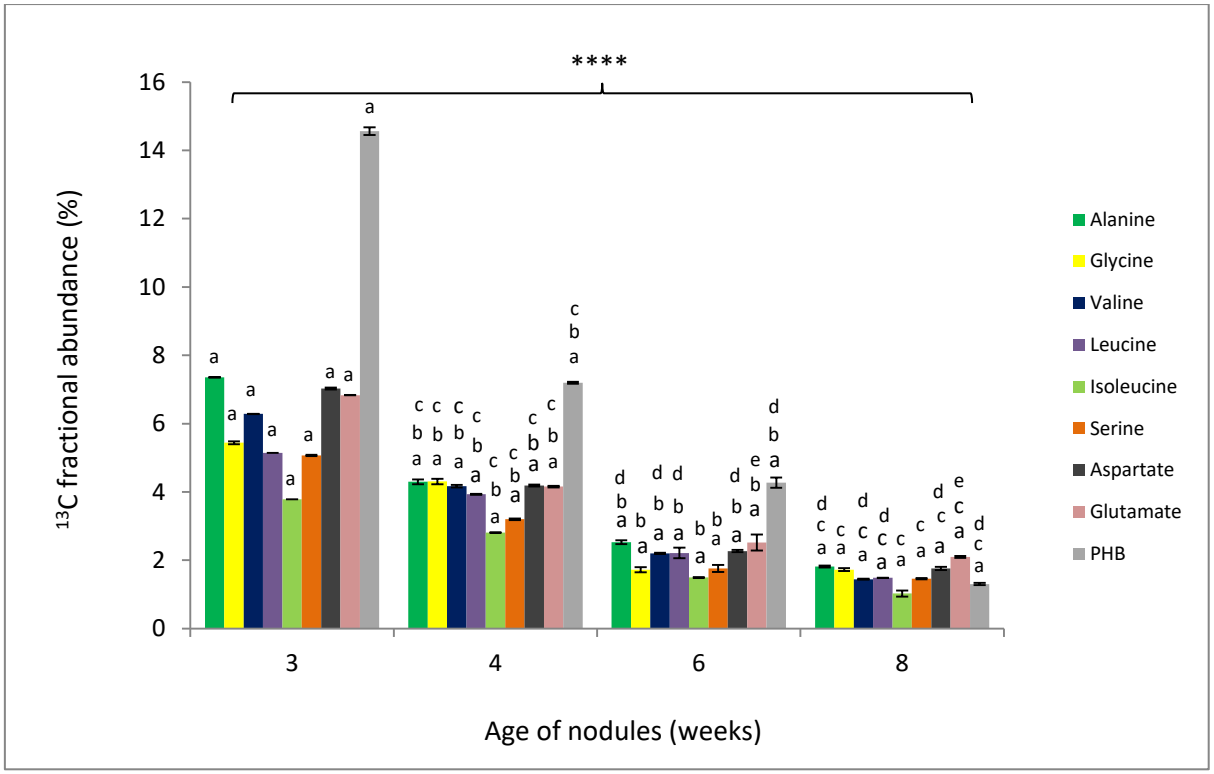

Figure 5.14: **Influence of nodule age on the ^{13}C incorporation of bacteroids isolated from root nodules**. Measurements are shown for bacteroids isolated from three, four, six and eight week old nodules of *S. rostrata*. The protein-derived amino acid molecular fragments used for this analysis are- alanine-2TBDMS, M-57, m/z 260; glycine-2TBDMS, M-57, 246; valine-2TBDMS, M-57, m/z 288; leucine-2TBDMS, M-85, m/z 274, C1-6; isoleucine-2TBDMS, M-159, m/z 200; aspartate-3TBDMS, M-57, m/z 418; serine-3TBDMS, M-57, m/z 390; glutamate-3TBDMS, M-57, m/z 432; PHB-2TBDMS, M-57, m/z 275. Significant differences between the measurements were determined by ANOVA test and are indicated: ***, p-value < 0.001. Significant differences for each amino acid between the nodules of four ages were determined by Tukey's multiple comparison test and are indicated: a, b, c, d, p-value < 0.0001; e, p-value < 0.01. Values are the mean ± SEM from three determinations.

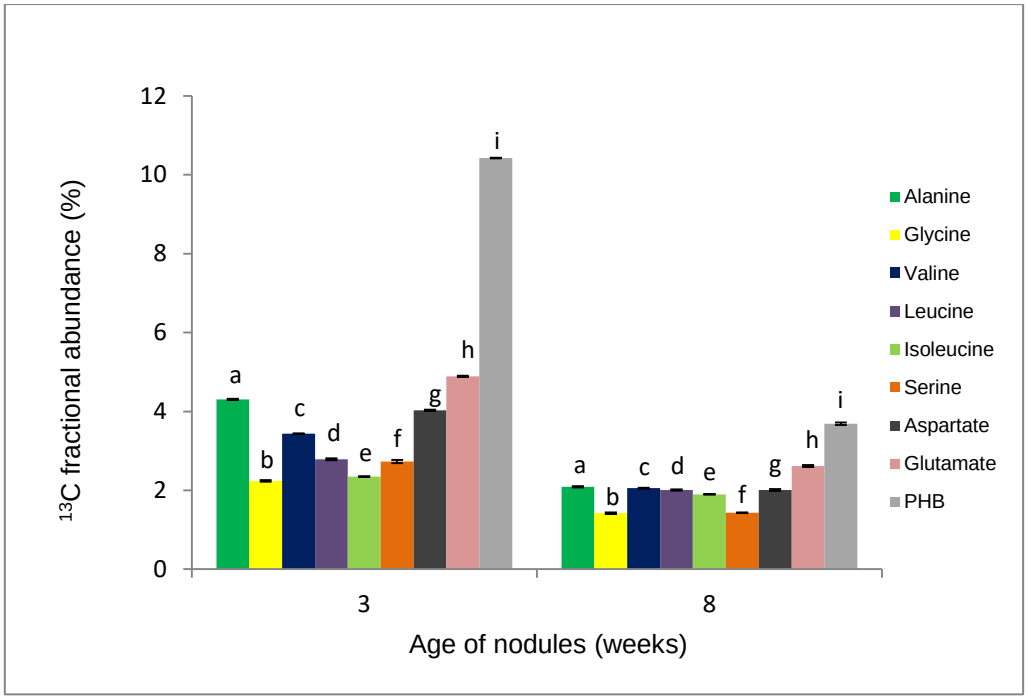

Figure 5.15: **Influence of nodule age on the ^{13}C incorporation of bacteroids isolated from stem nodules**. Measurements are shown for bacteroids isolated from three and eight week old stem nodules of *S. rostrata*. The protein-derived amino acid molecular fragments used for this analysis are- alanine-2TBDMS, M-57, m/z 260; glycine-2TBDMS, M-57, 246; valine-2TBDMS, M-57, m/z 288; leucine-2TBDMS, M-85, m/z 274, C1-6; isoleucine-2TBDMS, M-159, m/z 200; aspartate-3TBDMS, M-57, m/z 418; serine-3TBDMS, M-57, m/z 390; glutamate-3TBDMS, M-57, m/z 432; PHB-2TBDMS, M-57, m/z 275. Significant differences for each amino acid between the nodules of two ages were determined by t- tests and are indicated: a, b, c, d, e, f, g, h, i, p-value < 0.0001. Values are the mean ± SEM from three determinations.

5.5 Steady state ^{13}C-MFA of symbiotic ORS571

5.5.1 Establishment of metabolic and isotopic steady state

Bacteroids, post isolation from root and stem nodules did not show any significant increase in dry weight (Figure 5.4), implying that the bacteroids did not proliferate post isolation from the root and stem nodules. During symbiotic N_2 fixation, bacteroids are non-growing and act as nitrogen-fixing organelles inside the host (Goormachtig et al.,

2004; Oldroyd et al., 2011; Vercruysse et al., 2011). Also, the bacteroids inside the nodules have been reported to have reduced metabolism (Van de Velde et al., 2010). Since the bacteroids did not show a change in the dry weight post isolation, the non-growing bacteroids were considered to be in a metabolic pseudo-steady state. There are other instances where similar assumptions were made for non-proliferating mammalian cell cultures to be in metabolic pseudo-steady state (Buescher et al., 2015).

The labelling experiments were performed in triplicate using 20% [$^{13}C_4$]succinate as the tracer for isolated root and stem nodule bacteroids. To assess if the bacteroids incubated with 20% [$^{13}C_4$]succinate achieved isotopic steady state over the labelling period, the MID obtained from 13 protein-derived amino acids were compared for bacteroids incubated for 18 h and 24 h, using a line of best fit for the measurements (Figure 5.16). There was a displacement of the line of best fit from the origin and this was presumably caused by a substantial number of measurements with negligible labelling after 18 h and significant but still low labelling after 24 h. There was a positive correlation (R^2 value) between the MIDs at 18 h and 24 h, which indicated that the measurements were similar across the two time points. Based on this, an isotopic steady state was assumed was assumed for the corresponding fragments.

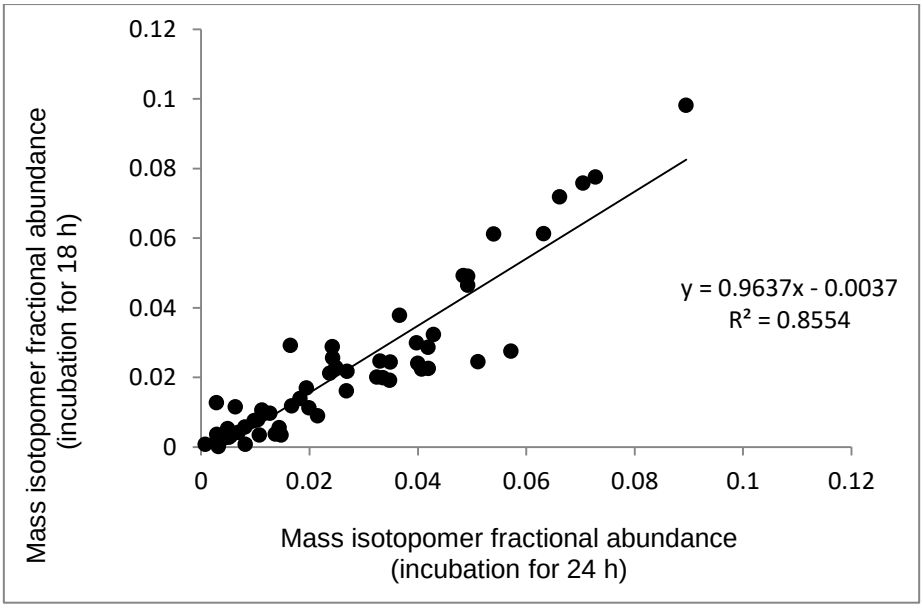

Figure 5.16: **Comparison of mass isotopomer distribution of protein-derived amino acids in the bacteroids incubated for 18 h and 24 h.** The amino acid fragments used in these analyses are: alanine-2TBDMS, M-57, m/z 261-263, C1-3; glycine-2TBDMS, M-57, 247-248, C1-2; valine-2TBDMS, M-57, m/z 289-293, C1-5; leucine-2TBDMS, M-57, m/z 303-308, C1-6; isoleucine-2TBDMS, M-57, m/z 303-308, C1-6; methionine-2TBDMS, M-57, m/z 321-325, C1-5; serine-3TBDMS, M-57, m/z 391-393, C1-3; C1-4; f302, m/z 302-304, C1-2; proline-2TBDMS, M-57, m/z 287-291, C1-5; phenylalanine-2TBDMS, M-57, m/z 337-345, C1-9; f302, m/z 302-304, C1-2; aspartate-3TBDMS, M-57, m/z 419-422, C1-4; glutamate-3TBDMS, M-57, m/z 433-437, C1-5;tyrosine-3TBDMS, f302, m/z 302-304, C1-2;. For clarity, the fractional abundance of unlabelled mass isotopomers are excluded from the plot. The MIDs at both time points are the mean of three determinations.

5.6 Generation of flux distributions

Metabolites were extracted from the bacteroids post incubation and MIDs of the labelled metabolites (protein-derived amino acids and PHB) were generated according to the methods established in section 3.7. Corrections were made for the MS measurements by using additional reactions in the model to compensate for the presence of naturally occurring ^{12}C pools that diluted the ^{13}C label incorporation in protein-derived amino acids and PHB (Masakapalli et al., 2013; Kruger et al., 2014).

The MS measurements used for ^{13}C-MFA of root and stem nodule bacteroids are included in the appendix (Table A13 and Table A14). The biomass equations used to constrain the models for root and stem nodule bacteroids were formulated as described in section 3.11.2 and the metabolic models are included in the appendix (Table A15). The flux distribution (net fluxes and their corresponding 95% confidence limits) for the bacteroids are listed in Table 5.1.

Table 5.1: **Flux distribution of N_2-fixing ORS571 bacteroids and their comparison to the free-living N_2-fixing cultures**

Reaction step (s) **Net fluxes**	**Symbol**	**Net flux (relative to succinate uptake)**		
		Root nodule bacteroid	**Stem nodule bacteroid**	**Free-living N_2-fixing ORS571**
Uptake fluxes				
Total uptake of succinate (constrained)	*upt3*	100	100	100
Tricarboxylic acid cycle				
Succinate dehydrogenase	*tca1*	**133 (128, 138)**	**135 (129, 142)**	165 (160, 168)
Fumarase	*tca2*	**133 (128, 138)**	**136.3 (130, 143)**	165 (160, 168)
Malate dehydrogenase	*tca3*	**133 (124, 138)**	**135 (126, 142)**	74.6 (72.5, 79.1)
Citrate synthase	*tca4*	**34 (28.7, 38.9)**	**37.1 (30.1, 43.7)**	66.4 (61.6, 69.5)
Aconitase	*tca5*	**34 (28.7, 38.9)**	**37.1 (30.1, 43.7)**	66.4 (61.6, 69.5)
Isocitrate dehydrogenase NADP-dependent	*tca6*	**34 (28.7, 38.9)**	**37.1 (30.1, 43.7)**	66.4 (61.6, 69.5)
2-Oxoglutarate dehydrogenase	*tca7*	**33.2 (28.7, 38.2)**	**35.9 (29.9, 42.6)**	65.0 (60.1, 68.2)
Succinyl-CoA synthetase	*tca8*	**32.9 (28.4, 38.0)**	**35.5 (29.5, 42.6)**	64.5 (59.4, 67.7)
Pyruvate dehydrogenase	*tca9*	0 (0, 7.3)	0 (0, 7.4)	87.9 (0, 89.2)
Anaplerotic pathways				
NAD-dependent malic enzyme	*mal*	0 (0, 7.6619)	0.75 (0, 6.8417)	90.8 (0, 91.6)
Phosphoenolpyruvate carboxykinase	*pepck*	**11 (9.75, 71.2)**	**10.08 (7.62, 69.8)**	5.71 (4.09, 6.09)
Methylmalonate semialdehyde dehydrogenase	*msdh*	**83.4 (28.3, 85.8)**	**86.1 (30.1, 87.5)**	0 (0, 1.36)
Glycolysis				
Pyruvate kinase	*gly1*	0 (0, 7.6619)	0.66 (0, 6.7454)	0 (0, 53.8)
Gluconeogenesis				
Phosphoglycerate kinase	*glu1*	11.50 (9.30, 21.24)	8.69 (6.97, 19.84)	4.85 (3.28, 15.2)

Reaction step (s) Net fluxes	Symbol	Net flux (relative to succinate uptake)		
		Root nodule bacteroid	Stem nodule bacteroid	Free-living N_2-fixing ORS571
Glyceraldehyde-3-phosphate dehydrogenase	*glu2*	10.14 (9.41, 19.03)	6.57 (6, 17.73)	2.98 (2.77, 13.3)
Triosephosphate isomerase	*glu3*	5.94 (5.58, 14.89)	3.84 (3.56, 15.38)	1.55 (1.47, 11.8)
Fructose-bisphosphate aldolase	*glu4*	5.24 (4.93, 14.19)	3.42 (3.19, 13.80)	1.46 (1.38, 11.7)
Fructose-1,6-bisphosphatase	*glu5*	5.24 (4.93, 14.19)	3.42 (3.19, 13.80)	1.46 (1.38, 11.7)
Phosphoglucose isomerase	*glu6*	4.23 (4.01, 213.48)	2.86 (2.71, 209.68)	1.85 (1.83, 17.6)
Pentose phosphate pathway				
Glucose-6-phosphate dehydrogenase	*ppp1*	1.64 (0.12, 213.67)	1.43 (0, 209)	1.59 (0, 17.4)
6-phosphogluconate dehydrogenase	*ppp2*	0 (0, 213)	0.32 (0, 209)	1.59 (0, 10.5)
Ribulose-phosphate 3-epimerase	*ppp3*	-1.01(-1.07, 142)	-0.55 (-0.64, 139)	0.38 (0.28, 6.35)
Ribose 5-phosphate isomerase	*ppp4*	1.01 (0.92, 71.12)	0.88 (0.80, 69.88)	1.20 (1.14, 4.19)
Transketolase- C5/C3 conversion	*ppp5*	-1.01 (-1.07, 142)	-0.55 (-0.64, 139)	0.38 (0.28, 6.35)
Transketolase- C6/C4 conversion	*ppp6*	0.62 (-71.2, 0.66)	0.46 (-69.8, 0.52)	0.02 (-2.95, 0.10)
Transketolase- C7/C5 conversion	*ppp7*	0.38 (-71.1, 0.41)	0.09 (-69.9, 0.11)	-0.41 (-3.39, -.39)
Transaldolase- C6/C3 conversion	*ppp8*	0.38 (-71.1, 0.41)	0.09 (-69.9, 0.11)	-0.41 (-3.39, -.39)
Transaldolase- C7/C4 conversion	*PPP9*	-0.38 (-0.41, 71.1)	-0.09 (-0.11, 69.92)	0.41 (0.39, 3.39)
Entner-Doudoroff pathway				
6-Phosphogluconate dehydratase	*ed1*	1.64 (0, 9.01)	1.11(0, 9.55)	0 (0, 7.92)
2-keto-3-deoxy-6-phosphogluconate aldolase	*ed2*	1.64 (0, 9.01)	1.11 (0, 9.55)	0 (0, 7.92)
Amino acid synthesis				
Glutamate dehydrogenase	*glt*	**6.18 (0, 6.60)**	7.06 (0, 9.26)	8.10 (7.39, 10.4)
Glutamine synthetase	*gln*	**0.50 (0, 0.53)**	0.76 (0, 0.85)	0.90 (0.82, 1.05)
Proline synthesis	*pro*	**0.13 (0, 0.14)**	0.20 (0, 0.22)	0.23 (0.21, 0.27)
Arginine synthesis	*arg*	**0.19 (0, 0.21)**	0.30 (0, 0.34)	0.36 (0.32, 0.42)
Aspartate transaminase	*asp*	3.53 (0, 3.80)	1.89 (0, 4.98)	2.22 (2.02, 4.66)
Asparagine synthase	*asn*	**0.17 (0, 0.18)**	0.26 (0, 0.29)	0.31 (0.28, 0.36)
Alanine aminotransferase	*ala*	**0.34 (0, 0.36)**	0.52 (0, 0.58)	0.62 (0.56, 0.72)

Reaction step (s) Net fluxes	Symbol	Net flux (relative to succinate uptake)		
		Root nodule bacteroid	Stem nodule bacteroid	Free-living N_2-fixing ORS571
Serine synthesis	*ser*	0.18 (0, 1.39)	1.39 (0, 1.52)	1.44 (0.54, 1.68)
Serine hydroxymethyltransferase	*glc1*	-0.19 (-0.24, 1)	0.81 (-0.60, 0.89)	0.76 (-0.14, 0.88)
MEETHF synthesis	*meethf*	1.79 (0, 1.92)	0.32 (0, 1.81)	0.19 (0.17, 1.25)
Threonine aldolase	*glc2*	2.29 (0, 2.49)	0 (0, 2.94)	0 (0, 2.07)
Cysteine synthesis	*cys*	**0.17 (0, 0.18)**	0.26 (0, 0.29)	0.31 (0.28, 0.36)
Lysine synthesis	*lys1*	**0.20 (0, 0.22)**	0.32 (0, 0.35)	0.37 (0.34, 0.43)
Lysine synthesis	*lys2*	**0.20 (0, 0.22)**	0.32 (0, 0.35)	0.37 (0.34, 0.43)
Threonine synthesis	*thr*	2.64 (0, 2.85)	0.53 (0, 3.50)	0.62 (0.56, 2.80)
Methionine synthesis	*met*	**0.07 (0, 0.08)**	0.11 (0, 0.13)	0.14 (0.12, 0.16)
Valine synthesis	*val*	**0.23 (0, 0.25)**	0.36 (0, 0.40)	0.42 (0.39, 0.50)
Leucine synthesis	*leu*	**0.28 (0, 0.30)**	0.43 (0, 0.48)	0.51 (0.46, 0.59)
Isoleucine synthesis	*ile*	**0.16 (0, 0.17)**	0.25 (0, 0.28)	0.29 (0.27, 0.34)
Phenylalanine synthesis	*phe*	**0.11 (0, 0.11)**	0.17 (0, 0.18)	0.20 (0.18, 0.23)
Tyrosine synthesis	*tyr*	**0.09 (0, 0.10)**	0.14 (0, 0.16)	0.17 (0.15, 0,20)
Tryptophan synthesis	*trp*	**0.03 (0, 0.03)**	0.04 (0, 0.05)	0.05 (0.05, 0.06)
Histidine synthesis	*his*	**0.05 (0, 0.06)**	0.08 (0, 0.09)	0.10 (0.09, 0.11)
Other outputs				
METHF synthesis	*methf*	**0.07 (0, 0.08)**	0.11 (0, 0.13)	0.14 (0.12, 0.16)
FTHF synthesis	*fthf*	**0.05 (0, 0.06)**	0.08 (0, 0.09)	0.10 (0.09, 0.11)
PHB synthesis	*accoa1*	20.2 (0, 21.56)	20.6 (0, 22.9)	9.41 (8.59, 11.0)
Biomass synthesis	*biomass*	3.60 (0, 3.85)	3.40 (0, 3.78)	1.85 (1.69, 2.17)
Lipid synthesis	*accoa2*	10.65 (0, 11.36)	6.65 (0, 7.40)	1.45 (1.32, 1.69)
DNA synthesis	*r5p1*	0.12 (0, 0.14)	0.06 (0, 0.11)	0.05 (0.05, 0.06)
RNA synthesis	*r5p2*	1.17 (0, 1.25)	0.74 (0, 0.82)	0.57 (0.53, 0.67)
Carbohydrates synthesis	*g6p1*	1.33 (0, 1.42)	0.38 (0, 0.43)	0.18 (0.17, 0.21)
EPS synthesis	*g6p2*	1.25 (0, 1.33)	1.04 (0, 1.16)	0.07 (0.06, 0.08)
Metabolic CO_2 output (net)	*co_2.out*	249 (238, 400)	258 (242, 414)	320 (306, 321)

Fluxes are presented as best-fit estimates calculated using MS measurements from three individual labelling experiments for bacteroids isolated from root and stem nodules. The 95% confidence limits for the fluxes were calculated using parameter continuation analysis in INCA and presented as (lower bound, upper bound) of the confidence limits. All fluxes were expressed on a molar basis relative to a succinate uptake flux of 100. Fluxes were considered to be significantly different if the confidence intervals associated with the fluxes do not overlap. Fluxes shown in **red** represent a significant increase in the fluxes of the bacteroids and those shown in **blue** represent a significant decrease in the fluxes of the bacteroids relative to those determined for free-living ORS571 (Table 4.1).

The biomass synthesis fluxes (amino acids, PHB, lipids, carbohydrates, EPS and nucleic acids) deduced for the bacteroid flux maps was poorly resolved; the confidence limits were large, where the lower limit stretched down to zero. The probable explaination for this was the comparatively lower ^{13}C abundance in the MS fragments used for flux estimation. For the root nodule bacteroids, the average ^{13}C measured in the amino acid and PHB was <8% and <15% respectively. For the stem nodule bacteroids, the measurements were <5% in the amino acid fragments and around 10% in the PHB. While the MS fragments used for the free-living cultures had a ^{13}C abundance of >15% and the biomass fluxes were comparatively well resolved as compared to that in the bacteroids. The low level of ^{13}C incorporation was due to the reduced turnover of the biomass in the non-dividing bacteroids.

5.6.1 Statistical analysis of the fluxes

The flux distributions obtained for bacteroids from root and stem nodules had statistically acceptable SSRs (Table 5.2). The assessment of goodness of fit for the flux distributions is included in the appendix (Figure A16-A17), where the experimentally derived MS measurements for amino acids and PHB are compared with the simulated measurements predicted by the corresponding flux distributions. The comparison confirmed that the measured and simulated isotopomer values were broadly

comparable; indicating that the deduced flux distributions provided a good explanation of the labelling data.

Table 5.2**: SSRs obtained for the fluxes of ORS571 bacteroids isolated from root and stem nodules**

Type of bacteroid	Obtained SSR	Expected SSR	Degrees of freedom (DOF)	Comment
Root nodule bacteroid	276.6	250.2 – 345.6	296	Fit accepted
Stem nodule bacteroid	195.6	151.9 – 227.9	188	Fit accepted

5.7 Influence of nodule phenotype on the metabolic behaviour of bacteroids

The fluxes determined for root and stem nodule bacteroids are shown as flux maps in Figure 5.17. There were no statistically significant differences in the distribution of fluxes between the root and stem nodule bacteroids. This comparison confirms that the metabolic fluxes of the bacteroids in the root and stem nodules are not affected by the different nodule phenotype. For root and stem nodules bacteroids, the flux distributions between the central carbon utilisation pathways- TCA cycle, PPP, gluconeogenesis and ED pathways followed a similar pattern as previously observed for free-living ORS571 under aerobic, micro-aerobic and N_2-fixing conditions.

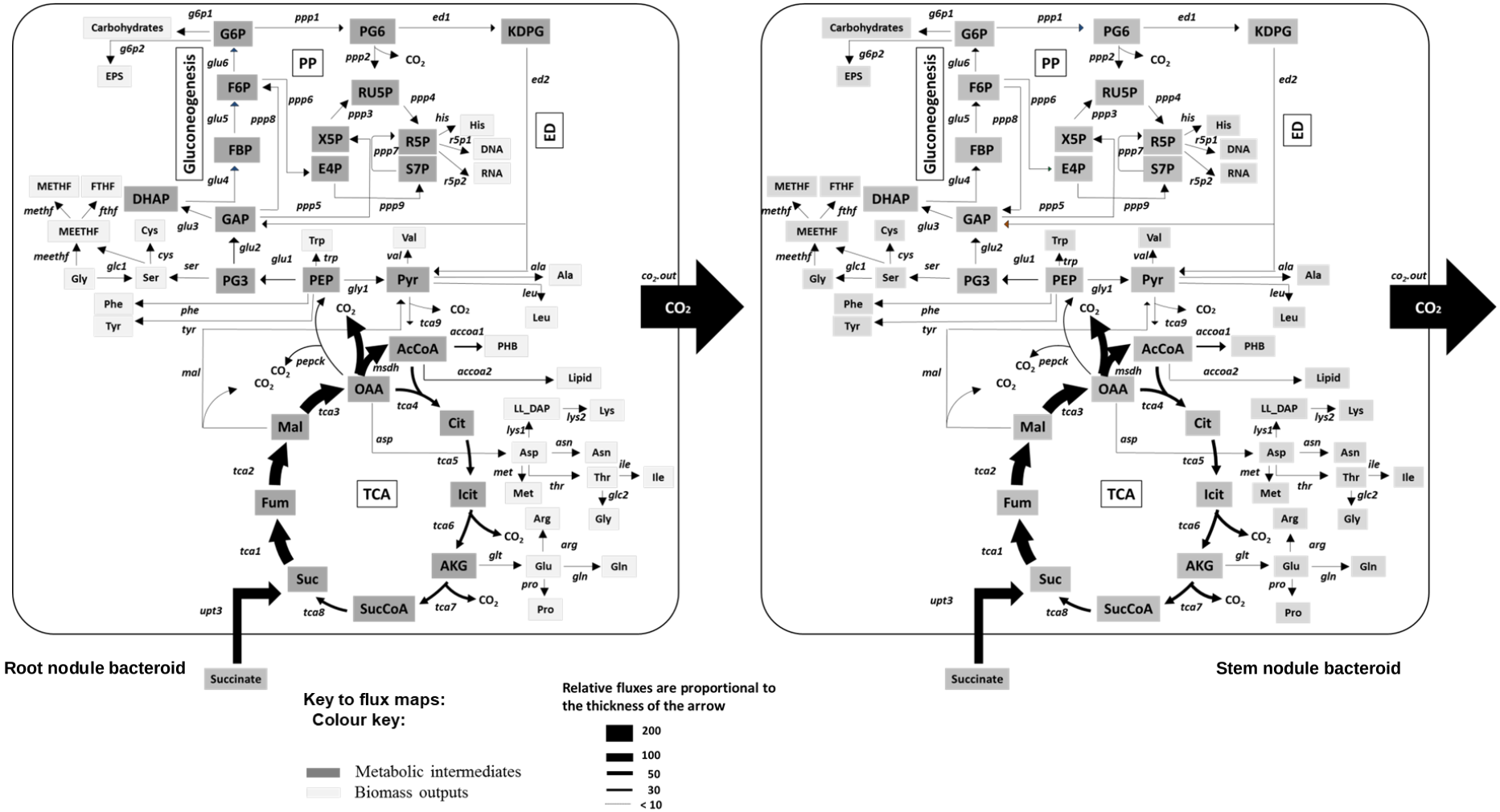

Figure 5.17: **Comparison of flux maps of ORS571 bacteroids in the two nodule types of *S. rostrata*.** The flux maps represent statistically valid best-fit models based on the redistribution of label following metabolism of [$^{13}C_4$] succinate by ORS571. The thickness of the each arrow in the flux maps is proportional to the relative molar flux. Metabolic intermediates and biomass outputs are shown in rectangular boxes with distinct colour key. The symbols for fluxes are shown in *italics* (defined in Table 5.1).

The TCA cycle fluxes (*tca1*, *tca2*, *tca3*, *tca4*, *tca5*, *tca6*, *tca7* and *tca8*) were substantially higher than the fluxes determined for PPP (*ppp1*, *ppp2*, *ppp3*, *ppp4*, *ppp5*, *ppp6*, *ppp7*, *ppp8* and *ppp9*); gluconeogenesis (*glu1*, *glu2*, *glu3*, *glu4*, *glu5* and *glu6*); glycolysis (*gly1*) and the ED (*ed1*, *ed2*) pathway. This was expected as the substrate succinate entered the metabolic network via TCA cycle. The flux distributions via the anaplerotic pathways in both the bacteroids was observed to differ from that previously determined for free-living ORS571. Flux *msdh,* through the additional pathway for AcCoA synthesis from OAA, was higher than the anaplerotic flux *mal* and *pepck*. Approximately 50% of the AcCoA synthesized by the *msdh* reaction was fed into the TCA cycle and the remainder was utilized for PHB and lipid synthesis. PHB occupied the largest proportion of the cell dry weight of the bacteroids. Consequently, the flux for PHB synthesis, *accoa1* was higher than the fluxes for amino acid synthesis (*glt*, *gln, pro*, *arg* , *asp*, *asn*, *ala*, *ser*, *glc1*, *meethf*, *glc2*, *cys*, *lys1*, *lys2*, *thr*, *met*, val, leu, *ile*, *phe*, *trp*, *his*), lipid synthesis (*accoa2*), nucleic acid synthesis (*r5p1*, *r5p2*), carbohydrate and EPS synthesis (*g6p1*, *g6p2*).

5.8 Changes in metabolic fluxes of bacteroids as compared to free-living ORS571

The flux distributions determined for root and stem nodule bacteroids (Table 5.1) were compared to the flux distributions previously determined for N_2-fixing free-living cultures (chapter 4, Table 4.1). This comparison highlights the changes in the metabolic fluxes that arose during symbiotic N_2-fixing conditions. The statistically significant changes in the fluxes of the bacteroids relative to the free-living ORS571 are shown in Figure 5.18.

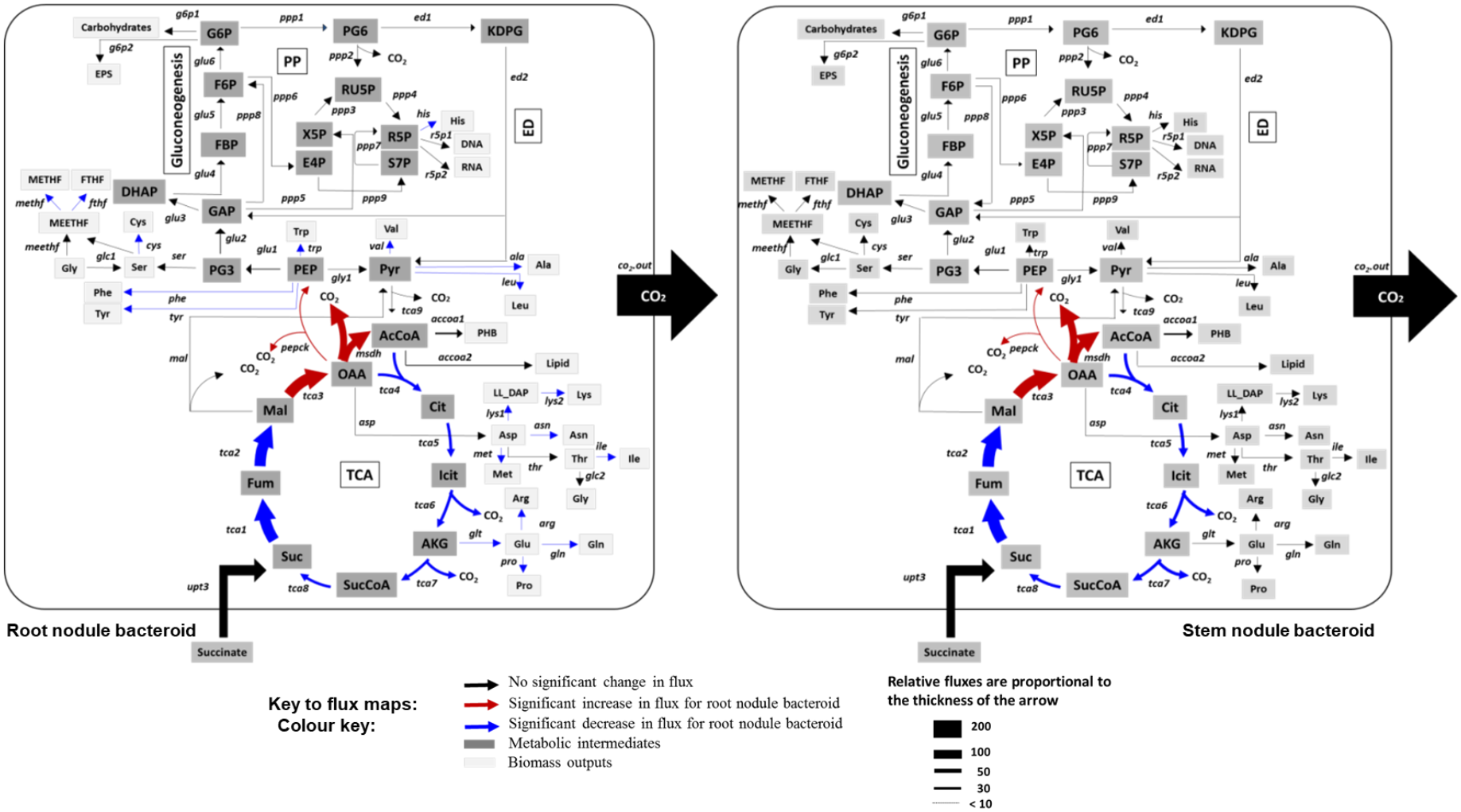

5.18: **Comparison of flux maps of root and stem nodule bacteroids with free-living ORS571.** The flux maps represent statistically valid best-fit models based on the redistribution of label following metabolism of [$^{13}C_4$] succinate by ORS571 bacteroids and cultures under N_2-fixing conditions. The thickness of the each arrow in the flux maps is proportional to the relative molar flux. Metabolic intermediates and biomass outputs are shown in rectangular boxes with distinct colour key. The symbols for fluxes are shown in *italics* (defined in Table 5.1). Significant increases in the fluxes for the the bacteroids (*tca3*, *pepck* and *msdh*) are shown in **red** and significant decrease in the fluxes (*tca1*, *tca2*, *tca4*, *tca5*, *tca6*, *tca7* and *tca8*) are shown in **blue**.

Fluxes *tca1*, *tca2*, *tca4*, *tca5*, *tca6*, *tca7* and *tca8* of the TCA cycle were significantly reduced in the bacteroids as compared to the free-living cultures. The TCA cycle is the major succinate utilising pathway that produced co-enzymes required for metabolic reactions, growth, biomass synthesis and N_2 fixation. Bacteroids did not show cell division and also lower rates of nitrogenase activity as compared to that of free-living cultures (section 5.2.1). Because of the comparatively reduced cellular activities, the co-enzyme demand will be lower in the bacteroids and hence the reduced TCA cycle fluxes (discussed in section 5.9).

Flux *tca3* via MDH which was significantly higher in the bacteroid as compared to the N_2-fixing free-living cultures. Flux *tca3* in the bacteroids directed flux via *msdh* which was an alternative route for AcCoA synthesis from malate. This was different to the route of malate utilisation in the free-living cultures, where malate was utilised by both *tca3* via MDH activity and *mal* via NAD(P)-ME activity. Flux *msdh* was significantly higher in the bacteroids, which implied that this pathway was the preferred route for AcCoA synthesis in the bacteroids. The rearrangement of fluxes for conversion of malate to AcCoA in the bacteroids resulted in a lower flux though the TCA cycle reactions (*tca1*, *tca2*, *tca4*, *tca5*, *tca6*, *tca7* and *tca8*) by diverting carbon away from the TCA cycle, and utilising it mainly to synthesize lipids and PHB.

Flux *pepck* via PEP carboxykinase that directs flux to gluconeogenesis, was higher in the bacteroids, which was probably because the higher amount of EPS synthesized in the bacteroids required a higher flux *pepck*. Anaplerotic flux, *mal* via NAD(P)-ME and flux *tca9* via pyruvate dehydrogenase (PDH) to synthesize AcCoA from pyruvate were reduced in the bacteroids. These observed alterations in the fluxes, *mal* and *tca9* were not statistically significant, primarily as a result of the large confidence intervals associated with these two values. However, since the fluxes *pepck* and *msdh* were significantly higher in the bacteroids, there must be associated decreases in the fluxes *mal* and *tca9*.

The fluxes for the synthesis of amino acids *glt*, *gln*, *pro*, *arg*, *asn*, *ala*, *cys*, *lys1*, *lys2*, *met*, *val*, *leu*, *ile*, *phe*, *tyr*, *trp*, *his*, *methf* and *fthf* were significantly reduced in the root nodule bacteroids. However there were no statistically significant changes in these fluxes for the stem nodule bacteroids; this was because these fluxes were not well-defined in the stem nodule bacteroids. Also, there were no statistically significant differences observed in the fluxes to PHB, lipid, nucleic acids, carbohydrate and EPS synthesis between free-living cultures and bacteroids. The 95% confidence limits associated with these fluxes were large and this masked any potential changes. Also, the fluxes to net CO_2 output, CO2.out and overall biomass synthesis, biomass were not well defined in the bacteroids. The possible explanation for the poorly defined fluxes is the limited range and number of informative MS measurements used for generation of bacteroid fluxes. Also, the measurements used for the bacteroid flux maps had a low ^{13}C incorporation, which affected the large confidence limits of these fluxes.

5.9 Co-enzyme analysis

This analysis was done to estimate the ATP, NADH, NADPH and $FADH_2$ utilisation in the bacteroids according to the method described in section 3.17. This analysis was done solely for the reactions that were included in the bacteroid model (Table A15) and does not include the reactions for oxidative phophorylation. Co-enzyme utilisation in the bacteroids was also compared to that in the N_2-fixing free-living cultures to identify the differences that arise under symbiotic conditions.

5.9.1 Comparison of co-enzyme production between bacteroids and free-living cultures

The production of co-enzymes by root and stem nodule bacteroids and their comparison to free-living cultures is shown in Figure 5.19. From this analysis, it is clear that the TCA cycle was the major source of the co-enzymes in the bacteroids. The

overall production of co-enzymes was reduced in the bacteroids; this was mainly due to the significantly reduced TCA cycle fluxes as compared to the free-living cultures.

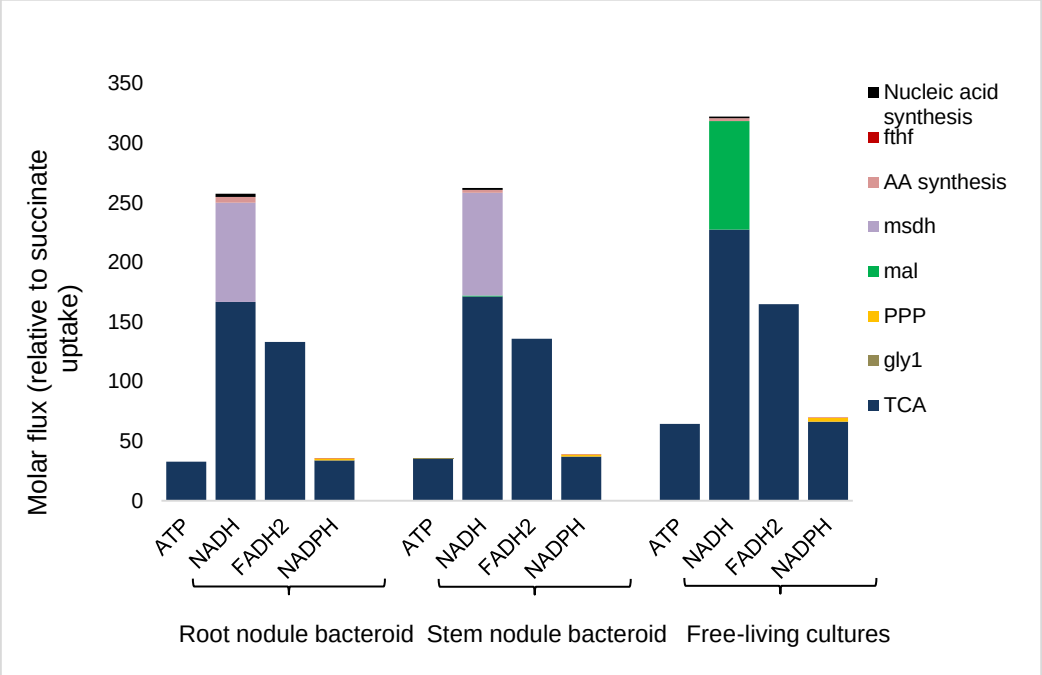

Figure 5.19: **Production of co-enzymes by ORS571 bacteroids and free-living cultures under N_2-fixing conditions.** The production of ATP, NADH, $FADH_2$ and NADPH by the network was determined from the sum of individual fluxes that produced co-enzymes in the flux distributions obtained for ORS571 bacteroids. The production of co-enzymes in the bacteroids was compared to that determined for N_2-fixing free-living cultures (section 4.10.1). All values are molar fluxes expressed relative to succinate uptake.

As in the free-living cultures, all of the ATP produced by the network arose from substrate phosphorylation in the TCA cycle (*tca8*). Flux *tca8* was significantly reduced in the bacteroids as compared to the free-living cultures and so, the ATP produced was also significantly reduced. There was a significant increase in the contribution of NADH by *msdh* in the bacteroids (33%) but the contribution by *msdh* in the free-living cultures was <1%. This was due to the significantly higher *msdh* flux in the bacteroids. $FADH_2$ produced solely by *tca1* reaction was significantly reduced in the bacteroids. The manner of NADPH production in the bacteroids was similar to that in the free-living

cultures. More than 95% of the total NADPH in both root and stem nodule bacteroids was produced by *tca6* and the remaining by *ppp1* and *ppp2* of the network. NADPH production was significantly reduced by 48.7% in the root nodule bacteroids and 44.1% in the stem nodule bacteroids as compared to the free-living cultures. This reflects the significantly higher *tca6* flux in the free-living cultures.

5.9.2 Comparison of co-enzyme consumption between bacteroids and free-living cultures

The consumption of co-enzymes by the root and stem nodule bacteroids is shown in Figure 5.20. The manner of co-enzyme consumption in the bacteroids by network reactions, biomass synthesis and nitrogenase reactions was similar to the free-living cultures. There were no significant differences between the overall co-enzyme consumption between the bacteroids and free-living cultures. This was because the biomass synthesis fluxes in the bacteroids were poorly defined and so, no significant differences were observed for these fluxes between the bacteroid and free-living forms.

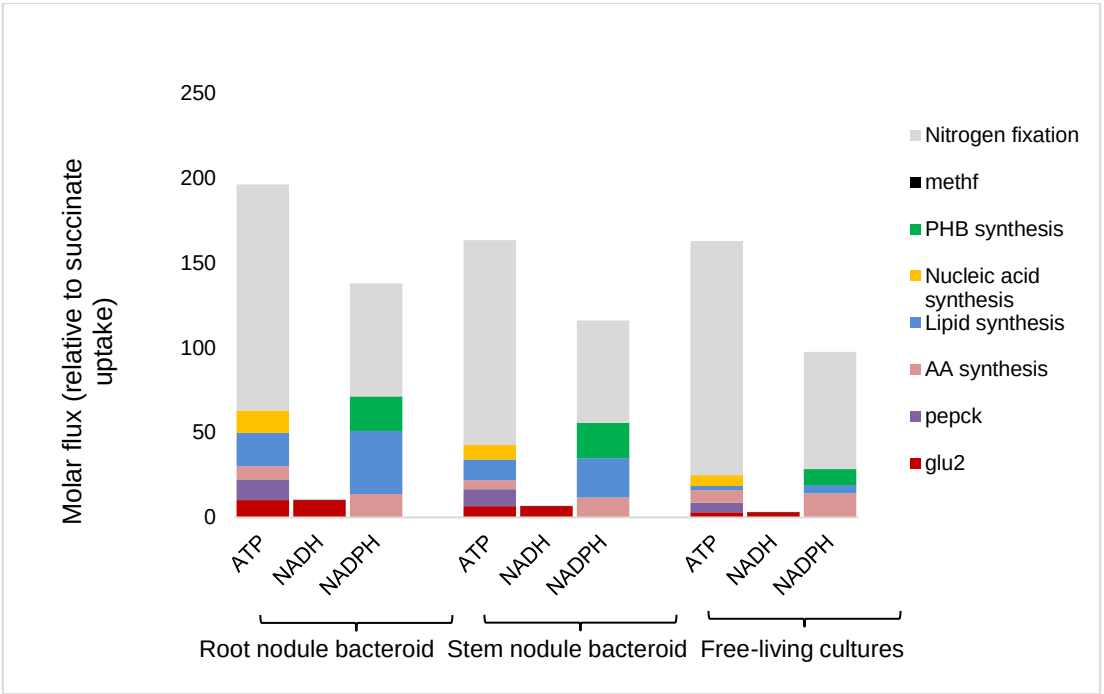

Figure 5.20: **Consumption of co-enzymes by the bacteroids and free-living cultures**. The consumption of ATP, NADH, $FADH_2$ and NADPH by the network reactions was determined from

the sum of individual fluxes that used co-enzymes in the flux distributions obtained for ORS571 bacteroids (Table 5.1). The consumption fluxes were compared to that determined for N_2-fixing free-living cultures (section 4.10.2). All values are molar fluxes expressed relative to succinate uptake.

The manner of ATP utilisation in the bacteroids was similar to that determined for free-living cultures. Out of the total ATP utilised by the network reactions, a large proportion was used by the nitrogenase reaction (68% in root nodule bacteroids and 74% in stem nodule bacteroids). The remaining ATP was used for *glu2*, *pepck*, amino acids, lipids and nucleic acid production. ATP consumed by *pepck* was significantly higher in the bacteroids (6.1%) as compared to the free-living cultures (3.5%). This reflects the significant increase in the flux via *pepck* in the bacteroids. ATP consumed for lipid synthesis was higher in the bacteroids (10% and 7.5% in the root and stem nodule bacteroids) in comparison to that in the free-living cultures (1.5%); this can be explained by the increased production of lipids in the bacteroids as a proportion of biomass.

There was no significant difference in NADH consumption between the bacteroids and free-living cultures. Out of all the NADH consumed, majority (> 98%) was used by *glu2* reaction and the remaining by *methf* in the bacteroids.

Majority of the NADPH (48% in root nodule bacteroids and 52% in the stem nodule bacteroids) was used by nitrogenase reaction in the bacteroids and the remaining for the synthesis of lipids, amino acids and PHB. The overall NADPH consumption in the bacteroids was higher than that in the free-living cultures (41% and 19% increase in the root and stem nodule bacteroids respectively). This was mainly due to the significant increase in the production of lipids as a proportion of biomass in the bacteroids. Around 27% and 20% of the total NADPH consumed by the network reactions was used for lipid synthesis in the root and stem nodule bacteroids, whereas only 5% was used for lipid synthesis in the free-living cultures.

For both bacteroids and free-living cultures, the total consumption of ATP exceeded the total production by the network (substrate level phosphorylation). The consumption of ATP for biomass production, nitrogenase reaction and network reaction, was over 5-fold and 4-fold higher than that produced by the network of root and stem nodule bacteroids respectively. Also, NADPH consumed by the bacteroid network was over 3-fold higher than that produced by the network. In contrast, co-enzymes NADH and $FADH_2$ were produced in excess by the network. Only a minor proportion (< 5%) of the total NADH produced was consumed for network reaction, while none of the $FADH_2$ produced by the network was used for net biosynthesis. The requirements for additional ATP could be met from the excess NADH and $FADH_2$ available (> 95%) via oxidative phosphorylation. Also, the excess NADH available could be used to produce NADPH via transhydrogenase activity, to fulfil the additional NADPH required for biomass production and nitrogenase reaction.

5.10 Discussion

The results presented in this chapter provide understanding about the metabolic adaptations in the N_2-fixing bacteroid form of ORS571 isolated from the root and stem nodules of the host, *S. rostrata*. The bacteroids isolated from root and stem nodules of *S. rostrata* maintained N_2-fixation after isolation but the rate of nitrogenase activity of the bacteroids was lower than that of the N_2-fixing free-living cultures. A previous study reported that the lower nitrogenase activity of the stem nodule bacteroids was because bacteroids lacked an O_2-tolerant N_2-fixing system present in N_2-fixing free-living micro-aerobic cultures (Bergersen, et al., 1988). In this study, both root and stem nodule bacteroids did not show cell division (no increase in cell dry weight) in comparison to the free-living cultures. These results agree with the previous reports about symbiotic bacteroids being in a non-growing state inside the nodules; that is to say, the bacteroids do not undergo cell division; but they differentiate into an elongated bacteroid form, where endoreduplication of the genome occurs (Reding & Lepo, 1989;

Vercruysse et al., 2011; Liu et al., 2011; Libault, 2014). These physiological changes in the bacteroids would probably influence the distribution of metabolic fluxes.

There were no significant differences in the biomass compositions between the root and stem nodule bacteroids; this confirms that the metabolic outputs in the bacteroids did not change due to different nodule phenotype. PHB constituted the largest proportion of the cell dry weight; around 50% in both root and stem nodule bacteroids. Previous studies have reported similar amounts of PHB accumulation in the bacteroids of bean and soybean plants, where PHB constituted more than 50% of the cell dry weight (Kim & Copeland, 1996; Lodwig et al., 2005). In the N_2-fixing free-living cultures of ORS571, PHB (39%) and protein (37%) formed the largest proportion of the cell dry weight. But in the bacteroids from root and stem nodules, PHB alone composed the largest proportion of the cell dry weight. There was a significant increase in the amount of lipids and EPS synthesized in the bacteroids with a significant decrease in the amount of protein. These changes in the biomass proportions of ORS571 bacteroids are a metabolic adaptation that arises under symbiotic conditions. In the free-living state, an increase in PHB synthesis was required to maintain the cellular redox balance and metabolic activity at low O_2 concentrations. Inside the nodules, the amount of O_2 available for the bacteroids was lower (in nanomolar range) than the O_2 concentration used to grow the N_2-fixing micro-aerobic cultures (in micromolar range) (Pauling et al., 2001). So, in addition to PHB, increased synthesis of lipids may also be necessary to sustain the metabolic activity of bacteroids at further reduced O_2 concentrations inside the nodules. Also, it has been hypothesized that increased accumulation of PHB in rhizobia serves as a carbon source during infection of the host and differentiation into bacteroids (Ludwig et al., 2005). The synthesis and accumulation of carbon storage compounds such as PHB, glycogen and lipids in N_2-fixing bacteroids has been shown in other rhizobial species. *R. leguminosarum* bacteroids from pea plant accumulated both PHB and lipids for carbon storage and redox balancing of the cell (Terpolili et al.,

2016). FBA analysis of *R. etli* bacteroids also predicted that PHB metabolism was active during N_2 fixation (Resendis-Antonio et al., 2007; Resendis-Antonio et al., 2011). In *S. meliloti* both PHB and glycogen were reported to be necessary for establishing effective nodulation and N_2 fixation in the host (Wang et al., 2007). From these previous studies, it can be said that the synthesis of carbon storage polymers in the bacteroids was essential for effective symbiosis.

The metabolic fluxes measured in the root and stem nodule bacteroids were not significantly different; so it is clear that the metabolic behaviour remains unchanged in the bacteroids from different nodule phenotypes. Well defined fluxes determined via the TCA cycle reactions confirm that the TCA cycle was active in ORS571 bacteroids and was the major carbon utilising pathway. This finding agrees with previous studies in *S. meliloti* and *R. etli* bacteroids, where the TCA cycle was predicted to be active during N_2-fixation (Resendis-Antonio et al., 2011; Zhao et al., 2012). The fluxes via all of the TCA cycle reactions were relatively higher than the sugar catabolism pathways (ED, PPP and gluconeogenesis). Similar manner of carbon utilisation was suggested for *Bradyrhizobium japonicum* bacteroids, where the researchers showed very low activities of enzymes for metabolism of sugars in comparison to the TCA cycle enzymes (Karr et al., 1984). It was also suggested that although the bacteroids metabolized sugars, the respiration rate of sugars was relatively lower than that of succinate and hence was inadequate to support N_2 fixation (Salminen & Streeter, 1987). In ORS571 bacteroids, gluconeogenic fluxes were detected; this finding was similar to the activity of gluconeogenesis predicted in *S. meliloti* and *R. etli* bacteroids (Resendis-Antonio et al., 2011; Zhao et al., 2012). Also in *S. meliloti* and *R. etli* bacteroids, PPP was reported to be active during N_2 fixation, while in ORS571 bacteroids, PPP fluxes were not well-defined and hence their involvement in bacteroid metabolism and N_2 fixation could not be determined in this study. The TCA cycle fluxes of the bacteroids.

There were significant changes in the metabolic fluxes of the bacteroids as compared to the N_2-fixing free-living cultures. This implies differences in the manner of carbon metabolism between the symbiotic bacteroids and free-living forms of ORS571 during N_2 fixation. One of the major metabolic adaptations in the symbiotic bacteroids was comparatively reduced TCA cycle fluxes as compared to that in the free-living cultures. This observation was similar to the previous report where, metabolite profiling showed lower amounts of pyruvate, acetyl-coA, free coenzyme A and citrate in bacteroids than in free-living cultures of *R. leguminosarum* (Terpolili et al., 2016). Therefore, it can be said that the bacteroids have a lower TCA cycle activity than the free-living form. There are three possible reasons for the reduced TCA cycle fluxes in ORS571 bacteroids. Firstly, the O_2 concentration inside the nodules was lower than the micro-aerobic condition used for the free-living cultures. Secondly, the TCA cycle produced a major proportion of the co-enzymes- ATP, NADH, NADPH and $FADH_2$ in both bacteroids and free-living cultures. From co-enzyme analysis, it was found that the overall production of co-enzymes was higher in the free-living cultures in comparison to that determined for the bacteroids. Due to the non-dividing state, the bacteroids will have a reduced demand for co-enzymes required for cell division and growth. The requirement for co-enzymes will be higher in the actively multiplying free-living cells and consequently the TCA cycle fluxes will be significantly higher in the free-living cultures than those in the non-growing bacteroids. Thirdly, the rate of N_2 fixation in the bacteroids was lower than that in the micro-aerobic free-living cultures. The higher rate of N_2 fixation in the micro-aerobic free-living cultures required a higher supply of energy and reducing equivalents, which was provided by the higher TCA cycle fluxes in the free-living cultures.

There were significant changes in the manner of malate and oxaloacetate utilisation, and AcCoA production in the bacteroid metabolic network. Flux *mal* via NAD(P)-ME was reduced in the bacteroids as compared to the free-living cultures. It was previously

shown that malic enzyme was essential for symbiotic N_2-fixation in the bacteroids isolated from stem nodules of *S. rostrata* (Suzuki et al., 2007). But in this study, malate oxidation was found to occur mainly via malate dehydrogenase (MDH) activity in the bacteroids, and the flux though this reaction was significantly higher in comparison to that determined for free-living cultures. This finding agrees with the previously reported MDH enzymatic activities in ORS571 bacteroids isolated from stem nodules of *S. rostrata* which was higher than the NAD(P)-ME activity (Trinchant & Rigaud, 1990). This indicates that although NAD(P)-ME activity has been shown to be crucial for N_2-fixation in ORS571 bacteroids, malate oxidation via MDH activity was the preferred route for malate utilisation. Alternate pathways for malic enzyme activity have also been reported in a different study on *R. leguminosarum* (Mulley et al., 2010). The researchers showed that the combined activity via PEP carboxykinase (pckA) and pyruvate kinase (pykA) substituted for the role of malic enzyme for pyruvate synthesis and still retained N_2 fixation on the host plant (Mulley et al., 2010).

The OAA generated by the MDH activity was utilised by the additional pathway via MSDH to produce AcCoA and the flux through this pathway was significantly higher in the bacteroids than the free-living cultures. Approximately half of the AcCoA produced via *msdh*, was utilised via the TCA cycle (*tca4*) and the remainder used for PHB and lipid synthesis. This contrasted with the free-living cultures in which flux via *mal* and *pdh* produced the majority of the AcCoA. A large proportion (86%) of this AcCoA was utilised via *tca4* and the remainder was used for PHB and lipid synthesis. It was previously shown that a PDH mutant in ORS571 was unable to fix N_2 during symbiosis with *S. rostrata* (Pauling et al., 2001). But the results from this study suggest that although PDH activity was essential for symbiotic N_2-fixation in ORS571 bacteroids, the flux through the pathway via MSDH activity was the primary route for AcCoA production. A different study using constraint based modelling in *R. etli* bacteroids showed that reduction in PDH enzymatic activity reduces the efficiency of N_2 fixation

but does not impair it (Resendis-Antonio et al., 2011). This flux-balance analysis suggested that the role of PDH in production of ACCoA can be replaced by alternative pathways, which is consistent with the current findings for the alternative pathway via *msdh* to be actively during symbiotic N_2 fixation in ORS571. There are previous studies, which reported MSDH to be involved in the catabolism of amino acids- valine, β-alanine in mammal and micro-organisms (Goodwin et al., 1989; Steele et al., 1992; Zhang et al., 1996). In *Pseudomonas aeruginosa*, the role of MSDH was hypothesized to catalyse energy production for activation of efflux pumps in ciprofloxacin resistance (Su et al., 2010). The researchers also postulated that the NADH produced during *msdh* activity prevented oxidative damage induced by ciprofloxacin (Su et al., 2010). For ORS571 bacteroids, it is possible that in addition to AcCoA production, the operation of the MSDH pathway might be important for other metabolic and cellular functions like utilization of plant derived substrates such as amino acids and/or survival against the host defence mechanisms. The role of this pathway during symbiotic metabolism and N_2 fixation of ORS571 needs to be confirmed using a mutagenesis approach.

The amount of EPS measured as a proportion of biomass was higher in the bacteroids as compared to the free-living N_2-fixing cultures. EPS biosynthesis genes were previously reported to be highly expressed in the stem nodule bacteroids, and EPS production were reported to play a role during infection and nodulation of the host by ORS571 (D'Haeze et al. 2004; Tsukada et al., 2009; Sato et al., 2016). EPS produced by ORS571 bacteroids has also been reported to provide protection against hydrogen peroxide generated by the host plant (D'Haeze et al., 2004). Lipopolysaccharides (LPS) of ORS571 were also reported to be essential for invasion, intracellular colonization and to establish compatible symbiotic interaction with *S. rostrata* (Mathis et al., 2005; Gao et al., 2001; Long, 1989). The synthesis of EPS, LPS and other carbohydrates was controlled mainly by the gluconeogenic fluxes which produced their

precursor glucose-6-phosphate. In this study, the flux through the reaction via PEP carboxykinase that directs flux to gluconeogenesis was significantly higher in the bacteroids than the free-living cultures. Increased flux via *pepck* was another metabolic adaptation in the bacteroid network, which was required to maintain a higher gluconeogenic flux and support increased production of EPS, and LPS in the bacteroids during symbiotic conditions.

5.11 Conclusion

The findings in this chapter demonstrate the successful use of ^{13}C-MFA to study the metabolism of a non-growing bacteroid system that maintained stable N_2-fixation post isolation from the host nodules and utilised succinate as the carbon source. Bacteroids in the root and stem nodule of *S. rostrata* did not show any significant differences in their metabolic phenotype irrespective of their different nodule phenotypes. The symbiotic forms of ORS571 showed reduced nitrogenase activity, changes in the biomass composition and distribution of metabolic fluxes as compared to the N_2-fixing free-living cultures. Significant changes in the metabolic fluxes of the bacteroids were the reduced TCA cycle fluxes and increased fluxes via malate dehydrogenae, methylmalonate-semialdehyde dehydrogenase and phosphoenolpyruvate carboxykinase catalysed reactions. The findings in this chapter provide a description of the metabolic adaptations that arise in the bacteroid forms of ORS571. This increases our knowledge of the metabolic phenotype of a rhizobial system during symbiotic N_2 fixation. This knowledge will be useful for studies aimed at establishing symbiotic N_2 fixation in non-legume plants.

6. Metabolic adjustments in a strain of ORS571 lacking PHB

6.1 Introduction

PHB is a polyester, stored as an intracellular granule in many bacterial species when growth is limited due to lack of nutrients like nitrogen, phosphorus and under low O_2 conditions such as inside a nodule (Dawes, 1988; Rehm, 2010; Aneja & Charles, 1999; Bonartsev et al., 2007). Several rhizobial species including *Sinorhizobium meliloti*, *Sinorhizobium fredii*, *Rhizobium etli*, *Bradyrhizobium japonicum*, and *Azorhizobium caulinodans* accumulate PHB during symbiotic N_2-fixation in the nodules of the host plant (Tombolini & Nuti, 1989; Kim & Copeland, 1996; Mandon et al., 1998; Pauling et al., 2001; Mercan et al., 2002; Wang et al., 2007; Ratcliff et al., 2008) . The role of PHB in rhizobia and its relationship to symbiotic N_2 fixation is debatable. PHB degradation can act as a carbon source under conditions of starvation in rhizobia and bacteroids (Lodwig et al., 2005; Ratcliff et al., 2008), and its synthesis can compete for carbon and reducing power with N_2-fixation. From this work, and previous studies, it was observed that PHB accumulation increased in N_2-fixing cultures and symbiotic bacteroids under low O_2 conditions (Stam et al., 1986; Ndoye et al., 1994). To further evaluate the metabolic role of PHB, it would be useful to study the metabolic consequences in the network, when the organism is unable to synthesize PHB. For this purpose, a PHB mutant in ORS571 was developed and the behaviour of the metabolic network in the PHB mutant was studied using ^{13}C-MFA. This chapter describes the construction of OPS0865 (*phbC* mutant in ORS571) using pK18*mob* insertional mutagenesis to disrupt PHB synthase, the enzyme that catalyses the polymerisation of β-hydroxybutyryl units to form the polyester molecule. The growth characteristics of OPS0865 under aerobic, micro-aerobic and N_2-fixing conditions are described, as well as the symbiotic properties of OPS0865 bacteroids when inoculated onto the host plant. ^{13}C-MFA was performed on OPS0865 free-living cultures under aerobic and micro-aerobic conditions using the methods established in chapter 3. The comparison of the OPS0865 flux

maps with the corresponding maps for the wildtype show the metabolic changes that arise in the absence of PHB synthesis. An increase in flux towards PHB biosynthesis was observed in ORS571 under micro-aerobic conditions (chapter 4), the significance of this diversion of carbon into PHB under O_2 limiting conditions can be assessed by examining the metabolic behaviour of OPS0865 in which PHB synthesis is prevented.

6.2 Construction of OPS0865

The open reading frame (ORF) encoding PHB synthase in ORS571 used for this study was the *phbC* gene previously identified and characterised by Mandon et al. (1998). The strategy for pK18 mutagenesis of the *phbC* gene followed the methods previously established for other rhizobial species (Karunakaran et al., 2010; Tett et al., 2014). The first step involved development of the construct pOPS0391 - a plasmid containing 1.1 kb of ORS571 *phbC* gene cloned into the pK18 mobilizable vector carrying the kanamycin/neomycin resistance (Kan^R/Neo^R) gene and *lacZ*. This was followed by transformation of *E. coli* with pOPS0391 and confirmation of the pOPS0391 construct. The next stage involved introduction of pOPS0391 into ORS571 via conjugation techniques using *E. coli* strains as donor and helper, and the final stage involved confirmation of the ORS571 conjugants carrying pK18 integration in the *phbC* region of the genome. The results obtained for each stage are described in the following sections.

6.2.1 Construction of pOPS0391

An internal region (~1.2 kb) of the *phbC* gene was PCR amplified (Figure 6.1) and cloned into the pK18*mob* vector to obtain the construct pOPS0391 (Figure 6.2) as described in section 2.18.1. *E. coli* DH5α was transformed using pOPS0391 as described in section 2.18.2 and the transformants were selected on the basis of their kanamycin resistance (Km^r). Colonies carrying pOPS0391 plasmid were confirmed by PCR analysis for the presence of the truncated *phbC* gene in pOPS0391 (Figure 6.3)

and by restriction digest analysis (Figure 6.4) using the method described in section 2.18.3. Plasmid S1 from one of the positive clones was checked by sequencing analysis, which confirmed it to be the construct pOPS0391, and this was conjugated into ORS571 as described in the following section.

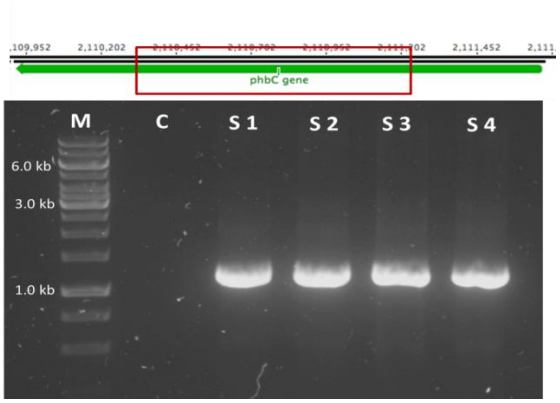

Figure 6.1: **DNA gel showing PCR amplified *phbC* gene.** Symbols are: M-DNA ladder; C-Control PCR with no DNA template used; S1, S2, S3 S4- *phbC* amplification using WT ORS571 genomic DNA as template). The numbers at left indicates the length of the fragments in the lanes S1, S2, S3 and S4 in kilobases.

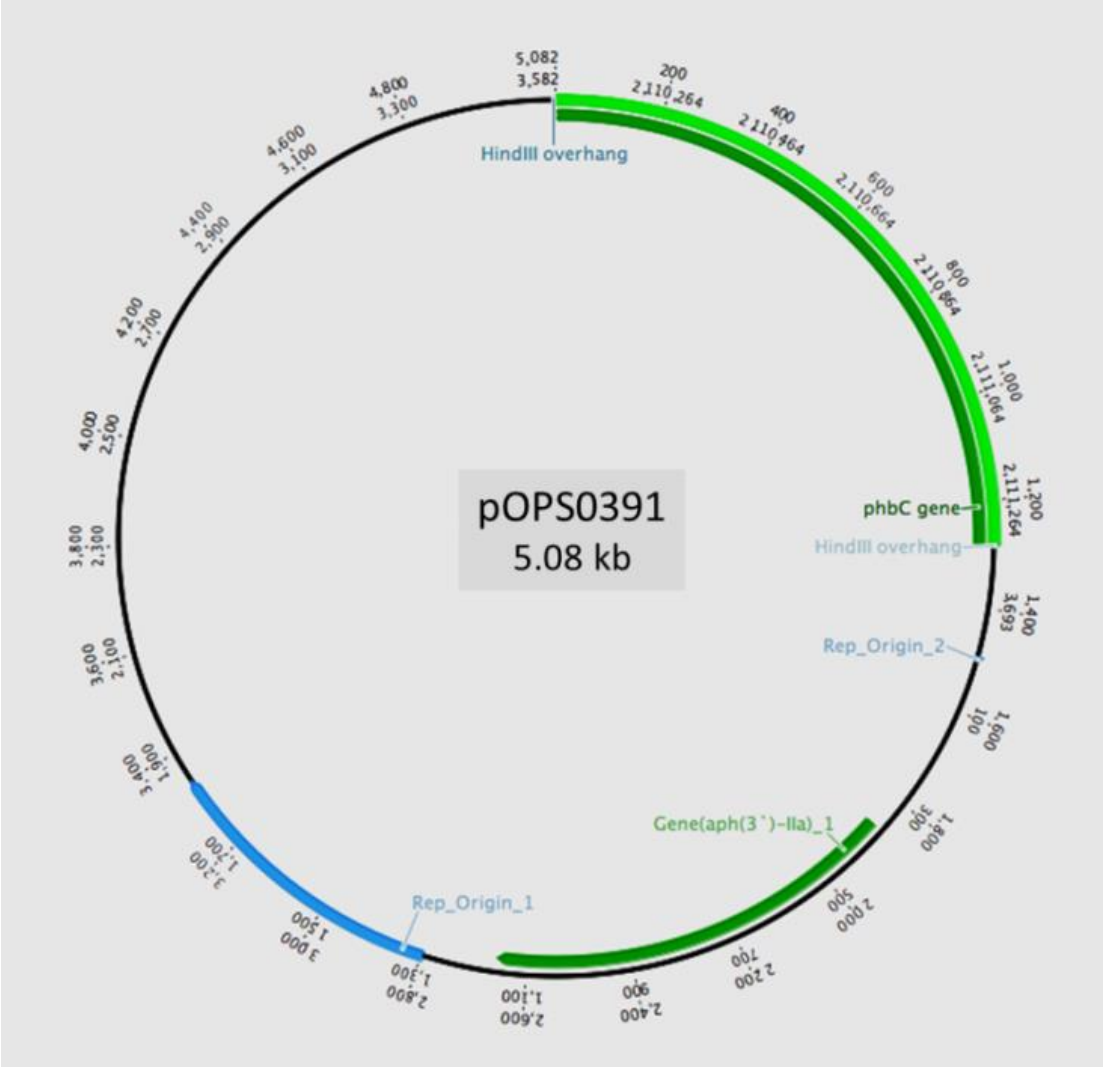

Figure 6.2: **Plasmid map of the pOPS0391 construct**

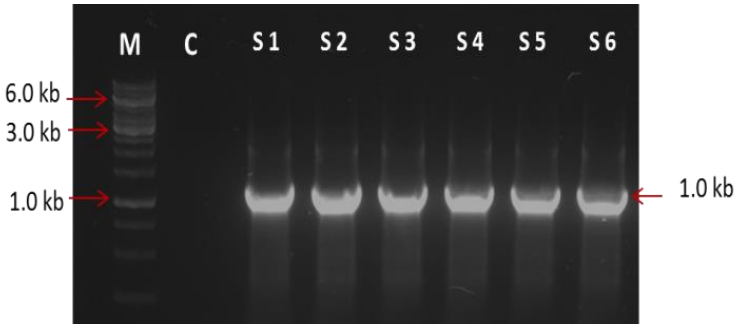

Figure 6.3: **DNA gel confirming *phbC* insert in pOPS0391.** Symbols are- M-DNA ladder; C-Control PCR with no template; S1-S6- *phbC* amplified using pOPS0391 plasmid isolated from six individual colonies as the template. The numbers at left indicates the size of the PCR fragment in kilobases.

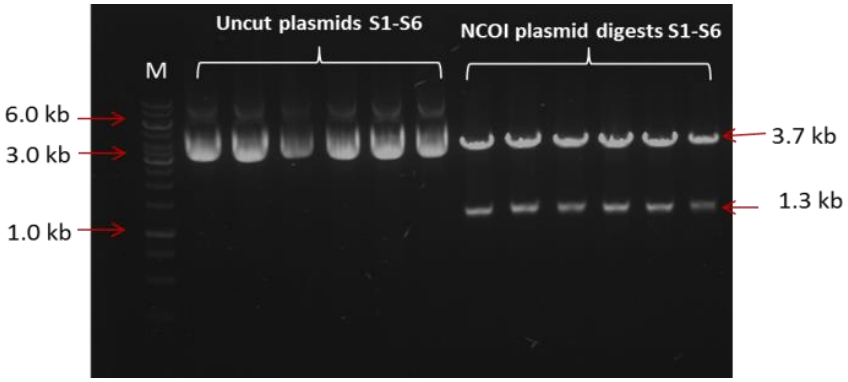

Figure 6.4: **DNA gel showing NCOI digests of pOPS0391.** Symbols are: M-DNA ladder; Uncut plasmids S1-S6 are not digested with NCOI; NCOI plasmid digests S1-S6 produces two fragments of the predicted sizes as indicated by numbers on the right. The numbers at left indicate sizes of the fragments of the DNA ladder.

6.2.2 Construction of ORS571 transconjugants

Plasmid pOPS0391 was introduced into ORS571 via the donor *E. coli* DH5α using the method described in section 2.18.4. pK18*mob* was integrated into the genome of ORS571 by homologous recombination between the *phbC* gene and the internal *phbC* fragment of pOPS0391. pK18*mob* integration disrupts the normal gene function and also confers kanamycin/neomycin resistance on ORS571 transconjugants. Two of the transconjugants isolated by selection on neomycin were first checked to be ORS571 using PCR and sequencing analysis of the *nif*A and 16SrRNA gene (2.18.5). PCR amplification of *nifA* (Figure 6.5) and sequencing analysis of the 16SrRNA gene (appendix A18) confirmed the transconjugants to be derived from the parent strain - ORS571.

Secondly, to confirm that pK18*mob* insertion was in the *phbC* gene, a mapping PCR analysis was done using the forward primer specific to the *phbC* gene and pK18*mob* specific primers. The PCR products obtained (Figure 6.6) were used for sequencing analysis and the sequences of the PCR products matched with the *phbC* region, which

confirmed the pK18 insertion in the appropriate region. The alignment of the sequences is included in the appendix (A19).

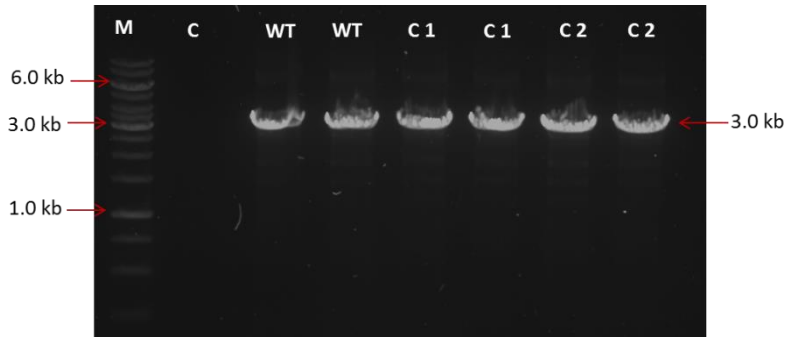

Figure 6.5: **DNA gel showing PCR amplification of *nifA***. Symbols are: M-DNA ladder; WT-*nifA* amplified from ORS571 genomic DNA; C 1, C2 – *nifA* amplified from OPS0865 genomic DNA (transconjugants). The numbers at right shows size of *nifA*. The numbers at left shows the sizes of the fragments in the ladder.

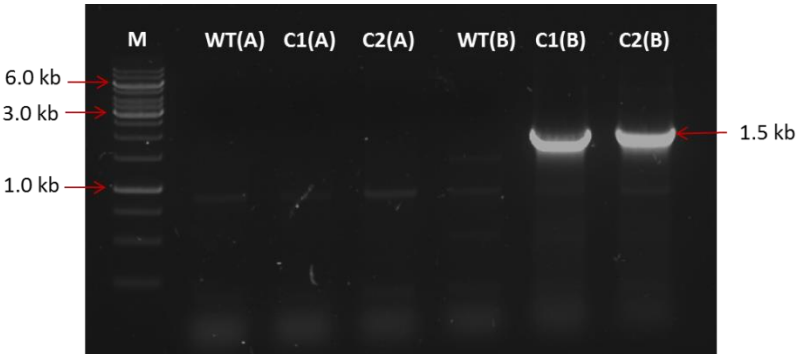

Figure 6.6: **DNA gel showing mapping PCR analysis**. Symbols are: M-DNA ladder; WT (A), C1 (A) and C2 (B) are PCR analysis using primers oxp1043 and pK18A; WT (B), C1 (B), C2 (B) PCR products using primers oxp1043 and pK18B. For WT (A) and WT (B), there was no PCR product in ORS571. For C1 (A) and C2 (A), there was no PCR product in OPS0865. PCR products in C1 (B) and C2 (B) confirms the pK18insertion and orientation in OPS0865. The numbers at right shows size of the mapping PCR product. The numbers at left shows the sizes of the fragments in the ladder.

6.2.3 Confirmation of *phbC* gene disruption in OPS0865

The disruption of the *phbC* gene in OPS0865 was checked by PCR amplification of the *phbC* region using primers Oxp1218 and Oxp1219 (section 2.18). There was no PCR product from the mutant which confirms the *phbC* gene disruption in OPS0865 (Figure 6.7).

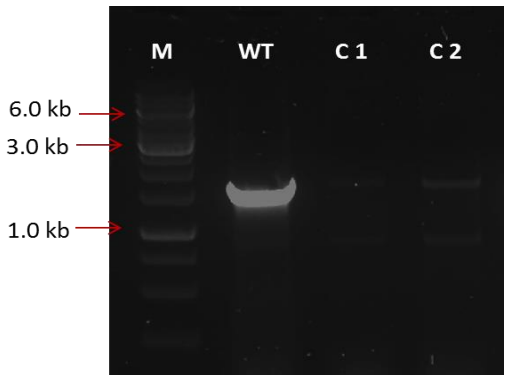

Figure 6.7: **PCR amplification of *phbC* in ORS571 and OPS086**. Symbols indicate: M-DNA ladder; WT-*phbC* amplification in ORS571; C1, C2 – *phbC* amplification in OPS0865. The numbers at left shows the fragment sizes of the ladder.

6.3 PHB synthesis in OPS0865

6.3.1 PHB detection

OPS0865 was grown in free-living cultures in the presence of the antibiotic neomycin using the growth conditions established in Chapter 3 for ORS571. PHB content in OPS0865 free-living cultures was measured using the Law and Slepecky's spectrophotometric method (Figure 6.8). Hydroxybutyrate fragments (PHB, m/z 275) produced from the hydrolysis of PHB was detected using GC-MS (Figure 6.9). Unlike the wildtype, there were no detectable hydroxybutyrate molecular fragments in the OPS0865 cultures.

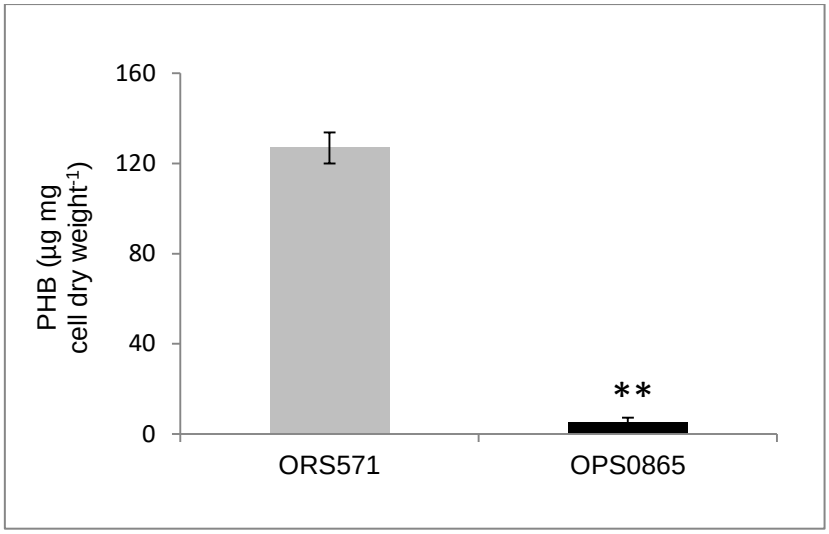

Figure 6.8: **PHB measured by Law and Slepecky's method in ORS571 and OPS0865**. The measurements are a mean ± SEM of three biological replicates. Significant reduction in PHB production by OPS0865 as determined by t-test is indicated: **, p-value < 0.01.

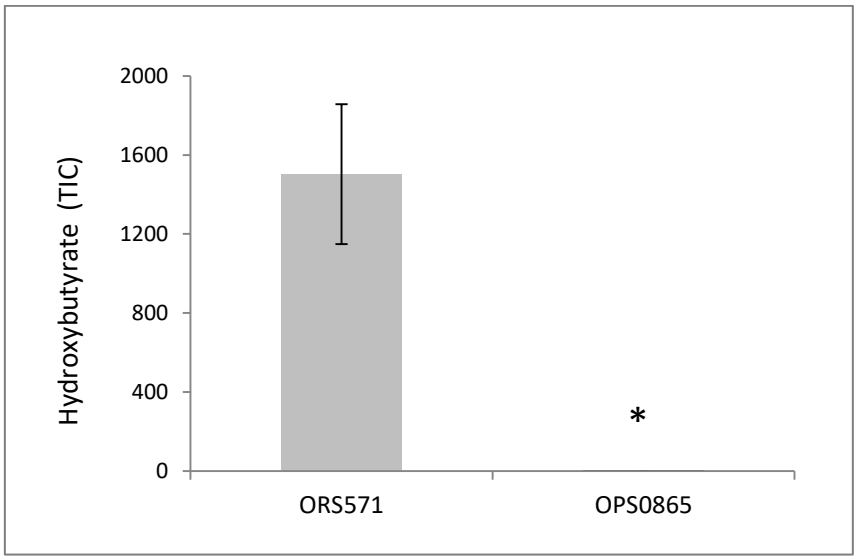

Figure 6.9: **Hydroxybutyrate detection in ORS571 and OPS0865 free-living cultures by GC-MS**. Values are the mean ± SEM of four biological replicates. Hydroxybutyrate molecular fragment of m/z 275 was used for this analysis. A statistically significant reduction in hydroxybutyrate detection in OPS0865 as determined by t-test is indicated: *, p-value < 0.05.

The results obtained from these assays show significantly reduced accumulation of PHB compared to the wild type. This confirms that the mutant OPS0865 was defective in PHB synthesis.

6.3.2 Utilisation of hydroxybutyrate

In this study, deletion of *phbC*, was observed to negatively affect the ability of ORS571 to utilise hydroxybutyrate. Hydroxybutyrate forms the monomeric unit of PHB and is also produced during PHB degradation (Han et al., 2004; Shabina et al., 2015). Unlike the wildtype, OPS0865 cultures failed to grow on hydroxybutyrate as the sole carbon source (Figure 6.10). This indicates that in addition to PHB synthesis, *phbC* was needed to metabolise hydroxybutyrate.

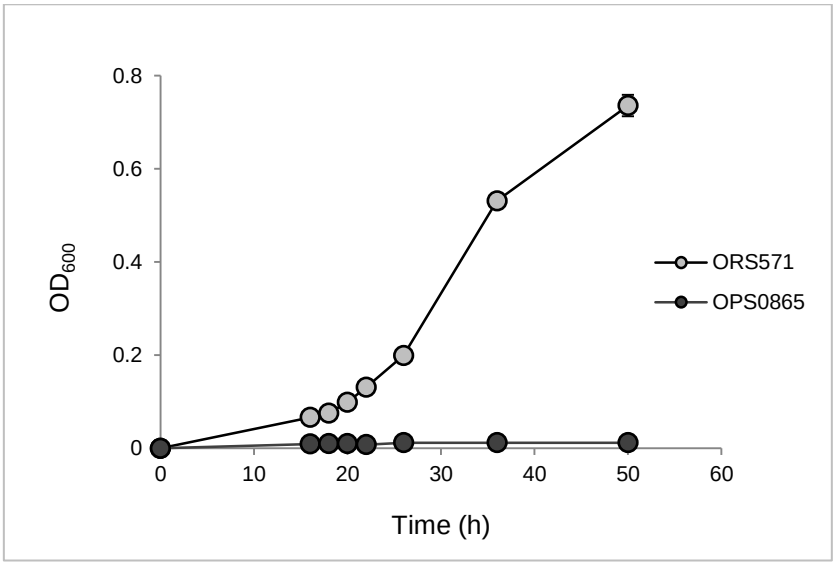

Figure 6.10: **Growth of OPS0865 and ORS571 on hydroxybutyrate**. The measurements are the mean ± SEM of three biological replicates.

6.4 Growth characteristics of OPS0865

6.4.1 Growth characteristics of free-living cultures

Free-living cultures of OPS0865 were able to grow on succinate as the carbon source, under both aerobic and micro-aerobic conditions, in the presence of NH_4Cl as the nitrogen source and neomycin. The doubling times of OPS0865 and ORS571 under aerobic and micro-aerobic conditions (Figure 6.11) were calculated as described in section 2.20. OPS0865 exhibited a slower growth with a significantly longer doubling time under aerobic conditions. Thus, the deletion of PHB had a negative effect on the

growth of ORS571 free-living cultures under aerobic conditions. Under micro-aerobic conditions, there was a significant increase in the doubling time between ORS571 and OPS0865. Thus, inhibition of PHB synthesis had a significant effect on the growth of ORS571 under micro-aerobic conditions. Also, the shift of OPS0865 free-living cultures from aerobic to micro-aerobic conditions resulted in a significantly slower growth. Thus, low O_2 conditions showed qualitatively (but not quantitatively) similar effects on the growth characteristics of OPS0865 to those observed for ORS571.

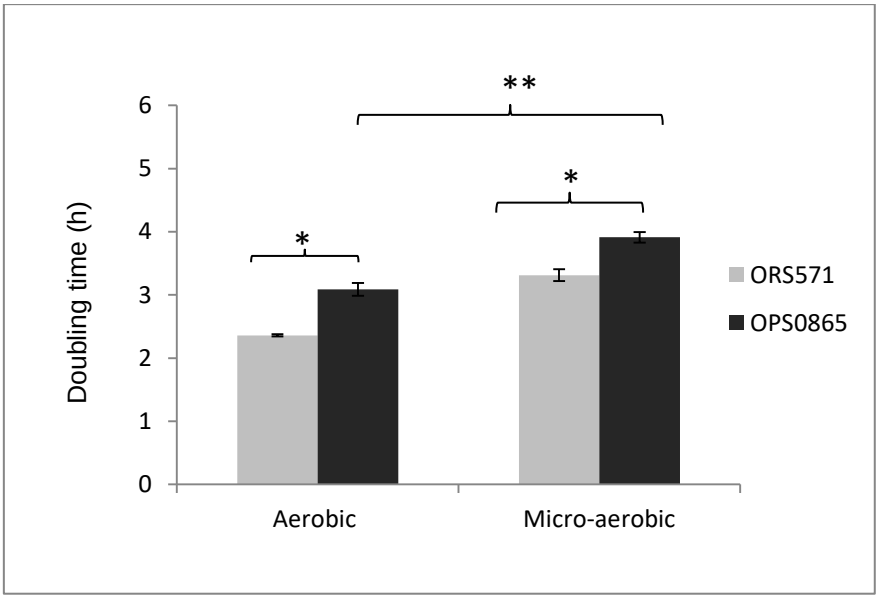

Figure 6.11: **Doubling times of ORS571 and OPS0865 free-living cultures**. Values are means of three biological replicates ± SEM. Significant differences between the doubling times as determined by t-test are indicated: *, p-value < 0.01.

OPS0865 free-living cultures exhibited restricted growth under N_2-fixing conditions (Figure 6.12), and showed a significant reduction in nitrogenase activity as compared to the wild type strain (Figure 6.13). The nitrogenase activity in OPS0865 cultures was approximately 16% of the wild type, which indicates that deletion of PHB synthesis inhibited the growth and N_2-fixing ability of ORS571. In a previous study, and in contrast to Figure 6.13, a PHB mutant in ORS571 was reported to be completely devoid of nitrogenase activity as free-living cultures (Mandon et al., 1998). To test if the

restricted growth and nitrogenase activity in OPS0865 was due to reversion to the wild type, PHB was measured using GC-MS. There was no PHB detected under N_2-fixing conditions (Figure 6.14) and the restricted growth in OPS0865 was probably due to the carry-over of nitrogen sources during inoculation of the cultures. Also, the cultures were able to grow in the presence of neomycin in the media, which confirmed that there had been no reversion of OPS0865 to wild type through selective loss of the exogenous DNA fragment used to disrupt the *phbC* gene.

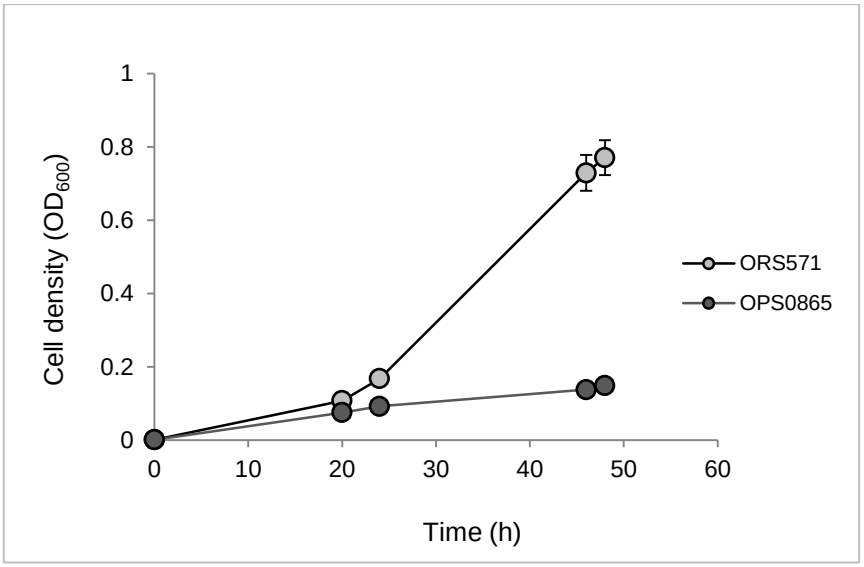

Figure 6.12: **Growth curves of ORS571 and OPS0865 under N_2-fixing conditions.** The measurements are the mean ± SEM of three biological replicates.

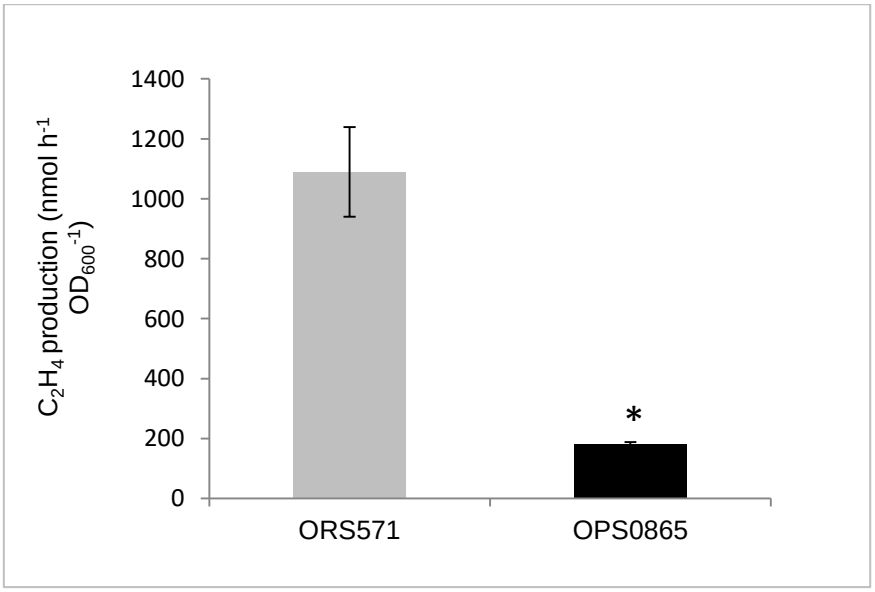

Figure 6.13: **Nitrogenase activity in ORS571 and OPS0865**. The measurements are the mean ± SEM of three biological replicates. A statistically significant reduction in C_2H_4 production by OPS0865 as determined by t-test is indicated: *, p-value < 0.05.

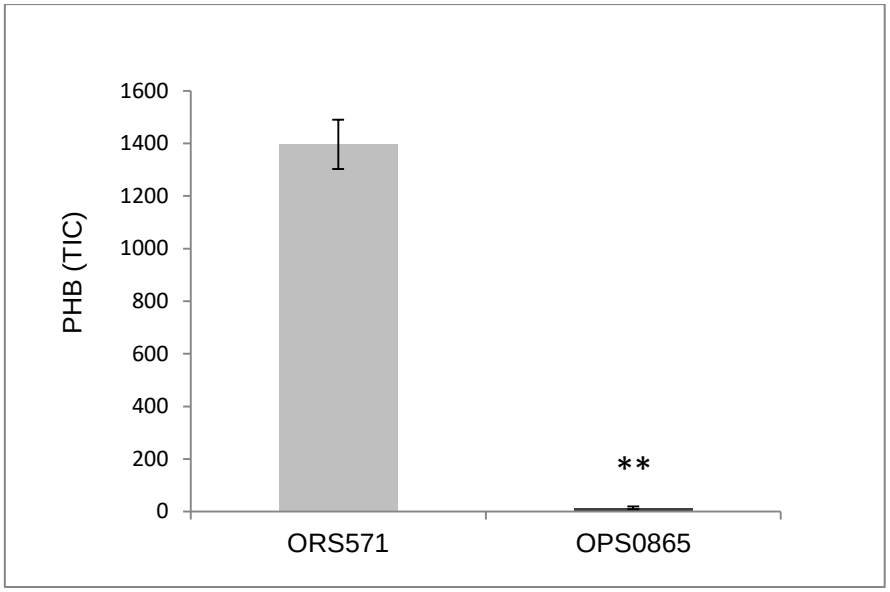

Figure 6.14: **PHB detection in ORS571 and OPS0865 under N_2-fixing condition**. The measurements are the mean ± SEM of three biological replicates. A statistically significant reduction in PHB production by OPS0865 as determined by t-test is indicated: **, p-value < 0.01.

6.4.2 Symbiotic performance of OPS0865

S. rostrata inoculated with OPS0865 showed slower growth and restricted nodulation relative to plants inoculated with ORS571 (Figure 6.15). The nitrogenase activity measured in symbiotic OPS0865 20 d post inoculation was only 40% of the activity found in symbiotic ORS571 (Figure 6.16). In contrast, a previous study on a PHB mutant in ORS571 reported no symbiotic N_2-fixation upon inoculation of the host plant (Mandon et al., 1998). N_2-fixation in the plants is unlikely to arise due to contamination by other rhizobial strains as ORS571 was the sole strain used in the lab that was able to nodulate *S. rotrata*. One possible cause for the difference could be the reversion of OPS0865 to the wild type form, in which PHB synthesis and symbiotic N_2-fixation ability have been restored. To investigate this, OPS0865 bacteroids were analysed for the

presence of *phbC* gene using the primers and the PCR amplification conditions described in section 2.18.5. Figure 6.17 shows the presence of *phbC* gene in OPS0865, suggesting that the restricted nitrogenase activity observed in symbiotic OPS0865, may be due to reversion. The plant assays in this study was not done using the selective antibiotic neomycin. This was because applying antibiotic to the plants during inoculation with OPS0865 would alter the growth conditions for the plants and would probably impact their growth. So, absence of the antibiotic removed the selective pressure that otherwise prevented loss of the integrated pK18 from OPS0865 and thus the nitrogenase activity was observed only because of the revertants in which PHB production was re-established. Nevertheless, the results obtained in this section confirm that inhibition of PHB synthesis in ORS571 reduced symbiotic N_2-fixation in the host.

Figure 6.15: **Growth characteristics of *S. rostrata* in symbiosis with OPS0865 and ORS571**. The images were recorded 20 d post inoculation of the plants with the strains.

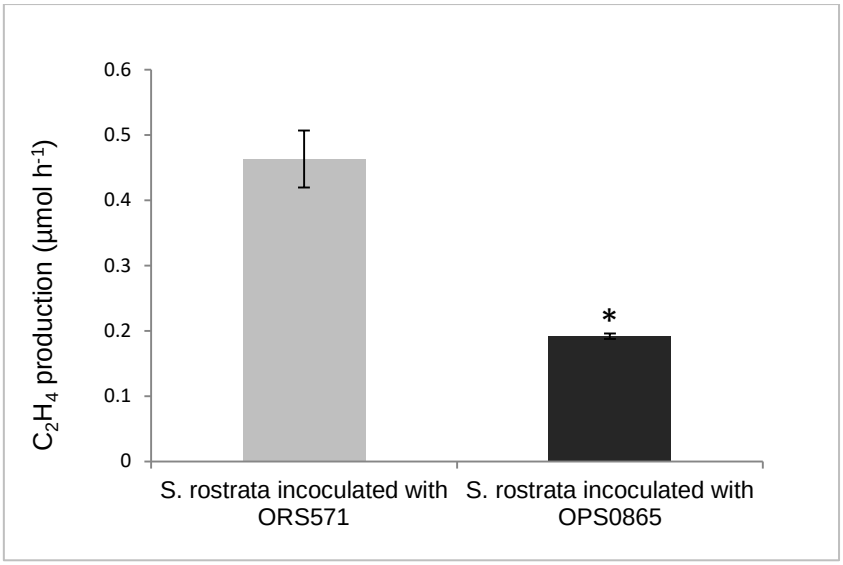

Figure 6.16: **Comparison of nitrogenase activity in ORS571 and OPS0865 during symbiosis with *S. rostrata***. The measurements are the mean ± SEM of three technical replicates. A statistically significant reduction in the nitrogenase activity of *S. rostrata* inoculated with OPS0865 as detected by t-test is indicated: *, p-value < 0.05.

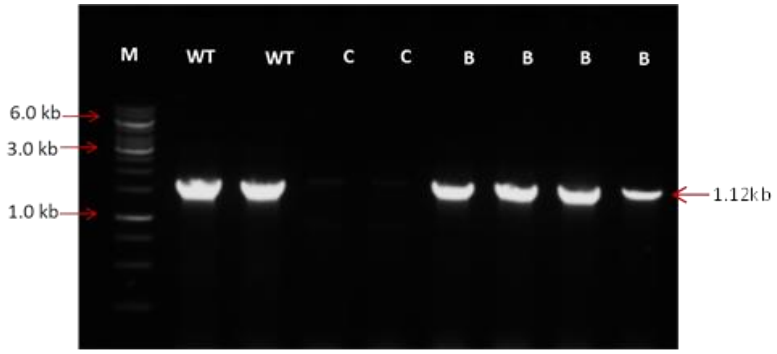

Figure 6.17: **Amplification of *phbC* in OPS0865 isolated from the nodules of *S. rostrata***. Symbols are: M-DNA ladder; WT-*phbC* amplification in ORS571; C – *phbC* amplification in OPS0865 free-living cultures; B- *phbC* amplification in OPS0865 isolated from *S. rostrata*. The numbers shown at left are the sizes of fragments in the DNA ladder. The umber shown at right indicates the size of *phbC* in lanes WT and B.

6.5 Biomass composition of OPS0865

The biomass composition of OPS0865 free-living cultures was measured under aerobic and micro-aerobic conditions according to the method described in section 2.8 and

each of the components was expressed as % of cell dry weight (Figure 6.18). Under both conditions, protein, lipid and RNA constituted the major proportions of the cell dry weight while, DNA, carbohydrates and EPS were present in minor proportions.

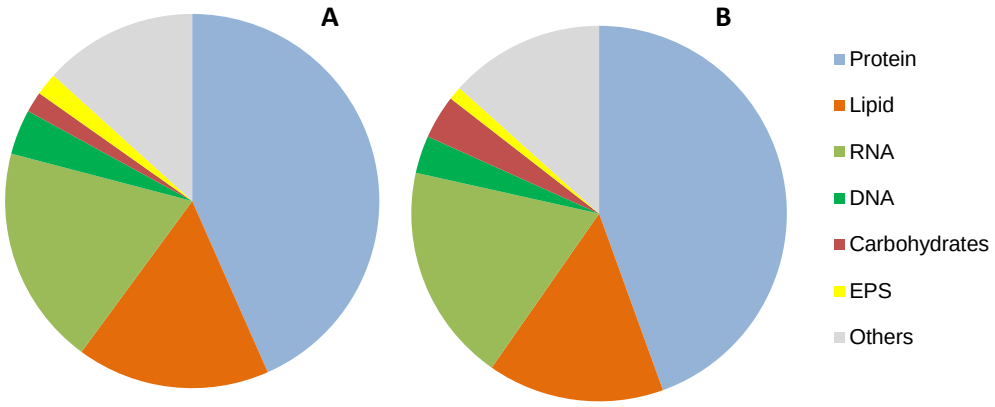

Figure 6.18: **Biomass composition of OPS0865 freeliving cultures**. The measurements are shown for OPS0865 under (A) aerobic and (B) micro-aerobic growth conditions. Values are the means of three biological replicates.

The biomass composition of aerobic and micro-aerobic OPS0865 was compared with the measurements determined for aerobic ORS571 (section 3.4.1) and micro-aerobic ORS571 (section 4.3) (Figure 6.19).

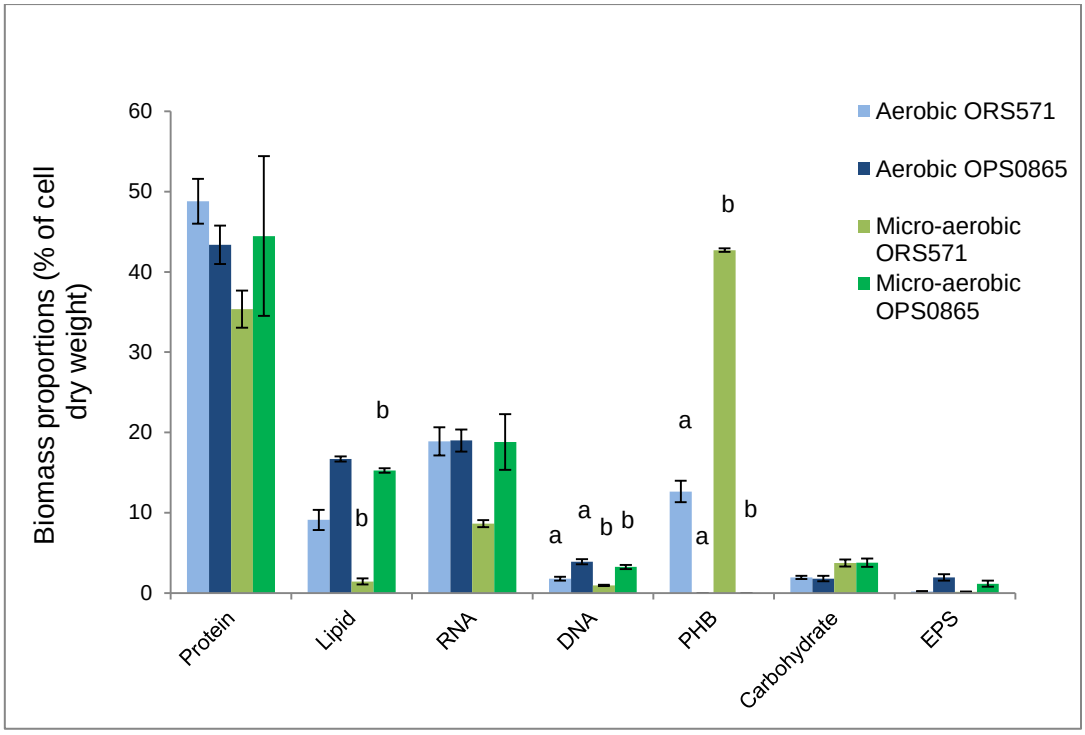

Figure 6.19: **Biomass composition of ORS571 and OPS0865** under aerobic and micro-aerobic conditions. Measurements for aerobic ORS571 are mean ± SEM from six biological replicates. Measurements for micro-aerobic ORS571, aerobic and micro-aerobic OPS0865 are mean ± SEM from three biological replicates. Significant differences between ORS571 and OPS0865 under aerobic and micro-aerobic conditions as determined by t-test are indicated: a, b; p-value < 0.05.

DNA content was significantly higher in OPS0865 than ORS571 under both aerobic and micro-aerobic growth conditions. In the current study, ORS571 was observed to accumulate a large amount of PHB under the micro-aerobic conditions; PHB alone occupied around 40% of the cell dry weight. OPS0865, devoid of PHB synthesis synthesized significantly higher amounts of lipid as compared to ORS571 under micro-aerobic conditions. The increase in the amount of lipids was over 10-fold in micro-aerobic OPS0865. The shift of OPS0865 from aerobic to micro-aerobic conditions did not cause any significant alterations in the biomass composition.

6.6 Steady state ^{13}C-MFA of OPS0865 under aerobic and micro-aerobic conditions

Labelling experiments were performed on free-living cultures in the mini-reactor set up using 20% [$^{13}C_4$]succinate under aerobic (21 % O_2) and micro-aerobic (3 % O_2) conditions with NH_4Cl as the nitrogen source. Labelling experiments and ^{13}C-MFA were not done under N_2-fixing conditions, as the OPS0865 cultures showed restricted growth under these conditions. The cultures were grown in triplicate and harvested at late exponential growth stage. The extraction of metabolites and MS measurement of isotopic labelling of biomass components were performed using the methods developed in chapter 3. The MS measurements used for ^{13}C-MFA are listed in the appendix (Table A20-A21). The metabolic model used for OPS0865 was essentially the same as that was used for ORS571 except for the biomass reaction and is presented in the appendix (Table A22). The biomass equation used to constrain the models for both the conditions was formulated according to the method established in section 3.11.2. The fluxes and their corresponding 95% confidence limits are listed in Table 6.1.

Table 6.1: **Net fluxes and their associated 95% confidence limits measured for OPS0865 free-living cultures under aerobic and micro-aerobic conditions**

Reaction step (s)		**Net flux (relative to succinate uptake)**	
Net fluxes	**Symbol**	**Aerobic**	**Micro-aerobic**
Uptake fluxes Total uptake of succinate (constrained)	*upt3*	100 (Fixed flux)	100 (Fixed flux)
Tricarboxylic acid cycle			
Succinate dehydrogenase	*tca1*	143 (139, 145)	**146 (142, 149)**
Fumarase	*tca2*	144 (140, 146)	**147 (143, 150)**
Malate dehydrogenase	*tca3*	71.4 (69.7, 147)	76.5 (72.7, 110)
Citrate synthase	*tca4*	45.5 (42.1, 48.1)	**48.2 (44.7, 51.2)**

Reaction step (s) Net fluxes	Symbol	Net flux (relative to succinate uptake) Aerobic	Micro-aerobic
Aconitase	*tca5*	45.5 (42.1, 48.1)	**48.2 (44.7, 51.2)**
Isocitrate dehydrogenase NADP-dependent	*tca6*	45.5 (42.1, 48.1)	**48.2 (44.7, 51.2)**
2-Oxoglutarate dehydrogenase	*tca7*	43.2 (39.7, 45.9)	**46.1 (42.6, 49.0)**
Succinyl-CoA synthetase	*tca8*	42.0 (38.4, 44.8)	**45.0 (41.5, 47.9)**
Pyruvate dehydrogenase	*tca9*	67.6 (3.78, 69.1)	66.1 (2.07, 67.4)
Anaplerotic pathways			
NAD-dependent malic enzyme	*mal*	72.9 (0, 75.8)	70.5 (0, 76.4)
Phosphoenolpyruvate carboxykinase	*pepck*	19.4 (16.3, 19.9)	22.5 (18.3, 22.9)
Methylmalonate-semialdehyde dehydrogenase	*msdh*	0 (0, 64.0)	0 (0, 66.3)
Glycolysis			
Pyruvate kinase	*gly1*	0.49 (0, 6.23),	0.26 (0, 50.2)
Gluconeogenesis			
Phosphoglycerate kinase	*glu1*	16.8 (14.2, 23.2)	**20.4 (15.7, 28.5)**
Glyceraldehyde-3-phosphate dehydrogenase	*glu2*	10.5 (8.83, 16.8)	**15.0 (9.59, 23.2)**
Triosephosphate isomerase	*glu3*	5.75 (4.30, 12.1)	**10.6 (8.91, 19.0)**
Fructose-bisphosphate aldolase	*glu4*	4.43 (3.03, 10.8)	**9.62 (6.67, 18.0)**
Fructose-1,6-bisphosphatase	*glu5*	4.43 (3.03, 10.8)	**9.62 (6.67, 18.0)**
Phosphoglucose isomerase	*glu6*	2.04 (0.76, 13.9)	**17.7 (15.4, 36.1)**
Pentose phosphate pathway			
Glucose-6-phosphate dehydrogenase	*ppp1*	1.24 (0, 13.0)	**16.7 (14.6, 35.2)***
6-phosphogluconate dehydrogenase	*ppp2*	0 (0, 8.68)	15.2 (0, 30.3)
Ribulose-phosphate 3-epimerase	*ppp3*	-2.38 (-2.53, 3.42)	8.11 (-2.39, 18.3)
Ribose 5-phosphate isomerase	*ppp4*	2.38 (2.27, 5.25)	**7.11 (7.01, 12.0)***
Transketolase- C5/C3 conversion	*ppp5*	-2.38 (-2.53, 3.42)	8.11 (-2.39, 18.3)
Transketolase- C6/C4 conversion	*ppp6*	1.70 (-1.21, 1.81)	-3.59 (-8.71, 1.73)
Transketolase- C7/C5 conversion	*ppp7*	0.67 (-1.46, 0.71)	-4.51 (-9.58, 0.65)

Reaction step (s) Net fluxes	Symbol	Net flux (relative to succinate uptake) Aerobic	 Micro-aerobic
Transaldolase- C6/C3 conversion	*ppp8*	0.67 (-1.46, 0.71)	-4.51 (-9.58, 0.65)
Transaldolase- C7/C4 conversion	*ppp9*	-0.67 (-0.71, 1.46)	4.51 (-0.65, 9.58)
Entner-Doudoroff pathway			
6-Phosphogluconate dehydratase	*ed1*	1.24 (0, 4.99)	1.57 (0, 6.11)
2-keto-3-deoxy-6-phosphogluconate aldolase	*ed2*	1.24 (0, 4.99)	1.57 (0, 6.11)
Amino acid synthesis			
Glutamate dehydrogenase	*glt*	18.9 (17.5, 20.7)	16.9 (15.8, 19.3)
Glutamine synthetase	*gln*	**1.23 (1.15, 1.31)**	1.11 (1.04, 1.19)
Proline synthesis	*pro*	0.56 (0.53, 0.60)	**0.50 (0.47, 0.54)**
Arginine synthesis	*arg*	0.85 (0.79, 0.90)	**0.76 (0.72, 0.82)**
Aspartate transaminase	*asp*	5.27 (4.89, 8.06)	4.73 (4.44, 8.35)
Asparagine synthase	*asn*	0.73 (0.68, 0.77)	**0.65 (0.61, 0.71)**
Alanine aminotransferase	*ala*	1.46 (1.37, 1.55)	**1.31 (1.23, 1.42)**
Serine synthesis	*ser*	4.03 (2.63, 4.28)	3.55 (2.13, 4.17)
Serine hydroxymethyltransferase	*glc1*	2.41 (1.03, 2.56)	2.09 (0.66, 2.46)
MEETHF synthesis	*meethf*	1.04 (0.97, 2.41)	0.87 (0.81, 2.49)
Threonine aldolase	*glc2*	0 (0, 2.71)	0 (0, 3.0275)
Cysteine synthesis	*cys*	0.73 (0.68, 0.77)	**0.65 (0.61, 0.71)**
Lysine synthesis	*lys1*	0.88 (0.83, 0.94)	**0.79 (0.74, 0.86)**
Lysine synthesis	*lys2*	0.88 (0.83, 0.94)	**0.79 (0.74, 0.86)**
Threonine synthesis	*thr*	1.47 (1.37, 4.21)	1.33 (1.24, 4.52)
Methionine synthesis	*met*	0.33 (0.31, 0.35)	**0.30 (0.28, 0.32)**
Valine synthesis	*val*	1.02 (0.95, 1.08)	**0.91 (0.85, 0.98)**
Leucine synthesis	*leu*	1.21 (1.13, 1.28)	**1.08 (1.02, 1.17)**
Isoleucine synthesis	*ile*	0.70 (0.66, 0.75)	**0.63 (0.59, 0.68)**
Phenylalanine synthesis	*phe*	0.47 (0.44, 0.50)	**0.42 (0.40, 0.46)**
Tyrosine synthesis	*tyr*	0.41 (0.38, 0.43)	**0.36 (0.34, 0.39)**

Reaction step (s) Net fluxes	Symbol	Net flux (relative to succinate uptake) Aerobic	 Micro-aerobic
Tryptophan synthesis	*trp*	0.13 (0.13, 0.14)	**0.12 (0.11, 0.13)**
Histidine synthesis	*his*	0.24 (0.22, 0.25)	**0.22 (0.20, 0.23)**
Other outputs			
METHF synthesis	*methf*	0.33 (0.31, 0.35)	**0.30 (0.28, 0.32)**
FTHF synthesis	*fthf*	0.24 (0.22, 0.25)	**0.22 (0.20, 0.23)**
PHB synthesis	*accoa1*	**0 (0, 0)**	**0 (0, 0)**
Biomass synthesis	*biomass*	3.76 (3.52, 3.99)	3.29 (3.09, 3.55)
Lipid synthesis	*accoa2*	**19.2 (17.9, 20.4)**	**15.3 (14.3, 16.5)***
DNA synthesis	*r5p1*	**0.47 (0.44, 0.50)**	**0.34 (0.32, 0.37)***
RNA synthesis	*r5p2*	2.20 (2.06, 2.33)	**1.90 (1.79, 2.06)**
Carbohydrates synthesis	*g6p1*	0.39 (0.37, 0.42)	0.72 (0.68, 0.78)*
EPS synthesis	*g6p2*	**0.40 (0.37, 0.42)**	**0.21 (0.19, 0.22)***
CO_2 output (net)	*co_2.out*	254 (251, 262)	**274 (264, 276)***

Fluxes are presented as best-fit estimates calculated using MS measurements from three individual labelling experiments for OPS0865 free-living cultures under aerobic and micro-aerobic conditions. The 95% confidence limits for the fluxes were calculated using parameter continuation analysis in INCA and presented as (lower bound, upper bound) of the confidence limits. All fluxes were expressed on a molar basis relative to a succinate uptake flux of 100. Fluxes measured under two different growth conditions were considered to be significantly different if the confidence intervals associated with the fluxes did not overlap. Fluxes shown in **red** represents a significant increase and **blue** represents a significant decrease in OPS0865 fluxes under aerobic and micro-aerobic conditions, relative to the fluxes determined for ORS571 under aerobic and micro-aerobic conditions (chapter 4) respectively. Fluxes indicated with * and * represents a significant increase and decrease respectively, for OPS0865 under micro-aerobic conditions relative to the fluxes determined for OPS0865 under aerobic conditions.

6.6.1 Statistical analysis of the flux maps

The flux maps obtained for OPS0865 free-living cultures had statistically acceptable SSRs as listed in Table 6.2. As found in earlier analyses (Chapter 3) SSR values lower than the anticipated range probably reflect under-estimation of the precision of the isotopomer measurements used to constrain the flux distributions deduced by MFA. The goodness of fit for the two flux maps was assessed by comparing the experimentally obtained MS measurements for amino acids and trehalose with the simulated measurements and is included in the appendix (Figure A23-24). There was a good agreement between the simulated and experimentally determined measurements, which confirms the reliability of the flux solutions.

Table 6.2: **SSRs obtained for flux maps of OPS0865 free-living cultures**

Growth condition	Obtained SSR	Expected SSR	Degrees of freedom (DOF)	Comment
Aerobic	216.9	318.6 - 425.2	370	Fit accepted
Micro-aerobic	173.1	260.4 – 357.4	307	Fit accepted

6.7 Changes in metabolic fluxes of OPS0865

The flux distributions determined for OPS0865 free-living cultures under aerobic and micro-aerobic conditions are represented as flux maps (Figure 6.20). The changes in the flux maps of OPS0865 relative to ORS571 and also the changes in OPS0865 under the two growth conditions are described in the subsequent sections.

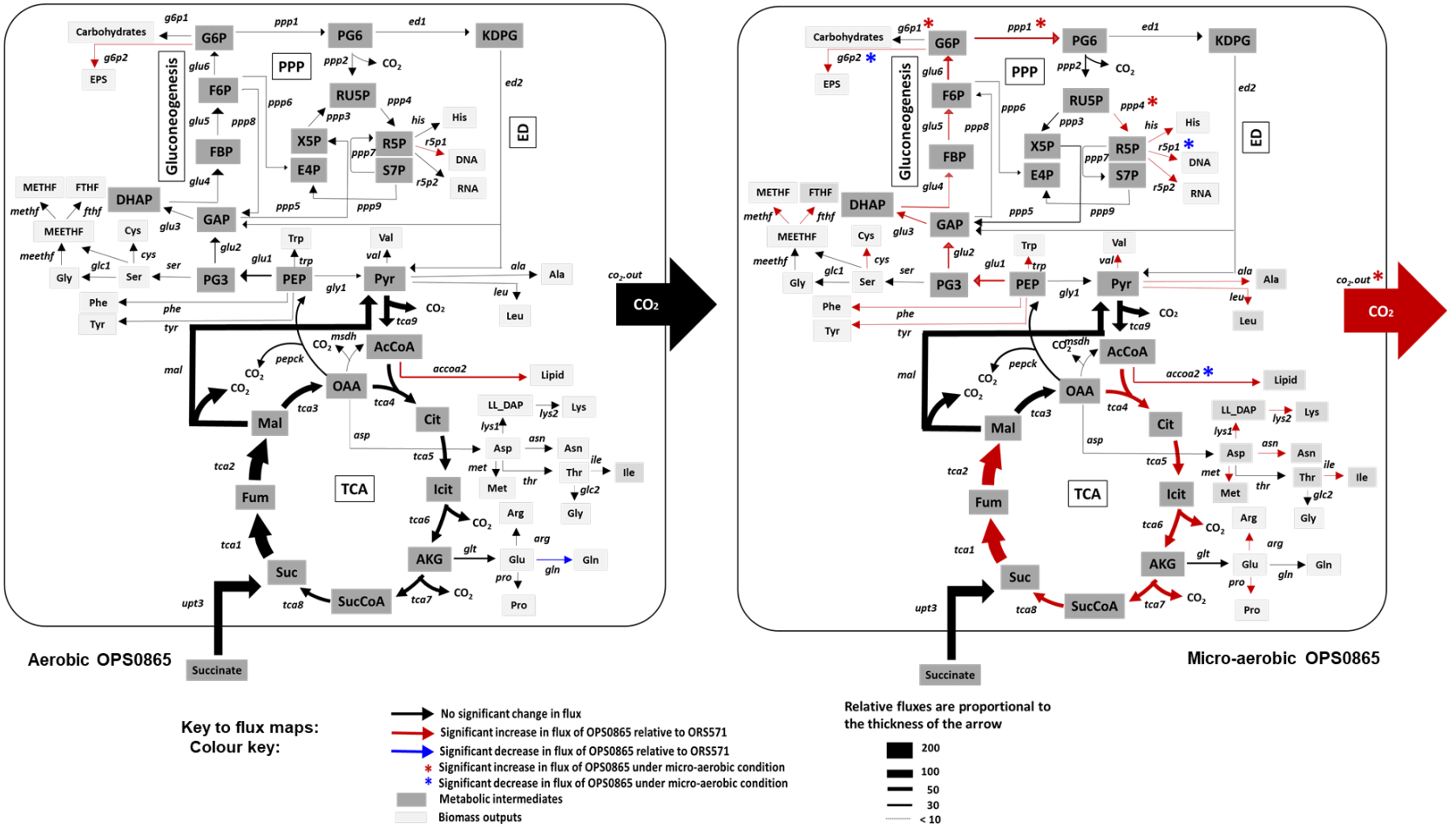

Figure 6.20: **Changes in the metabolic fluxes of OPS0865 free-living cultures under aerobic and micro-aerobic conditions**. The flux maps represent statistically valid best-fit models based on the redistribution of label following metabolism of [$^{13}C_4$] succinate by OPS0865 cultures under aerobic and micro-aerobic condition with NH_4Cl as the nitrogen source. The thickness of each arrow in the flux maps is proportional to the relative molar flux. Metabolic intermediates and biomass outputs are shown in rectangular boxes with distinct colour key. The symbols for fluxes are shown in *italics* (defined in Table 6.1). Statistically significantly changes in fluxes for OPS0865 as compared to ORS571 under aerobic and micro-aerobic condition are shown with distinct colour key (Table 6.1). Significant increase in fluxes for aerobic OPS0865 (*accoa2*, *g6p2 and r5p1*) are shown in **red** and significant decrease in fluxes (*gln*, *accoa1*) are in **blue** relative to aerobic ORS571. Significant increase in fluxes for micro-aerobic OPS0865 (*tca1, tca2, tca4, tca5, tca6, tca7, tca8, glu1, glu2, glu3, glu4, glu5, glu6, ppp1, ppp4, pro, arg, asn, ala, met, lys1, lys2, val, trp, tyr, phe, cys, methf, fthf, ile, his, r5p1, r5p2, g6p2, accoa2* and *co2.out*) are in **red** and significant decrease in flux (*accoa1*) are shown **blue** relative to micro-aerobic ORS571. Significant increase fluxes of micro-aerobic OPS0865 relative to aerobic OPS0865 is indicated by * and a significant decrease is indicated by *.

6.7.1 Changes in the metabolic fluxes of OPS0865 due to micro-aerobic conditions

The effect of the switch from aerobic to micro-aerobic growth conditions on the OP0865 flux distribution is shown in Figure 6.20 This comparison identified the fluxes that were significantly altered solely due to the micro-aerobic conditions. PPP fluxes *ppp1* and *ppp4* increased significantly under micro-aerobic conditions. The remaining PPP fluxes - *ppp2*, *ppp3*, *ppp5*, *ppp6*, *ppp7*, *ppp8* and *ppp9* were relatively poorly defined and so the estimates are not significantly different due to large confidence limits.

There were also significant changes in the biomass synthesis fluxes *accoa2*, *r5p1*, *g6p1* and *g6p2* synthesis under micro-aerobic conditions. The changes in these fluxes were directly influenced by the different amounts of lipid, DNA, carbohydrate and EPS synthesized under the two conditions. Flux co_2*.out* was also significantly higher in the micro-aerobic culture which was mainly affected by the increase in *ppp1* flux under micro-aerobic conditions.

Flux *ppp1* generates NADPH, which is primarily used for biosynthesis. Because the flux to lipid biosynthesis was reduced in micro-aerobic OPS0865, the increased NADPH by *ppp1* could not be accounted for the overall biosynthesis of lipids. A possible explanation for the increased *ppp1* flux could be due to the synthesis lipids which were different in structure and function, to the lipids synthesized under aerobic conditions. This hypothesis needs to be tested further by analysis of the lipids synthesized in OPS09865 under the two conditions. Flux *ppp4* generates R5P, which is the precursor for the nucleic acids-DNA and RNA. Flux *r5p1* was significantly reduced in micro-aerobic OPS0865 and there was no significant difference in *r5p2* between the two growth conditions, hence the increased *ppp4* flux cannot be explained in terms of nucleic acid synthesis. The increased *ppp4* could be required to maintain higher fluxes via *ppp5*, *ppp6*, *ppp7*, *ppp8* and *ppp9*. There were no statistically significant increases

in *ppp5*, *ppp6*, *ppp7*, *ppp8* and *ppp9* fluxes under micro-aerobic conditions because of the large confidence limits associated with these fluxes. However, because *ppp1* and *ppp4* fluxes were significantly higher under micro-aerobic conditions, it was very likely that there was an increase the remaining PPP fluxes. The increased *ppp1* and *ppp4* fluxes under micro-aerobic conditions could also be required to support the increased synthesis of carbohydrates (*g6p1*). In addition, micro-aerobic OPS0865 cultures showed a longer doubling time than aerobic cultures, which might increase the relative contribution of maintenance requirements to the overall metabolic activity of the central network.

6.7.2 Changes in fluxes between OS0865 and ORS571 under aerobic conditions

The significant changes in the fluxes of OPS0865 cultures relative to the wildtype under aerobic conditions (section 4.7, Table 4.1) are shown in Figure 6.20. There were changes in the fluxes to biomass outputs, which were influenced by the synthesis of different biomass proportions in the two strains. The fluxes- *accoa2*, *g6p2* and *r5p1* were higher in OPS0865, while fluxes- *accoa1* and *gln* were significantly reduced. The reduced *accoa1* flux for PHB synthesis in OPS0865 reflects the absence of PHB production in this strain. Under aerobic conditions, PHB occupied around 12% of the cell dry weight in ORS571; therefore an increased flux to lipid and EPS synthesis are the consequences of the loss of PHB in OPS0865. There was also an increase in flux to DNA synthesis in OPS0865. The construct pOPS0391containing pK18*mob* and *phbC* gene was introduced in ORS571 by conjugation with the donor *E. coli* strain (section 2.18) and such horizontal gene transfers has been previously reported by Vogan & Higgs (2011), to cause an increase in genome size. Similar genome rearrangements in bacteria have been previously reported to arise due to deletions, insertions, amplifications, duplications, inversions or translocations (Darmon & Leach,

2014). So, the integration of pK18 construct into the ORS571 genome contributed towards the increased nucleotide (DNA) production, but this contribution was unlikely to account for more than a very small proportion of the increased flux to DNA synthesis. A more likely explanation is, as for EPS and lipid that this arises from the way in which the flux data are expressed – relative to the rate of succinate consumption. Since PHB constitutes an appreciable proportion of the total dry mass of the wild type cells, preventing PHB accumulation will inevitably result in an increase in the proportions of all other biomass components even if their rates of production (relative to each other) are unaffected. Fluxes *accoa2* and *r5p1* in OPS0865 were nearly 2-fold higher than those in ORS571. Flux *g6p2* for EPS synthesis in OPS0865 was around 13-fold higher than that determined for ORS571. From these results a correlation can be proposed between the two polymers, PHB and EPS in ORS571, where the absence of PHB resulted in a striking increase in the production of EPS under aerobic growth conditions. The relationship between these two polymers has been previously studied in two *R. meliloti* strains, where the researchers suggested that the co-production was regulated by the type of carbon substrates used for growing the strains (Tavernier et al., 1997). Also, EPS production in ORS571 cultures was reported to increase under nitrogen-limiting conditions (D'Haeze et al., 2004). Here, there were no changes in the growth medium used for the two strains, so the increased EPS production in the absence of PHB cannot be explained by a change of growth substrates. The increased EPS production in OPS0865 was probably associated with the carbon and co-factor balance of the cell. Bacterial EPS synthesis required carbon and co-enzymes, mainly ATP (Schmid et al., 2015). Thus the central metabolic network responds flexibly to meet the demands of the cell for the precursors and coenzymes needed to produce the combination of products required to support growth and development.

There were no significant changes in the fluxes through the TCA cycle, gluconeogenesis, PPP and ED pathways. There are two possible explanations; one is

that the decrease in PHB production and changes in other biomass components precisely balance each other so that the withdrawal of intermediates for the network to provide the precursors for biomass production exactly balanced in the two strains; the alternative is that the estimates of fluxes through the central network lacked sufficient resolution to be able to detect any statistical significance in the differences needed to support the changes in biomass production.

6.7.3 Changes in fluxes between OS0865 and ORS571 under micro-aerobic conditions

The significant changes in the fluxes of OPS0865 relative to the wildtype (section 4.7, Table 4.1) under micro-aerobic growth conditions are shown in Figure 6.20. The major metabolic adjustment in ORS571 during micro-aerobic growth was the significant increase in flux to PHB synthesis (around 40% of the cell dry weight was composed of PHB). The accumulation of PHB under micro-aerobic conditions was previously rationalised as being needed to maintain the redox potential of the cell by acting as a sink for carbon and reducing equivalents (Senior et al, 1972; Jackson & Dawes, 1976; Trainer & Charles, 2006). The comparison between OPS0865 and ORS571 during micro-aerobic growth identified the changes in the network that were required to sustain micro-aerobic metabolism in the absence of the capacity to produce PHB. There were significant changes in the central carbon catabolic fluxes and output fluxes (biomass and metabolic CO_2 production) in OPS0865 cultures.

In micro-aerobic OPS0865, where as anticipated there was no synthesis of PHB, flux *accoa2* for lipid synthesis increased over 10-fold; additionally there was a 7-fold increase in flux to EPS synthesis (*g6p2*) and over 2-fold and 3-fold increases to RNA (*r5p2*) and DNA (*r5p1*) synthesis respectively. Fluxes for amino acid synthesis - *pro*, *arg*, *asn*, *lys1*, *lys2*, *ile*, *met*, *leu*, *ala*, *val*, *tr*p, *phe*, *tyr*, *his* and *cys* - were also higher in OPS0865.

Fluxes *tca1*, *tca2*, *tca4*, *tca5*, *tca6*, *tca7* and *tca8* through the TCA cycle were significantly higher in OPS0865. There were changes in AcCoA partitioning between the TCA cycle and lipid synthesis. The majority (i.e. over 50%) of AcCoA synthesized via *tca9* entered the TCA via *tca4* and the rest was utilised for lipid synthesis. In ORS571, *tca4* used 54%, while *accoa1* and *accoa2* used 21% and 2% respectively, and the remainder is released as CO_2. In OPS0865, 73% of AcCoA was used by *tca4,* 23% by *accoa2* for lipid synthesis, 4% was released as CO_2 and none by *accoa1*. Thus, elimination of PHB synthesis was accompanied by an increase in AcCoA utilized by the TCA cycle and lipid synthesis. Terpolilli et al. (2016) argued that a bacteroid incapable of PHB synthesis still retained symbiotic functionality because of the ability to use free fatty acids, glycerolipids and membrane phospholipids as alternative sinks for excess carbon and reductants. The significant increase in lipid synthesis for OPS0865 can be accepted as an alternative carbon and reductant sink in the absence of PHB.

The oxidative PPP flux *ppp1* catalysed by glucose 6-phosphate dehydrogenase (G6PD) was significantly higher in OPS0865 than ORS571 under micro-aerobic conditions; this reaction generates NADPH, which is primarily used for biosynthesis. The synthesis of lipids and amino acids required NADPH, hence an increased synthesis of these biomass components in OPS0865 required an increased flux through *ppp1* in addition to the increased TCA cycle fluxes. Flux *ppp4* catalysed by ribose-5-phosphate (R5P) isomerase produced ribose-5-phosphate - the precursor of nucleic acids. Under micro-aerobic conditions, OPS0865 produced increased amounts of nucleic acids, which may explain the increased flux through *ppp4*.

Gluconeogenic fluxes catalysed by the enzymes phosphoglycerate kinase (*glu1*), glyceraldehyde-3-phosphate dehydrogenase (*glu2*), triosephosphate isomerase (*glu3*), fructose-bisphosphate aldolase (*glu4*), fructose-1,6-bisphosphatase (*glu5*) and phosphoglucose isomerase (*glu6*) were significantly higher in OPS0865. Glucose 6-phosphate, the precursor for carbohydrates including EPS, was synthesized primarily

via the gluconeogenesis pathway. In OPS0865 cultures, the higher carbon flux via the gluconeogenesis pathway supported the increased production of EPS. The increased gluconeogenic flux was also needed to meet the increased demand for glucose-6-phosphate needed to support the increased *ppp1* flux.

Therefore, inhibition of PHB synthesis and low O_2 conditions in combination resulted in an increase in the fluxes via the carbon utilisation pathways - TCA, gluconeogenesis and PPP. The changes in these pathway fluxes can be explained by the altered requirements of precursors needed to support the observed changes in biomass composition during micro-aerobic growth.

6.8 Co-enzyme analysis

Co-enzyme analysis for the OPS0865 flux distributions determined under aerobic and micro-aerobic conditions was conducted according to the methods established in section 3.14. The analysis was done for the reactions defined in the metabolic model of OPS0865 - substrate level phosphorylation and amino acid, lipid, nucleic acid biosynthesis. The analysis does not include co-enzyme production by oxidative phosphorylation or consumption by functions such as growth and maintenance.

6.8.1 Co-enzyme production

The production of co-enzymes in OPS0865 free-living cultures under aerobic and micro-aerobic condition is shown in Figure 6.21.

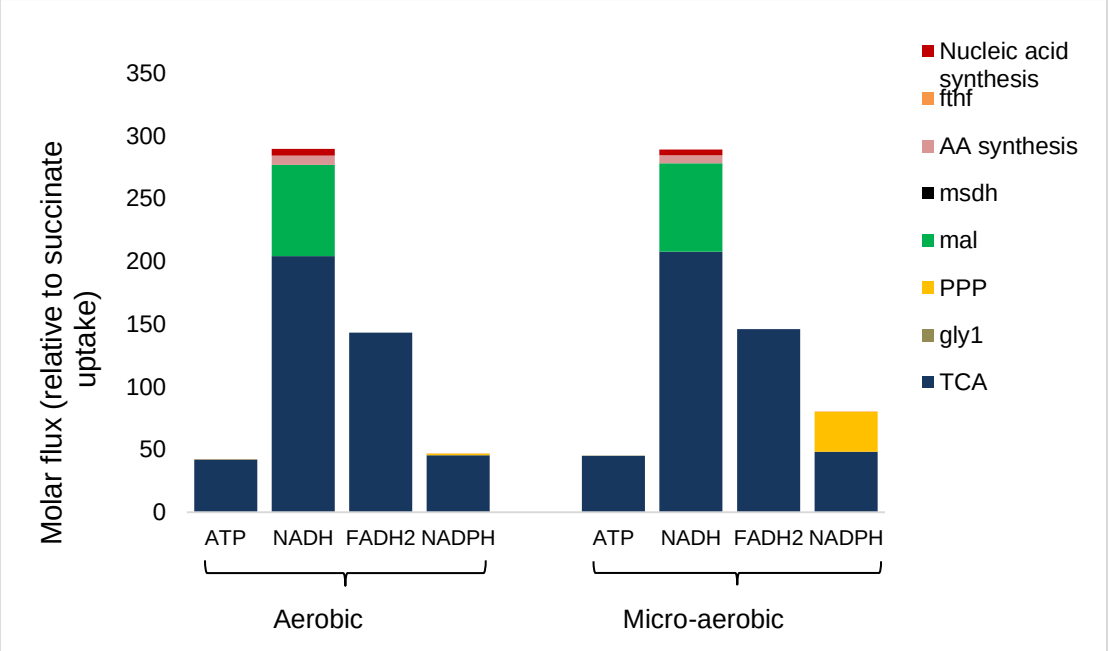

Figure 6.21: **Production of co-enzymes by OPS0865 growing under aerobic and micro-aerobic conditions**. The production of ATP, NADH, $FADH_2$ and NADPH by the network was determined from the sum of individual fluxes that produced co-enzymes in the flux distributions obtained for OPS0865 cultures under the two growth conditions (Table 6.1). All values are molar fluxes expressed relative to succinate uptake.

Around 97% of the NADPH in aerobic OPS0865 cultures was produced by *tca6*; whereas in micro-aerobic OPS0865 cultures, 60% of the NADPH was supplied by *tca6* and the rest (40%) by PPP reactions (*ppp1* and *ppp2*). The production of NADPH by PPP reactions in micro-aerobic OPS0865 was over 25-fold higher; this was mainly associated with the significantly higher *ppp1* flux under micro-aerobic conditions. Thus micro-aerobic conditions resulted in increased NADPH synthesis in OPS0865 cultures. This is in marked contrast to ORS571 in which micro-aerobic conditions did not produce any significant increase NADPH production (Figure 4.13) as there were no significant changes in the fluxes that produced NADPH in the network. There were no significant changes in ATP, NADH and $FADH_2$ production due to micro-aerobic condition in OPS0865 cultures.

Co-enzymes production in OPS0865 was also compared to that determined for ORS571 (Figure 4.14) under aerobic and micro-aerobic growth conditions. NADPH produced in micro-aerobic OPS0865 cultures was significantly higher (by 74%) than produced by the wildtype micro-aerobic ORS571. Inhibition of PHB synthesis during micro-aerobic growth resulted in significant increases in TCA cycle and PPP fluxes, and as a result, NADPH produced by these pathways also increased significantly.

Under aerobic conditions, there was no significant difference in ATP production between ORS571 and OPS0865 cultures. But under micro-aerobic conditions, ATP produced by OPS0865 metabolic network increased by 15% in comparison to ORS571. This was because of the significant increase in flux via *tca8* of OPS0865. There were no significant differences in NADH production between OPS0865 and ORS571 under aerobic growth conditions. But under micro-aerobic conditions, NADH production in OPS0865 increased by 8.5%, which was associated with the increase in the TCA cycle fluxes of OPS0865. Also, $FADH_2$ produced solely by *tca1* in the network, was 4.3% higher in micro-aerobic OPS0865 than micro-aerobic ORS571.

Overall, the differences in the metabolic network fluxes (mainly in the TCA cycle and PPP) between ORS571 and OPS0865 cultures under micro-aerobic growth conditions resulted in substantial changes in co-enzyme productions.

6.8.2 Co-enzyme consumption

Consumption of co-enzymes in the reaction network used for OPS0865 cultures under aerobic and micro-aerobic conditions is shown in Figure 6.22. Co-enzymes were utilised mainly for net biosynthesis (lipids, protein and nucleic acids) and only a minor proportion was used for network reactions that produced metabolic intermediates.

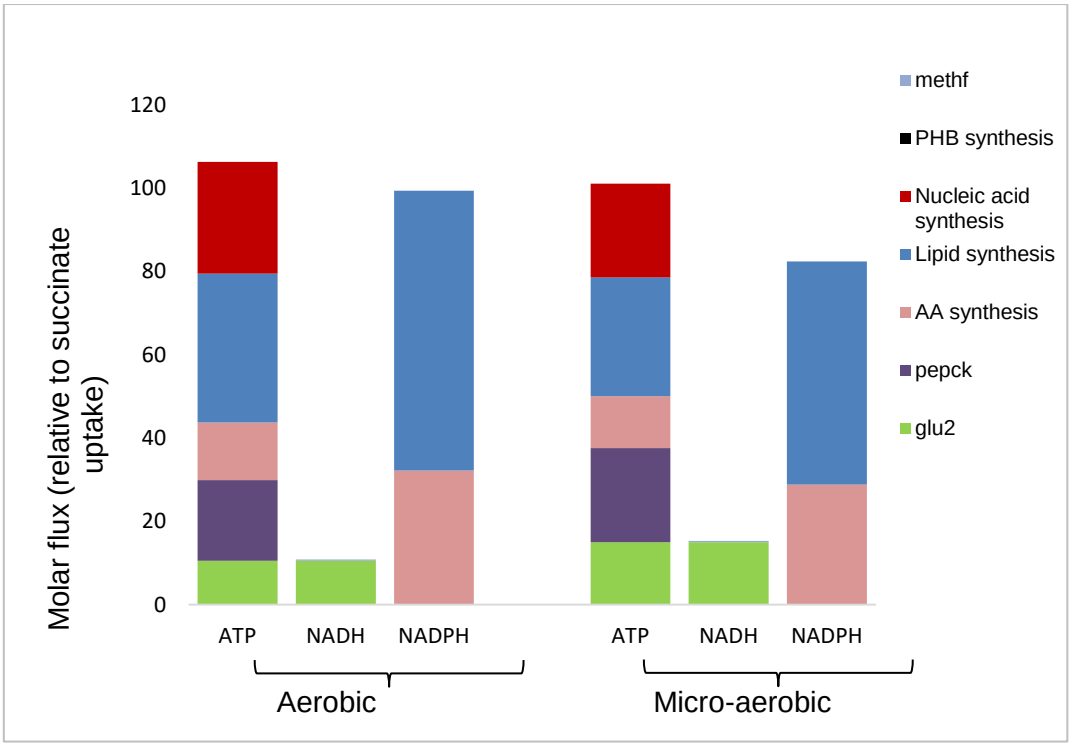

Figure 6.22: **Consumption of co-enzymes by OPS0865 growing under aerobic and micro-aerobic conditions**. The consumption of ATP, NADH, $FADH_2$ and NADPH by the network was determined from the sum of individual fluxes that consumed co-enzymes in the flux distributions obtained for OPS0865 cultures under the two growth conditions (Table 6.1). All values are molar fluxes expressed relative to succinate uptake.

ATP consumption in OPS0865 aerobic and micro-aerobic cultures followed a similar distribution: lipids > nucleic acids > amino acid synthesis > *pepck* > *glu2*. The overall ATP consumed was higher in OPS0865, largely as a consequence of the significantly higher *accoa2* flux for lipid synthesis under aerobic conditions. NADH was used mainly for the reaction *glu2* in the network; there was no significant difference in the proportion of NADH used in aerobic and micro-aerobic OPS0865. For both aerobic and micro-aerobic OPS0865, the overall consumption of co-enzymes ATP and NADPH was higher than produced by the network. The additional ATP and NADPH utilised for net biosynthesis could be generated by oxidation of NADH and $FADH_2$ that were produced in excess by the network. Only around 5% of the NADH generated by the network was used directly for production of biomass and the remaining 95% was available to

produce ATP via oxidative phosphorylation and NADPH via a transhydrogenase reaction. $FADH_2$ was not utilised for biomass production but could be utilised to produce ATP via oxidative phosphorylation.

The consumption of co-enzymes in OPS0865 was also compared to that determined for ORS571 (Figure 4.15) under aerobic and micro-aerobic conditions. ATP consumption in OPS0865 was significantly higher than that in ORS571; during aerobic growth, the overall ATP consumed increased by 21% and during micro-aerobic growth by 8%. NADPH consumption in OPS0865 cultures was significantly higher than that in ORS571; by 22% during aerobic and by 78% micro-aerobic growth respectively. In aerobic and micro-aerobic ORS571, amino acid synthesis consumed majority of the NADPH, and the rest by PHB and lipids synthesis. But in OPS0865, out of the total NADPH consumed, 60% was used for lipid synthesis and the rest for amino acid synthesis. The significant difference in NADPH consumption between OPS0865 and ORS571 under micro-aerobic conditions was because of the substantial increase (over-10 fold) in *accoa2* flux for lipid synthesis in OPS0865. Under aerobic growth conditions, NADH consumption in OPS0865 and ORS571 was not significantly different. But under micro-aerobic conditions, there was over 5-fold increase in NADH consumed by OPS0865; this was because of the increased gluconeogenic flux *glu2* in OPS0865. To summarise a greater proportion of the ATP, NADH and NADPH produced by the network is utilised for biomass production in micro-aerobic OPS0865 than micro-aerobic ORS571.

6.9 Discussion

The growth and metabolism of a PHB mutant (OPS0865) derived from ORS571 was studied in this chapter under aerobic and micro-aerobic growth conditions to identify the effect of preventing PHB synthesis on the flux distribution in central carbon metabolism. Under aerobic conditions, ORS571 was able to grow on hydroxybutyrate

as the carbon source. This observation confirmed previous reports on ORS571 free-living cultures being able to degrade PHB under aerobic growth conditions and then utilising it as a carbon and energy reserve during starvation in the soil (Stam et al., 1986; Ratcliff et al., 2008). PHB degradation in ORS571 also provided a competitive advantage in the rhizosphere (Stam et al., 1986). In *Azospirillum brasilense* PHB was utilised as the carbon and energy reserve during stress conditions (Kadouri et al., 2003). In azotobacters, PHB was reported to be utilised as the carbon and energy source for survival during encystment (Anderson & Dawes, 1990). It was also proposed that the advantage of an organism to be able to synthesize and degrade PHB was to inhibit degradation of other cellular components such as RNA and protein under nutrient starvation conditions (Anderson & Dawes, 1990).

The ability of OPS0865 to utilise β-hydroxybutyrate was inhibited due to deletion of *phbC*; this suggested that preventing PHB synthesis compromised the ability of ORS571 to catabolise PHB. In diazotrophs, *Azotobacter vinelandii* and *Azotobacter beijerinckii*, the activity of the β-hydroxybutyrate dehydrogenase that catalysed conversion of β-hydroxybutyrate into acetoacetate in the PHB degradation pathway was shown to increase with the polymer turn-over (Manchak & Page, 1994). It was suggested that PHB degradation was more likely to be active in the cells that utilised PHB as an endogenous carbon and energy reserve (Manchak & Page, 1994). In a different study on *Methylobacterium extorquens* AM1, involvements of *phbC* in β-hydroxybutyrate utilisation was also observed, where the deletion of *phbC* caused slower growth of the cultures on β-hydroxybutyrate as the sole carbon source (Korotkova & Lidstrom, 2001). There is no clear understanding about such effects of *phbC* in β-hydroxybutyrate utilisation pathway and this need to be further explored.

For OPS0865, an increase in the doubling time of the cultures was observed as compared to the wild type; this indicates that during growth on succinate, PHB synthesis was required to support normal growth of ORS571 cultures under aerobic

conditions. These results agreed with the previously studied growth defects in the PHB mutant of ORS571 (Mandon et al., 1998). Similar growth characteristics were also observed for PHB mutants in *R. leguminosarum* by. *viciae* and *R. leguminosarum* by. *phaseoli* which were growth defective on rich media under aerobic conditions (Lodwig et al., 2005).

Fluxes for lipids, EPS and DNA synthesis were significantly higher in OPS0865, while the fluxes via the TCA cycle, gluconeogenesis, PPP, ED and anaplerosis did not vary significantly from the wild type. In order to accommodate the loss of PHB under aerobic conditions the system increased the proportions of EPS and lipids produced. The net production of co-enzymes in both the strains was comparable, but there was a significant increase in the amounts of ATP and NADPH consumed by OPS0865 (mainly due to increased lipid synthesis). This reflects the fact the central metabolic fluxes that produced the co-enzymes in OPS0865 were unaffected by the loss of PHB that was synthesized in only a minor proportion in ORS571 under aerobic growth conditions.

Increase in PHB synthesis was the major metabolic adjustment in ORS571 cultures growing under micro-aerobic conditions, where around 40% of the cell dry weight was composed of the polymer. Previous studies have proposed PHB to act as the sink for excess carbon and reducing equivalents produced during micro-aerobic growth, which is required to maintain unrestricted activity of the TCA cycle (Senior et al., 1972; Trainer & Charles, 2006; Terpolilli et al., 2016). In a PHB mutant of *Rhizobium etli*, increased levels of reduced cofactors were argued to be related to the absence of PHB as the reductive sink and also, the higher amounts of reduced cofactors were suggested to cause reduction in glucose and succinate oxidation (Cevallos et al., 1996). Since PHB synthesis was important during micro-aerobic growth, it was expected that the deletion of PHB under micro-aerobic conditions would significantly affect the flux distributions through the network. The comparison of the flux maps for

OPS0865 and ORS571 under micro-aerobic conditions identified significant differences in the TCA cycle, gluconeogenesis and PPP fluxes. This confirms that inhibition of PHB synthesis affected the fluxes of the TCA cycle, gluconeogenesis, and PPP pathways. The fluxes through these pathways increased, resulting in greater amounts of coenzymes being synthesised through these reactions. There were increased amounts of lipids, nucleic acids, amino acids and EPS synthesized in OPS0865 micro-aerobic cultures; the proportional rise being highest for lipids. From co-enzyme analysis, it was clear that the consumption of ATP and NADPH for biomass production was significantly higher in OPS0865 than that in ORS571 under micro-aerobic conditions. The co-enzyme consumption analysis was calculated only for amino acids, lipids, PHB and nucleic acids and does not include those utilised for EPS and carbohydrate biosynthesis. This was because knowledge of the precise reactions for EPS biosynthesis in ORS571 is currently limited, and neither the individual carbohydrate components nor their synthesis were explored in this study. However, EPS and other carbohydrates were unlikely to have a large influence the consumption analysis for two reasons. Firstly, EPS constitutes only a small proportion of the biomass, and so, the overall co-enzyme used for its synthesis will be low in comparison to that used for amino acids, nucleic acids and lipid synthesis. Secondly, EPS fluxes were significantly higher in OPS0865, and thus including the EPS co-enzyme requirements in the analysis would result in an even the higher co-enzyme consumption in OPS0865 than ORS571.

Because of the significant rise in lipid production, lipids may be considered as an alternative sink for excess reductant generated particularly in micro-aerobic cultures thereby sustaining metabolism and allowing growth of OPS0865 under low O_2 conditions. In *Rhizobium leguminosarum* bacteroids, lipids were argued to act as the carbon and reductant (NAD(P)H) sink in addition to PHB, and balanced the oxidation of AcCoA in the TCA cycle (Terpolilli et al., 2016). Terpolilli et al. (2016) also explained

that in the absence of PHB in the bacteroids pea, alfalfa, soybean and common bean, multiple alternative lipids including free fatty acids, glycerolipids and membrane phospholipids may be exploited as the sink for excess reductants that maintained redox balance in these N_2-fixing symbioses. In ORS571, the deletion of PHB results in a significant increase in lipid production, and the lipids were likely to substitute for the role of PHB during micro-aerobic growth.

The comparison of the flux maps for OPS0865 under aerobic and micro-aerobic conditions identified PPP fluxes via G6PD and R5P isomerase and also *g6p1* for carbohydrate synthesis, which increased under micro-aerobic conditions. Micro-aerobic OPS0865 cultures also showed a comparatively longer doubling time than the aerobic cultures. This growth effect was similar to that observed for the wild type strain, where the doubling time of micro-aerobic cultures were significantly longer than the aerobic cultures.

In this study, it was observed that in ORS571 PHB was synthesised as the major component of biomass during N_2 fixation as free-living micro-aerobic cultures (~44% of DCW) (Figure 4.6) and as symbiotic bacteroids (> 50% of DCW) (Figure 5.5). Deletion of PHB had a severe effect on the growth and N_2-fixing ability of the micro-aerobic ORS571 cultures. PHB-less bacteroids also showed defects in their symbiotic N_2-fixation ability within the host plant. This suggests that PHB metabolism in ORS571 is necessary to support N_2-fixation under both free-living and symbiotic conditions. However, the precise role of PHB in supporting N_2-fixation is unclear and cannot be generalised for all rhizobial species. In soybean nodules, the excess carbon taken up by bacteroids resulted in an increase of ME activity and in AcCoA/CoA, NAD(P)H/$NAD(P)^+$ ratios, and AcCoA metabolism was partitioned between the TCA cycle and PHB synthesis (Bergersen et al., 1991). In contrast in chickpea bacteroids, which accumulated little or no PHB, the oxidation of malate to oxaloacetate and utilization of AcCoA in the TCA cycle was the alternative to PHB synthesis (Kim &

Copeland, 1996). Moreover, in pea bacteroids, PHB has been proposed to serve as a fuel for rhizobia during differentiation into N_2-fixing bacteroids (Lodwig et al., 2005). For some other rhizobial species like *R. etli,* deletion of PHB synthesis resulted in higher rates of symbiotic N_2-fixation (Cevallos et al., 1996). In the symbiosis between *S. meliloti* and *Medicago sativa*, a mutant of *S. meliloti* unable to synthesize PHB, retained its N_2-fixing ability in the nodules (Povolo et al., 1994; Cai et al., 2000). But a different study showed that PHB metabolism was important for both nodulation and N_2 fixing ability of *S. meliloti* during symbiosis with *Medicago truncatula* (Wang et al., 2006). Thus, the relationship between PHB metabolism and symbiotic N_2 fixation is varied amongst the rhizobial species and their symbiosis with their host plant. The defects in growth and nitrogenase activity observed in this study for ORS571 free-living and bacteroids agreed with the previous study by Mandon et al. (1998). These researchers proposed that the deletion of PHB in ORS571 altered the redox and ATP balance of the cell, which inhibited the synthesis of Nif A – an important regulatory protein for N_2-fixation. This characteristic was reported to be unique to ORS571, where PHB metabolism was required for the functions of Nif A.

6.10 Conclusion

This chapter characterised the growth and metabolic changes in ORS571 when it was unable to synthesize PHB. The results provide information about the link between PHB synthesis and other metabolic pathways of the network to sustain metabolism in ORS571 in the free-living state. The loss of PHB during aerobic conditions resulted in slow growth of ORS571 cultures and affected the synthesis of biomass mainly lipids and EPS. Under micro-aerobic conditions, inhibition of PHB synthesis also resulted in slower growth of the cultures, increased lipid and EPS synthesis and increased fluxes through the TCA cycle, gluconeogenesis, and PPP pathway. Inhibition of PHB synthesis severely affected the growth and N_2-fixing ability of ORS571 under both free-living and symbiotic conditions. Thus, PHB synthesis was dispensable for growth of

ORS571 cultures under aerobic and micro-aerobic growth conditions, where the system was able to accommodate the loss of PHB and sustain growth and metabolism. However, PHB synthesis was indispensable for diazotrophic growth of ORS571 free-living cultures. The deletions of PHB in ORS571 also affected its symbiotic capabilities to nodulate and fix N_2 on the host plant *S. rostrata*. The metabolic consequences of the deletion of PHB in micro-aerobic OPS0865, combined with its inability to fix N_2 under free-living and symbiotic conditions, suggests the non-feasibility of the metabolic network either to support the increased production of lipids (or other substitutes for PHB), or therefore to sustain nitrogenase activities.

7. General discussion

The metabolic integration of the microsymbiont in the nodules is important for establishment of a successful rhizobial-legume N_2-fixing symbiosis. This symbiosis in agricultural systems provides ecological and economic benefits and is extensively researched. This symbiosis has the potential to substitute for chemical nitrogen fertilizers for plant growth and productivity. To optimise this substitution, it is important to understand the metabolic phenotype of N_2-fixing rhizobia. The results in this study identified the metabolic adjustments in ORS571 required during free-living and symbiotic N_2 fixation using ^{13}C-MFA. The first set of results (chapter 3) shows successful establishment of ^{13}C-MFA in ORS571 and includes a detailed description of the establishment of MFA (metabolic modelling, biomass measurements, labelling experiments, mass isotopomer measurements and determination and comparison of fluxes) in the free-living cultures. The methodology established in chapter 3 is the first to provide a frame work for measuring fluxes in a N_2-fixing rhizobial system under free-living and symbiotic conditions. This method was employed in the subsequent results chapters (4, 5 and 6) to define the metabolic phenotype of the system under different conditions of growth and N_2 fixation.

7.1 The metabolic flux phenotype of ORS571 under free-living and symbiotic conditions

The results in chapter 4 and 5 showed in vitro and ex vivo central carbon fluxes in the free-living and symbiotic forms of ORS571 and highlighted TCA cycle as the major carbon utilising pathway operating during N_2 fixation. The significantly higher fluxes through the TCA cycle in the micro-aerobic free-living cultures and bacteroids confirm this pathway to be the major source of co-enzymes that met the requirements for nitrogenase activities. The TCA cycle provided the precursors for PHB, which was produced in the N_2 fixing cultures and bacteroids as the major component of biomass. PHB production in N_2-fixing ORS571 was necessary to maintain the redox balance of

the system and unrestricted activity of TCA cycle under low O_2 environment required for nitrogenase activity in micro-aerobic cultures and for bacteroids inside the nodules. The results in chapter 6 showed that the ORS571 mutant unable to synthesize PHB was able to survive and grow under low O_2 conditions. PHB was reported to be the redox regulator of the cell during low O_2 conditions and results confirm that PHB deficient ORS571 is able to survive by increasing synthesis of lipids. The results provide information about how the metabolic network copes when PHB- the major biomass component in micro-aerobic ORS57, is eliminated from the system. There were rearrangements in the network fluxes in the PHB deficient strain which indicates that the synthesis of lipids as substitutes for PHB could be expensive, and a further in depth analysis of these lipids (structure and function) will strengthen this hypothesis.

The knowledge about the active pathways operating during N_2-fixation highlights the targets of the metabolic network- the enzymes and the metabolic intermediates involved in the reactions of the TCA cycle, that can be engineered to enhance the efficiency of existing ORS571-sesbania symbiosis. ORS571 is able to establish an endophytic relationship with rice plants and this provides an opportunity to explore the metabolic state of ORS571 as an endophyte. The findings from this study will be useful because the metabolic phenotype of free-living and symbiotic ORS571 can be compared with that of the endophytic fate. Such comparison will provide an idea about the differences between ORS571 when associated with a legume and a cereal and will help to identify the gaps that exist in transferring nitrogen fixation to cereal crops.

7.2 Limitations of this study

The flux maps determined for the early and late exponential stage of a batch culture were metabolically indifferent. But measurements from the late exponential growth stages provided better resolution of fluxes, and so, were used as the appropriate growth stage for performing MFA in ORS571 in vitro growth conditions (chapters 4 and 6). The late exponential stage used throughout this study represents a growth stage

rather than a specific growth rate. Within this growth stage, free-living cultures under different conditions of study could possibly have different growth rates that were difficult to control or manipulate in batch cultures. So, in addition to the growth conditions, variations in the growth rates between the conditions probably have an effect on the metabolic fluxes. To minimise the variability between culture conditions and to perform labelling experiments at a specific growth rate, use of a chemostat will be more appropriate, as such a set up will allow controlled in vitro growth of the system for MFA. The ex vivo steady state metabolic fluxes of ORS571 bacteroids measured in chapter 5 will require further analysis to confirm the extent to which these fluxes are a true representation of the in vivo metabolic phenotype of ORS571. The establishment of metabolic and isotopic steady for bacteroids was difficult because of the fragile nature of the bacteroids and their decrease in nitrogenase activity following isolation from the host nodules. It is likely that the metabolic fluxes of the bacteroids might have changed after isolation from the host nodules. A possible alternative to avoid the compromised state of the bacteroids and to measure in vivo fluxes in the bacteroids will be to perform non-stationary flux analysis, where the strategy will be to incubate the host plant in a [^{13}C-CO_2] environment followed by isolation of bacteroids for measuring fluxes. Non-stationary ^{13}C-MFA is a technique used mainly for isotopic non-steady state photoautotrophic systems (Jazmin and Young, 2013); this technique will be appropriate for rhizobia-host symbiosis, since the isotopic substrate will be initially metabolised by the host plant and converted into different carbon compounds like dicarboxylic acids that are ultimately utilised by bacteroids inside the nodules. By using this technique, it will also be feasible to look at the metabolic fluxes in the host nodule cells that will provide us a picture of the metabolic state of the host when it accommodates and nourishes N_2-fixing rhizobia.

7.3 Future work

The pathways identified to be crucial for N_2 fixation in the free-living and symbiotic ORS571 cultures can be further evaluated; for instance, the TCA cycle reactions, the importance of each of the reactions can be individually studied by using mutagenesis approaches. The anaplerotic fluxes derived for free-living and symbiotic ORS571 were not well defined and this may mask changes in these fluxes under different conditions. The fluxes determined in this study can be complemented by using other omics approaches- transcriptomic and proteomic profiles of the system under different conditions of study. For instance, in the isolated bacteroids, a proteomic profile will confirm the presence of a particular protein that may imply a particular enzymatic capacity under the growth conditions being analysed of the metabolites involved in the less well resolved pathways. The issue of poorly resolved fluxes in the anaplerotic node can be addressed by targeted flux analysis strategies such as determining flux ratios for that particular node, which may help to improve the confidence on the flux estimates through the specific reactions for this study (Kokadeeva & Zamboni, 2016). The methodology for estimating flux ratios includes construction of stoichiometric model for the reactions in the anaplerotic node, information about the input ^{13}C-configuration of substrates for the node, measurement of ^{13}C isotope labelling patterns for metabolites malate, pyruvate and oxaloacetate of the node by mass spectrometry or nuclear magnetic mass spectrometry.

The MSDH catalysed pathway for synthesis of AcCoA from OAA, was found to have significantly higher fluxes in the bacteroid. There are reports on other microbial species such as *Streptomyces coelicolor* and *Pseudomonas aeruginosa*, where MSDH was involved in valine and β-alanine catabolism, and also the NADH produced by the reaction mitigated oxidative stress (Steele et al., 1992; Zhang et al., 1996; Su et al., 2010). Currently, there is limited knowledge about the role of this pathway in ORS571 and other rhizobial species. The metabolic importance of this pathway needs to be

explored. The mutants defective for this pathway can be isolated and then their effects on N_2 fixation and metabolic fluxes can be studied to establish the role of this pathway in bacteroids and free-living ORS571.

For bacteroids, the output fluxes to biomass were poorly defined in comparison to the free-living cultures. This was likely to be because of the low ^{13}C-label incorporation in the bacteroids. The nitrogenase activity of the bacteroids decreased with time post isolation and the incorporation of ^{13}C-label was dependent on the activity of the bacteroids. So, there is a need to refine the experimental techniques, perhaps by isolating symbiosomes (Gaude et al., 2004) and incubating them with the labelled substrate rather than the bacteroids. The bacteroids could then be isolated from the symbiosomes for further analysis. An alternative approach- non-stationary ^{13}C-MFA could potentially be used to avoid the compromised metabolic state of the isolated symbiosomes or bacteroids. This method will involve isotopic labelling of the host plant, followed by mass isotopomer measurements in bacteroids isolated from the host post labelling. This approach involves labelling the intact system (rather than isolated bacteroids or symbiosomes) the bacteroids will be in a more natural state and so the fluxes measured by this approach are more likely to reflect the metabolism of the bacteroids in situ in the natural system.

The potential for applying the ^{13}C-MFA approach developed in this work to other plant-rhizobial systems will be dependent on the extent to which the isolated bacteroids remain metabolically active. In this context, bacteroid forms of *R. leguminosarum* are reported to lose their nitrogenase activity (and thus the capacity for nitrogen assimilation) rapidly after isolation (Terpolilli et al., 2016). In contrast in preliminary studies, my work indicates that *S. fredii* bacteroids retain the ability to fix N_2 for 24 h) after isolation from soybean nodules, making this a potential system in which to analyse the central carbon metabolism associated with nitrogen fixation using ^{13}C-MFA. The initial measurements for N_2-fixation, biomass composition and a provisional

bacteroid flux map were generated for *S. fredii* bacteroids in this study (appendix A25-A27). The method can therefore be extended to study the metabolism of *S. fredii,* and a comparison with ORS571 would also be worthwhile. Ultimately, identification of other potential rhizobial-legume systems appropriate for flux analysis will be needed to establish if the metabolic phenotype of bacteroids varies across different rhizobial-legume associations. Such comparisons will provide a comprehensive understanding of symbiotic N_2-fixation in legumes and metabolic co-operation between the host plant and rhizobia.

7.4 Conclusion

The metabolic phenotype of a N_2-fixing rhizobium was obtained in this study using steady state ^{13}C-MFA. Under free-living conditions the TCA cycle and PHB biosynthesis were the two main pathways associated with N_2 fixation. Although PHB was required for redox balance during micro-aerobic growth, ORS571 was able to substitute for the inability to synthesise PHB by diverting carbon into synthesis of lipids which was able to serve as an alternative sink for reducing equivalent during micro-aerobic growth. PHB synthesis was essential for N_2 fixation under both free-living and symbiotic conditions in ORS571. In the bacteroids, in addition to the TCA cycle and PHB synthesis, the methyl malonate semialdehyde pathway was active under conditions of symbiotic N_2 fixation. The targets identified in this study can be extrapolated to other rhizobial systems such as *R. leguminosarum*, *S. fredii*, where the TCA cycle and PHB synthesis were reported to be essential for N_2 fixation (Krishnan et al., 2003; White et al., 2007). On the other hand, there are exceptions such as *B. japonicum* which do not require a full TCA cycle for N_2 fixation and those such as *R. etli* where PHB deletion did not affect N_2 fixation (Cevallos et al., 1996; Thonymeyer & Kunzler, 1996). Thus the metabolic phenotype of N_2-fixing ORS571 obtained in this study is species-specific and each rhizobial system needs to be studied individually.

The ORS571-Sesbania symbiosis is of particular interest because of the intercellular and intracellular modes of invasion by ORS571 and also development of different nodule types on the host. Also, ORS571 being an endosymbiont of cereal crops such as rice and wheat, this rhizobium and its symbiotic abilities can be further explored to establish symbiotic N_2 fixation in non-legumes, particularly cereal crops. The results from this study provide information about the metabolic phenotype of N_2-fixing rhizobia which will aid the researchers who are aiming to improve the existing symbioses and to design synthetic micro-symbiont for non-legume plants. Such research on legume symbiosis could provide for natural nitrogen fertilizers in agricultural systems that would substitute for the chemical nitrogen fertilizers, which are detrimental to the environment.

8. References

Adebiyi AO, Jazmin LJ, Young JD (2014) ^{13}C flux analysis of cyanobacterial metabolism. Photosynth Res **126**: 19-32

Ahn WS, Antoniewicz, MR (2011) Metabolic flux analysis of CHO cells at growth and non-growth phases using isotopic tracers and mass spectrometry. Metab Eng **5**: 598–609

Alagesan S, Gaudana SB, Sinha A, Wangikar PP (2013) Metabolic flux analysis of *Cyanothece* sp. ATCC 51142 under mixotrophic conditions. Photosynth Res **118**: 191–198

Allaway D, Lodwig EM, Crompton LA, Wood M, Parsons R, Wheeler TR, Poole, PS (2000) Identification of alanine dehydrogenase and its role in mixed secretion of ammonium and alanine by pea bacteroids. Mol Microbiol **36**: 508–15

Allen DK, Ratcliffe, RG (2009) Quantification of isotope label. Plant Metabolic Networks pp 105–149

Allen GC, Grimm DT, Elkan GH (1991) Oxygen uptake and hydrogen-stimulated nitrogenase activity from *Azorhizobium caulinodans* ORS571 grown in a succinate-limited chemostat. Appl Environ Microbiol **57**: 3220–3225

Allen DK, Young JD (2013) Carbon and nitrogen provisions alter the metabolic flux in developing soybean embryos. Plant Physiol **161**: 1458-75

Alonso AP, Dale, VL, Shachar-Hill Y (2010) Understanding fatty acid synthesis in developing maize embryos using metabolic flux analysis. Metab Eng **12**: 488–97

Anderson AJ, Dawes EA (1990) Occurrence, metabolism, metabolic role, and industrial uses of bacterial polyhydroxyalkanoates. Microbiol Rev **54:** 450-472

Aneja P, Charles TC (1999) Poly-3-hydroxybutyrate degradation in *Rhizobium* (*Sinorhizobium meliloti*: isolation and characterisation of a gene encoding 3-hydroxybutyrate dehydrogenase. J Bacteriol **181**: 849-857

Aneja P, Dai M, Lacorre DA, Pillon B, Charles TC (2004) Heterologous complementation of the exopolysaccharide synthesis and carbon utilization phenotypes of *Sinorhizobium meliloti* Rm1021 polyhydroxyalkanoate synthesis mutants. FEMS Microbiol Lett **239**: 277–283

Antoniewicz MR, Kelleher JK, Stephanopoulos G (2006) Determination of confidence intervals of metabolic fluxes estimated from stable isotope measurements. Metab Eng **8**: 324-337

Antoniewicz MR, Kelleher JK, Stephanopoulos G (2007a) Accurate assessment of amino acid mass isotopomer distributions for metabolic flux analysis. Anal Chem. **79**: 7554-9

Antoniewicz MR, Kraynie DF, Laffend LA, González-Lergier J, Kelleher JK, Stephanopoulos G (2007b) Metabolic flux analysis in a nonstationary system: fed-batch fermentation of a high yielding strain of *E. coli* producing 1,3-propanediol. Metab Eng **9:** 277-292

Antoniewicz MR, Kelleher JK, Stephanopoulos G (2007c) Elementary Metabolite Units (EMU): A novel framework for modelling isotopic distributions. Metab Eng **9**: 68-86

Antoniewicz MR (2015) Methods and advances in metabolic flux analysis: a mini review. J Ind Microbiol Biotechnol **42**: 317-325

Baginsky C, Palacios JM, Imperial J, Ruiz-Argüeso T, Brito B (2004) Molecular and functional characterization of the Azorhizobium caulinodans ORS571 hydrogenase gene cluster. FEMS Microbiol Lett **237:** 399–405

Bahar M, de Majnik J, Wexler M, Fry J, Poole PS, Murphy, PJ (1998) A model for the catabolism of rhizopine in *Rhizobium leguminosarum* involves a ferredoxin oxygenase complex and the inositol degradative pathway. Mol Plant Microbe Interact **11:** 1057–1068

Bar AR, Baggie I, Saninga N (2000) The use of Sesbania (*Sesbania rostrata*) and urea in lowland rice production in Sierra Leone. Agroforest Syst **48:** 111–118

Batut J, Boistard P (1994) Oxygen control in Rhizobium. Antonie van Leeuwenhoek **66**: 129-150

Bernardelli CE, Luna MF, Galar ML, Boiardi JL (2001) Periplasmic PQQ-dependent glucose oxidation in free-living and symbiotic rhizobia. Curr Microbiol **42:** 310–315

Bergersen FJ, Turner GL, Bogusz D, Wu Y, Appleby CA (1986) Effects of O_2 concentrations and various haemoglobins on respiration and nitrogenase activity of bacteroids from stem and root Nodules of *Sesbania rostrata* and of the same bacteria from continuous cultures. J Gen Microbiol **132**: 3325–3336

Bergersen FJ, Turner GL, Bogusz D, Appleby CA (1988) Fixation of N_2 by Bacteroids from Stem Nodules of *Sesbania rostrata*. J Gen Microbiol **134**: 1807–1810

Bergersen FJ, Turner GL (1990) Bacteroids from soybean root nodules: accumulation of poly-β-hydroxybutyrate during supply of malate and succinate in relation to N_2 fixation in flow-chamber reactions. Proc R Soc Lond Ser B **240**: 39–59

Bergersen FJ, Peoples MB, Turner GL (1991) A role for poly-β-hydroxybutyrate in bacteroids of soybean root nodules. Proc R Soc Lond Ser B **245**: 59–64

Berrada H, Fikri-Benbrahim K (2014) Taxonomy of the rhizobia: Current Perspectives. British Microbiology Research Journal **4**: 616-639

Beste DJV, Bonde B, Hawkins N, Ward JL, Beale MH, Noack S, Nöh K, Kruger NJ, Ratcliffe RG, McFadden J (2011) ^{13}C metabolic flux analysis identifies an unusual route for pyruvate dissimilation in mycobacteria which requires isocitrate lyase and carbon dioxide fixation. PLoS Pathog **7**: e1002091

Biswas JC, Ladha JK, Dazzo FB (2000) Rhizobia inoculation improves nutrient uptake and growth of lowland rice. Soil Sci Soc Amer J **64**: 1644-1650

Boddey R., Carlos De Moraes J, Alves BJR, Urquiaga S (1997) The contribution of biological nitrogen fixation for sustainable agricultural systems in the tropics. Soil Biol Biochem **29**: 787-799

Bonartsev AP, Myshkina V, Nikolaeva D, Furina EK, Makhina TA, Livshits VA, Boskhomdzhiev AP, Ivanov EA, Iordanskii AL, Bonartseva GA (2007) Biosynthesis, biodegradation, and application of poly (3-hydroxybutyrate) and its copolymers-natural polyesters produced by diazotrophic bacteria. Commun Curr Res Educ Top Trends Appl Microbiol **1**: 295–307

Boogerd FC, Pronk AF, Mashingaidze C, Affourtit C, Stouthamer AH, Van Verseveld HW, Westerhoff HV (1998) Oxygen protection of nitrogen fixation in free-living *Azorhizobium caulinodans*: the role of cytochrome *aa3*. Microbiology **144**: 1773–1782

Bothe H, Tennigkeit J, Eisbrenner G, Yates MG (1977) The hydrogenase-nitrogenase relationship in the blue-green alga *Anabaena cylindrica*. Planta **133:** 237-242

Brear EM, Day, DA, Smith PMC (2013) Iron: an essential micronutrient for the legume-rhizobium symbiosis. Front Plant Sci **4:** 359

Brown CM, Dilworth MJ (1975) Ammonia assimilation by rhizobium cultures and bacteroids. J Gen Microbiol **86**: 39-48

Buescher JM, Antoniewicz MR, Boros LG, Burgess SC, Brunengraber H, Clish C.B, DeBerardinis RJ, Feron O, Frezza C, Ghesquiere B, Gottlieb E, Hiller K, Jones RG, Kamphorst JJ, Kibbey RG, Kimmelman AC, Locasale JW, Lunt SY, Maddocks ODK, Malloy C, Metallo CM, Meuillet EJ, Munger J, Nöh K, Rabinowitz JD, Ralser M, Uwe S, Stephanopoulos G, St- Pierre J, Tennant DA, Wittmann C, Vander Heiden MG, Vazquez A, Vousden K, Young JD, Zamboni N, Fendt SM (2015) A roadmap for interpreting ^{13}C metabolite labeling patterns from cells. Curr Opin Biotechnol **34**: 189–201

Cai GQ, Driscoll BT, Charles TC (2000) Requirement for the enzymes acetoacetyl coenzyme A synthetase and poly- 3-hydroxybutyrate (PHB) synthase for growth of *Sinorhizobium meliloti* on PHB cycle intermediates. J Bacteriol **182**: 2113–2118

Capoen W, Goormachtig S, Holsters M (2010) Water-tolerant legume nodulation. J Exp Bot **61**: 1251-1255

Carranca C, Torres MO, Madeira M (2015) Underestimated role of legume roots for soil N fertility. Agron Sustain Dev **35**: 1095–1102

Cevallos MA, Encarnacion S, Leija A, Mora Y, Mora J (1996) Genetic and physiological characterization of a *rhizobium etli* mutant strain unable to synthesize poly-β-hydroxybutyrate. J Bacteriol **178**: 1646–1654

Chang C, Damiani I, Puppo A, Frendo P (2009) Redox changes during the legume-rhizobium symbiosis. Mol Plant **2**: 370-377

Cheung CYM, Williams TCR, Poolman MG, Fell DA, Ratcliffe RG, Sweetlove LJ (2013) A method for accounting for maintenance costs in flux balance analysis improves the prediction of plant cell metabolic phenotypes under stress conditions. Plant J **75**: 1050-1061

Chen G, Zhu H, Zhang Y (2003) Soil microbial activities and carbon and nitrogen fixation. Res Microbiol **154**: 393–398

Cheng Q (2008) Perspectives in biological nitrogen fixation research. J Integr Plant Biol **50**: 784–796

Chen X, Alonso AP, Allen DK, Reed JL, Shachar-Hill Y (2011) Synergy between ^{13}C-metabolic flux analysis and flux balance analysis for understanding metabolic adaptation to anaerobiosis in E*. coli*. Metab Eng. **13**: 38–48

Cheng Y, Zheng Y, Vander Gheynst JS (2011) Rapid quantitative analysis of lipids using a colorimetric method in a microplate format. Lipids **46**: 95–103

Chen X, Shachar-Hill Y (2012) Insights into metabolic efficiency from flux analysis. J Exp Bot **63**: 2343–2351

Cheng G, Karunakaran R, East AK, Poole PS (2016) Multiplicity of sulfate and molybdate transporters and their role in nitrogen fixation in *Rhizobium leguminosarum* bv. *viciae* Rlv3841. Mol Plant Microbe Interact **2**: 143-52

Christensen B, Nielsen J (1999) Isotopomer Analysis Using GC-MS. Metab Eng **1**: 282-90

Choma A, Komaniecka I, Turska-Szewczuk A, Danikiewicz W, Spolnik G (2012) Structure of lipid A from a stem-nodulating bacterium *Azorhizobium caulinodans*. Carbohydr Res **352**: 126–136

Choudhary MK, Yoon JM, Gonzalez R, Shanks JV (2011) Re-examination of metabolic fluxes in *Escherichia coli* during anaerobic fermentation of glucose using ^{13}C labeling experiments and 2-dimensional nuclear magnetic resonance (NMR) spectroscopy. Biotechnology and Bioprocess Engineering **16**: 419–437

Chohan SN, Copeland L (1998) Acetoacetyl coenzyme a reductase and polyhydroxybutyrate synthesis in *Rhizobium* (Cicer) sp. strain CC 1192. Appl Environ Microbiol **64**: 2859–2863

Clarke VC, Loughlin PC, Day DA, Smith PMC (2014) Transport processes of the legume symbiosome membrane. Front Plant Sci **5**: 699

Conley DJ (2012) Ecology: save the Baltic Sea. Nature **486**: 463-4

Crown SB, Antoniewicz MR (2013) Publishing ^{13}C metabolic flux analysis studies: A review and future perspectives. Metab Eng **20**: 42-48

Das A, Lodha ML (1998) Differential expression of uptake hydrogenase activity in free living cells and nodule bacteroids of *Azorhizobium caulinodans*. J Plant Biochem Biot **7**: 51–52

Dauner M, Sauer U (2000) GC-MS analysis of amino acids rapidly provides rich information for isotopomer balancing. Biotechnol Prog **16**: 642−649

Darmon E, Leach DR (2014) Bacterial Genome Instability. Microbiol Mol Biol Rev **78**: 1–39

Dawes EA (1988) Polyhydroxybutyrate: an intriguing biopolymer. Biosci Rep **8**: 537-547

de Vries W, Stam H, Stouthamer AH (1984) Hydrogen oxidation and nitrogen fixation in rhizobia, with special attention focused on strain ORS571. Ant van Leeuwenhoek **50**: 505-524

Denison RF, Kiers ET (2011) Life histories of symbiotic rhizobia and mycorrhizal fungi. Current Biology **21**: R775-R785

Denduluri S, Bal AK (1995) Fatty acid composition of oleosomes (lipid bodies) from stem and root nodules of *Sesbania rostrata*. J Plant Physiol **147**: 633-636

Dent D, Cocking E (2017) Establishing symbiotic nitrogen fixation in cereals and other non-legume crops: The greener nitrogen revolution. Agric Food Secur **6**: 7

D'Haeze W, Gao M, De Rycke R, Montagu MV, Engler G, Holsters M (1998) Roles for Azorhizobial nod factors and surface polysaccharides in intercellular invasion and nodule penetration, respectively. Mol Plant Microbe In **11**: 999–1008

Ding X, Boney-Montoya J, Owen BM, Bookout AL, Coate KC, Mangelsdorf DJ, Kliewer SA (2012) βKlotho is required for fibroblast growth factor 21 effects on growth and metabolism. Cell Metab **16**: 387–393

D'Haeze W, De Rycke R, Mathis R, Goormachtig S, Pagnotta S, Verplancke C, Capoen W, Holsters M (2003) Reactive oxygen species and ethylene play a positive role in lateral root base nodulation of a semiaquatic legume. Proc Natl Acad Sci U S A **100**: 11789–11794

D'Haeze W, Glushka J, De Rycke R, Holsters M, Carlson RW (2004) Structural characterization of extracellular polysaccharides of *Azorhizobium caulinodans* and importance for nodule initiation on *Sesbania rostrata*. Mol Microbiol **52**: 485–500

Donald RGK, Ludwig RA (1984) *Rhizobium* sp. strain ORS571 ammonium assimilation and nitrogen fixation. J Bacteriol **158**: 1144-1151

Downie JA (2014) Legume nodulation. Curr Biol **24**: R184-R190

Dreyfus BL, Dommergues YR (1981) Nitrogen fixing nodules induced by *Rhizobium* on the stem of the tropical legume *Sesbania rostrata*. FEMS Microbiol Lett **10**: 313-317

Dreyfus BL, Elmerich C, Dommergues YR (1983) Free-Living *Rhizobium* strain able to grow on N_2 as the sole nitrogen source. Appl Environ Microbiol **45**: 711–713

Dreyfus B, Rinaudo G, Dommergues Y (1985) Observations on the use of *Sesbania rostrata* as green manure in paddy fields. MIRCEN J Appl Microbiol Biotechnol **1**: 111–122

Dreyfus B, Garcia JL, Gillis M (1988) Characterization of *Azorhizobium caulinodans* gen. nov., sp. nov., a stem-nodulating nitrogen-fixing bacterium isolated from *sesbania rostrata*. Int J Syst Bacteriol. **38**: 89-98

Dunn MF (1998) Tricarboxylic acid cycle and anaplerotic enzymes in rhizobia. FEMS Microbiol Rev. **22**: 105-123

Edwards JS, Palsson BO (2000) Metabolic flux balance analysis and the *in silico* analysis of *Escherichia coli* K-12 gene deletions. BMC Bioinformatics **1**: 1

Elmerich C, Dreyfus BL, Reysset G, Aubert JP (1982) Genetic analysis of nitrogen fixation in a tropical fast-growing *Rhizobium*. Embo J **1**: 499–503

Elmerich C, Dreyfus B, Aubert JP (1983) Nicotinic acid requirement and degradation by *Sesbania rhizobium* strain ORS571. FEMS Microbiol Lett **19**: 281-284.

El-Sirafy ZM, Woodard HJ, El-Norjar EM (2005) Contribution of biofertilizers and fertilizer nitrogen to nutrient uptake and yield of Egyptian winter wheat. J Plant Nutr **29**: 587-599

Emerich DW, Krishnan HB (2014) Symbiosomes: temporary moonlighting organelles. Biochem J **460**: 1–11

Encarnación S, Dunn M, Willms K, Mora J (1995) Fermentative and aerobic metabolism in *Rhizobium etli*. J Bacteriol **177**: 3058-3066

Fagerquist CK, Hellerstein MK, Faubert D, Bertrand MJ (2001) Elimination of the concentration dependence in mass isotopomer abundance mass spectrometry of methyl palmitate using metastable atom bombardment. J Am Soc Mass Spectrom 2001 **12**: 754–761

Farkas A, Maróti G, Durgő H, Györgypál Z, Lima RM, Medzihradszky KF, Kereszt A, Mergaert P, Kondorosi É (2014) *Medicago truncatula* symbiotic peptide NCR247 contributes to bacteroid differentiation through multiple mechanisms. Proc Natl Acad Sci U S A **111**: 5183–5188

Feist AM, Henry CS, Reed JL, Krummenacker M, Joyce AR, Karp PD, Broadbelt LJ, Hatzimanikatis V, Palsson BØ (2007) A genome-scale metabolic reconstruction for *Escherichia coli* K-12 MG1655 that accounts for 1260 ORFs and thermodynamic information. Mol Syst Biol. **3**: 121

Finan TM, Wood JM Jordan DC (1983) C. Symbiotic properties of C,-dicarboxylic acid transport mutants of *Rhizobium leguminosarum*. J Bacteriol. **154**: 1403-1413

Fuhrer T, Fischer E, Sauer U (2005) Experimental Identification and Quantification of Glucose Metabolism in Seven Bacterial Species. J Bacteriol **187**: 1581-90

Fustec J, Lesuffleur F, Mahieu S, Cliquet JB (2010) Nitrogen rhizodeposition of legumes. A review. Agron Sustain Dev **30**: 57–66

Fraysse N, Couderc F, Poinsot V (2003) Surface polysaccharide involvement in establishing the rhizobium-legume symbiosis. Eur J Biochem **270**: 1365-1380

Fry J, Wood M, Poole PS (2001) Investigation of myo-inositol catabolism in *Rhizobium leguminosarum* bv. *viciae* and its effect on nodulation competitiveness. Mol Plant Microbe Interact **14**: 1016–25

Gage DJ (2004) Infection and invasion of roots by symbiotic, nitrogen fixing rhizobia during nodulation of temperate legumes. Microbiol Mol Biol Rev **68:** 280-300

Gao M, Haeze WD, Rycke RD, Wolucka B, Holsters M (2001) Knockout of an azorhizobial dTDP- L -rhamnose synthase affects lipopolysaccharide and extracellular polysaccharide production and disables symbiosis with *Sesbania rostrata*. Mol Plant Microbe Interact **14**: 857–66

Gaude N, Tippmann H, Flemetakis E, Katinakis P, Udvardi M, Dormann P (2004) The galactolipid digalactosyldiacylglycerol accumulates in the peribacteroid membrane of nitrogen-fixing nodules of soybean and *lotus*. J Biol Chem **279**: 34624–34630

Gebhardt C, Turner GL, Gibson AH, Dreyfus BL, Bergersen FJ (1984) Nitrogen-fixing growth in continuous culture of a strain of *Rhizobium* sp. isolated from stem nodules on *Sesbania rostrata*. Microbiol **130**: 843-848

Geelen D, Goethals K, Montagu MV, Holsters M (1995) The *nodD* locus from *Azorhizobium caulinodans* is flanked by two repetitive elements. Gene **164**: 107–111

Ghosh BC, Bhat R (1998) Environmental hazards of nitrogen loading in wetland rice fields. Environ Pollut **102**: 123-126

Gomes LC, Simoes M (2012) ^{13}C Metabolic flux analysis: From the principle to recent applications. Current Bioinformatics **7**: 77-86

Gonzalez JE, Long CP, Antoniewicz MR (2017) Comprehensive analysis of glucose and xylose metabolism in *Escherichia coli* under aerobic and anaerobic conditions by ^{13}C metabolic flux analysis. Metab Eng **39**: 9–18

Gopalakrishnan S, Sathya A, Vijayabharathi A, Varshney RK, Gowda CLL, Krishnamurthy L (2015) Plant growth promoting rhizobia: challenges and opportunities. 3 Biotech **5**: 355–377

Gordon AJ, Minchin FR, James CL, Komina O (1999) Sucrose synthase in legume nodules is essential for nitrogen fixation. Plant Physiol **120**: 867-877

Goodwin GW, Rougraff PM, Davis J, Harris RA (1989) Purification and characterization of methylmalonate-semialdehyde dehydrogenase from rat liver. J Biol Chem **264**: 14965-1497

Goormachtig S, Capoen W, Holsters M (2004) *Rhizobium* infection: lessons from the versatile nodulation behaviour of water-tolerant legumes. Trends Plant Sci **9**: 518-522

Görgens JF, van Zyl WH, Knoetze JH, Hahn-Hägerdal B (2005) Amino acid supplementation improves heterologous protein production by *Saccharomyces cerevisiae* in defined medium. Appl Microbiol Biotechnol **67**: 684–691

Gough C, Galera C, Vasse J, Webster G, Cocking EC, Dénarié J (1997) Specific flavonoids promote intercellular root colonization of *Arabidopsis thaliana* by *Azorhizobium caulinodans* ORS571. Mol Plant Microbe Interact **10**: 560–570

Graham PH, Vance CP (2000) Nitrogen fixation in perspective: an overview of research and extension needs. Fields Crops Research **65**: 93-106

Guo W, Sheng J, Feng X (2015) ^{13}C-Metabolic flux analysis: An accurate approach to demystify microbial metabolism for biochemical production. Bioengineering **3**: 3

Hakoyama T, Niimi K, Watanabe H, Tabata R, Matsubara J, Sato S, Nakamura Y, Tabata S, Jichun L, Matsumoto T, Tatsumi K, Nomura M, Tajima S, Ishizaka M, Yano K, Imaizumi-Anraku H, Kawaguchi M, Kouchi H, Suganuma N (2009) Host plant genome overcomes the lack of a bacterial gene for symbiotic nitrogen fixation. Nature **462**: 514–517

Halket JM, Waterman D, Przyborowska AM, Patel RKP, Fraser PD, Bramley PM (2005) Chemical derivatization and mass spectral libraries in metabolic profiling by GC/MS and LC/MS/MS. J Exp Bot **56**: 219–243

Handberg K, Stougaard J (1992) *Lotus japonicus*, an autogamous, diploid legume species for classical and molecular genetics. Plant J **2**: 487-496.

Han J, Qiu YZ, Liu DC, Chen GQ (2004) Engineered *Aeromonas hydrophila* for enhanced production of poly(3-hydroxybutyrate-*co*-3-hydroxyhexanoate) with alterable monomers composition. FEMS Microbiol Lett **239**: 195–201.

He L, Xiao Yi, Gebreselassie N, Zhang F, Antoniewiez MR, Tang YJ, Peng L (2014) Central metabolic responses to the overproduction of fatty acids in *Escherichia coli* based on ^{13}C-metabolic flux analysis. Biotechnol Bioeng **111**: 575-85

Herder GD, Schroeyers K, Holsters M, Goormachtig S (2006) Signaling and gene expression for water-tolerant legume nodulation. Critic Rev Plant Sci **25**: 367–380

Herridge DF, Peoples MB, Boddey RM (2008) Global inputs of biological nitrogen fixation in agricultural systems. Plant Soil **311**: 1–18

Hiller K, Metallo M (2012) Profiling metabolic networks to study cancer metabolism. Curr Opin Biotechnol **24**: 60–68

Hill S (1976) The apparent ATP requirement for nitrogen fixation in growing *Klebsiella pneumoniae*. J Gen Microbiol **95**: 297-312

Hill S, Viollet S, Smith AT, Anthony C (1990) Roles for enteric *d*-type cytochrome oxidase in N_2 fixation and microaerobiosis. J Bacteriol **172**: 2071-2078

Hungria M, Eaglesham ARJ, Hardy RWF (1992) Physiological comparisons of root and stem nodules of *Aeschynomene scabra* and *Sesbania rostrata*. Plant and Soil **139**: 7-13

Hunt S, Layzell DB (1993) Gas exchange of legume nodules and the regulation of nitrogenase activity. Annu. Rev Plant Physiol Plant Mol Biol **44**: 483-511

Igarashi RY, Seefeldt LC (2003) Nitrogen fixation: The mechanism of the Mo-dependent nitrogenase. Critic Rev Biochem Mol Biol **38**: 351-384

Iki T, Aono T, Oyaizu H (2007) Evidence for functional differentiation of duplicated *nifH* genes in *Azorhizobium caulinodans*. FEMS Microbiol Lett **274**: 173–179

Ionescu M, Shimshon B (2009) Simple quantification of bacterial envelope-associated extracellular materials. J Microbiol Methods **78**: 302-306

Izard J, Limberger RJ (2003) Rapid screening method for quantitation of bacterial cell lipids from whole cells. J Microbiol Methods **55**: 411–418

Jackson FA, Dawes, EA (1976) Regulation of the tricarboxylic acid cycle and poly-β-hydroxybutyrate metabolism in *Azotobacter beijerinckii* grown under nitrogen or oxygen limitation J Gen Microbiol **97**: 303–312

Jain V, Gupta K (2003) The flavonoid naringenin enhances intercellular colonization of rice roots by *Azorhizobium caulinodans*. Biol Fert Soils **38**: 119–123

Jazmin LJ, Young JD (2013) Isotopically Nonstationary 13C Metabolic Flux Analysis. Methods Mol Biol **985**: 367-390

Jiang L, Shestov AA, Swain P, Yang C, Parker SJ, Wang QA, Terada LS, Adams ND, McCabe MT, Pietrak B, Schmidt S, Metallo CM, Dranka BP, Schwartz B, DeBerardinis RJ (2016) Reductive carboxylation supports redox homeostasis during anchorage-independent growth. Nature **532**: 255–258

Kadouri D, Jurkevitch E, Okon Y (2003) Involvement of the reserve material poly- β -hydroxybutyrate in *Azospirillum brasilense* stress endurance and root colonization. Appl Environ Microb **69**: 3244-3250

Kaminski PA, Mandon K, Arigoni F, Desnoues N, Elmerich C (1991) Regulation of nitrogen fixation in *Azorhizobium caulinodans*: identification of a *fixK*-like gene, a positive regulator of *nifA*. Mol Microbiol **5**: 1983-1991

Kappelmann J, Wiechert W, Noack S (2015) Cutting the gordian knot: Identifiability of anaplerotic reactions in *Corynebacterium glutamicum* by means of ^{13}C-metabolic flux analysis. Biotechnol Bioeng **9999**: 1–14

Karr DB, Waters JK, Suzuki F, Emerich DW (1984) Enzymes of the poly-β-hydroxybutyrate and citric acid cycles of *Rhizobium japonicum* bacteroids. Plant Physiol **75**: 1158–1162

Karunakaran R, Haag AF, East AK, Ramachandran VK, Prell J, James EK, Scocchi M, Ferguson GP, Poole PS (2010) BacA is essential for bacteroid development in nodules of galegoid, but not phaseoloid, legumes. J Bacteriol **192**: 2920–2928

Kauffman KJ, Prakash P, Edwards JS (2003) Advances in flux balance analysis. Curr Opin Biotech **14:** 491–496

Kelly MJ, Poole RK, Yates MG, Kennedy C (1990) Cloning and mutagenesis of the genes encoding the cytochrome *bd* terminal oxidase complex in *Azotobacter vinelandii*: mutants deficient in the cytochrome *d* complex are unable to fix nitrogen in air. J Bacteriol **172:** 6010-6019

Kim SA, Copeland L (1996) Enzymes of poly-(beta)-hydroxybutyrate metabolism in soybean and chickpea bacteroids. Appl Environ Microbiol **62**: 4186–90

Kitts CL, Schaechter LE, Rabin RS, Ludwig RA (1989) Identification of cyclic intermediates in *Azorhizobium caulinodans* nicotinate catabolism. J. Bacteriol **171**: 3406-3411

Kitts CL, Ludwig RA (1994) *Azorhizobium caulinodans* respires with at least four terminal oxidases. J Bacteriol **176**: 886–895

Kohler PRA, Zheng JY, Schoffers E, Rossbach S (2010) Inositol catabolism, a key pathway in *Sinorhizobium meliloti* for competitive host nodulation. Appl Environ Microb **76**: 7972–80

Kogadeeva M, Zamboni N (2016) SUMOFLUX: A generalized method for targeted ^{13}C metabolic flux ratio analysis. PLoS Comput Biol **12**: e1005109

Korotkova N, Lidstrom ME (2001) Connection between Poly-β-Hydroxybutyrate Biosynthesis and Growth on C1 and C2 Compounds in the Methylotroph *Methylobacterium extorquens* AM1. J Bacteriol **183**:1038-1046

Krishnan HB, Kim WS, Sun-Hyung J, Kim KY, Jiang JQ (2003) Citrate synthase mutants of *Sinorhizobium fredii* USDA257 form ineffective nodules with aberrant ultrastructure. Appl Environ Microbiol **69**:3561– 3568.

Kruger NJ, Huddleston JE, Le Lay P, Brown ND, Ratcliffe RG (2007) Network flux analysis: impact of ^{13}C-substrates on metabolism in *Arabidopsis thaliana* cell suspension cultures. Phytochemistry **68**: 2176–2188

Kruger NJ, Masakapalli SK, Ratcliffe RG (2014) Optimization of steady-state ^{13}C-labeling experiments for metabolic flux analysis. Plant Metabolic Flux Analysis 53-72

Kruger NJ, Masakapalli S, Ratcliffe, RG (2012) Strategies for investigating the plant metabolic network with steady-state metabolic flux analysis: lessons from an *Arabidopsis* cell culture and other systems. J Exp Bot **63**: 2309-2323

Kruger NJ, Ratcliffe RG (2009) Insights into plant metabolic networks from steady-state metabolic flux analysis. Biochimie **91**: 697–702

Kruger NJ, Ratcliffe RG (2015) Fluxes through plant metabolic networks: measurements, predictions, insights and challenges. Biochem J **465**: 27-38

Lane DJ (1991) 16S/23S rRNA sequencing. In: Nucleic acid techniques in bacterial systematics. Stackebrandt, E. & Goodfellow, M., eds., John Wiley and Sons, New York, NY 115-175

Lang E, Schumann P, Adler S, Sproer C, Sahin N (2013) *Azorhizobium oxalatiphilum* sp. nov., and emended description of the genus *Azorhizobium*. Int J Syst Evol Micr **63**: 1505–1511

Law JH, Slepecky R (1961) Assay of poly-β-hydroxybutyric acid. J. Bacteriol **82**: 33-36

Leighty RW, Antoniewicz MR (2012) Parallel labeling experiments with [U-^{13}C] glucose validate *E. coli* metabolic network model for ^{13}C metabolic flux analysis. Metab Eng **14**: 533-541

Libault M (2014) The carbon-nitrogen balance of the nodule and its regulation under elevated carbon dioxide concentration. BioMed Research International 507946

Liu CT, Lee KB, Wang YS, Peng MH, Lee KT, Suzuki S, Suzuki T, Oyaizu H (2011) Involvement of the azorhizobial chromosome partition gene (*parA*) in the onset of bacteroid differentiation during *Sesbania rostrata* stem nodule development. Appl Environ Microbiol **77**: 4371–4382

Lira Jr MA, Nascimento LRS, Fracetto GGM (2015) Legume-rhizobia signal exchange: promiscuity and environmental effects. Front Microbiol **6:** 945

Lee KB, De Backer P, Aono T, Liu CT, Suzuki S, Suzuki T, Kaneko T, Tabata S, Kupfer DM, Najar FZ, Wiley GB, Roe B, Binnewies TT, Ussery DW, D'Haeze W, Herder JD, Gevers D, Vereecke D, Holsters M, Oyaizu H (2008) The genome of the versatile nitrogen fixer *Azorhizobium caulinodans* ORS571. BMC genomics. **9**: 271

Lommen A (2009) Metalign: Interface-driven, versatile metabolomics tool for hyphenated full-scan mass spectrometry data preprocessing. Anal Chem **81**: 3079–3086

López-López A, Rosenblueth M, Martinez J, Martinez-Romero E (2010) Rhizobial symbiosis in tropical legumes and non-legumes. Soil Biology and Agriculture in the Tropics **21**: 163-183

Lodwig E, Poole PS (2003) Metabolism of rhizobium bacteroids. Crit Rev Plant Sci **22:** 37–78

Lodwig EM, Leonard M, Marroqui S, Wheeler TR, Findla K, Downie JA, Poole PS (2005) Role of polyhydroxybutyrate and glycogen as carbon storage compounds in pea and bean bacteroids. Mol Plant Microbe Interact **18**: 67–74

Long CP, Antoniewicz MR (2014) Quantifying biomass composition by gas chromatography/mass spectrometry. Anal Chem **86**: 9423-7

Long CP, Au J, Gonzalez JE, Antoniewicz MR (2016) ^{13}C metabolic flux analysis of microbial and mammalian systems is enhanced with GC–MS measurements of glycogen and RNA labelling. MetabEng **38**: 65-72

Long SR (1989) Rhizobium-legume nodulation: Life together in the underground. Cell **56**: 203-214

Manchak J, Page WJ (1994) Control of polyhydroxyalkanoate synthesis in *Azotobacter vinelandii* strain UWD. Microbiol 140: 953-963

Mandon K, Kaminski PA, Elmerich C (1994) Functional analysis of the *fixNOQP* region of *Azorhizobium caulinodans*. J Bacteriol **176**: 2560–2568

Mandon K, Michel-Reydellet N, Encarnación S, Kaminski PA, Leija A, Cevallos MA, Elmerich C, Mora J (1998) Poly-β-hydroxybutyrate turnover in *Azorhizobium caulinodans* is required for growth and affects *nifA* expression. J Bacteriol **180**: 5070–6

Maroti G, Kondorosi E (2014) Nitrogen-fixing *Rhizobium*-legume symbiosis: Are polyploidy and host peptide-governed symbiont differentiation general principles of endosymbiosis? Front Microbiol **5**: 326

Masakapalli SK, Bryant FM, Kruger NJ, Ratcliffe RG (2014) The metabolic flux phenotype of heterotrophic Arabidopsis cells reveals a flexible balance between the cytosolic and plastidic contributions to carbohydrate oxidation in response to phosphate limitation. Plant J **78**: 964–977

Masakapalli SK, Kruger NJ, Ratcliffe RG (2013) The metabolic flux phenotype of heterotrophic Arabidopsis cells reveals a complex response to changes in nitrogen supply. Plant J **74**: 569-582

Masakapalli SK, Le Lay P, Huddleston JE, Pollock NL, Kruger NJ, Ratcliffe RG (2010) Subcellular flux analysis of central metabolism in a heterotrophic Arabidopsis cell suspension using steady-state stable isotope labeling. Plant Physiol **152**: 602–19

Mathis R, Van Gijsegem F, De Rycke R, D'Haeze W, Van Maelsaeke E, Anthonio E, Montagu MV, Holsters M, Vereecke D (2005) Lipopolysaccharides as a

communication signal for progression of legume endosymbiosis. Proc Natl Acad Sci USA **102**: 2655–2660

McAllister CF, Lepo JE (1983) Succinate transport by free-living forms of *Rhizobium japonicum*. J Bacteriol **153**: 1155-1162

McKay IA, Dilworth MJ, Glenn AR (1988) C_4-dicarboxylatemetabolismin free-living and bacteroid forms of *Rhizobium leguminosarum* MNF3841. J Gen Microbiol **134**: 1433–1440

McKinlay JB, Shachar-Hill Y, Zeikus JG, Vieille C (2007) Determining *Actinobacillus succinogenes* metabolic pathways and fluxes by NMR and GC-MS analyses of ^{13}C-labeled metabolic product isotopomers. Metab Eng **9**: 177–92

McMahon A, Lu H, Butovich IA (2013) The spectrophotometric sulfo-phospho-vanillin assessment of total lipids in human meibomian gland secretions. Lipids **48**: 513–525

Metallo CM, Walther JL, Stephanopoulos G (2009) Evaluation of ^{13}C isotopic tracers for metabolic flux analysis in mammalian cells. J Biotechnol **144**: 167–174

Mercan N, Aslim B, Yuksekdag & Z N.,Beyatli, Y (2002) Production of poly-β-hydroxybutyrate (PHB) by some Rhizobium bacteria. Turkish Journal of Biology **26:** 215-219

Molnár-Perl I, Katona ZsF (2000) GC-MS of amino acids as their trimethylsilyl/t-butyldimethylsilyl Derivatives: In model solutions III. Chromatographia **51**: S228-S236

Montiel J, Arthikala MK, Cárdenas L, Quinto C (2016) Legume NADPH oxidases have crucial roles at different stages of nodulation. Int J Mol Sci **17**: 680

Mulley G, White JP, Karunakaran R, Prell J, Bourdes A, Bunnewell S, Hill L, Poole PS (2011) Mutation of GOGAT prevents pea bacteroid formation and N_2 fixation by globally downregulating transport of organic nitrogen sources. Mol Microbiol **80**: 149-67

Mulley G, Lopez-Gomez M, Zhang Y, Terpolilli J, Prell J, Finan T, Poole PS (2010) Pyruvate is synthesized by two pathways in pea bacteroids with different efficiencies for nitrogen fixation. J Bacteriol **192**: 4944–4953

Murphy PJ, Wexler W, Grzemski W, Rao JP, Gordon D (1995) Rhizopines—Their role in symbiosis and competition. Soil Biol Biochem **27**: 525–529

Mus F, Crook MB, Garcia K, Garcia Costas A, Geddes BA, Kouri ED, Paramasivan P, Ryu MH, Oldroyd GED, Poole PS, Udvardi MK, Voigt CA, Ané JM, Peters JW (2016) Symbiotic nitrogen fixation and challenges to extending it to non-legumes- Appl Environ Microbiol **82**: 3698-3710

Mylona P, Pawlowski K, Bisseling T (1995) Symbiotic Nitrogen Fixation. The Plant cell **7:** 869-885

Ndoye I, De Billy F, Vasse J, Dreyfus B, Truchet G (1994) Root nodulation of *Sesbania rostrata*. J Bacteriol **176:** 1060-1068

Neidhardt FC (1987) *Escherichia coli* and *Salmonella typhimurium*: Cellular and Molecular Biology 1st ed. (ASM Press, Washington, DC)

Neidhardt FC, Ingraham JL, Schaechter **M** (1990) Physiology of the bacterial cell: a molecular approach. Sinauer associates, Sunderland, MA ISBN 0–87893–608–4 pp 507

Norel F, Elmerich C (1987) Nucleotide Sequence and functional analysis of the two *nifH* copies of *Rhizobium* ORS571. J Gen Microbiol **133**: 1563-1 576

O'Callaghan KJ, Davey MR, Cocking EC (1997) Xylem colonization of the legume *Sesbania rostrata* by *Azorhizobium caulinodans*. Proc R Soc Lond B **264**: 1821-1826

O'Callaghan KJ, Stone PJ, Hu X, Griffiths DW, Davey MR, Cocking EC (2000) Effects of glucosinolates and flavonoids on colonization of the roots of Brassica napus by *Azorhizobium caulinodans* ORS571. Appl Environ Microbiol **66**: 2185–2191

Okazaki S, Tittabutr P, Teulet A, Thouin J, Fardoux J, Chaintreuil C, Gully D, Arrighi JF, Miwa FH, Yasuda M, Nouwen N, Teaumroong N, Giraud E (2016) Rhizobium-legume symbiosis in the absence of Nod factors: two possible scenarios with or without the T3SS. ISME J **10**: 64-74

Okahashi N, Kajihata S, Furusawa C, Shimizu H (2014) Reliable metabolic flux estimation in *Escherichia coli* central carbon metabolism using intracellular free amino acids. Metabolites **4**: 408-420

Oldroyd GED, Murray JD, Poole PS, Downie JA (2011) The rules of engagement in the legume-rhizobial symbiosis. Annu Rev Genet **45**: 119-144

Oldroyd GED (2013) Speak, friend, and enter: signalling systems that promote beneficial symbiotic associations in plants. Nat Rev Microbiol **11**: 252-63

Orata F (2012) Derivatization reactions and reagents for gas chromatography analysis. Advanced gas chromatography-Progress in agricultural, biomedical and industrial applications 83-156

Pacovsky RS, Bayne HG, Bethlenfalvay GJ (1984) Symbiotic Interactions between Strains of *Rhizobium phaseoli* and Cultivars of *Phaseolus vulgaris* L. Crop Sci **24**: 101-105

Pauling DC, Lapointe JP, Paris CM, Ludwig RA (2001) *Azorhizobium caulinodans* pyruvate dehydrogenase activity is dispensable for aerobic but required for microaerobic growth. Microbiology **147:** 2233–45

Patriarca EJ, Tatè R, Iaccarino M (2002) Key role of bacterial NH_4^+ metabolism in rhizobium-plant symbiosis. Microbiol Mol Biol Rev **66**: 203–222

Pawlowski K, Klosse U, de Bruijn FJ (1991) Characterization of a novel *Azorhizobium caulinodans* ORS571 two-component regulatory system, NtrY/NtrX, involved in nitrogen fixation and metabolism. Mol Gen Genet **231**: 124–38

Pawlowski K, Ratet P, Schell J, de Bruijn FJ (1987) Cloning and characterization of *nifA* and *ntrC* genes of the stem nodulating bacterium ORS571, the nitrogen fixing

symbiont of *Sesbania rostrata*: Regulation of nitrogen fixation (*nif*) genes in the free living versus symbiotic state. Mol Gen Genet. **206**: 207-219

Peoples M, Herridge DF, Ladha JK (1995) Biological nitrogen fixation: An efficient source of nitrogen for sustainable agricultural production. Plant and soil **174:** 3-28

Peng S, Biswas JC, Ladha JK, Gyaneshwar P, Chen Y (2002) Influence of rhizobial inoculation on photosynthesis and grain yield ofrice. Agron J **94**: 925-929

Peoples MB, Brockwell J, Herridge DF, Rochester IJ, Alves BJR, Urquiaga S, Boddey RM, Dakora FD, Bhattarai S, Maskey SL, Sampet C, Rerkasem B, Khan DF, Hauggaard-Nielsen H, Jensen ES (2009) The contributions of nitrogen-fixing crop legumes to the productivity of agricultural systems. Symbiosis **48**: 1-17

Pfau T, Christian N, Masakapalli SK, Sweetlove LJ, Mark G, Ebenh O (2016). The intertwined metabolism of *Medicago truncatula* and its nitrogen fixing symbiont *Sinorhizobium meliloti* elucidated by genome-scale metabolic models. bioRxiv 067348

Poole PS, Blyth A, Reid CJ, Walters K (1994) Myo-inositol catabolism and catabolite regulation in *Rhizobium leguminosarum* bv. *viciae*. Microbiology **140**: 2787-2795

Povolo S, Tombolini R, Morea A, Anderson AJ, Casella S, Nuti MP (1994) Isolation and characterization of mutants of *Rhizobium meliloti* unable to synthesize poly-β-hydroxybutyrate (PHB). Candian Journal of Microbiology. **40**: 823–829

Pronk AF, Boogerd FC, Stoof C, Oltmann LF, Stouthamer AH, van Verseveld HW (1993) *In situ* determination of the reduction levels of cytochromes *b* and *c* in growing bacteria: a case study with N,-fixing *Azorhizobium caulinodans*. Anal Biochem **214**: 149-155

Quelas JI, Mongiardini EJ, Pérez-Giménez J, Parisi G, Lodeiro AR (2013) Analysis of two polyhydroxyalkanoate synthases in *Bradyrhizobium japonicum* USDA 110. J bacterial **195**: 3145–3155

Rae AL, Bonfante-Fasolo P, Brewin NJ (1992) Structure and growth of infection threads in the legume symbiosis with *Rhizobium leguminosarum*. Plant J **2**: 385-395

Ratcliffe RG, Shachar-Hill Y (2006) Measuring multiple fluxes through plant metabolic networks. Plant J **45**: 490–511

Ratcliff WC, Kadam SV, Denison RF (2008) Poly-β-hydroxybutyrate (PHB) supports survival and reproduction in starving rhizobia. FEMS Microbiol Ecol **65**: 391–399

Ratet P, Pawlowski K, Schell J, de Bruijn FJ (1989) The *Azorhizobium caulinodans* nitrogen-fixation regulatory gene, *nifA*, is controlled by the cellular nitrogen and oxygen status. Mol Microbiol **3**: 825–38

Reding HK, Lepo JE (1989) Physiological characterization of dicarboxylate-induced pleomorphic forms of *Bradyrhizobium japonicum*. Appl Environ Microbiol **55**: 666-671

Rehm BHA (2010) Bacterial polymers: biosynthesis, modifications and applications. Nat Rev Microbiol **8**: 578-592

Reid CJ, Walshaw DL, Poole PS (1996) Aspartate transport by the Dct system in *Rhizobium leguminosarum* negatively affects nitrogen-regulated operons. Microbiology **142**: 2603-2612

Resendis-Antonio O, Reed JL, Encarnación S, Collado-Vides J, Palsson, BØ (2007) Metabolic reconstruction and modeling of nitrogen fixation in *Rhizobium etli*. PLoS Computational Biology **3**: 1887–95

Resendis-Antonio O, Hernández M, Salazar E, Contreras S, Batallar G, Mora Y, Encarnación S (2011) Systems biology of bacterial nitrogen fixation: High-throughput technology and its integrative description with constraint-based modelling. BMC Syst Biol **5:** 120

Robson RL, Postgate JR (1980) Oxygen and hydrogen in biological nitrogen fixation. A Rev Microbiol **34**: 183-207

Romanov VI, Hernández-Lucas I, Martínez-Romero E (1994) Carbon metabolism enzymes of *Rhizobium tropici* cultures and bacteroids. Appl Environ Microbiol **60**: 2339–2342

Roscher A, Kruger NJ, Ratcliffe RG (2000) Strategies for metabolic flux analysis in plants using isotope labelling. J Biotechnol **77**: 81–102

Rosenblatt J, Chinkes D,Wolfe M, Wolfe, RR (1992) Stable isotope tracer analysis by GC-MS, including quantification of isotopomer effects. Am J Physiol **263**: E584-96

Rout ME (2014) The Plant Microbiome. Advances in Botanical Research **69**: 279-309

Sabry SR, Saleh SA, Batchelor CA, Jones J, Jotham J, Webster G, Kothari SL, Davey MR, Cocking EC (1997) Endophytic establishment of *Azorhizobium caulinodans* in wheat. Proc R Soc Lond B **264**: 341–346

Saraswati R, Matoh T, Sekiya J (1992) Nitrogen Fixation of *Sesbania rostrata*: Contribution of stem nodules to nitrogen acquisition. Soil Sci Plant Nutr **38**: 775-780

Salminen SO, Streeter JG (1987) Uptake and metabolism of carbohydrates by *Bradyrhizobium japonicum* bacteroids. Plant Physiol **83**: 535-540

Sato S, Siarot L, Matsuoka J, Aono T, Yaizu H (2016) An *Azorhizobium caulinodans* ORS571 mutant with deletion of a gene encoding a TIGR02302 family protein overproduces exopolysaccharides and is defective in infection into plant host cells. Soil Sci Plant Nutr **62**: 392-398

Sauer U, Lasko DR, Fiaux J, Hochuli M, Glaser R, Szyperski T, Wüthrich K, Bailey JE (1999) Metabolic flux ratio analysis of genetic and environmental modulations of *Escherichia coli* central carbon metabolism. J Bacteriol **181**: 6679–6688

Schäfer A, Tauch A, Jäger W, Kalinowski J, Thierbach G, Pühler A (1994) Small mobilizable multi-purpose cloning vectors derived from the *Escherichia coli* plasmids pK18 and pK19: selection of defined deletions in the chromosome of *Corynebacterium glutamicum*. Gene. **145**: 69 – 73

Schmid J, Sieber V, Rehm B (2015) Bacterial exopolysaccharides: biosynthesis pathways and engineering strategies. Front Microbiol **6**: 496

Scott JD, Ludwig RA (2004) *Azorhizobium caulinodans* electron-transferring flavoprotein N electrochemically couples pyruvate dehydrogenase complex activity to N_2 fixation. Microbiology **150**: 117–126

Schubert KR, Evans HJ (1976) Hydrogen evolution: A major factor affecting the efficiency of nitrogen fixation in nodulated symbionts. Proc Nat Acad Sci USA **73**: 1207-1211

Schöder H, Knight RJ, Kofoed KF, Schelbert HR (1998) Regulation of pyruvate dehydrogenase activity and glucose metabolism in post-ischaemic myocardium. Biochim Biophys Acta **1406**: 62-72

Seifter S, Dayton S, Nonic B, Muntwyler E (1950) The estimation of glycogen with anthrone reagent. Arch Biochem **25**: 191–200

Senior PJ, Dawes EA (1971) Poly-β-hydroxybutyrate biosynthesis and the regulation of glucose metabolism in *Azotobacter beijerinckii*. Biochem J **125**: 55–66

Senior PJ, Beech GA, Ritchie GAF, Dawes EA (1972) The role of oxygen limitation in the formation of poly-3-hydroxybutyrate during batch and continuous culture of *Azotobacter beijerinckii*. Biochem J **128**: 1193–1201

Senior PJ, Dawes EA (1973) The Regulation of poly-β-hydroxybutyrate metabolism in *Azotobacter beijerinckii*. Biochem J **134**: 225-238

Sessions AL (2006) Isotope-ratio detection for gas chromatography. J Sep Sci **29**: 1946 – 1961

Shabina M, Afzal M, Hameed S (2015) Bacterial polyhydroxyalkanoates-eco-friendly next generation plastic: Production, biocompatibility, biodegradation, physical properties and applications. Green Chem Lett Rev **8**: 56-77

Shah R, Emerich DW (2006) Isocitrate dehydrogenase of *Bradyrhizobium japonicum* is not required for symbiotic nitrogen fixation with soybean. J Bacteriol **188**: 7600–7608

Sharma RS, Mishra V, Mohmmed A, Babu CR (2011) Variations in outer-membrane characteristics of two stem-nodulating bacteria of *Sesbania rostrata* and its role in tolerance towards diverse stress. Curr Microbiol **63**: 81-6

Smith A, Hill S, Anthony C (1990) The purification, characterization and role of the *d*-type cytochrome oxidase of *Klebsiella pneumonaie* during nitrogen fixation. J Gen Microbiol **136**: 171-180

Smith CM, Bryla J, Williamsony JR (1974) Regulation of mitochondrial α-ketoglutarate metabolism by product inhibition at α-ketoglutarate dehydrogenase. J Biol chem **249**: 1497-1505

Smith PK, Krohn RI, Hermanson GT, Mallia AK, Gartner FH, Provenzano MD, Fujimoto EK, Goeke NM, Olson BJ, Klenk DC (1985) Measurement of protein using bicinchoninic acid. Anal Biochem **19**: 76-85

Srour O, Young JD, Eldar YC (2011) Fluxomers: a new approach for ^{13}C metabolic flux analysis. BMC Syst Biol **5**: 129

Stam H, van Verseveld HW, de Vries W, Stouthamer AH (1984) Hydrogen oxidation and efficiency of nitrogen fixation in succinate-limited chemostat cultures of *Rhizobium* ORS 571. Archives of Microbiology **139**: 53-60

Stam H, van Verseveld HW, de Vries W, Stouhamer AH (1986) Utilization of poly-β-hydroxybutyrate in free-living cultures of *Rhizobium* ORS571. FEMS Microbiol Lett **35**: 215–220

Stam H, Stouthamer AH, van Verseveld HW (1987) Hydrogen metabolism and energy costs of nitrogen fixation. FEMS Microbiol Rev **46**: 73-92

Steele MI, Lorenz D, Hatter K, Park A, Sokatch JR (1992) Characterization of the *mmsAB* operon of *Pseudomonas aeruginosa* PA0 Encoding Methylmalonate-semialdehyde Dehydrogenase and 3-hydroxyisobutyrate dehydrogenase. J Biol Chem **267**: 13585-13592

Steinbuchel A, Schlegel HG (1991) Physiology and molecular genetics of poly(β-hydroxy-alkanoic- acid) synthesis in *Alcaligenes eutrophus*. Mol Microbiol **5**: 535–542

Stigter J, Schneider M, de Bruijn FJ (1993) *Azorhizobium caulinodans* nitrogen fixation (*nif/fix*) gene regulation: mutagenesis of the *nifA* - 24/-12 promoter element, characterization of a *ntrA* (*rpoN*) gene, and derivation of a model. Mol. Plant-Microbe Interact **6:** 238-252

Stone PJ, O'Callaghan KJ, Davey MR, Cocking EC (2001) *Azorhizobium caulinodans* ORS571 colonizes the xylem of *Arabidopsis thaliana*. Mol Plant Microbe Interact **14**: 93–7

Stowers MD (1985) Carbon metabolism in rhizobium. Ann Rev Microbiol **39**: 89–108

Stowers MD, Elkan GH (1985) Regulation of hexose catabolism in *Rhizobium* sp. 32H1. FEMS Microbiol Lett **26**:45-48

Stovall I, Cole M (1978) Organic acid metabolism by isolated *Rhizobium japonicum* bacteroids. Plant Physiol **61**, 787–90

Su HC, Ramkissoon K, Doolittle J, Clark M, Khatun J, Secrest A, Wolfgang MC, Giddings MC (2010) The development of ciprofloxacin resistance in Pseudomonas aeruginosa involves multiple response stages and multiple proteins. Antimicrob Agents Chemother **54**: 4626-35

Suzuki S, Aono T, Lee KB, Suzuki T, Liu CT, Miwa H, Wakao S, Iki T, Oyaizu, H (2007) Rhizobial factors required for stem nodule maturation and maintenance in *Sesbania rostrata-Azorhizobium caulinodans* ORS571 symbiosis. Appl Environ Microbiol. **73**,6650–6659

Suzuki T, Aono T, Liu CT, Suzuki S, Iki T, Yokota K, Oyaizu H (2008) An outer membrane autotransporter, AoaA, of *Azorhizobium caulinodans* is required for sustaining high N_2-fixing activity of stem nodules. FEMS Microbiol Lett **285**: 16–24

Tavernier P, Portais JC, Saucedo JEN, Courtois J, Courtois B, Barbotin JN (1997) Exopolysaccharide and poly-β-hydroxybutyrate coproduction in two *Rhizobium meliloti* strains. Appl Environ Microbiol. **63**: 21–26

Tkacz A, Poole PS (2015) Role of root microbiota in plant productivity. J Exp Bot **66**: 2167-2175

Terpolilli JJ, Hood GA, Poole PS (2012) What determines the efficiency of N_2-fixing *Rhizobium*-legume symbioses? Adv Microb Physiol **60**1; 325–389

Terpolilli JJ, Masakapalli SK, Karunakaran R, Webb I, Green R, Watmough NJ, Kruger NJ, Ratcliffe RG, Poole PS (2016) Lipogenesis and redox balance in nitrogen-fixing pea bacteroids. J Bacteriol **198**: 2864-2875

Tett AJ, Karunakaran R, Poole PS (2014) Characterisation of SalRAB a salicylic acid inducible positively regulated efflux system of *Rhizobium leguminosarum* bv *viciae* 3841. PLoS ONE **9**: e103647

Thöny-Meyer L, Kunzler P (1996) The *Bradyrhizobium japonicum* aconitase gene (*acnA*) is important for free- living growth but not for an effective root nodule symbiosis. J Bacteriol **178**: 6166–6172

Timmers ACJ, Auriac MC, Truchet G (1999) Refined analysis of early symbiotic steps of the *Rhizobium-Medicago* interaction in relationship with microtubular cytoskeleton rearrangements. Development **126**: 3617-3628

Tombolini R, Nuti MP (1989) Poly(β-hydroxyalkanoate) biosynthesis and accumulation by different *Rhizobium* species. FEMS Microbiol Lett **60**: 299-304

Toya Y, Kono N, Arakawa K, Tomita M (2011) Metabolic flux analysis and visualization. J Proteome Res **10**: 3313–23

Toya Y, Shimizu H (2013) Flux analysis and metabolomics for systematic metabolic engineering of microorganisms. Biotechnology Advances **31**: 818–26

Trainer MA, Charles TC (2006) The role of PHB metabolism in the symbiosis of rhizobia with legumes. Appl Microbiol Biotechnol **71**: 377–86

Tremblay J, Singh K, Fern A, Kirton ES, He S, Woyke T, Lee J, Chen F, Dangl JL, Tringe SG (2015). Primer and platform effects on 16S rRNA tag sequencing. Front Microbiol **6**: 771.

Trinchant JC, Rigaud J (1990) Occurrence of two pathways for malate oxidation in bacteroids isolated from *Sesbania rostrata* stem nodules during C_2H_2 reduction. Plant Physiol **94**: 1002-1008

Trinick MJ, Dilworth MJ, Grounds M (1976) Factors affecting the reduction of acetylene by root nodules of *Lupinus* species. New Phytol **77**: 359-370

Tsukada S, Aono T, Akiba N, Lee KB, Liu CT, Toyazaki H, Oyaizu H (2009) Comparative genome-wide transcriptional profiling of *Azorhizobium caulinodans* ORS571 grown under free-living and symbiotic conditions. Appl Environ Microbiol **75**: 5037–5046

Turner TR, James EK, Poole PS (2013) The plant microbiome. Genome Biology **14**: 209

Udvardi M, Poole PS (2013) Transport and metabolism in legume-rhizobia symbioses. Annu Rev Plant Biol **64**: 781-805

Van de Velde W, Zehirov G, Szatmari A, Debreczeny M, Ishihara H, Kevei Z, Farkas A, Mikulass K, Nagy A, Tiricz H, Satiat-Jeunemaître B, Alunni B, Bourge M, Kucho K, Abe M, Kereszt A, Maroti G, Uchiumi T, Kondorosi E, Mergaert P (2010) Plant peptides govern terminal differentiation of bacteria in symbiosis. Science **327:** 1122–1126

Vogan AA, Higgs PG (2011) The advantages and disadvantages of horizontal gene transfer and the emergence of the first species. Biology Direct **6**: 1

Vercruysse M, Fauvart M, Beullens S, Braeken K, Cloots L, Engelen K, Marchal K, Michiels J (2011) A comparative transcriptome analysis of *Rhizobium etli* bacteroids: specific gene expression during symbiotic nongrowth. Mol Plant Microbe Interact **24**: 1553–1561

Wahl SA, Dauner M, Wiechert W (2004) New tools for mass isotopomer data evaluation in ^{13}C flux analysis: mass isotope correction, data consistency checking, and precursor relationships. Biotechnol Bioeng **85**: 259-268

Walther JL, Metallo CM, Zhang J, Stephanopoulos G (2012) Optimization of ^{13}C isotopic tracers for metabolic flux analysis in mammalian cells. Metab Eng **14**: 162–171

Wang C, Saldanha M, Sheng X, Shelswell KJ, Walsh KT, Sobral BWS, Charles TC (2007) Roles of poly-β-hydroxybutyrate (PHB) and glycogen in symbiosis of *Sinorhizobium meliloti* with *Medicago* sp. Microbiology **153**: 388–98

Webb KJ, Cookson A, Allison G, Sullivan ML, Winters AL (2014) Polyphenoloxidase affects normal nodule development in red clover (*Trifolium pratense* L.). Front Plant Sci **5**: 700

Weitzel M, Wiechert W, Nöh K (2007) The topology of metabolic isotope labeling networks. BMC Bioinformatics **8:** 315

Wendisch VF, de Graaf AA, Sahm H (1997) Accurate determination of ^{13}C enrichments in nonprotonated carbon atoms of isotopically enriched amino acids by ^{1}H nuclear magnetic resonance. Anal Biochem **245**: 196–202

White J, Prell J, James EK, Poole PS (2007) Nutrient sharing between symbionts. Plant Physiol **144**: 604–614

Wiechert W (2001) ^{13}C metabolic flux analysis. Metab Eng **3**: 195–206

Wiechert W, Möllney M, Petersen S, de Graaf AA (2001) A universal framework for ^{13}C metabolic flux analysis. Metab Eng **3**: 265–83

Williams TCR, Miguet L, Masakapalli SK, Kruger NJ, Sweetlove LJ, Ratcliffe RG (2008) Metabolic network fluxes in heterotrophic arabidopsis cells: stability of the flux distribution under different oxygenation conditions. Plant Physiol **148**: 704-718

Xiao TT, Schilderink S, Moling S, Deinum EE, Kondorosi E, Franssen H, Kulikova

O, Andreas NA, Bisseling T (2014) Fate map of *Medicago truncatula* root nodules. Development **141**: 3517-3528

Yanni YG, Rizk RY, Corich V, Squartini A, Ninke K, Philip-Hollingsworth S, Orgambide G, de Bruijn F, Stoltzfus J, Buckley D, Schmidt TM, Mateos PF, Ladha JK, Dazzo FB (1997) Natural endophyticassociation between *Rhizobium leguminosarum* bv. *trifolii* and rice roots and assessment of its potential to promote rice growth. Plant and Soil **194:** 99-114

Yoch DC (1974) Electron transport carriers involved in nitrogen fixation by the coliform, *Klebsiella pneumoniae*. J Gen Microbiol **83**: 153-164

Young JD, Walther JL, Antoniewicz MR, Yoo H, Stephanopoulos G (2008) An elementary metabolite unit (EMU) based method of isotopically nonstationary flux analysis. Biotechnol Bioeng **99**: 686–99

Young JD (2013) Metabolic flux rewiring in mammalian cell cultures. Curr Opin Biotechnol **24**: 1108-1115

Young JD (2014) INCA: A computational platform for isotopically non-stationary metabolic flux analysis. Bioinformatics **30**: 1333–1335

Young JD, Allen DK, Morgan JA (2014) Isotopomer measurement techniques in metabolic flux analysis II: mass spectrometry. Methods Mol Biol **1083**: 85-108

Zamboni N, Fendt SM, Rühl M, Sauer U (2009) ^{13}C-based metabolic flux analysis. Nat Protoc **4**: 878 – 892

Zevenhuizen LPTM (1971) Chemical composition of exopolysaccharides of *Rhizobium* and *Agrobacterium*. J Gen Microbiol **68**: 239-243

Zhang Y, Tang L, Hutchinson CR (1996) Cloning and characterization of a gene (*msdA*) encoding methylmalonic acid semialdehyde dehydrogenase from *Streptomyces coelicolor*. J Bacteriol **178**: 490-495

Zhang Y, Aono T, Poole P, Finan TM (2012a) $NAD(P)^+$-malic enzyme mutants of *Sinorhizobium* sp. strain ngr234, but not *Azorhizobium caulinodans* ORS571, maintain symbiotic N_2 fixation capabilities. Appl Environ Microbiol **78**: 2803–2812

Zhang Y, Tobias HJ, Sacks G, Brenna JT (2012b) Calibration and Data Processing in Gas Chromatography Combustion Isotope Ratio Mass Spectrometry. Drug Test Anal **4**: 912-922

Zhao H, Li M, Fang K, Chen W, Wang J (2012) In silico insights into the symbiotic nitrogen fixation in *Sinorhizobium meliloti* via metabolic reconstruction. PLoS One **7:** e31287

9. Appendices

A1. **The alignment statistics for the best match obtained for 16SrRNA analysis of the strain used for this study using BLAST analysis is shown below.**

Method:- The analysis was done using BLAST (Basic local alignment tool) of NCBI. “Query” refers to the sequence of OPS0865 for which the best match was obtained and “Sbjct” refers to the best match found in the database of NCBI (National centre for biotechnology information).
Best match:- *Azorhizobium caulinodans* strain ORS 571 16S ribosomal RNA gene, complete sequence (Length: 1468). This analysis confirms the phylogeny of the strain used for this study was *Azorhizobium caulinodans*, ORS571.

Score	Expect	Identities	Gaps	Strand
2486 bits(1346)	**0.0**	**1346/1346(100%)**	**0/1346(0%)**	**Plus/Plus**

```
Query  1    TCGAGCGCCCAGCAATGGGAGCGGCAGACGGGTGAGTAACGCGTGGGGATGTGCCCAATG  60
           ||||||||||||||||||||||||||||||||||||||||||||||||||||||||||||
Sbjct  52   TCGAGCGCCCAGCAATGGGAGCGGCAGACGGGTGAGTAACGCGTGGGGATGTGCCCAATG  111

Query  61   GTGCGGAATAACCCAGGGAAACTTGGATTAATACCGCATGTGCCCTTCGGGGGAAAGATT  120
           ||||||||||||||||||||||||||||||||||||||||||||||||||||||||||||
Sbjct  112  GTGCGGAATAACCCAGGGAAACTTGGATTAATACCGCATGTGCCCTTCGGGGGAAAGATT  171

Query  121  TATCGCCATTGGATCAACCCGCGTCTGATTAGCTAGTTGGTGAGGTAAAGGCTCACCAAG  180
           ||||||||||||||||||||||||||||||||||||||||||||||||||||||||||||
Sbjct  172  TATCGCCATTGGATCAACCCGCGTCTGATTAGCTAGTTGGTGAGGTAAAGGCTCACCAAG  231

Query  181  GCGACGATCAGTAGCTGGTCTGAGAGGATGATCAGCCACACTGGGACTGAGACACGGCCC  240
           ||||||||||||||||||||||||||||||||||||||||||||||||||||||||||||
Sbjct  232  GCGACGATCAGTAGCTGGTCTGAGAGGATGATCAGCCACACTGGGACTGAGACACGGCCC  291

Query  241  AGACTCCTACGGGAGGCAGCAGTGGGGAATATTGGACAATGGGCGCAAGCCTGATCCAGC  300
           ||||||||||||||||||||||||||||||||||||||||||||||||||||||||||||
Sbjct  292  AGACTCCTACGGGAGGCAGCAGTGGGGAATATTGGACAATGGGCGCAAGCCTGATCCAGC  351

Query  301  CATGCCGCGTGAGTGATGAAGGCCTTAGGGTTGTAAAGCTCTTTCGCCGGTGAAGATAAT  360
           ||||||||||||||||||||||||||||||||||||||||||||||||||||||||||||
Sbjct  352  CATGCCGCGTGAGTGATGAAGGCCTTAGGGTTGTAAAGCTCTTTCGCCGGTGAAGATAAT  411

Query  361  GACGGTAACCGGAGAAGAAGCCCCGGCTAACTTCGTGCCAGCAGCCGCGGTAATACGAAG  420
           ||||||||||||||||||||||||||||||||||||||||||||||||||||||||||||
Sbjct  412  GACGGTAACCGGAGAAGAAGCCCCGGCTAACTTCGTGCCAGCAGCCGCGGTAATACGAAG  471

Query  421  GGGGCAAGCGTTGCTCGGAATCACTGGGCGTAAAGCGCACGTAGGCGGATCGTTAAGTCA  480
           ||||||||||||||||||||||||||||||||||||||||||||||||||||||||||||
Sbjct  472  GGGGCAAGCGTTGCTCGGAATCACTGGGCGTAAAGCGCACGTAGGCGGATCGTTAAGTCA  531

Query  481  GGGGTGAAAGCCTGGAGCTCAACTCCAGAACTGCCCTTGATACTGGCGATCTTGAGTTCG  540
           ||||||||||||||||||||||||||||||||||||||||||||||||||||||||||||
Sbjct  532  GGGGTGAAAGCCTGGAGCTCAACTCCAGAACTGCCCTTGATACTGGCGATCTTGAGTTCG  591

Query  541  AGAGAGGTTGGTGGAACTCCGAGTGTAGAGGTGAAATTCGTAGATATTCGGAAGAACACC  600
           ||||||||||||||||||||||||||||||||||||||||||||||||||||||||||||
Sbjct  592  AGAGAGGTTGGTGGAACTCCGAGTGTAGAGGTGAAATTCGTAGATATTCGGAAGAACACC  651

Query  601  AGTGGCGAAGGCGGCCAACTGGCTCGATACTGACGCTGAGGTGCGAAAGCGTGGGGAGCA  660
```

```
                ||||||||||||||||||||||||||||||||||||||||||||||||||||||||||||||||
Sbjct  652   AGTGGCGAAGGCGGCCAACTGGCTCGATACTGACGCTGAGGTGCGAAAGCGTGGGGAGCA  711

Query  661   AACAGGATTAGATACCCTGGTAGTCCACGCCGTAAACGATGGATGCTAGCCGTTGGGGAG  720
                ||||||||||||||||||||||||||||||||||||||||||||||||||||||||||||||||
Sbjct  712   AACAGGATTAGATACCCTGGTAGTCCACGCCGTAAACGATGGATGCTAGCCGTTGGGGAG  771


Query  721   CTTGCTCTTCAGTGGCGCAGCTAACGCCTTAAGCATCCCGCCTGGGGAGTACGGTCGCAA  780
                ||||||||||||||||||||||||||||||||||||||||||||||||||||||||||||||||
Sbjct  772   CTTGCTCTTCAGTGGCGCAGCTAACGCCTTAAGCATCCCGCCTGGGGAGTACGGTCGCAA  831

Query  781   GATTAAAACTCAAAGGAATTGACGGGGGCCCGCACAAGCGGTGGAGCATGTGGTTTAATT  840
                ||||||||||||||||||||||||||||||||||||||||||||||||||||||||||||||||
Sbjct  832   GATTAAAACTCAAAGGAATTGACGGGGGCCCGCACAAGCGGTGGAGCATGTGGTTTAATT  891

Query  841   CGAAGCAACGCGCAGAACCTTACCAGCCTTTGACATGGCAGGACGACTTCCGGAGACGGA  900
                ||||||||||||||||||||||||||||||||||||||||||||||||||||||||||||||||
Sbjct  892   CGAAGCAACGCGCAGAACCTTACCAGCCTTTGACATGGCAGGACGACTTCCGGAGACGGA  951

Query  901   TTTCTTCCAGCAATGGACCTGCACACAGGTGCTGCATGGCTGTCGTCAGCTCGTGTCGTG  960
                ||||||||||||||||||||||||||||||||||||||||||||||||||||||||||||||||
Sbjct  952   TTTCTTCCAGCAATGGACCTGCACACAGGTGCTGCATGGCTGTCGTCAGCTCGTGTCGTG
1011

Query  961   AGATGTTGGGTTAAGTCCCGCAACGAGCGCAACCCTCGCCTTTAGTTGCCATCATTCAGT
1020
                ||||||||||||||||||||||||||||||||||||||||||||||||||||||||||||||||
Sbjct  1012  AGATGTTGGGTTAAGTCCCGCAACGAGCGCAACCCTCGCCTTTAGTTGCCATCATTCAGT
1071

Query  1021  TGGGCACTCTAAAGGGACTGCCGGTGATAAGCCGCGAGGAAGGTGGGGATGACGTCAAGT
1080
                ||||||||||||||||||||||||||||||||||||||||||||||||||||||||||||||||
Sbjct  1072  TGGGCACTCTAAAGGGACTGCCGGTGATAAGCCGCGAGGAAGGTGGGGATGACGTCAAGT
1131

Query  1081  CCTCATGGCCCTTACGGGCTGGGCTACACACGTGCTACAATGGCGGTGACAATGGGATGC
1140
                ||||||||||||||||||||||||||||||||||||||||||||||||||||||||||||||||
Sbjct  1132  CCTCATGGCCCTTACGGGCTGGGCTACACACGTGCTACAATGGCGGTGACAATGGGATGC
1191

Query  1141  GAGCCTGCGAGGGTGAGCAAATCTCCAAAAGCCGTCTCAGTTCGGATTGCACTCTGCAAC
1200
                ||||||||||||||||||||||||||||||||||||||||||||||||||||||||||||||||
Sbjct  1192  GAGCCTGCGAGGGTGAGCAAATCTCCAAAAGCCGTCTCAGTTCGGATTGCACTCTGCAAC
1251

Query  1201  TCGAGTGCATGAAGTTGGAATCGCTAGTAATCGTGGATCAGCATGCCACGGTGAATACGT
1260
                ||||||||||||||||||||||||||||||||||||||||||||||||||||||||||||||||
Sbjct  1252  TCGAGTGCATGAAGTTGGAATCGCTAGTAATCGTGGATCAGCATGCCACGGTGAATACGT
1311

Query  1261  TCCCGGGCCTTGTACACACCGCCCGTCACACCATGGGAGTTGGCTTTACCCGAAGGCGTT
1320
                ||||||||||||||||||||||||||||||||||||||||||||||||||||||||||||||||
Sbjct  1312  TCCCGGGCCTTGTACACACCGCCCGTCACACCATGGGAGTTGGCTTTACCCGAAGGCGTT
1371

Query  1321  GCGCTAACCGCAAGGAGGCAGGCGAC  1346
                |||||||||||||||||||||||||
Sbjct  1372  GCGCTAACCGCAAGGAGGCAGGCGAC  1397
```

Figure A2: GC-MS mass spectra of 16 protein-derived amino acids, trehalose and hydroxybutyrate from late exponential cultures of ORS571 under aerobic growth conditions.

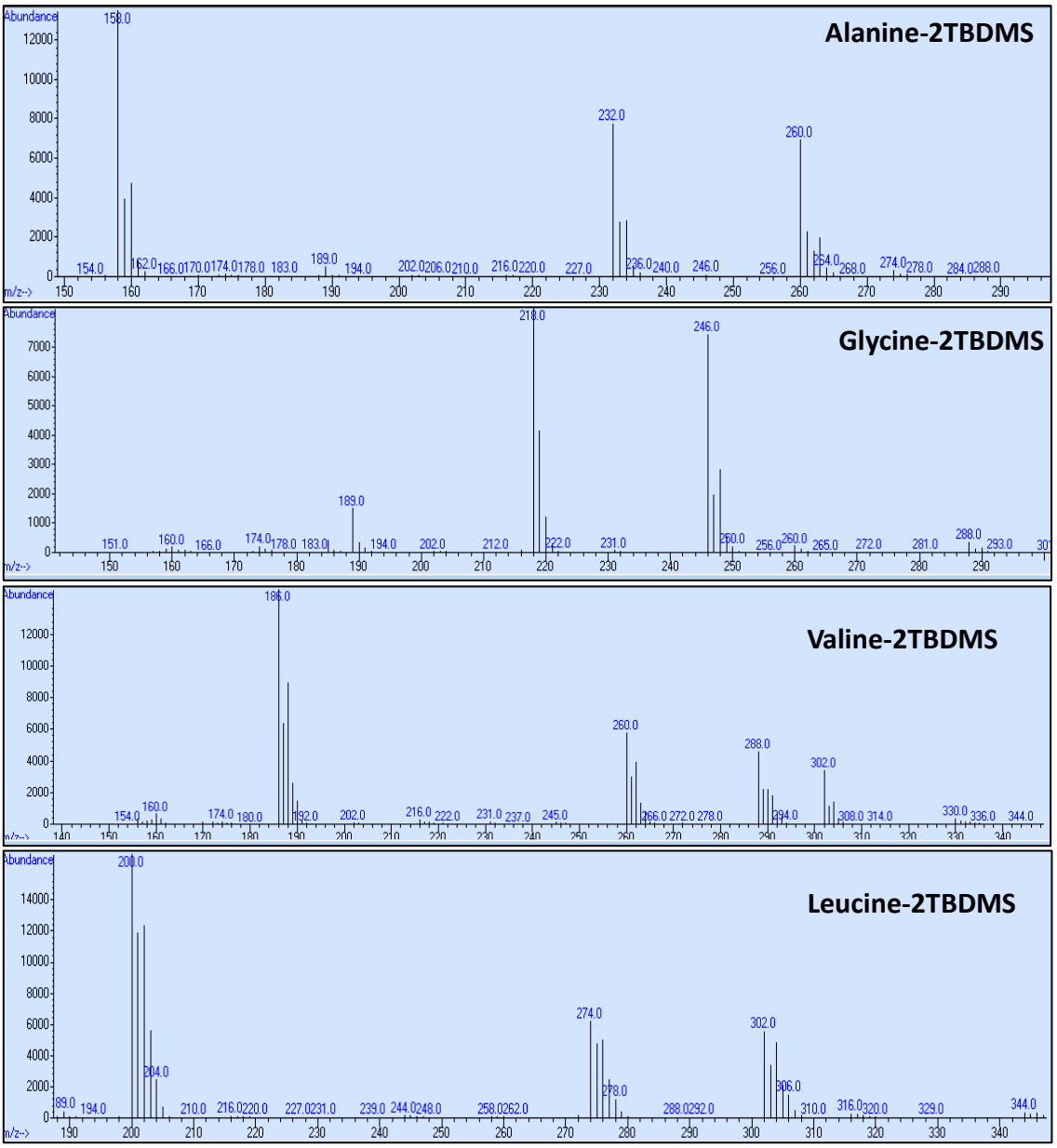

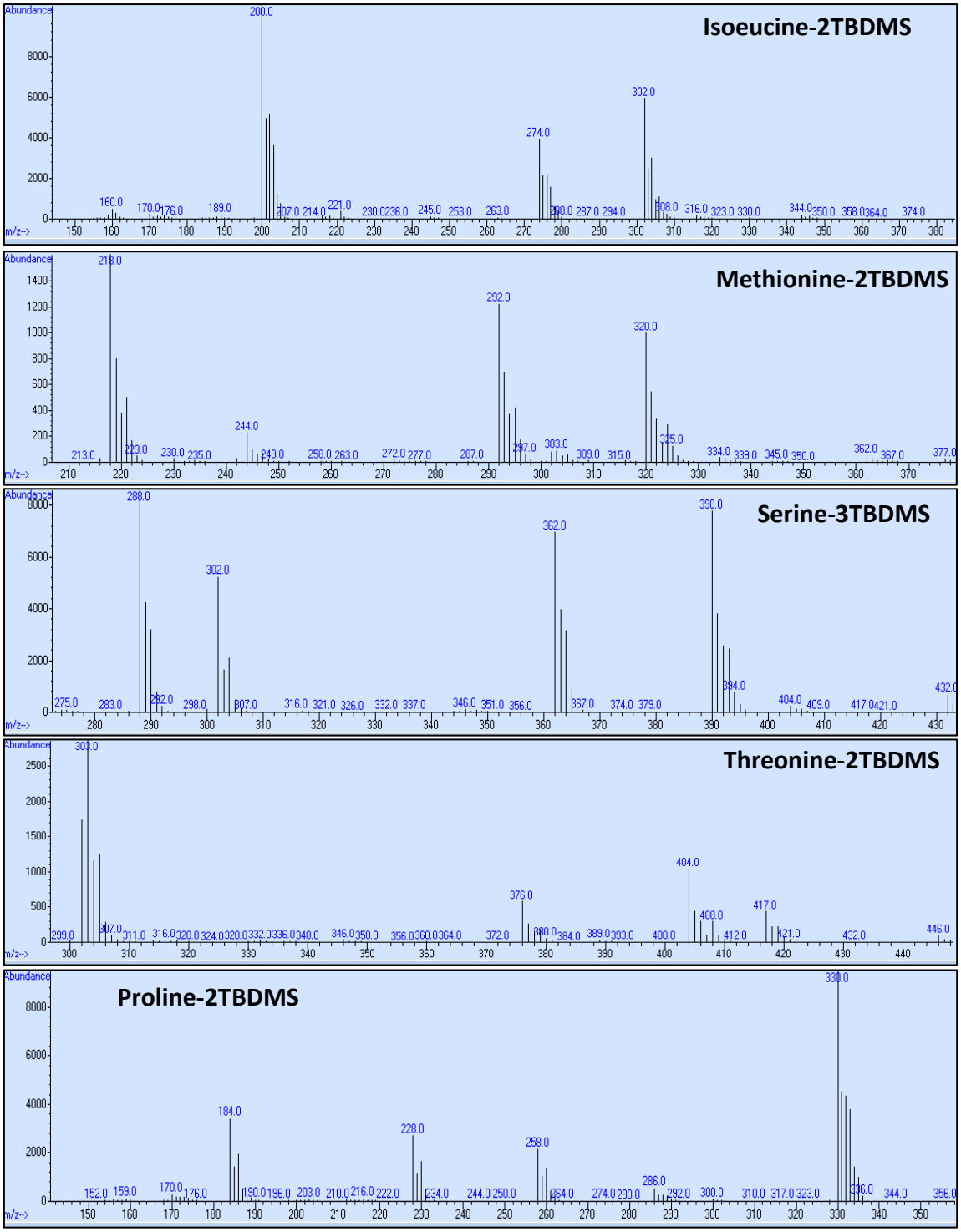
Isoeucine-2TBDMS
Methionine-2TBDMS
Serine-3TBDMS
Threonine-2TBDMS
Proline-2TBDMS

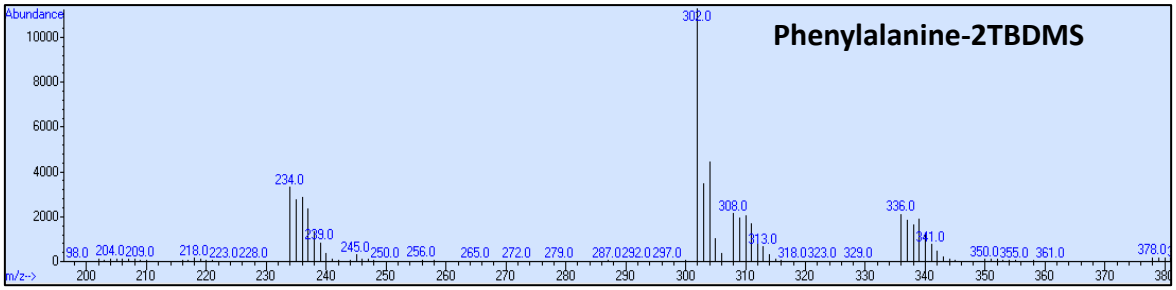
Phenylalanine-2TBDMS
Abundance
m/z-->

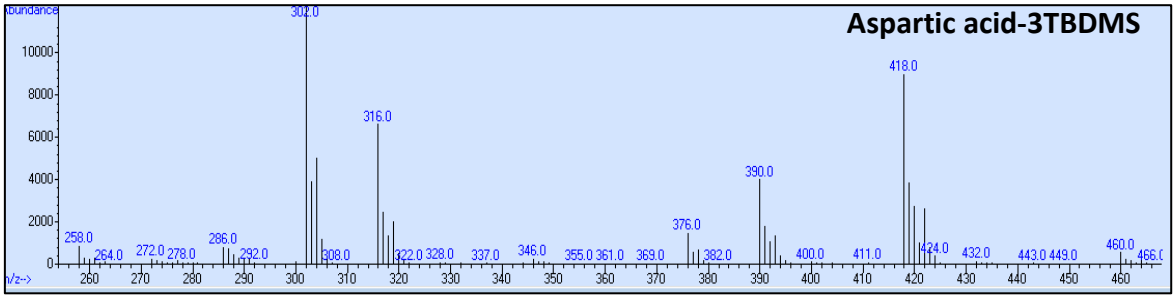
Aspartic acid-3TBDMS
Abundance
m/z-->

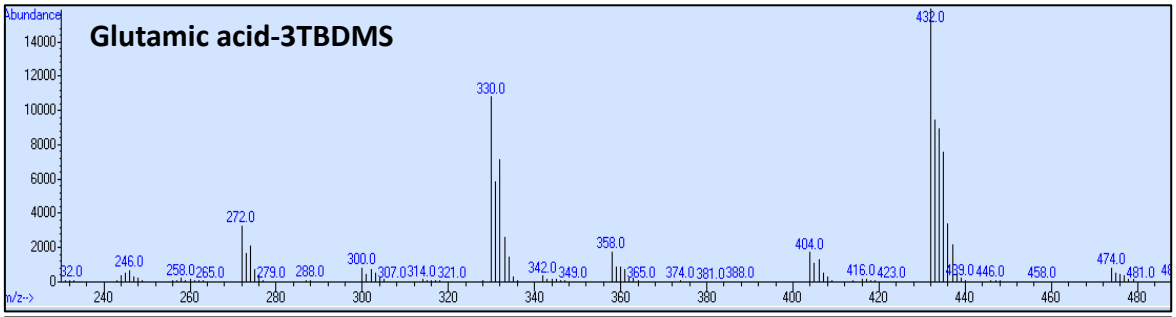
Glutamic acid-3TBDMS
Abundance
m/z-->

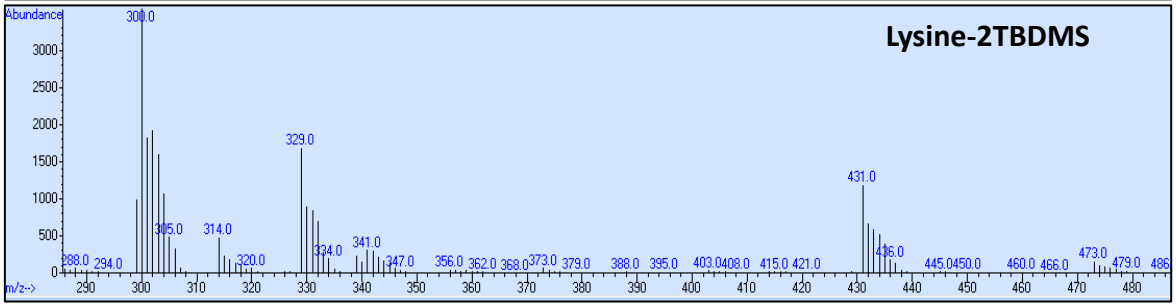
Lysine-2TBDMS
Abundance
m/z-->

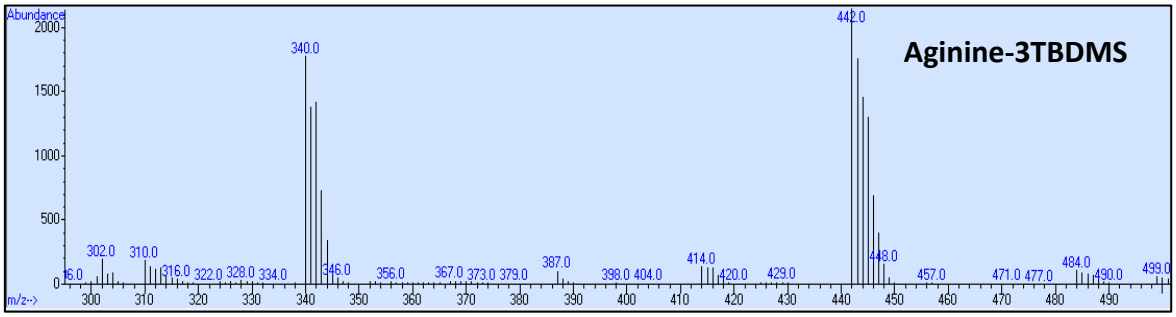
Aginine-3TBDMS
Abundance
m/z-->

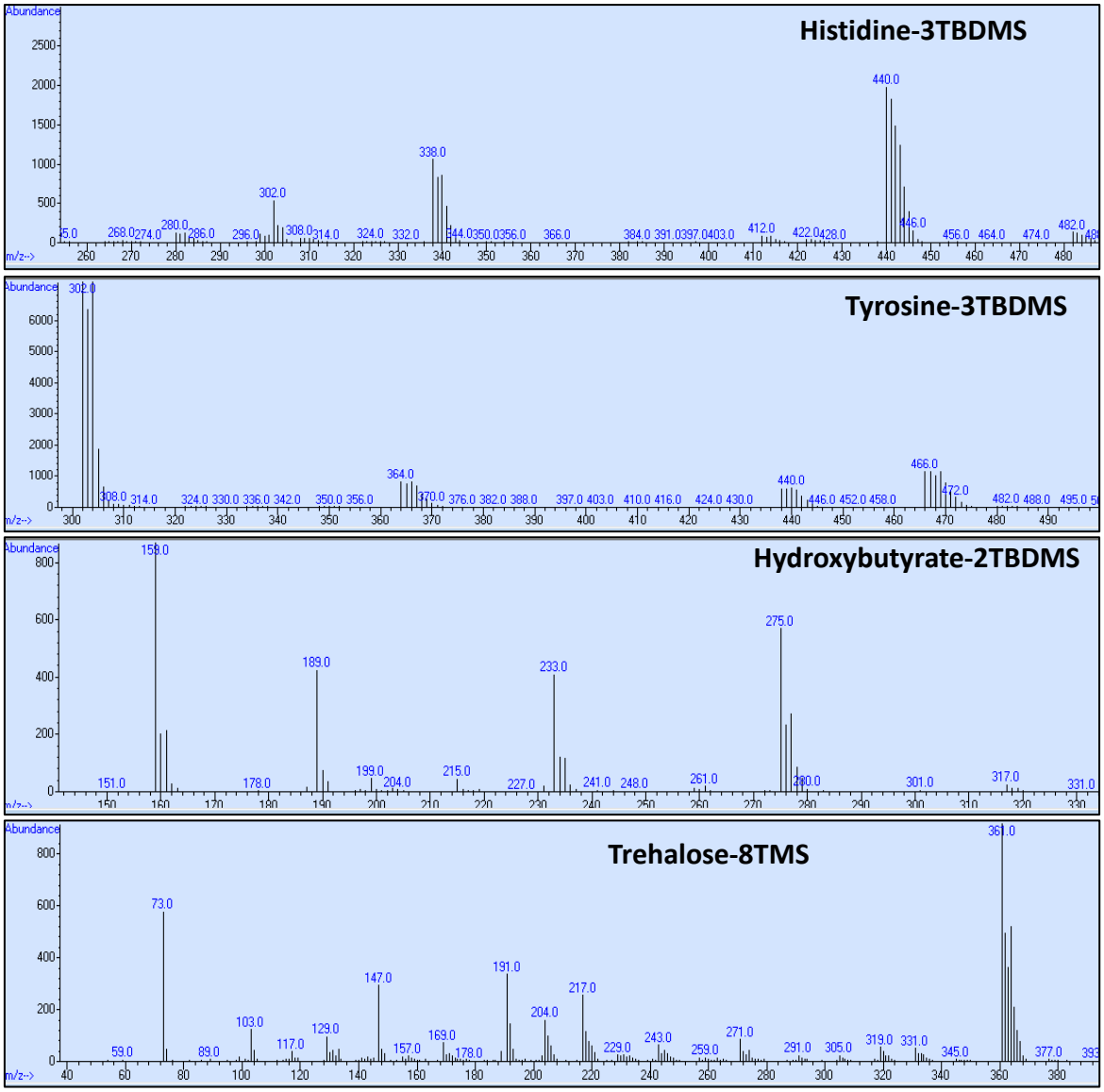

Table A3: MS measurements of valid molecular fragments used for ^{13}C-MFA of early and late exponential cultures of ORS571.

Molecular fragments	MI	Mass isotopomer distribution (fractional abundance)					
		Early exponential cultures			Late exponential cultures		
		Replicate 1	Replicate 2	Replicate 3	Replicate 1	Replicate 2	Replicate 3
Ala 260	M + 0 M + 1 M + 2 M + 3	0.7182 0.0772 0.0402 0.1644	0.7147 0.0757 0.0434 0.1662	0.7125 0.0811 0.0418 0.1647	0.6942 0.0887 0.0499 0.1709	0.6895 0.0900 0.0502 0.1703	0.6870 0.0892 0.0510 0.1728
Ala 232	M + 0 M + 1 M + 2	0.7244 0.1084 0.1672	0.7192 0.1073 0.1735	0.7265 0.1046 0.169	0.7082 0.1146 0.1772	0.7076 0.1150 0.1773	0.7054 0.1159 0.1788

Molecular fragments	MI	Mass isotopomer distribution (fractional abundance)					
		Early exponential cultures			Late exponential cultures		
		Replicate 1	Replicate 2	Replicate 3	Replicate 1	Replicate 2	Replicate 3
Gly 246	M + 0	0.7676	0.765	0.7769	0.7415	0.7422	0.7378
	M + 1	0.0439	0.0444	0.0456	0.0516	0.0508	0.0528
	M + 2	0.1885	0.1905	0.1775	0.2069	0.2071	0.2094
Gly 218	M + 0	0.797	0.7814	0.798	0.7682	0.7659	0.7659
	M + 1	0.203	0.2186	0.202	0.2318	0.2341	0.2341
Val288	M + 0	0.5126	0.518	0.5156	0.4958	0.4962	0.4934
	M + 1	0.13	0.1318	0.1303	0.1360	0.1359	0.1371
	M + 2	0.1597	0.16	0.159	0.1669	0.1652	0.1665
	M + 3	0.1395	0.1354	0.1386	0.1427	0.1439	0.1437
	M + 4	0.0258	0.0254	0.0266	0.0272	0.0274	0.0608
	M + 5	0.0323	0.0294	0.0298	0.0313	0.0314	0.0279
Val260	M + 0				0.5001	0.4989	0.4983
	M + 1				0.1587	0.1570	0.1594
	M + 2				0.2631	0.2618	0.2650
	M + 3				0.0459	0.0497	0.0448
	M + 4				0.0323	0.0326	0.0325
Val186	M + 0				0.5012	0.5032	0.4982
	M + 1				0.1543	0.1535	0.1551
	M + 2				0.2640	0.2647	0.2657
	M + 3				0.0477	0.0457	0.0476
	M + 4				0.0328	0.0330	0.0334
Leu 274	M + 0	0.4244	0.4259	0.4237	0.3993	0.4002	0.3984
	M + 1	0.2184	0.2235	0.2204	0.2301	0.2302	0.2305
	M + 2	0.2334	0.2289	0.2343	0.2405	0.2394	0.2406
	M + 3	0.0826	0.0828	0.083	0.0341	0.0893	0.0896
	M + 4	0.0338	0.032	0.0323	0.0341	0.0339	0.0338
	M + 5	0.0074	0.007	0.0062	0.0069	0.0070	0.0071
Leu200	M + 0				0.3984	0.3945	0.3910
	M + 1				0.2305	0.2284	0.2288
	M + 2				0.2406	0.2439	0.2456
	M + 3				0.0896	0.0912	0.0918
	M + 4				0.0338	0.0350	0.0357
	M + 5				0.0071	0.0070	0.0071
Ile274	M + 0				0.4650	0.4662	0.4614
	M + 1				0.1643	0.1637	0.1658
	M + 2				0.1874	0.1864	0.1877
	M + 3				0.1297	0.1292	0.1303
	M + 4				0.0291	0.0297	0.0302
	M + 5				0.0244	0.0248	0.0246
Ile 200	M + 0	0.4788	0.4882	0.4896	0.4652	0.4660	0.4631
	M + 1	0.1541	0.1551	0.1581	0.1619	0.1623	0.1625
	M + 2	0.181	0.1818	0.1806	0.1885	0.1871	0.1878
	M + 3	0.121	0.1204	0.1189	0.1296	0.1294	0.1310
	M + 4	0.0301	0.025	0.025	0.0299	0.0299	0.0302
	M + 5	0.035	0.0295	0.0278	0.0249	0.0252	0.0253
PHB 275	M + 0	0.8227	0.7784	0.8010	0.6546	0.6174	0.6176
	M + 1	0.0808	0.0826	0.0894	0.1195	0.1284	0.1286
	M + 2	0.1140	0.1300	0.1191	0.1838	0.2048	0.2032
	M + 3	-0.0118	0.0119	-0.0096	0.0252	0.0276	0.0283
	M + 4	-0.0057	-0.0029	0.0002	0.0169	0.0220	0.0224
Met 320	M + 0	0.5516	0.5480	0.5709	0.5443	0.5344	0.5456
	M + 1	0.1781	0.1779	0.1719	0.1841	0.1934	0.1831
	M + 2	0.0628	0.0520	0.0602	0.0711	0.0691	0.0686
	M + 3	0.0365	0.0381	0.0325	0.0280	0.0278	0.0291
	M + 4	0.1348	0.1397	0.1294	0.1377	0.1397	0.1395
	M + 5	0.0362	0.0443	0.0351	0.0348	0.0356	0.0340

Molecular fragments	MI	Mass isotopomer distribution (fractional abundance)					
		Early exponential cultures			Late exponential cultures		
		Replicate 1	Replicate 2	Replicate 3	Replicate 1	Replicate 2	Replicate 3
Met 292	M + 0	0.5864	0.5780	0.5725	0.5594	0.5487	0.5585
	M + 1	0.1914	0.1953	0.1881	0.2040	0.2113	0.2020
	M + 2	0.0414	0.0444	0.0466	0.0549	0.0549	0.0546
	M + 3	0.1427	0.1549	0.1588	0.1462	0.1481	0.1502
	M + 4	0.0381	0.0274	0.0340	0.0356	0.0371	0.0347
Met 218	M + 0	0.5587	0.5712	0.5653	0.5609	0.5480	0.5576
	M + 1	0.1794	0.1783	0.1868	0.2026	0.2125	0.2053
	M + 2	0.0966	0.0615	0.0787	0.0587	0.0612	0.0579
	M + 3	0.1414	0.1559	0.1415	0.1454	0.1435	0.1459
	M + 4	0.0239	0.0331	0.0277	0.0324	0.0348	0.0334
Ser 390	M + 0				0.6579	0.6586	0.6525
	M + 1				0.1173	0.1173	0.1185
	M + 2				0.0814	0.0807	0.0820
	M + 3				0.1434	0.1434	0.1470
Ser 362	M + 0	0.7320	0.7100	0.7032	0.6769	0.6795	0.6723
	M + 1	0.1354	0.1449	0.1497	0.1731	0.1713	0.1753
	M + 2	0.1327	0.1451	0.1471	0.1500	0.1492	0.1523
Ser288	M + 0	0.7274	0.7100	0.7101	0.6801	0.6815	0.6735
	M + 1	0.1385	0.1468	0.1475	0.1714	0.1715	0.1756
	M + 2	0.1341	0.1431	0.1424	0.1485	0.1469	0.1509
Ser302	M + 0	0.7101	0.7737	0.7701	0.7343	0.7363	0.7305
	M + 1	0.1475	0.0473	0.0424	0.0538	0.0544	0.0545
	M + 2	0.1424	0.1789	0.1875	0.2120	0.2093	0.2150
Thr404	M + 0	0.6754	0.6880	0.6786	0.6711	0.6765	0.6728
	M + 1	0.0705	0.0777	0.0676	0.0728	0.0661	0.0695
	M + 2	0.0568	0.0649	0.0808	0.0717	0.0719	0.0699
	M + 3	0.0286	0.0119	0.0082	0.0160	0.0173	0.0196
	M + 4	0.1686	0.1575	0.1648	0.1683	0.1681	0.1682
Thr376	M + 0				0.6908	0.6924	0.6905
	M + 1				0.0880	0.0900	0.0900
	M + 2				0.0506	0.0449	0.0479
	M + 3				0.1706	0.1727	0.1715
Phe336	M + 0	0.2985	0.2918	0.2808	0.2694	0.2687	0.2646
	M + 1	0.1751	0.1747	0.1715	0.1818	0.1815	0.1830
	M + 2	0.1347	0.1404	0.1302	0.1465	0.1454	0.1468
	M + 3	0.1770	0.1870	0.1829	0.1918	0.1924	0.1926
	M + 4	0.0907	0.0898	0.0885	0.0956	0.0954	0.0971
	M + 5	0.0593	0.0595	0.0765	0.0594	0.0606	0.0604
	M + 6	0.0405	0.0341	0.0410	0.0373	0.0369	0.0371
	M + 7	0.0135	0.0146	0.0171	0.0115	0.0117	0.0116
	M + 8	0.0081	0.0066	0.0086	0.0054	0.0061	0.0058
	M + 9	0.0026	0.0015	0.0029	0.0012	0.0013	0.0011
Phe308	M + 0				0.2766	0.2764	0.2734
	M + 1				0.1959	0.1959	0.1953
	M + 2				0.2039	0.2044	0.2062
	M + 3				0.1618	0.1611	0.1619
	M + 4				0.0828	0.0838	0.0839
	M + 5				0.0538	0.0527	0.0547
	M + 6				0.0180	0.0182	0.0178
	M + 7				0.0062	0.0067	0.0056
	M + 8				0.0009	0.0007	0.0013

Molecular fragments	MI	Mass isotopomer distribution (fractional abundance)					
		Early exponential cultures			Late exponential cultures		
		Replicate 1	Replicate 2	Replicate 3	Replicate 1	Replicate 2	Replicate 3
Phe234	M + 0				0.2772	0.2774	0.2735
	M + 1				0.1966	0.1959	0.1969
	M + 2				0.2041	0.2049	0.2052
	M + 3				0.1629	0.1615	0.1631
	M + 4				0.0825	0.0833	0.0831
	M + 5				0.0534	0.0536	0.0541
	M + 6				0.0176	0.0174	0.0179
	M + 7				0.0051	0.0053	0.0055
	M + 8				0.0005	0.0008	0.0006
Phe302	M + 0	0.7553	0.7553	0.7590			
	M + 1	0.0464	0.0464	0.0440			
	M + 2	0.1983	0.1983	0.1970			
Asp418	M + 0	0.6962	0.6916	0.6872	0.6641	0.6627	0.6590
	M + 1	0.0657	0.0631	0.0630	0.0744	0.0742	0.0762
	M + 2	0.0625	0.0664	0.0699	0.0751	0.0755	0.0757
	M + 3	0.0153	0.0157	0.0152	0.0177	0.0175	0.0180
	M + 4	0.1602	0.1632	0.1647	0.1687	0.1699	0.1711
Asp390	M + 0	0.7144	0.7067	0.7071	0.6848	0.6855	0.6839
	M + 1	0.0808	0.0863	0.0801	0.0922	0.0922	0.0921
	M + 2	0.0405	0.0413	0.0426	0.0506	0.0499	0.0514
	M + 3	0.1642	0.1657	0.1702	0.1724	0.1724	0.1726
Asp316	M + 0	0.7092	0.7058	0.7059	0.6849	0.6833	0.6814
	M + 1	0.0801	0.0835	0.0785	0.0904	0.0918	0.0915
	M + 2	0.0435	0.0420	0.0475	0.0516	0.0500	0.0516
	M + 3	0.1672	0.1687	0.1680	0.1731	0.1749	0.1755
Asp302	M + 0	0.7577	0.7577	0.7482	0.7304	0.7295	0.7281
	M + 1	0.0430	0.0430	0.0459	0.0551	0.0555	0.0556
	M + 2	0.1994	0.1994	0.2058	0.2145	0.2150	0.2163
Glu432	M + 0	0.5383	0.5349	0.5294	0.4971	0.4971	0.4926
	M + 1	0.1218	0.1251	0.1244	0.1394	0.1382	0.1398
	M + 2	0.1522	0.1477	0.1522	0.1590	0.1599	0.1611
	M + 3	0.1481	0.1423	0.1416	0.1478	0.1482	0.1492
	M + 4	0.0223	0.0229	0.0235	0.0268	0.0266	0.0270
	M + 5	0.0265	0.0270	0.0288	0.0299	0.0300	0.0303
Glu404	M + 0	0.5513	0.5487	0.5443	0.5172	0.5161	0.5142
	M + 1	0.1509	0.1421	0.1442	0.1569	0.1576	0.1573
	M + 2	0.2373	0.2466	0.2474	0.2589	0.2567	0.2604
	M + 3	0.0296	0.0365	0.0355	0.0378	0.0380	0.0390
	M + 4	0.0309	0.0260	0.0286	0.0292	0.0317	0.0292
Glu330	M + 0	0.5544	0.5505	0.5433	0.5176	0.5165	0.5136
	M + 1	0.1440	0.1434	0.1469	0.1571	0.1576	0.1588
	M + 2	0.2397	0.2434	0.2481	0.2565	0.2567	0.2584
	M + 3	0.0344	0.0339	0.0326	0.0387	0.0380	0.0388
	M + 4	0.0275	0.0289	0.0291	0.0302	0.0309	0.0304
Lys329	M + 0	0.5279	0.5691	0.5298	0.4937	0.4952	0.4902
	M + 1	0.1358	0.1189	0.1340	0.1398	0.1389	0.1407
	M + 2	0.1627	0.1673	0.1615	0.1667	0.1681	0.1677
	M + 3	0.1317	0.1215	0.1318	0.1416	0.1413	0.1433
	M + 4	0.0215	0.0141	0.0258	0.0266	0.0265	0.0278
	M + 5	0.0204	0.0090	0.0171	0.0318	0.0300	0.0303
Arg442	M + 0	0.4509	0.4423	0.4374	0.4076	0.4051	0.4023
	M + 1	0.1832	0.1946	0.1975	0.2047	0.2066	0.2054
	M + 2	0.1406	0.1477	0.1472	0.1491	0.1507	0.1518
	M + 3	0.1436	0.1361	0.1385	0.1547	0.1521	0.1540
	M + 4	0.0385	0.0418	0.0472	0.0493	0.0492	0.0510
	M + 5	0.0340	0.0340	0.0329	0.0285	0.0304	0.0289
	M + 6	0.0092	0.0035	-0.0008	0.0061	0.0061	0.0066

Molecular fragments	MI	Mass isotopomer distribution (fractional abundance)					
		Early exponential cultures			Late exponential cultures		
		Replicate 1	Replicate 2	Replicate 3	Replicate 1	Replicate 2	Replicate 3
Arg414	M + 0				0.4002	0.4129	0.4004
	M + 1				0.2416	0.2300	0.2574
	M + 2				0.2333	0.2291	0.2261
	M + 3				0.0860	0.0877	0.0856
	M + 4				0.0287	0.0279	0.0258
	M + 5				0.0103	0.0123	0.0073
Arg340	M + 0				0.4153	0.4159	0.4108
	M + 1				0.2199	0.2190	0.2223
	M + 2				0.2378	0.2372	0.2389
	M + 3				0.0837	0.0840	0.0835
	M + 4				0.0317	0.0324	0.0334
	M + 5				0.0115	0.0114	0.0111
His440	M + 0				0.3834	0.3711	0.3750
	M + 1				0.2283	0.2355	0.2329
	M + 2				0.1555	0.1477	0.1565
	M + 3				0.1431	0.1445	0.1436
	M + 4				0.0566	0.0583	0.0577
	M + 5				0.0281	0.0328	0.0296
	M + 6				0.0050	0.0101	0.0047
His412	M + 0				0.4162	0.4000	0.4183
	M + 1				0.2232	0.2330	0.2187
	M + 2				0.2602	0.2463	0.2411
	M + 3				0.0683	0.0822	0.0820
	M + 4				0.0367	0.0382	0.0342
	M + 5				0.0046	0.0002	0.0057
His338	M + 0				0.4077	0.4068	0.4020
	M + 1				0.2206	0.2234	0.2233
	M + 2				0.2356	0.2342	0.2370
	M + 3				0.0912	0.0903	0.0917
	M + 4				0.0367	0.0364	0.0368
	M + 5				0.0082	0.0089	0.0093
Tyr466	M + 0	0.3107	0.2954	0.2917	0.2730	0.2739	0.2666
	M + 1	0.1828	0.1891	0.1962	0.1827	0.1822	0.1837
	M + 2	0.1330	0.1381	0.1409	0.1458	0.1470	0.1484
	M + 3	0.1679	0.1839	0.1792	0.1902	0.1891	0.1899
	M + 4	0.0892	0.0840	0.0808	0.0943	0.0928	0.0942
	M + 5	0.0594	0.0558	0.0576	0.0599	0.0593	0.0597
	M + 6	0.0354	0.0308	0.0325	0.0350	0.0360	0.0363
	M + 7	0.0091	0.0131	0.0130	0.0114	0.0112	0.0116
	M + 8	0.0075	0.0047	0.0057	0.0062	0.0063	0.0076
	M + 9	0.0050	0.0052	0.0024	0.0016	0.0021	0.0020
Tyr364	M + 0				0.2825	0.2831	0.2771
	M + 1				0.1947	0.1988	0.1978
	M + 2				0.2023	0.2012	0.2047
	M + 3				0.1608	0.1569	0.1603
	M + 4				0.0810	0.0831	0.0832
	M + 5				0.0531	0.0522	0.0542
	M + 6				0.0179	0.0175	0.0171
	M + 7				0.0065	0.0061	0.0052
	M + 8				0.0011	0.0010	0.0003
Tyr302	M + 0	0.7616	0.7578	0.7605	0.7375	0.7364	0.7316
	M + 1	0.0446	0.0421	0.0423	0.0518	0.0514	0.0538
	M + 2	0.1938	0.2001	0.1972	0.2108	0.2123	0.2146
Pro286	M + 0	0.5009	0.4943	0.5175	0.4989	0.5069	0.5024
	M + 1	0.1417	0.1388	0.1279	0.1362	0.1345	0.1301
	M + 2	0.1505	0.1639	0.1582	0.1607	0.1567	0.1648
	M + 3	0.1497	0.1532	0.1443	0.1493	0.1503	0.1492
	M + 4	0.0286	0.0209	0.0215	0.0276	0.0231	0.0247
	M + 5	0.0286	0.0289	0.0306	0.0273	0.0285	0.0287

Molecular fragments	MI	Mass isotopomer distribution (fractional abundance)					
		Early exponential cultures			Late exponential cultures		
		Replicate 1	Replicate 2	Replicate 3	Replicate 1	Replicate 2	Replicate 3
Pro258	M + 0	0.5480	0.5406	0.5328	0.5172	0.5166	0.5125
	M + 1	0.1448	0.1438	0.1422	0.1523	0.1542	0.1561
	M + 2	0.2472	0.2506	0.2480	0.2584	0.2610	0.2623
	M + 3	0.0363	0.0398	0.0520	0.0410	0.0372	0.0390
	M + 4	0.0237	0.0251	0.0251	0.0312	0.0309	0.0302
Pro184	M + 0	0.5451	0.5354	0.5464	0.5231	0.5247	0.5221
	M + 1	0.1407	0.1404	0.1385	0.1517	0.1519	0.1513
	M + 2	0.2588	0.2528	0.2536	0.2606	0.2613	0.2643
	M + 3	0.0310	0.0404	0.0332	0.0349	0.0334	0.0348
	M + 4	0.0244	0.0310	0.0283	0.0297	0.0287	0.0275
Tre361	M + 0	0.5117	0.4938	0.4821	0.4685	0.4801	0.4704
	M + 1	0.1359	0.1361	0.1385	0.1396	0.1343	0.1391
	M + 2	0.0811	0.0780	0.0887	0.0881	0.0895	0.0912
	M + 3	0.2378	0.2293	0.2126	0.2211	0.2150	0.2184
	M + 4	0.0166	0.0271	0.0367	0.0398	0.0362	0.0359
	M + 5	0.0034	0.0137	0.0167	0.0186	0.0189	0.0197
	M + 6	0.0135	0.0220	0.0246	0.0244	0.0260	0.0254
Tre271	M + 0				0.4902	0.5324	0.5428
	M + 1				0.1229	0.1328	0.1354
	M + 2				0.1047	0.0900	0.1022
	M + 3				0.1916	0.1888	0.1728
	M + 4				0.0448	0.0269	0.0241
	M + 5				0.0126	0.0055	0.0070
	M + 6				0.0333	0.0236	0.0156

Table A4: Reactions in the metabolic model of ORS571 used for flux analysis in early and late exponential under aerobic growth conditions

Reaction ID	Reaction step (s)	Symbol	Reactions
	Uptake fluxes		
R1	Uptake of $^{13}C_4$-succinate	*upt1*	Suc_$^{13}C_4$ -> Suc_in
R2	Uptake of ^{12}C-succinate	*upt2*	Suc_nat -> Suc_in
R3	Total uptake of succinate (constrained)	*upt3*	Suc_in -> Suc
	Tricarboxylic acid cycle		
R4	Succinate dehydrogenase	*tca1*	Suc <-> Fum
R5	Fumarase	*tca2*	Fum <-> Mal
R6	Malate dehydrogenase	*tca3*	Mal <-> OAA
R7	Citrate synthase	*tca4*	OAA + AcCoA -> Cit
R8	Aconitase	*tca5*	Cit <-> ICit
R9	Isocitrate dehydrogenase NADP-dependent	*tca6*	ICit <-> AKG + CO_2
R10	2-Oxoglutarate dehydrogenase	*tca7*	AKG -> SucCoA + CO_2

Reaction ID	Reaction step (s)	Symbol	Reactions
R11	Succinyl-CoA synthetase	*tca8*	SucCoA <-> Suc
R12	Pyruvate dehydrogenase	*tca9*	Pyr -> AcCoA + CO_2
R13	Anaplerotic pathways NAD-dependent malic enzyme	*mal*	Mal -> Pyr + CO_2
R14	Phosphoenolpyruvate carboxykinase	*pepck*	PEP + CO2 <-> OAA
R15	Methylmalonate-semialdehyde dehydrogenase	*msdh*	OAA -> AcCoA + CO_2 + CO_2
R16	Glycolysis Pyruvate kinase	*gly1*	PEP -> Pyr
R17	Gluconeogenesis Phosphoglycerate kinase	*glu1*	PEP <-> PG3
R18	Glyceraldehyde-3-phosphate dehydrogenase	*glu2*	PG3 <-> GAP
R19	Triosephosphate isomerase	*glu3*	GAP <-> DHAP
R20	Fructose-bisphosphate aldolase	*glu4*	DHAP + GAP <-> FBP
R21	Fructose-1,6-bisphosphatase	*glu5*	FBP -> F6P
R22	Phosphoglucose isomerase	*glu6*	F6P <-> G6P
R23	Pentose phosphate pathway Glucose-6-phosphate dehydrogenase	*ppp1*	G6P -> PG6
R24	6-phosphogluconate dehydrogenase	*ppp2*	PG6 -> Ru5P + CO2
R25	Ribulose-phosphate 3-epimerase	*ppp3*	Ru5P <-> X5P
R26	Ribose 5-phosphate isomerase	*ppp4*	Ru5P <-> R5P
R27	Transketolase- C5/C3 conversion	*ppp5*	X5P <-> GAP + EC2
R28	Transketolase- C6/C4 conversion	*ppp6*	F6P <-> E4P + EC2
R29	Transketolase- C7/C5 conversion	*ppp7*	S7P <-> R5P + EC2
R30	Transaldolase- C6/C3 conversion	*ppp8*	F6P <-> GAP + EC3
R31	Transaldolase- C7/C4 conversion	*PPP9*	S7P <-> E4P + EC3
R32	Entner-Doudoroff pathway 6-Phosphogluconate dehydratase	*ed1*	PG6 -> KDPG
R33	2-keto-3-deoxy-6-phosphogluconate aldolase	*ed2*	KDPG -> Pyr + GAP
R34	Amino acid synthesis Glutamate dehydrogenase	*glt*	AKG -> Glu
R35	Glutamine synthetase	*gln*	Glu -> Gln
R36	Proline synthesis	*pro*	Glu -> Pro

Reaction ID	Reaction step (s)	Symbol	Reactions
R37	Arginine synthesis	*arg*	Glu + CO2 + Gln + Asp + AcCoA -> Arg + AKG + Fum + Ac
R38	Aspartate transaminase	*asp*	OAA + Glu -> Asp + AKG
R39	Asparagine synthase	*asn*	Asp -> Asn
R40	Alanine aminotransferase	*ala*	Pyr + Glu -> Ala + AKG
R41	Serine synthesis	*ser*	PG3 + Glu -> Ser + AKG
R42	Serine hydroxymethyltransferase	*glc1*	Ser <-> Gly + MEETHF
R43	MEETHF synthesis	*meethf*	Gly <-> CO2 + MEETHF
R44	Threonine aldolase	*glc2*	Thr -> Gly + AcCoA
R45	Cysteine synthesis	*cys*	Ser + AcCoA -> Cys + Ac
R46	Lysine synthesis	*lys1*	Asp + Pyr + Glu + SucCoA -> LL_DAP + AKG + Suc
R47	Lysine synthesis	*lys2*	LL_DAP -> Lys + CO2
R48	Threonine synthesis	*thr*	Asp -> Thr
R49	Methionine synthesis	*met*	Asp + METHF + Cys + SucCoA -> Met + Pyr + Suc
R50	Valine synthesis	*val*	Pyr + Pyr + Glu -> Val + CO2 + AKG
R51	Leucine synthesis	*leu*	AcCoA + Pyr + Pyr + Glu -> Leu + CO2 + CO2 + AKG
R52	Isoleucine synthesis	*ile*	Thr + Pyr + Glu -> Ile + CO2 + AKG
R53	Phenylalanine synthesis	*phe*	PEP + PEP + E4P + Glu -> Phe + CO2 + AKG
R54	Tyrosine synthesis	*tyr*	PEP + PEP + E4P + Glu -> Tyr + CO2 + AKG
R55	Tryptophan synthesis	*trp*	Ser + R5P + PEP + E4P + PEP + Gln -> Trp + CO2 + GAP + Pyr + Glu
R56	Histidine synthesis	*his*	R5P + FTHF + Gln + Asp -> His + AKG + Fum
R57	METHF synthesis	*methf*	MEETHF -> METHF
R58	FTHF synthesis	*fthf*	MEETHF -> FTHF
R59	Metabolic CO_2 output (net)	*co2.out*	CO2 -> CO2.ext
R60	PHB synthesis	*accoa1*	AcCoA + AcCoA -> PHB + 2CoA

Reaction ID	Reaction step (s)	Symbol	Reactions
R61	Biomass synthesis	*biomass*	Biomass reaction for early exponential cultures: 0.424*Ala + 0.395*Gly + 0.294*Val + 0.349*Leu + 0.204*Ile + 0.163*Pro + 0.096*Met + 0.215*Ser + 0.223*Thr + 0.137*Phe + 0.212*Asn + 0.212*Asp + 0.262*Glu + 0.262*Gln + 0.256*Lys + 0.07*His + 0.119*Tyr + 0.247*Arg + 0.115*Cys + 0.039*Trp + 2.78*AcCoA + 0.184*DHAP + 0.604*PG3 + 0.284*OAA + 0.749*MEETHF + 0.667*R5P + 0.117*G6P + 1.13*PHB = 38.95*Biomass Biomass reaction for late exponential cultures:0.439*Ala + 0.408*Gly + 0.304*Val + 0.362*Leu + 0.211*Ile + 0.169*Pro + 0.1*Met + 0.223*Ser + 0.231*Thr + 0.142*Phe + 0.219*Asn + 0.219*Asp + 0.271*Glu + 0.271*Gln + 0.265*Lys + 0.073*His + 0.123*Tyr + 0.255*Arg + 0.119*Cys + 0.041*Trp + 2.9*AcCoA + 0.192*DHAP + 0.482*PG3 + 0.801*MEETHF + 0.272*OAA + 0.638*R5P + 0.117*G6P + 1.46*PHB -> 40.73*Biomass
R62	Reaction to compensate for naturally occurring ^{12}C pools		0*Ala -> Ala.S
R63	Reaction to compensate for naturally occurring ^{12}C pools		0*Ala_nat -> Ala.S
R64	Reaction to compensate for naturally occurring ^{12}C pools		0*Gly -> Gly.S
R65	Reaction to compensate for naturally occurring ^{12}C pools		0*Gly_nat -> Gly.S
R66	Reaction to compensate for naturally occurring ^{12}C pools		0*Asp -> Asp.S
R67	Reaction to compensate for naturally occurring ^{12}C pools		0*Asp_nat -> Asp.S
R68	Reaction to compensate for naturally occurring ^{12}C pools		0*Val -> Val.S
R69	Reaction to compensate for naturally occurring ^{12}C pools		0*Val_nat -> Val.S
R70	Reaction to compensate for naturally occurring ^{12}C pools		0*Leu -> Leu.S
R71	Reaction to compensate for naturally occurring ^{12}C pools		0*Leu_nat -> Leu.S
R72	Reaction to compensate for naturally occurring ^{12}C pools		0*Ile -> Ile.S
R73	Reaction to compensate for naturally occurring ^{12}C pools		0*Ile_nat -> Ile.S
R74	Reaction to compensate for naturally occurring ^{12}C pools		0*Pro -> Pro.S
R75	Reaction to compensate for naturally occurring ^{12}C pools		0*Pro_nat -> Pro.S
R76	Reaction to compensate for naturally occurring ^{12}C pools		0*Met -> Met.S
R77	Reaction to compensate for naturally occurring ^{12}C pools		0*Met_nat -> Met.S
R78	Reaction to compensate for naturally occurring ^{12}C pools		0*Ser -> Ser.S
R79	Reaction to compensate for naturally occurring ^{12}C pools		0*Ser_nat -> Ser.S
R80	Reaction to compensate for naturally occurring ^{12}C pools		0*Thr -> Thr.S

Reaction ID	Reaction step (s)	Symbol	Reactions
R81	Reaction to compensate for naturally occurring ^{12}C pools		0*Thr_nat -> Thr.S
R82	Reaction to compensate for naturally occurring ^{12}C pools		0*Phe -> Phe.S
R83	Reaction to compensate for naturally occurring ^{12}C pools		0*Phe_nat -> Phe.S
R84	Reaction to compensate for naturally occurring ^{12}C pools		0*Glu -> Glu.S
R85	Reaction to compensate for naturally occurring ^{12}C pools		0*Glu_nat -> Glu.S
R86	Reaction to compensate for naturally occurring ^{12}C pools		0*Lys -> Lys.S
R87	Reaction to compensate for naturally occurring ^{12}C pools		0*Lys_nat -> Lys.S
R88	Reaction to compensate for naturally occurring ^{12}C pools		0*Arg -> Arg.S
R89	Reaction to compensate for naturally occurring ^{12}C pools		0*Arg_nat -> Arg.S
R90	Reaction to compensate for naturally occurring ^{12}C pools		0*His -> His.S
R91	Reaction to compensate for naturally occurring ^{12}C pools		0*His_nat -> His.S
R92	Reaction to compensate for naturally occurring ^{12}C pools		0*Tyr -> Tyr.S
R93	Reaction to compensate for naturally occurring ^{12}C pools		0*Tyr_nat -> Tyr.S
R94	Reaction to compensate for naturally occurring ^{12}C pools		0*PHB -> PHB.S
R95	Reaction to compensate for naturally occurring ^{12}C pools		0*PHB_nat -> PHB.S

Table A5: MS measurements of valid molecular fragments used for ^{13}C-MFA of ORS571 free-living cultures under aerobic growth conditions in the mini reactor set up.

Molecular fragments	Mass isotopomer	Mass isotopomer distribution (fractional abundance)		
		Replicate 1	Replicate 2	Replicate 3
Ala 260	M + 0	0.7109	0.7116	0.7086
	M + 1	0.0796	0.0792	0.0907
	M + 2	0.0436	0.0429	0.0475
	M + 3	0.1659	0.1663	0.1531
Ala 232	M + 0	0.7275	0.7278	0.7282
	M + 1	0.1021	0.1019	0.1127
	M + 2	0.1703	0.1703	0.1591
Gly 246	M + 0	0.7571	0.7597	0.7602
	M + 1	0.0430	0.0427	0.0496
	M + 2	0.1999	0.1976	0.1902
Gly 218	M + 0	0.7798	0.7815	0.7865
	M + 1	0.2202	0.2185	0.2135

Molecular fragments	Mass isotopomer	Mass isotopomer distribution (fractional abundance)		
		Replicate 1	Replicate 2	Replicate 3
Val288	M + 0	0.5285	0.5317	0.5370
	M + 1	0.1260	0.1254	0.1282
	M + 2	0.1585	0.1565	0.1555
	M + 3	0.1366	0.1356	0.1321
	M + 4	0.0229	0.0230	0.0213
	M + 5	0.0275	0.0278	0.0258
Val260	M + 0	0.5300	0.5327	0.5403
	M + 1	0.1447	0.1435	0.1478
	M + 2	0.2523	0.2527	0.2456
	M + 3	0.0439	0.0428	0.0395
	M + 4	0.0291	0.0284	0.0268
Val186	M + 0	0.5333	0.5357	0.5415
	M + 1	0.1428	0.1417	0.1450
	M + 2	0.2543	0.2537	0.2476
	M + 3	0.0402	0.0397	0.0381
	M + 4	0.0294	0.0292	0.0278
Leu 274	M + 0	0.4287	0.4314	0.4377
	M + 1	0.2224	0.2224	0.2250
	M + 2	0.2322	0.2303	0.2260
	M + 3	0.0808	0.0800	0.0777
	M + 4	0.0298	0.0296	0.0279
	M + 5	0.0061	0.0062	0.0057
Leu200	M + 0	0.4237	0.4273	0.4309
	M + 1	0.2217	0.2200	0.2229
	M + 2	0.2358	0.2347	0.2318
	M + 3	0.0835	0.0822	0.0795
	M + 4	0.0303	0.0304	0.0294
	M + 5	0.0050	0.0054	0.0056
Ile274	M + 0	0.4826	0.4821	0.5088
	M + 1	0.1681	0.1723	0.1532
	M + 2	0.1927	0.1936	0.1740
	M + 3	0.1122	0.1104	0.1203
	M + 4	0.0264	0.0254	0.0231
	M + 5	0.0181	0.0163	0.0206
Ile 200	M + 0	0.5088	0.4804	0.5081
	M + 1	0.1532	0.1704	0.1522
	M + 2	0.1740	0.1940	0.1744
	M + 3	0.1203	0.1112	0.1207
	M + 4	0.0231	0.0262	0.0230
	M + 5	0.0206	0.0178	0.0215
PHB 275	M + 0	0.5986	0.5877	0.6751
	M + 1	0.1284	0.1436	0.1054
	M + 2	0.2369	0.2283	0.2163
	M + 3	0.0196	0.0115	0.0028
	M + 4	0.0166	0.0288	0.0005
Met 320	M + 0	0.5716	0.5833	0.5882
	M + 1	0.1753	0.1731	0.1733
	M + 2	0.0628	0.0603	0.0621
	M + 3	0.0224	0.0179	0.0233
	M + 4	0.1376	0.1345	0.1275
	M + 5	0.0304	0.0309	0.0257
Met 292	M + 0	0.5871	0.5966	0.5961
	M + 1	0.1936	0.1861	0.1919
	M + 2	0.0479	0.0440	0.0488
	M + 3	0.1425	0.1442	0.1375
	M + 4	0.0289	0.0291	0.0257
Met 218	M + 0	0.5872	0.5951	0.5988
	M + 1	0.1958	0.1901	0.1915
	M + 2	0.0483	0.0471	0.0508
	M + 3	0.1384	0.1390	0.1315
	M + 4	0.0303	0.0287	0.0273

Molecular fragments	Mass isotopomer	Mass isotopomer distribution (fractional abundance)		
		Replicate 1	Replicate 2	Replicate 3
Ser 390	M + 0	0.6793	0.6798	0.6788
	M + 1	0.1094	0.1090	0.1169
	M + 2	0.0745	0.0747	0.0758
	M + 3	0.1368	0.1365	0.1285
Ser 362	M + 0	0.6951	0.6986	0.7017
	M + 1	0.1616	0.1604	0.1646
	M + 2	0.1433	0.1410	0.1337
Ser288	M + 0	0.6962	0.6994	0.7024
	M + 1	0.1620	0.1609	0.1641
	M + 2	0.1417	0.1396	0.1335
Ser302	M + 0	0.7511	0.7554	0.7551
	M + 1	0.0465	0.0466	0.0509
	M + 2	0.2023	0.1981	0.1940
Thr404	M + 0	0.7020	0.7019	0.6991
	M + 1	0.0618	0.0632	0.0703
	M + 2	0.0609	0.0638	0.0681
	M + 3	0.0127	0.0111	0.0151
	M + 4	0.1626	0.1600	0.1473
Thr376	M + 0	0.7193	0.7199	0.7182
	M + 1	0.0772	0.0770	0.0839
	M + 2	0.0402	0.0390	0.0464
	M + 3	0.1633	0.1640	0.1515
Phe336	M + 0	0.3004	0.3067	0.3083
	M + 1	0.1815	0.1794	0.1828
	M + 2	0.1407	0.1393	0.1419
	M + 3	0.1883	0.1878	0.1874
	M + 4	0.0850	0.0855	0.0828
	M + 5	0.0550	0.0537	0.0513
	M + 6	0.0326	0.0319	0.0305
	M + 7	0.0102	0.0095	0.0090
	M + 8	0.0051	0.0048	0.0046
	M + 9	0.0011	0.0015	0.0014
Phe308	M + 0	0.3072	0.3135	0.3137
	M + 1	0.1943	0.1920	0.1973
	M + 2	0.1998	0.1994	0.1996
	M + 3	0.1539	0.1540	0.1513
	M + 4	0.0747	0.0739	0.0725
	M + 5	0.0488	0.0476	0.0457
	M + 6	0.0149	0.0146	0.0145
	M + 7	0.0056	0.0045	0.0052
	M + 8	0.0008	0.0004	0.0003
Phe234	M + 0	0.3070	0.3124	0.3144
	M + 1	0.1950	0.1930	0.1974
	M + 2	0.2000	0.1990	0.2008
	M + 3	0.1546	0.1533	0.1519
	M + 4	0.0742	0.0744	0.0713
	M + 5	0.0489	0.0482	0.0462
	M + 6	0.0146	0.0145	0.0136
	M + 7	0.0045	0.0045	0.0039
	M + 8	0.0011	0.0008	0.0005
Phe302	M + 0	0.7567	0.7575	0.7602
	M + 1	0.0460	0.0458	0.0478
	M + 2	0.1973	0.1967	0.1920
Asp418	M + 0	0.6880	0.6879	0.6769
	M + 1	0.0665	0.0675	0.0844
	M + 2	0.0660	0.0660	0.0733
	M + 3	0.0140	0.0135	0.0184
	M + 4	0.1655	0.1651	0.1470

Molecular fragments	Mass isotopomer	Mass isotopomer distribution (fractional abundance)		
		Replicate 1	Replicate 2	Replicate 3
Asp316	M + 0	0.7060	0.7080	0.7011
	M + 1	0.0819	0.0806	0.0977
	M + 2	0.0436	0.0434	0.0504
	M + 3	0.1685	0.1680	0.1509
Asp390	M + 0	0.7091	0.7089	0.7020
	M + 1	0.0810	0.0821	0.0982
	M + 2	0.0424	0.0427	0.0504
	M + 3	0.1674	0.1662	0.1495
Asp302	M + 0	0.7458	0.7465	0.7480
	M + 1	0.0489	0.0495	0.0597
	M + 2	0.2053	0.2040	0.1923
Glu432	M + 0	0.5224	0.5242	0.5179
	M + 1	0.1282	0.1276	0.1411
	M + 2	0.1536	0.1533	0.1607
	M + 3	0.1443	0.1434	0.1328
	M + 4	0.0234	0.0235	0.0228
	M + 5	0.0280	0.0279	0.0248
Glu404	M + 0	0.5431	0.5449	0.5409
	M + 1	0.1408	0.1421	0.1566
	M + 2	0.2553	0.2529	0.2430
	M + 3	0.0326	0.0322	0.0341
	M + 4	0.0281	0.0278	0.0253
Glu330	M + 0	0.5390	0.5435	0.5415
	M + 1	0.1448	0.1432	0.1572
	M + 2	0.2534	0.2511	0.2406
	M + 3	0.0339	0.0334	0.0346
	M + 4	0.0288	0.0287	0.0262
Lys329	M + 0	0.5222	0.5306	0.5285
	M + 1	0.1321	0.1288	0.1381
	M + 2	0.1601	0.1552	0.1569
	M + 3	0.1360	0.1351	0.1295
	M + 4	0.0224	0.0226	0.0217
	M + 5	0.0271	0.0277	0.0252
Arg442	M + 0	0.4600	0.4598	0.4567
	M + 1	0.1785	0.1821	0.1881
	M + 2	0.1475	0.1438	0.1488
	M + 3	0.1457	0.1438	0.1397
	M + 4	0.0381	0.0406	0.0361
	M + 5	0.0279	0.0270	0.0269
	M + 6	0.0023	0.0028	0.0037
Arg414	M + 0	0.4703	0.4518	0.4508
	M + 1	0.1953	0.2108	0.2131
	M + 2	0.2280	0.2304	0.2262
	M + 3	0.0675	0.0686	0.0734
	M + 4	0.0332	0.0368	0.0231
	M + 5	0.0056	0.0017	0.0134
Arg340	M + 0	0.4682	0.4675	0.4712
	M + 1	0.1942	0.1941	0.1977
	M + 2	0.2377	0.2357	0.2332
	M + 3	0.0649	0.0657	0.0646
	M + 4	0.0283	0.0297	0.0265
	M + 5	0.0067	0.0073	0.0068
His440	M + 0	0.4137	0.4138	0.4209
	M + 1	0.2248	0.2242	0.2253
	M + 2	0.1457	0.1464	0.1469
	M + 3	0.1366	0.1358	0.1316
	M + 4	0.0493	0.0508	0.0480
	M + 5	0.0271	0.0256	0.0243
	M + 6	0.0029	0.0033	0.0030

Molecular fragments	Mass isotopomer	Mass isotopomer distribution (fractional abundance)		
		Replicate 1	Replicate 2	Replicate 3
His412	M + 0	0.4425	0.4509	0.4514
	M + 1	0.2228	0.2077	0.2235
	M + 2	0.2188	0.2259	0.2204
	M + 3	0.0911	0.0781	0.0780
	M + 4	0.0248	0.0295	0.0234
	M + 5	0.0001	0.0080	0.0033
His338	M + 0	0.4280	0.4280	0.4454
	M + 1	0.2153	0.2153	0.2130
	M + 2	0.2270	0.2270	0.2268
	M + 3	0.0870	0.0870	0.0779
	M + 4	0.0331	0.0331	0.0303
	M + 5	0.0095	0.0095	0.0067
Tyr466	M + 0	0.3011	0.3076	0.3056
	M + 1	0.1826	0.1808	0.1867
	M + 2	0.1417	0.1411	0.1437
	M + 3	0.1874	0.1849	0.1826
	M + 4	0.0853	0.0852	0.0840
	M + 5	0.0541	0.0534	0.0505
	M + 6	0.0324	0.0314	0.0307
	M + 7	0.0092	0.0096	0.0090
	M + 8	0.0048	0.0048	0.0057
	M + 9	0.0013	0.0013	0.0014
Tyr364	M + 0	0.3085	0.3143	0.3130
	M + 1	0.1932	0.1932	0.1959
	M + 2	0.2019	0.1971	0.2005
	M + 3	0.1533	0.1525	0.1523
	M + 4	0.0752	0.0733	0.0726
	M + 5	0.0477	0.0482	0.0461
	M + 6	0.0148	0.0152	0.0142
	M + 7	0.0050	0.0053	0.0050
	M + 8	0.0004	0.0008	0.0005
Tyr302	M + 0	0.7506	0.7504	0.7539
	M + 1	0.0480	0.0489	0.0522
	M + 2	0.2013	0.2007	0.1940
Pro286	M + 0	0.5143	0.5143	0.5347
	M + 1	0.1340	0.1340	0.1335
	M + 2	0.1476	0.1476	0.1536
	M + 3	0.1410	0.1410	0.1316
	M + 4	0.0326	0.0326	0.0228
	M + 5	0.0306	0.0306	0.0239
Pro258	M + 0	0.5422	0.5462	0.5471
	M + 1	0.1414	0.1412	0.1447
	M + 2	0.2559	0.2525	0.2472
	M + 3	0.0327	0.0325	0.0348
	M + 4	0.0279	0.0275	0.0262
Pro184	M + 0	0.5473	0.5491	0.5510
	M + 1	0.1391	0.1393	0.1416
	M + 2	0.2557	0.2555	0.2507
	M + 3	0.0297	0.0288	0.0295
	M + 4	0.0282	0.0273	0.0272
Tre361	M + 0	0.4667	0.5399	0.5337
	M + 1	0.2161	0.1572	0.1320
	M + 2	0.1322	0.0872	0.0830
	M + 3	0.1356	0.1644	0.1948
	M + 4	0.0297	0.0265	0.0276
	M + 5	0.0105	0.0113	0.0136
	M + 6	0.0091	0.0137	0.0153

Table A6 MS measurements of valid molecular fragments used for ^{13}C-MFA of ORS571 free-living cultures grown under micro-aerobic conditions in the mini reactor set up.

Molecular fragments	Mass isotopomer	Mass isotopomer distribution (fractional abundance)		
		Replicate 1	Replicate 2	Replicate 3
Ala 260	M + 0	0.7353	0.7381	0.7386
	M + 1	0.0782	0.0757	0.0698
	M + 2	0.0408	0.0405	0.0358
	M + 3	0.1458	0.1458	0.1558
Ala 232	M + 0	0.7534	0.7524	0.7528
	M + 1	0.0953	0.0972	0.0874
	M + 2	0.1513	0.1504	0.1598
Gly 246	M + 0	0.7822	0.7794	0.7797
	M + 1	0.0443	0.0426	0.0401
	M + 2	0.1734	0.1780	0.1802
Gly 218	M + 0	0.8039	0.8008	0.7974
	M + 1	0.1961	0.1992	0.2026
Val288	M + 0	0.5718	0.5612	0.5659
	M + 1	0.1170	0.1276	0.1106
	M + 2	0.1461	0.1463	0.1491
	M + 3	0.1259	0.1235	0.1308
	M + 4	0.0165	0.0193	0.0189
	M + 5	0.0227	0.0220	0.0247
Val260	M + 0	0.5712	0.5651	0.5663
	M + 1	0.1342	0.1443	0.1270
	M + 2	0.2347	0.2316	0.2418
	M + 3	0.0352	0.0363	0.0394
	M + 4	0.0247	0.0226	0.0255
Val186	M + 0	0.5777	0.5678	0.5726
	M + 1	0.1296	0.1407	0.1246
	M + 2	0.2380	0.2337	0.2472
	M + 3	0.0294	0.0340	0.0286
	M + 4	0.0253	0.0238	0.0271
Leu 274	M + 0	0.4700	0.4747	0.4626
	M + 1	0.2156	0.2157	0.2122
	M + 2	0.2169	0.2165	0.2221
	M + 3	0.0688	0.0647	0.0713
	M + 4	0.0238	0.0243	0.0263
	M + 5	0.0049	0.0041	0.0055
Leu 200	M + 0	0.4669	0.4694	0.4588
	M + 1	0.2130	0.2123	0.2112
	M + 2	0.2215	0.2231	0.2272
	M + 3	0.0692	0.0666	0.0715
	M + 4	0.0251	0.0247	0.0268
	M + 5	0.0042	0.0038	0.0045
Ile274	M + 0	0.5587	0.5142	0.5563
	M + 1	0.1251	0.1712	0.1203
	M + 2	0.1502	0.1837	0.1538
	M + 3	0.1234	0.0946	0.1279
	M + 4	0.0196	0.0221	0.0184
	M + 5	0.0230	0.0142	0.0233
Ile 200	M + 0	0.5597	0.5144	0.5538
	M + 1	0.1222	0.1708	0.1189
	M + 2	0.1509	0.1836	0.1549
	M + 3	0.1247	0.0951	0.1281
	M + 4	0.0191	0.0224	0.0190
	M + 5	0.0234	0.0137	0.0253

Molecular fragments	Mass isotopomer	Mass isotopomer distribution (fractional abundance)		
		Replicate 1	Replicate 2	Replicate 3
PHB 275	M + 0	0.5932	0.6658	0.5791
	M + 1	0.1193	0.1172	0.1230
	M + 2	0.2384	0.1906	0.2470
	M + 3	0.0241	0.0165	0.0254
	M + 4	0.0250	0.0099	0.0255
Met 320	M + 0	0.6538	0.6385	0.6541
	M + 1	0.1269	0.1380	0.1207
	M + 2	0.0553	0.0569	0.0512
	M + 3	0.0179	0.0183	0.0180
	M + 4	0.1297	0.1321	0.1402
	M + 5	0.0164	0.0164	0.0158
Ser 390	M + 0	0.7122	0.7099	0.7063
	M + 1	0.1019	0.0999	0.0969
	M + 2	0.0648	0.0627	0.0687
	M + 3	0.1210	0.1275	0.1280
Ser 362	M + 0	0.7296	0.7250	0.7191
	M + 1	0.1448	0.1429	0.1488
	M + 2	0.1255	0.1321	0.1321
Ser288	M + 0	0.7314	0.7276	0.7246
	M + 1	0.1442	0.1406	0.1463
	M + 2	0.1245	0.1318	0.1291
Ser302	M + 0	0.7745	0.7704	0.7698
	M + 1	0.0493	0.0472	0.0451
	M + 2	0.1761	0.1824	0.1851
Thr404	M + 0	0.7244	0.7206	0.7262
	M + 1	0.0626	0.0651	0.0557
	M + 2	0.0601	0.0602	0.0542
	M + 3	0.0147	0.0074	0.0127
	M + 4	0.1382	0.1466	0.1512
Thr376	M + 0	0.7438	0.7383	0.7380
	M + 1	0.0712	0.0748	0.0750
	M + 2	0.0414	0.0375	0.0371
	M + 3	0.1435	0.1494	0.1498
Phe336	M + 0	0.3437	0.3369	0.3387
	M + 1	0.1832	0.1864	0.1787
	M + 2	0.1368	0.1377	0.1316
	M + 3	0.1802	0.1797	0.1864
	M + 4	0.0726	0.0757	0.0746
	M + 5	0.0455	0.0446	0.0477
	M + 6	0.0254	0.0267	0.0288
	M + 7	0.0078	0.0077	0.0085
	M + 8	0.0040	0.0035	0.0040
	M + 9	0.0008	0.0010	0.0011
Phe308	M + 0	0.3555	0.3449	0.3455
	M + 1	0.1942	0.1995	0.1878
	M + 2	0.1922	0.1938	0.1954
	M + 3	0.1414	0.1415	0.1448
	M + 4	0.0616	0.0655	0.0645
	M + 5	0.0399	0.0394	0.0430
	M + 6	0.0110	0.0108	0.0129
	M + 7	0.0037	0.0040	0.0049
	M + 8	0.0006	0.0006	0.0013
Phe234	M + 0	0.3520	0.3440	0.3458
	M + 1	0.1954	0.2006	0.1909
	M + 2	0.1941	0.1954	0.1939
	M + 3	0.1427	0.1429	0.1457
	M + 4	0.0627	0.0634	0.0650
	M + 5	0.0395	0.0397	0.0432
	M + 6	0.0102	0.0104	0.0112
	M + 7	0.0033	0.0034	0.0040
	M + 8	0.0001	0.0002	0.0004

Molecular fragments	Mass isotopomer	Mass isotopomer distribution (fractional abundance)		
		Replicate 1	Replicate 2	Replicate 3
Phe302	M + 0	0.7862	0.7812	0.7812
	M + 1	0.0411	0.0424	0.0399
	M + 2	0.1727	0.1765	0.1790
Asp418	M + 0	0.7125	0.7160	0.7221
	M + 1	0.0713	0.0649	0.0588
	M + 2	0.0612	0.0602	0.0535
	M + 3	0.0145	0.0121	0.0137
	M + 4	0.1405	0.1469	0.1518
Asp390	M + 0	0.7293	0.7321	0.7371
	M + 1	0.0857	0.0800	0.0700
	M + 2	0.0406	0.0390	0.0371
	M + 3	0.1445	0.1489	0.1558
Asp316	M + 0	0.7301	0.7312	0.7365
	M + 1	0.0827	0.0783	0.0691
	M + 2	0.0421	0.0402	0.0374
	M + 3	0.1450	0.1502	0.1569
Asp302	M + 0	0.7724	0.7717	0.7711
	M + 1	0.0495	0.0454	0.0429
	M + 2	0.1782	0.1828	0.1860
Glu432	M + 0	0.5545	0.5741	0.5588
	M + 1	0.1270	0.1233	0.1139
	M + 2	0.1532	0.1336	0.1484
	M + 3	0.1242	0.1314	0.1351
	M + 4	0.0188	0.0177	0.0184
	M + 5	0.0224	0.0200	0.0255
Glu404	M + 0	0.5690	0.5882	0.5712
	M + 1	0.1453	0.1395	0.1347
	M + 2	0.2287	0.2284	0.2364
	M + 3	0.0322	0.0251	0.0322
	M + 4	0.0249	0.0189	0.0255
Glu330	M + 0	0.5708	0.5878	0.5724
	M + 1	0.1459	0.1398	0.1318
	M + 2	0.2286	0.2250	0.2355
	M + 3	0.0314	0.0267	0.0343
	M + 4	0.0233	0.0207	0.0261
Lys329	M + 0	0.5581	0.5581	0.5604
	M + 1	0.1235	0.1290	0.1194
	M + 2	0.1516	0.1445	0.1484
	M + 3	0.1262	0.1274	0.1289
	M + 4	0.0179	0.0193	0.0196
	M + 5	0.0227	0.0216	0.0233
Arg442	M + 0	0.4598	0.4705	0.4468
	M + 1	0.2002	0.2051	0.2018
	M + 2	0.1346	0.1288	0.1415
	M + 3	0.1381	0.1319	0.1386
	M + 4	0.0422	0.0402	0.0424
	M + 5	0.0220	0.0205	0.0249
	M + 6	0.0032	0.0030	0.0039
Arg414	M + 0	0.4344	0.4515	0.4300
	M + 1	0.2362	0.2444	0.2474
	M + 2	0.2153	0.1969	0.2015
	M + 3	0.0553	0.0647	0.0731
	M + 4	0.0463	0.0305	0.0377
	M + 5	0.0125	0.0120	0.0103
Arg340	M + 0	0.4682	0.4752	0.4608
	M + 1	0.2139	0.2187	0.2147
	M + 2	0.2120	0.2089	0.2154
	M + 3	0.0705	0.0662	0.0734
	M + 4	0.0258	0.0220	0.0264
	M + 5	0.0068	0.0090	0.0092

Molecular fragments	Mass isotopomer	Mass isotopomer distribution (fractional abundance)		
		Replicate 1	Replicate 2	Replicate 3
His440	M + 0	0.4463	0.4446	0.4372
	M + 1	0.2307	0.2246	0.2256
	M + 2	0.1317	0.1393	0.1378
	M + 3	0.1250	0.1241	0.1270
	M + 4	0.0423	0.0439	0.0451
	M + 5	0.0191	0.0195	0.0210
	M + 6	0.0048	0.0040	0.0064
His338	M + 0	0.4675	0.4659	0.4533
	M + 1	0.2166	0.2121	0.2168
	M + 2	0.2041	0.2148	0.2177
	M + 3	0.0765	0.0730	0.0774
	M + 4	0.0270	0.0271	0.0282
	M + 5	0.0083	0.0070	0.0066
Tyr466	M + 0	0.3450	0.3378	0.3353
	M + 1	0.1831	0.1891	0.1779
	M + 2	0.1343	0.1353	0.1345
	M + 3	0.1793	0.1791	0.1857
	M + 4	0.0718	0.0767	0.0760
	M + 5	0.0450	0.0432	0.0474
	M + 6	0.0266	0.0250	0.0279
	M + 7	0.0065	0.0078	0.0091
	M + 8	0.0057	0.0045	0.0046
	M + 9	0.0027	0.0016	0.0016
Tyr364	M + 0	0.3488	0.3428	0.3380
	M + 1	0.1927	0.1979	0.1899
	M + 2	0.1945	0.1949	0.1941
	M + 3	0.1408	0.1439	0.1440
	M + 4	0.0634	0.0634	0.0675
	M + 5	0.0440	0.0405	0.0480
	M + 6	0.0106	0.0122	0.0128
	M + 7	0.0037	0.0041	0.0048
	M + 8	0.0014	0.0003	0.0008
Tyr302	M + 0	0.7826	0.7775	0.7788
	M + 1	0.0415	0.0437	0.0381
	M + 2	0.1759	0.1788	0.1831
Pro286	M + 0	0.5549	0.5702	0.5453
	M + 1	0.1206	0.1220	0.1220
	M + 2	0.1548	0.1421	0.1539
	M + 3	0.1135	0.1180	0.1358
	M + 4	0.0276	0.0258	0.0192
	M + 5	0.0250	0.0219	0.0238
Pro258	M + 0	0.5721	0.5856	0.5740
	M + 1	0.1288	0.1368	0.1293
	M + 2	0.2339	0.2240	0.2349
	M + 3	0.0411	0.0335	0.0366
	M + 4	0.0241	0.0200	0.0252
Pro184	M + 0	0.5754	0.5939	0.5747
	M + 1	0.1259	0.1327	0.1300
	M + 2	0.2334	0.2257	0.2325
	M + 3	0.0405	0.0284	0.0353
	M + 4	0.0247	0.0193	0.0275
Tre361	M + 0	0.5005	0.4342	0.4560
	M + 1	0.1824	0.2249	0.1907
	M + 2	0.1002	0.1344	0.1152
	M + 3	0.1635	0.1531	0.1776
	M + 4	0.0282	0.0312	0.0323
	M + 5	0.0095	0.0119	0.0134
	M + 6	0.0157	0.0103	0.0148
Tre271	M + 0	0.5569	0.4425	0.4691
	M + 1	0.1602	0.2286	0.1860
	M + 2	0.1009	0.1395	0.1185
	M + 3	0.1477	0.1470	0.1737
	M + 4	0.0258	0.0268	0.0292
	M + 5	0.0056	0.0058	0.0090
	M + 6	0.0030	0.0099	0.0146

Table A7: MS measurements of valid molecular fragments used for ^{13}C-MFA of ORS571 free-living cultures grown under micro-aerobic N_2-fixing conditions in the mini reactor set up.

Molecular fragments	Mass isotopomer	Mass isotopomer distribution (fractional abundance)		
		Replicate 1	Replicate 2	Replicate 3
Ala 260	M + 0	0.7519	0.7558	0.7528
	M + 1	0.0912	0.0902	0.0902
	M + 2	0.0417	0.0415	0.0425
	M + 3	0.1153	0.1125	0.1144
Ala 232	M + 0	0.7693	0.7733	0.7713
	M + 1	0.1120	0.1090	0.1089
	M + 2	0.1187	0.1177	0.1198
Gly 246	M + 0	0.8113	0.8122	0.8075
	M + 1	0.0515	0.0520	0.0528
	M + 2	0.1371	0.1358	0.1397
Gly 218	M + 0	0.8359	0.8386	0.8346
	M + 1	0.1641	0.1614	0.1654
Val288	M + 0	0.6054	0.6071	0.6064
	M + 1	0.1448	0.1404	0.1403
	M + 2	0.1227	0.1222	0.1223
	M + 3	0.0936	0.0992	0.0996
	M + 4	0.0191	0.0170	0.0164
	M + 5	0.0144	0.0142	0.0148
Val260	M + 0	0.5656	0.6062	0.5971
	M + 1	0.1501	0.1537	0.1542
	M + 2	0.1699	0.1831	0.1810
	M + 3	0.0945	0.0407	0.0513
	M + 4	0.0199	0.0163	0.0165
Val186	M + 0	0.6060	0.6193	0.6176
	M + 1	0.1541	0.1492	0.1523
	M + 2	0.1835	0.1854	0.1876
	M + 3	0.0400	0.0296	0.0248
	M + 4	0.0164	0.0165	0.0177
Leu 274	M + 0	0.5529	0.5592	0.5531
	M + 1	0.2078	0.1983	0.2036
	M + 2	0.1726	0.1777	0.1774
	M + 3	0.0478	0.0468	0.0475
	M + 4	0.0163	0.0162	0.0163
	M + 5	0.0017	0.0018	0.0021
Ile 200	M + 0	0.5689	0.5833	0.5760
	M + 1	0.1793	0.1747	0.1805
	M + 2	0.1543	0.1590	0.1594
	M + 3	0.0659	0.0609	0.0619
	M + 4	0.0174	0.0158	0.0154
	M + 5	0.0141	0.0063	0.0068
PHB 275	M + 0	0.6248	0.6595	0.6500
	M + 1	0.1504	0.1317	0.1276
	M + 2	0.1871	0.1790	0.1867
	M + 3	0.0222	0.0179	0.0202
	M + 4	0.0155	0.0119	0.0155

Molecular fragments	Mass isotopomer	Mass isotopomer distribution (fractional abundance)		
		Replicate 1	Replicate 2	Replicate 3
Met 320	M + 0	0.6488	0.6756	0.6691
	M + 1	0.1643	0.1363	0.1359
	M + 2	0.0632	0.0622	0.0629
	M + 3	0.0171	0.0209	0.0258
	M + 4	0.0905	0.0921	0.0938
	M + 5	0.0161	0.0128	0.0125
Met 292	M + 0	0.6681	0.7018	0.6972
	M + 1	0.1731	0.1470	0.1459
	M + 2	0.0435	0.0435	0.0460
	M + 3	0.0998	0.0987	0.1004
	M + 4	0.0155	0.0090	0.0105
Met 218	M + 0	0.6673	0.6986	0.7003
	M + 1	0.1750	0.1499	0.1478
	M + 2	0.0484	0.0429	0.0445
	M + 3	0.0939	0.0981	0.0969
	M + 4	0.0154	0.0105	0.0105
Ser 390	M + 0	0.7484	0.7509	0.7440
	M + 1	0.1019	0.0993	0.1022
	M + 2	0.0564	0.0558	0.0556
	M + 3	0.0933	0.0939	0.0981
Ser 362	M + 0	0.7688	0.7724	0.7642
	M + 1	0.1313	0.1321	0.1339
	M + 2	0.0999	0.0955	0.1019
Ser288	M + 0	0.7702	0.7727	0.7690
	M + 1	0.1338	0.1303	0.1317
	M + 2	0.0960	0.0970	0.0993
Ser302	M + 0	0.8042	0.8082	0.7998
	M + 1	0.0546	0.0488	0.0530
	M + 2	0.1412	0.1430	0.1472
Thr404	M + 0	0.7158	0.7399	0.7272
	M + 1	0.0934	0.0784	0.0952
	M + 2	0.0669	0.0632	0.0553
	M + 3	0.0070	0.0118	0.0158
	M + 4	0.1170	0.1068	0.1065
Thr376	M + 0	0.7594	0.7714	0.7539
	M + 1	0.0932	0.0874	0.0873
	M + 2	0.0334	0.0378	0.0477
	M + 3	0.1139	0.1034	0.1111
Phe336	M + 0	0.4037	0.4147	0.4033
	M + 1	0.1980	0.1942	0.1962
	M + 2	0.1253	0.1273	0.1297
	M + 3	0.1445	0.1448	0.1477
	M + 4	0.0648	0.0608	0.0612
	M + 5	0.0360	0.0337	0.0363
	M + 6	0.0171	0.0170	0.0167
	M + 7	0.0071	0.0047	0.0058
	M + 8	0.0029	0.0022	0.0027
	M + 9	0.0007	0.0005	0.0006
Phe302	M + 0	0.8117	0.8139	0.8142
	M + 1	0.0509	0.0478	0.0481
	M + 2	0.1375	0.1383	0.1377
Asp418	M + 0	0.7314	0.7321	0.7339
	M + 1	0.0797	0.0818	0.0796
	M + 2	0.0660	0.0634	0.0629
	M + 3	0.0110	0.0122	0.0111
	M + 4	0.1119	0.1105	0.1126
Asp390	M + 0	0.7515	0.7557	0.7517
	M + 1	0.0941	0.0929	0.0940
	M + 2	0.0386	0.0389	0.0386
	M + 3	0.1159	0.1125	0.1157

Molecular fragments	Mass isotopomer	Mass isotopomer distribution (fractional abundance)		
		Replicate 1	Replicate 2	Replicate 3
Asp316	M + 0	0.7490	0.7512	0.7505
	M + 1	0.0919	0.0933	0.0903
	M + 2	0.0402	0.0404	0.0416
	M + 3	0.1189	0.1151	0.1176
Asp302	M + 0	0.7985	0.8007	0.7988
	M + 1	0.0536	0.0534	0.0533
	M + 2	0.1506	0.1460	0.1479
Glu432	M + 0	0.6114	0.6240	0.6189
	M + 1	0.1410	0.1351	0.1344
	M + 2	0.1132	0.1085	0.1111
	M + 3	0.1066	0.1055	0.1077
	M + 4	0.0143	0.0149	0.0145
	M + 5	0.0135	0.0120	0.0135
Glu404	M + 0	0.6260	0.6447	0.6323
	M + 1	0.1589	0.1472	0.1496
	M + 2	0.1766	0.1750	0.1811
	M + 3	0.0263	0.0208	0.0229
	M + 4	0.0122	0.0123	0.0141
Glu330	M + 0	0.6292	0.6434	0.6384
	M + 1	0.1548	0.1497	0.1488
	M + 2	0.1789	0.1722	0.1781
	M + 3	0.0238	0.0225	0.0214
	M + 4	0.0133	0.0122	0.0132
Lys329	M + 0	0.6014	0.6014	0.5948
	M + 1	0.1569	0.1522	0.1541
	M + 2	0.1275	0.1219	0.1232
	M + 3	0.0928	0.0951	0.0982
	M + 4	0.0139	0.0161	0.0158
	M + 5	0.0075	0.0133	0.0138
Arg442	M + 0	0.5408	0.5697	0.5519
	M + 1	0.2200	0.1959	0.2063
	M + 2	0.1009	0.0974	0.1039
	M + 3	0.0924	0.0996	0.0972
	M + 4	0.0334	0.0236	0.0284
	M + 5	0.0151	0.0118	0.0102
	M + 6	-0.0025	0.0020	0.0021
His338	M + 0	0.5152	0.5487	0.5163
	M + 1	0.2115	0.1996	0.2019
	M + 2	0.1559	0.1717	0.1714
	M + 3	0.0777	0.0614	0.0758
	M + 4	0.0224	0.0164	0.0210
	M + 5	0.0173	0.0022	0.0135
Tyr466	M + 0	0.4009	0.4200	0.4069
	M + 1	0.1983	0.1945	0.1942
	M + 2	0.1261	0.1239	0.1297
	M + 3	0.1413	0.1447	0.1481
	M + 4	0.0652	0.0606	0.0617
	M + 5	0.0335	0.0320	0.0334
	M + 6	0.0204	0.0170	0.0152
	M + 7	0.0071	0.0047	0.0046
	M + 8	0.0036	0.0017	0.0045
	M + 9	0.0034	0.0009	0.0017
Tyr302	M + 0	0.8111	0.8130	0.8082
	M + 1	0.0504	0.0496	0.0523
	M + 2	0.1385	0.1374	0.1395
Pro286	M + 0	0.6011	0.6211	0.5930
	M + 1	0.1539	0.1371	0.1495
	M + 2	0.1149	0.1073	0.1140
	M + 3	0.1030	0.1109	0.1106
	M + 4	0.0203	0.0159	0.0208
	M + 5	0.0069	0.0076	0.0121

Molecular fragments	Mass isotopomer	Mass isotopomer distribution (fractional abundance)		
		Replicate 1	Replicate 2	Replicate 3
Pro258	M + 0	0.6483	0.6449	0.6140
	M + 1	0.1509	0.1490	0.1395
	M + 2	0.1684	0.1606	0.1580
	M + 3	0.0218	0.0343	0.0773
	M + 4	0.0106	0.0113	0.0112
Pro184	M + 0	0.6485	0.0668	0.6222
	M + 1	0.1502	0.1395	0.1440
	M + 2	0.1708	0.1639	0.1588
	M + 3	0.0219	0.0208	0.0611
	M + 4	0.0086	0.0080	0.0139
Tre361	M + 0	0.4580	0.4776	0.4551
	M + 1	0.2006	0.1769	0.2023
	M + 2	0.1180	0.1030	0.1170
	M + 3	0.1591	0.1773	0.1603
	M + 4	0.0378	0.0364	0.0382
	M + 5	0.0161	0.0152	0.0161
	M + 6	0.0104	0.0136	0.0109
Tre271	M + 0	0.4711	0.4882	0.4695
	M + 1	0.1960	0.1716	0.1970
	M + 2	0.1243	0.1092	0.1214
	M + 3	0.1611	0.1761	0.1611
	M + 4	0.0283	0.0302	0.0320
	M + 5	0.0079	0.0109	0.0089
	M + 6	0.0112	0.0139	0.0102

Table A8: Reactions in the metabolic model used for ^{13}C-MFA of ORS571 free-living cultures under aerobic, micro-aerobic and micro-aerobic N_2-fixing conditions

Reaction ID	Reaction step (s)	Symbol	Reactions
	Uptake fluxes		
R1	Uptake of $^{13}C_4$-succinate	*upt1*	Suc_$^{13}C_4$ -> Suc_in
R2	Uptake of ^{12}C-succinate	*upt2*	Suc_nat -> Suc_in
R3	Total uptake of succinate (constrained)	*upt3*	Suc_in -> Suc
	Tricarboxylic acid cycle		
R4	Succinate dehydrogenase	*tca1*	Suc <-> Fum
R5	Fumarase	*tca2*	Fum <-> Mal
R6	Malate dehydrogenase	*tca3*	Mal <-> OAA
R7	Citrate synthase	*tca4*	OAA + AcCoA -> Cit
R8	Aconitase	*tca5*	Cit <-> ICit
R9	Isocitrate dehydrogenase NADP-dependent	*tca6*	ICit <-> AKG + CO_2
R10	2-Oxoglutarate dehydrogenase	*tca7*	AKG -> SucCoA + CO_2
R11	Succinyl-CoA synthetase	*tca8*	SucCoA <-> Suc

Reaction ID	Reaction step (s)	Symbol	Reactions
R12	Pyruvate dehydrogenase	*tca9*	Pyr -> AcCoA + CO_2
R13	Anaplerotic pathways NAD-dependent malic enzyme	*mal*	Mal -> Pyr + CO_2
R14	Phosphoenolpyruvate carboxykinase	*pepck*	PEP + CO2 <-> OAA
R15	Methylmalonate-semialdehyde dehydrogenase	*msdh*	OAA -> AcCoA + CO_2 + CO_2
R16	Glycolysis Pyruvate kinase	*gly1*	PEP -> Pyr
R17	Gluconeogenesis Phosphoglycerate kinase	*glu1*	PEP <-> PG3
R18	Glyceraldehyde-3-phosphate dehydrogenase	*glu2*	PG3 <-> GAP
R19	Triosephosphate isomerase	*glu3*	GAP <-> DHAP
R20	Fructose-bisphosphate aldolase	*glu4*	DHAP + GAP <-> FBP
R21	Fructose-1,6-bisphosphatase	*glu5*	FBP -> F6P
R22	Phosphoglucose isomerase	*glu6*	F6P <-> G6P
R23	Pentose phosphate pathway Glucose-6-phosphate dehydrogenase	*ppp1*	G6P -> PG6
R24	6-phosphogluconate dehydrogenase	*ppp2*	PG6 -> Ru5P + CO2
R25	Ribulose-phosphate 3-epimerase	*ppp3*	Ru5P <-> X5P
R26	Ribose 5-phosphate isomerase	*ppp4*	Ru5P <-> R5P
R27	Transketolase- C5/C3 conversion	*ppp5*	X5P <-> GAP + EC2
R28	Transketolase- C6/C4 conversion	*ppp6*	F6P <-> E4P + EC2
R29	Transketolase- C7/C5 conversion	*ppp7*	S7P <-> R5P + EC2
R30	Transaldolase- C6/C3 conversion	*ppp8*	F6P <-> GAP + EC3
R31	Transaldolase- C7/C4 conversion	*PPP9*	S7P <-> E4P + EC3
R32	Entner-Doudoroff pathway 6-Phosphogluconate dehydratase	*ed1*	PG6 -> KDPG
R33	2-keto-3-deoxy-6-phosphogluconate aldolase	*ed2*	KDPG -> Pyr + GAP
R34	Amino acid synthesis Glutamate dehydrogenase	*glt*	AKG -> Glu
R35	Glutamine synthetase	*gln*	Glu -> Gln
R36	Proline synthesis	*pro*	Glu -> Pro
R37	Arginine synthesis	*arg*	Glu + CO2 + Gln + Asp + AcCoA -> Arg + AKG + Fum + Ac

Reaction ID	Reaction step (s)	Symbol	Reactions
R38	Aspartate transaminase	*asp*	OAA + Glu -> Asp + AKG
R39	Asparagine synthase	*asn*	Asp -> Asn
R40	Alanine aminotransferase	*ala*	Pyr + Glu -> Ala + AKG
R41	Serine synthesis	*ser*	PG3 + Glu -> Ser + AKG
R42	Serine hydroxymethyltransferase	*glc1*	Ser <-> Gly + MEETHF
R43	MEETHF synthesis	*meethf*	Gly <-> CO2 + MEETHF
R44	Threonine aldolase	*glc2*	Thr -> Gly + AcCoA
R45	Cysteine synthesis	*cys*	Ser + AcCoA -> Cys + Ac
R46	Lysine synthesis	*lys1*	Asp + Pyr + Glu + SucCoA -> LL_DAP + AKG + Suc
R47	Lysine synthesis	*lys2*	LL_DAP -> Lys + CO2
R48	Threonine synthesis	*thr*	Asp -> Thr
R49	Methionine synthesis	*met*	Asp + METHF + Cys + SucCoA -> Met + Pyr + Suc
R50	Valine synthesis	*val*	Pyr + Pyr + Glu -> Val + CO2 + AKG
R51	Leucine synthesis	*leu*	AcCoA + Pyr + Pyr + Glu -> Leu + CO2 + CO2 + AKG
R52	Isoleucine synthesis	*ile*	Thr + Pyr + Glu -> Ile + CO2 + AKG
R53	Phenylalanine synthesis	*phe*	PEP + PEP + E4P + Glu -> Phe + CO2 + AKG
R54	Tyrosine synthesis	*tyr*	PEP + PEP + E4P + Glu -> Tyr + CO2 + AKG
R55	Tryptophan synthesis	*trp*	Ser + R5P + PEP + E4P + PEP + Gln -> Trp + CO2 + GAP + Pyr + Glu
R56	Histidine synthesis	*his*	R5P + FTHF + Gln + Asp -> His + AKG + Fum
R57	METHF synthesis	*methf*	MEETHF -> METHF
R58	FTHF synthesis	*fthf*	MEETHF -> FTHF
R59	Metabolic CO_2 output (net)	*co2.out*	CO2 -> CO2.ext
R60	PHB synthesis	*accoa1*	AcCoA + AcCoA -> PHB + 2CoA
R61	Biomass synthesis	*biomass*	Biomass reaction for ORS571 under aerobic condition: 0.439*Ala + 0.408*Gly + 0.304*Val + 0.362*Leu + 0.211*Ile + 0.169*Pro + 0.1*Met + 0.223*Ser + 0.231*Thr + 0.142*Phe + 0.219*Asn + 0.219*Asp + 0.271*Glu + 0.271*Gln + 0.265*Lys + 0.073*His + 0.123*Tyr + 0.255*Arg + 0.119*Cys + 0.041*Trp + 2.9*AcCoA + 0.192*DHAP + 0.482*PG3 + 0.801*MEETHF + 0.272*OAA + 0.638*R5P +

			0.117*G6P + 1.46*PHB -> 40.73*Biomass
			Biomass reaction for ORS571 under micro-aerobic condition: 0.318*Ala + 0.296*Gly + 0.221*Val + 0.262*Leu + 0.154*Ile + 0.123*Pro + 0.073*Met + 0.162*Ser + 0.168*Thr + 0.103*Phe + 0.159*Asn + 0.159*Asp + 0.197*Glu + 0.197*Gln + 0.193*Lys + 0.053*His + 0.089*Tyr + 0.185*Arg + 0.087*Cys + 0.03*Trp + 0.455*AcCoA + 0.03*DHAP + 0.188*PG3 + 0.127*OAA + 0.33*MEETHF + 0.296*R5P + 0.225*G6P + 4.96*PHB -> 40.5*Biomass
			Biomass reaction for ORS571 under micro-aerobic N_2-fixing condition: 0.334*Ala + 0.31*Gly + 0.231*Val + 0.275*Leu + 0.161*Ile + 0.128*Pro + 0.076*Met + 0.169*Ser + 0.175*Thr + 0.108*Phe + 0.167*Asn + 0.167*Asp + 0.206*Glu + 0.206*Gln + 0.202*Lys + 0.055*His + 0.093*Tyr + 0.194*Arg + 0.091*Cys + 0.031*Trp + 0.781*AcCoA + 0.051*DHAP + 0.227*PG3 + 0.145*OAA + 0.384*MEETHF + 0.342*R5P + 0.14*G6P + 5.07*PHB -> 42.39*Biomass
R62	Reaction to compensate for naturally occurring ^{12}C pools		0*Ala -> Ala.S
R63	Reaction to compensate for naturally occurring ^{12}C pools		0*Ala_nat -> Ala.S
R64	Reaction to compensate for naturally occurring ^{12}C pools		0*Gly -> Gly.S
R65	Reaction to compensate for naturally occurring ^{12}C pools		0*Gly_nat -> Gly.S
R66	Reaction to compensate for naturally occurring ^{12}C pools		0*Asp -> Asp.S
R67	Reaction to compensate for naturally occurring ^{12}C pools		0*Asp_nat -> Asp.S
R68	Reaction to compensate for naturally occurring ^{12}C pools		0*Val -> Val.S
R69	Reaction to compensate for naturally occurring ^{12}C pools		0*Val_nat -> Val.S
R70	Reaction to compensate for naturally occurring ^{12}C pools		0*Leu -> Leu.S
R71	Reaction to compensate for naturally occurring ^{12}C pools		0*Leu_nat -> Leu.S
R72	Reaction to compensate for naturally occurring ^{12}C pools		0*Ile -> Ile.S
R73	Reaction to compensate for naturally occurring ^{12}C pools		0*Ile_nat -> Ile.S
R74	Reaction to compensate for naturally occurring ^{12}C pools		0*Pro -> Pro.S
R75	Reaction to compensate for naturally occurring ^{12}C pools		0*Pro_nat -> Pro.S

Reaction ID	Reaction step (s)	Symbol	Reactions
R76	Reaction to compensate for naturally occurring ^{12}C pools		0*Met -> Met.S
R77	Reaction to compensate for naturally occurring ^{12}C pools		0*Met_nat -> Met.S
R78	Reaction to compensate for naturally occurring ^{12}C pools		0*Ser -> Ser.S
R79	Reaction to compensate for naturally occurring ^{12}C pools		0*Ser_nat -> Ser.S
R80	Reaction to compensate for naturally occurring ^{12}C pools		0*Thr -> Thr.S
R81	Reaction to compensate for naturally occurring ^{12}C pools		0*Thr_nat -> Thr.S
R82	Reaction to compensate for naturally occurring ^{12}C pools		0*Phe -> Phe.S
R83	Reaction to compensate for naturally occurring ^{12}C pools		0*Phe_nat -> Phe.S
R84	Reaction to compensate for naturally occurring ^{12}C pools		0*Glu -> Glu.S
R85	Reaction to compensate for naturally occurring ^{12}C pools		0*Glu_nat -> Glu.S
R86	Reaction to compensate for naturally occurring ^{12}C pools		0*Lys -> Lys.S
R87	Reaction to compensate for naturally occurring ^{12}C pools		0*Lys_nat -> Lys.S
R88	Reaction to compensate for naturally occurring ^{12}C pools		0*Arg -> Arg.S
R89	Reaction to compensate for naturally occurring ^{12}C pools		0*Arg_nat -> Arg.S
R90	Reaction to compensate for naturally occurring ^{12}C pools		0*His -> His.S
R91	Reaction to compensate for naturally occurring ^{12}C pools		0*His_nat -> His.S
R92	Reaction to compensate for naturally occurring ^{12}C pools		0*Tyr -> Tyr.S
R93	Reaction to compensate for naturally occurring ^{12}C pools		0*Tyr_nat -> Tyr.S
R94	Reaction to compensate for naturally occurring ^{12}C pools		0*PHB -> PHB.S
R95	Reaction to compensate for naturally occurring ^{12}C pools		0*PHB_nat -> PHB.S

Figure A9: Comparison of the simulated and experimental MS measurements for the flux map showing the metabolic behaviour of ORS571 under aerobic condition. The simulated (black bars) and measured (grey bars) are plotted with MI on X-axis and abundance of MI on Y-axis. There was no significant difference between the simulated and experimentally obtained MS measurements, which confirms the goodness of fit of the flux map. The MS measurements from 46 valid molecular fragments of amino acids, PHB and trehalose used for generating the flux map are– alanine (Ala 232, Ala 260), glycine (Gly 218, Gly 246), valine (Val 186, Val 260, Val 288), leucine (Leu 200, Leu 274), isoleucine (Ile 200, Ile 274), methionine (Met 218, Met 292, Met 320), serine (Ser 288, Ser 302, Ser 362, Ser 390), threonine (Thr 376, Thr 404), proline (Pro 184, Pro 258, Pro 286), phenylalanine (Phe 302, Phe 308, Phe 234, Phe 336),

aspartate (Asp 302, Asp 316, Asp 390, Asp 418), glutamate (Glu 330, Glu 404, Glu 432), lysine (Lys 329), arginine (Arg 340, Arg 414, Arg 442), histidine (His 338, His 412, His 440), tyrosine (Tyr 302, Tyr 364, Tyr 466), PHB (Hb 275) and trehalose (Tre 361).

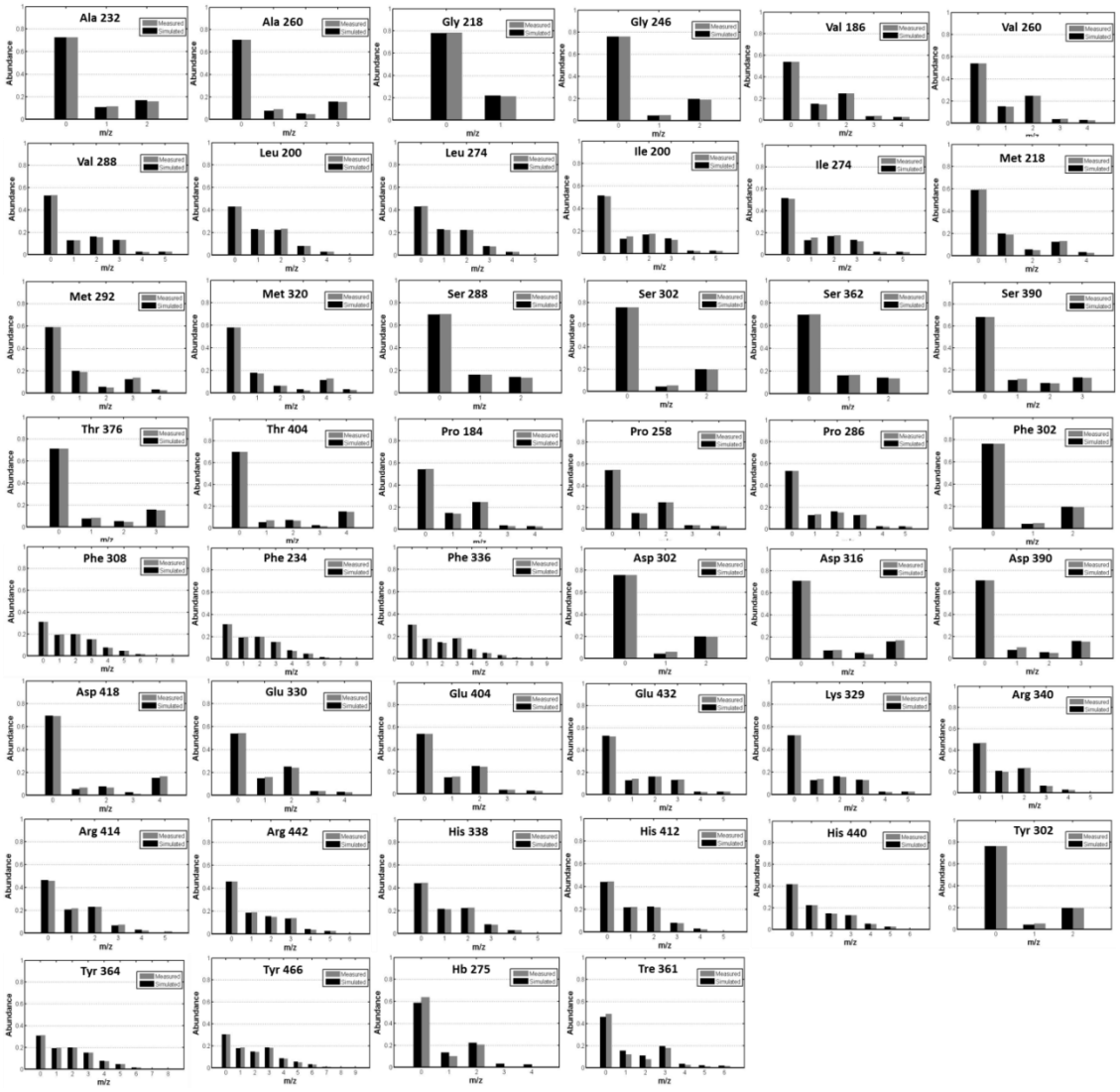

Figure A10: **Comparison of simulated and experimental MS measurements for the flux map showing metabolism of ORS571 under micro-aerobic condition**. The simulated (black bars) and measured (grey bars) are plotted with MI on X-axis and abundance of MI on Y-axis. There was no significant difference between the simulated and experimentally obtained MS measurements, which confirms the goodness of fit of the flux map. The MS measurements from 44 valid molecular fragments of amino acids, PHB and trehalose used for generating te flux map are– alanine (Ala 232, Ala 260), glycine (Gly 218, Gly 246), valine (Val 186, Val 260, Val 288), leucine (Leu 200, Leu 274), isoleucine (Ile 200, Ile 274), methionine (Met 320), serine (Ser 288, Ser 302, Ser 362, Ser 390), threonine (Thr 376, Thr 404), proline (Pro 184, Pro 258, Pro 286), phenylalanine (Phe 302, Phe 308, Phe 234, Phe 336), aspartate (Asp 302, Asp 316, Asp 390, Asp 418), glutamate (Glu 330, Glu 404, Glu 432), lysine (Lys 329), arginine (Arg 340, Arg

414, Arg 442), histidine (His 338, His 440), tyrosine (Tyr 302, Tyr 364, Tyr 466), poly-hydroxybutyrate (PHB 275) and trehalose (Tre 361, Tre 271).

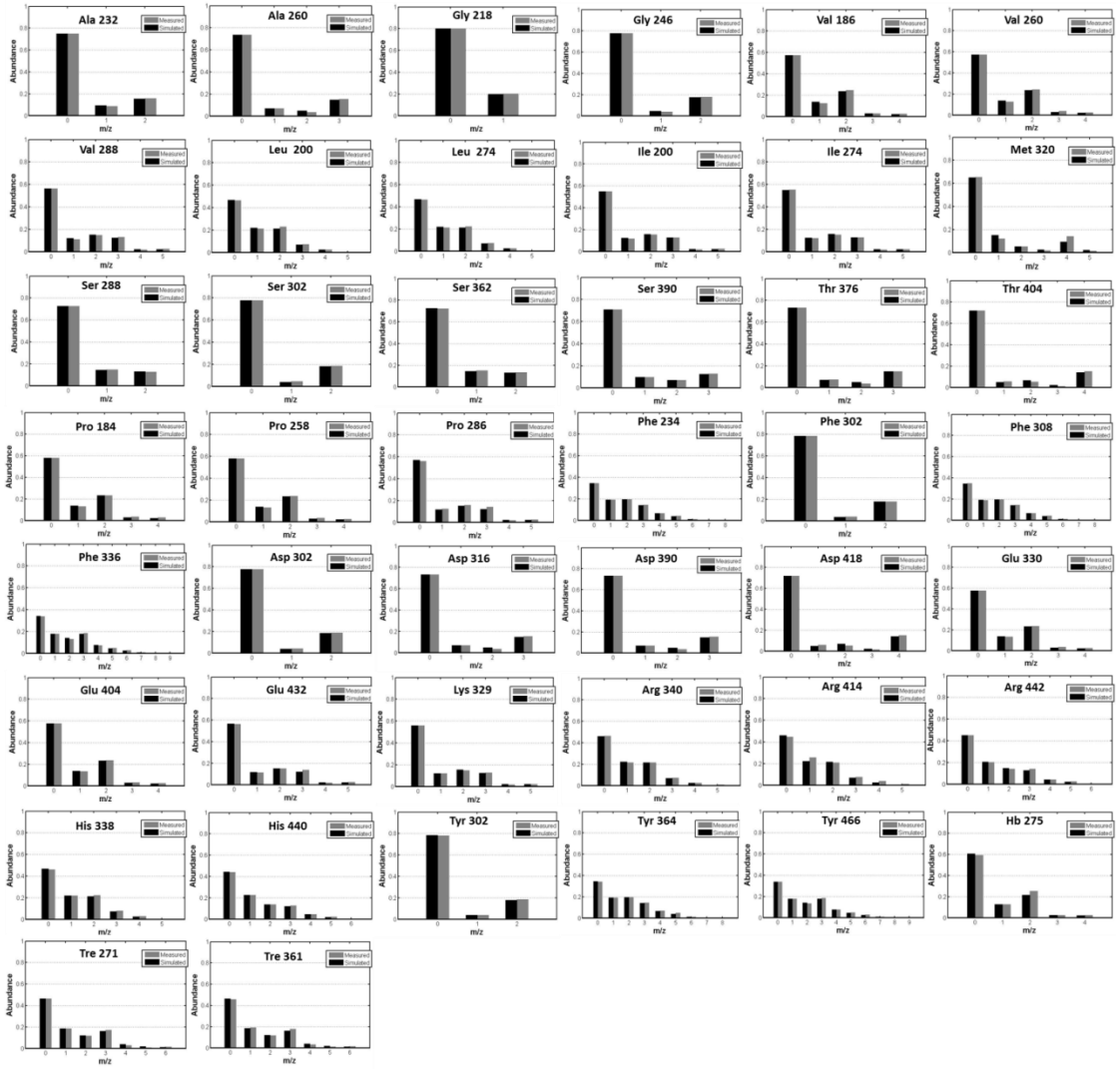

Figure A11: **Comparison of simulated and experimental MS measurements for the flux map showing metabolism of ORS571 under micro-aerobic N_2 fixing conditions**. The simulated (black bars) and measured (grey bars) are plotted with MI on X-axis and abundance of MI on Y-axis. There was no significant difference between the simulated and experimentally obtained MS measurements, which confirms the goodness of fit of the flux map. The MS measurements from 37 valid molecular fragments of amino acids, PHB and trehalose used to generate the flux map are – alanine (Ala 232, Ala 260), glycine (Gly 218, Gly 246), valine (Val 186, Val 260, Val 288), leucine (Leu 274), isoleucine (Ile 200), methionine (Met 218, Met 292, Met 320), serine (Ser 288, Ser 302, Ser 362, Ser 390), threonine (Thr 376, Thr 404), proline (Pro 258, Pro 286), phenylalanine (Phe 302, Phe 336), aspartate (Asp 302, Asp 316, Asp 390, Asp 418), glutamate (Glu 330, Glu 404, Glu 432), lysine (Lys 329), arginine (Arg 442), histidine (His 338), tyrosine (Tyr 302, Tyr 466), poly-hydroxybutyrate (PHB 275) and trehalose (Tre 361, Tre 271).

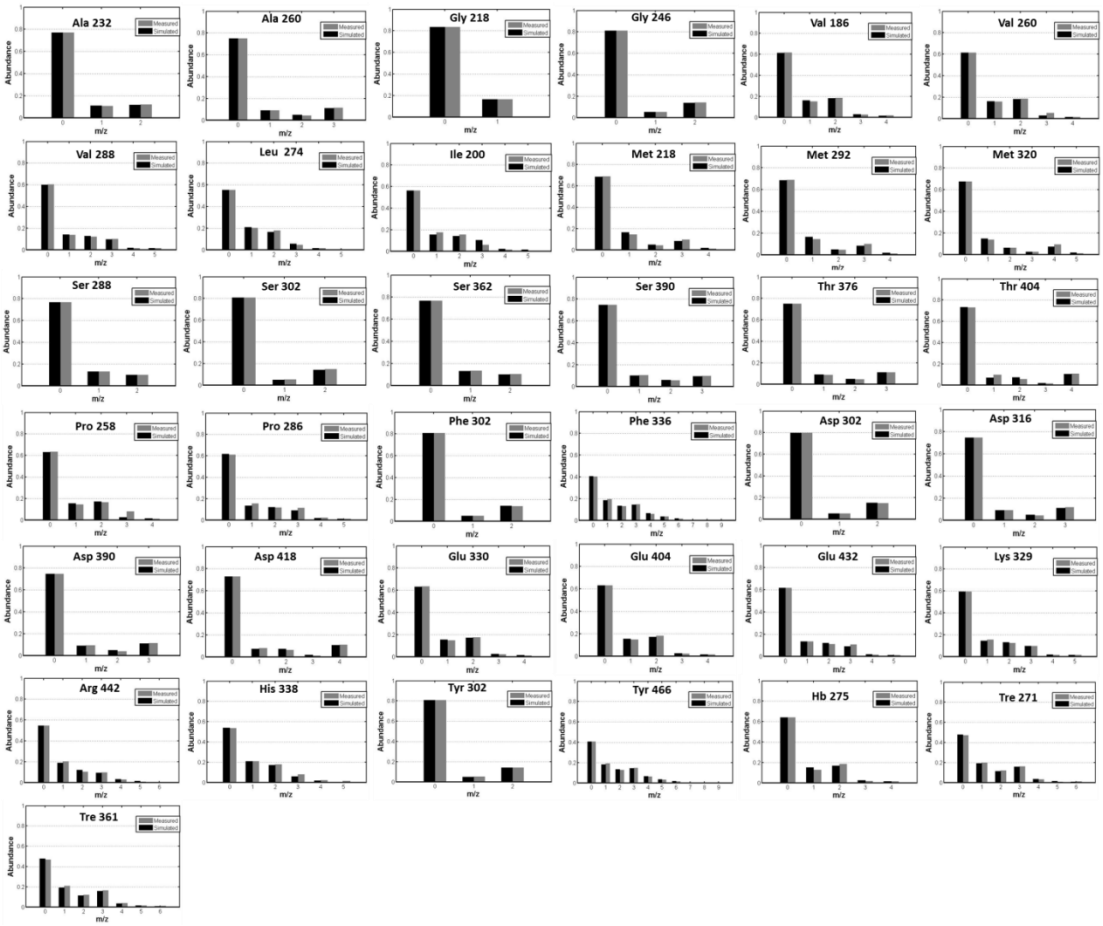

Table A12: Absolute fluxes calculated for ORS571 free-living cultures under aerobic, micro-aerobic and micro-aerobic N_2-fixing conditions

Pathway	Symbol	Net fluxes (µmol h^{-1} g dry $weight^{-1}$)		
		Aerobic condition	Microaerobic condition	Micro-aerobic N_2-fixing condition
Uptake fluxes Uptake of $^{13}C_4$-succinate	*upt1*	20.16837	19.914003	20.222711
Uptake of ^{12}C-succinate	*upt2*	69.83163	77.085997	82.777289
Total uptake of succinate (constrained)	*upt3*	100	100	100
Tricarboxylic acid cycle Succinate dehydrogenase	*tca1*	128.0318	135.898455	170.047335
Fumarase	*tca2*	129.0785	136.672709	170.523504
Malate dehydrogenase	*tca3*	63.32328	106.81446	76.906804
Citrate synthase	*tca4*	41.11479	41.182223	68.451019
Aconitase	*tca5*	41.11479	41.182223	68.451019
Isocitrate dehydrogenase NADP-dependent	*tca6*	41.11479	41.182223	68.451019
2-Oxoglutarate dehydrogenase	*tca7*	38.03175	38.898455	67.047335

Pathway	Symbol	Net fluxes (μmol h^{-1} g dry $weight^{-1}$)		
		Aerobic condition	Microaerobic condition	Micro-aerobic N_2-fixing condition
Succinyl-CoA synthetase	*tca8*	36.86679	38.033118	66.515649
Pyruvate dehydrogenase	*tca9*	60.8103	76.908972	90.553068
Anaplerotic pathways NAD-dependent malic enzyme	*mal*	65.75535	29.858346	93.6167
Phosphoenolpyruvate carboxykinase	*pepck*	60.8103	76.908972	90.553068
Methylmalonate-semialdehyde dehydrogenase	*msdh*	0	0	0
Glycolysis Pyruvate kinase	*gly1*	0.26667	52.021585	0.000000103
Gluconeogenesis Phosphoglycerate kinase	*glu1*	12.55221	8.031309	5.001886
Glyceraldehyde-3-phosphate dehydrogenase	*glu2*	8.04087	5.051372	3.077022
Triosephosphate isomerase	*glu3*	4.42152	2.46186	1.606388
Fructose-bisphosphate aldolase	*glu4*	3.8088	2.364278	1.508847
Fructose-1,6-bisphosphatase	*glu5*	3.8088	2.364278	1.508847
Phosphoglucose isomerase	*glu6*	1.88316	2.440617	1.910238
Pentose phosphate pathway Glucose-6-phosphate dehydrogenase	*ppp1*	1.50975	1.708655	1.642438
6-phosphogluconate dehydrogenase	*ppp2*	0	1.708655	1.642438
Ribulose-phosphate 3-epimerase	*ppp3*	-1.92555	0.076436	0.401391
Ribose 5-phosphate isomerase	*ppp4*	1.92564	1.632316	1.241047
Transketolase- C5/C3 conversion	*ppp5*	-1.92555	0.076436	0.401391
Transketolase- C6/C4 conversion	*ppp6*	1.45107	0.322913	0.021115
Transketolase- C7/C5 conversion	*ppp7*	0.47448	-0.399349	-0.422506
Transaldolase- C6/C3 conversion	*ppp8*	0.47448	-0.399349	-0.422506
Transaldolase- C7/C4 conversion	*PPP9*	-0.47448	0.399349	0.422506
Entner-Doudoroff pathway 6-Phosphogluconate dehydratase	*ed1*	1.50975	0	0
2-keto-3-deoxy-6-phosphogluconate aldolase	*ed2*	1.50975	0	0

Pathway	Symbol	Net fluxes (μmol h^{-1} g dry $weight^{-1}$)		
		Aerobic condition	**Microaerobic condition**	**Micro-aerobic N_2-fixing condition**
Amino acid synthesis Glutamate dehydrogenase	*glt*	19.56285	13.507347	8.344854
Glutamine synthetase	*gln*	2.04264	1.512715	0.929472
Proline synthesis	*pro*	0.53937	0.400125	0.244831
Arginine synthesis	*arg*	0.81387	0.601885	0.371006
Aspartate transaminase	*asp*	6.5682	3.721696	2.289175
Asparagine synthase	*asn*	0.69894	0.517301	0.319403
Alanine aminotransferase	*ala*	1.40112	1.034505	0.638703
Serine synthesis	*ser*	2.97306	2.368352	1.490719
Serine hydroxymethyltransferase	*glc1*	1.43154	1.22317	0.788877
MEETHF synthesis	*meethf*	1.67715	0.260251	0.196009
Threonine aldolase	*glc2*	1.54782	0.000000097	0.000000103
Cysteine synthesis	*cys*	0.69894	0.520502	0.319403
Lysine synthesis	*lys1*	0.84573	0.627881	0.386353
Lysine synthesis	*lys2*	0.84573	0.627881	0.386353
Threonine synthesis	*thr*	2.95848	1.047503	0.642617
Methionine synthesis	*met*	0.31914	0.237456	0.145333
Valine synthesis	*val*	0.9702	0.718964	0.441767
Leucine synthesis	*leu*	1.15533	0.852339	0.525918
Isoleucine synthesis	*ile*	0.67347	0.501005	0.307867
Phenylalanine synthesis	*phe*	0.45324	0.335038	0.206515
Tyrosine synthesis	*tyr*	0.39258	0.289545	0.177881
Tryptophan synthesis	*trp*	0.13086	0.097582	0.059328
Histidine synthesis	*his*	0.23301	0.172466	0.105163
METHF synthesis	*methf*	0.31914	0.237456	0.145333
FTHF synthesis	*fthf*	0.23301	0.172466	0.105163
Metabolic CO_2 output (net)	*co_2.out*	227.1244	253.987225	329.656341
PHB synthesis	*accoa1*	4.65975	16.13595	9.696008

Pathway	Symbol	Net fluxes (μmol h^{-1} g dry $weight^{-1}$)		
		Aerobic condition	Microaerobic condition	Micro-aerobic N_2-fixing condition
Biomass synthesis	*biomass*	3.19158	3.253186	1.912401
Lipid synthesis	*accoa2*	9.18	1.4744	1.4935
DNA synthesis	*r5p1*	0.18	0.097	0.0515
RNA synthesis	*r5p2*	1.854	0.8633	0.5871
Carbohydrates synthesis	*g6p1*	0.342	0.6984	0.1854
EPS synthesis	*g6p2*	0.027	0.0291	0.0721

Table A13: MS measurements of valid molecular fragments used for ^{13}C-MFA of ORS571 bacteroids isolated from root nodules of *S.rotrata* under micro-aerobic conditions.

Molecular fragments	Mass isotopomer	Mass isotopomer distribution (fractional abundance)		
		Replicate 1	Replicate 2	Replicate 3
Ala 232	M + 0	0.9076	0.9105	0.9086
	M + 1	0.0335	0.0303	0.0320
	M + 2	0.0590	0.0592	0.0594
Gly 246	M + 0	0.9341	0.9327	0.9349
	M + 1	0.0243	0.0251	0.0233
	M + 2	0.0416	0.0423	0.0418
Val288	M + 0	0.8573	0.8597	0.8599
	M + 1	0.0559	0.0522	0.0539
	M + 2	0.0344	0.0365	0.0339
	M + 3	0.0328	0.0322	0.0323
	M + 4	0.0049	0.0049	0.0049
	M + 5	0.0147	0.0146	0.0151
Val186	M + 0	0.8522	0.8562	0.8546
	M + 1	0.0489	0.0453	0.0495
	M + 2	0.0647	0.0660	0.0640
	M + 3	0.0179	0.0174	0.0157
	M + 4	0.0162	0.0151	0.0161
Leu 274	M + 0	0.8548	0.8544	0.8544
	M + 1	0.0704	0.0705	0.0705
	M + 2	0.0426	0.0430	0.0430
	M + 3	0.0182	0.0183	0.0183
	M + 4	0.0107	0.0108	0.0108
	M + 5	0.0033	0.0031	0.0031
Ile274	M + 0	0.8715	0.8677	0.8677
	M + 1	0.0638	0.0673	0.0673
	M + 2	0.0387	0.0403	0.0403
	M + 3	0.0170	0.0166	0.0166
	M + 4	0.0059	0.0053	0.0053
	M + 5	0.0030	0.0028	0.0028
Ile 200	M + 0	0.8619	0.8655	0.8655
	M + 1	0.0653	0.0628	0.0628
	M + 2	0.0409	0.0401	0.0401
	M + 3	0.0175	0.0177	0.0177
	M + 4	0.0078	0.0077	0.0077
	M + 5	0.0066	0.0062	0.0062

Molecular fragments	Mass isotopomer	Mass isotopomer distribution (fractional abundance)		
		Replicate 1	Replicate 2	Replicate 3
PHB 275	M + 0	0.7178	0.7148	0.7207
	M + 1	0.0562	0.0557	0.0556
	M + 2	0.1848	0.1887	0.1855
	M + 3	0.0104	0.0080	0.0081
	M + 4	0.0309	0.0327	0.0301
Met 320	M + 0	0.8633	0.8646	0.8659
	M + 1	0.0716	0.0707	0.0761
	M + 2	0.0063	0.0056	0.0071
	M + 3	0.0165	0.0160	0.0108
	M + 4	0.0283	0.0229	0.0293
	M + 5	0.0140	0.0133	0.0108
Met 292	M + 0	0.8916	0.8890	0.8922
	M + 1	0.0668	0.0708	0.0664
	M + 2	0.0063	0.0033	0.0045
	M + 3	0.0259	0.0294	0.0275
	M + 4	0.0094	0.0074	0.0094
Met 218	M + 0	0.8872	0.8896	0.8929
	M + 1	0.0692	0.0672	0.0653
	M + 2	0.0081	0.0085	0.0075
	M + 3	0.0278	0.0275	0.0263
	M + 4	0.0077	0.0072	0.0080
Ser 390	M + 0	0.9077	0.9110	0.9094
	M + 1	0.0503	0.0486	0.0488
	M + 2	0.0208	0.0189	0.0200
	M + 3	0.0212	0.0215	0.0218
Ser 362	M + 0	0.9209	0.9208	0.9205
	M + 1	0.0589	0.0573	0.0571
	M + 2	0.0202	0.0219	0.0224
Ser288	M + 0	0.9181	0.9196	0.9197
	M + 1	0.0581	0.0568	0.0579
	M + 2	0.0238	0.0236	0.0224
Ser302	M + 0	0.9377	0.9283	0.9354
	M + 1	0.0218	0.0282	0.0229
	M + 2	0.0405	0.0436	0.0417
Thr404	M + 0	0.9151	0.9069	0.9194
	M + 1	0.0335	0.0398	0.0361
	M + 2	0.0105	0.0050	0.0062
	M + 3	0.0008	0.0061	0.0017
	M + 4	0.0401	0.0421	0.0365
Thr376	M + 0	0.9074	0.9062	0.9277
	M + 1	0.0415	0.0435	0.0319
	M + 2	0.0068	0.0100	0.0054
	M + 3	0.0443	0.0403	0.0350
Phe302	M + 0	0.9430	0.9399	0.9417
	M + 1	0.0239	0.0254	0.0254
	M + 2	0.0330	0.0347	0.0329
Asp418	M + 0	0.8864	0.8880	0.8866
	M + 1	0.0499	0.0484	0.0493
	M + 2	0.0097	0.0100	0.0097
	M + 3	0.0029	0.0027	0.0031
	M + 4	0.0511	0.0509	0.0513
Asp390	M + 0	0.9040	0.9041	0.9013
	M + 1	0.0383	0.0370	0.0399
	M + 2	0.0069	0.0069	0.0067
	M + 3	0.0509	0.0520	0.0521
Asp316	M + 0	0.8964	0.8986	0.8969
	M + 1	0.0397	0.0371	0.0397
	M + 2	0.0082	0.0095	0.0086
	M + 3	0.0557	0.0548	0.0548

Molecular fragments	Mass isotopomer	Mass isotopomer distribution (fractional abundance)		
		Replicate 1	Replicate 2	Replicate 3
Asp302	M + 0	0.9111	0.9117	0.9110
	M + 1	0.0303	0.0293	0.0305
	M + 2	0.0586	0.0590	0.0586
Glu432	M + 0	0.8456	0.8434	0.8438
	M + 1	0.0622	0.0639	0.0635
	M + 2	0.0327	0.0333	0.0330
	M + 3	0.0405	0.0406	0.0410
	M + 4	0.0053	0.0050	0.0051
	M + 5	0.0137	0.0139	0.0136
Glu404	M + 0	0.8676	0.8600	0.8651
	M + 1	0.0474	0.0548	0.0495
	M + 2	0.0642	0.0634	0.0640
	M + 3	0.0072	0.0062	0.0073
	M + 4	0.0136	0.0156	0.0141
Glu330	M + 0	0.8597	0.8602	0.8575
	M + 1	0.0548	0.0542	0.0568
	M + 2	0.0637	0.0640	0.0645
	M + 3	0.0075	0.0072	0.0073
	M + 4	0.0143	0.0144	0.0140
Lys329	M + 0	0.8669	0.8676	0.8697
	M + 1	0.0593	0.0597	0.0571
	M + 2	0.0308	0.0313	0.0324
	M + 3	0.0273	0.0267	0.0267
	M + 4	0.0038	0.0028	0.0027
	M + 5	0.0119	0.0119	0.0114
Arg442	M + 0	0.8689	0.8702	0.8711
	M + 1	0.0732	0.0718	0.0708
	M + 2	0.0163	0.0178	0.0164
	M + 3	0.0232	0.0250	0.0244
	M + 4	0.0102	0.0086	0.0095
	M + 5	0.0062	0.0058	0.0065
	M + 6	0.0020	0.0008	0.0013
Arg340	M + 0	0.8666	0.8727	0.8643
	M + 1	0.0656	0.0622	0.0671
	M + 2	0.0384	0.0356	0.0373
	M + 3	0.0175	0.0180	0.0176
	M + 4	0.0084	0.0082	0.0088
	M + 5	0.0035	0.0033	0.0049
His440	M + 0	0.8804	0.8777	0.8798
	M + 1	0.0674	0.0702	0.0695
	M + 2	0.0174	0.0178	0.0178
	M + 3	0.0221	0.0196	0.0204
	M + 4	0.0062	0.0076	0.0076
	M + 5	0.0065	0.0051	0.0044
	M + 6	0.0000	0.0019	0.0006
Tyr302	M + 0	0.9391	0.9380	0.9376
	M + 1	0.0262	0.0274	0.0273
	M + 2	0.0346	0.0346	0.0351
Pro258	M + 0	0.8878	0.8865	0.8867
	M + 1	0.0489	0.0480	0.0483
	M + 2	0.0407	0.0414	0.0379
	M + 3	0.0145	0.0168	0.0181
	M + 4	0.0081	0.0073	0.0090
Pro184	M + 0	0.9043	0.9060	0.9076
	M + 1	0.0451	0.0452	0.0420
	M + 2	0.0410	0.0403	0.0417
	M + 3	0.0031	0.0009	0.0018
	M + 4	0.0065	0.0075	0.0070

Table A14: MS measurements of valid molecular fragments used for ^{13}C-MFA of ORS571 bacteroids isolated from stem nodules of *S.rotrata* under micro-aerobic conditions.

Molecular fragments	Mass isotopomer	Mass isotopomer distribution (fractional abundance)		
		Replicate 1	Replicate 2	Replicate 3
Ala 260	M + 0	0.9348	0.9325	0.9325
	M + 1	0.0324	0.0350	0.0350
	M + 2	0.0033	0.0025	0.0025
	M + 3	0.0296	0.0300	0.0300
Ala 232	M + 0	0.9440	0.9435	0.9434
	M + 1	0.0261	0.0261	0.0268
	M + 2	0.0299	0.0305	0.0298
Ala158	M + 0	0.9053	0.9056	0.9054
	M + 1	0.0292	0.0304	0.0322
	M + 2	0.0655	0.0604	0.0624
Gly 246	M + 0	0.9654	0.9672	0.9660
	M + 1	0.0227	0.0216	0.0225
	M + 2	0.0119	0.0112	0.0115
Gly 218	M + 0	0.9733	0.9731	0.9749
	M + 1	0.0267	0.0269	0.0251
Val288	M + 0	0.9064	0.9063	0.9065
	M + 1	0.0524	0.0535	0.0541
	M + 2	0.0171	0.0169	0.0163
	M + 3	0.0155	0.0150	0.0145
	M + 4	0.0019	0.0017	0.0019
	M + 5	0.0067	0.0067	0.0067
Val260	M + 0	0.9089	0.9080	0.9111
	M + 1	0.0519	0.0521	0.0497
	M + 2	0.0288	0.0296	0.0295
	M + 3	0.0037	0.0036	0.0031
	M + 4	0.0066	0.0066	0.0067
Val186	M + 0	0.9052	0.9047	0.9053
	M + 1	0.0444	0.0451	0.0448
	M + 2	0.0329	0.0328	0.0334
	M + 3	0.0096	0.0106	0.0096
	M + 4	0.0079	0.0069	0.0069
Leu 274	M + 0	0.9086	0.9082	0.9072
	M + 1	0.0630	0.0641	0.0633
	M + 2	0.0162	0.0162	0.0170
	M + 3	0.0071	0.0071	0.0073
	M + 4	0.0039	0.0036	0.0039
	M + 5	0.0011	0.0010	0.0013
Leu200	M + 0	0.8976	0.8966	0.8967
	M + 1	0.0631	0.0636	0.0627
	M + 2	0.0261	0.0262	0.0267
	M + 3	0.0075	0.0077	0.0081
	M + 4	0.0045	0.0046	0.0043
	M + 5	0.0012	0.0013	0.0015
Ile274	M + 0	0.9262	0.9203	0.9227
	M + 1	0.0543	0.0586	0.0531
	M + 2	0.0130	0.0123	0.0144
	M + 3	0.0034	0.0043	0.0056
	M + 4	0.0013	0.0022	0.0016
	M + 5	0.0018	0.0024	0.0026
PHB 275	M + 0	0.7910	0.7910	0.7909
	M + 1	0.0505	0.0505	0.0511
	M + 2	0.1299	0.1299	0.1298
	M + 3	0.0068	0.0068	0.0069
	M + 4	0.0217	0.0217	0.0213
Ser 390	M + 0	0.9412	0.9408	0.9396
	M + 1	0.0442	0.0451	0.0443
	M + 2	0.0082	0.0075	0.0088
	M + 3	0.0064	0.0066	0.0074

Molecular fragments	Mass isotopomer	Mass isotopomer distribution (fractional abundance)		
		Replicate 1	Replicate 2	Replicate 3
Ser 362	M + 0	0.9533	0.9492	0.9504
	M + 1	0.0407	0.0439	0.0424
	M + 2	0.0060	0.0069	0.0072
Ser288	M + 0	0.9539	0.9521	0.9510
	M + 1	0.0384	0.0403	0.0405
	M + 2	0.0077	0.0075	0.0085
Ser302	M + 0	0.9564	0.9561	0.9573
	M + 1	0.0264	0.0261	0.0254
	M + 2	0.0172	0.0179	0.0173
Phe302	M + 0	0.9660	0.9663	0.9415
	M + 1	0.0253	0.0254	0.0286
	M + 2	0.0086	0.0082	0.0299
Asp418	M + 0	0.9240	0.9228	0.9228
	M + 1	0.0446	0.0470	0.0470
	M + 2	0.0044	0.0031	0.0031
	M + 3	0.0010	0.0013	0.0013
	M + 4	0.0261	0.0257	0.0257
Asp390	M + 0	0.9364	0.9364	0.9356
	M + 1	0.0362	0.0362	0.0352
	M + 2	0.0023	0.0023	0.0025
	M + 3	0.0251	0.0251	0.0267
Asp316	M + 0	0.9287	0.9283	0.9294
	M + 1	0.0350	0.0343	0.0348
	M + 2	0.0045	0.0054	0.0049
	M + 3	0.0318	0.0319	0.0309
Asp302	M + 0	0.9420	0.9399	0.9416
	M + 1	0.0288	0.0305	0.0283
	M + 2	0.0292	0.0297	0.0301
Glu432	M + 0	0.8797	0.8760	0.8772
	M + 1	0.0578	0.0609	0.0604
	M + 2	0.0232	0.0244	0.0239
	M + 3	0.0280	0.0272	0.0276
	M + 4	0.0027	0.0028	0.0023
	M + 5	0.0086	0.0087	0.0086
Glu404	M + 0	0.8975	0.8969	0.8969
	M + 1	0.0475	0.0475	0.0475
	M + 2	0.0441	0.0435	0.0435
	M + 3	0.0030	0.0032	0.0032
	M + 4	0.0080	0.0089	0.0089
Glu330	M + 0	0.8915	0.8915	0.8924
	M + 1	0.0487	0.0487	0.0484
	M + 2	0.0463	0.0463	0.0455
	M + 3	0.0050	0.0050	0.0055
	M + 4	0.0085	0.0085	0.0083
Lys329	M + 0	0.9306	0.9277	0.9362
	M + 1	0.0540	0.0541	0.0592
	M + 2	0.0037	0.0095	0.0025
	M + 3	0.0091	0.0070	0.0036
	M + 4	0.0006	0.0004	-0.0011
	M + 5	0.0021	0.0014	-0.0004
Tyr302	M + 0	0.9740	0.9728	0.9740
	M + 1	0.0232	0.0240	0.0236
	M + 2	0.0027	0.0033	0.0025

Table A15: Metabolic model used for ^{13}C-MFA of ORS571 bacteroids isolated from root and stem nodules of *S. rostrata*.

Reaction ID	Reaction step (s)	Symbol	Reactions
	Uptake fluxes		
R1	Uptake of $^{13}C_4$-succinate	*upt1*	Suc_$^{13}C_4$ -> Suc_in
R2	Uptake of ^{12}C-succinate	*upt2*	Suc_nat -> Suc_in
R3	Total uptake of succinate (constrained)	*upt3*	Suc_in -> Suc
	Tricarboxylic acid cycle		
R4	Succinate dehydrogenase	*tca1*	Suc <-> Fum
R5	Fumarase	*tca2*	Fum <-> Mal
R6	Malate dehydrogenase	*tca3*	Mal <-> OAA
R7	Citrate synthase	*tca4*	OAA + AcCoA -> Cit
R8	Aconitase	*tca5*	Cit <-> ICit
R9	Isocitrate dehydrogenase NADP-dependent	*tca6*	ICit <-> AKG + CO_2
R10	2-Oxoglutarate dehydrogenase	*tca7*	AKG -> SucCoA + CO_2
R11	Succinyl-CoA synthetase	*tca8*	SucCoA <-> Suc
R12	Pyruvate dehydrogenase	*tca9*	Pyr -> AcCoA + CO_2
	Anaplerotic pathways		
R13	NAD-dependent malic enzyme	*mal*	Mal -> Pyr + CO_2
R14	Phosphoenolpyruvate carboxykinase	*pepck*	PEP + CO2 <-> OAA
R15	Methylmalonate-semialdehyde dehydrogenase	*msdh*	OAA -> AcCoA + CO_2 + CO_2
	Glycolysis		
R16	Pyruvate kinase	*gly1*	PEP -> Pyr
	Gluconeogenesis		
R17	Phosphoglycerate kinase	*glu1*	PEP <-> PG3
R18	Glyceraldehyde-3-phosphate dehydrogenase	*glu2*	PG3 <-> GAP
R19	Triosephosphate isomerase	*glu3*	GAP <-> DHAP
R20	Fructose-bisphosphate aldolase	*glu4*	DHAP + GAP <-> FBP
R21	Fructose-1,6-bisphosphatase	*glu5*	FBP -> F6P
R22	Phosphoglucose isomerase	*glu6*	F6P <-> G6P
	Pentose phosphate pathway		
R23	Glucose-6-phosphate dehydrogenase	*ppp1*	G6P -> PG6
R24	6-phosphogluconate dehydrogenase	*ppp2*	PG6 -> Ru5P + CO2

Reaction ID	Reaction step (s)	Symbol	Reactions
R25	Ribulose-phosphate 3-epimerase	*ppp3*	Ru5P <-> X5P
R26	Ribose 5-phosphate isomerase	*ppp4*	Ru5P <-> R5P
R27	Transketolase- C5/C3 conversion	*ppp5*	X5P <-> GAP + EC2
R28	Transketolase- C6/C4 conversion	*ppp6*	F6P <-> E4P + EC2
R29	Transketolase- C7/C5 conversion	*ppp7*	S7P <-> R5P + EC2
R30	Transaldolase- C6/C3 conversion	*ppp8*	F6P <-> GAP + EC3
R31	Transaldolase- C7/C4 conversion	*PPP9*	S7P <-> E4P + EC3
R32	Entner-Doudoroff pathway 6-Phosphogluconate dehydratase	*ed1*	PG6 -> KDPG
R33	2-keto-3-deoxy-6-phosphogluconate aldolase	*ed2*	KDPG -> Pyr + GAP
R34	Amino acid synthesis Glutamate dehydrogenase	*glt*	AKG -> Glu
R35	Glutamine synthetase	*gln*	Glu -> Gln
R36	Proline synthesis	*pro*	Glu -> Pro
R37	Arginine synthesis	*arg*	Glu + CO2 + Gln + Asp + AcCoA -> Arg + AKG + Fum + Ac
R38	Aspartate transaminase	*asp*	OAA + Glu -> Asp + AKG
R39	Asparagine synthase	*asn*	Asp -> Asn
R40	Alanine aminotransferase	*ala*	Pyr + Glu -> Ala + AKG
R41	Serine synthesis	*ser*	PG3 + Glu -> Ser + AKG
R42	Serine hydroxymethyltransferase	*glc1*	Ser <-> Gly + MEETHF
R43	MEETHF synthesis	*meethf*	Gly <-> CO2 + MEETHF
R44	Threonine aldolase	*glc2*	Thr -> Gly + AcCoA
R45	Cysteine synthesis	*cys*	Ser + AcCoA -> Cys + Ac
R46	Lysine synthesis	*lys1*	Asp + Pyr + Glu + SucCoA -> LL_DAP + AKG + Suc
R47	Lysine synthesis	*lys2*	LL_DAP -> Lys + CO2
R48	Threonine synthesis	*thr*	Asp -> Thr
R49	Methionine synthesis	*met*	Asp + METHF + Cys + SucCoA -> Met + Pyr + Suc
R50	Valine synthesis	*val*	Pyr + Pyr + Glu -> Val + CO2 + AKG
R51	Leucine synthesis	*leu*	AcCoA + Pyr + Pyr + Glu -> Leu + CO2 + CO2 + AKG
R52	Isoleucine synthesis	*ile*	Thr + Pyr + Glu -> Ile + CO2 + AKG

Reaction ID	Reaction step (s)	Symbol	Reactions
R53	Phenylalanine synthesis	*phe*	PEP + PEP + E4P + Glu -> Phe + CO2 + AKG
R54	Tyrosine synthesis	*tyr*	PEP + PEP + E4P + Glu -> Tyr + CO2 + AKG
R55	Tryptophan synthesis	*trp*	Ser + R5P + PEP + E4P + PEP + Gln -> Trp + CO2 + GAP + Pyr + Glu
R56	Histidine synthesis	*his*	R5P + FTHF + Gln + Asp -> His + AKG + Fum
R57	METHF synthesis	*methf*	MEETHF -> METHF
R58	FTHF synthesis	*fthf*	MEETHF -> FTHF
R59	Metabolic CO_2 output (net)	*co2.out*	CO2 -> CO2.ext
R60	PHB synthesis	*accoa1*	AcCoA + AcCoA -> PHB + 2CoA
R61	Biomass synthesis	*biomass*	Biomass reaction for root nodule bacteroid: 0.095*Ala + 0.088*Gly + 0.066*Val + 0.078*Leu + 0.046*Ile + 0.037*Pro + 0.022*Met + 0.048*Ser + 0.05*Thr + 0.031*Phe + 0.048*Asn + 0.048*Asp + 0.059*Glu + 0.059*Gln + 0.058*Lys + 0.016*His + 0.027*Tyr + 0.055*Arg + 0.026*Cys + 0.009*Trp + 2.95*AcCoA + 0.195*DHAP + 0.325*PG3 + 0.405*MEETHF + 0.155*OAA + 0.362*R5P + 0.717*G6P + 5.6*PHB -> 41.65*Biomass
			Biomass reaction for stem nodule bacteroid: 0.155*Ala + 0.144*Gly + 0.107*Val + 0.128*Leu + 0.075*Ile + 0.06*Pro + 0.035*Met + 0.079*Ser + 0.081*Thr + 0.05*Phe + 0.077*Asn + 0.077*Asp + 0.096*Glu + 0.096*Gln + 0.094*Lys + 0.026*His + 0.043*Tyr + 0.09*Arg + 0.042*Cys + 0.014*Trp + 1.954*AcCoA + 0.123*DHAP + 0.215*PG3 + 0.273*MEETHF + 0.106*OAA + 0.247*R5P + 0.42*G6P + 6.069*PHB -> 41.15*Biomass
R62	Reaction to compensate for naturally occurring ^{12}C pools		0*Ala -> Ala.S
R63	Reaction to compensate for naturally occurring ^{12}C pools		0*Ala_nat -> Ala.S
R64	Reaction to compensate for naturally occurring ^{12}C pools		0*Gly -> Gly.S
R65	Reaction to compensate for naturally occurring ^{12}C pools		0*Gly_nat -> Gly.S
R66	Reaction to compensate for naturally occurring ^{12}C pools		0*Asp -> Asp.S
R67	Reaction to compensate for naturally occurring ^{12}C pools		0*Asp_nat -> Asp.S
R68	Reaction to compensate for naturally occurring ^{12}C pools		0*Val -> Val.S
R69	Reaction to compensate for naturally occurring ^{12}C pools		0*Val_nat -> Val.S

Reaction ID	Reaction step (s)	Symbol	Reactions
R70	Reaction to compensate for naturally occurring ^{12}C pools		0*Leu -> Leu.S
R71	Reaction to compensate for naturally occurring ^{12}C pools		0*Leu_nat -> Leu.S
R72	Reaction to compensate for naturally occurring ^{12}C pools		0*Ile -> Ile.S
R73	Reaction to compensate for naturally occurring ^{12}C pools		0*Ile_nat -> Ile.S
R74	Reaction to compensate for naturally occurring ^{12}C pools		0*Pro -> Pro.S
R75	Reaction to compensate for naturally occurring ^{12}C pools		0*Pro_nat -> Pro.S
R76	Reaction to compensate for naturally occurring ^{12}C pools		0*Met -> Met.S
R77	Reaction to compensate for naturally occurring ^{12}C pools		0*Met_nat -> Met.S
R78	Reaction to compensate for naturally occurring ^{12}C pools		0*Ser -> Ser.S
R79	Reaction to compensate for naturally occurring ^{12}C pools		0*Ser_nat -> Ser.S
R80	Reaction to compensate for naturally occurring ^{12}C pools		0*Thr -> Thr.S
R81	Reaction to compensate for naturally occurring ^{12}C pools		0*Thr_nat -> Thr.S
R82	Reaction to compensate for naturally occurring ^{12}C pools		0*Phe -> Phe.S
R83	Reaction to compensate for naturally occurring ^{12}C pools		0*Phe_nat -> Phe.S
R84	Reaction to compensate for naturally occurring ^{12}C pools		0*Glu -> Glu.S
R85	Reaction to compensate for naturally occurring ^{12}C pools		0*Glu_nat -> Glu.S
R86	Reaction to compensate for naturally occurring ^{12}C pools		0*Lys -> Lys.S
R87	Reaction to compensate for naturally occurring ^{12}C pools		0*Lys_nat -> Lys.S
R88	Reaction to compensate for naturally occurring ^{12}C pools		0*Arg -> Arg.S
R89	Reaction to compensate for naturally occurring ^{12}C pools		0*Arg_nat -> Arg.S
R90	Reaction to compensate for naturally occurring ^{12}C pools		0*His -> His.S
R91	Reaction to compensate for naturally occurring ^{12}C pools		0*His_nat -> His.S
R92	Reaction to compensate for naturally occurring ^{12}C pools		0*Tyr -> Tyr.S
R93	Reaction to compensate for naturally occurring ^{12}C pools		0*Tyr_nat -> Tyr.S
R94	Reaction to compensate for naturally occurring ^{12}C pools		0*PHB -> PHB.S
R95	Reaction to compensate for naturally occurring ^{12}C pools		0*PHB_nat -> PHB.S

Figure A16: **Comparison of the simulated and experimental MS measurements for the flux map of bacteroids isolated from root nodules of *S. rotrata***. The simulated (black bars) and measured (grey bars) are plotted with MI on X-axis and abundance of MI on Y-axis. There was no significant difference between the simulated and experimentally obtained MS measurements, which confirms the goodness of fit of the flux map. The MS measurements from 33 valid molecular fragments of amino acids, and PHB used for generating the flux map are– alanine (Ala 232), glycine (Gly 218, Gly 246), valine (Val 186, Val 288), leucine (Leu 274), isoleucine (Ile 200, Ile 274), methionine (Met 218, Met 292, Met 320), serine (Ser 288, Ser 302, Ser 362, Ser 390), threonine (Thr 376, Thr 404), proline (Pro 184, Pro 258, Pro 286), phenylalanine (Phe 302), aspartate (Asp 302, Asp 316, Asp 390, Asp 418), glutamate (Glu 330, Glu 404, Glu 432), lysine (Lys 329), arginine (Arg 340, Arg 442), histidine (His 440), tyrosine (Tyr 302), and poly-hydroxybutyrate (PHB 275).

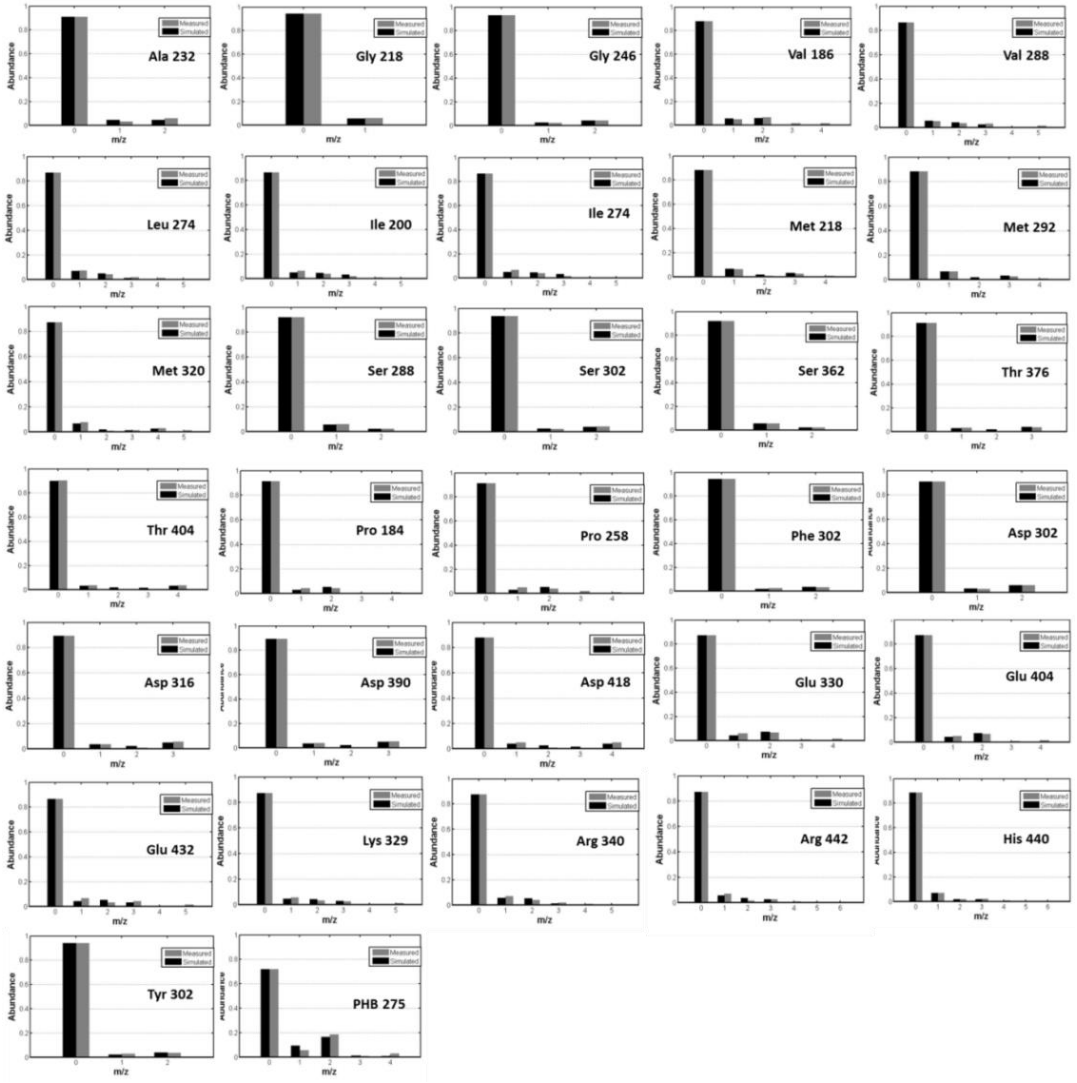

Figure A17: **Comparison of the simulated and experimental MS measurements for the flux map of bacteroids isolated from the stem nodules of *S. rostrata*.** The simulated (black bars) and measured (grey bars) are plotted with MI on X-axis and abundance of MI on Y-axis. There was no significant difference between the simulated and experimentally obtained MS measurements, which confirms the goodness of fit of the flux map. The MS measurements from 26 valid molecular fragments of amino acids, and PHB used for generating the flux map are– alanine (Ala 158, Ala 232, Ala 260), glycine (Gly 218, Gly 246), valine (Val 186, Val 260, Val 288), leucine (Leu 200, Leu 274), isoleucine (Ile 200), serine (Ser 288, Ser 302, Ser 362, Ser 390), aspartate (Asp 302, Asp 316, Asp 390, Asp 418), glutamate (Glu 330, Glu 404, Glu 432), lysine (Lys 329), tyrosine (Tyr 302), and poly-hydroxybutyrate (PHB 275).

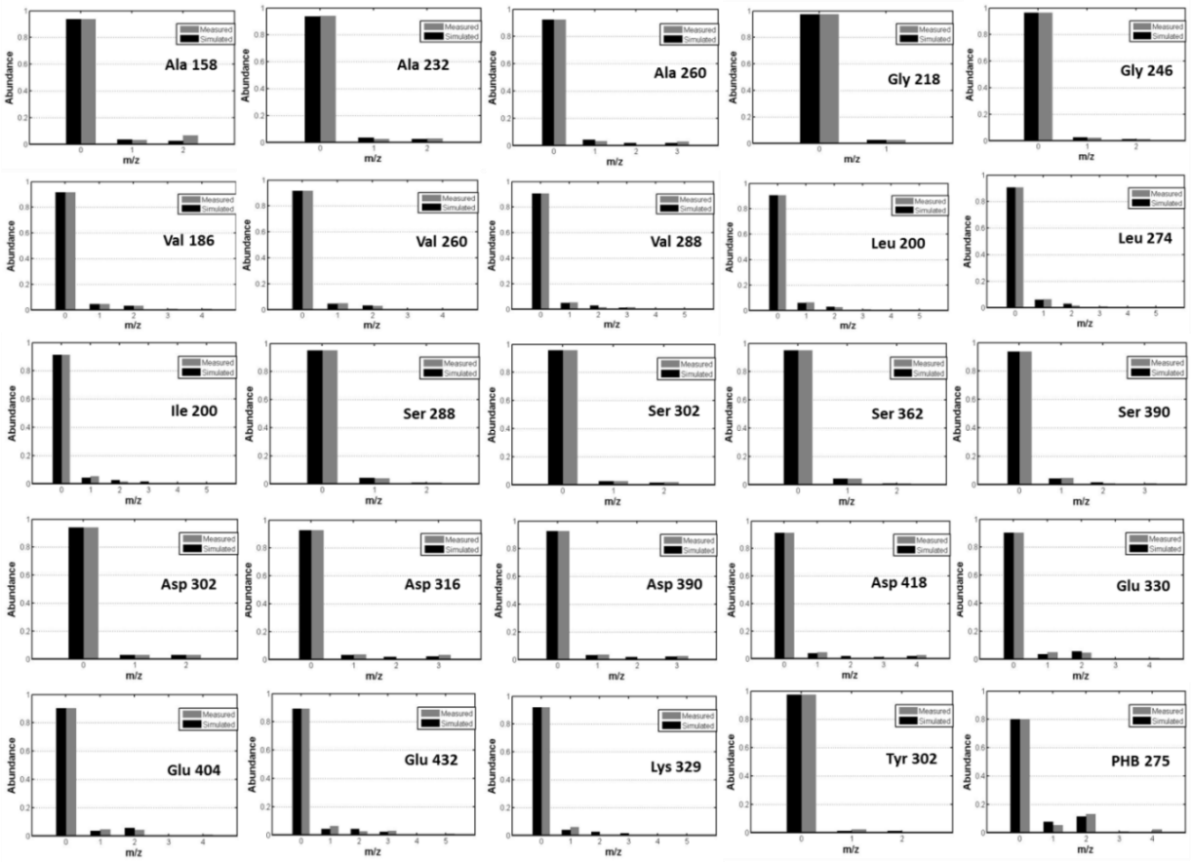

A18. **The alignment statistics for the best match obtained for 16SrRNA analysis of OPS0865**

Best match:- *Azorhizobium caulinodans* strain ORS 571 16S ribosomal RNA gene, complete sequence (Length: 1020).

Score	Expect	Identities	Gaps	Strand
1136 bits(615)	**0.0**	**644/656(98%)**	**9/656(1%)**	**Plus/Plus**

```
Query  2    ACAATGGGCGCAAGCCTGATCCAGCCATGCCGCGTGAGTGATGAAGGCCTTAGGGTTGTA  61
           ||||||||||||||||||||||||||||||||||||||||||||||||||||||||||||
Sbjct  310  ACAATGGGCGCAAGCCTGATCCAGCCATGCCGCGTGAGTGATGAAGGCCTTAGGGTTGTA  369
```

```
Query  62   AAGCTCTTTCGCCGGTGAAGATAATGACGGTAACCGGAGAAGAAGCCCCGGCTAACTTCG  121
            ||||||||||||||||||||||||||||||||||||||||||||||||||||||||||||
Sbjct  370  AAGCTCTTTCGCCGGTGAAGATAATGACGGTAACCGGAGAAGAAGCCCCGGCTAACTTCG  429

Query  122  TGCCAGCAGCCGCGGTAATACGAAGGGGGCAAGCGTTGCTCGGAATCACTGGGCGTAAAG  181
            ||||||||||||||||||||||||||||||||||||||||||||||||||||||||||||
Sbjct  430  TGCCAGCAGCCGCGGTAATACGAAGGGGGCAAGCGTTGCTCGGAATCACTGGGCGTAAAG  489

Query  182  CGCACGTAGGCGGATCGTTAAGTCAGGGGTGAAAGCCTGGAGCTCAACTCCAGAACTGCC  241
            ||||||||||||||||||||||||||||||||||||||||||||||||||||||||||||
Sbjct  490  CGCACGTAGGCGGATCGTTAAGTCAGGGGTGAAAGCCTGGAGCTCAACTCCAGAACTGCC  549

Query  242  CTTGATACTGGCGATCTTGAGTTCGAGAGAGGTTGGTGGAACTCCGAGTGTAGAGGTGAA  301
            ||||||||||||||||||||||||||||||||||||||||||||||||||||||||||||
Sbjct  550  CTTGATACTGGCGATCTTGAGTTCGAGAGAGGTTGGTGGAACTCCGAGTGTAGAGGTGAA  609

Query  302  ATTCGTAGATATTCGGAAGAACACCAGTGGCGAAGGCGGCCAACTGGCTCGATACTGACG  361
            ||||||||||||||||||||||||||||||||||||||||||||||||||||||||||||
Sbjct  610  ATTCGTAGATATTCGGAAGAACACCAGTGGCGAAGGCGGCCAACTGGCTCGATACTGACG  669

Query  362  CTGAGGTGCGAAAGCGTGGGGAGCAAACAGGATTAGATACCCTGGTAGTCCACGCCGTAA  421
            ||||||||||||||||||||||||||||||||||||||||||||||||||||||||||||
Sbjct  670  CTGAGGTGCGAAAGCGTGGGGAGCAAACAGGATTAGATACCCTGGTAGTCCACGCCGTAA  729

Query  422  ACGATGGATGCTAGCCGTTGGGGAGCTTGCTCTTCAGTGGCGCAGCTAACGCCTTAAGCA  481
            ||||||||||||||||||||||||||||||||||||||||||||||||||||||||||||
Sbjct  730  ACGATGGATGCTAGCCGTTGGGGAGCTTGCTCTTCAGTGGCGCAGCTAACGCCTTAAGCA  789

Query  482  TCCCGCCTGGGGAGTACGGTCGCAAGATT-AAACTCAAAGGAATTGACGGGGGCCCGCAC  540
            |||||||||||||||||||||||||||||| ||||||||||||||||||||||||||||||
Sbjct  790  TCCCGCCTGGGGAGTACGGTCGCAAGATTAAAACTCAAAGGAATTGACGGGGGCCCGCAC  849

Query  541  AAGCGGTGGAGCATGTGGTTTA-TTCCAAGC-ACGCGCAAAACC-TACCAGCCTTTGA-A  596
            |||||||||||||||||||||| ||| |||| ||||||| |||| |||||||||||||  |
Sbjct  850  AAGCGGTGGAGCATGTGGTTTAATTCGAAGCAACGCGCAGAACCTTACCAGCCTTTGACA  909

Query  597  TGGCAGGACG-CTTCCGGAGACGGATT-CTTCCACCA-TGGACCTGC-CACAGGTG  648
            |||||||||| ||||||||||||||| |||||| || ||||||||| ||||||||
Sbjct  910  TGGCAGGACGACTTCCGGAGACGGATTTCTTCCAGCAATGGACCTGCACACAGGTG  965
```

A19. **The alignment statistics for the best match obtained for the mapping PCR analysis of OPS0865**

Best match:- Azorhizobium caulinodans phbC gene

Length: 1752

Score	Expect	Identities	Gaps	Strand
1110 bits(601)	**0.0**	**604/605(99%)**	**1/605(0%)**	**Plus/Plus**

```
Query  1    CGGC-AGGCCGTCGCCGCTTACATGCGTCCGCGCGAGGAGGGCAAGCCGGACGACATGAC  59
            |||| ||||||||||||||||||||||||||||||||||||||||||||||||||||||
Sbjct  45   CGGCAAGGCCGTCGCCGCTTACATGCGTCCGCGCGAGGAGGGCAAGCCGGACGACATGAC  104

Query  60   GGACGATATCGCCGATGCGCTCAAGACCATCGGCGAGGTGGCCAATTACTGGATGTCCGA  119
            ||||||||||||||||||||||||||||||||||||||||||||||||||||||||||||
Sbjct  105  GGACGATATCGCCGATGCGCTCAAGACCATCGGCGAGGTGGCCAATTACTGGATGTCCGA  164

Query  120  TCCAAAGCGCTCCTTCGAGGCCCAGTCGCGCCTCATGATGGGCTACATGGGCGTCTGGGC  179
            ||||||||||||||||||||||||||||||||||||||||||||||||||||||||||||
Sbjct  165  TCCAAAGCGCTCCTTCGAGGCCCAGTCGCGCCTCATGATGGGCTACATGGGCGTCTGGGC  224

Query  180  GGGGGCGCTCCAGAAGCTCTCCGGCGAGAAGGCCGAGCCCATCGCGAAGGCCGACCCCAA  239
            ||||||||||||||||||||||||||||||||||||||||||||||||||||||||||||
Sbjct  225  GGGGGCGCTCCAGAAGCTCTCCGGCGAGAAGGCCGAGCCCATCGCGAAGGCCGACCCCAA  284

Query  240  GGACGGCCGCTTCAAGGACCCGGAATGGGAAAGCCCGTTCTTCGACGCCCTGAAGCAGAC  299
            ||||||||||||||||||||||||||||||||||||||||||||||||||||||||||||
Sbjct  285  GGACGGCCGCTTCAAGGACCCGGAATGGGAAAGCCCGTTCTTCGACGCCCTGAAGCAGAC  344

Query  300  CTATCTCGTGACCAGCAACTGGGCCGAGTCCATGGTCAAGGAGGCCGAGGGGCTCGATCC  359
            ||||||||||||||||||||||||||||||||||||||||||||||||||||||||||||
Sbjct  345  CTATCTCGTGACCAGCAACTGGGCCGAGTCCATGGTCAAGGAGGCCGAGGGGCTCGATCC  404

Query  360  CCACACCAAGCACAAGGCCGAATTCCTGGTGCGCCAGCTCTCGAATGCGGTGGCGCCCTC  419
            ||||||||||||||||||||||||||||||||||||||||||||||||||||||||||||
Sbjct  405  CCACACCAAGCACAAGGCCGAATTCCTGGTGCGCCAGCTCTCGAATGCGGTGGCGCCCTC  464

Query  420  GAACTTCCTCATGACCAACCCGGAGCTGATCCGCGAAACGCTCTCCTCCAGCGGCGAGAA  479
            ||||||||||||||||||||||||||||||||||||||||||||||||||||||||||||
Sbjct  465  GAACTTCCTCATGACCAACCCGGAGCTGATCCGCGAAACGCTCTCCTCCAGCGGCGAGAA  524

Query  480  CCTCGTGCGCGGCATGAAGAATCTGGCCGAGGATCTGGTGGAGGGCAAAGGCGATCTCAA  539
            ||||||||||||||||||||||||||||||||||||||||||||||||||||||||||||
Sbjct  525  CCTCGTGCGCGGCATGAAGAATCTGGCCGAGGATCTGGTGGAGGGCAAAGGCGATCTCAA  584

Query  540  GATCCGCCAGACGGACATGAGCGCCTTCGAGGTGGGCCGCAATCTGGCGCTCAGCCCCGG  599
```

```
            ||||||||||||||||||||||||||||||||||||||||||||||||||||||||||||||||
Sbjct  585  GATCCGCCAGACGGACATGAGCGCCTTCGAGGTGGGCCGCAATCTGGCGCTCAGCCCCGG  644

Query  600  CAAGG  604
            |||||
Sbjct  645  CAAGG  649
```

Table A20: **MS measurements of valid molecular fragments used for ^{13}C-MFA of OPS0865 free-living cultures under aerobic conditions.**

Molecular fragments	Mass isotopomer	Mass isotopomer distribution (fractional abundance)		
		Replicate 1	Replicate 2	Replicate 3
Ala260	M + 0	0.7464	0.7383	0.7394
	M + 1	0.0746	0.082	0.082
	M + 2	0.0382	0.042	0.0408
	M + 3	0.1409	0.1377	0.1378
Ala 232	M + 0	0.7595	0.7547	0.7554
	M + 1	0.0927	0.1011	0.1007
	M + 2	0.1479	0.1441	0.1439
Gly 246	M + 0	0.7891	0.7878	0.7894
	M + 1	0.0435	0.0449	0.0455
	M + 2	0.1673	0.1673	0.1651
Gly218	M + 0	0.8098	0.8096	0.8098
	M + 1	0.1902	0.1904	0.1902
Val288	M + 0	0.58	0.572	0.5728
	M + 1	0.1192	0.1292	0.1293
	M + 2	0.1442	0.1432	0.1422
	M + 3	0.1194	0.1185	0.1183
	M + 4	0.0174	0.0186	0.0182
	M + 5	0.0198	0.0185	0.0191
Val260	M + 0	0.5794	0.5742	0.5756
	M + 1	0.1366	0.1483	0.146
	M + 2	0.2264	0.2243	0.2231
	M + 3	0.037	0.0341	0.0354
	M + 4	0.0205	0.019	0.0199
Val186	M + 0	0.5823	0.574	0.5758
	M + 1	0.1357	0.1451	0.144
	M + 2	0.2284	0.2256	0.2252
	M + 3	0.0323	0.0342	0.0338
	M + 4	0.0213	0.0211	0.0212
Leu 274	M + 0	0.4953	0.4869	0.4883
	M + 1	0.2099	0.217	0.217
	M + 2	0.212	0.2107	0.2095
	M + 3	0.0285	0.0618	0.0609
	M + 4	0.0213	0.0207	0.0212
	M + 5	0.003	0.003	0.0032
Leu200	M + 0	0.4905	0.4828	0.4836
	M + 1	0.208	0.2149	0.2141
	M + 2	0.2179	0.2159	0.2162
	M + 3	0.0615	0.0634	0.0626
	M + 4	0.0208	0.0211	0.0213
	M + 5	0.0013	0.002	0.0021
Met 320	M + 0	0.6435	0.6445	0.6722
	M + 1	0.126	0.154	0.1307
	M + 2	0.0741	0.0446	0.044
	M + 3	0.0032	0.017	0.0217
	M + 4	0.1283	0.1226	0.1207
	M + 5	0.0248	0.0173	0.0108

Molecular fragments	Mass isotopomer	Mass isotopomer distribution (fractional abundance)		
		Replicate 1	Replicate 2	Replicate 3
Met 218	M + 0	0.6689	0.6535	0.6689
	M + 1	0.1571	0.1586	0.1509
	M + 2	0.0423	0.0504	0.0526
	M + 3	0.1132	0.1255	0.1127
	M + 4	0.0185	0.0138	0.0149
Ser 390	M + 0	0.7075	0.7063	0.7046
	M + 1	0.1148	0.1187	0.1214
	M + 2	0.0828	0.0773	0.0789
	M + 3	0.0949	0.0977	0.095
Ser 362	M + 0	0.7224	0.718	0.7184
	M + 1	0.1781	0.1813	0.1787
	M + 2	0.0995	0.1008	0.1029
Ser288	M + 0	0.723	0.7223	0.7222
	M + 1	0.1748	0.1793	0.1735
	M + 2	0.1023	0.0984	0.1044
Ser302	M + 0	0.7943	0.7884	0.786
	M + 1	0.0415	0.0456	0.0453
	M + 2	0.1642	0.166	0.1688
Thr404	M + 0	0.743	0.7384	0.714
	M + 1	0.0537	0.0509	0.0746
	M + 2	0.0608	0.0708	0.0624
	M + 3	0.0073	0.0093	0.0148
	M + 4	0.1352	0.1306	0.1343
Thr376	M + 0	0.762	0.7439	0.7665
	M + 1	0.0571	0.078	0.056
	M + 2	0.0373	0.0376	0.0468
	M + 3	0.1436	0.1405	0.1307
Phe336	M + 0	0.359	0.3515	0.3532
	M + 1	0.1912	0.1918	0.1944
	M + 2	0.1332	0.1374	0.1361
	M + 3	0.1738	0.1739	0.1711
	M + 4	0.0689	0.0727	0.0711
	M + 5	0.0418	0.0412	0.0416
	M + 6	0.0228	0.0219	0.0225
	M + 7	0.0065	0.0068	0.0071
	M + 8	0.0026	0.0027	0.0026
	M + 9	0.0002	0.0002	0.0003
Phe302	M + 0	0.7954	0.7898	0.7892
	M + 1	0.0407	0.045	0.044
	M + 2	0.1639	0.1652	0.1668
Asp418	M + 0	0.7347	0.7246	0.7258
	M + 1	0.0639	0.0714	0.0682
	M + 2	0.054	0.06	0.0613
	M + 3	0.0105	0.0122	0.0119
	M + 4	0.137	0.1318	0.1329
Asp390	M + 0	0.75	0.7418	0.744
	M + 1	0.074	0.0827	0.081
	M + 2	0.0337	0.0405	0.0395
	M + 3	0.1422	0.135	0.1355
Asp316	M + 0	0.7458	0.7405	0.7416
	M + 1	0.0746	0.0833	0.0821
	M + 2	0.0359	0.0401	0.0391
	M + 3	0.141	0.1361	0.1372
Asp302	M + 0	0.7872	0.783	0.7831
	M + 1	0.0429	0.0478	0.0477
	M + 2	0.1698	0.1693	0.1692

Molecular fragments	Mass isotopomer	Mass isotopomer distribution (fractional abundance)		
		Replicate 1	Replicate 2	Replicate 3
Glu404	M + 0	0.609	0.5994	0.5991
	M + 1	0.1343	0.143	0.1458
	M + 2	0.2169	0.2158	0.2141
	M + 3	0.0196	0.0252	0.0245
	M + 4	0.0201	0.0166	0.0164
Glu330	M + 0	0.6067	0.596	0.5958
	M + 1	0.1335	0.1472	0.1482
	M + 2	0.2181	0.2156	0.2137
	M + 3	0.0233	0.0246	0.0246
	M + 4	0.0184	0.0166	0.0177
Lys329	M + 0	0.5807	0.5797	0.5728
	M + 1	0.1278	0.1374	0.1326
	M + 2	0.1424	0.1409	0.1472
	M + 3	0.1186	0.1136	0.1175
	M + 4	0.0155	0.0148	0.0167
	M + 5	0.0149	0.0136	0.0132
Arg340	M + 0	0.5575	0.5393	0.523
	M + 1	0.1762	0.1904	0.1945
	M + 2	0.2002	0.2026	0.2036
	M + 3	0.0428	0.0472	0.0546
	M + 4	0.0183	0.0155	0.0153
	M + 5	0.005	0.0051	0.009
His440	M + 0	0.462	0.4571	0.4584
	M + 1	0.2289	0.2307	0.2309
	M + 2	0.1273	0.1303	0.1333
	M + 3	0.1211	0.1196	0.1158
	M + 4	0.0401	0.0421	0.0428
	M + 5	0.0179	0.0168	0.017
	M + 6	0.0027	0.0034	0.0018
His338	M + 0	0.4845	0.4774	0.4768
	M + 1	0.2097	0.2181	0.2167
	M + 2	0.201	0.2077	0.2084
	M + 3	0.0734	0.0679	0.0707
	M + 4	0.025	0.0238	0.0243
	M + 5	0.0065	0.0052	0.0031
Tyr466	M + 0	0.3582	0.3523	0.3589
	M + 1	0.1881	0.1935	0.1966
	M + 2	0.1394	0.1379	0.1292
	M + 3	0.1758	0.1722	0.1718
	M + 4	0.0688	0.0717	0.0741
	M + 5	0.0382	0.0398	0.0403
	M + 6	0.0228	0.0227	0.0199
	M + 7	0.0073	0.0066	0.0063
	M + 8	0.0018	0.0026	0.0027
	M + 9	-0.0003	0.0007	0.0001
Tyr302	M + 0	0.79	0.7847	0.7863
	M + 1	0.0431	0.046	0.0468
	M + 2	0.1669	0.1693	0.1668
Pro286	M + 0	0.5883	0.5796	0.5855
	M + 1	0.1206	0.1373	0.1329
	M + 2	0.1281	0.1332	0.1345
	M + 3	0.1106	0.118	0.1073
	M + 4	0.0324	0.0085	0.0331
	M + 5	0.02	0.0234	0.0068

Molecular fragments	Mass isotopomer	Mass isotopomer distribution (fractional abundance)		
		Replicate 1	Replicate 2	Replicate 3
Pro184	M + 0	0.6142	0.6056	0.6071
	M + 1	0.1311	0.1363	0.1369
	M + 2	0.2198	0.2195	0.2166
	M + 3	0.0196	0.023	0.0229
	M + 4	0.0153	0.0155	0.0164
Tre361	M + 0	0.5036	0.478	0.4744
	M + 1	0.1628	0.1927	0.1955
	M + 2	0.0967	0.1114	0.1132
	M + 3	0.176	0.1617	0.156
	M + 4	0.0323	0.032	0.0366
	M + 5	0.015	0.0132	0.0147
	M + 6	0.0136	0.0109	0.0097

Table A21: MS measurements of valid molecular fragments used for ^{13}C-MFA of OPS0865 free-living cultures under micro-aerobic conditions.

Molecular fragments	Mass isotopomer	Mass isotopomer distribution (fractional abundance)		
		Replicate 1	Replicate 2	Replicate 3
Ala260	M + 0	0.7302	0.7306	0.7307
	M + 1	0.0867	0.0854	0.086
	M + 2	0.0449	0.0438	0.0432
	M + 3	0.1382	0.1402	0.1402
Ala 232	M + 0	0.7508	0.7507	0.748
	M + 1	0.1053	0.1022	0.1047
	M + 2	0.1439	0.147	0.1472
Gly 246	M + 0	0.7837	0.7833	0.7814
	M + 1	0.0489	0.0465	0.0475
	M + 2	0.1675	0.1702	0.1712
Gly218	M + 0	0.8084	0.8051	0.8065
	M + 1	0.1916	0.1949	0.1935
Val288	M + 0	0.561	0.5624	0.5589
	M + 1	0.1351	0.1337	0.1352
	M + 2	0.1446	0.1451	0.1474
	M + 3	0.1212	0.1206	0.1193
	M + 4	0.0186	0.0184	0.0195
	M + 5	0.0195	0.0198	0.0197
Val260	M + 0	0.5657	0.5693	0.5637
	M + 1	0.15	0.1492	0.1527
	M + 2	0.2224	0.2251	0.2221
	M + 3	0.0413	0.0358	0.0402
	M + 4	0.0207	0.0207	0.0213
Val186	M + 0	0.5685	0.567	0.5643
	M + 1	0.1502	0.1479	0.1502
	M + 2	0.2231	0.2275	0.2272
	M + 3	0.0371	0.0359	0.0367
	M + 4	0.0211	0.0216	0.0216
Leu 274	M + 0	0.489	0.4817	0.4777
	M + 1	0.2184	0.2176	0.221
	M + 2	0.2093	0.2135	0.2124
	M + 3	0.0601	0.0626	0.0638
	M + 4	0.0206	0.022	0.0221
	M + 5	0.0026	0.0025	0.003

Molecular fragments	Mass isotopomer	Mass isotopomer distribution (fractional abundance)		
		Replicate 1	Replicate 2	Replicate 3
Met 218	M + 0	0.6709	0.6624	0.6788
	M + 1	0.1452	0.1486	0.1416
	M + 2	0.0486	0.0384	0.0476
	M + 3	0.1214	0.138	0.1328
	M + 4	0.014	0.0126	-0.0009
Ser 390	M + 0	0.6869	0.7047	0.7087
	M + 1	0.1336	0.1138	0.1093
	M + 2	0.0935	0.0747	0.0697
	M + 3	0.0859	0.1067	0.1123
Ser 362	M + 0	0.7064	0.7204	0.7204
	M + 1	0.203	0.1668	0.1605
	M + 2	0.0906	0.1128	0.119
Ser288	M + 0	0.7105	0.7222	0.7265
	M + 1	0.1971	0.1648	0.1553
	M + 2	0.0924	0.113	0.1182
Ser302	M + 0	0.7846	0.7838	0.7816
	M + 1	0.0503	0.0459	0.0475
	M + 2	0.165	0.1703	0.1709
Thr404	M + 0	0.7247	0.7287	0.7223
	M + 1	0.0647	0.0633	0.0681
	M + 2	0.0693	0.0645	0.0628
	M + 3	0.0121	0.012	0.009
	M + 4	0.1292	0.1323	0.1379
Thr376	M + 0	0.7463	0.7513	0.7405
	M + 1	0.0851	0.0735	0.0753
	M + 2	0.0384	0.0425	0.0398
	M + 3	0.1302	0.1327	0.1444
Phe336	M + 0	0.3476	0.342	0.3399
	M + 1	0.1967	0.1936	0.1945
	M + 2	0.141	0.1394	0.1407
	M + 3	0.1674	0.175	0.1739
	M + 4	0.074	0.0732	0.0749
	M + 5	0.0409	0.0427	0.0436
	M + 6	0.0226	0.0238	0.0226
	M + 7	0.0065	0.007	0.0069
	M + 8	0.0026	0.0029	0.0028
	M + 9	0.0006	0.0003	0.0002
Phe302	M + 0	0.791	0.7819	0.7848
	M + 1	0.0467	0.0504	0.046
	M + 2	0.1623	0.1677	0.1692
Asp418	M + 0	0.7184	0.7186	0.7186
	M + 1	0.0715	0.0691	0.069
	M + 2	0.0642	0.0627	0.0644
	M + 3	0.0123	0.012	0.0137
	M + 4	0.1336	0.1376	0.1343
Asp390	M + 0	0.7388	0.7358	0.7354
	M + 1	0.0844	0.0857	0.0821
	M + 2	0.0394	0.0391	0.0415
	M + 3	0.1374	0.1394	0.1409
Asp316	M + 0	0.736	0.7328	0.7358
	M + 1	0.0857	0.0839	0.0836
	M + 2	0.0405	0.0417	0.0409
	M + 3	0.1378	0.1416	0.1398
Asp302	M + 0	0.7811	0.7763	0.7792
	M + 1	0.0491	0.0479	0.0462
	M + 2	0.1698	0.1759	0.1745

Molecular fragments	Mass isotopomer	Mass isotopomer distribution (fractional abundance)		
		Replicate 1	Replicate 2	Replicate 3
Glu404	M + 0	0.5865	0.5882	0.5877
	M + 1	0.1507	0.147	0.1537
	M + 2	0.2199	0.2184	0.2139
	M + 3	0.0259	0.0268	0.0258
	M + 4	0.017	0.0196	0.0189
Glu330	M + 0	0.5886	0.5863	0.5876
	M + 1	0.153	0.1497	0.1497
	M + 2	0.2147	0.2183	0.2169
	M + 3	0.0262	0.0271	0.0269
	M + 4	0.0175	0.0186	0.0189
Lys329	M + 0	0.5615	0.5622	0.5579
	M + 1	0.1451	0.1395	0.1455
	M + 2	0.1486	0.1513	0.1493
	M + 3	0.1127	0.1168	0.1126
	M + 4	0.0193	0.0158	0.0175
	M + 5	0.0128	0.0143	0.0171
Arg442	M + 0	0.4731	0.4641	0.4739
	M + 1	0.2187	0.2253	0.2043
	M + 2	0.1204	0.1277	0.1299
	M + 3	0.1234	0.1243	0.1297
	M + 4	0.0411	0.039	0.04
	M + 5	0.0204	0.0184	0.0206
	M + 6	0.0029	0.0012	0.0015
Tyr466	M + 0	0.3532	0.3447	0.3435
	M + 1	0.1929	0.1975	0.1978
	M + 2	0.1445	0.1389	0.1406
	M + 3	0.1667	0.1708	0.1701
	M + 4	0.0779	0.0732	0.0764
	M + 5	0.0382	0.0416	0.0398
	M + 6	0.0212	0.0237	0.0265
	M + 7	0.0039	0.0066	0.0042
	M + 8	0.0032	0.0025	0.0026
	M + 9	-0.0016	0.0005	-0.0015
Tyr302	M + 0	0.7866	0.7807	0.7831
	M + 1	0.0477	0.0478	0.0471
	M + 2	0.1657	0.1715	0.1698
Pro258	M + 0	0.6059	0.5909	0.5868
	M + 1	0.1545	0.1452	0.1509
	M + 2	0.1993	0.2178	0.2155
	M + 3	0.0226	0.0293	0.0289
	M + 4	0.0176	0.0168	0.0179
Pro184	M + 0	0.5881	0.5999	0.5975
	M + 1	0.1512	0.1419	0.1452
	M + 2	0.2269	0.2212	0.218
	M + 3	0.0209	0.022	0.0237
	M + 4	0.013	0.015	0.0156
Tre361	M + 0	0.4613	0.4764	0.48
	M + 1	0.1962	0.1789	0.1769
	M + 2	0.1163	0.1094	0.1026
	M + 3	0.1585	0.1703	0.1774
	M + 4	0.0401	0.0356	0.0344
	M + 5	0.0189	0.0173	0.015
	M + 6	0.0087	0.0122	0.0137

Table A22: **Metabolic model used for ^{13}C-MFA of OPS0865 free-living cultures**

Reaction ID	Reaction step (s)	Symbol	Reactions
	Uptake fluxes		
R1	Uptake of $^{13}C_4$-succinate	*upt1*	Suc_$^{13}C_4$ -> Suc_in
R2	Uptake of ^{12}C-succinate	*upt2*	Suc_nat -> Suc_in
R3	Total uptake of succinate (constrained)	*upt3*	Suc_in -> Suc
	Tricarboxylic acid cycle		
R4	Succinate dehydrogenase	*tca1*	Suc <-> Fum
R5	Fumarase	*tca2*	Fum <-> Mal
R6	Malate dehydrogenase	*tca3*	Mal <-> OAA
R7	Citrate synthase	*tca4*	OAA + AcCoA -> Cit
R8	Aconitase	*tca5*	Cit <-> ICit
R9	Isocitrate dehydrogenase NADP-dependent	*tca6*	ICit <-> AKG + CO_2
R10	2-Oxoglutarate dehydrogenase	*tca7*	AKG -> SucCoA + CO_2
R11	Succinyl-CoA synthetase	*tca8*	SucCoA <-> Suc
R12	Pyruvate dehydrogenase	*tca9*	Pyr -> AcCoA + CO_2
	Anaplerotic pathways		
R13	NAD-dependent malic enzyme	*mal*	Mal -> Pyr + CO_2
R14	Phosphoenolpyruvate carboxykinase	*pepck*	PEP + CO2 <-> OAA
R15	Methylmalonate-semialdehyde dehydrogenase	*msdh*	OAA -> AcCoA + CO_2 + CO_2
	Glycolysis		
R16	Pyruvate kinase	*gly1*	PEP -> Pyr
	Gluconeogenesis		
R17	Phosphoglycerate kinase	*glu1*	PEP <-> PG3
R18	Glyceraldehyde-3-phosphate dehydrogenase	*glu2*	PG3 <-> GAP
R19	Triosephosphate isomerase	*glu3*	GAP <-> DHAP
R20	Fructose-bisphosphate aldolase	*glu4*	DHAP + GAP <-> FBP
R21	Fructose-1,6-bisphosphatase	*glu5*	FBP -> F6P
R22	Phosphoglucose isomerase	*glu6*	F6P <-> G6P
	Pentose phosphate pathway		
R23	Glucose-6-phosphate dehydrogenase	*ppp1*	G6P -> PG6
R24	6-phosphogluconate dehydrogenase	*ppp2*	PG6 -> Ru5P + CO2
R25	Ribulose-phosphate 3-epimerase	*ppp3*	Ru5P <-> X5P

Reaction ID	Reaction step (s)	Symbol	Reactions
R26	Ribose 5-phosphate isomerase	*ppp4*	Ru5P <-> R5P
R27	Transketolase- C5/C3 conversion	*ppp5*	X5P <-> GAP + EC2
R28	Transketolase- C6/C4 conversion	*ppp6*	F6P <-> E4P + EC2
R29	Transketolase- C7/C5 conversion	*ppp7*	S7P <-> R5P + EC2
R30	Transaldolase- C6/C3 conversion	*ppp8*	F6P <-> GAP + EC3
R31	Transaldolase- C7/C4 conversion	*PPP9*	S7P <-> E4P + EC3
R32	Entner-Doudoroff pathway 6-Phosphogluconate dehydratase	*ed1*	PG6 -> KDPG
R33	2-keto-3-deoxy-6-phosphogluconate aldolase	*ed2*	KDPG -> Pyr + GAP
R34	Amino acid synthesis Glutamate dehydrogenase	*glt*	AKG -> Glu
R35	Glutamine synthetase	*gln*	Glu -> Gln
R36	Proline synthesis	*pro*	Glu -> Pro
R37	Arginine synthesis	*arg*	Glu + CO2 + Gln + Asp + AcCoA -> Arg + AKG + Fum + Ac
R38	Aspartate transaminase	*asp*	OAA + Glu -> Asp + AKG
R39	Asparagine synthase	*asn*	Asp -> Asn
R40	Alanine aminotransferase	*ala*	Pyr + Glu -> Ala + AKG
R41	Serine synthesis	*ser*	PG3 + Glu -> Ser + AKG
R42	Serine hydroxymethyltransferase	*glc1*	Ser <-> Gly + MEETHF
R43	MEETHF synthesis	*meethf*	Gly <-> CO2 + MEETHF
R44	Threonine aldolase	*glc2*	Thr -> Gly + AcCoA
R45	Cysteine synthesis	*cys*	Ser + AcCoA -> Cys + Ac
R46	Lysine synthesis	*lys1*	Asp + Pyr + Glu + SucCoA -> LL_DAP + AKG + Suc
R47	Lysine synthesis	*lys2*	LL_DAP -> Lys + CO2
R48	Threonine synthesis	*thr*	Asp -> Thr
R49	Methionine synthesis	*met*	Asp + METHF + Cys + SucCoA -> Met + Pyr + Suc
R50	Valine synthesis	*val*	Pyr + Pyr + Glu -> Val + CO2 + AKG
R51	Leucine synthesis	*leu*	AcCoA + Pyr + Pyr + Glu -> Leu + CO2 + CO2 + AKG
R52	Isoleucine synthesis	*ile*	Thr + Pyr + Glu -> Ile + CO2 + AKG
R53	Phenylalanine synthesis	*phe*	PEP + PEP + E4P + Glu -> Phe + CO2 + AKG

Reaction ID	Reaction step (s)	Symbol	Reactions
R54	Tyrosine synthesis	*tyr*	PEP + PEP + E4P + Glu -> Tyr + CO2 + AKG
R55	Tryptophan synthesis	*trp*	Ser + R5P + PEP + E4P + PEP + Gln -> Trp + CO2 + GAP + Pyr + Glu
R56	Histidine synthesis	*his*	R5P + FTHF + Gln + Asp -> His + AKG + Fum
R57	METHF synthesis	*methf*	MEETHF -> METHF
R58	FTHF synthesis	*fthf*	MEETHF -> FTHF
R59	Metabolic CO_2 output (net)	*co2.out*	CO2 -> CO2.ext
R60	PHB synthesis	*accoa1*	AcCoA + AcCoA -> PHB + 2CoA
R61	Biomass synthesis	*biomass*	Biomass reaction for OPS0865 grown under aerobic conditions: 0.39*Ala + 0.363*Gly + 0.271*Val + 0.322*Leu + 0.188*Ile + 0.151*Pro + 0.089*Met + 0.199*Ser + 0.205*Thr + 0.127*Phe + 0.195*Asn + 0.195*Asp + 0.241*Glu + 0.241Gln + 0.236*Lys + 0.065*His + 0.11*Tyr + 0.227*Arg + 0.106*Cys + 0.037*Trp + 5.11*AcCoA + 0.352*DHAP + 0.614*PG3 + 0.31*OAA + 0.765*MEETHF + 0.712*R5P + 0.212*G6P -> 38.88*Biomass
			Biomass reaction for OPS0865 grown under micro-aerobic conditions: 0.4*Ala + 0.372*Gly + 0.277*Val + 0.33*Leu + 0.193*Ile + 0.154*Pro + 0.091*Met + 0.204*Ser + 0.211*Thr + 0.13*Phe + 0.2*Asn + 0.2*Asp + 0.248*Glu + 0.248Gln + 0.242*Lys + 0.067*His + 0.112*Tyr + 0.233*Arg + 0.109*Cys + 0.037*Trp + 4.656*AcCoA + 0.321*DHAP + 0.581*PG3 + 0.296*OAA + 0.744*MEETHF + 0.684*R5P + 0.284*G6P -> 38.47*Biomass
R62	Reaction to compensate for naturally occurring ^{12}C pools		0*Ala -> Ala.S
R63	Reaction to compensate for naturally occurring ^{12}C pools		0*Ala_nat -> Ala.S
R64	Reaction to compensate for naturally occurring ^{12}C pools		0*Gly -> Gly.S
R65	Reaction to compensate for naturally occurring ^{12}C pools		0*Gly_nat -> Gly.S
R66	Reaction to compensate for naturally occurring ^{12}C pools		0*Asp -> Asp.S
R67	Reaction to compensate for naturally occurring ^{12}C pools		0*Asp_nat -> Asp.S
R68	Reaction to compensate for naturally occurring ^{12}C pools		0*Val -> Val.S

Reaction ID	Reaction step (s)	Symbol	Reactions
R69	Reaction to compensate for naturally occurring ^{12}C pools		0*Val_nat -> Val.S
R70	Reaction to compensate for naturally occurring ^{12}C pools		0*Leu -> Leu.S
R71	Reaction to compensate for naturally occurring ^{12}C pools		0*Leu_nat -> Leu.S
R72	Reaction to compensate for naturally occurring ^{12}C pools		0*Ile -> Ile.S
R73	Reaction to compensate for naturally occurring ^{12}C pools		0*Ile_nat -> Ile.S
R74	Reaction to compensate for naturally occurring ^{12}C pools		0*Pro -> Pro.S
R75	Reaction to compensate for naturally occurring ^{12}C pools		0*Pro_nat -> Pro.S
R76	Reaction to compensate for naturally occurring ^{12}C pools		0*Met -> Met.S
R77	Reaction to compensate for naturally occurring ^{12}C pools		0*Met_nat -> Met.S
R78	Reaction to compensate for naturally occurring ^{12}C pools		0*Ser -> Ser.S
R79	Reaction to compensate for naturally occurring ^{12}C pools		0*Ser_nat -> Ser.S
R80	Reaction to compensate for naturally occurring ^{12}C pools		0*Thr -> Thr.S
R81	Reaction to compensate for naturally occurring ^{12}C pools		0*Thr_nat -> Thr.S
R82	Reaction to compensate for naturally occurring ^{12}C pools		0*Phe -> Phe.S
R83	Reaction to compensate for naturally occurring ^{12}C pools		0*Phe_nat -> Phe.S
R84	Reaction to compensate for naturally occurring ^{12}C pools		0*Glu -> Glu.S
R85	Reaction to compensate for naturally occurring ^{12}C pools		0*Glu_nat -> Glu.S
R86	Reaction to compensate for naturally occurring ^{12}C pools		0*Lys -> Lys.S
R87	Reaction to compensate for naturally occurring ^{12}C pools		0*Lys_nat -> Lys.S
R88	Reaction to compensate for naturally occurring ^{12}C pools		0*Arg -> Arg.S
R89	Reaction to compensate for naturally occurring ^{12}C pools		0*Arg_nat -> Arg.S
R90	Reaction to compensate for naturally occurring ^{12}C pools		0*His -> His.S
R91	Reaction to compensate for naturally occurring ^{12}C pools		0*His_nat -> His.S
R92	Reaction to compensate for naturally occurring ^{12}C pools		0*Tyr -> Tyr.S
R93	Reaction to compensate for naturally occurring ^{12}C pools		0*Tyr_nat -> Tyr.S
R94	Reaction to compensate for naturally occurring ^{12}C pools		0*PHB -> PHB.S
R95	Reaction to compensate for naturally occurring ^{12}C pools		0*PHB_nat -> PHB.S

Figure A23: **Comparison of the simulated and experimental MS measurements for the flux map of OPS0865 under aerobic condition**. The simulated (black bars) and measured (grey bars) are plotted with MI on X-axis and abundance of MI on Y-axis. There was no significant difference between the simulated and experimentally obtained MS measurements, which confirms the goodness of fit of the flux map. The MS measurements from 37 valid molecular fragments of amino acids, PHB and trehalose used for generating the flux map are– alanine (Ala 232, Ala 260), glycine (Gly 218, Gly 246), valine (Val 186, Val 260, Val 288), leucine (Leu 200, Leu 274), methionine (Met 218, Met 292, Met 320), serine (Ser 288, Ser 302, Ser 362, Ser 390), threonine (Thr 376, Thr 404), proline (Pro 184, Pro 258, Pro 286), phenylalanine (Phe 302, Phe 336), aspartate (Asp 302, Asp 316, Asp 390, Asp 418), glutamate (Glu 330, Glu 404, Glu 432), lysine (Lys 329), arginine (Arg 340), histidine (His 338, His 440), tyrosine (Tyr 302, Tyr 466), and trehalose (Tre 361).

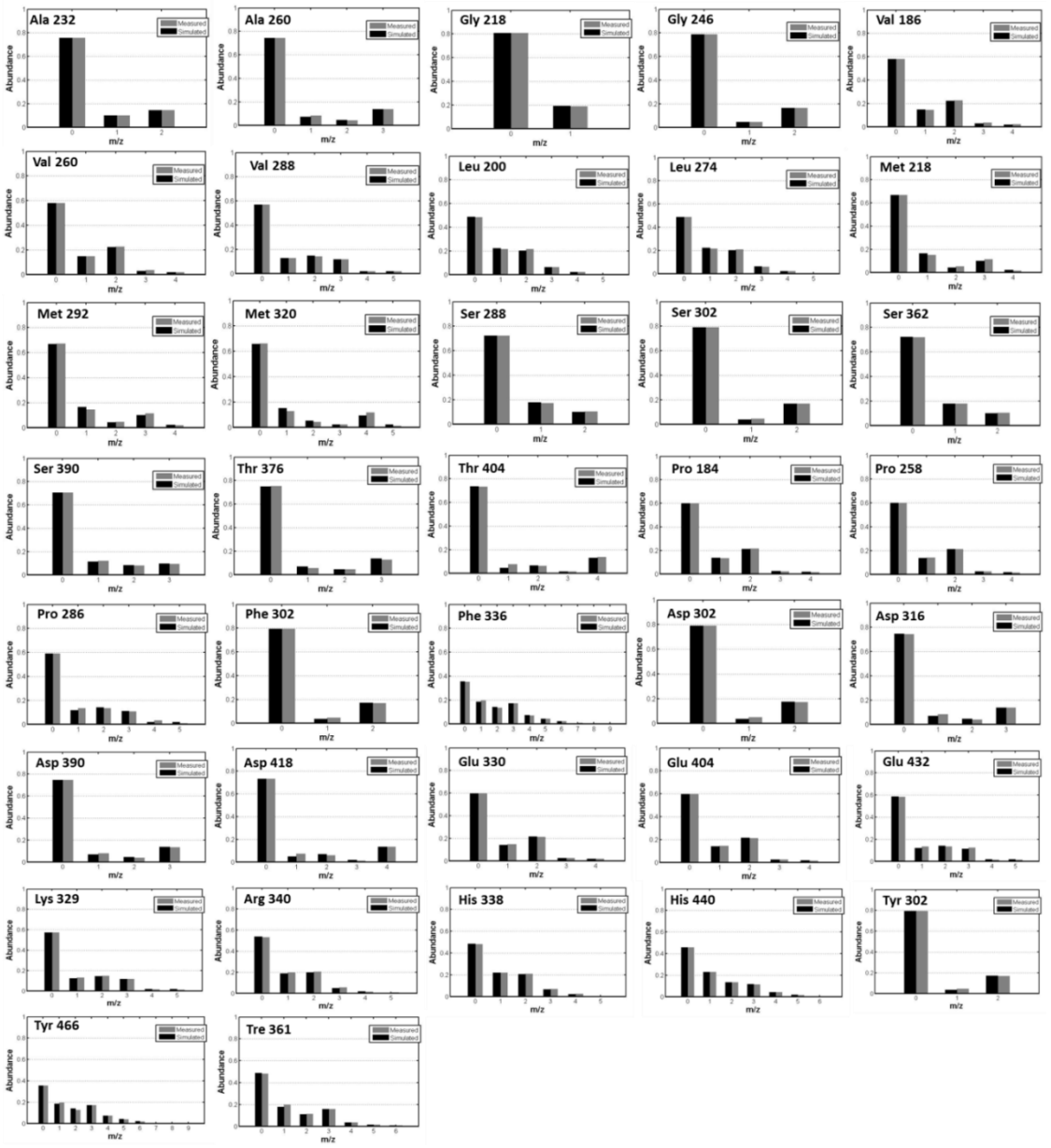

Figure A24: **Comparison of the simulated and experimental MS measurements for the flux map of OPS0865 under micro-aerobic condition**. The simulated (black bars) and measured (grey bars) are plotted with MI on X-axis and abundance of MI on Y-axis. There was no significant difference between the simulated and experimentally obtained MS measurements, which confirms the goodness of fit of the flux map. The MS measurements from 32 valid molecular fragments of amino acids, PHB and trehalose used for generating the flux map are– alanine (Ala 232, Ala 260), glycine (Gly 218, Gly 246), valine (Val 186, Val 260, Val 288), leucine (Leu 200, Leu 274), methionine (Met 218), serine (Ser 288, Ser 302, Ser 362, Ser 390), threonine (Thr 376, Thr 404), proline (Pro 184, Pro 258), phenylalanine (Phe 302, Phe 336), aspartate (Asp 302, Asp 316, Asp 390, Asp 418), glutamate (Glu 330, Glu 404, Glu 432), lysine (Lys 329), arginine (Arg 442), tyrosine (Tyr 302, Tyr 466), and trehalose (Tre 361).

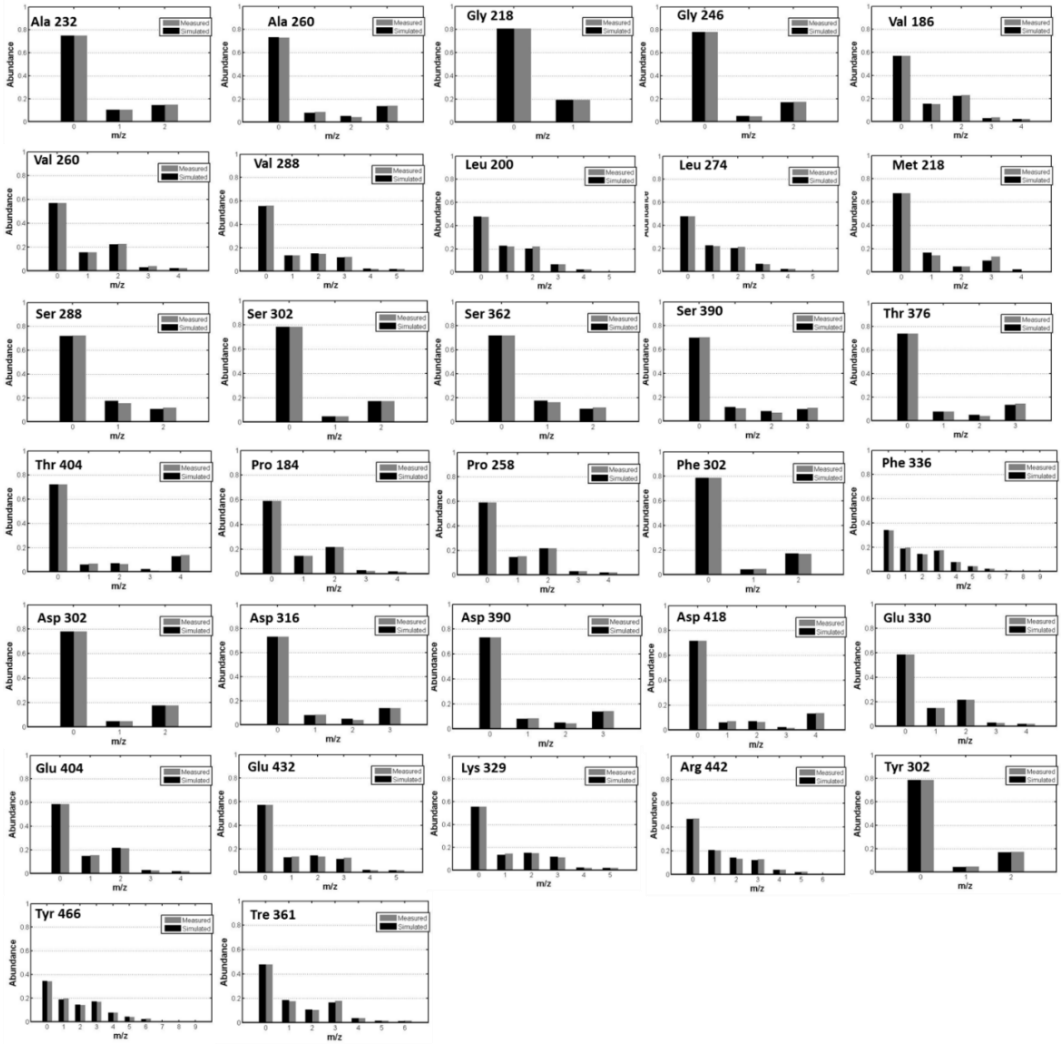

Figure A25: **Nitrogenase activity of *S. fredii* HH103 bacteroids isolated from soybean plants**

Measurements are mean ± SEM from three determinations.

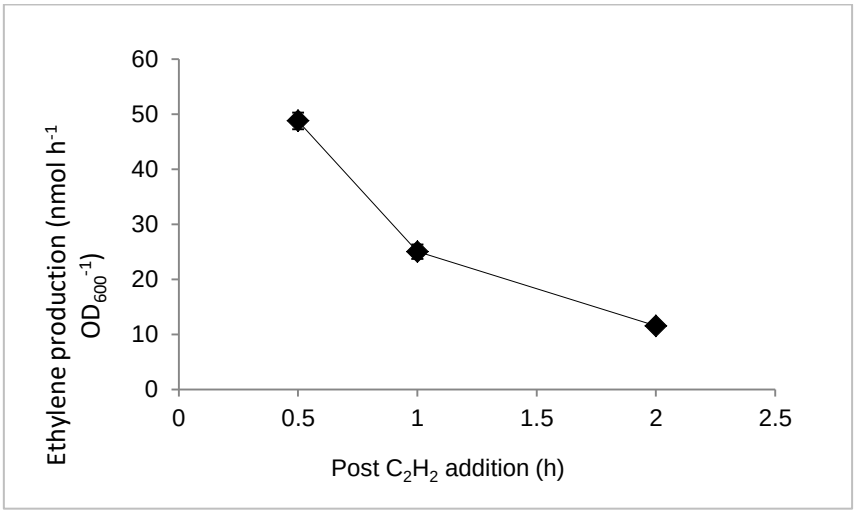

Figure A26: **Biomass composition of *S. fredii* HH103 isolated from soybean plants.** The measurements are mean ± SEM from three determinations.

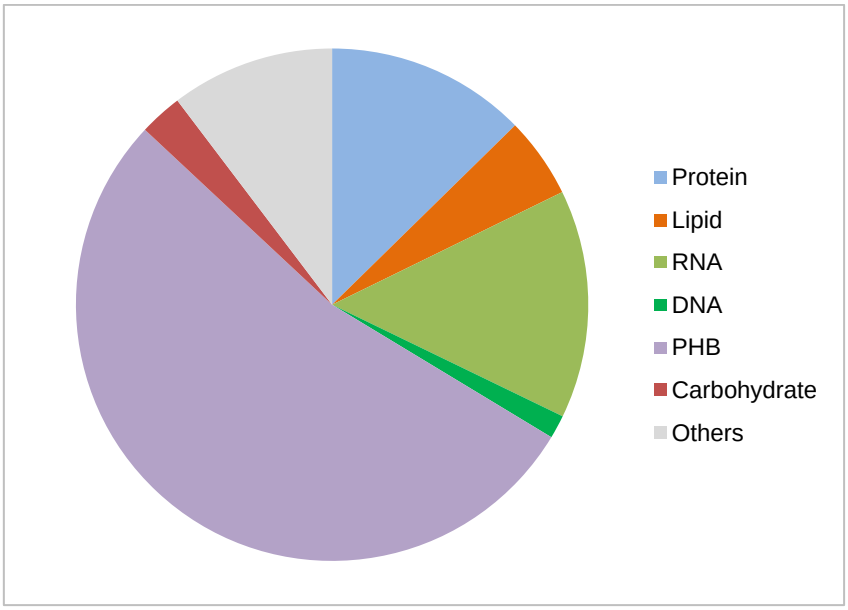

Figure A27: **Flux map of S fredii HH103 bacteroids isolated from soybean plants.** The flux maps represent statistically valid best-fit models based on the redistribution of label following metabolism of [$^{13}C_4$]succinate by HH103 bacteroids. The thickness of the each arrow in the flux maps is proportional to the relative molar flux. Metabolic intermediates and biomass outputs are shown in rectangular boxes with distinct colour key.

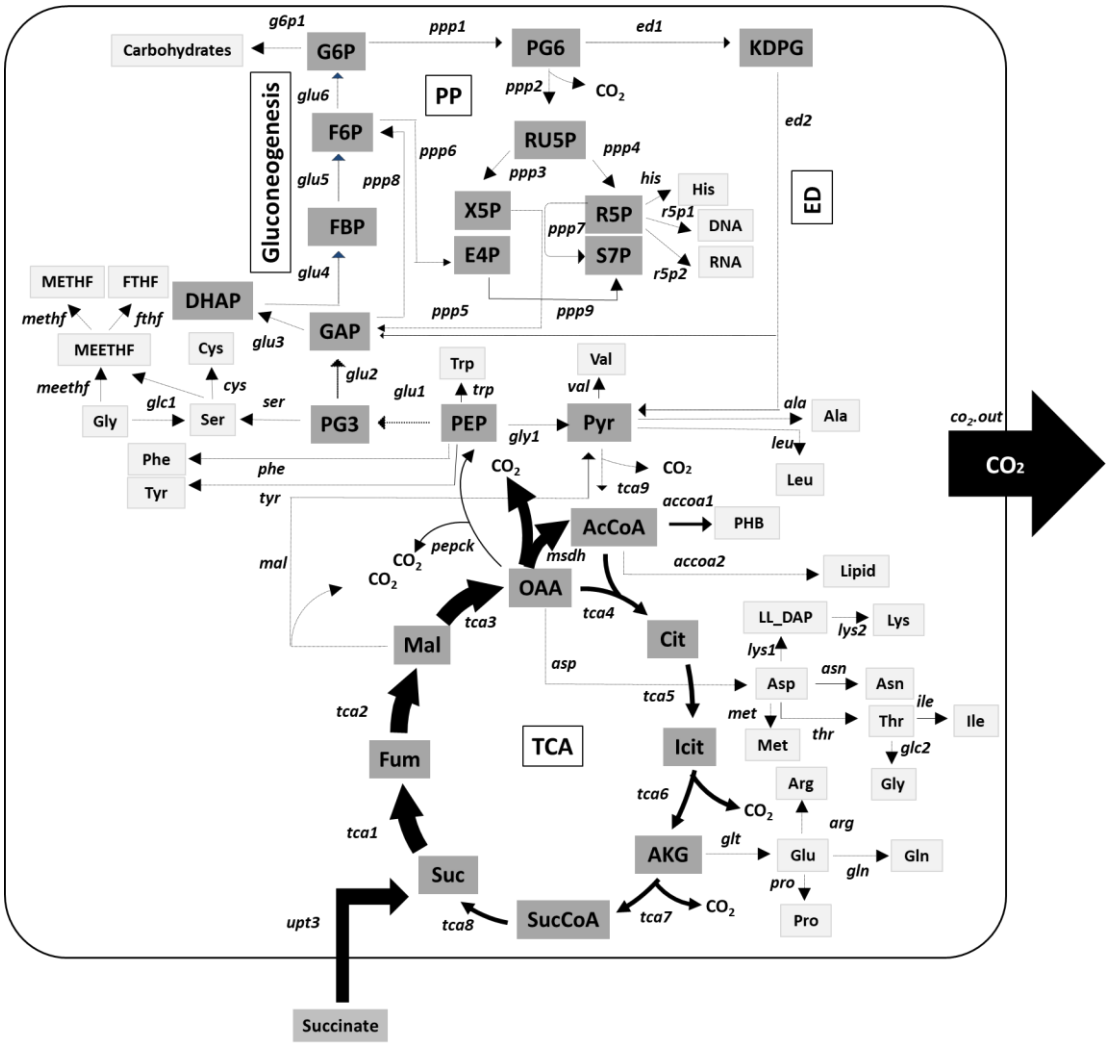

Key to flux maps:
Colour key:

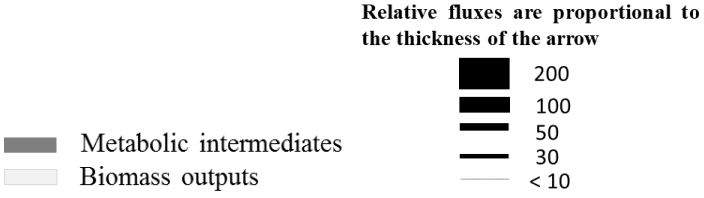

Figure A28: **Comparison of growth curves of ORS571 cultures grown with various carbon sources.** Values are calculated from the growth curves shown in Figure 3.10 and using methods described in section 2.20. Values are the mean ± SEM from three biological replicates.

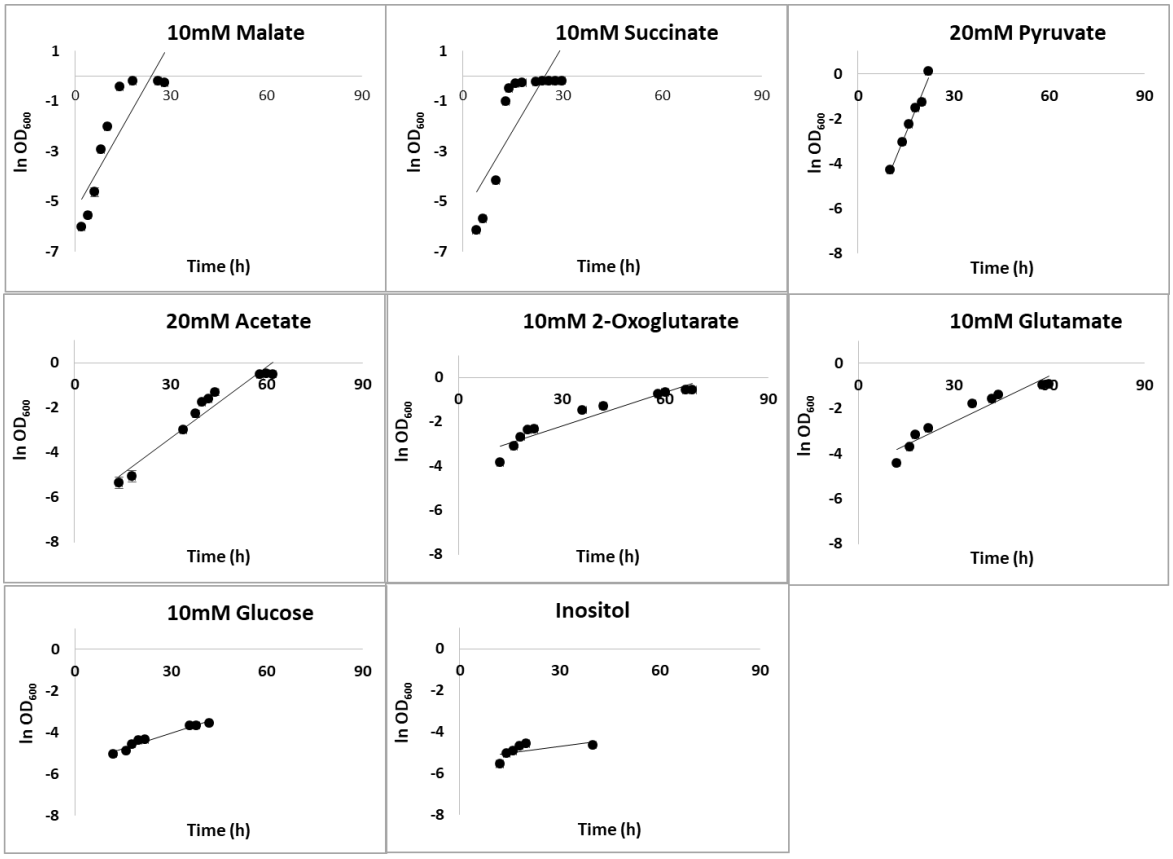

Figure A29: **Comparison of growth rates of ORS571 cultures grown with various carbon sources.** Values are calculated from the growth curves shown in Figure 3.10 and using methods described in section 2.20. Values are the mean ± SEM from three biological replicates.

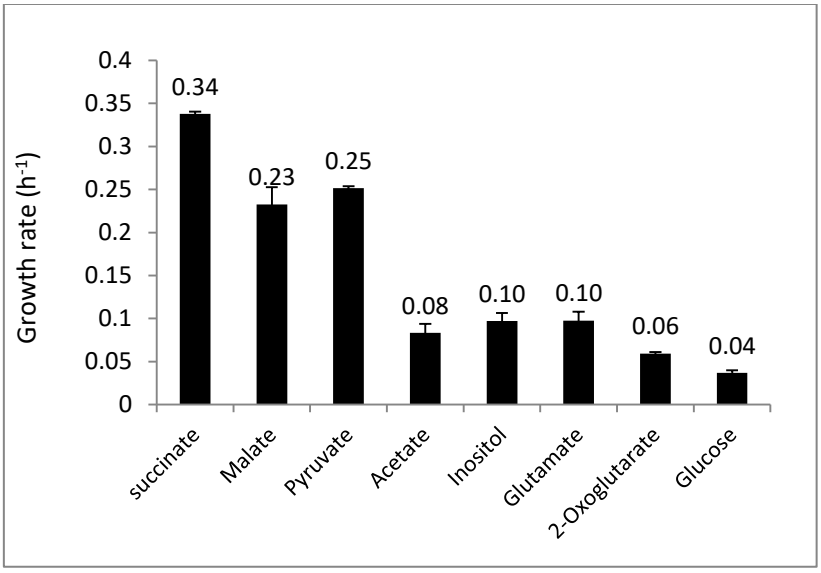

Figure A30: **Comparison of growth of ORS571 cultures grown with various oxygen concentrations.** Values are calculated from the growth curves shown in Figure 4.2 and using methods described in section 2.20. Values are the mean ± SEM from three biological replicates.

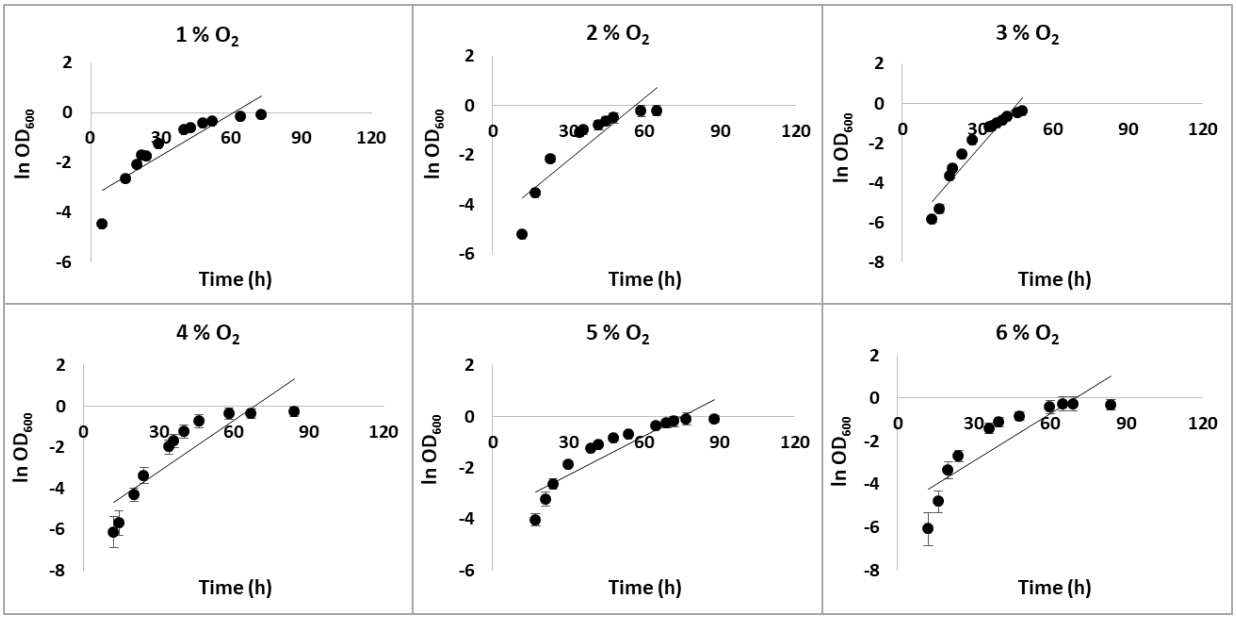

Figure A31: **Comparison of growth of ORS571 cultures grown with various oxygen concentrations.** Values are calculated from the growth curves shown in Figure 4.2 and using